A MODEL OF THE ION CHEMISTRY OF ELECTRIFIED CONVECTION

by

ROBERT A. BOLDI

B.S., Biology
Boston College, Chestnut Hill, MA, 1974

M.S., Environmental Studies
University of Montana, Missoula, MT, 1981

Submitted to the Department of
Earth, Atmospheric, and Planetary Sciences
in Partial Fulfillment of the Requirements for the Degree of

DOCTOR OF PHILOSOPHY
IN METEOROLOGY

at the

MASSACHUSETTS INSTITUTE OF TECHNOLOGY

September 1992

Signature of Author _____
Department of Earth, Atmospheric, and Planetary Sciences
Center for Meteorology and Physical Oceanography
11 September, 1992

Certified by _____
Ronald G. Prinn, Thesis Supervisor

Accepted by _____
Thomas H. Jordan, Department Chairman

A MODEL OF THE ION CHEMISTRY OF ELECTRIFIED CONVECTION

by

ROBERT A. BOLDI

Submitted to the Department of Earth, Atmospheric, and Planetary Sciences
on 11 September, 1992 in partial fulfillment of the requirements for the
degree of Doctor of Philosophy in Meteorology

ABSTRACT

Electrified convection provides a unique setting for atmospheric chemistry. While the chemistry of lightning is sometimes thought of as predominantly the chemistry of the hot ($\approx 30,000$K) lightning channel, the large radial electric fields (>breakdown strength of air) surrounding the lightning channel result in high ion and electron production rates in the "corona sheath". Additionally, the high-temperature lightning channel releases large amounts of short-wavelength, ionizing, UV radiation ($\lambda_{max} \approx$ 100nm) that is absorbed in the surrounding region. The relative volumes of the hot lightning channel and the surrounding corona sheath are also noteworthy. If a typical lightning channel has a radius of a few centimeters and the surrounding corona sheath is a few tens of meters then the ratio of the volume of the corona sheath to that of the lightning channel is $10^6 : 1$.

The fate of the highly reactive, charged products formed outside of the hot channel determine, in part, the net chemical effect of electrified convection. These products can dominate over the hot-channel chemistry and alter the local concentrations of all the major chemical families considered in standard photochemical studies. Additionally, it is of interest to know whether electron-capturing gases with very long tropospheric lifetimes, such as SF_6, may be removed by in-cloud ion chemistry at a rate sufficient to materially alter their total atmospheric lifetime.

To examine the chemical effects of the reactions induced by the ions, electrons, and photons produced in and around a lightning channel, a two-dimensional, axisymmetric dynamical/chemical model of electrified convection has been developed. This model represents the first effort to model the physical/chemical phenomena associated with the production of corona, the subsequent chemical reactions, and these reactions' integrated effects on the chemistry of electrified convection. This model considers ≈ 800 thermal and photochemical reactions among 165 neutrals, ions, water clusters, and electrons; effects of pressure, temperature, and electric fields upon the reaction coefficients are explicitly considered. Because the aim of this thesis is to focus on ion production and their subsequent gas-phase reactions, aqueous-phase chemistry has not been considered (although heteroge-

neous loss is represented) and the dynamics and microphysics are specified in a relatively simple manner.

The in-cloud lifetimes and storm-averaged production rates for each species considered in the (Electrified) model are computed and compared with their corresponding values computed by the model with all electrical processes turned off (the Base Case model run). Additionally, the relative chemical-source strengths of the hot channel *vis-à-vis* the surrounding regions are compared for selected chemical species.

The ion and UV-photon generation mechanisms dominate the overall production of many neutrals such as atomic O, N, and H, and are responsible for elevated mixing ratios of the sparingly soluble or short-lived chemical families that derive from these species (*i.e.* NO_x, O_x). For example, the average mixing ratio of NO_x is increased from 20 ppt in the Base Case model run to 100 ppb in the Electrified model run. Similarly, the maximum OH mixing ratio in the Electrified model run (5×10^{-10}) is 5 orders of magnitude higher than in the Base Case model run, and the domain-average mixing ratio is one order of magnitude larger.

The model-domain-averaged effect of lightning on the highly soluble chemical families such as HO_x, is relatively small because of high in-cloud scavenging rates that mask locally-high rates of production. For example, the model-domain-average concentration of HO_x changes by less than 2% between the Base Case & Electrified model runs, yet the maximum HO_x mixing ratios in the main ionization regions of the Electrified model are four orders of magnitude larger than in the Base Case model run.

In general, the ion and UV-induced reactions contribute equally to the production of both $O(^3P)$ and $O(^1D)$ and consequently are equally important in the overall chemistry of O_3 and OH and other derivative chemical species. Ion processes dominate the production of both the neutral N (and consequently its derivative species, *e.g.* NO) as well as charged species such as O_2^+, O_4^+, N_2^+, N_4^+, and the ions that ultimately derive from them, primarily water clusters $H_3O^+ \cdot (H_2O)_n$.

Extrapolating the results of this model to the global average number of thunderstorms ($\approx$ 1000 at any given time) results in an annual, global production of 20 Tg of O_3, 0.64 Tg of Nitrogen as NO_x, and 0.34 Tg of Nitrogen as N_2O. These values can be compared to the currently estimated global stratospheric source of O_3 of 680 $Tg \cdot yr^{-1}$ and to the currently estimated tropospheric source strengths of 6.8 Tg of Nitrogen as NO_x, and 9.7 Tg of Nitrogen as N_2O. The predicted mixing ratios of NO in the outflow of this model thunderstorm agrees with corresponding observations.

The Electrified model represents a net-loss process for some chemical species, primarily due to enhanced in-cloud OH levels. On a global basis this model accounts for the annual destruction of 1.8 Tg of CO, 0.45 Tg of CH_4, and 2×10^{-4} Tg of OCS. Once again, these are small fractions of the currently estimated annual source strengths of these species (1600 Tg CO, 525 Tg CH_4, and 0.4 Tg OCS).

Although the global budgets of the major chemical families and compounds are not greatly affected by electrified convection, the meso-scale regime in which the thunderstorms are embedded certainly are affected to a greater or lesser extent depending on the assumptions regarding the heterogeneous-loss rates of sparingly soluble species in the outflow.

In addition to the meso-scale chemical effects of the thunderstorm outflow, the electric-field-driven capture of ions and the heterogeneous loss of neutrals to cloud particles greatly alters the normal aqueous-phase chemistry of clouds, although this model does not accurately quantify the extent of this perturbation. Nevertheless, high levels (millimolar concentrations) of water-soluble oxidants such as H_2O_2 can reasonable be expected to occur in the vicinity (< 100's of meters) of corona and lightning events.

The quantities of almost all chemical species formed in the cooling hot channel are of little importance when compared with the corresponding quantities formed in the surrounding regions. The only exception is NO_x; while the local mixing ratios of NO and NO_2 can approach 0.01 in the cooled lightning channel, the relatively small volume of the hot lightning channel ($\approx$ 10 m^3) compared to the much larger volume of air surrounding the channel dominated by ion chemistry ($\approx 5 \times 10^7$ m^3) results in $\approx$ 50% of the in-cloud production of NO_x coming from the hot channel. The ion-induced processes occurring in the regions surrounding the lightning channel dominate the production or loss of all other species and chemical families (*e.g.* N_2O, O_x, HO_y).

For the cases of CF_4, SF_6, and $CC\ell_4$ their mean in-cloud chemical lifetimes are reduced by a factor of ≈ 2 from their base-case lifetimes of 6.1×10^7, 6.1×10^5, 2.2×10^4 years respectively. Given the small fraction of the Earth's troposphere that is in electrified convection ($\approx 6 \times 10^{-4}$), this in-cloud loss cannot compete with other known loss mechanisms, such as stratospheric or mesospheric photodissociation and electron impact that result in these gases having global lifetimes estimated to be of order centuries for CF_4 and SF_6, and decades for $CC\ell_4$.

This model is now being refined to include (1) a better representation of heterogeneous loss to the ice phase and (2) feedback between space charge (ions) and the electric field and it is being expanded to include the full range of aqueous-phase chemistry. Additionally (1) a better understanding of the electric-field-strength dependent reactions of e^- and O_2 with water would be valuable in quantifying the production of the HO_y family and (2) modeling the production of corona from water would improve the simulation of aqueous-phase ion chemistry. With these modifications in hand it will then become possible to make a complete first-principles model of the chemistry of lightning and its impact upon cloud chemistry.

Thesis supervisor: Dr. Ronald G. Prinn
Title: Professor of Atmospheric Chemistry

Acknowledgments

I would like to thank all people that I have come to know and respect for selflessly sharing their company and ideas. I would especially like to thank my thesis committee for their guidance. Finally I would like to thank my family and friends for the moral support that made this emotionally possible, and the John Lyons' Fund and the NSF Atmospheric Chemistry Program Grant ATM-87-10102 to MIT for the financial support that made all this economically possible.

Table of Contents

List of Figures

List of Tables

1 Introduction

1.1 The Global Electric Circuit

Lightning has long interested atmospheric scientists. It is presently thought to be the primary (if not sole) electrical generator that maintains the 250 kV potential gradient existing between the ground and the ionosphere in the presence of a 1kA discharge rate. An electrical schematic of the global electrical circuit is given in Figure 1. The data in this Figure and the discussion that follows reflect the summaries of the atmospheric electric circuit and findings as given in *Williams* [1985], *Ogawa* [1985], *Makina & Ogawa* [1985], and *Markson* [1985,1986].

The belief that thunderstorms are responsible for maintaining the ionospheric potential is supported by two lines of reasoning. The first line is based on calculations that demonstrate that if the global current generator, depicted in Figure 1 as a thunderstorm, were to cease operating then the potential gradient would decay with a time scale of tens of minutes. To explain why this decay is never observed, it is postulated that it is the relatively constant number of thunderstorms active at any one time over the globe ($\approx$ 1000, *cf.* page 9-4, *U.S.A.F.*, 1961) that is responsible for the relatively constant currents flowing in the global electrical circuit. The second line of reasoning links the observation that the slight daily variations in the ionospheric potential (the "*Carnegie*" curve) is synchronous with the slight daily variations in the global-average areal extent of thunderstorms to the idea that thunderstorms are indeed responsible for maintaining the ionospheric potential.

1.2 Ions are Charge Carriers

Fortunately for atmospheric chemists, an electrical schematic is **not** a complete

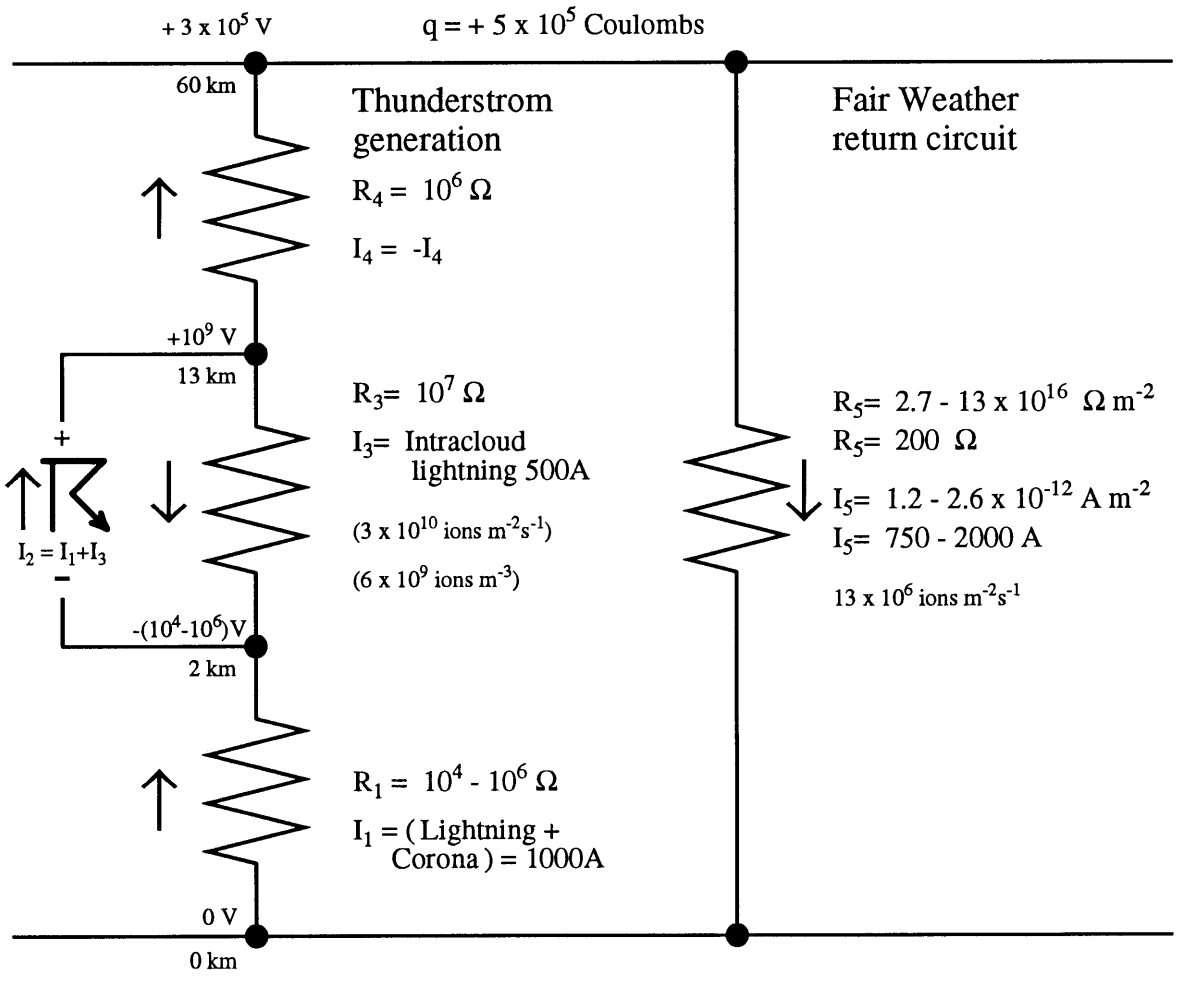

Figure 1. An electrical schematic representation of the global electric circuit. Adapted from *Williams* [1985], *Ogawa* [1985], and *Markson* [1985,1986]. In this electrical circuit, the arrows indicate the direction of current flow and each node (•) has indicated its voltage and height with respect to ground. Following the current around the loop, we begin at the lower left left node (ground potential/ground level). In this Figure, the currents are considered positive when in the direction of the arrows. Ground-to-cloud currents (I_1) are composed of lightning and corona. Intra-cloud lightning (I_3) can be viewed as internal resistance (loss) to to main generator: lightning (I_2). The net current, presumably generated by lightning, is the Wilson above-cloud current (I_4), that maintains the 3×10^5 Volt potential of the stratosphere. This potential drives the fair-weather return current (I_5). Kirchhoff's first rule states that $I_1 = (I_2 - I_3) = I_4 = I_5$ and $I_2 = I_1 + I_3$. The corresponding ion densities and fluxes are indicated where applicable.

representation of the global electric circuit. Ions (by definition) must be the carriers of this charge, but what ions are they? In the first mass spectrometric measurement of atmospheric

ions at ground level, *Perkins & Eisele* [1984] reported that the dominant positive ion was $NH_4^+ \cdot (H_2O)_2$ and the dominant negative ions were NO_3^- and $NO_3^- \cdot (H_2O)_2$. These same ions were also found by *Eisele & McDaniel* [1986] in their ground level studies of atmospheric ions. Eisele has studied atmospheric ions for many years and tentatively identified water clusters that have core ions derived from methylpyridine, dimethylpyridine (*Eisele*, 1986) and ethylpyridine (*Eisele*, 1988) in addition to the above mentioned ions. As discussed by *Ziereis & Arnold* [1986], these ions are mostly stable, secondary ions (*e.g.* NH_4^+), formed by the subsequent reactions of reactive, primary ions (*e.g.* N_2^+) in reaction sequences such as

$$N_2 \rightarrow N_2^+ + e^- \tag{1a}$$

$$N_2^+ + H_2O \rightarrow N_2 + H_2O^+ \tag{1b}$$

$$H_2O^+ + H_2O \rightarrow H_3O^+ + OH \tag{1c}$$

$$H_3O^+ + NH_3 \rightarrow NH_4^+ + H_2O\ , \tag{1d}$$

that can be summarized as

$$H_2O + NH_3 \rightarrow NH_4^+ + OH + e^-\ . \tag{1}$$

The ion chemistry of the electron similarly results in stable, negative ions such as NO_3^-. This study will focus on the generation of these reactive, primary ions (*e.g.* N_2^+, e^-) as well as their subsequent chemistry and loss mechanisms inside clouds.

What are the magnitudes of ion currents and densities in thunderstorms? The most relevant findings in studies regarding the generation of ions in thunderstorms are summarized by *Williams* [1985] who reports current densities of $\approx 10\ nA \cdot m^{-2}$ within the cloud (mainly on hydrometeors) and charge densities of $1\ nC \cdot m^{-3}$; similar values have also been found by *Byrne et al.* [1983]. Expressing these values in terms of ion fluxes and densities

gives 3×10^{10} ions$\cdot$m$^{-2}\cdot$s^{-1} and 6×10^{9} ions$\cdot$m^{-3} respectively. These values are shown on Figure 1 in their locations relative to the global circuit.

Not only is lightning a potent source of ions, it is also a strong UV emitter: the peak temperatures in the lightning channel have been measured by *Orville* [1986a,b] to be $\approx$ 30,000K, with the peak emissions occurring at UV wavelengths $\approx$ 100nm. The radiative, peak-power output of a lightning channel has been estimated to be 3×10^{9} Watts per meter (*Paxton et al.* [1986]). What then is the resulting atmospheric chemistry of the lightning-induced ion and photon production and how does it compare with the neutral chemistry of the hot lightning channel?

1.3 Previous Studies of Lightning Chemistry

Individual aspects of the chemistry of lightning have been studied for many years. These studies have focused on identifying the products of lightning, thought to originate mainly from reactions among neutral species in the hot lightning channel with lesser contributions from the corona and lightning-induced photon flux that also exists near and within lightning channels. A review of the major studies performed on these various types of chemistry will serve to place in perspective the ion chemistry considered in this study.

1.3.1 Hot-Channel Chemistry

The dominant processes of the hot-channel chemistry can be considered to be the dissociation and ionization of N_2 and O_2 upon ohmic heating by the lightning current and the subsequent recombination of N and O upon the cooling of the hot channel. The most common chemical species whose chemistries in the hot channel have been studied are NO_x and O_3 (ozone) and to a lesser extent N_2O (nitrous oxide) and CO (carbon monoxide).

1.3.1.1 Studies of NO_x Production

Perhaps the most widely studied product of the hot lightning channel is the NO_x family, herein defined to be the sum of NO (nitrogen oxide) and NO_2 (nitrogen dioxide). This family is relatively insoluble in water, so it should be fairly easy to detect in the gas phase if it is produced in large quantities within clouds. *Noxon* [1976] spectroscopically detected increased concentrations of NO_2 in electrically active clouds (0.1 ppb $< NO_2 <$ 6 ppb); these increases and the observed lightning-stroke rate yielded a production rate of 10^{26} NO_2 molecules per lightning stroke. Using a global lightning-stroke rate of 200 per second (*cf.* page 9-4, *U.S.A.F.*, 1961), this production rate results in an annual global production rate of 14 Tg N·yr^{-1}.

Taking a rather different approach, *Tuck* [1976] used energetic arguments and analogies to nuclear bomb detonations to arrive at a very crude estimate of 4 Tg N·yr^{-1} as the global production rate of fixed nitrogen due to the expanding shock front of the heated lightning channel. In a similar fashion *Chameides et al.* [1977], considering the hot channel to be the sole source of NO_x, estimated the global production rate of fixed nitrogen to be 30 – 40 Tg N·yr^{-1} or about 50% of the total global production (*cf.* Table 9, Chemical boundary conditions / Assumed global budgets; Section 6.3, page 121). Also considering just the hot-channel chemistry, *Hill et al.* [1980] computed a global annual production rate of 4 Tg N·yr^{-1} and found this value to be sensitive to the rate at which the hot channel cools.

While these studies suggest that lightning can be an important contributor to the global budget of NO_x, these estimates must viewed with more than a little caution for, as detailed by *Dawson* [1980], they are no more than order of magnitude estimates.

1.3.1.2 Studies of O_3 Production

Just as the recombination of O with N can lead to the production of NO_x, the recombination of O with O_2 can lead to the production of O_3. The production of O_3 by lightning was observed spectroscopically by *Orville* [1967] although the processes responsible for the increased ozone were not determined in that study. There has been considerable speculation over time as to the origin and fate of the O_3 formed in thunderstorms. This speculation derives from the facts that (1) the maximum thermodynamic mixing ratio of O_3 occurs between 4000K and 3000K (*cf.* Appendix C , page 213) and (2) the short-wavelength UV photons created in the hot lightning channel can photolyze O_2, thereby creating O and subsequently O_3. Using a highly parameterized production rate tied to energy deposition, *Griffing* [1977] found O_3 to be formed with the same efficiency as NO_x. This result is in contrast to the findings of *Levine et al.* [1981] who found, in laboratory discharges, that all the NO_x produced to be NO (*i.e.* no NO_2) and found no evidence of O_3 production.

1.3.1.3 Studies of N_2O & CO Production

In addition to NO_x, other species, specifically N_2O, and CO, having maximum thermodynamic mixing ratios at elevated temperatures (*cf.* Appendix C , page 213), are also thought to originate in the hot lightning channel. *Levine et al.* [1979] found enhanced levels of both N_2O and CO in tropospheric air samples exposed to laboratory discharges. These results were interpreted in terms of a rapidly cooling gas model that permits a "freezing out" of these compounds at a concentration above their thermodynamic equilibrium value. By varying the assumed rate of cooling, a wide range of final concentrations of N_2O and CO can be obtained.

This study raises the questions: "Is the hot core of the lightning channel necessary

to produce N_2O and CO?" and "Do we need to cool the channel rapidly to "freeze out" compounds not otherwise producible?"

1.3.2 Corona & Photon Chemistry

High-temperature processing of air is not the only method to create oxides and CO. Another method to produce these compounds is *via* ion chemistry. This ion chemistry is a result of the breakdown of air near the hot lightning channel caused by the large **radial**† electric fields present there. As discussed in Section 4.2.1.2, page 98, these ion processes result in the creation of the reactive O and N atoms. Additionally, in natural lightning ($\approx$ 30,000K) but not in cooler laboratory arcs ($\approx$ 8,000K) there is a radially outward flux and subsequent adsorption of short-wavelength UV photons created in the hot channel. How important is this ion and photon chemistry?

1.3.2.1 Studies of NO_x Production

It has long been suspected that in-cloud corona can produce oxides of nitrogen. *Reiter* [1970] showed that the time integral of the electric field at 3,000m was positively correlated with the NO_3^- (nitrate) concentration in rains at that altitude and found no correlation between the NO_3^- concentration in rain and the average rate of lightning strokes. The nitrate content of rain water collected at 3,000m increased by a factor of 3 as the storm

† Why are the radial electric fields generally larger than the vertical fields near lightning channels? As discussed in Section 3.3.1, page 74, the hot lightning channel is conductive and can be crudely considered to be a wire hanging vertically in an ambient vertical electric field. This causes an induced charge on the channel such that the electric field lines are perpendicular to the (conductive) channel's outer perimeter. This charge on the channel in turn causes a large radial electric field that causes the surrounding region to go into corona.

classification changed from non-electrified to electrified. These findings were interpreted as suggesting that corona was responsible for the enhanced nitrate levels. This type of result is not generally accepted, however, and others have not found such correlations (*Viemeister*, 1960).

That ions can produce NO_x was also appreciated by *Griffing* [1977] who used a highly parameterized production rate based on the energy deposited by lightning processes and calculated the production rate of fixed nitrogen to be 10^{26} molecules NO_2 per lightning flash, in agreement with the value computed by *Noxon* [1976] as discussed above.

1.3.2.2 Studies of N_2O & O_3 Production

Just as NO_x can be created by corona processes, so too can N_2O and O_3. Studies (*e.g. Hill et al.*, 1988) have been performed on laboratory-scale electrical discharges, examining the production rates of N_2O and O_3. In this particular study, the N_2O produced by lightning is assumed to come from the reaction of an excited state of molecular nitrogen $N_2(A^3\Sigma)$ with molecular oxygen with an adjustable yield.

$$O_2 + N_2(A^3\Sigma) \rightarrow N_2O + O(^3P) \quad (2)$$

These types of studies raise another question: To what extent are studies of laboratory discharges applicable to lightning in thunderstorms where the radial electric fields are much larger than in laboratory arcs? Not only are these large radial electric fields able to cause the surrounding air to go into corona, but also the so liberated electrons can acquire high kinetic energies in the electric field, and many reactions involving electrons are dependent on the electron's energy.

1.4 Production of HO_y in lightning

In addition to the chemical species discussed above, there is also another chemical family deserving attention, namely the HO_y family, herein defined to be OH (hydroxyl radical), HO_2 (hydroperoxy radical), and twice the H_2O_2 (hydrogen peroxide) concentration.

Given that H_2O (water) is present in air at the percent concentration level, it is not surprising that atomic H is observed in lightning channels. The chemistry of ion-water interactions results in two separate paths to produce HO_y: ion-produced H can recombine with O_2 forming HO_2, and the ion-induced production of OH can result in the production of H_2O_2. What are the relative contributions of these two paths?

1.5 The Goals of this Study

To summarize then, I once again ask the questions: What is the resulting atmospheric chemistry of the lightning-induced ion and photon production, and how does it compare with the chemistry of the hot lightning channel itself? What are the chemical species most influenced by lightning on both the local and global scales? To what extent and by what mechanism is the HO_y family produced in electrified convection?

1.6 The Approach Taken to Attain the Goals

This study answers these questions by creating a detailed chemical, but relatively crude dynamical and microphysical model of electrified convection. This model focuses on the chemistry of both the hot lightning channel as well as the region surrounding the hot channel.

This model includes $\approx$ 800 thermal and photochemical reactions among $\approx$ 165 neutrals, ions, water clusters, and electrons; the pressure, temperature, and electric field effects upon the reaction coefficients are explicitly considered. To focus on the gas-phase processes, aqueous-phase chemistry has not been considered in this study although heterogeneous loss is included.

To determine the net chemical effects of electrified convection, given a specified dynamical and microphysical parameterization, the in-cloud lifetimes τ_{storm} and production rates of the chemical species are computed and compared with their tropospheric chemical lifetimes $\tau_{\text{trop.}}$ and background production rates, determined by turning off all electrical processes in the model.

To assess the relative importance of the hot-channel chemistry *vis-à-vis* the cold ion processes, the relative source strengths of the hot channel and the surrounding regions are compared for selected chemical species in a one-box, explicit time-marching model of a cooling lightning channel. Finally, to assess the adequacy of a steady-state representation of a thunderstorm, an explicit, time-marching model of a lightning flash was also performed for one grid point from the inner model domain that is subject to a high rate of ion production.

2 Formulation of the Ion Model

In this chapter is presented (1) a description of the physical events that are begin simulated by this model, (2) the derivation and scale analysis of the basic equation governing the atmospheric concentration of a chemical species in the model, and (3) the establishment of a grid structure on which to execute the model.

2.1 Physical Basis of the Model

The focus of this study is the chemistry of a lightning channel and the surrounding corona regions that are embedded in electrified convection (a "thunderstorm"). I therefore begin with a physical description of the lightning channel and its environs and proceed radially outward toward the surrounding thunderstorm and its associated features. The reader is referred to the next chapter (Chapter 3, page 55) for the details of the implementation of the features described here and to *Uman* [1987,1969] for an introduction to lightning in general.

2.1.1 Lightning Channel

Along the inner wall of the model domain is a (model) segmented lightning channel. This channel has two main sections: starting at the ground there is the ground–lowercloud segment and above that there is the lowercloud–uppercloud segment. These segments represent cloud-to-ground and intracloud lightning respectively. These sections are subject to prescribed flash rates that are meant to represent "storm average" cloud-to-ground and intracloud flash rates.

While the chemistry of this channel (as it cools) is modeled in a 1-box, time dependent model (described in Section 6.1.3, page 116), this channel is not otherwise directly

considered. Rather, this channel serves as (1) a direct source of photons and (2) an indirect source of ions in the following manners. (1) The photons (50nm $< \lambda <$ 10,000nm) emitted by the lightning channel are assumed to follow the theoretical emission spectrum of a cooling gray body (30,000K $<$ T $<$ 300K); these photons stream radially outward from the inner domain wall and cause the photolysis of O_2 and O_3. (2) When active, these lightning channels are considered conductive and following the lines of *Heckman & Williams* [1989] acquire net charges of order 1 C·km^{-1}. This charge serves as the origin of large radial electric fields that cause the surrounding region to go into corona and produce ions in the following manner.

2.1.2 Corona Sheath

Surrounding the lightning channel is a region of space that extends outward for some meters that has a (radial) electric field that is above the breakdown strength of air (E_{BD}), herein assumed to be 500 kV·m^{-1} (*cf.* Figure 20, in Section 3.3.1.2, page 77). The response of the ambient air is to produce a weak plasma, thereby reducing the electric field back to it maximally permitted value (E_{BD}). This plasma consists of positive ions and electrons (N_2^+, N^+, O_2^+, O^+, and e^-) whose subsequent reactions are modeled.

Inasmuch as this model will primarily be a steady-state one, I average the photon and ion production of a flash over the basic interflash interval used in this model: one second. The validity of this steady-state approximation is tested with a 1-box, time-dependent model of a lightning flash, described in Section 6.1.2, page 115.

2.1.3 Surrounding Thunderstorm

The above lightning processes are embedded in a highly simplified thunderstorm

that extends throughout the entire model domain. Due to the moderate level of axial symmetry of an "average" thunderstorm and the desire for a simple kinematic representation, the thunderstorm is represented by a steady-state, 2-D (axially symmetric), model that has impermeable lower, inner and upper boundaries.

For the sake of simplicity, the wind field of the thunderstorm $\vec{V}(r,z)$ is represented by a relatively simple function of radial position r and altitude z whose vertical component $W(r,z)$ is everywhere non-negative and whose radial component $U(r,z)$ preserves the non-divergence of mass. There is a maximum updraft velocity of 12 $\mathrm{m{\cdot}s^{-1}}$ at the center of the inner portions of the model domain that decays above, below and radially outward. Crudely speaking the air comes into the model domain at (model) altitudes of $0-2$km along the outer model boundary. The air is then drawn into the up-draft regions and exits out of the model domain at (model) altitudes of $2-15$km along the outer model boundary.

The "cloudness" of the model is determined by the rate of liquid water production and an assumed cloud-particle size distribution. (The local vertical velocity and water-vapor content determine the rate of liquid-water production). The rates of all heterogeneous-loss processes are scaled to the local cloud-particle size distribution, mean free path and "sticking coefficient". For ions, there is also capture by cloud particles due to ion drift driven by the applied electric field. While there is heterogeneous loss of most chemical species in this model, there is no explicit representation of the resulting aqueous-phase chemistry, nor is washout of compounds considered.

2.1.4 Chemistry

The chemistry of this model is designed to represent the "global average" chemi-

cal fluxes (sources) of various natural and anthropogenic compounds through the lower and upper model boundaries (there is also deposition along these boundaries). The air entering the model domain is assumed to have the chemical composition as determined by a 1-D steady-state photochemical of the "globally, diurnally averaged" troposphere. The (altitude dependent) rates of photolytic reactions are determined using a separate 1-D radiative transfer model and published wavelength-dependent absorption cross-sections (reaction probabilities).

2.2 Continuity Equation

Having reviewed the physical situation to be simulated, I now present the derivation and scale analysis of the basic equation governing the atmospheric concentration of a chemical species in the model.

2.2.1 Derivation of the Continuity Equation

The fundamental equation governing the conservation of mass of species i in a parcel of air is given by

$$\frac{d\chi_i}{dt} = (P_i - L_i)\left(\frac{\mathrm{MW_{AIR}}}{\rho_{\mathrm{air}}\,\mathrm{N_A}}\right), \quad \mathrm{s}^{-1} \tag{3}$$

where χ_i is the mixing ratio of species i, and P_i and L_i are, respectively, the chemical production and loss of species i ($\mathrm{molec}_i \cdot \mathrm{m}^{-3} \cdot \mathrm{s}^{-1}$), $\mathrm{MW_{AIR}}$ is the molecular weight of air ($\mathrm{kg \cdot mol}^{-1}$), ρ_{air} is the density of air ($\mathrm{kg \cdot m}^{-3}$), and $\mathrm{N_A}$ is Avogadro's constant ($\mathrm{molec \cdot mol}^{-1}$) †. The ratio on the right-hand side of Eq.(3) is an inverse number den-

† All symbols and their definitions are listed in Appendix F , page 279.

sity and can be represented as $\varrho_{\text{air}}^{-1}$ (molec·m^{-3})$^{-1}$. Eq.(3) then becomes

$$\frac{d\chi_i}{dt} = \frac{P_i - L_i}{\varrho_{\text{air}}}. \tag{4}$$

To express this conservation relation at a point in space, we expand the total derivative as

$$\frac{d\bullet}{dt} = \frac{\partial \bullet}{\partial t} + \vec{V} \cdot \vec{\nabla} \bullet \tag{5}$$

If the air is not static and there are spatial gradients in the mixing ratio of species i, then the mixing ratio can also change *via* the turbulent mixing of neighboring parcels. The change in the local mixing ratio due to this "turbulent diffusion" is given as

$$\frac{\partial \chi_i}{\partial t} = +\vec{\nabla} \cdot \left(\vec{\vec{D}} \cdot \vec{\nabla} \chi_i \right), \tag{6}$$

where $\vec{\vec{D}}$ is the diffusion tensor (m^2·s^{-1}). In the parameterization of this model, I replace $\vec{\vec{D}}$ with K_{eddy}.

We must also consider the possibility that the species in question may have a net electric charge q_i and that electric fields $\vec{E}$ (V·m^{-1}) may be present. In this case, charged particles will move in an electric field with a velocity $\vec{V_i}$, according to

$$\vec{V_i} = q_i \, \vec{\vec{\mu_i}} \cdot \vec{E}, \tag{7}$$

where $\vec{\vec{\mu_i}}$ is a diagonal tensor whose non zero elements μ_{jj} are functions of $\vec{E}$, as well as the local pressure and temperature and have the dimensions m·s^{-1}/V·m^{-1}. Specifically,

$$\mu_{jj} = \begin{cases} \frac{e^- \ell}{mV}, & \text{low field limit,} \\ \sqrt{\frac{e^- \ell}{2mE}}, & \text{high field limit;} \end{cases} \tag{8}$$

where ℓ is the local mean free path of air and m and V are respectively the mass and (kinetic) velocity of the ion.

Spatial gradients in χ_i, $\vec{\mu}_i$, or $\vec{E}$ will therefore cause the local value of χ_i to change over time according to

$$\frac{\partial \chi_i}{\partial t} = -q_i \vec{\nabla} \cdot \left(\chi_i \vec{\mu}_i \cdot \vec{E} \right). \tag{9}$$

External forcing factors also exist that can modify χ_i. Because this model will simulate the chemistry inside a cloud, there will be heterogeneous loss processes H_i that can be most simply represented by a loss frequency f_i or an inverse lifetime τ_h^{-1} (s^{-1}). These heterogeneous-loss processes are diffusional driven for the case of neutral species and electric-field driven for the case of charged species. Additionally, for grid points near the boundaries of the domain, there can be a flux F_i of compound i expressed as the specific rate of influx into a region ($molec_i \cdot m^{-3} \cdot s^{-1}$) divided by the influx region's air number density ϱ_{air}. These two processes will then cause χ_i to change over time according to

$$\frac{\partial \chi_i}{\partial t} = -H_i \chi_i + \frac{F_i}{\varrho_{air}}. \tag{10}$$

Adding the right-hand sides of Eqs.(10), (9), and (6) to Eq.(4) and expanding the total derivative as in Eq.(5) results in

$$\frac{\partial \chi_i}{\partial t} = \frac{P_i - L_i}{\varrho_{air}} - \vec{V} \cdot \vec{\nabla} \chi_i - q_i \vec{\nabla} \cdot \left(\chi_i \vec{\mu}_i \cdot \vec{E} \right) + \vec{\nabla} \cdot \left(\vec{\vec{D}} \cdot \vec{\nabla} \chi_i \right) - H_i \chi_i + \frac{F_i}{\varrho_{air}}. \tag{11}$$

Equation (11) represents the time evolution of χ_i at a point in space. In the discretization of this continuous variable, a multi-dimensional grid of points is established and Equation (11) is solved at every node (or grid point).

2.2.2 Scale Analysis of Continuity Equation

Because the magnitudes of some of the terms in Eq.(11) are directly related to the grid structure, while others are only indirectly so related, I now consider the dominant terms of the continuity equation (Eq.(11)) in order to determine the type of grid system most appropriate for this model. Because there are many different types of chemical compounds, each with its own characteristic behavior, different terms will be important for different classes of compounds. For this reason, I will discuss the scale analysis on a chemical class basis, starting with short-lived species (τ_c order minutes or less) and proceeding to the long-lived ones.

2.2.2.1 Short-Lived Species

The chemical production and loss term in Eq.(11)

$$\frac{P_i - L_i}{\varrho_{\text{air}}}, \qquad (11-1)$$

dominates the continuity equation for the short-lived, neutral compounds in the model such as $O(^1D)$ or $O(^3P)$ as no reasonable amount of advection, turbulent diffusion, nor electrically-induced flow will directly alter their concentration: they will always be in steady-state equilibrium with their longer lived source (or parent) compounds (*i.e.* O_3 for the above examples) and reactants (H_2O and O_2). For this reason, the details of the grid structure will not directly affect their computed concentrations in the model.

The grid structure is, however, critical to the modeling of the production of short-lived ions during the lightning flash. As will be discussed in the section on the parameterization of ion generation (Section 3.3.2, page 77), the production rate of small ions is directly related to the square of the strength of the local electric field; hence the grid must have its

inner boundary very near the lightning channel. The ions so produced are uniformly distributed over the node's domain (grid point's control volume)†; hence the (radial) resolution of the domain must be sufficiently fine to permit the accurate evaluation of the average of the square of the local electric field in order to accurately represent the local ion production.

What terms of the continuity equation will be in balance in these regions of intense ion production? In these regions, the ion production rate P_i will be shown to be (*cf.* Section 3.3.2.3, page 80) of order 10^{20} ions m^{-3} per lightning stroke. Taking typical values of $\chi_i \sim 10^{-9}$, $\partial\chi_i/\partial r \sim 10^{-10}\ m^{-1}$, $\partial^2\chi_i/\partial r^2 \sim 10^{-11}\ m^{-2}$, $\partial\chi_i/\partial z \sim 10^{-12}\ m^{-1}$, $\partial^2\chi_i/\partial z^2 \sim 10^{-15}\ m^{-2}$, $\partial\chi_i/\partial t \sim 0\ s^{-1}$, $\vec{V} \sim 10\ m{\cdot}s^{-1}$, $\mu_{jj} \sim 10^{-4}\ m^2{\cdot}V^{-1}{\cdot}s^{-1}$, $\partial E_r/\partial r \sim 10^5\ V{\cdot}m^{-2}$, $D_r \sim 10^2\ m^2{\cdot}s^{-1}$, $\varrho_{air} \sim 10^{25}\ m^{-3}$, $H_i \sim 10^{-1}\ s^{-1}$, and $F_i \sim 0\ s^{-1}$, Equation (11) then becomes

$$\underbrace{\frac{\partial\chi_i}{\partial t}}_{0} = \underbrace{\frac{P_i - L_i}{\varrho_{air}}}_{\frac{10^{20}-L_i}{10^{25}}} - \underbrace{\vec{V}\cdot\vec{\nabla}\chi_i}_{10^{-9}} - \underbrace{q_i\,\vec{\nabla}\cdot\left(\chi_i\,\vec{\mu}_i\cdot\vec{E}\right)}_{10^{-8}} + \underbrace{\vec{\nabla}\cdot\left(\vec{\vec{D}}\cdot\vec{\nabla}\chi_i\right)}_{10^{-9}} - \underbrace{H_i\chi_i}_{10^{-10}} + \underbrace{\frac{F_i}{\varrho_{air}}}_{0},$$

where the the two terms most likely to balance the chemical production of ions P_i are: (1) the chemical loss term L_i, and (2) the gradient of the radial drift velocity term $\vec{\nabla}\cdot\chi_i\,\vec{\mu}_i\cdot\vec{E}$ (11–3).

This scale analysis of the continuity equation permits the identification of those terms that require the closest attention in the subsequent parameterizations.

2.2.2.2 Long-Lived Species

Long-lived neutral species, such as CH_4 or CO, are not greatly affected by the details of the grid structure; rather it is the parameterizations of their heterogeneous loss, the magnitudes of their boundary fluxes, the velocity field, and to a lesser extent the assumed

† These terms will be explained more fully in Section 2.5.1, page 48.

turbulent diffusion coefficient that tend to dominate their concentration at a specific grid point.

2.3 Other Constraints Upon Grid Systems

2.3.1 Constraints at Small Radial Distances

For reasons to be discussed in the section on computer resources available (Section 2.6.1, page 50), the models primarily utilized in this study are steady-state ones; if these models were to be run in an explicit, time-marching mode, then having a high resolution grid near the lightning channel would impose the following constraint upon the maximum time step allowed.

Ions move in electric fields at a rate given by Eq.(8); for our purposes we pick a typical value of 3×10^{-4} for the magnitude of μ_{jj} (*Rosen et al.*, 1985)†. The condition that the radial spacing δ of the inner grid points be greater than the distance that ions can travel during one time step Δt of the model requires that

$$\Delta t \leq \frac{\delta}{E_r \mu_{jj}}, \tag{12}$$

where E_r is the radial component of the electric field, and μ_{jj} is the ion mobility ($m \cdot sec^{-1}$ / $V \cdot m^{-1}$)

If the inner grid has a spacing of order 1m, then the minimum time step Δt is order 0.01 seconds for a radial electric field of 500,000 $V \cdot m^{-1}$. This minimum time step increases as the radial distance away from the lightning channel increases; therefore any explicit scheme must have a variable time step with the inner grid points being evaluated

† Note that 3×10^{-4} (m/s)/(V/m) equals 3 (cm/s)/(V/cm)

at more closely spaced points in model-time than the outer grid points. It is noted however that this may be unnecessarily conservative as ions can be captured by cloud particles, and the distance that an ion can travel before capture is of order centimeters, not meters.

The magnitude of the local electric field also directly influences those reaction coefficients that depend on the magnitude of the electric field. To obtain a good estimate of the average reaction coefficient in a region of space, the electric field must be well represented and the radial variations in the electric field are the largest in the inner domain of the model. These considerations argue in favor of having the preponderance of grid points in the regions of the greatest spatial variation of the electric field.

Having established the basic radial structure of the grid system, there are some other considerations that also bear upon the grid construction. These are the considerations of how well the far field and the vertical structure of the thunderstorm must be represented. I now discuss each of these in turn.

2.3.2 Constraints at Large Radial Distances

Another condition imposed upon the grid generation process is that the separation between the outer points in the grid must not be too large. This is required to ensure faithful calculation of functions that have a constant spatial scale of variation. Choosing the maximum separation between the outermost grid points to be L leads to the following constraint on N (the total number of grid points in the radial direction):

$$N \geq 1 + \frac{\ln(R_{\text{inner}}/R_{\text{outer}})}{\ln(R_{\text{outer}}/(R_{\text{outer}} - L))}. \tag{13}$$

It is noted that in order to accurately compute ($\approx 1\%$ error) the derivatives of a function such as sin(r/L), approximately 25 grid points per cycle of length L are required. This requirement for a rather large number of grid points required per cycle can be understood

by considering the Taylor-series expansion of the error in approximating the derivative of the $\sin(x)$ with its finite-difference representation:

$$\text{Error} = \underbrace{\left| \frac{d\sin(x)}{dx} - \frac{\sin(x+\delta x) - \sin(x-\delta x)}{2\,\delta x} \right|}_{\text{finite-difference error}} \approx \underbrace{\left| \left(\frac{\delta x^2}{6} - \frac{\delta x^4}{120} \right) \cos(x) \right|}_{\substack{\text{Taylor series} \\ \text{expansion of error}}} . \qquad (14)$$

This error is maximal at $x = 0$, where a 1% error requires $\delta x < 0.25$ radians, or ≈ 25 grid points per 2π radians. In this model, the kinematics are specified, so this issue is not very important in the present context but would clearly be important in any model in which the dynamics are explicitly computed.

Another constraint in the far field is that the outer boundary should be sufficiently far away from the lightning channel so that the spatial derivatives in χ_i induced by the storm are small enough so that the particular outer-boundary condition does not influence the model very much. In this model, the background-tropospheric photochemistry is considered as the outer-boundary condition in the inflow sections of the domain, and either the constant gradient condition or the zero-gradient condition is used in the outflow regions.

2.3.3 Vertical Constraints

Just as the model's grid should faithfully compute the radial gradients in the electric field, so too should it be able to represent the vertical variations of the electric field (*i.e.* $\partial E_z/\partial z$ and $\partial E_r/\partial z$). This should not be a very difficult condition to meet as the electric fields are, as will be shown later, more slowly varying functions of z than they are of r, *i.e.*

$$\frac{\partial E_z}{\partial z} \sim \frac{\partial E_z}{\partial r} \sim \frac{\partial E_r}{\partial z} << \frac{\partial E_r}{\partial r} \qquad (15)$$

What vertical spacing is required to represent the di/tripole structure of a thunderstorm? The magnitude of the vertical electric field at a (horizontal) distance r away from the centerline, and in the equator of, a dipole is

$$E_z(r) = \frac{q_i}{4\pi\varepsilon_o}\frac{2a}{(a^2+r^2)^{3/2}}, \tag{16}$$

where a is half the separation between the charge centers of the dipole. As discussed in Section 2.4.1, page 41, the error introduced into a calculation by using a finite-difference representation of a function is the truncation error of the Taylor-series expansion of that function. The truncation error in the Taylor-series expansion of Eq.(16) can be estimated by comparing the magnitude of the last retained term in the expansion to the first excluded term; in our case, they are the first and second terms respectively. The ratio (Δ) of the third term to the second term in the Taylor expansion of Eq.(16) is

$$\Delta = \frac{\frac{\delta^2}{2}\frac{d^2E(r)}{dr^2}}{\delta\frac{dE(r)}{dr}} = -\frac{\delta(4r^2-a^2)}{2r(r^2+a^2)}. \tag{17}$$

Non-dimensionalizing r by defining $y = r/a$, and scaling δ as ϵa results in

$$\Delta = -\frac{\epsilon(4y^2-1)}{2a(y^2+1)} \tag{18}$$

or $\Delta = 3\epsilon/4a$ when $y = 1$. For Δ to be $\leq 1\%$, we therefore need the grid spacing to be $\approx 1\%$ of the dipole separation a. If the dipole (or tripole) structure of the thunderstorm is to be accurately modeled, then a vertical spacing on the order of tens of meters would be required. This constraint is not a very strong one however, as the largest electric fields in the model will be the radial fields due to the net charge on the lightning channel, and this radial field varies slowly with height (*i.e.* along the lightning channel).

2.4 Establishment of a Grid System

Having examined the terms of the continuity equation and seen that it is the spatial variations of the (radial) electric field in the inner regions of the model that are the most important to resolve, the construction of the grid on which this equation is to be solved is now considered.

2.4.1 Errors of the Finite-Difference Approximation

The error introduced into a calculation as a consequence of using the finite-difference approximation to the first derivative of a continuous function

$$\underbrace{\frac{\partial F(r)}{\partial r}}_{\substack{\text{True}\\ \text{Derivative}}} \approx \underbrace{\frac{F(r+\delta)-F(r-\delta)}{2\delta}}_{\substack{\text{Finite-Difference}\\ \text{Estimate}}}, \tag{19}$$

can be determined by subtracting the Taylor-series expansions of $F(r)$ at the points $F(r+\delta)$ (Eq.20a) and $F(r-\delta)$ (Eq.20b) to produce Eq.(21a) and then dividing by 2δ to obtain Eq.(21b).

$$F(r+\delta) = F(r) + \delta\frac{\partial F(r)}{\partial r} + \frac{\delta^2}{2!}\frac{\partial^2 F(r)}{\partial r^2} + \frac{\delta^3}{3!}\frac{\partial^3 F(r)}{\partial r^3} + \cdots \tag{20a}$$

$$F(r-\delta) = F(r) - \delta\frac{\partial F(r)}{\partial r} + \frac{\delta^2}{2!}\frac{\partial^2 F(r)}{\partial r^2} - \frac{\delta^3}{3!}\frac{\partial^3 F(r)}{\partial r^3} + \cdots \tag{20b}$$

$$F(r+\delta) - F(r-\delta) = 2\delta\frac{\partial F(r)}{\partial r} + 2\frac{\delta^3}{3!}\frac{\partial^3 F(r)}{\partial r^3} + \cdots \tag{21a}$$

$$\underbrace{\frac{\partial F(r)}{\partial r}}_{\substack{\text{True}\\ \text{Derivative}}} = \underbrace{\frac{F(r+\delta)-F(r-\delta)}{2\delta}}_{\substack{\text{Finite-Difference}\\ \text{Estimate}}} \underbrace{-\frac{\delta^2}{3!}\frac{\partial^3 F(r)}{\partial r^3} - \cdots}_{\text{Error Terms}} \tag{21b}$$

Similarly, the error introduced by approximating the second derivative of a continuous function with its finite-difference form

$$\frac{\partial^2 F(r)}{\partial r^2} \approx \frac{F(r+\delta) - 2F(r) + F(r-\delta)}{\delta^2}, \tag{22}$$

can be derived by adding Eqs.(20a) and (20b) together to produce

$$F(r+\delta)+F(r-\delta)=2F(r)+2\frac{\delta^2}{2!}\frac{\partial^2F(r)}{\partial r^2}+2\frac{\delta^4}{4!}\frac{\partial^4F(r)}{\partial r^4}+\cdots\ , \tag{23a}$$

and then subtracting $2F(r)$ and dividing by δ to yield

$$\underbrace{\frac{\partial^2F(r)}{\partial r^2}}_{\substack{\text{True}\\\text{Derivative}}}=\underbrace{\frac{F(r+\delta)-2F(r)+F(r-\delta)}{\delta^2}}_{\substack{\text{Finite-Difference}\\\text{Estimate}}}\ \underbrace{-2\frac{\delta^2}{4!}\frac{\partial^4F(r)}{\partial r^4}-\cdots}_{\text{Error Terms}}\ . \tag{23b}$$

In Eqs.(21b) and (23b), the numerical error is seen to be directly related to the magnitude of the higher derivatives of $F(r)$ and to the spacing of the grid δ. We can anticipate that the physical parameter with the largest spatial non-linearity (and therefore the largest higher derivatives) will be the electric field $\vec{E}(r,z)$, as it will vary as $r^{-\epsilon}$ where r is the distance away from the space charge responsible for the electric field. The exact value of ϵ will be a function of the geometry of the space charge and reduces to simple values for simple arrangements of space charge. In order of increasing spatial gradients we have: $\epsilon =$ 0 for a plane charge, 1 for a line charge, 2 for a point charge, and 3 for a dipole charge.

Each of these limiting cases of charge distribution exists within the domain of an electrified storm; near the ground, far from lightning, the electric field can be represented by a plane charge overhead; near a lightning channel, the electric field approximates that due to a line charge; and in the far field, a thunder-cloud can be represented as an electric dipole or tripole. Except for the case of a plane charge, all of the above derivatives of $\vec{E}(r) \rightarrow \infty$ as $r \rightarrow 0$. This places limits on the inner radius permissible in the model. Additionally, to have a relatively constant error at each grid point, the spacing between the grid points must decrease as r decreases.

We must therefore find an efficient system of grid spacing; it must be parsimonious in its allocation of grid points yet maintain accuracy throughout the model's domain.

2.4.2 Exponentials and Positive Polynomials

Two systems of grid spacing seem reasonable: one in which the radial distance r away from the model's origin R_{inner} is a function of the grid number n to some power, and another wherein the distance from the origin increases exponentially with increasing grid number. An explicit formula for a grid point's radial position as a function of its grid number for the first system (herein called the polynomial system) is given by Eq.(24a). In this system, for a fixed total number of grid points N, increasing the value of β increases the density of grid points near the origin and decreases the density of points in the outer regions. The requirements that $r(1) = R_{\text{inner}}$ and $r(N) = R_{\text{outer}}$ lead to the values of the coefficients of this equation as shown in Equations (24b,c).

$$r(n) = \alpha_0 + \alpha_1 n^{\beta} \tag{24a}$$

$$\alpha_0 = \frac{R_{\text{inner}} N^{\beta} - R_{\text{outer}}}{N^{\beta} - 1} \quad \text{and} \quad \alpha_1 = \frac{R_{\text{outer}} - R_{\text{inner}}}{N^{\beta} - 1} \tag{24b,c}$$

The generating equations for the second candidate grid system, the exponential system, are given by Eq.(25a), and the above boundary conditions on $r(1)$ and $r(N)$ lead to Equations (25b,c).

$$r(n) = e^{\alpha_0 + \alpha_1 n} \tag{25a}$$

$$\alpha_0 = \frac{N \ln(R_{\text{inner}}) - \ln(R_{\text{outer}})}{N - 1} \quad \text{and} \quad \alpha_1 = \frac{\ln(R_{\text{outer}}) - \ln(R_{\text{inner}})}{N - 1} \tag{25b,c}$$

Taking typical values of R_{inner}, R_{outer}, and N, to be 0.1 meters, 1000 meters, and 250 points, respectively, the relative locations of grid points for these two systems can be plotted together for comparison. Figure 2 shows the distribution of the grid points for the two systems; in the polynomial system, the values of β ranging from 3 to 6 are shown as

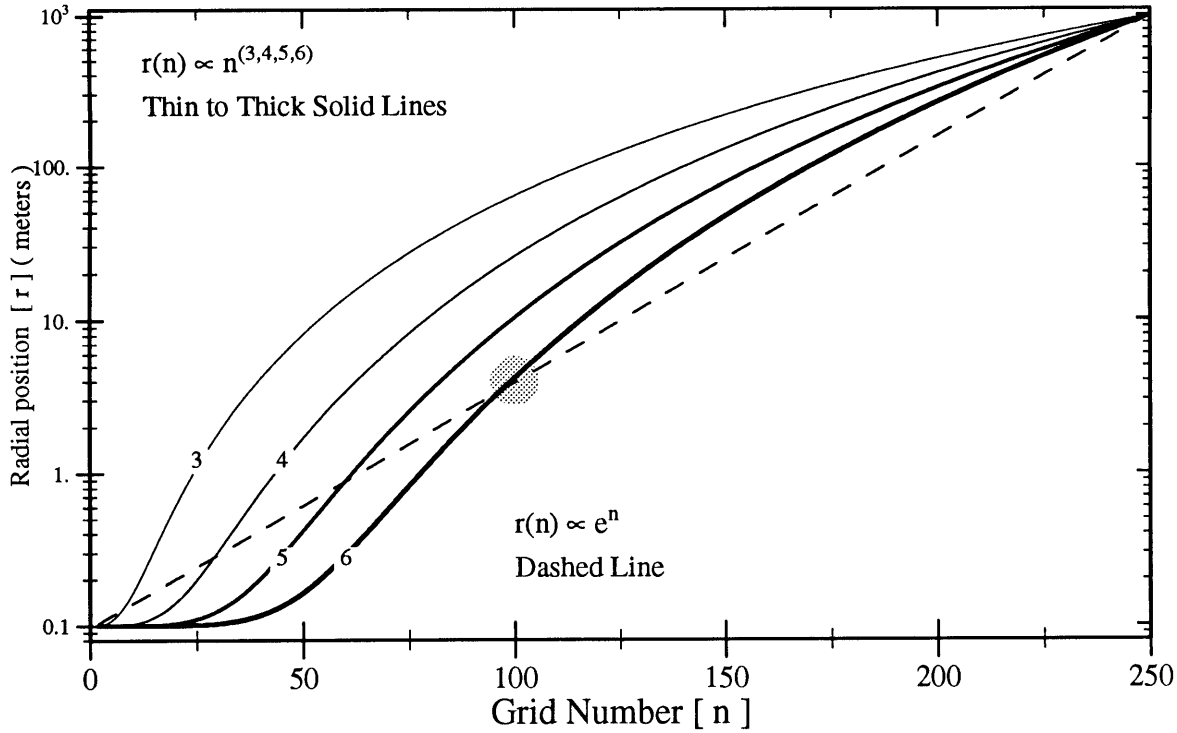

Figure 2. Radial position *vs.* Grid number for the two proposed grid spacing systems with typical values for R_{inner}, R_{outer}, and N. Solid and dashed lines represent the polynomial and exponential systems respectively. The solid gray circle at the point (100,4) represents grid point # 100 at a radial distance of 4 meters in both the e^n and n^6 systems.

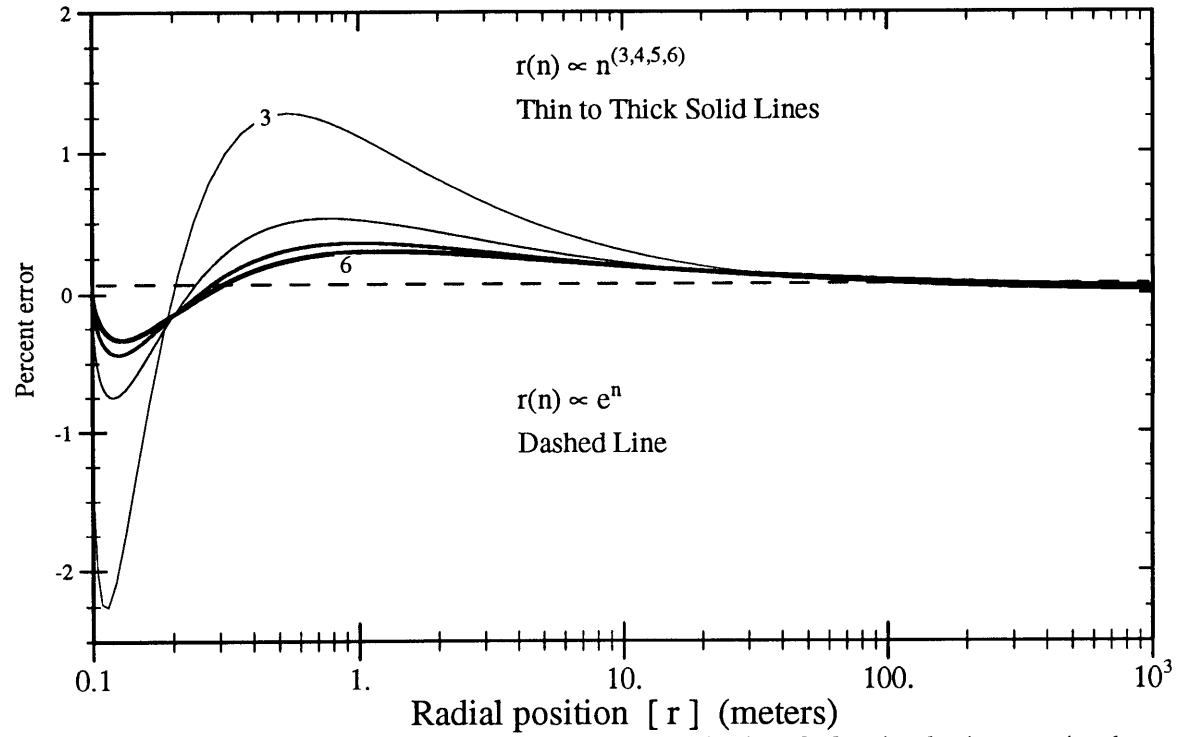

Figure 3. Radial position *vs.* Percent error in evaluating the first derivative of a function that is proportional to r to the -2 power in the two proposed grid spacing systems. Solid and dashed lines represent the polynomial and exponential systems respectively.

solid lines of increasing thickness; the exponential system is shown as a dashed line. It can be seen from this Figure that the polynomial grid system has a greater density of points near the origin, than the exponential grid system. For example, grid point number 50 is 0.15 meters away from the inner domain wall in the polynomial system with $\beta = 6$, represented by the thickest solid line, while the corresponding grid point number 50 is 0.60 meters from the inner domain wall in the exponential system. The average density of points is, of course, the same in both systems. For example, grid point number 100 is approximately the same distance (4 meters) away from the origin in both systems; this point is indicated by the solid gray circle at the point (100,4).

What is the magnitude of the errors introduced into the continuity equation (Eq.(11)) by the use of either of these grids? We can explicitly evaluate the error in estimating the first derivative of a function varying as $r^{-\varepsilon}$ in either coordinate system by using the above values for R_{inner}, R_{outer}, and N, and choosing the value 2 as a typical value of ε. These assumptions result in the following equations:

$$F\left(r\left(n\right)\right) \propto r\left(n\right)^{-2} \quad \text{and} \quad \begin{cases} r(n) = \mathrm{e}^{\alpha_0+\alpha_1 n} & \text{in the exponential system} \\ r(n) = \alpha_0 + \alpha_1 n^{\beta} & \text{in the polynomial system} \end{cases} . \qquad (26a, b, c)$$

The finite-difference estimation of the first derivative then becomes

$$\frac{\Delta F}{\Delta r} = \frac{F\left(r\left(n+1\right)\right) - F\left(r\left(n-1\right)\right)}{r\left(n+1\right) - r\left(n-1\right)}, \qquad (27)$$

and the relative error introduced by making this approximation is

$$\text{Error} = \frac{\frac{\Delta F}{\Delta r} - \frac{\partial F(r)}{\partial r}}{\frac{\partial F(r)}{\partial r}}. \qquad (28)$$

We can plot the magnitude of this error as a function of the radial distance from the origin (or grid number) for the two proposed grid systems. The results of this analysis are shown in Figure 3, where the exponential system (dashed line) is seen to have a more uniform error than the polynomial system although it does have a slight bias (non-zero mean value). This small bias can be overlooked given other approximations in the model.

2.4.3 Negative Polynomials

Just as positive values of β can produce a grid structure, negative values of β can also produce polynomial grids. How do these grids compare with the first two grids examined? Figure 4 shows a few negative values of β between -0.5 and -2 (with increasing line widths) along with the exponential system (dashed line) for comparison. It can be seen in this graph that the negative polynomial grid system has a very uneven density of points. For example in the $\beta = -2$ system (thinnest solid line), grid point number 100 is essentially still at the domain's inner boundary, and the very last few points span most of the domain's radial domain.

How do the numerical errors vary on such a grid? Using the same values for R_{inner}, R_{outer}, N, and ε, as used before, we can explicitly evaluate the error in estimating the first derivative of $F(r)$ in a manner similar to that done for the positive polynomial system. The results of this analysis are shown in Figure 5, where this system is shown to produce very large errors in the inner regions of the model's domain for values of $\beta > -1$ and very large errors in the outer regions of the model's domain for all negative values of β.

Because the errors are more uniform (and in general smaller) for the exponential system than the polynomial system, we choose the exponential grid system and now investigate the relationship between the relative error in evaluating a derivative and the fineness of this exponential grid.

2.4.4 Errors on Exponential Grid

The relative error in using the finite-difference approximation to the first derivative of a function was given in Eq.(28). Substituting Equations (26a) and (26b) into Eq.(27)

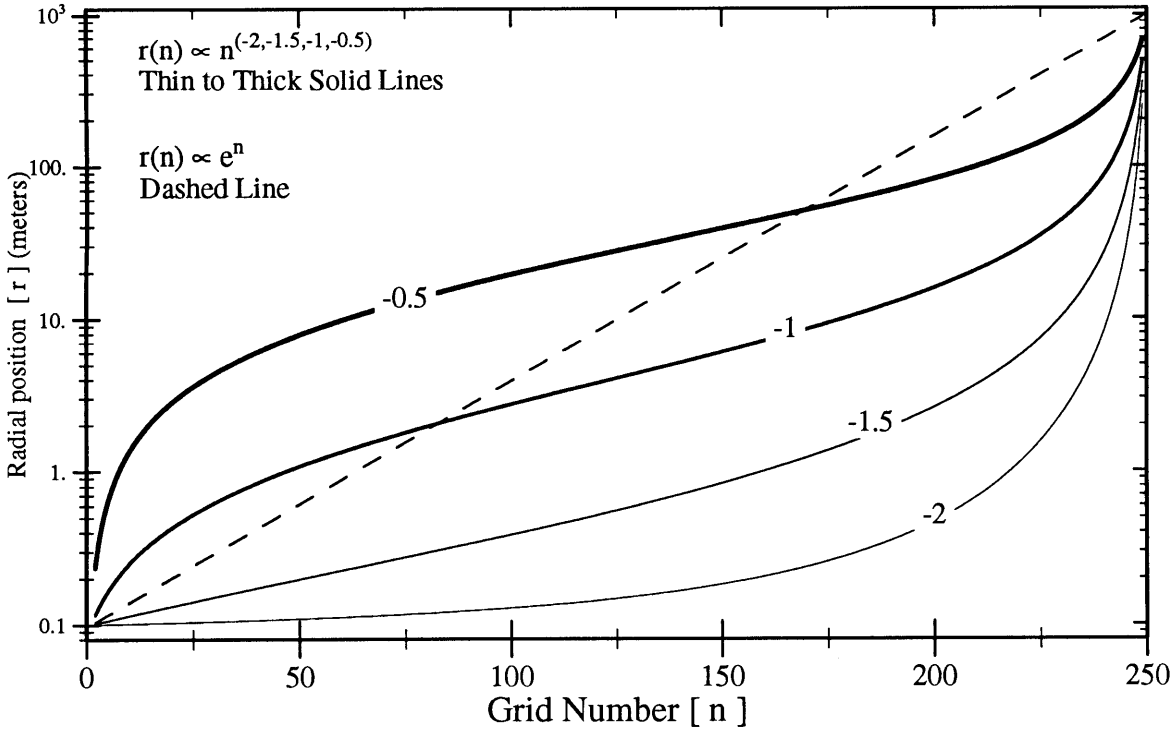

Figure 4. Radial position *vs.* Grid number for the negative values of β in the polynomial system (solid lines) and the exponential system (dashed lines) for comparison.

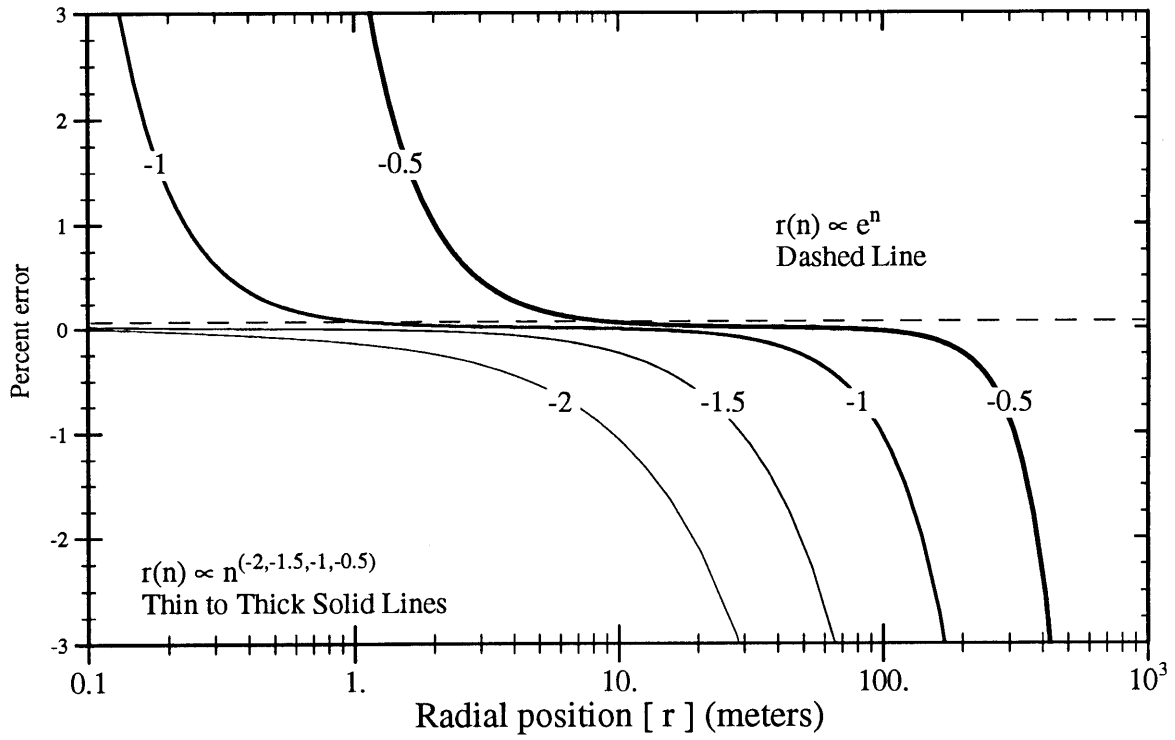

Figure 5. Radial position *vs.* Percent error in evaluating the first derivative of a function that is proportional to r to the -2 power for negative values of β in the two proposed grid spacing systems.

and then substituting Eq.(27) into Eq.(28) we obtain

$$\text{Percent Error} = 100 \times \left(\frac{e^{\alpha_1(1+\varepsilon)} - e^{\alpha_1(1-\varepsilon)}}{\varepsilon \left(e^{2\alpha_1} - 1 \right)} - 1 \right). \tag{29}$$

This function of α_1 and ε is graphed in Figure 6 where it can be seen that the error introduced by the finite-difference approximation approaches 0 as $\varepsilon \rightarrow 1$ or $\alpha_1 \rightarrow 0$. Of course we have no direct control over ε because it is a function of the charge structure inside of a thunderstorm; only α_1 is available to us as a variable parameter of the model. I have shaded the proposed operating region of the model on this Figure. Specifically, ε is expected to vary up to 3, and as will be discussed in the section on computer resources (Section 2.6.1, page 50), $\alpha_1 = 0.4$ is the finest grid that is practicably achievable with the computer resources at hand.

A graph of the error resulting from using the finite-difference approximation to the second derivative of a function (*cf.* Eq.23*b*) on an exponential grid is very similar in structure. Noting that there is a bias in the error when evaluating the first and second derivatives on the exponential grid (the dashed line representing the error is offset from 0 in Figures 3 and 5), one could derive a weighting factor designed to give no error for a particular pair of α_1 and ε values. There is little profit in extensive analysis of this point, however, as there is uncertainty in the exact value of ε at any particular point on the grid, and, as discussed earlier (Section 2.4.1, page 42), ε certainly varies over the model domain.

2.5 Finite-Difference Models on Non-uniform Grids

Having established the desirability of a non-uniform grid in the radial direction, the precise formulation of a grid point's control volume and the coefficients in the finite-difference approximations to the continuity equation (Eq.11) must be considered.

2.5.1 Definition of the Control Volume

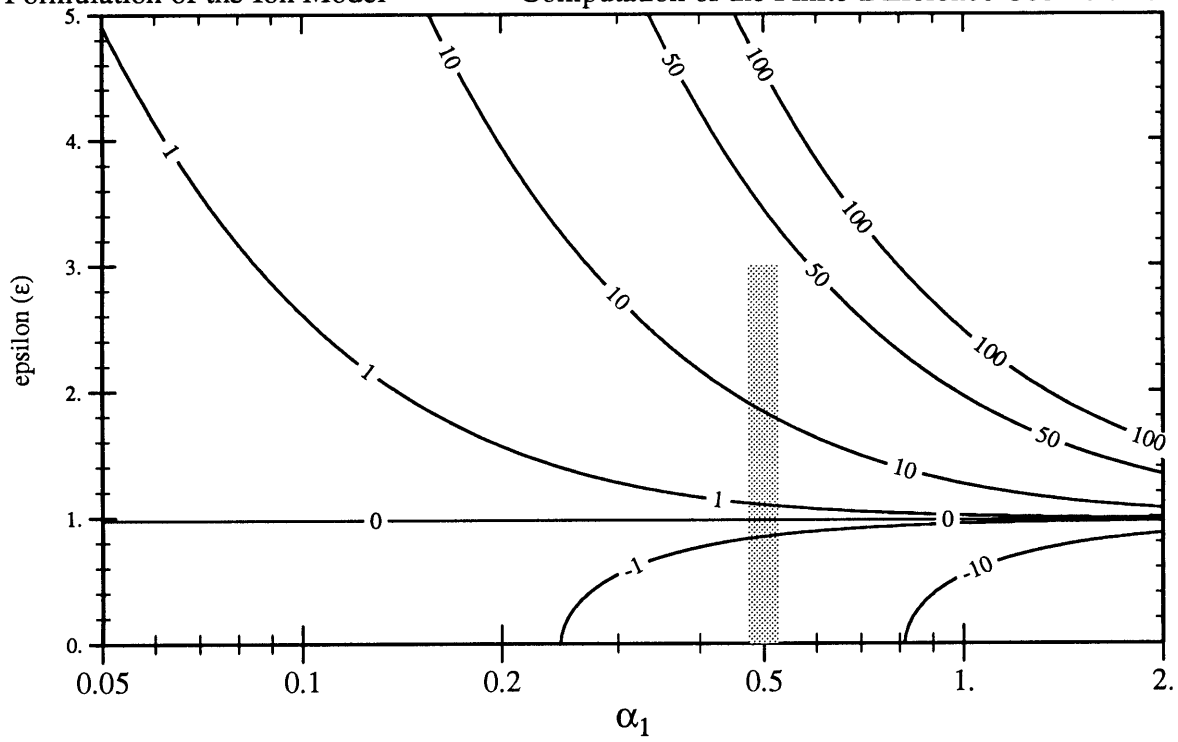

Figure 6. Radial position *vs.* Percent error in evaluating the first derivative of a function that is proportional to r to the $-\varepsilon$ power in an exponential system of grid spacing α_1. The parameter space of the model is shaded; ε is expected to vary up to 3, and $\alpha_1 = 0.4$ is the finest grid spacing that is practicable.

The control volume of a grid point is defined to be that volume of model space that is represented by the grid point in question. The innermost wall of the innermost grid points' control volume is the inner wall of the model domain, R_{inner} and the outermost wall of the outermost grid points' control volume is the outermost region of the model domain, R_{outer}. Similarly, the lower wall of the lowermost grid points is the ground and the upperwall of the uppermost grid points is the model tropopause. The grid point is centered in the control volume in the vertical and at the logarithmic center in the radial direction. The volumes and wall surface areas of the control volumes are therefore functions of a grid point's position in the model. These volumes and areas are used in computing the coefficients of the finite-difference approximation to Eq.(11).

2.5.2 Computation of the Finite-Difference Coefficients

To compute the coefficients of the finite-difference approximation of Eq.(11) the following direct approach is taken. Consider for example the turbulent diffusion term of Eq.(11)

$$+\vec{\nabla}\cdot\left(\vec{\vec{D}}\cdot\vec{\nabla}\chi_i\right). \qquad (11-4)$$

In this model at a grid point (r_i, z_j) or simply the grid point (i, j), this term becomes a function of the mixing ratios of the grid point itself, $\chi_{i,j}$, and those of its four nearest neighbors $\chi_{i\pm1,j\pm1}$. By explicitly considering the geometry of the control volume for grid point (i, j), (that volume of space bounded above and below by horizontal planes at $Z = j \pm 1/2$ and lying between concentric cylinders with radii $R = i \pm 1/2$) and defining the total diffusive flux into the control volume as the sum of the diffusive fluxes through each wall, then the above term, Eq.(11–4) becomes

$$\vec{\nabla}\cdot\left(\vec{\vec{D}}\cdot\vec{\nabla}\chi_i\right) = \alpha_{i-1,j}\cdot\chi_{i-1,j} + \begin{matrix}\alpha_{i,j+1}\cdot\chi_{i,j+1}\\ +\\ \alpha_{i,j}\cdot\chi_{i,j}\\ +\\ \alpha_{i,j-1}\cdot\chi_{i,j-1}\end{matrix} + \alpha_{i+1,j}\cdot\chi_{i+1,j} \qquad (11-4\,a)$$

where the α's are dependent on the control volume's dimensions as well as other physical paramterizations, such as $\vec{\vec{D}}$. Note that the spatial arrangement of the terms in this equation correspond to their spatial arrangement in the 2-D model.

2.6 Computer Resources Required for the Model

2.6.1 Explicit, Time-Marching Model

If computer resources were not limiting, then a grid 100 points wide in both the radial and vertical directions would seem to be a good starting point for an explicit time-

marching model of a lifecycle of a thunderstorm. A 100×100 grid, time-marched for 2 model-hours with 0.01 model-second time steps would result in 7.2×10^9 grid point calculations. At each grid point the continuity equation (Eq.11) is to be solved for $O[200]$ † chemical species. This equation requires about 50 floating point operations (FLOP's) for a chemical species with very simple chemical production P_i and loss L_i terms (*e.g.* DMS, SF_6) and over 500 FLOP's for a species with a complicated atmospheric chemistry (*e.g.* OH, H_2O). Taking 200 as the average number of floating point operations per evaluation of Eq.(11) brings the overall number of floating point operations to $\approx 288 \times 10^{12}$. Because a fast IBM-PC performs about 1×10^6 floating point operations per second (FLOPS), this model would then take 3300 days (9 yrs) to run. On a CRAY-class machine, being about 100 times faster, the model would still take a month of CPU time - hardly an inexpensive undertaking. It should be pointed out that as of this writing (September 1992), the 1G FLOPS barrier has been broken by advanced parallel processors, so this type of model could be run in a reasonable amount of time ($\approx$ few days) on such a machine.

2.6.2 Steady-State Model

To avoid the above unacceptable computer run times, I seek a simplification: replacing the time-evolving model with a steady-state model reduces the number of grid point calculations to the number of grid points times the average number of iterative approximations required to find a steady-state solution for a grid point. Given the exploratory nature of this work I wanted to be able to run the model on an IBM-PC class machine. If the maximum practicable run time for a model is 1 week on an IBM-PC, then the model must converge using about 6×10^{11} floating point operations. Using the above values of the

† Read as Order 200.

number of compounds and the number of FLOP's per compound and assuming 10,000 successive approximations at each grid point to obtain a 0.01% convergence, the model must have <2000 grid points, or a grid size of about 45×45. This is not the only limiting factor however.

2.6.3 Maximum Number of Grid Points in the Model

For long lived compounds such as CF_4 or O_3, the relatively low rate of chemical processing results in the boundary conditions influencing their concentration throughout the model domain. This necessitates using matrix solutions to the concentrations of the long lived species. A 45×45 grid has 2025 grid points; this translates into a system of non-linear equations having 2025 equations inter-relating 2025 unknowns. The solution of this system of equations requires computing the inverse of a 2025×2025 matrix. Because finding the inverse of an $N \times N$ matrix takes on order N^3 FLOP's, this inversion would require $O[10^{10}]$ FLOP's; on an IBM-PC, this would take $\approx$ 3 hrs. The size alone of such a matrix is daunting: using double-precision arithmetic, it is about 40 Mbytes. Unless we emply sparse matrix techniques, a matrix of this size is too large for any but the largest of supercomputers; given the constraints on the IBM-PC, a 15×15 model grid is the largest that can be readily manipulated. The matrices resulting from this grid are of dimension 225×225, and can be inverted in about 2 minutes.

2.7 Adequacy of the Model's Grid

I therefore establish a steady-state model of a storm on a 15×15 grid and later will discuss (*cf.* Section 8.1.2, page 135) the differences between this steady-state model and the equivalent time dependent one. I now consider the overall accuracy that can be

achieved with a 15 × 15 grid.

2.7.1 Radial Accuracy

A two-dimensional, 15 × 15 grid is established with horizontal nodes placed at equal intervals over the range of $\ln(R_{\text{inner}})$ to $\ln(R_{\text{outer}})$, where R_{inner} = 2m and R_{outer} = 2000m (*cf.* Section 2.7, page 52). In other words, the grid is a semi-logarithmic one, which has been be shown earlier (*cf.* Section 2.4, page 41) to minimize numerical errors in evaluating fields such as the electric field that have radial power dependencies. As shown on Figure 6 in Section 2.4.4, page 49, the radial errors in evaluating the first derivative of the radial electric field are expected to be on order of 10% to 50%. These errors affect only those terms of the continuity equation (Eq.11) that depend on the gradient of the electric field *i.e.* the gradient of the radial drift velocity term $\vec{\nabla} \cdot \chi_i \vec{\mu_i} \cdot \vec{E}$ (11– 3).

Another source of inaccuracy due to the radial grid spacing relates to the evaluation of the integral over the control volume of a grid point of the square of the electric field that is in excess of breakdown, as to be discussed in Section 3.3.2.1, page 78. The radial grid spacing does not affect the integral, as that integral is done analytically. Rather, due to the fact that the ions produced in a control volume are uniformly distributed over the control volume, large gradients in the electric field over the control volume would produce gradients in the rate of ion production in the control volume that are not considered in the model. Fortunately, as to be shown in Section 8.1.2, page 135, the ion number densities are sufficiently low, relative to the neutrals with which they react, such that the model can be considered a linear one and the errors in the distribution function will produce errors no greater that those already discussed *i.e.* 10% - 50%.

2.7.2 Vertical Accuracy

As discussed in Section 2.3.3, page 39, to achieve accuracy in vertical derivatives comparable to that of radial derivatives requires that the grid spacing be between 10% and 50% of the di/tripole spacing. This would demand vertical grid spacing between 0.4 and 1.0km for a dipole separation of 2km, the characteristic dipole separation in this model (*cf.* Section 3.3.1.1, page 74). This requirement is met using 15 grid points in the vertical with a model domain of 15 km. This is perhaps an overestimate of the error contributed to the evaluation of the continuity equation Eq.(11) as the vertical derivatives are smaller than the radial ones, so a 50% error in the evaluation of a derivative in the vertical is a smaller contributor to the overall accuracy than a 50% error in the evaluation of a radial gradient.

3 Model Parameterizations

Because this model focuses upon the ion chemistry of electrified convection, the dynamics, microphysics, electrical environment, and lightning-induced ion and photon production of the storm are are specified (parameterized). I now describe each of these in turn.

3.1 Kinematic Parameterizations

3.1.1 Meteorological Setting

Because most of the global lightning occurs in, or equatorward of, the mid-latitudes (*cf. Orville & Henderson*, 1986), I choose a sub-tropical equinox environment for the meteorological setting of the model. The vertical temperature structure is taken from *Fels* [1986], and the vertical pressure structure is computed by numerically integrating the hydrostatic equation. The resulting vertical pressure and temperature structures are shown in Figure 7.

3.1.2 Specification of the Wind Field

Given that this is a chemical rather than a dynamical model of a thunderstorm, I wish to represent the "mean" velocities of a "typical" thunderstorm in a simple manner. Perhaps the zeroth order description of the air motions in a thunderstorm is "in–up–out". While it is recognized that there are also downdrafts, sometimes in close proximity to the updrafts, we may envisage our model as that of an updraft region relatively isolated from any downdrafts. The chemical consequences of ignoring the downdrafts will be discussed in Chapter 9, page 172.

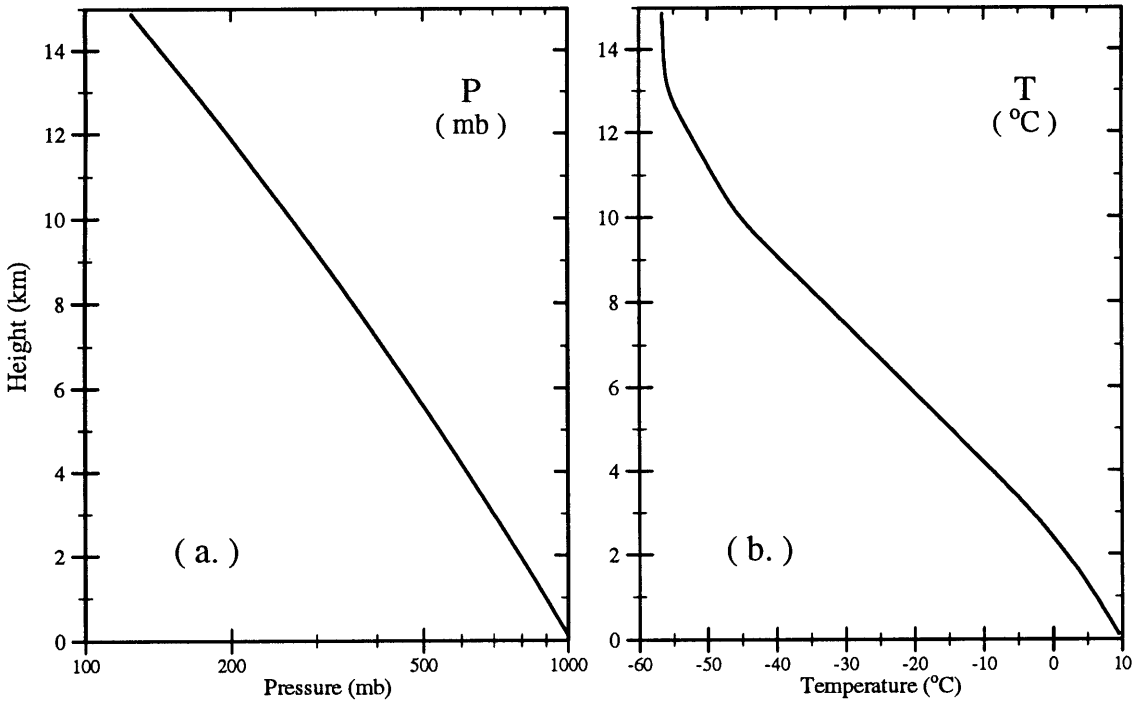

Figure 7. Pressure (a.) and Temperature (b.) *vs.* Height in the model. These distributions correspond to sub-tropical equinox conditions, although the model is not very sensitive to the exact model troposphere chosen.

The vertical motions can be characterized by a maximum updraft speed and a radial distance over which the updraft occurs. Given the wide range in thunderstorm velocity fields, a maximum updraft of 12 $m \cdot s^{-1}$ and a radial decay constant of 1km seem reasonable values to begin with (*cf. Mueller & Carbone*, 1986). Variations in these parameters will not greatly affect the mixing ratios of most compounds for the following reasons. If a species is short-lived then, as noted in Section 2.2.2.1, page 35, chemical production and loss will dominate the terms of the continuity equation for its mixing ratio. Long-lived compounds can be divided into two groups, those that have have significant chemical production or chemical loss within the cloud and those that do not. The domain-averaged mixing ratio of long-lived compounds that have relatively feeble in-cloud chemical production and loss processes is determined by their mixing ratio in the inflow air as the nominal 12 $m \cdot s^{-1}$ up-

draft velocity sets a dynamic time scale too short for the mixing ratio of these compounds to be altered by in-cloud chemistry. Those long-lived compounds that have significant in-cloud chemistry tend to be produced by the storm (*e.g.* O_3); while changing the vertical velocity will change their average mixing ratio, it will not greatly alter their total production. Only in the case of long-lived, water soluble compounds (*e.g.* HNO_3) will the average mixing ratio be affected by the wind field. In this case advection balances heterogeneous loss so changing the velocity field will change the mixing ratios. This case will be examined more closely in Section 8.2.5.1, page 154.

I therefore prescribe a vertical wind velocity $W(r, z)$ *via*

$$W(r,z) = \alpha_W \, W_{\max} \frac{z}{H_o} \frac{15 - z}{7.5} \exp\left[\frac{1}{2}\left(1 - \left(\frac{z}{1.125 H_o}\right)^2 - \left(\frac{r}{R_o}\right)^2\right)\right], \qquad (30)$$

where z is the height above the ground expressed in km, r is the radial distance away from the lightning channel expressed in meters, $W_{\max}$ is the maximum vertical velocity (12 $m \cdot s^{-1}$), R_o is the radial decay constant (1 km), H_o determines the height of the maximum velocity ($H_o = 5$, results in $W_{\max}$ occurring at 4 km), and α_W is a constant required such that $W(0, H_o) = W_{\max}$. The radial components of the wind field are then chosen to satisfy the conservation of mass for each grid node's control region. This is done by integrating the divergence of the wind radially outward starting from the inner boundary of the domain; this results in the wind field as shown in Figure 8 where the thick gray line indicates the impermeable walls of the model's domain. The U and W components are also plotted separately in Figure 9.

3.1.3 Dynamic Lifetimes in Model

The specification of the wind field specifies a dynamic lifetime τ_d (expressed in seconds) that can be defined either locally $\tau_d^{r,z}$ or in a vertically averaged sense τ_d^r. In the

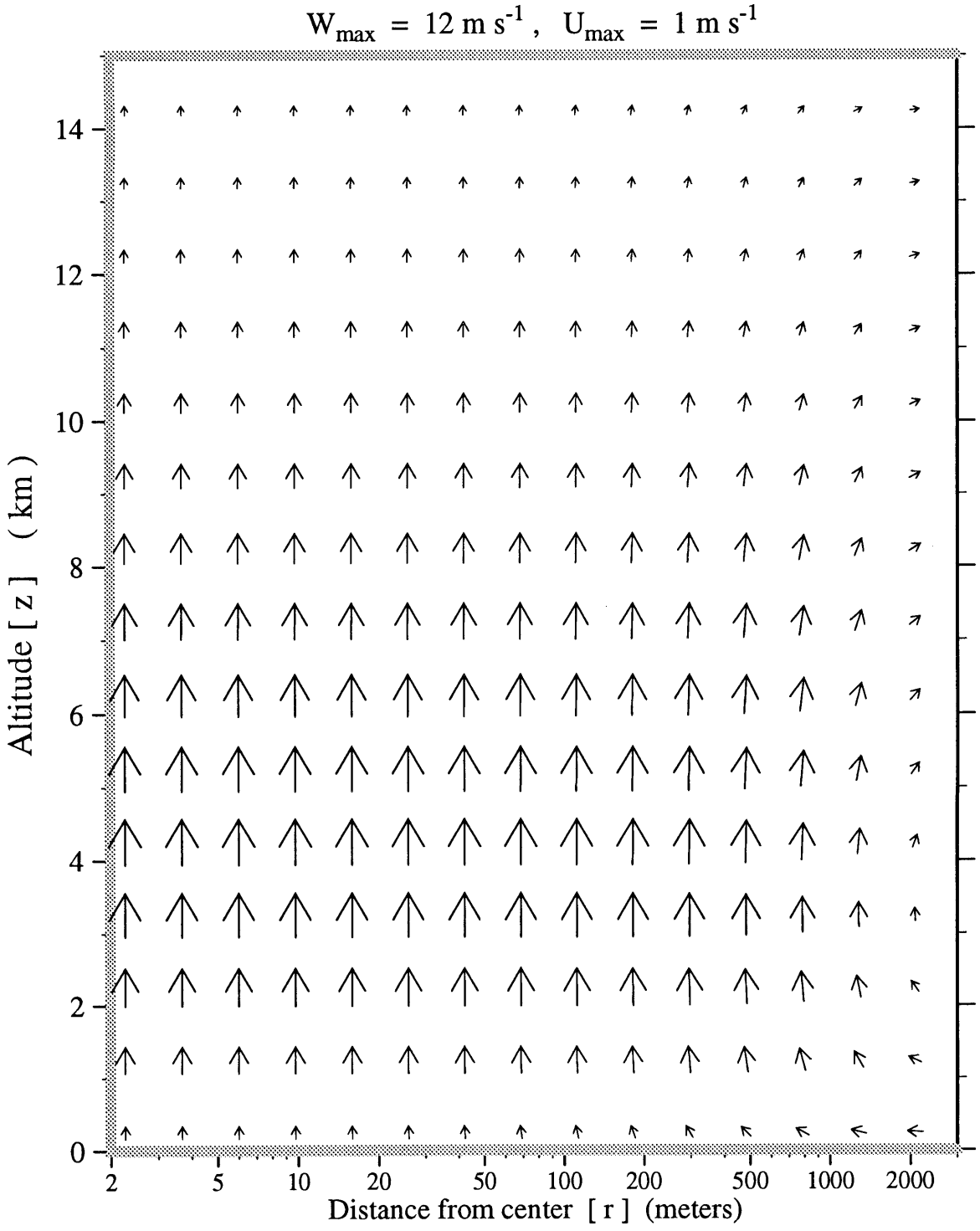

Figure 8. Vectorial representation of the wind field utilized in the model. The vertical component is specified, and the horizontal component is chosen to satisfy conservation of mass. The thick gray line indicates the impermeable walls of the model's domain.

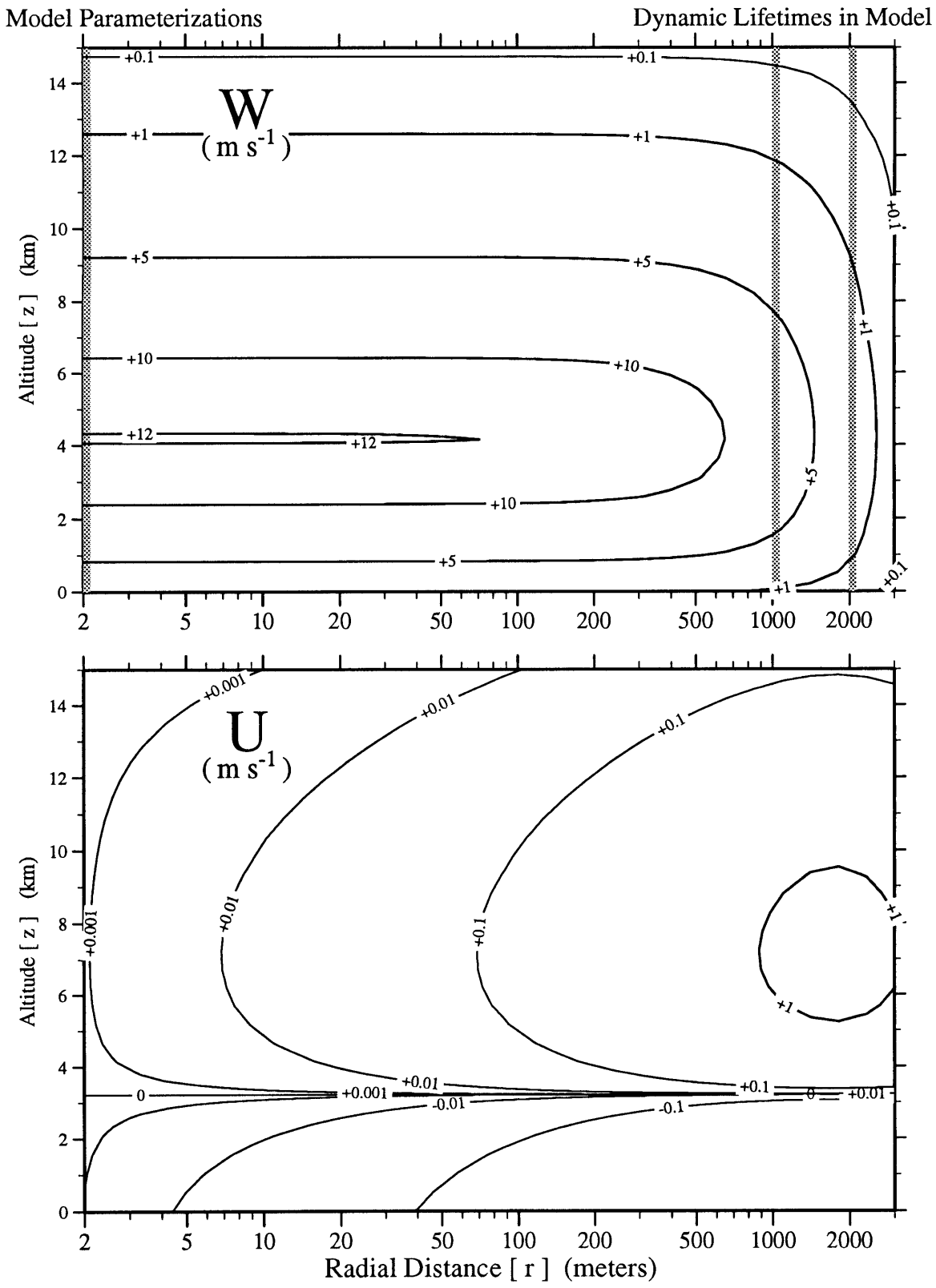

Figure 9. Spatial distribution of the horizontal and vertical components of the wind field. The shaded regions correspond to the vertical profiles shown in Figure 12 a,b. Positive values of U correspond to radial outward motions.

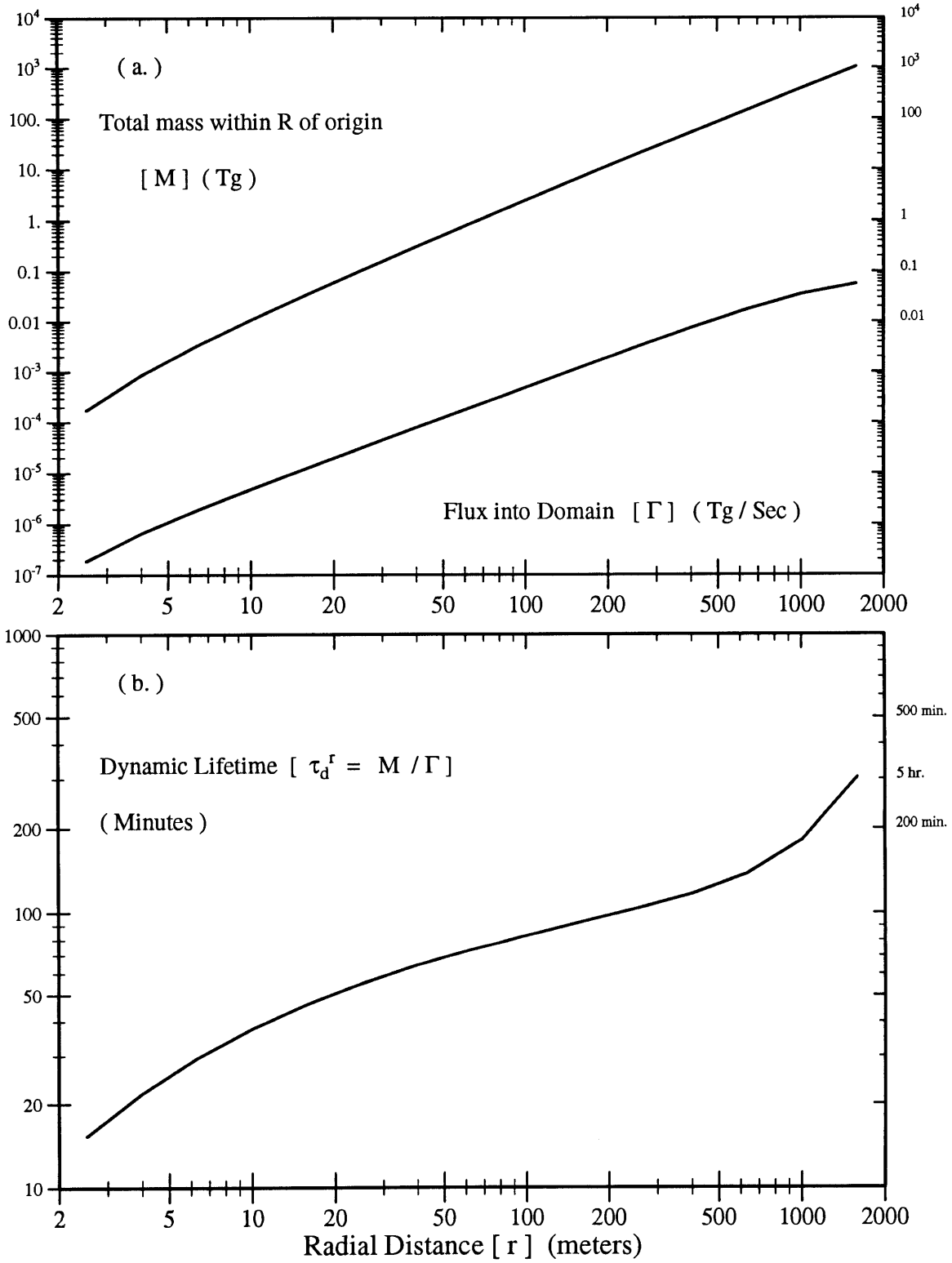

Figure 10. **a.**) Radial variations in the vertically integrated Mass M, and Flux Γ, over the model's domain. **b.**) The vertically averaged Dynamic lifetimes (τ_d^r) in the model. Here τ_d^r is defined to be the mass M of air in a cylinder concentric with the model's origin divided by the flux Γ of air into that cylinder.

vertically averaged sense, τ_d^r is defined to be the mass of air M in a cylinder concentric with the model's origin divided by the mass flux of air Γ into that cylinder. In the outermost portions of the model's domain τ_d^r is of order hours, while in the inner regions of the model's domain it is of order minutes. The vertically integrated mass and fluxes, as well as the vertically averaged dynamic lifetimes as a function of radial position, are shown in Figure 10. It is noted in this Figure that the total mass flux into the model domain is 0.1 $Tg \cdot sec^{-1}$ or 10^8 $kg \cdot sec^{-1}$, which is also the mean estimate of the mass of air advected through a "typical" thunderstorm as reported by *Chameides et al.* [1987].

Alternatively, one can also define the dynamic lifetime as the mass of air in a node's control region divided by the average flux of air into that control region. Figure 11 shows the distribution of $\tau_d^{r,z}$ throughout the model domain.

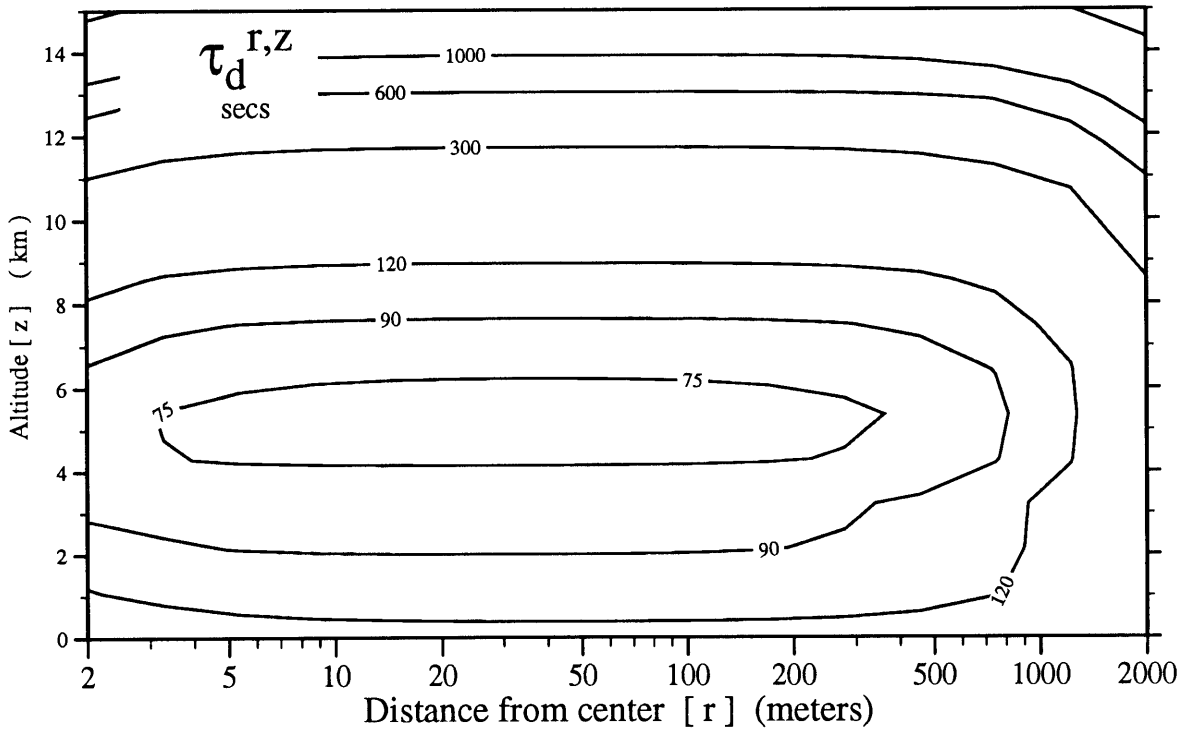

Figure 11. Spatial distribution of the local dynamic lifetimes, $\tau_d^{r,z}$, over the model's domain. $\tau_d^{r,z}$ is defined to be the mass M of air in a control region divided by the flux Γ of air into that region.

These dynamic lifetimes are a useful measure of the time required to establish a dynamical steady state in the dynamical/chemical environment. In a survey of continental thunderstorm durations, *Robinson & Easterling* [1988] found mean durations of between 30 mins and 1 hour for *continental* thunderstorms *at a given location* and about 6% of all storms lasted 3 hours or longer. Storm durations following the motion of the storm itself can be longer than a locally observed lifetime, and convection associated with monsoons can be much more persistent than an air mass thunderstorm (*Keenan & Carbone*, 1989), so even the longest dynamic lifetimes occurring in this model (12 hours) are achievable in the real world under some conditions.

3.1.4 Turbulent Diffusion

The eddy diffusion coefficient $K_{\text{eddy}}(r, z)$ varies throughout the model domain in a rather simple manner. I take an average vertical profile of $K_{\text{eddy}}(z)$ from *Thompson & Cicerone* [1982] and increase the value of $K_{\text{eddy}}(z)$ according to the local value of the vertical wind velocity $W(r, z)$. Specifically, the spatial variation in $K_{\text{eddy}}(z, r)$ is scaled to the variations in $W(r, z)$ according to

$$K_{\text{eddy}}(r, z) = K_{\text{eddy}}(\infty, z) \times \left(1 + \alpha_K \frac{W(r, z)}{W_{\text{max}}}\right), \tag{31}$$

where α_K is a scaling constant that is initially 10 but was varied to 50 in some sensitivity tests and where the results were found to be rather insensitive to its precise value.

This scaling procedure can be visualized *via* reference to Figure 12. In Figure 12a, the vertical profiles of the vertical wind velocity for three selected radial positions are shown and in Figure 12b, the corresponding vertical profiles of $K_{\text{eddy}}(r, z)$ are shown. (These regions correspond to the shaded regions on Figures 10.) As shown in Figure 12b, the values of $K_{\text{eddy}}(r, z)$ decrease from a value of 50 $\text{m}^2 \cdot \text{s}^{-1}$ near the ground to 5 $\text{m}^2 \cdot \text{s}^{-1}$

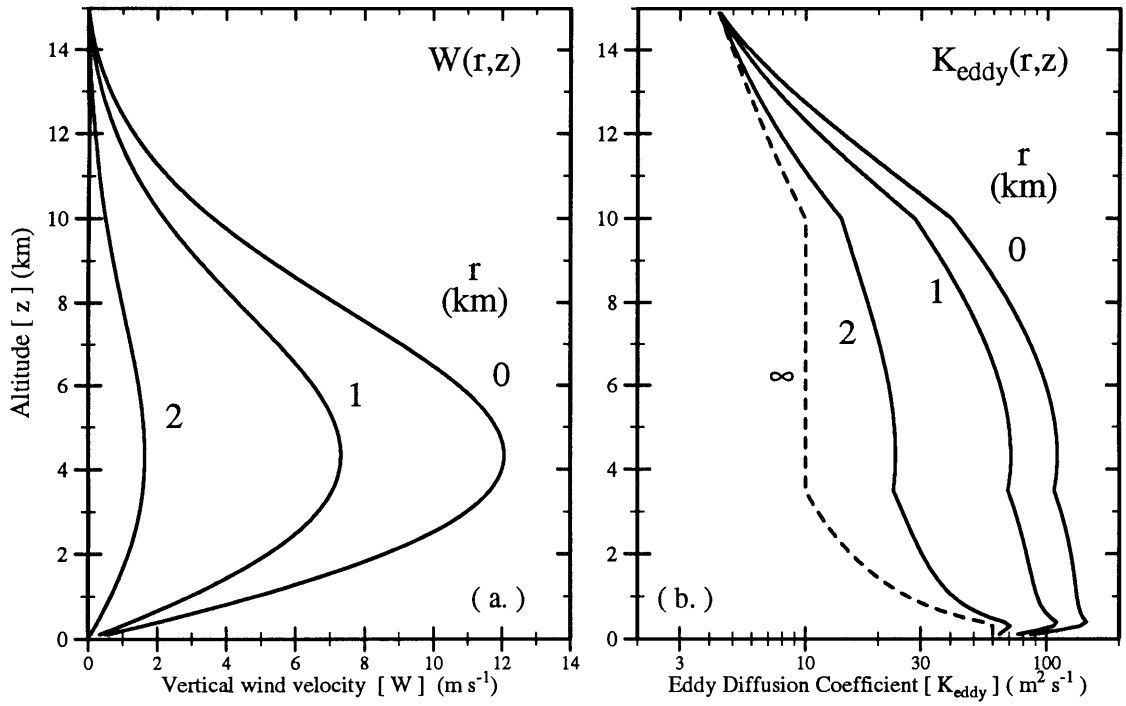

Figure 12. (a.) $W(r, z)$ *vs.* z and (b.) $K_{\text{eddy}}(r, z)$ *vs.* z for selected values of r. These profiles correspond to the shaded regions in Figure 10.

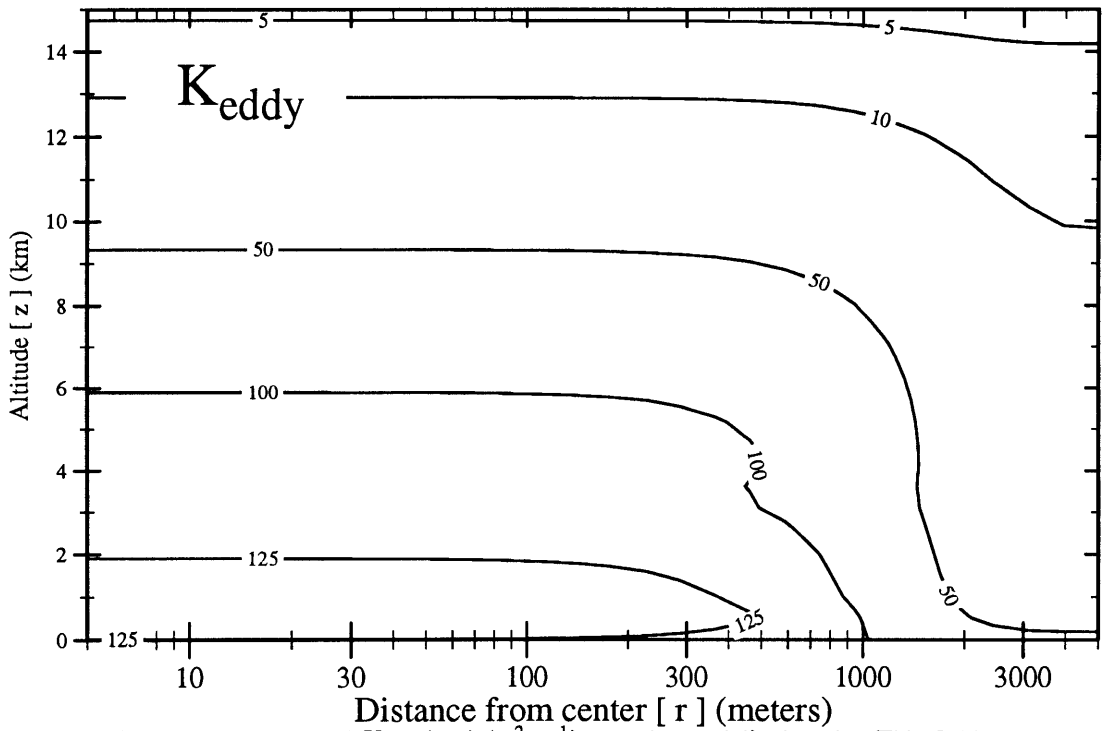

Figure 13. Spatial distribution of $K_{\text{eddy}}(r, z)$ ($\text{m}^2 \cdot \text{s}^{-1}$) over the model's domain. This field corresponds to α_K = 10 in Eq. 31.

near the tropopause in the far field of the model ($r = \infty$), while in the inner regions of the storm, the value of $K_{\text{eddy}}(r, z)$ varies less with height and is approximately 150 $\text{m}^2 \cdot \text{s}^{-1}$. In their simulation of convective storm dynamics, *Klemp & Wilhelmson* [1978] obtained a maximum value of K_{eddy} of $\approx$ 800 $\text{m}^2 \cdot \text{s}^{-1}$ near the shear zone between the updrafts and downdrafts in their model, with mean values near 200 $\text{m}^2 \cdot \text{s}^{-1}$ in the updrafts themselves. The entire field of $K_{\text{eddy}}(r, z)$ is shown in Figure 13.

3.2 Microphysical Parameterizations

I turn now from the dynamical parameterizations of the model to the microphysical parameterizations. Chief among the microphysical parameterizations is the representation of the interaction of the modeled chemical species with cloud particles. This interaction is dominantly one of an irreversible loss to cloud particles, and is normally called heterogeneous loss in order to differentiate it from chemical loss.

3.2.1 1-D Steady-State Model's Heterogeneous-Loss Rates

To initialize the storm model, and to provide boundary conditions for the model's inflow regions, a standard 1-D steady-state photochemical model of the "average" low-latitude troposphere is run. The heterogeneous-loss processes in this model run are scaled to the local atmospheric pressure and generally have the sea level values as used in *Thompson & Cicerone* [1982] and *Thompson & Cicerone* [1986]. heterogeneous-loss rates in this 1-D steady-state model are listed in Table 10, Section 6.3, page 122. Because the loss processes in a cloudy, convective region will be a strong function of the specific surface area of the cloud particles, a different method is used to estimate the heterogeneous-loss rates in the convective model runs, describe next.

3.2.2 2-D Steady-State Model's Heterogeneous-Loss Rates

In the two-dimensional, convective model runs, the heterogeneous-loss processes are scaled to the local specific surface area of cloud particles as well as the sticking coefficient ξ of each chemical species. There is also an electric-field-driven loss process for ions. This loss process is called ion capture and is proportional to the local specific surface area of cloud particles, the local electric field, and the ion mobility. The local specific surface

area of cloud particles is determined from the local size distribution function. I now detail the steps in this process.

3.2.2.1 Cloud-Particle Size Distributions

The size distribution function at each grid point is determined as follows. At each node $W(r, z)$, the lapse rate, and the relative humidity RH are specified; this allows the computation of the rate of conversion of H_2O from the vapor to the liquid state (expressed as grams H_2O $m^{-3} \cdot s^{-1}$). This rate of liquid generation is then converted into a drop-size distribution having the property such that the integral of the liquid water content of the drop-size distribution is equal to the rate of liquid water production dictated by the local values of $W(r, z)$ and RH. This size distribution is then broken down into 50 size classes, spanning the range of sizes from 1 μm to 10 mm. For each size, the fall speed of the class median is computed, and the steady-state concentration of each class size over the model domain is determined using the wind fields and eddy diffusivity as discussed in the previous sections.

The overall size distribution used is the sum of a cloud-particle size distribution and a raindrop size distribution. The cloud-particle size distribution used here is the one used in *Chameides & Davis* [1982], *i.e.* a Khrgian and Mazin size distribution such that

$$N(D) = 0.1 D^2 e^{-0.125D}. \quad \text{cm}^{-3} \cdot \text{cm}^{-1} \tag{32}$$

Two different raindrop size distribution functions were used. The first is the "standard" Marshall–Palmer drop size distribution (*Marshall & Palmer*, 1948)

$$N(D) = N_o e^{-\Lambda D}, \tag{33}$$

where D is the particle diameter, $N(D)\delta D$ is the number of drops of diameters between D and $D + \delta D$ per unit volume of space, N_o is the value of $N(D)$ at $D = 0$ (0.08 cm^{-4}), and Λ is a function of the rainfall rate R expressed in $\text{mm} \cdot \text{hr}^{-1}$ ($\Lambda = 41 R^{-0.21}$ cm^{-1}).

The second raindrop size distribution used was a modified Marshall–Palmer drop size distribution of *Willis & Tattelman* [1989]:

$$N(D) = N_G D^{\alpha} e^{-\Lambda D}, \tag{34}$$

where $N_G = 512.85M \times 10^{-6} D_o^{-(4+\alpha)}$, $\alpha = 2.160$, $\Lambda = 5.5880 D_o^{-1}$, $D_o = 0.1571 M^{0.1681}$, $M = 0.062 R^{0.913}$, and M is the specific liquid water content. The results of these two raindrop size distributions were averaged, based on the following considerations: (1) the two distributions gave very similar results for raindrops with diameters ≥ 0.1 mm, and (2) the "standard" Marshall-Palmer distribution is known to overestimate the number density of small raindrops while the "modified" Marshall-Palmer distribution underestimates them.

The resulting overall size distributions can be seen by reference to Figure 14a and 14b where, respectively, the specific number density (particles·cm^{-3} per cm interval) and the specific surface area (cm^2·cm^{-3}·cm^{-1}) are shown for the inner regions of the model domain. Note that these distributions result in smaller particles higher in the domain. This is due to the lower vertical wind velocities in the upper regions of the domain, and hence the larger particles tend to drop out because their fall speeds are larger than the local magnitude of W.

3.2.2.2 Sticking Coefficients and Scavenging Rates

There are two primary heterogeneous-loss mechanisms considered; diffusion-driven loss and, for ions, a larger, electric-field-driven loss. I discuss now the diffusional-loss process that represents the transfer of material from the gas phase to the surface of a cloud particle and its subsequent incorporation into (or loss to) that particle.

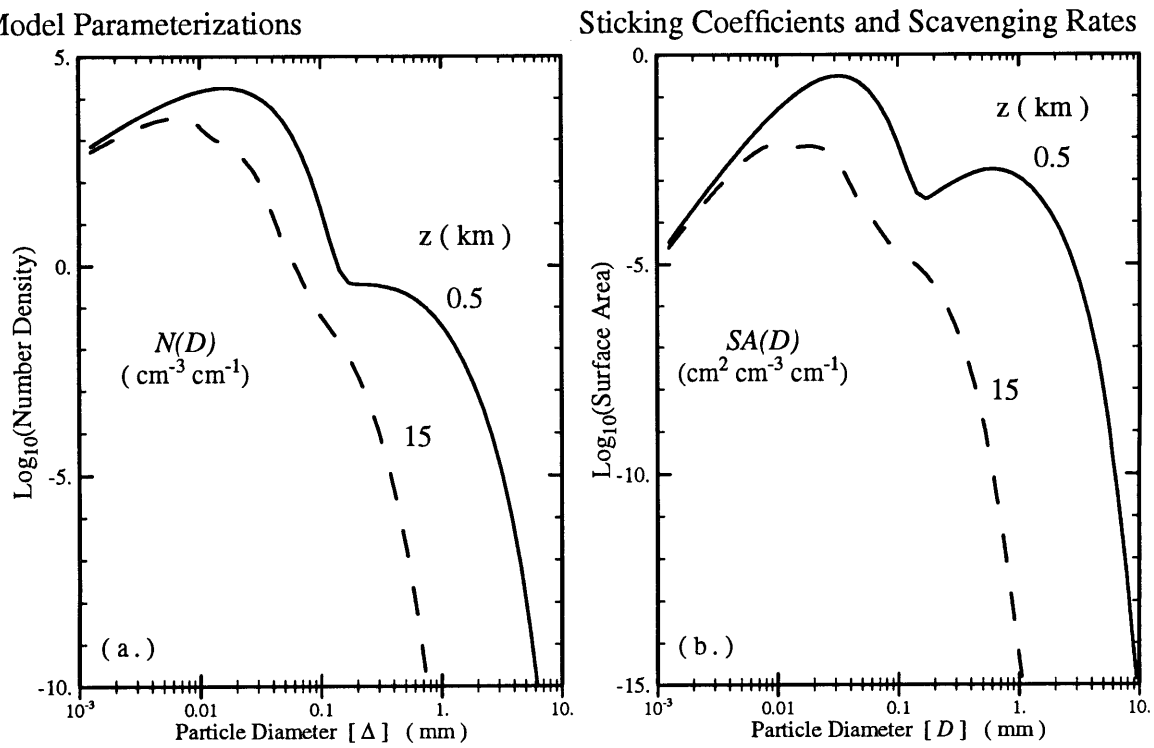

Figure 14. a.) Size distributions of Specific number density, N(D), and b.) Specific surface area, SA(D), at r = 10 m, for two altitudes. The solid lines correspond to z = 500 m, and the dashed lines correspond to z = 15 km.

The above computed steady-state size distribution of cloud particles is used to compute a heterogeneous-loss rate, often called the scavenging rate ϕ. I use the scavenging function that was derived by *Fuchs & Sutugin* [1971] and utilized by *Chameides & Davis* [1982] in their model of (non-electrified) cloud chemistry. In this formulation, the scavenging rate of a compound by a cloud drop of radius a is given by

$$\phi(a,\xi)da = \frac{4}{3}\pi\ell\left(\frac{8kT}{m\pi}\right)^{1/2}\frac{aN(a)da}{1+\left(0.7+\frac{4(1-\xi)}{3\xi}\right)\frac{\ell}{a}}, \qquad s^{-1} \tag{35}$$

where ℓ is the free mean path, ξ is the sticking coefficient, and m is the molecular mass. This function is integrated across all size classes considered in the model to produce an overall loss rate at each grid point.

$$\phi(\xi) = \frac{4}{3}\pi\ell\left(\frac{8kT}{m\pi}\right)^{1/2}\int_{1\mu m}^{10mm}\frac{aN(a)da}{1+\left(0.7+\frac{4(1-\xi)}{3\xi}\right)\frac{\ell}{a}} \qquad s^{-1} \tag{36}$$

This procedure results in a field of heterogeneous lifetimes τ_h, expressed in seconds and shown in Figure 15 for $\xi = 0.1$, $\xi = 0.01$, $\xi = 0.001$, and $\xi = 10^{-4}$. In the model $\xi = 0.1$ is used for ions and small water clusters, $\xi = 0.01$ is used for water soluble chemical species such as HNO_3, $\xi = 0.001$ is used as a default value, and $\xi = 10^{-4}$ is used for sparingly soluble compounds such as O_3.

It is noted here that the cloud particles would exist as ice at temperatures corresponding to the upper model domain. Although there are undoubtedly differences between the sticking coefficients of some compounds to ice and liquid water, this effect is not included here, as other uncertainties in the cloud-water chemistry are expected to be larger than any error introduced by neglecting the freezing of the cloud-particles aloft (*e.g.* specifically the saturation of cloud-drops by sparingly soluble compounds such as O_3).

3.2.2.3 Heterogeneous-Loss Rates of Ions

In addition to the above loss mechanism, driven in some sense by Browian motion, charged species (ions and electrons) have another loss mechanism, specifically an electric-field-driven loss. As discussed in *Griffiths et al.* [1974], this term is very much larger than the diffusional capture of ions by cloud droplets.

An ion of charge q_i will move in an electric field $\vec{E}$ with a velocity $\vec{V_i} = q_i \, \vec{\mu_i} \cdot \vec{E}$, where $\vec{\mu_i}$ is the ion mobility (*cf.* Section 2.2.1, page 33). As the ion moves through the control volume surrounding a grid point, the specific surface area SA ($m^2 \cdot m^{-3}$) of the cloud particles in the control volume are struck by the ions at a rate given by

$$\tau_{IC}^{-1} = \mu_{jj} \times SA \times \{f_\ell E_\ell + (1 - f_\ell) E_a\} \tag{37}$$

where τ_{IC}^{-1} is the overall loss rate due to ion capture (s^{-1}), f_ℓ is the fraction of the time that the channel is conductive (0.01), E_ℓ is the local electric field when the channel **is**

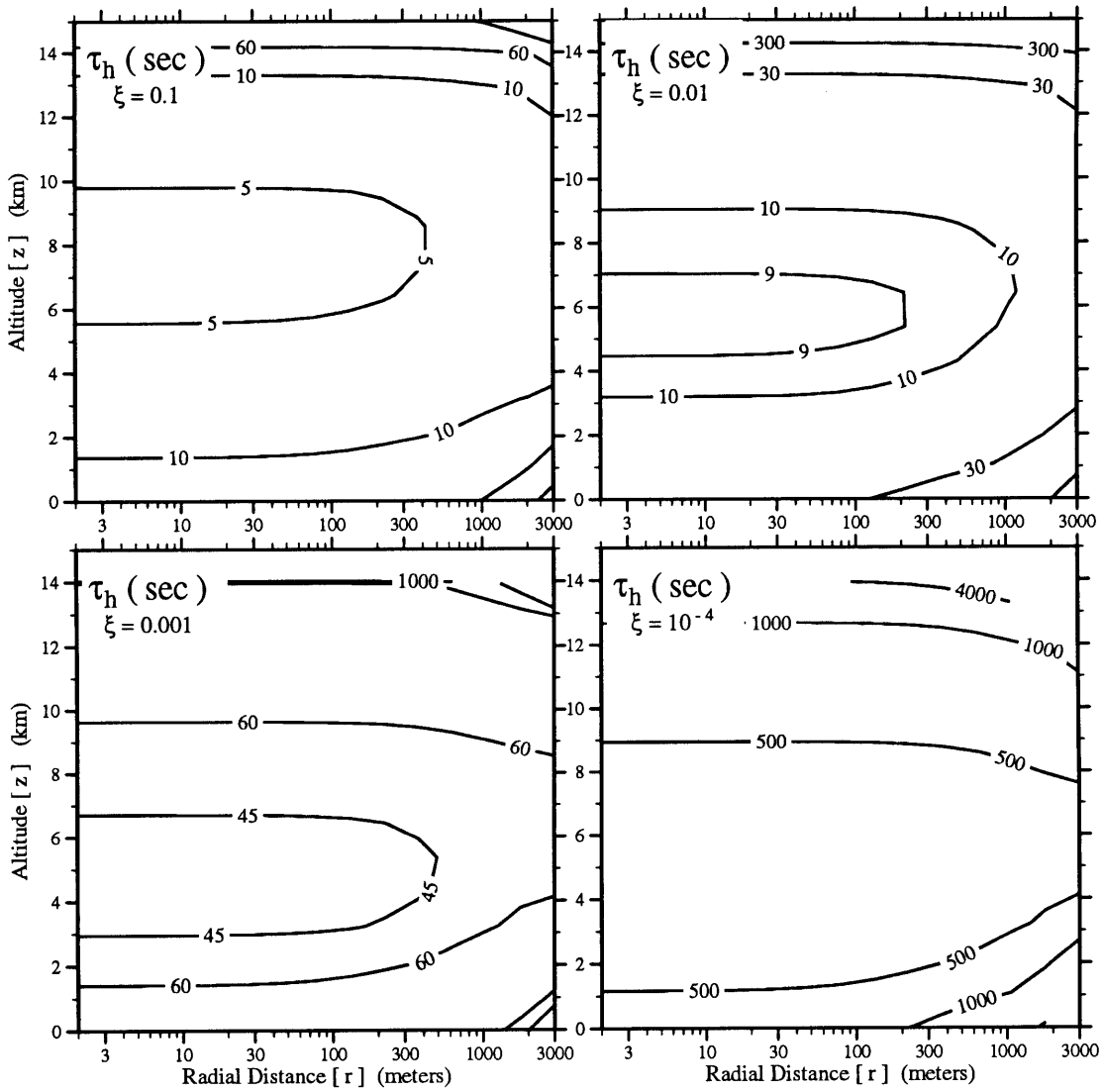

Figure 15. Fields of heterogeneous lifetimes τ_h (seconds) for selected values of the sticking coefficient ξ. In the model $\xi = 0.1$ is used for ions and small water clusters, $\xi = 0.01$ is used for water-soluble chemical species such as HNO_3, $\xi = 0.001$ is used as a default value, and $\xi = 10^{-4}$ is used for sparingly soluble compounds such as O_3.

conductive, and E_a is the local electric field when the channel **is not** conductive.

The distributions of ion-capture loss rates, expressed as a lifetime τ_{IC}, are shown in Figure 16 for the 2-D model runs. The 1-D steady-state model run utilized the ion-capture rates corresponding to the outer domain of the 2-D Base Case model run.

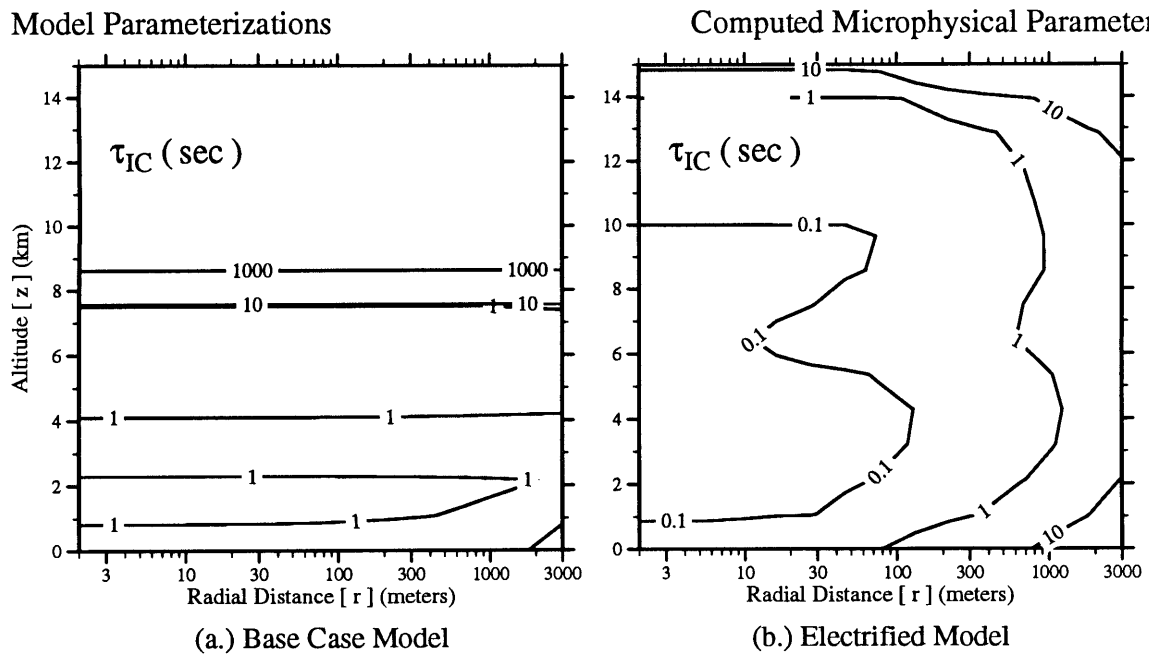

Figure 16. Fields of ion-capture lifetimes τ_{IC} in the 2-D models.

3.2.3 Computed Microphysical Parameters

For ease of comparison with typical storm values, six fields of diagnostic statistics are also computed from the cloud-particle size distributions: (1) the rate of liquid water generation R (mg $H_2O \cdot m^{-3} \cdot s^{-1}$), (2) the average drop diameter D (μm), (3) number density N (cm^{-3}), (4) the surface area SA ($cm^2 \cdot cm^{-3}$), (5) the liquid water content M (g $H_2O \cdot m^{-3}$), and (6) the radar reflectivity dBZ ($10*Log_{10}(mm^6 \cdot m^{-3})$). These fields are shown in Figure 17. In general, these values are consistent with those found in continental thunderstorms and maritime cumulus (*e.g. Musil & Smith*, 1989 and *Pruppacher & Klett*, 1978).

The ratio of the rate of liquid water generation R to the total liquid water content of an air parcel M also determines a time scale of water overturning in the model τ_R. Specifically, τ_R is the time required to replenish M, the standing crop of liquid water (g $H_2O \cdot m^{-3}$), by R, the production of liquid water (mg $H_2O \cdot m^{-3} \cdot s^{-1}$). $\tau_R = 1000M/R$. This

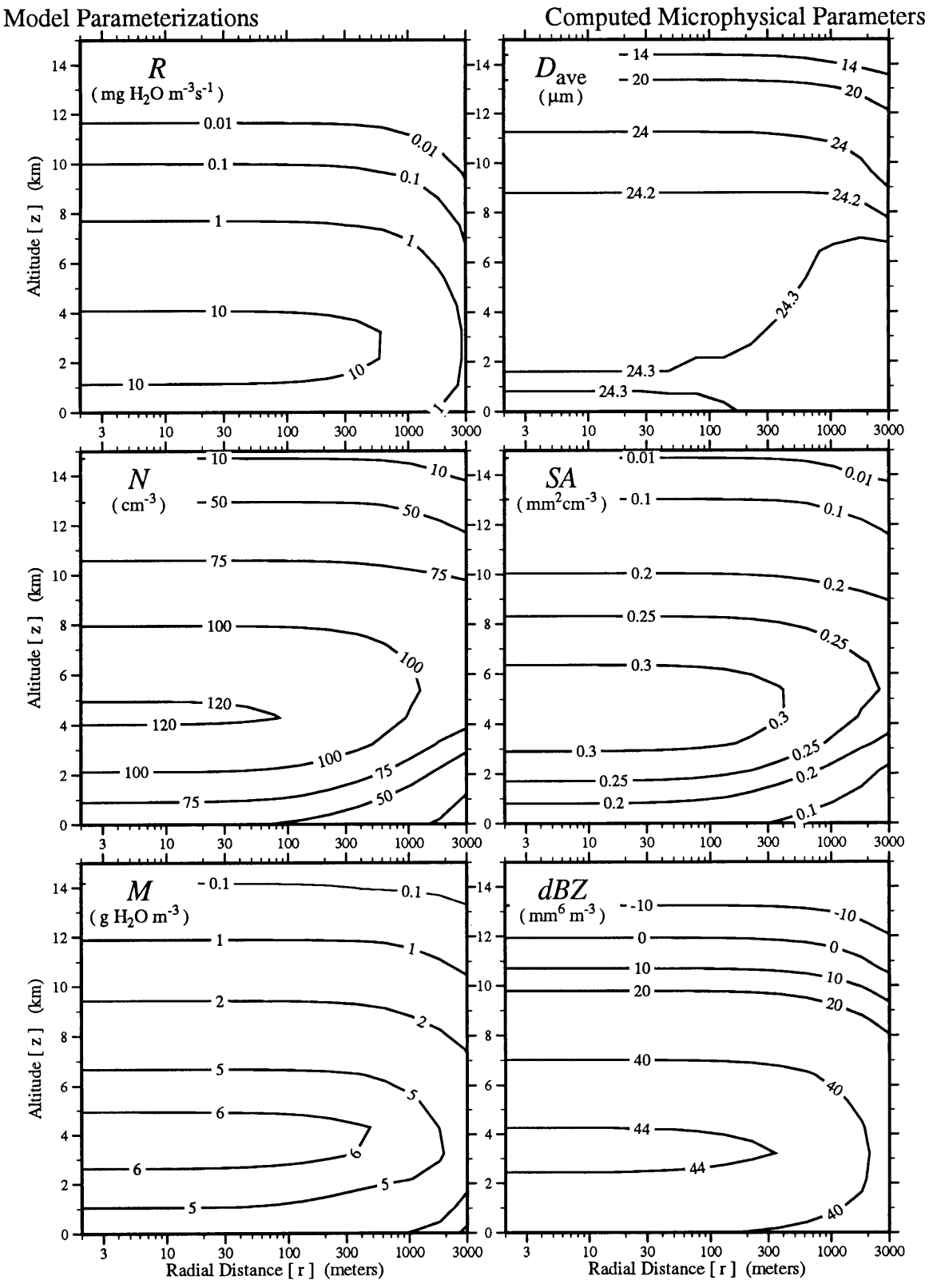

Figure 17. Fields of Liquid water generation rate R, Average drop diameter D, Drop number density N, Specific surface area SA, Liquid water content M, and Radar reflectivity dBZ.

time scale is used to determine the steady-state aqueous phase concentration and to ensure that the drops are not saturated with the sparingly soluble materials such as NO *etc.* The spatial distribution of τ_R over the model's domain is shown in Figure 18.

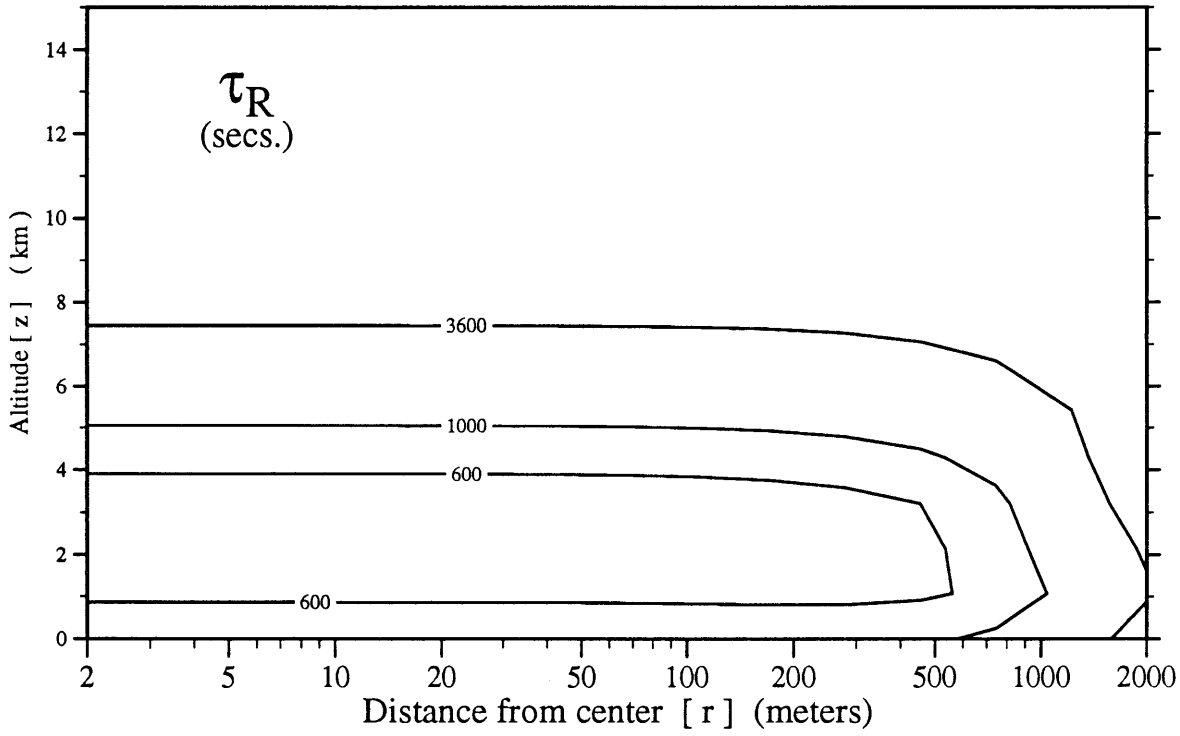

Figure 18. The lifetime of liquid water drops in the model (τ_R). This is the time required to replenish M, the standing crop of liquid water (g $H_2O \cdot m^{-3}$) by R, the production of liquid water (mg $H_2O \cdot m^{-3} \cdot s^{-1}$). Specifically, $\tau_R = 1000M/R$.

3.3 Electrical Parameterizations

I now turn to the parameterization of the electrical environment of the various models. The electrical environment can be considered to be comprised of two main features, electric fields and ions (charged particles). Electric fields exist in both fair weather and foul. The electric fields in thunderstorms ($> 100\text{kV}\cdot\text{m}^{-1}$) are, of course, much larger than the fair weather electric field ($< 0.1\text{kV}\cdot\text{m}^{-1}$). Ion production also occurs in both fair weather and foul. Cosmic rays and radioactive decays are responsible for the maintaining the fair weather population of ions; thunderstorms produce ions via their large electric fields in a manner to be describe below.

In this model, in an effort to simplify the computations, the electric field is specified as is the resulting ion-production rate. As a result of this parameterization, there is no feedback between the produced ions and the local electric field. This interaction needs to be explicitly considered in a more general, explicit, time-dependent model of ion production.

3.3.1 Electric Fields

There are two contributions to the model's electric field $\vec{E}(r, z)$. The first is the vertical field $E_z(r, z)$ caused by the vertical charge distribution within the model. The second is the radial field $E_r(r, z)$ produced by the conductive lightning channel embedded in the vertical electric field. I now discuss each of these in turn.

3.3.1.1 Vertical Electric Field

In the absence of electrification processes within the model domain, the electric field is represented by the fair-weather electric field. This is a vertical electric field which

has a magnitude of -100 V·m^{-1} at the ground† and decreases with a scale height of 2000 m.

In the model runs representing electrified convection, the electric fields are computed from a specified charge structure. The large-scale electric structure of thunderstorms has been reviewed in *Williams* [1989] where a tripole structure is suggested with the heights of the lower positive, central negative, and upper positive centers at 0°C, -10°C, and -30°C respectively. Using a composite of the charge densities seen by *Marshall & Rust* [1991], I derive a "typical" vertical charge structure that is shown in Figure 19(a), where the lower positive, main negative, and upper positive charge regions have net charge densities of approximately 500, 2200, and 1400 nC·m^2 respectively, with a net charge overhead of -250 nC·m^{-2}.

This charge density is then integrated using the one-dimensional version of Gauss' law

$$\rho_{\pm} = \varepsilon_0 \frac{\Delta E_z}{\Delta z}, \quad \left(\text{C}\cdot\text{m}^{-3}\right) \tag{38}$$

to produce the vertical component of the electric field (Figure 19b). This charge distribution produces a field at the ground of +29 kV·m^{-1}, a maximum positive field of +84 kV·m^{-1} at the lower sign reversal level (-2°C), and a maximum negative field of -160 kV·m^{-1} at the upper sign reversal level (-20°C).

3.3.1.2 Radial Electric Field

This vertical electric field then produces a much larger radial electric field for the following reason. During a lightning flash, the lightning channel is conductive; the charge

† The sign convention used here is such that in positive fields, a positive charge will tend to rise (increase in altitude). Under this convention, a negative field ("fair weather field") at the ground corresponds to positive charge overhead.

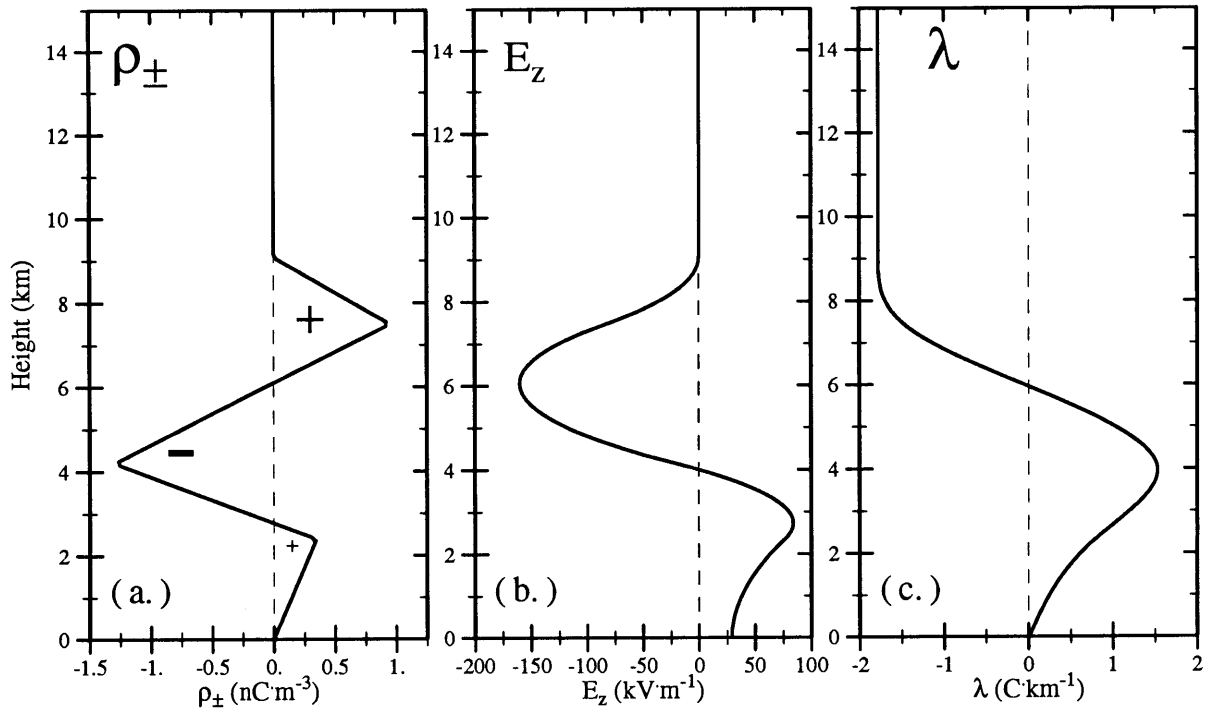

Figure 19. Vertical variations in (a.) Space charge density $\rho_{\pm}$ (nC·m^{-3}), (b.) Vertical electric field E_z (kV·m^{-1}), and (c.) Induced channel charge λ (C·km^{-1}).

per unit length on a long thin conductive channel† in a parallel electric field was shown by *Heckman & Williams* [1989] to be

$$\lambda \approx \frac{2\pi\varepsilon_o}{\ln\left(L/R_{\text{channel}}\right)} \int_0^z E_z dz, \quad \left(\text{C}\cdot\text{m}^{-1}\right) \tag{39}$$

where L is the channel length and R_{channel} is the channel radius. This charge deposited on the channel induces a radial electric field in excess of the breakdown strength of air in the inner region of the model domain during the time that a lightning channel is conductive (order milliseconds). The resulting electric field is shown in Figure 20, where the shading corresponds to the region where the electric field is above the breakdown strength of air

† In this simple model, the lightning channel is represented by a vertical line segment along the inner model domain; any tortuosity will only serve to increase the total (parameterized) ion production as the specific channel length will increase accordingly.

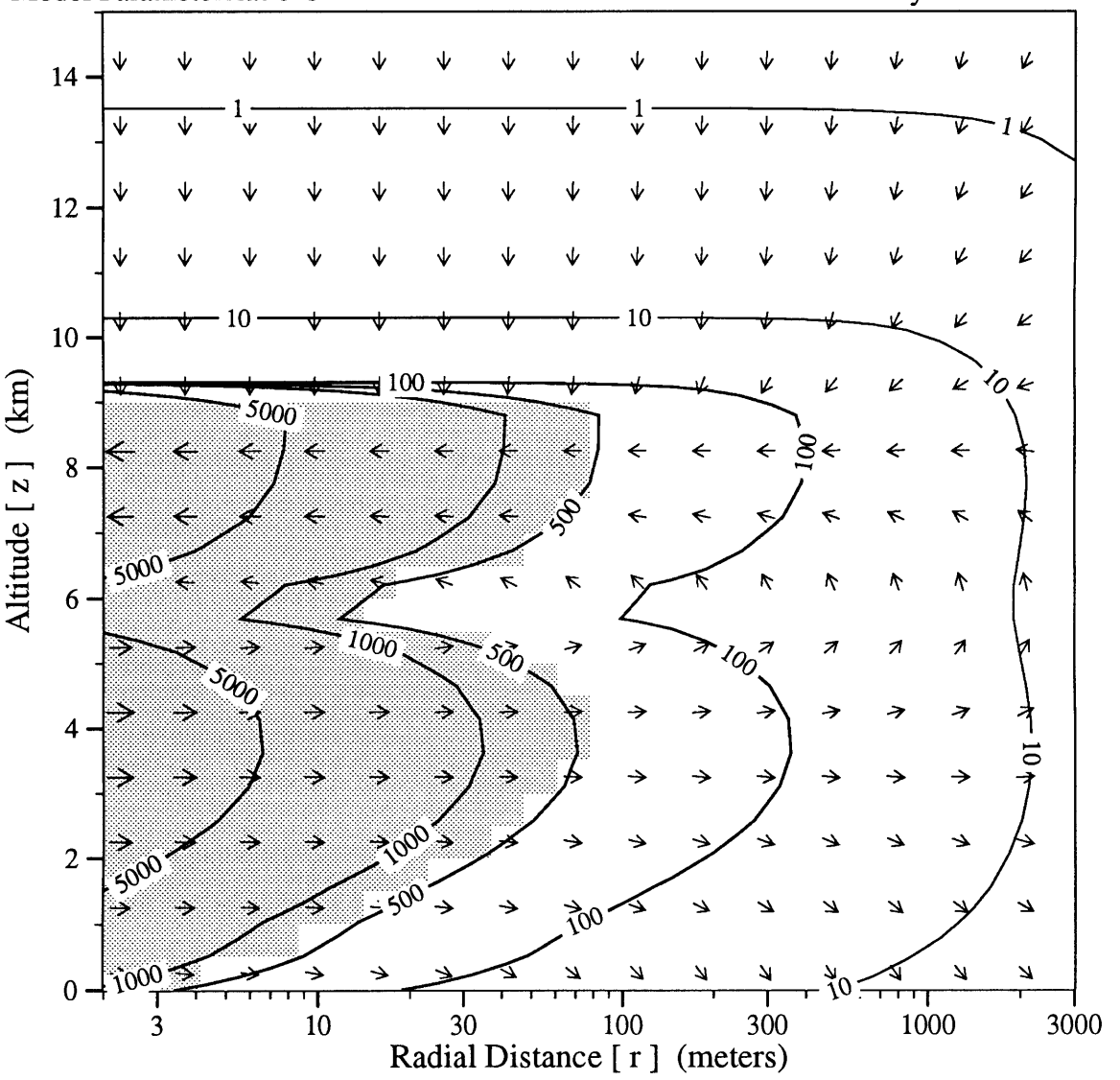

Figure 20. Spatial distribution of the induced electric field resulting from the conductive lightning channel located at the model's inner domain wall. The units are kv·m^{-1} and the shaded region corresponds to regions above the breakdown strength of air.

(assumed herein to be $\approx$ 500 kV·m^{-1}).

It is this radial electric field that is assumed to produce the bulk of the ionization during a lightning flash in this model.

3.3.2 Primary-Ion Production

How many ions are produced per flash? This number is highly uncertain but is bounded by a maximum that can be computed based on energetics and a minimum that is based on field neutralization.

3.3.2.1 Maximum Rate of Ion Production

The maximum number of ions that can be created by an electric field, based on energetics, is roughly equal to that number allowed by taking all the energy of the electric field in excess of breakdown in a given region and using this energy to create ions. The available energy density in a given region of space μ ($\mathrm{J{\cdot}m^{-3}}$) is proportional to the square of that part of the amplitude of the electric field that is above the breakdown strength of air E_{BD} ($\approx 0.5 \times 10^6$ $\mathrm{V{\cdot}m^{-1}}$) and is given by

$$\mu = \frac{1}{2}\varepsilon_o \left(E(r) - E_{BD}\right)^2, \quad \left(\mathrm{J{\cdot}m^{-3}}\right) \tag{40}$$

where the electric field is given by

$$E(r) \approx \frac{\lambda}{2\pi\varepsilon_o r} \quad \left(\mathrm{V{\cdot}m^{-1}}\right) \tag{41}$$

for a line charge, and λ is the charge density on the lightning channel ($\mathrm{C{\cdot}m^{-1}}$). Integrating Eq.(40) over the control volume of a grid point results in

$$\mu^* = \int_{z_l}^{z_u} \int_0^{2\pi} \int_{r_i}^{r_o} \frac{1}{2}\varepsilon_o \left(E - E_{BD}\right)^2 r\,dr\,d\theta\,dz \quad \text{(Joules)} \tag{42}$$

where μ^* represents the total electrostatic energy over the control volume of a grid point. This value of μ^* is then converted into the total number of ions produced throughout the entire control volume by dividing by the average amount of energy required to produce one ion pair,

$$\#\mathrm{IONS}_{max} = \frac{\mu^*}{E_{\pm}}, \quad \text{(Ion Pairs)} \tag{43}$$

where $E_{\pm}$ is the average energy required to produce one ion pair.

We now compute the average amount of energy it takes to produce one ion pair. This is a function of the reactions that are postulated to be the primary ionizations. Following a similar line as that in *Dalgarno* [1967], the primary products of ionization are those due to the breakdown of air and are shown in Table 1 along with their ionization energies.

Table 1. Primary Ionization events.

relative frequency	Reaction	eV per ion pair	total eV required
0.75×0.8	$N_2 \rightarrow N_2^+ + e^-$	15	9.00
0.75×0.2	$O_2 \rightarrow O_2^+ + e^-$	12	1.80
0.25×0.8	$N_2 \rightarrow N + N^+ + e^-$	14 + 9.8	4.76
0.25×0.2	$O_2 \rightarrow O + O^+ + e^-$	14 + 5.2	0.96
$\Sigma = 1$			16.52

Using the conversion factor of 1 eV $\equiv 1.6 \times 10^{-19}$ Joules, we arrive at a value of 2.6×10^{-18} J·Ion Pair^{-1} for $E_{\pm}$ and use this value to compute the number of ions produced per lightning stroke in the control volume of a grid point.

3.3.2.2 Minimum Rate of Ion Production

The minimum number of ions that can be created by an electric field is roughly equal to that number required to just cancel the applied electric field. These ions can be imagined as being created at some point within the control volume of a grid point, starting to move in the applied electric field, and soon being captured by a cloud drop particle, forming a small dipole (the positive and negative ions moving in opposite directions). The magnitude of the electric field produced by the dipole is proportional to the distance that the ions can travel before they are captured. If they travel a short distance, the dipole is weak and a lot of ions are required; conversely, if the ions travel a large distance prior to

being captured, then fewer will be required than in the former case. In other words we are creating a macroscopic-scale dielectric whose dielectric strength κ is proportional to the average distance that an ion can travel prior to capture. The reduction in the electric field due to the creation of the dielectric is then $E = E_o/\kappa$.

This minimum number can be represented by

$$\upsilon = \frac{\varepsilon_o (E - E_{BD})}{a\, e^-}, \quad \left(\text{Ion Pairs}\cdot\text{m}^{-3}\right) \tag{44}$$

where υ is the number of ion pairs per cubic meter required to reduce the field from E to E_{BD}, a is the dipole separation, and e^- is the charge on one ion (1.6×10^{-19}C). This value can vary between an upper limit based on the previously discussed energetic limit and a minimum when the ions can drift a distance comparable to the dimensions of a control region's width (an unlikely prospect); I therefore assume that a is of order 1cm. This function is then integrated over the control volume of a grid point in a manner analogous to that done for μ to obtain the minimum total number of ions produced in that region,

$$\#\text{IONS}_{\text{min}} = \int_{z_l}^{z_u} \int_0^{2\pi} \int_{r_i}^{r_o} \upsilon \; r dr \, d\theta \; dz. \quad \text{(Ion Pairs)} \tag{45}$$

3.3.2.3 Computation of Reaction Coefficient

The number of ions created per lightning flash should lie somewhere between these values ($\#\text{IONS}_{\text{min}}$ and $\#\text{IONS}_{\text{max}}$). Having reason to believe that each bound is an extreme one and wishing to use a conservative ion production rate, I use the geometric mean of these two bounds (given in Eqs.45, and 43) as the number of ions created per lightning flash and uniformly distribute them over the grid's control volume,

$$\text{Volume} = \int_{z_l}^{z_u} \int_0^{2\pi} \int_{r_i}^{r_o} r dr \, d\theta \; dz. \quad \left(\text{m}^3\right) \tag{46}$$

Table 2. Typical values of ion-pair-production rates.

Induced charge λ ($C \cdot km^{-1}$)	Breakdown distance r_{BD} (m)	Maximum Ion Pairs (m^{-1})	Minimum Ion Pairs (m^{-1})	Average Ion Pairs (m^{-1})
0.1	3.6	2.3×10^{20}	6.0×10^{14}	3×10^{17}
1.0	36	3.1×10^{22}	6.0×10^{15}	1×10^{19}
2.0	72	1.3×10^{23}	1.2×10^{16}	4×10^{19}

An example of the results of these calculations are shown in Table 2. In this table is shown the maximum, minimum, and average number of ion pairs created, per meter of lightning channel, per lightning flash as a function of the charge on the lightning channel.

The first column shows typical values of the charge on the lightning channel; the second column lists the radial distance away from the channel that has the (radial) electric field at the assumed breakdown value (the electric field is above E_{BD} for all $r < r_{BD}$); the third column and fourth columns represent the maximum and minimum number of ions produced per meter of lightning channel between $r_i = 0$ and $r_o = r_{BD}$. It is noted that these average values are similar to the value of 4×10^{19} used by *Hill* [1980] in his study of corona currents.

3.3.3 Ground Corona

Estimates of the current density in ground corona underneath thunderstorms are of the order of 1×10^{-9} $A \cdot m^{-2}$ (*Williams*, 1989 and *Standler*, 1980). This current density amounts to 1 A of corona ion current beneath the inner 2000 m of the model domain. This ion current is distributed uniformly throughout the control volumes of the first row of grid points (the lowermost level in the model) in proportion to their ground surface area.

3.3.4 Cosmic Rays & Radioactive decay

In the absence of electrification processes, the primary source of ions in the atmosphere is (1) cosmic rays and (2) radioactive decays. Because the primary chemical reactions leading to ion creation in the regions around lightning channels are similar to the ion production reactions in cosmic-ray bombardment and radioactive decay these latter sources of ions were easily included in all model runs.

There is a latitudinal gradient in incident energy due to cosmic-ray bombardment because the Earth's magnetic field deflects the less energetic particles. Values of total radiance range from $\approx 5 \times 10^6$ MeV $m^{-2} \cdot s^{-1} \cdot sr^{-1}$ near the geomagnetic equator to $\approx 15 \times 10^6$ MeV $m^{-2} \cdot s^{-1} \cdot sr^{-1}$ near the geomagnetic poles (*Hayakawa*, 1969). Cosmic rays dissipate their energy in the atmosphere via ionization (64%), nuclear reactions (13%), and neutrino production (20%); the residual 3% being deposited on the Earth. The incident flux for 30^o latitude is estimated to be 10×10^6 MeV $m^{-2} \cdot s^{-1} \cdot sr^{-1}$. This results in the estimates of the amount of energy dissipated in the atmosphere by cosmic rays shown in Table 3.

Table 3. Estimated Distribution of Energy Dissipation at Latitude 30°

Process	(MeV $m^{-2} \cdot s^{-1} \cdot sr^{-1}$) Dissipation	%
Ionization in the atmosphere	6.35×10^6	64
Neutrinos	2.00×10^6	20
Nuclear Reactions	1.30×10^6	13
Residual energy at sea level	0.35×10^6	3
Total (j_o)	10.00×10^6	

This energy is not deposited uniformly in the vertical, however, as the density of the atmosphere varies exponentially with height, and energy deposition (per unit length)

is proportional to density, with an energy-averaged mass-absorption cross section (k) of 5.5×10^{-4} m^2 kg^{-1} . The cosmic-ray unidirectional intensity as a function of height (z) and zenith angle (θ) is (I assume no azimuthal dependence) therefore

$$j(\theta, z) = j_o \exp\left(\frac{-k}{cos\theta} \int_z^\infty \rho(z)\, dz\right). \quad \text{MeV}\cdot\text{m}^{-2}\cdot\text{s}^{-1}\cdot\text{sr}^{-1} \tag{47}$$

Note that j_o, the omnidirectional cosmic-ray intensity at the top of the atmosphere, can be estimated as twice the downward flux shown in Table 3 or 20×10^6 MeV·m^{-2}·s^{-1}·sr^{-1}. The total, unidirectional (downward) flux at altitude $J(z)$ is found by integrating $j(\theta, z)$ over the upper hemisphere (of a plane parallel atmosphere)†

$$J(z) = 2\pi \int_0^{\pi/2} j(\theta, z)\, \sin\theta\, d\theta\,, \quad \text{MeV}\cdot\text{m}^{-2}\cdot\text{s}^{-1} \tag{48}$$

and the vertical derivative of $J(z)$ is the specific rate of energy deposition at altitude z (MeV·m^{-3}·s^{-1}).

When multiplied by the proportion of the energy dissipation that is due to ionization events ($P_i \approx 0.64$), and divided by the average amount of energy required to create one ion pair ($E_\pm \approx 16$ eV per ion pair), the number of ion pairs produced per m^3 per second can be calculated as a function of height $I(z)$

$$I(z) = \frac{dJ(z)}{dz} \times \left(\frac{P_i}{E_i}\right). \quad \text{ion pairs}\cdot\text{m}^{-3}\cdot\text{s}^{-1} \tag{49}$$

This equation can be most readily solved numerically and yields the solid line shown in Figure 21. As can be seen in this figure, the ionization produced by cosmic rays reaches a maximum near 20 km, where the atmospheric "optical depth" is unity, *i.e.* 1800

† Here I am speaking of the total flux and not just the downward component. The downward component of radiation incident (omnidirectional from above) on a hemisphere is just $\frac{1}{2}$ of the total. The plane parallel approximation is made as altitudes considered will be small ($\leq$ 50 km).

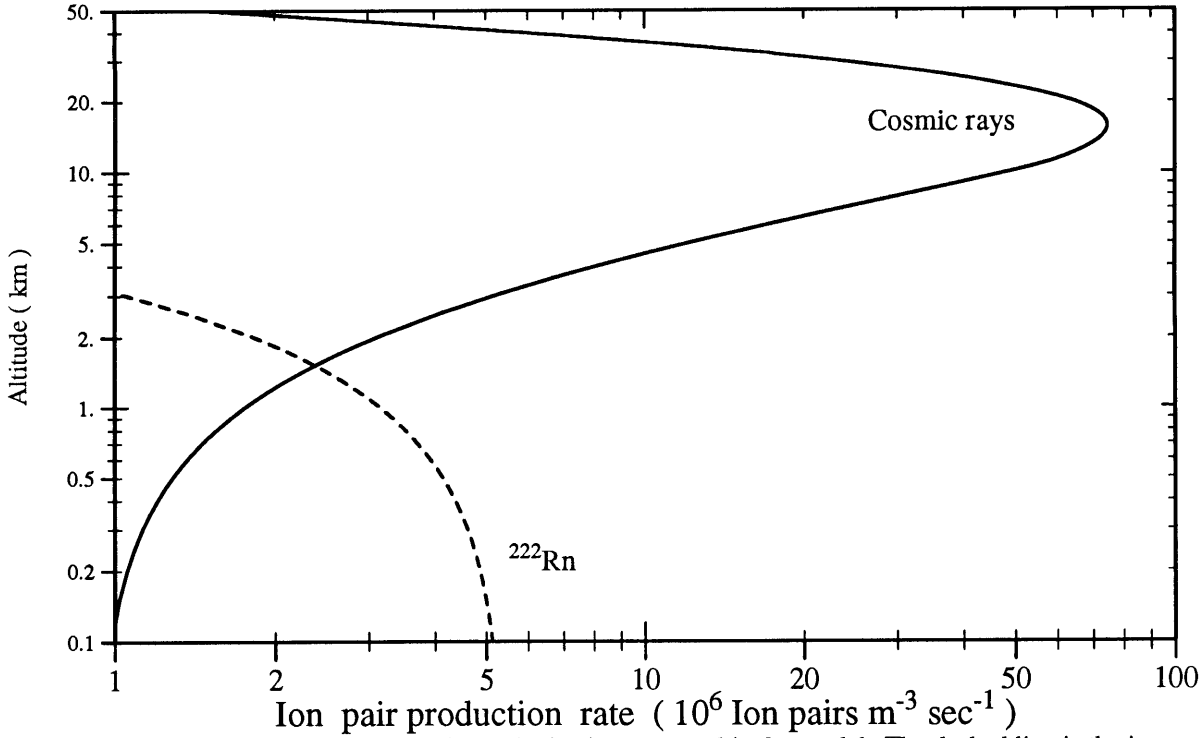

Figure 21. Vertical distribution of cosmic-ray ionization rate used in the model. The dashed line is the ionization rate due to ^{222}Rn and the solid line is the ionization rate due to cosmic rays. The ionization rate used is the sum of these two processes.

$kg \cdot m^{-2}$. This naive integration ignores the interaction of the "hard" component of the cosmic rays (primarily muons) and also ignores the slight energy dependence of the absorption cross section, as well as other subtleties, but it gives values of $I(z)$ good to within a factor of 2 of generally accepted distributions (*cf.* Fig. 18-6 in *U.S.A.F.*, 1961). As seen in Figure 21, the cosmic-ray ion production rate below 1 km is of the order of 1 to 2 $\times 10^6$ $m^{-3} \cdot s^{-1}$. In this region, radioactive emanations from the ground also contribute to the ionization rate and are considered next.

Radioactive decay of naturally occurring uranium and thorium result in long chains of daughter isotopes, ultimately leading to lead. The fact that radon is a noble gas allows it to percolate through the soil and escape to the air. In addition, as *Martell* [1985] points out, plant transpiration can increase the flux of radon from soils by almost an order

of magnitude over the rate for "bare" soils. Martell further summarizes reported values of radon fluxes as $^{222}Rn \approx 1 \times 10^4$ atoms$\cdot m^{-2} \cdot s^{-1}$, $^{220}Rn \approx 2.4 \times 10^2$ atoms$\cdot m^{-2} \cdot s^{-1}$, while the fluxes of ^{219}Rn are insignificant due to the fact that it has a 3.9 sec half life and its parent (^{235}U) has an abundance relative to ^{238}U of 0.72%.

When the average energy released in the decay of radon and its short-lived daughters (6 MeV) are combined with the energy requirement of 16 eV per Ion pair created, approximately 2×10^5 ion pairs are produced per disintegration of radon. The density of ^{222}Rn decreases exponentially with height, averaging 500 dpm (disintegrations per minute) at ground level and having a scale height of 1.76 km. This ionization rate is shown on Figure 21 as a dashed line. As seen by this line, radon dominates over cosmic rays as the chief source of ionization below 2 km and creates a ground-level† ion-production rate of some 5×10^6 ion pairs$\cdot m^{-3} \cdot s^{-1}$. Because most lightning occurs over land (*Orville & Henderson*, 1978), these two sources of ionizing radiation are added together to produce the net background ionization.

3.4 Ultraviolet-Light Production

Due to the very high temperatures of the lightning channel ($\approx$ 30,000K) and the facts that (1) the photon flux output by a black body varies as the third power of the temperature‡, (2) the wavelength of maximum emission varies as $1/T$ (Wien's displacement law), and (3) the photolysis of molecular oxygen O_2 and O_3 are chemically important events, the production of copious quantities of ultraviolet light by the lightning flash must

† Radon is emitted only over land in any substantial quantities, as its precursors are insoluble in seawater and so the radon concentration of the sea is very low and its half life is too short for diffusion from the sea floor to be important.

‡ This result is derived in Appendix A , page 183 .

be considered and accounted for in some manner if it in any way resembles a black body.

The approach that I took can be summarized as the following seven stage analysis: **(1)** Establish to what extent the lightning channel can be considered as a gray body (and consider the errors resulting from this assumption) and **(2)** compute the gray body emissivity required to give the same total radiance as an actual lightning channel with emphasis on the vacuum-UV (< 200 nm). I then **(3)** compute the time-temperature profile of an average lightning channel and based on this, **(4)** compute the total radiance for the standard *WMO* [1985] spectral bins† (and the shorter wavelengths emitted as a consequence of the high temperatures of the lightning channel). This wavelength dependent photon flux is then **(5)** coupled to intra-cloud loss processes and **(6)** given estimates of the average lightning-flash rate as a function of position within the model domain, **(7)** determine reaction coefficients for selected wavelength-dependent photolytic reactions, specifically the photolysis of O_2 and O_3. The details of each of the preceding steps are now presented.

3.4.1 Black-Body Analysis of a Lightning Channel

We begin the analysis with the first point to consider, namely **(1)** To what extent can the hot channel can be considered to be a gray body of radius 1 cm? Lightning is certainly **not** a perfect black body (nor perhaps even a very good gray body) emitter. However, the radiative considerations are simplified considerably if the gray body assumption can be made. How poor an approximation is this?

The answer is based on two considerations. The first is an analysis of the spectra of relatively cold laboratory arcs ($\approx 8,000$K) obtained by *Palva* [1974] (Figs. 3.8.2 and 3.8.3 therein) and the spectra of return strokes recorded by *Orville* [1968a] (Figs. 9–12

† Standard wavelength intervals used in the computation of absorption cross-sections and photolysis rates.

therein). These spectra clearly indicate that in some parts of the spectrum lines dominate, while in other regions the continuum dominates. Although none of these spectra show the UV spectrum of an actual return stroke, that spectrum can be expected to have a similar mix of continuum and lines. The lines will perhaps be even broader because the temperatures are higher.

The second consideration derives from the recognition that it is not the exact spectral distribution of photons that we are ultimately interested in. Rather it is the integral of the product of the emission spectrum and the absorption cross-sections of O_2 and O_3 (*cf.* Section 4.1, page 95). These cross-sections do show some line features but are generally relatively smooth; hence the integral may be (hopefully) less sensitive to the details of the emission spectrum than it is to the integrated photon flux within the regions of strongest absorption.

I therefore conclude that a gray body is an acceptable assumption provided that I pick an emissivity ϵ for the gray body such that it emits the same amount of radiant energy as an actual channel at 30,000K, especially in the ultraviolet.

3.4.2 Determination of a Gray-Body Emissivity

We come now to the second stage of the analysys **(2)**: Assign a gray body emissivity.

The total radiant energy flux of a lightning channel at 30,000K can be estimated from the measurements of the long-wavelength (400 – 1200 nm) light output of lightning strokes as observed by *Guo & Krider* [1982] and computed in *Paxton et al.*'s [1986] model of the energy balance of a 20 kA return stroke (Fig. 9 therein). Figure 22 shows the distribution of radiant energy as a function of wavelength for a "black body" 1 cm lightning

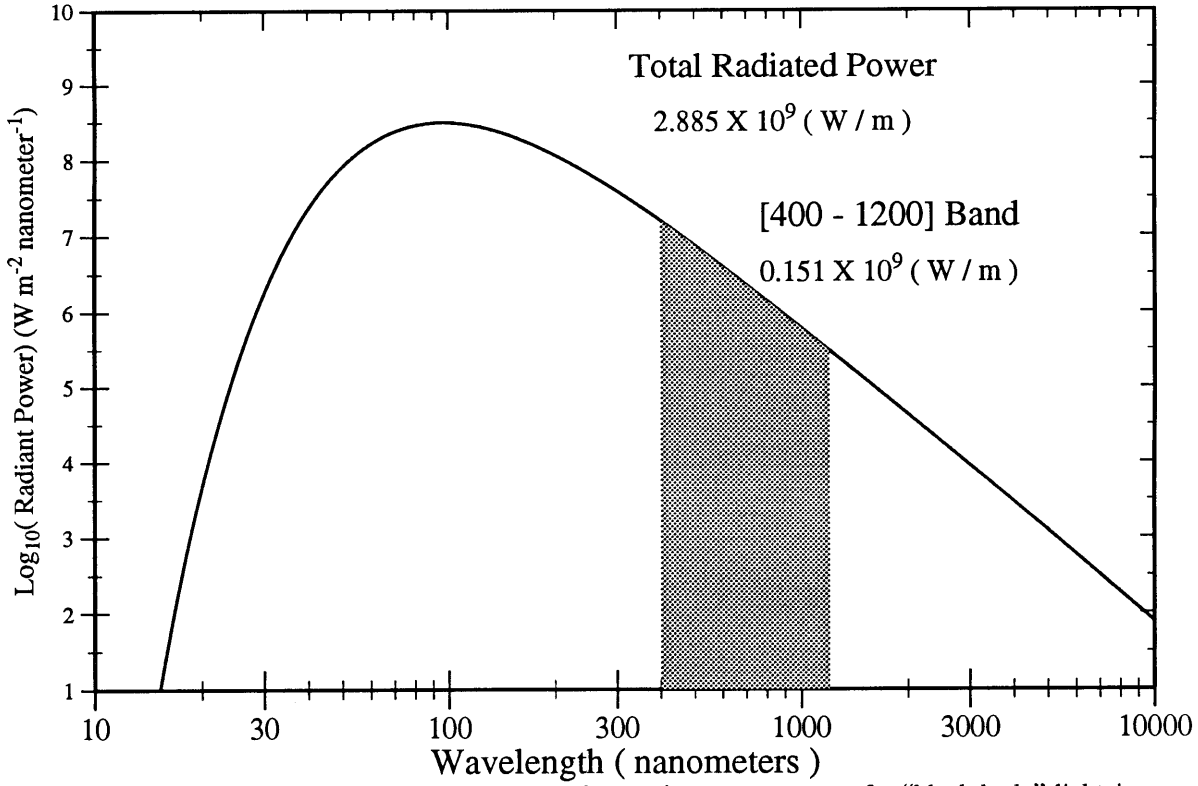

Figure 22. Spectral distribution of the radiative flux from a 1 meter segment of a "black body" lightning channel 1-cm in diameter at 30,000K. The shaded region corresponds to the region observed by *Guo & Krider* [1982].

channel at 30,000K. The output in the 400 to 1200 micron band is shaded.

As seen from this figure, most of the energy output of a black body has wavelengths shorter that the 400 micron limit to the observations of *Guo & Krider* [1982], and the total power is 2885×10^6 W·m^{-1} with 151×10^6 or 5.2% in the 400 to 1200 micron region. *Guo & Krider* [1982]'s measured optical output in the 400 to 1200 micron band was $1.0 \pm 0.9 \times 10^6$ W·m^{-1}. If we assume that the lightning channel at the time of its observation was at 30,000K and had a 1-cm radius, then this "black body" lightning channel would have a total radiation output of 2885×10^6 W·m^{-1}, with 151×10^6 W·m^{-1} of that output in the 400 to 1200 micron window. This implies an emissivity in this region of 0.67%.

Another estimate of the emissivity of the lightning channel can be obtained from

the 20kA lightning return stroke modeled by *Paxton et al.* [1986]. This channel radiated 1600 $J \cdot m^{-1}$ during a 8 μsec time interval or 200×10^6 $W \cdot m^{-1}$. This corresponds to an emissivity of 6.9%. The dependence of the emissivity upon temperature is apparent here as a black body should radiate 5.2% of its power in the 400 to 1200 micron window: in the model of *Paxton et al.* [1986] it radiates 0.5% with 1×10^6 $W \cdot m^{-1}$ of the total power in the 400 to 1200 micron band.

Considering the fact that most of the radiation will be from the very hot early moments of the flash, the 6.9% gray body is more appropriate than the 0.67% derived from the 400 - 1200 nanometer region. I therefore choose 5% as the emissivity of the channel.

Having derived an estimate of the emissivity of the lightning channel, I now determine the time-temperature characteristic of a cooling lightning channel in order to permit the computation of the total photon flux.

3.4.3 Rate of Channel Cooling

The third stage of the analysis is **(3)**: Estimate the time evolution of the temperature of the lightning channel. The time-temperature relationships observed by *Orville* [1968b] and the model computations of *Uman & Voshall* [1968] were combined and fitted to a power-law time-temperature profile. These data and the fitted curve are shown in Figure 23. The channel begins at 30,000K at 1 μsec and cools to 2,000K in 1 sec.

3.4.4 Total Photon Flux

The fourth stage of the analysis is **(4)**: Compute the photon flux in each spectral bin as defined in *WMO* [1985] and in the vacuum-UV wavelengths.

The total number of photons emitted per meter of lightning channel per light-

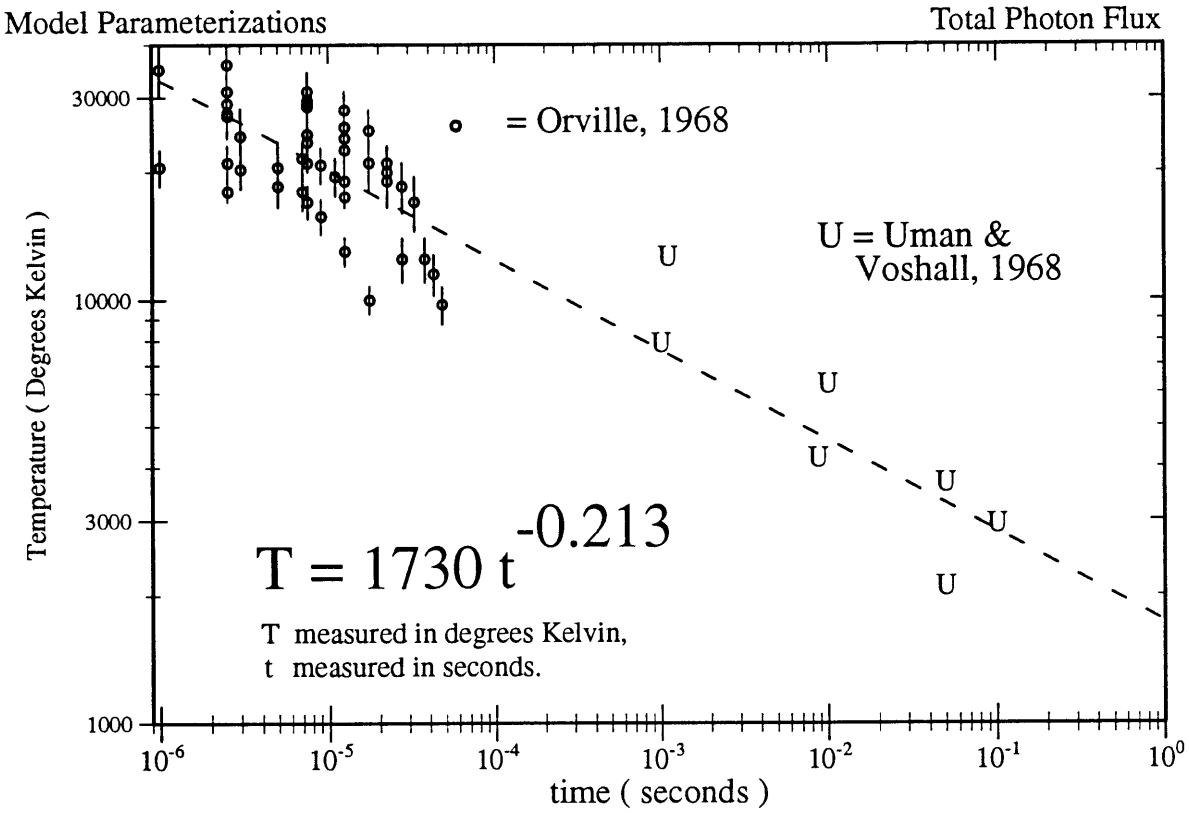

Figure 23. The time evolution of channel temperature (dashed line) that is used to compute the radiation flux. The circles are observed temperatures (*Orville* [1968b]), the U's are various models of (*Uman & Voshall* [1968]).

ning flash $\Gamma(\delta\lambda)$ can be computed by successively integrating the outward photon flux over (a) the specific surface area of the lightning channel, (b) wavelength interval, and (c) time. The outward photon flux $\Gamma(T, \lambda)$ is found by integrating the outward component $\cos(\theta)$ of the channel's radiance, given by the channel's emissivity ϵ times Planck's function ($\mathrm{J \cdot m^{-2} \cdot s^{-1} \cdot sr^{-1} \cdot m^{-1}}$) over a hemisphere σ (2π sr) and dividing by the energy per photon $h\nu (= hc/\lambda$ $\mathrm{J \cdot photon^{-1}})$

$$\Gamma(T,\lambda) = \int_{\sigma} \frac{\lambda\epsilon}{hc} \mathrm{B}\,(T(t),\lambda)\,\cos\theta\; d\sigma \quad = \pi \frac{\lambda\epsilon}{hc} \mathrm{B}\,(T(t),\lambda) \;\; . \;\; \frac{\text{photons}}{\mathrm{s \cdot m^2 \cdot m}} \tag{50}$$

where h is Planck's constant ($\mathrm{J \cdot Hz^{-1}}$), c is the speed of light, $T(t)$ is the prescribed temperature T at time t, and $\mathrm{B}(T(t), \lambda)$ is the Planck function at temperature $T(t)$ and wavelength

λ. The remaining integrations are then

$$\Gamma(\delta\lambda) = \pi \frac{\epsilon}{hc} 2\pi R_{\text{channel}} \delta Z \int_{1\mu\text{sec}}^{1\text{ sec}} \int_{\lambda_i}^{\lambda_f} \lambda \, \text{B}(T(t),\lambda) \, d\lambda \, dt, \quad \frac{\text{photons}}{\text{m}} \qquad (51)$$

where R_{channel} is the channel radius, δZ is one meter of channel length and $\delta\lambda$ is the wavelength interval between the limits of a WMO [1985] spectral bin λ_i, and λ_f. The wavelength intervals are 2nm's in width for wavelengths shorter than the first WMO standard spectral bin ($\lambda < 175$ nm) and 5nm's in width for wavelengths longer than the last WMO standard spectral bin ($\lambda > 850$ nm). Figure 24 shows this total photon flux as a function of wavelength.

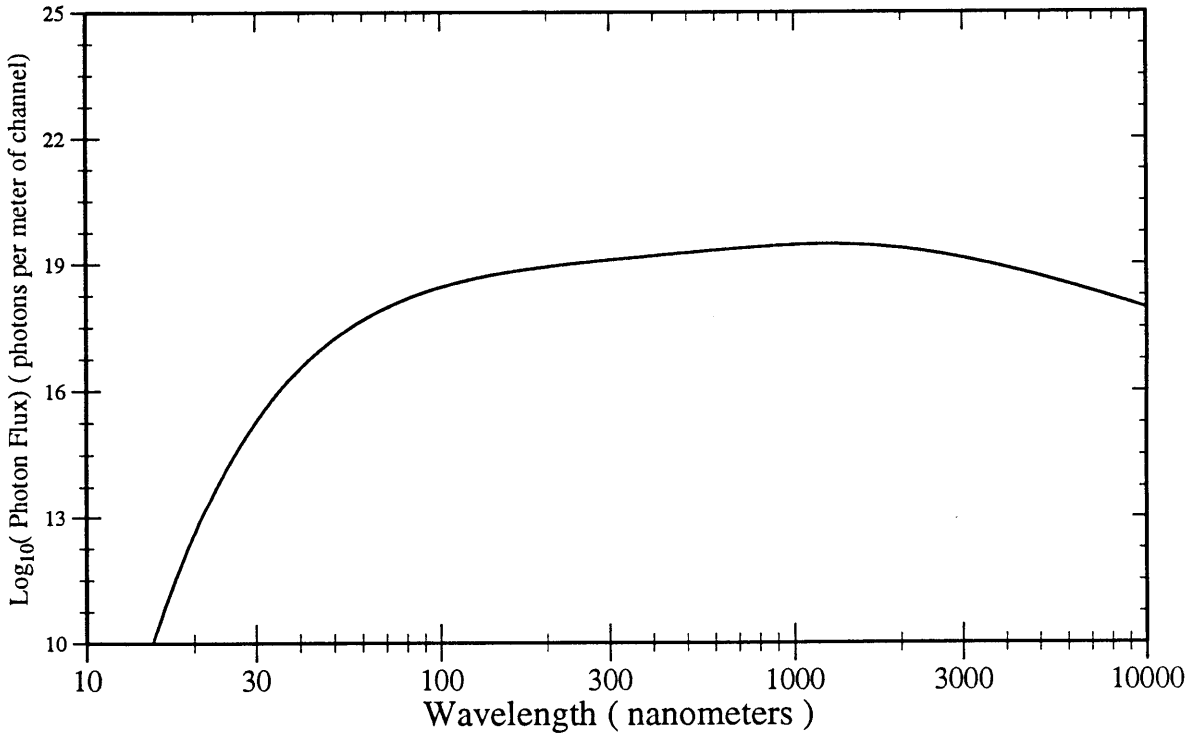

Figure 24. Spectral distribution of the total photon flux from one meter of a cooling lightning channel.

3.4.5 Photon Loss

The fifth stage of the analysis is: **(5)** Determine the nature of the intra-cloud photon loss processes. Photons in the visible spectral region have a rather low loss rate inside clouds; as noted by *Thomason & Krider* [1982], the single-scattering albedo ($\bar{\omega}_0$) of clouds is very near 1.0 throughout the visible region and decreases very slightly in the infrared ($1.000 \leq \bar{\omega}_0 \leq 0.99997$ in the region 450 nm $\leq \lambda \leq$ 870 nm). For water drops much greater than the wavelength of light, the extinction efficiency of a spherical drop is approximately 2 (*van de Hulst*, 1957) and the interaction mean free path of photons Ψ with a uniform population of drops is approximately

$$\Psi \approx \frac{1}{2\pi a^2 N}$$

where a is the mean radius and N is the number density of drops. Choosing characteristic values of a and N of 10μm and 500 cm^{-3} respectively results in a Λ of 3.2 meters. Taking a value of $\bar{\omega}_0 \leq 0.9999$ as the average for the visible/near-UV region gives and using the above value of Λ yields a photon "e-folding" distance of 32 km.

The scattering of vacuum-UV photons ($\lambda <$ 200nm) is much greater. However, they are also strongly absorbed by O_2 and O_3, and are removed within a meter for the vacuum-UV and on a scale of tens of meters for the longer wavelength UV photons ($>$ 200 nm).

3.4.6 Lightning-Flash Rate

The penultimate stage of the analysis is: **(6)** Derive an average lightning-flash rate as a function of height for the model. To derive the lightning-flash rates for the electrified convection model run, I consider two regions of the model, the region below the main lower

charge center that is assumed to have cloud-to-ground lightning flashes, and the region between the main charge centers that is assumed to have cloud-to-cloud lightning flashes (*cf.* Section 3.3.1.1, page 75 and Figure 19).

I begin with an estimate of the average global lightning-flash rate of $O[100]$ per second (*Borucki & Chameides*, 1984) and a consertative average number of thunderstorms in existence at any one time over the globe of $O[1000]$ (*cf.* page 9-4, *U.S.A.F.*, 1961). I assume that these flashes represent cloud to ground flashes. This results in an average cloud to ground flash rate in any particular thunderstorm of $O[0.1]$ per second. Most flashes are composed of multiple strokes, so I then (conservatively) multiply the flash rate by 2 to account for multiple strokes per flash (*Uman*, page 4, 1969 gives range of $3-4$ strokes per flash as representative). This yields a cloud to ground stroke rate of 0.2 per second.

It is known that cloud to cloud flashes are more common than cloud to ground flashes, and much of the ion model represents intra-cloud lightning; therefore, between the main charge centers of the model (*cf.* Section 3.3.1.1, page 75 and Figure 19) I use a global average cloud-cloud stroke rate. To compute the average cloud-cloud stroke rate I multiply the average cloud to ground stroke rate by 5, the average ratio of cloud-cloud flashes to cloud-ground flashes reported by *Rutledge et al.* [1992]; this yields a cloud to cloud stroke rate of 1 per second.

3.4.7 Computation of Photolysis Rates

The final stage of the analysis is (**7**): Compute an effective reaction coefficient for the photolysis of O_2 and O_3.

The computed photon flux is then turned into an equivalent photolysis rate for the photolytic reactions via a 1-D Beer-Lambert type analysis of the photons absorbed as they

stream radially outward from the lightning channel. To accomplish this, the photon flux per meter of channel $\Gamma(\delta\lambda)$ (photons$\cdot$m$^{-1}\cdot$flash^{-1}) is first divided by the specific surface of the channel (m^2/m) and then multiplied by the assumed lightning-flash rate (flash per second) to obtain a radial flux $d\Gamma$ expressed as photons$\cdot$m$^{-2}\cdot$s^{-1}. The photons (of a given wavelength interval) absorbed in the control region of a grid point then becomes a function of the intensity of the incoming photon flux and the optical depth of the control region of the grid point (*cf.* Section 4.1, page 95). The number of photons absorbed is then divided by the local atmospheric number density to obtain an effective $J(r, z, \delta\lambda)$.

4 Chemistry of the Model

In this chapter I discuss the compounds and reactions included in the model as well as the methods used to create and test the model. Generally, when setting out to create a chemical / dynamical model on a grid, two distinct problems arise. The first is the creation of the grid, and that has already been dealt with in the chapter detailing the creation of the grid (Section 2.4, page 41). I now discuss the procedure to select the compounds and reactions to include in the model.

4.1 Overview of the Chemistry of the Model

As this is a model of the ion chemistry of electrified convection embedded in a tropical atmosphere, it begins with a standard photochemical model, patterned closely after those of *Logan et al.*, 1981, *Thompson & Cicerone*, 1982, and *Thompson & Cicerone*, 1986). I therefore begin with the major reactions ($\approx$ 150) and compounds ($\approx$ 50) found in standard photochemical models.

The altitude-dependent diurnally-averaged, photolysis rates used in the model (J_n's) were computed by integrating across all wavelengths the product of the UV photon flux at altitude z, represented by $\varphi(\lambda, z)$ ($\mathrm{cm}^{-2}\cdot\mathrm{s}^{-1}$) times the temperature-dependent reaction cross-section $\sigma(\lambda, T(z))$ (cm^{-2}) *i.e.*,

$$J_n(z) = \int_{\lambda_i}^{\lambda_f} \varphi(\lambda, z)\, \sigma(\lambda, T)\ d\lambda\,. \tag{52}$$

The altitude-dependent diurnally-averaged UV fluxes are calculated in a separate model. In this model, the atmosphere is divided into 1km thick layers, from the surface to 50km. Given prescribed concentrations of ozone and Rayleigh scatters for each layer and

a top-of-the-atmosphere solar flux, the UV flux at each level is computed for each of the spectral intervals in *WMO* [1985]. In this model, the Rayleigh-scattering phase function is bi-directional, *i.e.* either directly forward or backward, the surface albedo is 0.06, and the column ozone concentration is 250 Dobson units (DU).

Given the debate over the importance of the atmospheric oxidation of the sulfur-containing species OCS and DMS to the generation of CCN (Cloud Condensation Nuclei), I add the chemistry of OCS, DMS and their degradation products on down to H_2SO_4. This adds another $\approx$ 150 reactions and $\approx$ 20 compounds. The addition of these reactions permits an understanding of the vertical distribution of possible CCN generating reactions.

To compare the importance of the hot-channel chemistry to the ion chemistry occurring in the cooler regions surrounding the lighting channel, the standard chemistry of high-temperature air must be included in the model. Adding this high temperature adds another $\approx$ 150 reactions and $\approx$ 25 compounds to the model. These reactions focus on the dissociation and recombination of the major atmospheric constituents.

We now come to the focus of this study – the atmospheric chemistry of ions. The major ion reactions will be reviewed in the next section and it suffices to state here that the inclusion of this ion chemistry adds another $\approx$ 300 reactions and $\approx$ 75 compounds to the model. Of these reactions, about 1/3 deal with the basic ion chemistry of air, 1/3 are reactions of water clusters, and 1/3 are reactions of the long-lived gases SF_6, CF_4, and $CC\ell_4$.

We arrive at the final model with a rather large number of reactions and compounds. The methods used to manage such a relatively complicated chemical model will be dealt with in detail later in this chapter, beginning at Section 5.1, page 102.

4.2 Ion Chemistry

I now describe the basic ion chemistry of the model. The ion reactions will be discussed in an order parallel with the life history of an ion, *i.e.* its production, reaction, and loss.

4.2.1 Ion-Producing Reactions

We begin with the reactions that produce ions from neutral species; these reactions can be characterized as being driven by either cosmic rays or high electric fields.

4.2.1.1 Cosmic-Ray-Induced Reactions

The reactions induced by cosmic rays are considered to be similar to those estimated by *Dalgarno* [1967] and used by *Hill et al.* [1984] and are listed in Table 4 . As seen in this table, the immediate products of ionization are electrons, N_2^+, N^+, O_2^+, and O^+. I also added the cosmic-ray-induced destruction of the long-lived trace gases SF_6, CF_4, and $CC\ell_4$ in order to obtain an estimate of their tropospheric (chemical) lifetime in the absence of electrified convection.

The cosmic-ray reaction-rate coefficient, referred to in Table 4 as **Ionization-Rate**, was computed by taking the total ion production rate ($I(z)$) as shown in Figure 21 and dividing by the number density of the local air ϱ_{air}. This produces an effective j that varies with height. Rates computed in this manner are indicated by **X3** in the rate tables. It is noted that the reactions that break chemical bonds as well as ionize are given less weight (occur less often) to account for the greater energy requirement of these reactions (*cf.* Table 1).

Table 4. Cosmic-ray-induced reactions.

Rx	Ref	Reaction	Rate Coefficient
R_{114}	X3	$O_2 \rightarrow O_2^+ + e$	$j_{114} = 0.50 \times$ IonizationRate
R_{115}	X3	$O_2 \rightarrow O + O^+ + e$	$j_{115} = 0.25 \times$ IonizationRate
R_{116}	X3	$N_2 \rightarrow N_2^+ + e$	$j_{116} = 0.50 \times$ IonizationRate
R_{117}	X3	$N_2 \rightarrow N + N^+ + e$	$j_{117} = 0.25 \times$ IonizationRate
R_{118}	X3	$CO_2 \rightarrow CO_2^+ + e$	j_{118} = IonizationRate
R_{119}	X3	$H_2O \rightarrow H_2O^+ + e$	j_{119} = IonizationRate
R_{120}	X3	$SF_6 \rightarrow SF_5 + F$	j_{120} = IonizationRate
R_{121}	X3	$CC\ell_4 \rightarrow CC\ell_3 + C\ell$	j_{121} = IonizationRate
R_{122}	X3	$CF_4 \rightarrow CF_3 + F$	j_{122} = IonizationRate

4.2.1.2 High-Electric-Field Production

The reactions that comprise the initial creation of ions (primary ions) by the electric field in excess of breakdown are are listed in Table 5. As seen in this table, the immediate products of ionization due to high fields are the same as for cosmic ray induced reactions, namely electrons, N_2^+, N^+, O_2^+, and O^+.

Table 5 . High-Field-Induced Reactions.

Rx	Ref	Reaction	Rate Coefficient
R_{129}	X5	$O_2 \rightarrow O_2^+ + e$	$j_{129} = 0.79 \times$ L_Ion_P
R_{130}	X5	$N_2 \rightarrow N_2^+ + e$	$j_{130} = 0.79 \times$ L_Ion_P
R_{131}	X5	$O_2 \rightarrow O + O^+ + e$	$j_{131} = 0.21 \times$ L_Ion_P
R_{132}	X5	$N_2 \rightarrow N + N^+ + e$	$j_{132} = 0.21 \times$ L_Ion_P

The reaction rate coefficient, referred to in Table 5 as **L_Ion_P**, was computed by taking the local value of the average ion production rate as discussed in Section 3.3.2, page 77 and listed in Table 2 and dividing by the local air number density ϱ_{air}. This produces

an effective j that varies with height and the strength of the local electric field. This rate is 0 for any grid point whose control volume is sufficiently away from the lightning channel such that the magnitude of the electric field is less than the assumed breakdown strength of air ($E_{BD} = 0.5 \times 10^6$ V·m^{-1}). The grid points for which this rate is non zero are indicated by the shaded region of Figure 20 as discussed in Section 3.3.1.2, page 77. Rates computed in this manner are indicated by **X5** in the rate tables. It is noted that the reactions that break chemical bonds as well as ionize are given less weight (occur less often) to account for the greater energy requirement of these reactions (*cf.* Table 1).

4.2.2 Secondary-Ion Production

The reactions that comprise the secondary creation of ions are those that are due to the electrons previously created by the primary-ion reactions in conjunction with the ambient electric field. Specifically, these are the various electron-energy-dependent reactions of O_2 and N_2. The energy dependencies were accounted for by fitting polynomials to the energy-dependent cross-section data of *Itikawa et al.* [1986], referred to as **II** in the reaction tables and *Itikawa et al.* [1989], referred to as *IH* in the reaction tables. In increasing order of electron energy required for the reactions are Ionization, Dissociation, and Dissociation & Ionization. These are represented by the (energy dependent) functions **X2**_Ion, **X2**_Dis, and **X2**_DisIon respectively where **X2** represents either N_2 or O_2. These reactions are summarized by Table 6.

4.2.3 Reactions With Water

Unlike the ion chemistry of the stratosphere and ionosphere, the ion chemistry of the troposphere is dominated by reactions with water. Water reacts rapidly with positive

Table 6 . Lightning-Induced-Ionization Reactions

Rx	Ref	Reaction	Rate Coefficient
R_{209}	II	$O_2 + e \rightarrow O_2^+ + e + e$	k_{208} = O2_Ion
R_{210}	II	$O_2 + e \rightarrow O + O + e$	k_{209} = O2_Dis
R_{211}	II	$O_2 + e \rightarrow O + O^+ + e + e$	k_{210} = O2_DisIon
R_{309}	IH	$N_2 + e \rightarrow N_2^+ + e + e$	k_{308} = N2_Ion
R_{310}	IH	$N_2 + e \rightarrow N + N + e$	k_{309} = N2_Dis
R_{311}	IH	$N_2 + e \rightarrow N^+ + N + e + e$	k_{310} = N2_DisIon

ions to produce OH, H_3O^+. As discussed by *Good et al.* [1970a] the presence of water causes the primary positive ion loss mechanism to be

$$N_2^+ + N_2 + \{M\} \rightarrow N_4^+ + \{M\}, \qquad (53\ a)$$

$$N_4^+ + H_2O \rightarrow 2N_2 + H_2O^+, \qquad (53\ b)$$

$$H_2O^+ + H_2O \rightarrow H_3O^+ + OH\ . \qquad (53\ c)$$

The analogous reactions also occur with O_2 instead of N_2 (*Good et al.* [1970a]).

The fate of negative ions is less interesting. The primary (first created) negative species is the electron. It undergoes three-body collisions with O_2 to produce O_2^- and O_4^-. If, as discussed in *Hameka et al.* [1987], the electron or O_2^- impacts H_2O with sufficient energy then the following reactions could occur

$$e^- + H_2O \rightarrow OH^- + H\ , \qquad (54\ a)$$

$$O_2^- + H_2O \rightarrow OH^- + H + O_2\ . \qquad (54\ b)$$

These reactions are indicated by **XX** in the reaction tables and are given in Table 7. These rates should be considered as upper limits to the rates applicable to atmospheric studies.

Table 7 . Primary reactions with water

Rx	Ref	Reaction	Rate Coefficient
R_{314}	MP	$N_4^+ + H_2O \rightarrow H_2O^+ + N_2 + N_2$	$k_{313} = 1.9 \times 10^{-9}$
R_{316}	MP	$N_2^+ + H_2O \rightarrow H_2O^+ + N_2$	$k_{315} = 1. \times 10^{-10}$
R_{216}	ZN	$O_4^+ + H_2O \rightarrow WO_2^+ + O_2$	$k_{215} = 2.2 \times 10^{-9}$
R_{225}	XX	$O_2^+ + H_2O \rightarrow H_2O^+ + O_2$	$k_{224} = 1. \times 10^{-10}$
R_{242}	XX	$e + H_2O \rightarrow OH^- + H$	$k_{241} = 1. \times 10^{-12}$
R_{340}	ZN	$H_2O^+ + O_2 \rightarrow O_2^+ + H_2O$	$k_{339} = 2. \times 10^{-10}$
R_{341}	ZN	$H_2O^+ + H_2O \rightarrow H_3O^+ + OH$	$k_{340} = 1.8 \times 10^{-9}$

4.3 Lightning-Induced Photolysis

As discussed in Section 3.4, page 85, the lightning channel also is an emitter of vacuum-UV radiation; the primary reactions driven by this photon flux are listed in Table 8. As discussed in Section 3.4.7, page 93, the effective photolysis rates for these reactions are computed via a 1-D Beer-Lambert procedure; these reactions are indicated by the reference **X4**. The wavelength specific cross-sections σ were taken from *WMO* [1985] for O_2 and O_3 and from *McEwan & Philips* [1975] for O^-, O_2^- and O_3^-.

Table 8 . Lightning-Induced-Photolysis Reactions.

Rx	Ref	Reaction	Rate Coefficient
R_{123}	X4	$O_3 \rightarrow O_2 + O$	J_{123}= 0.05× O3_L_Photo
R_{124}	X4	$O_3 \rightarrow O_2 + O(^1D)$	J_{124}= 0.95× O3_L_Photo
R_{125}	X4	$O_2 \rightarrow O + O$	J_{125}= O2_L_Photo
R_{126}	X4	$O^- \rightarrow O + e$	J_{126}= O_L_PhotoFrag
R_{127}	X4	$O_2^- \rightarrow O_2 + e$	J_{127}= O2_L_PhotoFrag
R_{128}	X4	$O_3^- \rightarrow O_3 + e$	J_{128}= O3_L_PhotoFrag

5 Creating and Testing the Model

This chapter explains the methods utilized to create and test (validate) the ion model herein developed. I begin with the methods used to physically create the model and then discuss the methods used to test the model.

5.1 Methods Used to Create the Model

Given the wide range of chemistry being modeled in this study, it should not be unexpected that there are many more reactions and chemical species included in this model than in others; over 800 reactions among 200 compounds are included in this model. With this number of reactions and compounds there is no feasible way to manually produce all the subroutines needed to compute the sources and sinks of all the compounds in the model.

It was necessary therefore to write first a computer program whose input was a standard ASCII listing of the reactions to be included in the model and whose output was all the subroutines necessary to compute the sources and sinks of all the compounds in the model. The first version of this program, herein called the model builder (BUILDER), was written in 1989 by Neil Donahue in his study of the hydrocarbon chemistry of the marine troposphere (*Donahue & Prinn*, 1990). This program has been modified in this study to create a more efficient computer code, and it is now a quick and easy method to reliably create chemical models of arbitrary complexity. The use of BUILDER has allowed the user to focus upon the chemistry to be utilized (or ignored) in the model and not worry about mistakes in the coding of the sources and sinks; the most error-prone task in building chemical models.

In addition to the automatic generation of the source and sink subroutines, equally simple and flexible methods were developed to allow the specification of the various bound-

ary conditions of the models. The boundary conditions could then be specified at a "high level" of the model generation rather than actually "hard-wiring in" these conditions.

The above two tasks were considerably facilitated by the selection of a highly structured language for the model builder (BUILDER) and for the model builder's output (the chemistry model itself); in this study, Turbo Pascal® was chosen for both BUILDER and BUILDER's output. The output of BUILDER could just as easily be i860 assembler code or any other code that a target platform requires for maximum efficiency.

5.2 Methods Used to Check the Reactions & Errors Encountered

Due to the large number of reactions included in this study, it was necessary to exclude as many errors as possible from the table of reactions (Appendix B , page 184). I now describe these errors and the methods used to eliminate them.

Because the subroutines used to calculate the sources and sinks of all the compounds were created by BUILDER, little could go wrong in this phase that would get past the language compiler used for this study (Turbo Pascal® V5). The errors were therefore primarily in the table of reactions itself; the errors encountered during the construction and testing of the models were of four different types; **mistakes, invalid extrapolations, missing reactions**, and **inconsistencies**. These errors are now discussed in turn.

5.2.1 Mistakes

Mistakes in entering the original kinetic data are of two types. The first is a mistake in the names of the compounds that are involved in the reaction, and the second is a mistake in the expression for the rate constant. The following reaction has both types of

mistakes:

$$CH_4 + OH \rightarrow CH_2 + H_2O \quad k = 2.4 \times 10^{-12} e^{+1720/T} \quad . \tag{55}$$

The first mistake in this equation is that it does not conserve hydrogen atoms; there are 5 on the left and only 4 on the right. This type of mistake is automatically checked by BUILDER and is corrected in the input files manually after having been flagged as questionable by BUILDER. The second mistake in (55) is that the exponential value should be -1720 rather than +1720; this type of mistake is harder to find but does often show up as either a very large or a very small rate constant at either high or low temperatures. The range of rate coefficients at 5000K and 500K are automatically checked and suspicious values are flagged for manual examination.

Because many sources of data were referenced in the construction of the tables, mistakes in the original sources were common. In general these errors were picked up by the above methods as well as through a comparison of corresponding rates from varying sources. Another way to notice bad rate constants is that they cause a well characterized chemical species to misbehave, (*e.g.* if the OH number density was very different from $1 \times 10^6 \cdot cm^{-3}$ or if its chemical lifetime τ was very different from 1 sec, then a mistake would be suspected in the dominant reactions controlling its atmospheric mixing ratio and lifetime).

As a result of the above checks, the following statement can be made regarding any residual mistakes still in the input data table: *The mistake (1) does not violate conservation of charge nor mass, (2) produces a reasonable rate coefficient, and (3) does not perturb the chemistry of any well characterized chemical species.*

5.2.2 Invalid Extrapolation

A second type of error encountered was using a rate coefficient outside its range of validity. Most chemical reactions show some temperature dependency, and rate coefficients generally reflect this dependency. Sometimes a rate coefficient is measured at just one temperature, 300K being the most common temperature cited. If the rate of the reaction has a relatively large temperature dependency that is not reflected in the cited rate coefficient, then extrapolations to other temperatures will be in error. This type of error is called an **invalid extrapolation**. This type of error is unimportant in the standard model runs since the runs are performed at temperatures similar to those at which the rate coefficients were computed. It is noticed, however, in the high temperature chemistry runs when neglecting the actual temperature dependency causes a deviation from the independently computed thermodynamic equilibrium mixing ratio of air.

This requirement that the kinetic models be able to reproduce thermodynamic equilibrium under certain conditions is an important test of the chemistry of the model. Why this is so is discussed, next followed by the types of errors this type of comparison reveals.

5.2.3 Missing Reactions

Discrepancies between the computed compositions of the thermodynamic equilibrium and kinetic steady state are, in general, caused by either **missing reactions** or **inconsistent rates**. Missing reactions are generally the reverse of a reaction that becomes important at some temperature. Inconsistent rates are found when the forward and reverse rate coefficients k_f and k_r have been independently computed (or measured) and the temperature dependent ratio of k_f to k_r does not match the temperature dependency of K_{TE}.

The relatively large amount of scatter shown in Figure 5b is an example of this discrepancy. For reactions such as this that were of importance to the high temperature cooling model, I took the better characterized of either the forward or reverse reaction and a polynomial fit to the thermodynamic equilibrium coefficient to obtain a consistent value for the less well characterized reaction of the pair. Although rate coefficients in the reaction tables do not reflect this approach, *i.e.* the raw forward and reverse rates are listed, the equilibrium data required can be found in Baulch *et al.* [1972].

5.3 Methods Used to Check the Model

In addition to checking the individual reactions comprising the model, it is also necessary to test them collectively. This task was accomplished by comparing the output of the model with other models of differing types, specifically (1) two thermodynamic equilibrium models and (2) generic 1-D photochemical models.

5.3.1 Thermodynamic Equilibrium *vs.* Kinetic Steady State

There is an intimate relationship between thermodynamic equilibrium and kinetic steady state: they are two different paths to the same place. In other words, both methods should give exactly the same mixing ratios of all the compounds for any specified temperature, pressure, and elemental composition.

For the kinetic steady state to precisely match the thermodynamic equilibrium composition, every elemental reaction must be balanced by the reverse reaction, and at kinetic steady state these two reactions must be occurring at the same rate. For example, given the pair of reactions

$$aA + bB \underset{k_r}{\overset{k_f}{\rightleftharpoons}} cC + dD, \tag{56}$$

the thermodynamic equilibrium between A, B, C, and D can be expressed as

$$K_{TE} = \frac{[C]^c[D]^d}{[A]^a[B]^b}, \tag{57}$$

where K_{TE} is the thermodynamic equilibrium coefficient and generally is a function of temperature. Because the rate of the forward reaction ($k_f[A]^a[B]^b$) must equal the rate of the reverse reaction ($k_r[C]^c[D]^d$) at kinetic steady state (or thermodynamic equilibrium), we have

$$k_f[A]^a[B]^b = k_r[C]^c[D]^d, \tag{58}$$

and therefore

$$K_{TE} = \frac{k_f}{k_r} = \frac{[C]^c[D]^d}{[A]^a[B]^b}. \tag{59}$$

As an example of this inter-relationship of kinetics and thermodynamics, the National Institude of Standards and Technology (N.I.S.T.) summary (*NIST*, [1992]) of the $H + O_2 \overset{k_f}{\underset{k_r}{\rightleftharpoons}} OH + O$ system is shown in Figure 25. As noted on this Figure, $k_f = 2.12 \times 10^{-10} e^{-8065/T}$ and $k_r = 1.55 \times 10^{-11} e^{+218/T}$. A fit of the thermodynamic equilibrium data of *Baulch et al.* [1972] gives $K_{TE} = 2.25e^{-9960/T}$; this value is to be compared to the value of $k_f/k_r = 13.7e^{-8283/T}$ derived from the N.I.S.T. estimates shown on Figure 25. By way of introduction to these data, the National Institute of Standards and Technology (the old National Bureau of Standards) produces computerized data bases based on a survey of the chemical kinetic literature.

5.3.2 Thermodynamic Equilibrium Models

To determine the initial conditions of the high temperature channel cooling model, and to test the consistency of the kinetic code, the thermodynamic equilibrium composition of air as a function of temperature over the range 6,000K – 500K was required.

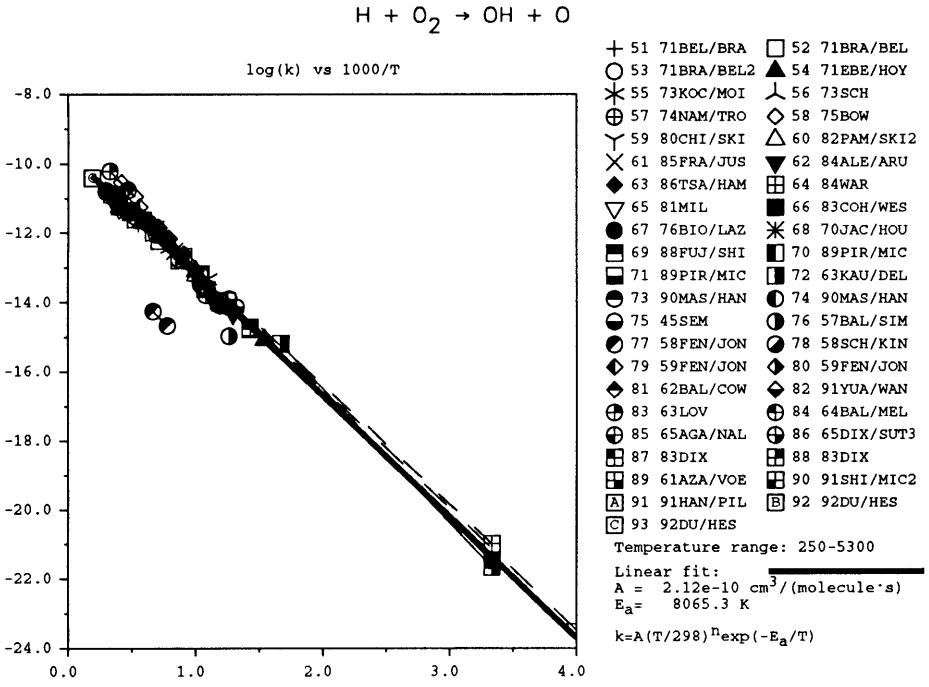

Figure 25a. *N.I.S.T.*, 1992 summary of $H + O_2 \rightarrow OH + O$ reaction.

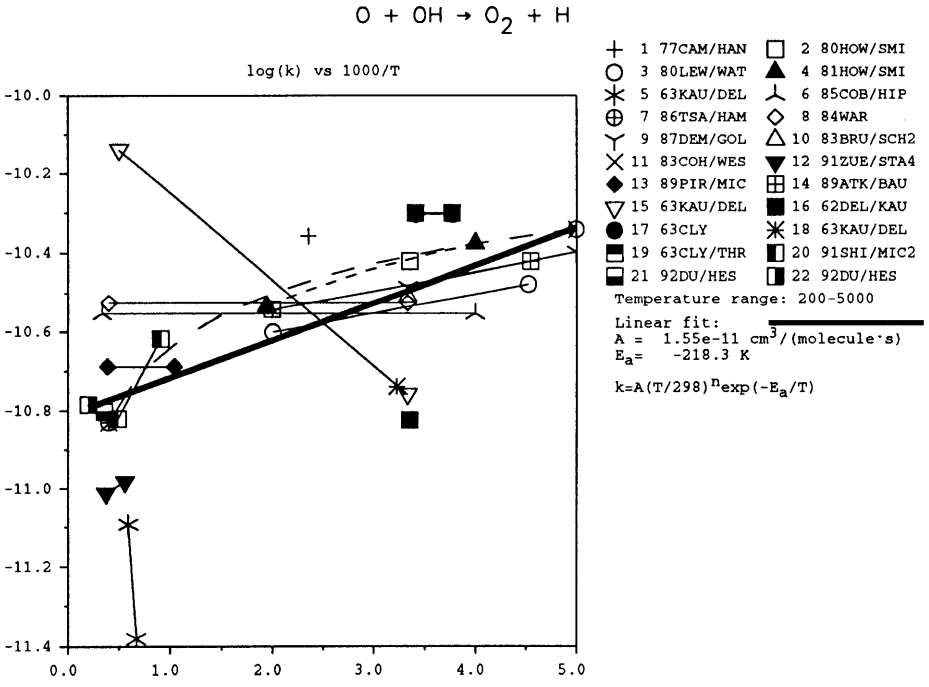

Figure 25b. *N.I.S.T.*, 1992 summary of $OH + O \rightarrow H + O_2$ reaction.

To accomplish this, two different thermodynamic equilibrium models (identified herein as SPLUNGER and STANJAN) were tested and their results compared for consistency. The two models differ in both the manner in which the thermodynamic equilibrium composition is found, and in the basic thermodynamic data used as input. The input to both models is the same: the temperature, pressure and mole fraction elemental composition of the atmosphere. Both models then find a chemical composition that is in thermodynamic equilibrium with the specified physical parameters and chemical composition.

I consider the results of the two models to be no more accurate than their degree of agreement and I now relate brief descriptions of the two models as given by their authors.

5.3.2.1 SPLUNGER

The first model used was the SPLUNGER model first written by L. K. Thrasher, B. Fegley, and M. Camitta in 1986 and later revised by B. Fegley and K. Ehlers in April 1989. This program uses the method of successive approximation to thermodynamic equilibrium by simultaneously considering constraints of mass balance and chemical equilibrium. The method was described by *Barshay & Lewis* [1978] as

> "The workings of the program can best be illustrated with a simplified example. Consider a gas of pure hydrogen where the ideal gases H and H_2 are the only molecules assumed to be present. We can write the equilibrium expression
>
> $$\frac{1}{2}H_2 \rightleftharpoons H \qquad (B\&L-3)$$
>
> and define the equilibrium constant $K_H(T)$ for the formation of H as
>
> $$K_H(T) = f_H / \left(f_{H_2}\right)^{1/2}, \qquad (B\&L-4)$$
>
> where $K_H(T)$ is a function of the temperature T only. We thus calculate f_H, the fugacity of atomic hydrogen gas, by
>
> $$f_H = K_H(T) \times \left(f_{H_2}\right)^{1/2}, \qquad (B\&L-5)$$

where f_{H_2} is the fugacity of molecular hydrogen gas.
The computer program solves the "mass balance" for hydrogen; beginning with a fixed total abundance of hydrogen atoms, ΣH, it finds, by an iterative technique, that value of f_{H_2} such that

$$f_H + f_{H_2} = \Sigma H." \qquad (B\&L - 6)$$

The thermodynamic data required by this program are polynomial approximations to $K_H(T)$.

5.3.2.2 STANJAN

The second model utilized was STANJAN, version 5.90 written by W. Reynolds of Stanford University during the period 1981 – 1987, and the author's description of the method is:

"The method of element potentials is used to find the state of minimum Gibbs function for the system, subject to the atom population constraints. Treating the phases as either ideal gases or ideal solutions,

$$G\text{ibbs}/RT = \Sigma\{[G(j) + \ln X(j)] * M(j)\}$$

where $G(j) = g(T,P)/RT$, $X(j)$ is the phase mol fraction and $M(j)$ is the mols of species j. The atom constraints are $\Sigma\{N(i,j) * M(j)\} = A(i)$, where $A(i)$ is the mols of i atoms present and $N(i,j)$ is the number of i atoms in a molecule of j. Other constraints are $\Sigma\{X(j)\} = 1$ for each phase. Using Lagrange multipliers, one finds that

$$X(j) = \exp\{-G(j) + sum[L(i) * N(i,j)]\}$$

where $L(i)$ is the element potential for the i^{th} atom (Lagrange multiplier).
This ... formula is the key to the method of element potentials. Note that $L(i)$ represents $G\text{ibbs}/RT$ per mol of the i^{th} ATOM in ANY species! $L(i)$ and the TOTAL mols in each phase are iterated to meet the constraints."

The required thermodynamic data for this model are the temperature dependent values of entropy and enthalpy as given in the JANAF tables†.

† Joint Army, Navy, and Air Force thermodynamic tables.

5.3.3 1-D Photochemical Models

A few 1-D photochemical models have been published that can serve as a basis of comparison with the output of this model when run in a 1-D mode with similar boundary conditions. To this end, the 1-D photochemical models of *Logan et al.* [1981], *Thompson & Cicerone* [1982], and *Thompson & Cicerone* [1986] are used as fiducial marks for this work. To facilitate the comparison with those models, very similar boundary conditions are used (*cf.* Table 9, Chemical boundary conditions; Section 6.3, page 121 and Table 10, Heterogeneous-loss rates; Section 6.3, page 122).

6 Description of the Models

I now describe modes in which the model developed herein was operated. Two fundamentally different modes of operation (or models) were utilized in this study: (1) a time-dependent model, and (2) various steady-state models. The primary differences in these models is in the outer "driver" that controlled the behavior of the chemistry "module". In the time-dependent model runs, an initial chemical composition was specified and the evolution of the chemical composition was explicitly evaluated; in the steady-state models, the core chemistry "module" was used as a basis for a successive approximation to a steady-state solution. The only differences in the chemistry of the two different modes of operation was that in the time-dependent models, in the interest of speed, all compounds containing S, Cℓ, and F were eliminated from consideration.

6.1 Time-Dependent Models

6.1.1 Description of Time-Marching Procedure

This method was described in *Donahue & Prinn* [1990], and the discussion therein is reproduced now with a commentary on the slight differences between that study and this one.

> "We use a novel and very flexible prognostic code in which the time-step is continually adjusted to be appropriate to the time scale for chemical change intrinsic to the system. The equation solved for each compound, i, is
>
> $$\begin{aligned}\frac{dC_i}{dt} &= \left(Source_i + \frac{\Phi_i}{H}\right) - \left(sink_i + \nu_i + \frac{v_i}{H}\right) C_i \\ &= P_i(t;\tau_{P_i}) - l_i(t;\tau_{P_i}) \cdot C_i(t;\tau_{C_i})\end{aligned} \tag{60}$$
>
> where C_i is the concentration of i (molec·cm^{-3}), H is the thickness of the layer (cm), $Source_i$ is the homogeneous chemical source strength of i (molec ·cm^{-3}

$\cdot s^{-1}$), Φ_i is the flux of i into the layer (molec$\cdot cm^{-2}\cdot s^{-1}$), $sink_i$ is the homogeneous chemical sink strength of i (s^{-1}), ν_i is the removal frequency of i from the layer through ventilation or heterogeneous reactions (s^{-1}), and v_i is the deposition velocity of i to the ocean surface (cm$\cdot s^{-1}$)."

Expressing this equation in terms of our one-box model, Eq.(11),

$$\begin{aligned}\frac{dC_i}{dt} &= \left(Source_i + \Phi_i'\right) - \left(sink_i + v_i'\right) C_i \\ &= P_i(t;\tau_{P_i}) - l_i(t;\tau_{P_i})\cdot C_i(t;\tau_{C_i})\end{aligned} \tag{61}$$

where Φ_i' is the average rate of advective/ diffusive gain or loss from the 2-D steady-state model results, and v_i' is the heterogeneous-loss rate, scaled (for ions) by the instantaneous value of the electric field. I continue now the discussion of the time stepping time scales.

"There are four time scales pertinent to the evolution of C_i: **(1)** τ_{C_i} = the time scale $(d\ln C_i/dt)^{-1}$ on which C_i changes, **(2)** τ_i = the chemical lifetime of i $(1/l_i)$, **(3)** τ_{P_i} and **(4)** τ_{l_i} = the characteristic times [$(d\ln P_i/dt)^{-1}$ and $(d\ln l_i/dt)^{-1}$], for changes in the production and loss terms of i.
The scale τ_{C_i} is a function of the other three time scales. Jointly, the production and loss terms constitute the chemical forcing of i, and we call τ_{P_i} and τ_{l_i} together the forcing time scales of i. The behavior of i depends strongly on whether the chemical lifetime τ_i is shorter or longer than the forcing time scales. To determine the time evolution of the system, we assume a constant coefficient solution, rather than a finite-difference solution, because the former allows longer time steps and because errors will be more evenly distributed about the true solutions."

The equation (62) is derived from the fact that the evolution of C_i will always tend toward its steady-state concentration C_{ss_i},

$$C_i(t+\delta t) = C_i(t)e^{-\delta t/\tau_i} + C_{ss_i}(1 - e^{-\delta t/\tau_i}). \tag{62}$$

"Given a known concentration at time t, the concentration at $(t+\delta t)$ is thus

$$C_i(t+\delta t) = C_{ss_i}((t+\delta t);\tau_{fi}) + \{C_i(t) - C_{ss_i}((t+\delta t);\tau_{f_i})\}e^{-\delta t/\tau_i} \tag{63}$$

where $C_{ss_i} = P_i\cdot\tau_i$, $\tau_i = 1/l_i$, and τ_{f_i} (found *after* a model step of time δt) is the "reduced" forcing timescale, derived from the production and loss terms,

i.e.

$$\tau_{f_i} = \left(\frac{\tau_{P_i} \cdot \tau_{l_i}}{\tau_{P_i} + \tau_{l_i}} \right), \text{ where}$$

$$\tau_{P_i} = \left(\frac{min(P_i)}{\Delta P_i} \right) \delta t, \qquad \tau_{l_i} = \left(\frac{min(l_i)}{\Delta l_i} \right) \delta t,$$

and $min(x)$ is the minimum value obtained by x in the interval δt (a numerically safer choice than the average value).
The timescale over which the coefficients of our "constant" coefficient solution actually changes is τ_{f_i}. For a species i, the constant coefficient assumption is therefore valid for times small compared to τ_{f_i}. Specifically, the constant coefficient solution for i will be within a desired accuracy, ϵ, of the actual solution for all times from t to $(t + \epsilon\tau_{f_i})$; we therefore find the time-step appropriate for each compound *following* each model-step:

$$\delta t_i = \epsilon \tau_{f_i}. \tag{64}$$

The "optimal" time-step for the (just passed) model step is then the shortest δt_i, excluding those compounds whose lifetimes, τ_i, are sufficiently shorter than τ_{f_i} (these are *always* within ϵ of $C_{ss_i}(t)$ hence they do not limit δt and are treated separately, as discussed below). If, after a model step, the optimal time-step for that step was significantly shorter (we use a factor of 2) than the one actually used, the step is repeated with the optimal time-step. Otherwise, this optimal time-step is used for the next step. The time-steps used by the model are thus determined internally, and are continually adjusted based on the accuracy being demanded of the model and the rates of the chemical change intrinsic to the system being modeled."

Simply stated, in as much as the electron-production rates dominated the system at short times, the initial time steps were on the order of of 10^{-12} model-seconds at model-time = 3.0×10^{-3} seconds (model-temperature = 6000K) and increased to 10^{-4} model-seconds at model-time = 300.0 seconds (model-temperature = 500K). This model took approximately 48 hours of CPU time on a 1MFLOP machine, and has all compounds containing S, F, and Cℓ excluded from consideration.

"Not all compounds are solved with the constant coefficient solution. Those with lifetimes (τ_i) much smaller than the timescale for changes in their chemical forcing ($\tau_i < \epsilon\tau_{f_i}$) will always be within ϵ of the asymptotic, or steady-state concentration (C_{ss_i}), excepting transient behavior associated with initial conditions. These compounds are therefore identified by the model and excluded from the determination of the optimal time-step. Their concentrations are then

> iterated until the source and sink terms for each balance to within ϵ, subject to the constraint that the total concentrations of certain selected families (HO_y = $OH + H + HO_2 + 2H_2O_2$, for example) agree with values determined for those families by the explicit, constant coefficient coefficient solution."

The iteration scheme used when $\tau_i < \epsilon\tau_{f_i}$ is Jacobian iteration with under-relaxation, *i.e.* repeat

$$C_i^{n+1} = \beta \cdot (P_i^n \cdot \tau_i^n) + (1 - \beta) \cdot C_i^n \tag{65}$$

until $C_i^{n+1} = C_i^n$ to within the desired accuracy, normally ϵ (10^{-6}), and β is the under-relaxation factor, normally 1/2.

6.1.2 Lightning-Flash Model

To ascertain how good an approximation to an actual lightning-flash sequence the steady-state models are, an explicit, time-dependent model was also run. The primary result to be obtained from this model is an understanding of the degree of non-linearity of the steady-state models. This is of concern since the rate of ion recombination is proportional to the square of the ion density and if there is excessive ion recombination during the first few milliseconds of a return stroke, then a steady-state model that averages the ion-production rates over 1 second will systematically underestimate the average amount of ion recombination and consequently overestimate the average ion density.

This model was initialized with the results from the 2-D steady-state Electrified model run for the node position r = 2 m, z = 4 km. This corresponds to a very active location in the domain, with an intra-cloud lightning-stroke rate of one per second. The results from this node were time-marched forward (in the manner described above) for one model-second using a variable time step that is always short compared to the time scale over which the environment is changing.

I then computed the time-average mixing ratio of all the compounds during this

interval and compared those averages to the corresponding steady-state averages as determined in the 2-D Electrified model run.

6.1.3 Cooling-Channel Model.

To determine how important the chemistry of the hot-lightning channel is relative to the ion chemistry occurring simultaneously in the region outside of the lightning channel, I examine the behavior of compounds that have large thermodynamic equilibrium (T.E.) mixing ratios at high temperatures and small T.E. mixing ratios at low temperatures. The net amount of this compound that is produced by the lightning channel will depend on the rate of cooling of the channel. If the channel cools slowly enough, then the chemical kinetics have time to keep the system in thermodynamic equilibrium. If the channel cools very rapidly, then some chemical reactions whose rates have very large temperature dependencies may not have time to keep the system in chemical equilibrium and one or more compounds can "freeze" out of the system.

This examination of cooling rates and chemical dynamics can be approached in two different ways. The first, and simplest, is to determine a "freeze out temperature" of the cooling channel for a chemical species of interest and take the thermodynamic composition at this temperature as the final concentration of the species. This "freeze out temperature" can be defined, following the lines of *Fegley & Prinn* [1985], as that temperature such that

$$\left(\frac{1}{T}\frac{dT}{dt}\right)^{-1} > \left(\frac{1}{[X]}\Sigma r_i\right)^{-1} = \tau_c \tag{66}$$

where τ_c is the chemical lifetime and r_i is the rate of a reaction between X and compound i

$$r_i = k_{i\mathrm{X}}[i][\mathrm{X}] \tag{67}$$

The drawbacks of this approach are that: (1) it leads (in principle) to a different "freeze out temperature" for each compound, and (2) it cannot take into account the dependence of one compound's "freeze out temperature" on the concentration of another species that has already "frozen out".

The second approach avoids these two limitations at the cost of more computations. The second method is to time-march a kinetic model forward in time with the temperature the prescribed function of time shown in Figure 23 in Section 3.4.3, page 90. This approach has the advantage that the interaction of various "quenched" compounds is explicitly accounted for. The starting point for this kinetic model is the highest temperature at which kinetic rate data are available (and valid): about 6000K. Thermodynamic equilibrium is assumed to have been attained by the lightning channel at this temperature.

6.2 Steady-State Photochemical Models

6.2.1 1-D Model

The model begins as a 15-level 1-D steady-state photochemical model of the "global average" atmosphere. The vertical nodes are placed at equal distances between the ground and 15 km. The 1-D steady-state model boundary conditions and $K_{\text{eddy}}(z)$ are similar to those of *Thompson & Cicerone* [1982,1986]. In this model, O_2, N_2, H_2O, and H_2 are fixed, all other compounds attain a vertical mixing ratio profile determined by either ground level sources (*e.g.* CH_4, OCS, and DMS), stratospheric sources (*e.g.* O_3 and NO_x), photochemical equilibrium (*e.g.* OH, NO, and NO_2), or some combination of these processes (*e.g.* CO). These boundary fluxes are listed in Table 9 in Section 6.3, page 121.

Surface deposition is specified for most water soluble species (*e.g.* HNO_3 and

H_2O_2); stratospheric deposition is used to simulate stratospheric exchange and is the major sink for the very long lived, inert trace gases (*e.g.* CF_4, SF_6, and $CC\ell_4$). Heterogeneous loss scales as pressure and is set for most species to be 10^{-6} s^{-1} at sea level, with the exception of all charged species, which are given a value of 10^{-3} s^{-1} at sea level. Inert gases such as SF_6 and N_2O have no (known) heterogeneous loss. A summary of the various loss processes and their corresponding rates is given in Table 10 in Section 6.3, page 122.

The wavelength dependent photon flux is computed at each model level using a two-stream approximation and a diurnally averaged incident solar photon flux typical of tropical equinox conditions (vertical photon fluxes do not vary during the model runs). The resulting altitude dependent spectrum is utilized to compute the J's for the photolysis reactions in the chemical "module".

As shown in Figure 21, in Section 3.3.4, page 84, there is a cosmic ray flux that produces 5 ion pairs·cm^{-3}·s^{-1} at sea level and increases slowly with altitude to a maximum of 50 cm^{-3}·s^{-1} at the top of the model domain (15 km). There is also a vertical electric field that has a ground level value of 100 V/M and decays aloft with a scale height of 2000 m, although it is sufficiently weak to be unimportant in the ion chemistry of the general troposphere.

This photochemical steady-state model is then iterated, using a successive approximation technique, until no compound changes by more than 1.0×10^{-6} per iteration.

6.2.2 2-D Base Case Model

A two-dimensional, cylindrically symmetrical, 15 X 15 grid is established with horizontal nodes placed at equal intervals over the range of Log(R_{inner}) to Log(R_{outer}), where R_{inner} = 2 m and R_{outer} = 2000 m (*cf.* Section 2.7, page 52). The vertical nodes

are equally spaced between the ground and 15km. In other words, it is a semi-logarithmic grid; which has been be shown earlier (see Section 2.4, page 41) to minimize numerical errors in evaluating fields such as the electric field that have radial power dependencies.

An axisymmetric convective cell is established by specifying the vertical component of the wind $W(r, z)$ and then fixing the horizontal component $U(r, z)$ to ensure a non-divergent flow. These fields were shown in Section 3.1.2, page 58. This model assumes that inflowing air is of the 1-D Steady-State photochemical composition, and the outflowing air is assumed to have a constant mixing ratio gradient on the inward side of the outer boundary. The model also uses upwind differencing to improve stability. This model is iterated, using a successive approximation technique (Jacobian iteration) until no compound changes by more than 1 part in 10^6 per iteration, When convergence is achieved, this model result is used as the reference state and is called the Base Case model run.

6.2.3 2-D Electrified Model

The Base Case model is then electrified and run once again to steady-state convergence; this is the Electrified model run. The model is electrified by turning on the time-averaged lightning flash and ground-corona processes, replacing the fair-weather electric field $E_z(z)$ with the (generally larger and primarily radial) electric field caused by the charge on the lightning channel (*cf.* Figure 20 in Section 3.3.1.2, page 77). This electrification generally involves activating the reactions listed in Tables 5, 6, and

6.3 Chemical Boundary Conditions

I now discuss the chemical boundary conditions used in the models. As this model is designed to represent in some sense a "global average" thunderstorm, global aver-

age emissions are used throughout. Inspired by the modeling approach of *Hough* [1991], as few compounds as possible are held fixed. Specifically, only O_2, N_2, H_2, and H_2O are prescribed and held fixed in the 1-D photochemical steady-state models, and no compounds are held fixed in the high-temperature and high-field explicit time-marching model runs. When held fixed O_2, N_2, and H_2 are held to their average tropospheric concentrations, and the concentration of water vapor is determined by the assumption of a constant 80% relative humidity (This slight in-cloud undersaturation is of no chemical importance). All other compounds are either injected into the model at a boundary or are produced within the model domain. Compounds injected into the model are released into the lowermost or uppermost row of grid points. Those compounds released into the top-most row represent compounds injected into the troposphere from the stratosphere; those injected into the bottom-most row represent compounds with ground level sources. Table 9 lists those compounds injected into the model.

In addition to injection of compounds, there is heterogeneous loss throughout the model domain. Heterogeneous loss is here considered to be the irreversible loss of gas-phase material to a cloud particle. In the 1-D photochemical-model run, the heterogeneous loss is scaled to the local atmospheric pressure and has a ground-level value as shown in Table 10. In the 2-D steady-state-model runs, the heterogeneous loss of compounds is determined by computing the cloud-particle specific surface area and the sticking coefficient for each compound (diffusional loss). For charged compounds (ions), there is an additional, electric-field driven loss mechanism (ion capture by cloud particles). These processes were detailed in Section 3.2.2, page 65 and the lifetimes due to diffusional loss were shown in Figure 15 of Section 3.2.2.2, page 70; the lifetimes for ion capture are much shorter, generally < 0.5 seconds.

Table 9. Chemical boundary conditions / Assumed global budgets.

Compound	Emission Rates: Molecules $cm^{-2} \cdot s^{-1}$	Emission Rates: Global $Tg \cdot yr^{-1}$	Reference / Note
	Stratospheric Sources		Note 1
O_3	5.30×10^{10}	680	*Thompson & Stewart*, [1991]
O	4.0×10^{5}	1.7×10^{-3}	"
HNO_3	1.37×10^{8}	2.3	"
NO_x	1.13×10^{8}	1.15	"
	Tropospheric Sources		Note 2
CO	2.14×10^{11}	1600	*Warneck*, [1988]
CH_4	1.23×10^{11}	526	"
SO_2	1.17×10^{10}	200	"
HNO_3	7.27×10^{9}	122	"
NH_3	2.67×10^{10}	121	"
$(CH_3)_2S$ (DMS)	4.55×10^{9}	75.4	"
NO_x	1.82×10^{9}	18.5	"
N_2O	1.39×10^{9}	15.3	*Hough*, [1991]
H_2S	4.36×10^{8}	3.96	*Warneck*, [1988]
$CC\ell_3CH_3$	1.68×10^{7}	0.6	*Prinn et al.*, [1992]
CS_2	2.34×10^{7}	0.475	*Warneck*, [1988]
OCS	4.36×10^{7}	0.375	"
$CC\ell_4$	2.82×10^{6}	0.116	Note 3
CF_4	9.27×10^{4}	2.18×10^{-3}	Note 4
SF_6	6.73×10^{2}	2.63×10^{-5}	Note 5

Notes:
1) Stratospheric sources are injected into the uppermost boxes of the model (z = 15km).
2) Tropospheric sources are injected into the lowermost boxes of the model (z = 0km).
3) Required to produce average mixing ratio of 150 ppt and lifetime of 30 years.
4) Required to produce average mixing ratio of 70 ppt and lifetime of 750 years.
5) Required to produce average mixing ratio of 0.5 ppt and lifetime of 750 years.

Table 10. Heterogeneous-loss rates in the 1-D photochemical model .

Sea Level (Ground) Value of the Heterogeneous-Loss Frequency Compound	(s^{-1})	Reference / Note
Default	1.0×10^{-6}	Note 1
Intert/Insoluble	0	Note 2
Soluble	2.0×10^{-6}	Note 3
All Water Clusters ($W_n \cdot H_2O$)	1.0×10^{-3}	Note 4
All Small Ions	1.0×10^{-2}	"
The electron	1.0×10^{-1}	"
Deposition Velocity (to ground) Compound	($cm\ s^{-1}$)	
Default	0.0025	Note 1
Inert/Insoluble	0	Note 2
Soluble	1.0	Note 3
NO_3, N_2O_5, N_2O_4, N_2O_3	0.5	*Thompson & Cicerone* [1982]
CH_3SCH_2OOH, CH_3SCH_2OH, CH_3SCHO, CH_3OH	0.5	*Kasting & Singh* [1986]
CH_2O	0.3	*Thompson & Cicerone* [1982]
NH_3	0.25	Note 4
HNO_2, HNO_3	0.2	*Thompson & Cicerone* [1982]
O_3, SO_2	0.1	"
NO, NO_2	0.01	"
CO	0.009	"
troposphere → stratosphere transfer rate	(s^{-1})	
Default	0	Note 1
CO	0.1	*Thompson & Cicerone* [1982]
DMS, H_2S, NH_3, OCS	0.003	Note 5
CH_4	0.0003	*Thompson & Cicerone* [1982]
OCS, CF_4, SF_6	0.0003	Note 5
$CC\ell_4$	0.00439	"
N_2O	0.000775	"

Note 1.) This is the value given to any compound not otherwise listed.

Note 2.) The Inert/Insoluble compounds are: O_2, N_2, H_2, Ar, CO_2, CO, CH_4, OCS, DMS, CF_4, SF_6, $CC\ell_4$, N_2O, and $CC\ell_3CH_3$.

Note 3.) The Soluble compounds are: H_2O_2, H_2SO_4, HF, $HC\ell$, $HONO_2$, HONO, NH_3

Note 4.) Estimate based on mean molecular weight and solubility considerations.

Note 5.) Required to produce observed atmospheric lifetime.

7 Model Validation

7.1 Thermodynamic Validation

As discussed in Section 5.3, page 106, a good check of the accuracy of the reactions considered in this study is a comparision of the results of this model with thermodynamic equilibrium models. The two thermodynamic equilibrium models used (STANJAN and SPLUNGER) were run for a range of temperatures between 10,000K and 500K at a pressure of 1bar. The results are shown in Figure 26 where the o's are results for STANJAN and the +'s are results for SPLUNGER. In general the results of the two thermodynamic equilibrium models, SPLUNGER and STANJAN, agree very closely for all compounds at all temperatures. The only notable dissimilarities between the two model's results are: (1) an increasing disparity in the mixing ratios of a few compounds above 5000K (*e.g.* O^+, O_2^+, and NO^+) and (2) a systematic difference in the mixing ratios of HO_2 and HNO_2.

To check the internal consistency of reactions comprising the chemical kinetic models, I then ran the time-dependent channel cooling model in a mode wherein it was allowed to reach chemical steady state at every time step prior to advancing model time (and thereby changing the prescribed temperature). This permits a comparison of the computed atmospheric composition as a function of temperature with the two thermodynamic equilibrium models. The results of this model run are also shown in Figure 26 where the kinetic model's results are indicated by the thin solid line. It is noted that the agreement is not quite as good as was the case with the two thermodynamic models. For example, picking the worst case, the computed mixing ratios of HNO_3 computed by the kinetic code are about a factor of 10 lower than computed by the thermodynamic models. The other chemical species agree much better and some amount of disagreement is unavoidable given the

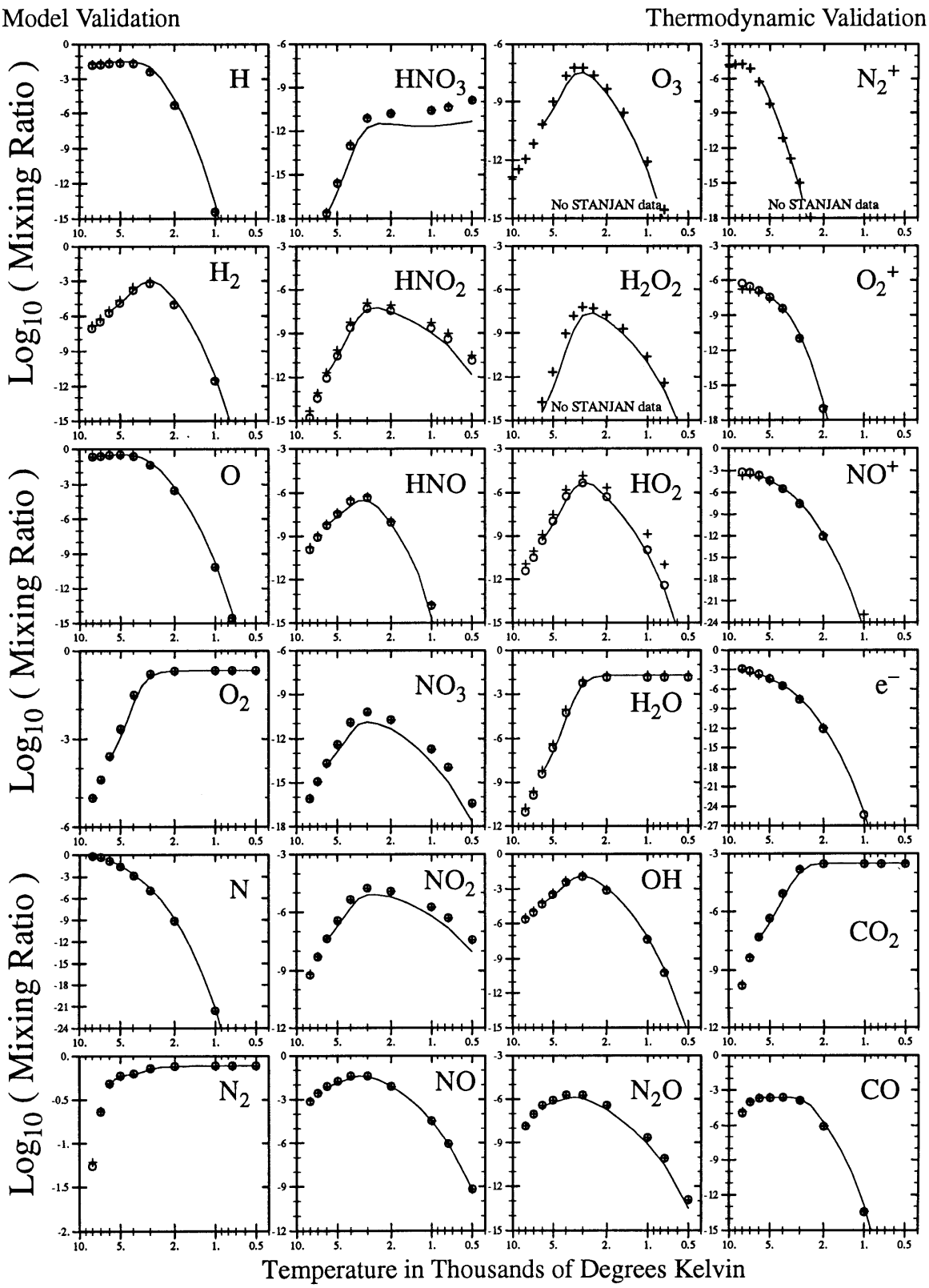

Figure 26. Thermodynamic equilibrium composition of air at 1 bar as a function of Temperature. Only the major chemical species common to all three models are shown. The o's are results for STANJAN, +'s are results for SPLUNGER and the line is the ion model's steady state model run. Note that the ordinate varies from graph to graph.

independent sources of the data that comprised these models.

To see the differences between the three models more clearly, Figure 27 presents the ratios of the mixing ratios computed by SPLUNGER, STANJAN and the kinetic model as a function of temperature. In this figure the mixing ration of a compound as determined by the SPLUNGER model is arbitrarily called the reference value and the corresponding mixing ratio as computed by either the kinetic model or STANJAN is divided by the reference value to yield a ratio of mixing ratios. These ratios are then plotted as a function of temperature to see if there is any tendency for the disparities between the models to show up at either high or low temperatures. In this figure, the mixing ratio as computed by the kinetic model divided by the corresponding mixing ratio as computed by SPLUNGER is indicated by + and the corresponding ratio of STANJAN's result to that of SPLUNGER is indicated by •. In Figure 28 these same ratios are shown as a function of average mixing ratio with the results of the various model runs indicated as before.

Given the general agreement of the two thermodynamic models, I consider from now on just the results of SPLUNGER when referring to thermodynamic equilibrium results. A complete set of graphs of the computed thermodynamic equilibrium composition of air as a function of temperature as computed by SPLUNGER is presented in Appendix C , page 213.

Another method to check the reactions utilized in this model is to run a 1-D photochemical steady-state model using boundary conditions very similar to other such models.

7.2 Steady-State Photochemical Models

Therefore I now present the results of the one-dimensional steady-state photo-

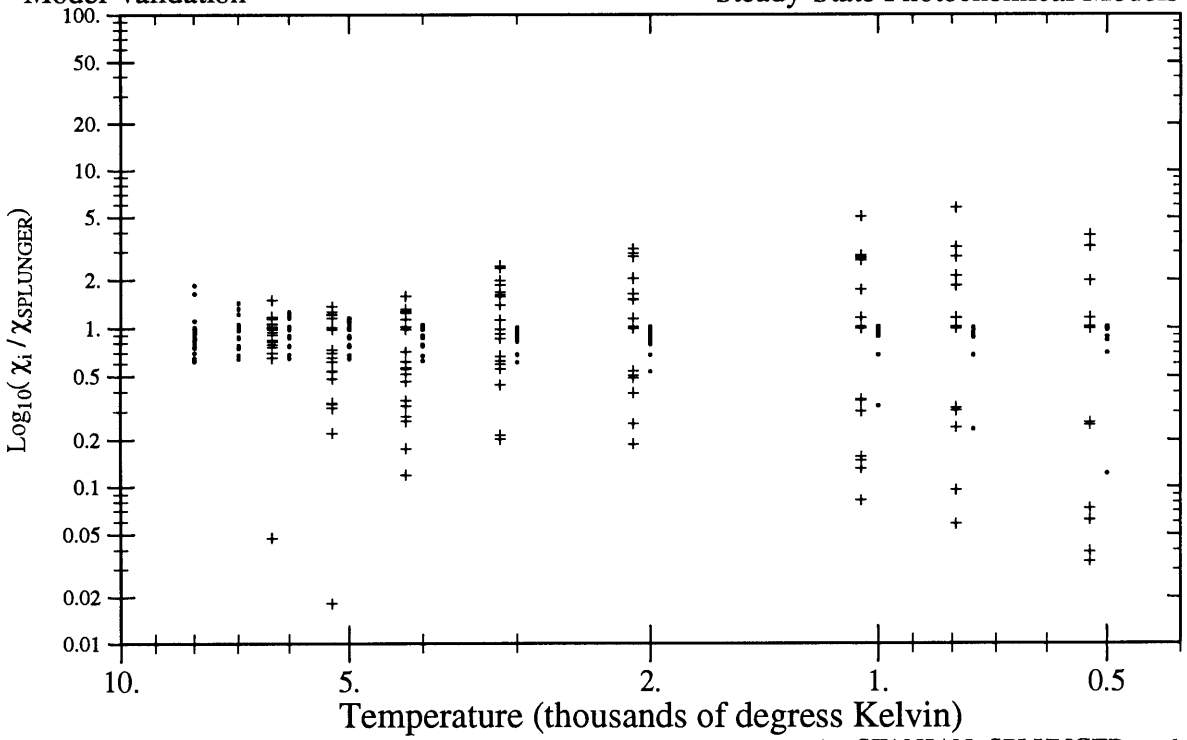

Figure 27. Comparison of mixing ratios as calculated by the computer codes STANJAN, SPLUNGER, and the kinetic code as a function of temperature. The ratios are computed only for compounds having average mixing ratios $> 10^{-25}$. The ratios for the kinetic model are indicated by + and those for STANJAN are indicated by •.

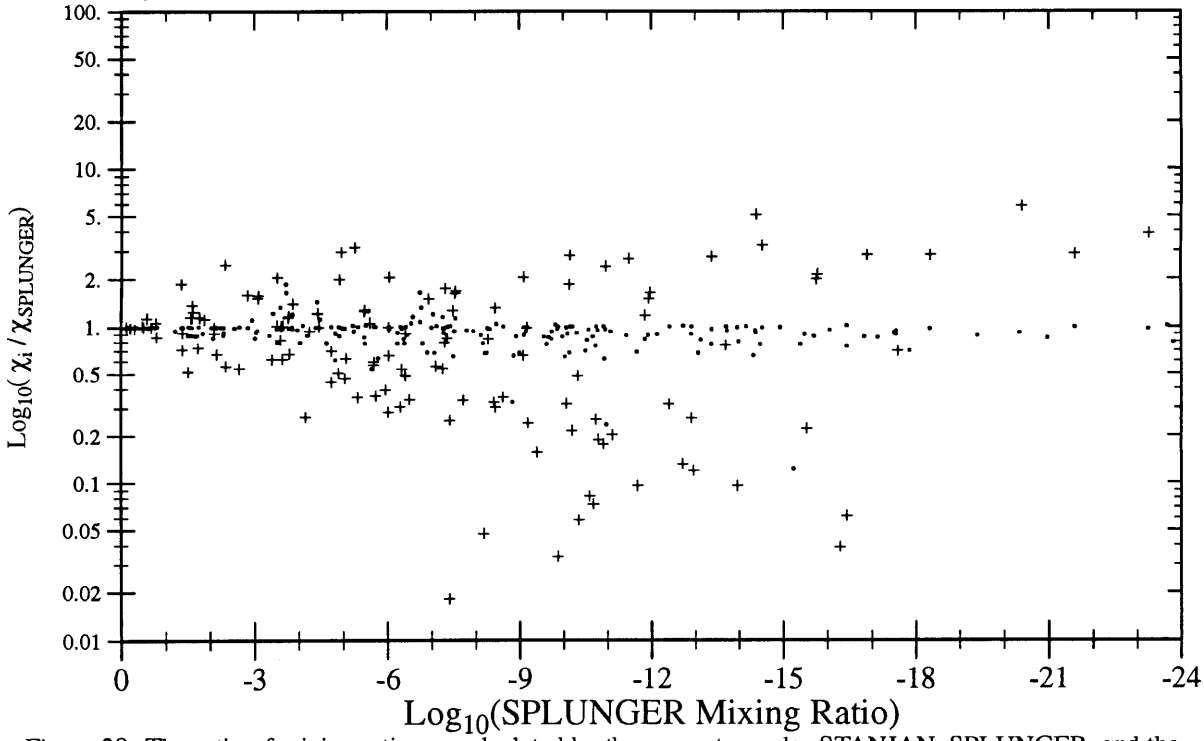

Figure 28. The ratio of mixing ratios as calculated by the computer codes STANJAN, SPLUNGER, and the kinetic code as a function of average mixing ratio. The ratios for the kinetic model are indicated by + and those for STANJAN are indicated by •.

chemical steady-state model run for comparison purposes with other such models (*e.g. Logan et al.*, 1981, *Thompson & Cicerone*, 1982, *Thompson & Cicerone*, 1986). Figure 29a presents the vertical distribution of the compounds held fixed (H_2O and H_2) and Figure 29b shows the calculated vertical distribution of OH.

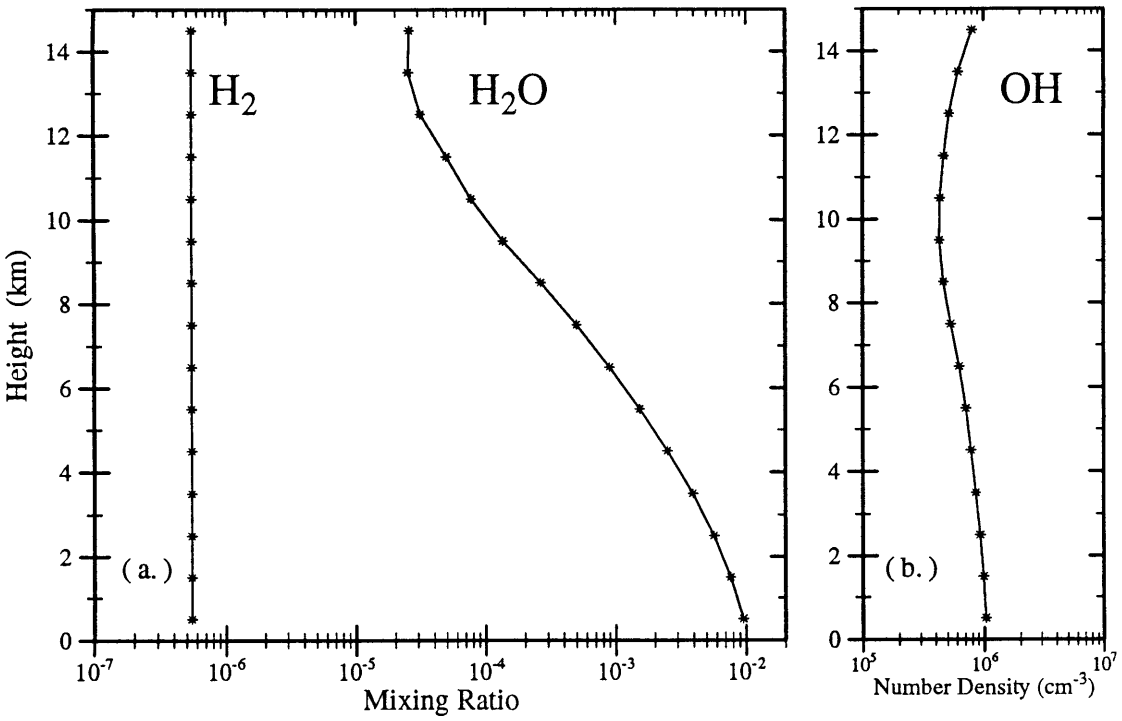

Figure 29. Vertical variations of the fixed compounds (a.) and OH (b.) in the model. The H_2O profile represents a fixed 80% relative humidity. Note that H_2 is fixed in the 1-D SS model run only.

Figure 30 presents the vertical distribution of the major long-lived compounds of the model, O_3, CH_4, CO, and Figure 31 presents the vertical distribution of the minor long-lived compounds of the model, OCS, $CH_3CC\ell_3$, $CC\ell_4$, CF_4 and SF_6.

The chemical families O_x, NO_x, NO_z, and HO_y were treated as pseudo- compounds; Figure 32 presents the vertical distribution of the major chemical families in the model, O_x, NO_x, NO_z, HO_y. O_x is defined as the sum of $[O_3]$, $[O(^3P)]$ and $[O(^1D)]$, $NO_x = \Sigma([NO] + [NO_2])$, $NO_z = \Sigma([NO_x] + [N_iO_j] + [HNO_3])$, and $HO_y = \Sigma([OH] +$

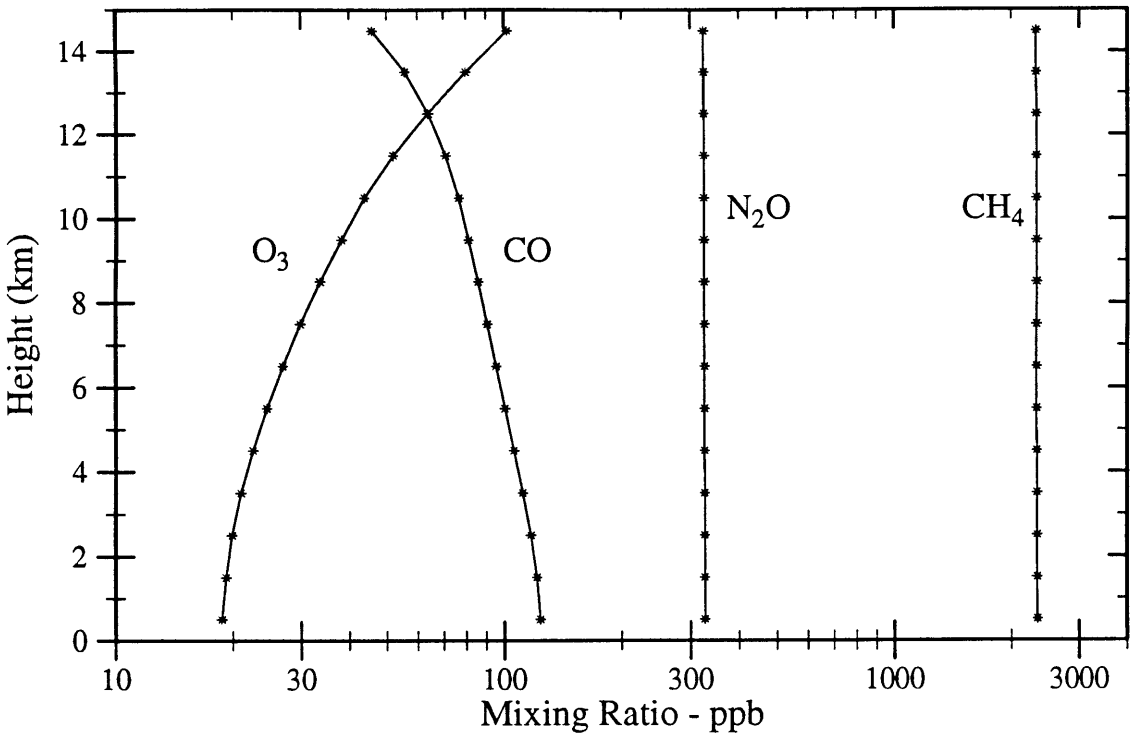

Figure 30. Vertical variations of the major long-lived compounds of the model.

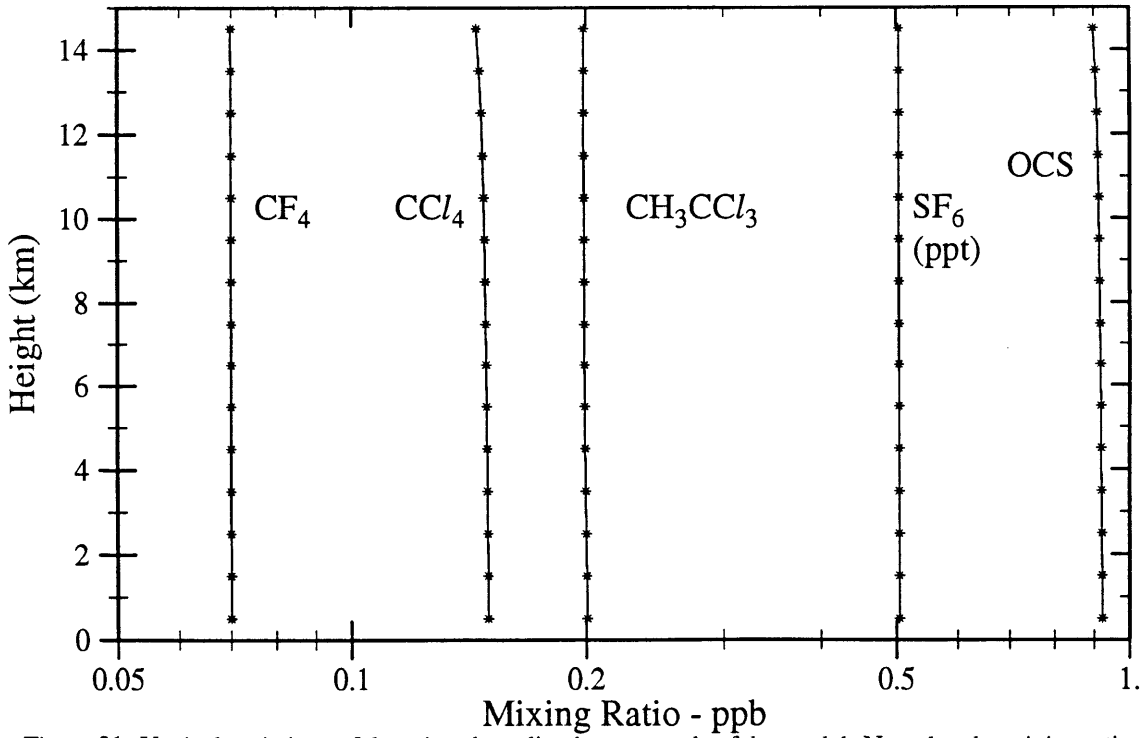

Figure 31. Vertical variations of the minor long-lived compounds of the model. Note that the mixing ratios of the long-lived CF_4 and SF_6 reflect the steady-state values, not their current atmospheric mixing ratios. Note too that the scale for SF_6 is ppt.

$[H] + [HO_2] + 2\times[H_2O_2]$). Figure 33 presents the vertical distribution of the major sulfur containing compounds in the model.

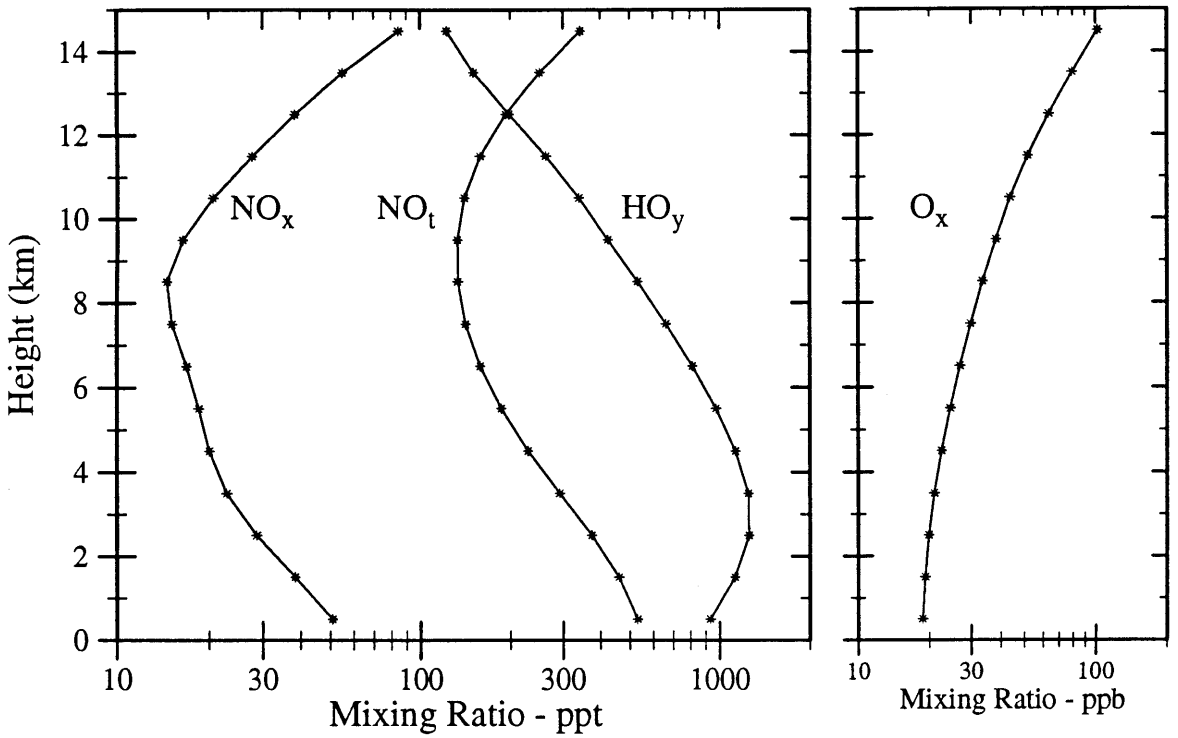

Figure 32. Vertical variations of the chemical families of the model.

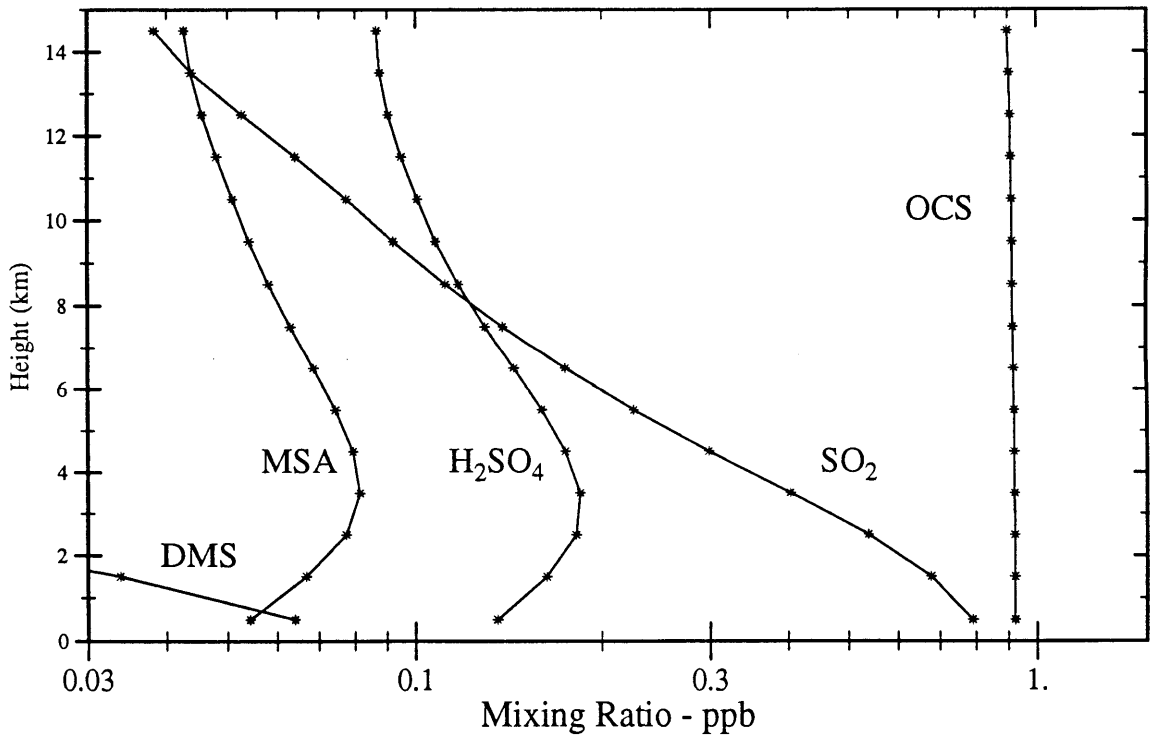

Figure 33. Vertical variations of the major sulfur containing compounds of the model.

8 Results and Discussion

There are two basic types of models developed and used in this study, they are (1) explicit, time-marching models of both a cooling lightning channel and a lightning flash and (2) 2-dimensional steady-state photochemical/ion model of the tropical troposphere. Given the different types of models that were utilized in this study, it seems that the greatest degree of clarity can be achieved by presenting the model results on a model by model basis. I therefore discuss the model results beginning with the models of high temperature air; I then consider the lightning-flash model and finally the steady-state models.

8.1 Time-Dependent Models

8.1.1 Cooling-Channel model

I now turn to the results of then time-dependent model of a cooling lightning channel. The time evolution of the major chemical species as computed by the time-dependent model of the cooling channel are shown in Figure 34. As can be seen in this figure, all of the compounds remain in thermodynamic equilibrium at high temperatures and most of the compounds remain very near to their steady-state, thermodynamic equilibrium (T.E.) concentration, as the temperature decreases. This behavior can be understood *via* reference to the chemical lifetimes of these compounds compared with the characteristic cooling time of the channel, as before (Section 6.1.3, page 116).

The chemical lifetimes of the major chemical species as computed by the time-dependent model of the cooling channel are shown in Figure 35. As can be seen in this figure, those compounds that have their chemical lifetime exceed the cooling time of the channel are the ones that are seen to deviate from thermodynamic equilibrium concentration

as shown on Figure 34. If we assume that the mixing ratio at 300K represents the net production from the hot lightning channel, and estimate that the lightning channel has a radius of 10 cm when it reaches 300K, the we can compute the contribution of the hot channel to the overall chemistry of lightning. Additionally, we can use the lifetime data to ascertain wether or not varying the prescribed cooling rate of the channel will materially affect the net production of any chemical compound.

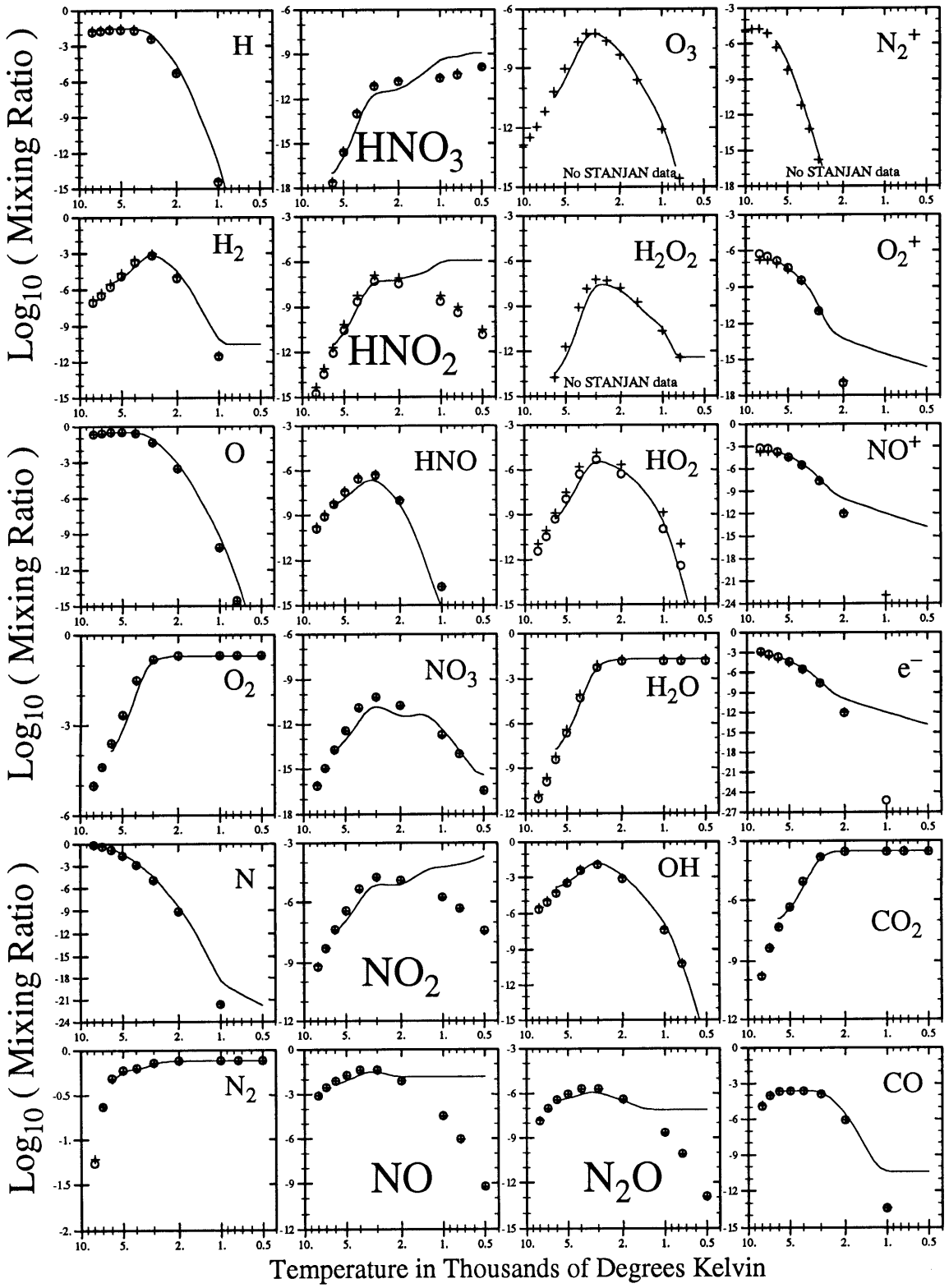

Figure 34. The time evolution of the mixing ratios of selected compounds in the Cooling-channel model. The circles are the thermodynamic equilibrium as computed by STANJAN, the crosses are the thermodynamic equilibrium as computed by SPLUNGER.

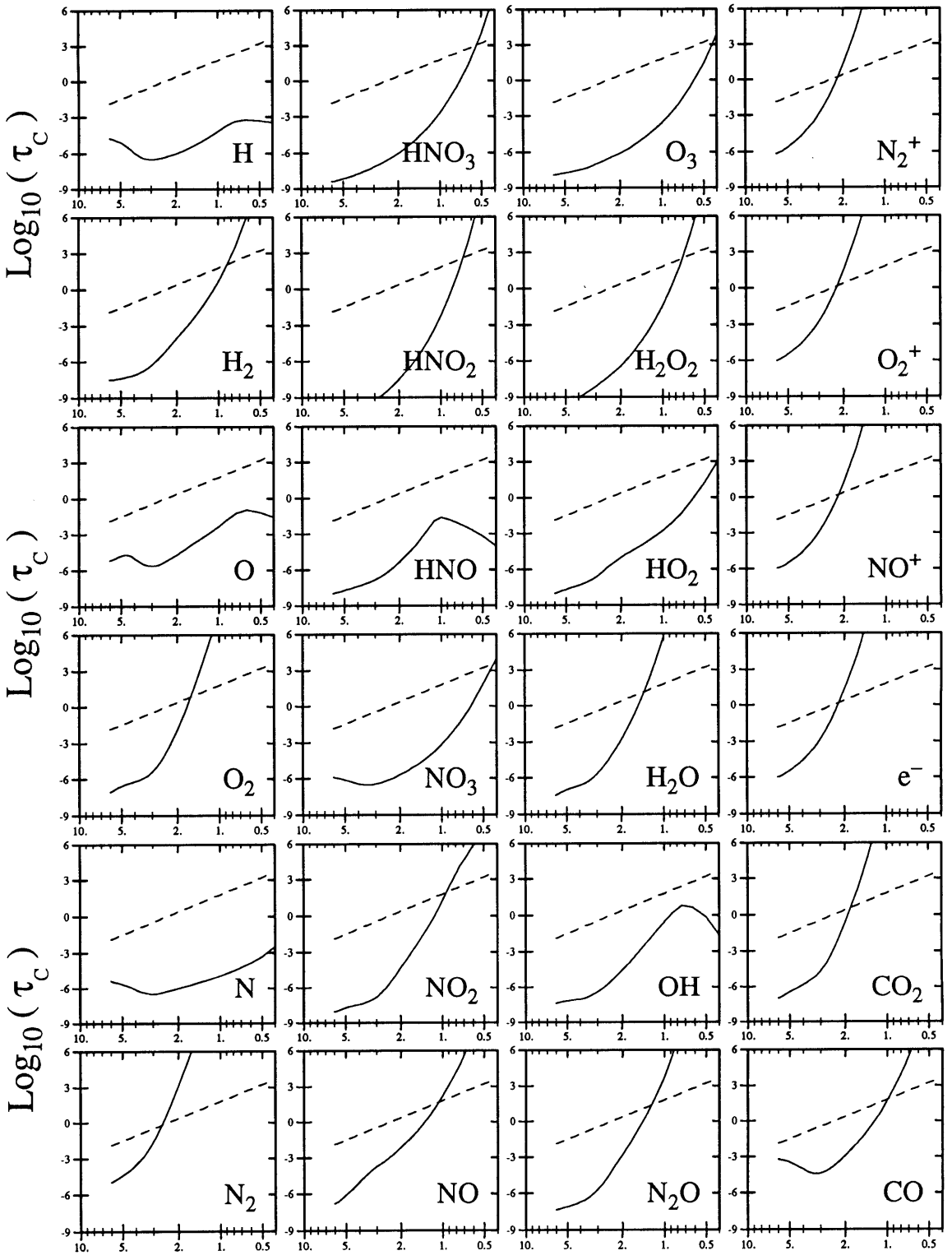

Figure 35. The chemical lifetimes of selected compounds as a function of temperature in the Cooling-channel model. The dashed line is the characteristic cooling time of the channel and the solid line is the local value of the chemical lifetime as computed by the kinetic code.

8.1.2 Lightning-Flash Model

I now turn to the results of the second explicit, time-dependent model used in this study: a model of a lightning flash. The 1-box, time-dependent model of an active lightning region of the 2-D Steady-State model was time-marched forward for one model-second in the manner discussed earlier (Section 6.1.1, page 112). The results are shown for some ions and neutrals in Figure 36.

In this figure, the shaded thick line is the instantaneous value of the primary forcing function, (proportional to the square of the instantaneous channel temperature) divided by the average value of that function. On each figure is shown the Log_{10} of the chemical lifetime τ_i, as well as the ratio of the average concentration C to the steady state concentration C_{ss}. As can be seen from these figures, those chemical species with short lifetimes follow the forcing function quite closely; those with longer lifetimes, change from their average concentration by small amounts and in both cases, their average concentrations are within 10% of their steady state concentrations. This is indicative of a linear system. The degree of linearity is suggestive of the validity of the steady state runs and is in accord with the same conclusion reached by *Griffing* [1977] in his study of the chemistry of the lightning channel.

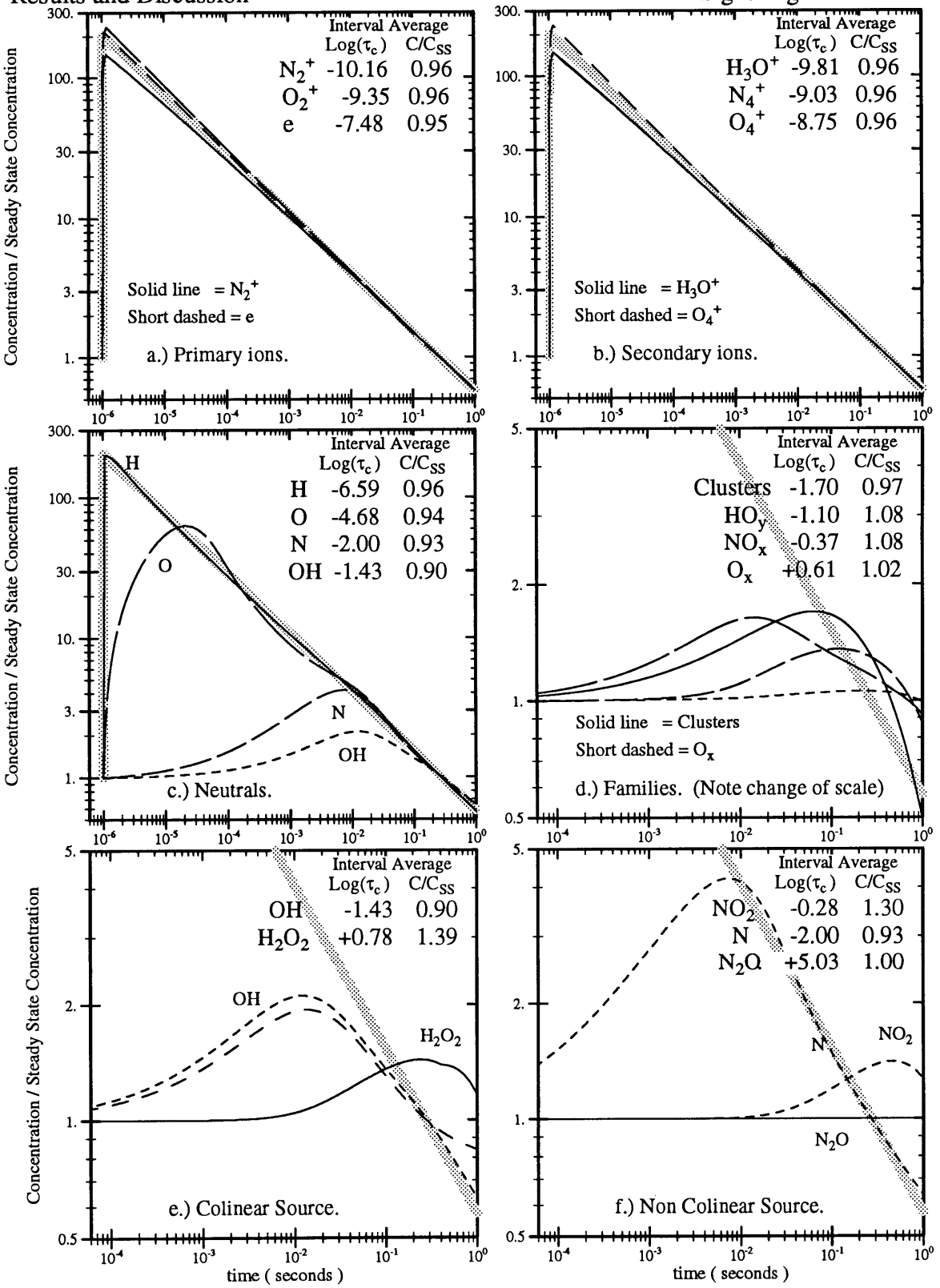

Figure 36. The time evolution of selected compounds in the lightning flash model of grid point (2,4). The thick gray line represents the forcing function for which the average value is unity. See text for more details.

8.2 Two-Dimensional Steady-State Ion Model

8.2.1 Introduction

To facilitate the discussion of the chemical compounds, I first introduce the typical layout of the summary of the data for a chemical compound. Each compound is summarized on two pages of data; one page is comprised primarily of a 3 by 3 grid of half-tone maps (*e.g.* Figure 37) and the other page is comprised of a set of 3 tables (*e.g.* Table 11).

8.2.1.1 Layout of Half-tone Maps

Each half-tone map page displays summaries of the mixing ratios χ, chemical lifetimes τ, and **term weights** (defined below) for the particular chemical species, the name of which is at the top of the page. These summaries are laid out in a 3 by 3 grid in the following manner. Each of the rows represents a different parameter being summarized, and each of the columns represents a different model run. Specifically the top row of half-tone maps represent the distribution of mixing ratio of the species throughout the domains of each of the model runs; the second row displays the corresponding chemical lifetimes, and the bottom row shows the relative importance of the different types of processes in the continuity equation (**term weights**, described below) for the species in question. Each of the three columns represents a different model run; the left-most column is the 1-D steady-state model, the center column is the Base Case model run (*i.e.* the 2-D steady state model with no lightning produced ions nor ultra-violet light included), and the right most column is the Electrified model run, (*i.e.* the 2-D steady state run with lightning-produced ions and ultra-violet light included).

This 3 by 3 grid is bounded on the right-most edge by the legends for each of the

three rows. Immediately above the 3 by 3 grid are the mass-weighted-average mixing ratios $\bar{\chi}$ and chemical lifetimes $\bar{\tau}_c$ for each of the three model runs. Above these summaries are the net mass production (outflow - inflow) of the chemical species in question in both the Base Case and Electrified model runs (there is no transport in the 1-D model). Here P_{BC} is the net production in the Base Case model and P_{IM} is the net production in the Electrified model case. Above these figures is presented the difference in the net production between these two model runs (Differential Net Production; P_{IM} - P_{BC}).

The meaning of the phrase **term weights** is explained as follows. All processes in the models (or terms in the continuity equation Eq.(11)) are classified as belonging to one of the three following realms: **Chemistry**, **Dynamics**, or **Heterogeneous Processes**. Because these models are Steady State models, the sum of all the source processes (or sources) must equal the sum of all the loss processes (or sinks)

$$\begin{aligned} 0 = &\text{Chemistry\_Sources} + \text{Chemistry\_Losses} \\ &+ \text{Dynamic\_Sources} + \text{Dynamic\_Losses} \\ &+ \text{Hetero.\_Sources} + \text{Hetero.\_Losses} \ . \end{aligned} \tag{68}$$

We now define the total "Reactive Flux" $\Re_f$ as the sum of the absolute magnitude of all of these terms

$$\begin{aligned} \Re_f = &|\text{Chemistry\_Sources}| + |\text{Chemistry\_Losses}| \\ &+ |\text{Dynamic\_Sources}| + |\text{Dynamic\_Losses}| \\ &+ |\text{Hetero.\_Sources}| + |\text{Hetero.\_Losses}| \ , \end{aligned} \tag{69}$$

and the relative importance of chemical processes ($\Im_C$) can be defined as

$$\Im_C = \frac{|\text{Chemistry\_Sources}| + |\text{Chemistry\_Losses}|}{\Re_f} \tag{70}$$

with similar terms for the importance of the Heterogeneous and Dynamic processes ($\Im_H$ and $\Im_D$ respectively).

Given the requirement that $\Im_C + \Im_H + \Im_D = 1$, any particular combination of $\Im_C, \Im_H$, and $\Im_D$ can be considered as a point located on or within the perimeter of an equilateral triangle having Chemistry, Dynamics and Heterogeneous Processes as its vertices. Maps of **term weights** result from representing this point with various symbols for each grid point in the model domain. In these figures, the domains are represented by slanted and horizontal lines. In the center, where all three processes are about equal, the lines are not plotted and the region is blank.

8.2.1.2 Layout of Summary Tables

On the page after the 3 by 3 grid of half-tone maps are 3 tables that summarize the major sources and sinks for the compound in question (*e.g.* Table 11). Beginning at the top, the first table **(a.)** lists the major source terms in each of the three model runs; **(b.)** lists the major sink terms in each of the three model runs. These terms have units molec·cm^{-3}·s^{-1} and can be considered the specific production (or loss) rate $\Re$ of the compound in question. Because these models are steady state ones, the sum of the source $\Re$'s (shown at the bottom of each column in the source **(a.)** table must equal sum of the sink $\Re$'s (shown at the bottom of each column in the sink **(b.)** table.

The lower-most table **(c.)** summarizes the domain averaged mixing ratio χ, number density [..] and total specific production rate $\Sigma\Re$ in each of the three steady state model runs. As noted at the bottom of this table, τ = [..] / $\Sigma\Re$ or Log(τ) = Log([..]) − Log($\Sigma\Re$). Because non-chemical terms (*e.g.* Advection/Diffusion) are sometimes the dominant ones, also listed in the final two columns of this table are the chemical lifetime τ_c

of the compound in question for both source and sink processes.

8.2.1.3 Chemical Species Summarized

I will here discuss just the most important chemical species and major chemical families of the models. The individual members of the chemical families as well as some interesting minor compounds are similarly displayed in Appendix D , page 218.

8.2.2 Primary-Ion Production

The primary ions formed in the electrified models have been shown to be the electron, O_2^+, and N_2^+. Given that they all have very short lifetimes, and are produced together, they are expected to have similar spatial distributions of mixing ratio and chemical lifetimes. I therefore focus on the results for the electron and refer the reader to Appendix D , page 218, specifically pages 219 and 221 for the corresponding summaries of O_2^+ and N_2^+ respectively.

8.2.2.1 Electron

The strong in-cloud source of electrons in the 2-D Electrified model run can be seen by reference to Figure 37 where the top row of half-tone pictures depict the mixing ratio of the electron in the 1-D steady-state, 2-D Base Case and 2-D Electrified model runs. The large increase in the mixing ratio in the 2-D Electrified model between the ground and 10km and from the inner domain wall out to 50m is readily apparent.

The dominant source of the electron in the 2-D Base Case model run is cosmic ray ionizations (Rxn's 114–117, Table 4, Section 4.2.1.1, page 98) while in the 2-D Electrified model run the dominant source is the parameterization of the ion-production processes

due to the large radial fields surrounding the lightning channel (Rxn's 129–132, Table 5, Section 4.2.1.2, page 98). The fact that it is these reactions that are responsible for the high electron density can be seen by referring to the second and third columns of Table 11**a** where the major reactions producing the electron are listed.

That the electron has a very short chemical lifetime (this is the reason that the high-electric-field time-dependent model runs were linear in the average-electron-mixing ratio) can be seen by reference to the second row of half-tone maps of Figure 37; note that the lifetime does not change from model run to model run. This is due to the fact that its primary loss mechanism is reactions with O_2 and the rate of this loss does not change materially between model runs. It is the decreasing number density of O_2 with increasing altitude that casues an increase in the lifetime of the free electron from $\approx 10^{-8}$ secs at ground level to $\approx 10^{-7}$ secs at 15km.

The fact that chemical processes (reaction with O_2) dominate the mixing ratio of the electron is borne out by the third row of maps. By reference to the legend at the right hand side of this row it can be seen that the chemistry symbol is present throughout the model domain.

Turning now to the tabular summary of the major sources and sinks of the electron in the three model runs, we see that the dominant source of the electron changes from cosmic rays (RX's $j_{114} - j_{117}$) to lightning (RX's $j_{129} - j_{131}$). Additionally, the reactive flux $\Sigma\Re$ of electrons increases from $10^{0.654}$ reactions$\cdot$cm$^{-3}\cdot$s^{-1} in the 2-D Base Case run to $10^{10.72}$ reactions$\cdot$cm$^{-3}\cdot$s^{-1} in the 2-D Electrified model run.

Finally, in the third, summary table (**c.**), it is noted that the average mixing ratio of the electron increases by 10 orders of magnitude. This is reasonable as the lifetime of the electron does not change very much and the source strength increases dramatically in

Electron

Differential Net Production ($P_{I.M.} - P_{B.C.}$) = 5.240×10^{-12} (Moles Year^{-1})

	$P_{B.C.} = 7.226 \times 10^{-8}$	$P_{I.M.} = 7.226 \times 10^{-8}$	(Moles Year^{-1})
$\overline{\tau}_c = 1.055 \times 10^{-7}$	$\overline{\tau}_c = 1.055 \times 10^{-7}$	$\overline{\tau}_c = 1.055 \times 10^{-7}$	(Seconds)
$\overline{\chi} = 2.310 \times 10^{-25}$	$\overline{\chi} = 2.310 \times 10^{-25}$	$\overline{\chi} = 5.980 \times 10^{-20}$	(Mixing Ratio)

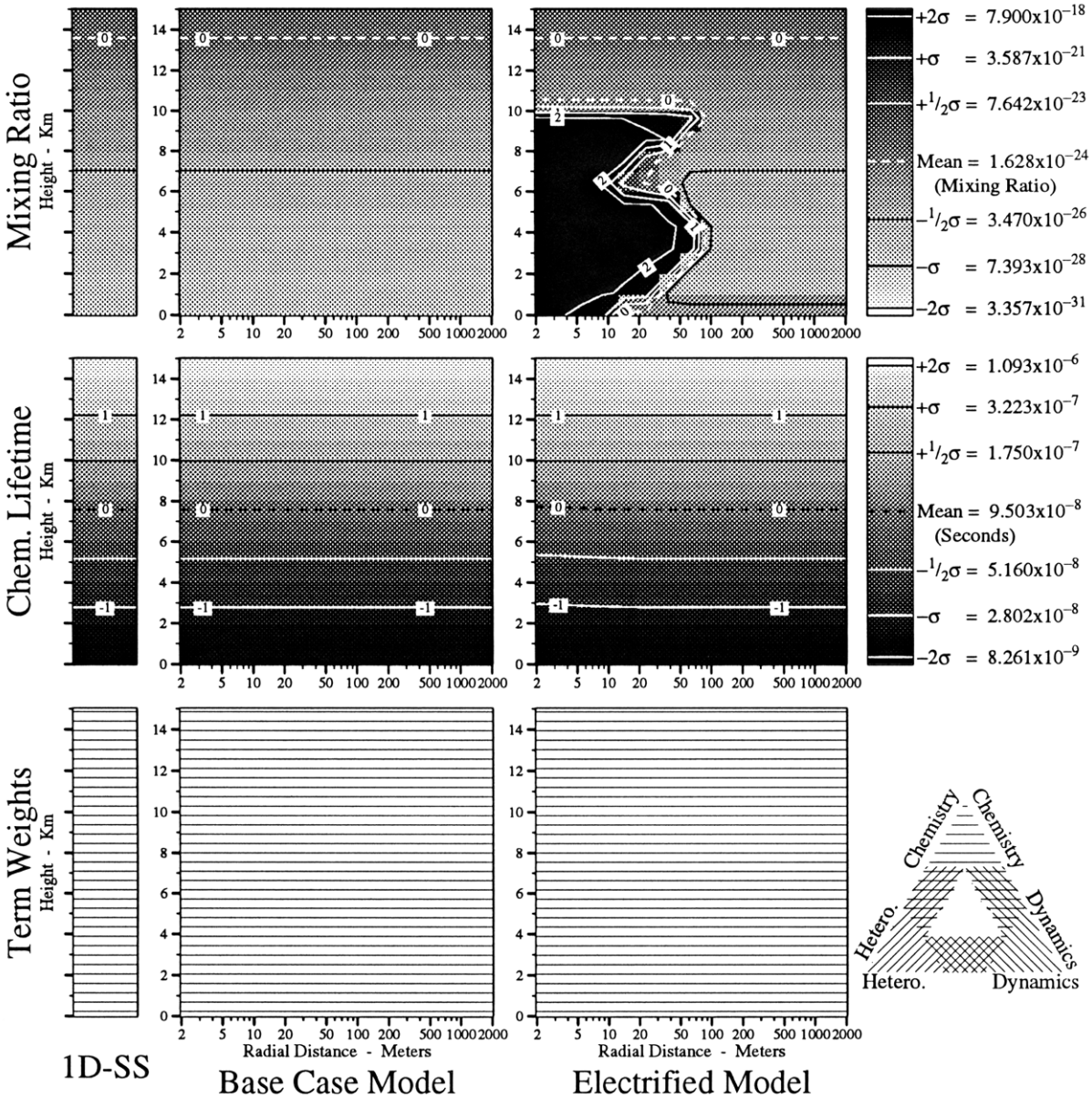

Figure 37. Mixing ratios (χ), lifetimes (τ_c), and term weights of e^-. See text for definitions of terms and other details.

the Electrified model run.

Inasmuch as the ionizing contribution from ground corona is small compared to that from lightning, it is included in the lightning reactions.

8.2.2.2 Positive-Ion Reaction-Sequence Summary

In principle, the complete chemistry of the subsequent reactions of the primary ions created can be worked out from just the Tables of the major sources and sinks. In the interest of clarity however I summarize these data in a "flow diagram" shown in Figure 38.

This Figure has two main columns of reaction paths, the left-most column summarizes the reactions of the N_2 family, and the right-most column summarizes the reactions of the O_2 family. Each box represents the steady-state concentration of a chemical species in the 2-D Electrified model run; below the name of the species is the common logarithm of the domain-average number density. The arrows that connect the boxes represent reactions. At the origin of each arrow is given first the other reactant involved the reaction in question, as well as the reaction number. Following these data is then given the common logarithm of the specific production rate $\Re$. For example, in this Figure, N_2 has an average number density of $10^{19.204}$ molec·cm^{-3}, Lightning (Reaction number 130) causes a reaction that turns $10^{10.51}$ molecules of N_2 into N_2^+ per cm^{-3} per second. The thickness of the lines representing the reaction paths is proportional to $\Re$. In the center of the above mentioned columns are the products of the positive ion chemistry; at upper most box in the center represent the ion exchange/rearrangement of N_2 and O_2 yielding NO^+ and NO. The NO^+ so produced becomes hydrated, and ultimately reacts with water to produce H_3O^+ and HONO.

The lightning-induced dissociative ionizations (Rx's 132, 132) also produce a similar sequence of reactions, shown in Figure 39, and ultimately leading to O_2^+, and NO^+

Table 11. Summary of the chemistry of the electron in the **inner domain** of the three models. (**a**,**b**) The major terms in the continuity equations for e^- in the three model runs and (**c**) a summary of its mixing ratios χ and lifetimes τ in the three model runs. In these tables $\Re$ is the specific rate of production of e^- (molec·cm^{-3}·s^{-1}), τ is the total lifetime (sec) of e^- and τ_c is its lifetime due to chemical processes (sec). J_i, j_i, k_i, and l_i are photolytic, unimolecular, bimolecular and termolecular rate coefficients respectively for reaction number i as listed in Appendix B , page 184.

a.) The major source terms for the electron in the inner domain of the three model runs.

1-D Steady-State Model		2-D Base Case Model		2-D Electrified Model	
Log ($\Re$)	Reaction Rate $\Re = k_{yz}[y][z]$	Log ($\Re$)	Reaction Rate $\Re = k_{yz}[y][z]$	Log ($\Re$)	Reaction Rate $\Re = k_{yz}[y][z]$
0.37	$j_{116}[N_2]$	0.37	$j_{116}[N_2]$	10.51	$j_{130}[N_2]$
0.07	$j_{117}[N_2]$	0.07	$j_{117}[N_2]$	9.94	$j_{129}[O_2]$
-0.20	$j_{114}[O_2]$	-0.20	$j_{114}[O_2]$	9.94	$j_{132}[N_2]$
-0.50	$j_{115}[O_2]$	-0.50	$j_{115}[O_2]$	9.36	$j_{131}[O_2]$
-1.82	$j_{119}[H_2O]$	-1.82	$j_{119}[H_2O]$	8.47	$k_{211}[O_2][e^-]$
-2.74	$j_{118}[CO_2]$	-2.74	$j_{118}[CO_2]$	7.22	$k_{209}[O_2][e^-]$
...	37 More Reactions	...	37 More Reactions	...	37 More Reactions
0.654 = Log($\Sigma\Re$)		0.654 = Log($\Sigma\Re$)		10.719 = Log($\Sigma\Re$)	

b.) The major sink terms for the electron in the inner domain of the three model runs.
The reaction rate $\Re$ implicitly contains $[e^-]$.

1-D Steady-State Model		2-D Base Case Model		2-D Electrified Model	
Log ($\Re$)	Reaction Rate $\Re = k_{yz}[y][e^-]$	Log ($\Re$)	Reaction Rate $\Re = k_{yz}[y][e^-]$	Log ($\Re$)	Reaction Rate $\Re = k_{yz}[y][e^-]$
0.53	$l_{243}[O_2][O_2]$	0.53	$l_{243}[O_2][O_2]$	10.58	$l_{243}[O_2][O_2]$
-0.09	$l_{244}[O_2][N_2]$	-0.09	$l_{244}[O_2][N_2]$	9.94	$l_{244}[O_2][N_2]$
-0.49	$l_{245}[O_2][H_2O]$	-0.49	$l_{245}[O_2][H_2O]$	9.64	$l_{245}[O_2][H_2O]$
-1.99	$l_{246}[O_2][CO_2]$	-1.99	$l_{246}[O_2][CO_2]$	9.18	$k_{347}[W_2H_3O^+]$
-2.20	$k_{242}[H_2O]$	-2.20	$k_{242}[H_2O]$	8.04	$l_{246}[O_2][CO_2]$
-5.87	$k_{347}[W_2H_3O^+]$	-5.25	Heterogeneous Loss	7.95	$k_{242}[H_2O]$
...	45 More Reactions	...	45 More Reactions	...	45 More Reactions
0.654 = Log($\Sigma\Re$)		0.654 = Log($\Sigma\Re$)		10.719 = Log($\Sigma\Re$)	

Note: Read **W** as H_2O.

c.) Summary of the lifetimes of the electron in the inner domain of the three model runs.

	Log(χ)	Log($[e^-]$) cm^{-3}	Log($\Sigma\Re$) cm^{-3}·s^{-1}	Log(τ) sec	Source Log(τ_c) sec	Sink Log(τ_c) sec
1-D Steady-State Model	−25.738	−6.546	0.654	−7.200	−7.200	−7.200
2-D Base Case Model	−25.738	−6.546	0.654	−7.200	−7.200	−7.200
2-D Electrified Model	−15.845	3.347	10.719	−7.373	−7.373	−7.373

Note: $\tau = [e^-] / \Sigma\Re$ or $\text{Log}(\tau) = \text{Log}([e^-]) - \text{Log}(\Sigma\Re)$.

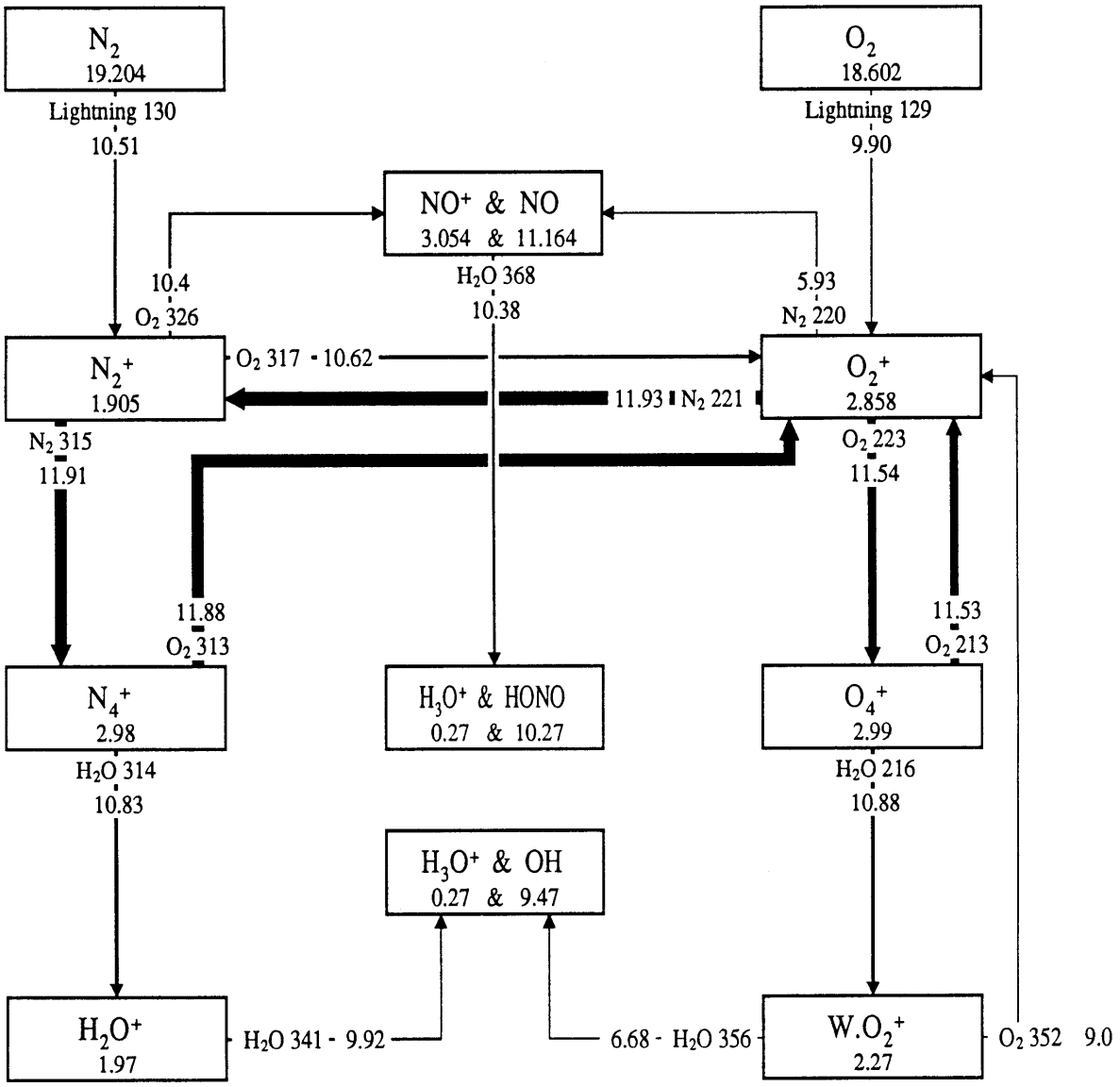

Figure 38. O_2^+ & N_2^+ Reaction-sequence summary. See text for definitions of terms and other details.

whose fates are described above. It is note in this Figure that the reactions of N^+ and O^+ also produce atomic N and O, the fates of which, as discussed below are NO and O_3 respectively.

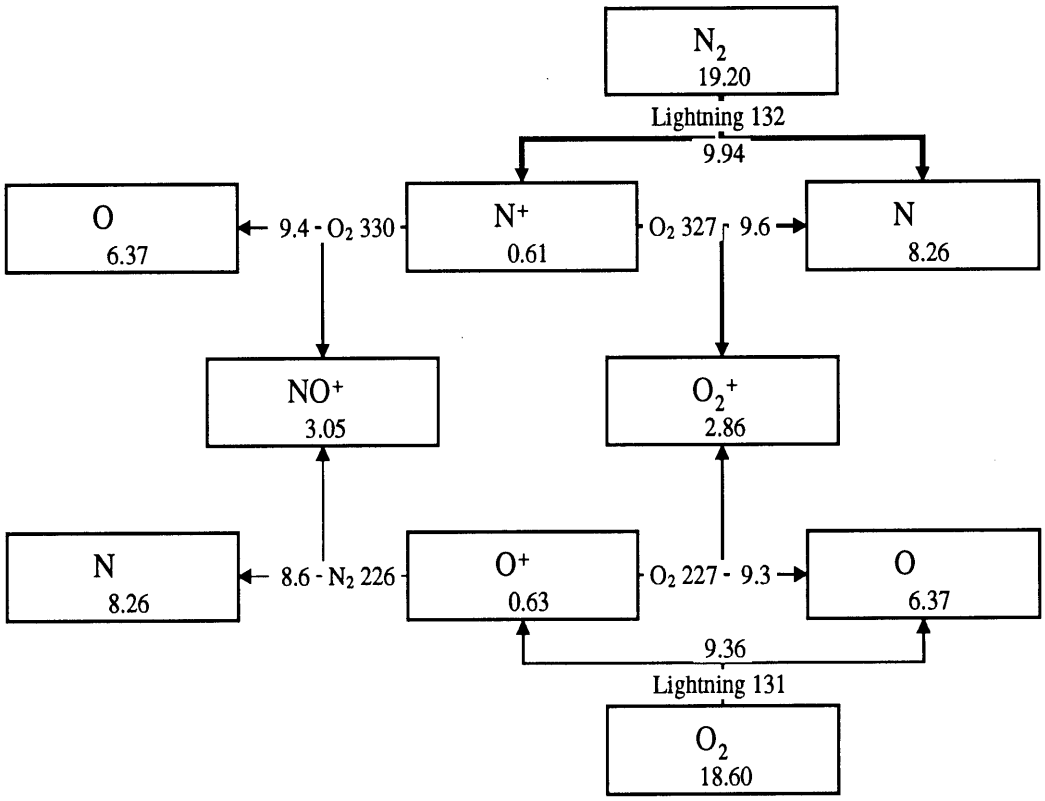

Figure 39. O^+ & N^+ Reaction-sequence summary. See text for definitions of terms and other details.

The overall reaction of these reactions can be expressed as

$$2H_2O \rightarrow OH + H_3O^+ + e^- \qquad (71a)$$

and

$$N_2 + O_2 + 2H_2O \rightarrow NO + HONO + H_3O^+ + e^- . \qquad (71b)$$

8.2.2.3 Negative-Ion Reaction-Sequence Summary

The fate of the electron that is produced along with the positive ions is dominated by its three body collision with O_2, resulting in O_2^-. The fate of O_2^- is dominated by its

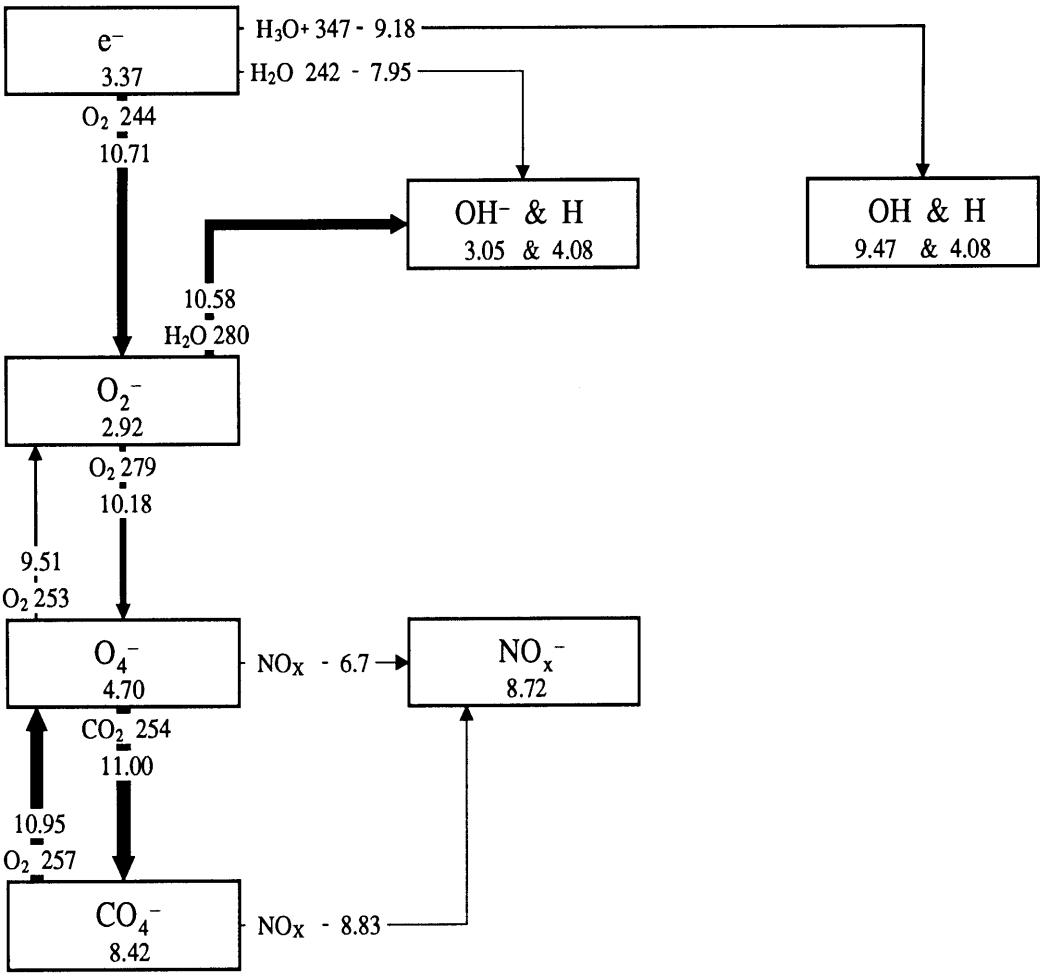

Figure 40. Negative-ion reaction-sequence summary. See text for definitions of terms and other details.

assumed rate of reaction with H_2O, herein given the maximal gas kinetic rate, a rather high rate. Otherwise, O_2^- goes on to form O_4^- and CO_4^-. These negative ions are relatively stable and ultimately react with NO_3 to form NO_3^-. The negative ion system is shown schematically in Figure 40 where the reactions of the electron and the subsequent electron carriers are shown in the first column, the stable negative ions are shown in the second column and the products of electron / ion dissociative recombination are shown in the third column.

8.2.3 Neutral-Atomic Production

The primary atomic species formed are, in order of average concentration, N, O, and H. I now discuss these as a group, and here present the summaries of N. The reader is referred to Appendix D , page 218 for the summaries of O (page 239) and H (page 243). In the 2-D Electrified model run, the neutrals N and O are mostly formed via the parameterization of the lightning flash (Reactions 131 and 132), along with O^+, N^+ and the electron, while the dominant sources of atomic H are the reactions of the electron and O_2^- with water. The dominant reactions of the mono-atomic ions O^+ and N^+ are with O_2 to form O, N, NO, NO^+, and O_2^+.

The dominant loss mechanism of atomic N is with molecular oxygen, O_2 to form NO and O. The dominant loss mechanism of atomic O is, of course, also with reaction with molecular oxygen to form O_3 (ozone). The dominant loss mechanism of atomic H is the three body reaction with O_2 to form HO_2. The map of term weights also indicates that chemical production balances chemical loss throughout most of the model domain in all the model runs.

N

Differential Net Production ($P_{I.M.} - P_{B.C.}$) = -1.966×10^{-6} (Kg Year^{-1})

$P_{B.C.} = 4.530 \times 10^{-4}$ $P_{I.M.} = 4.511 \times 10^{-4}$ (Kg Year^{-1})

$\overline{\tau}_c = 0.11630$ $\overline{\tau}_c = 0.11676$ $\overline{\tau}_c = 0.11551$ (Seconds)

$\overline{\chi} = 1.195 \times 10^{-19}$ $\overline{\chi} = 1.201 \times 10^{-19}$ $\overline{\chi} = 4.889 \times 10^{-15}$ (Mixing Ratio)

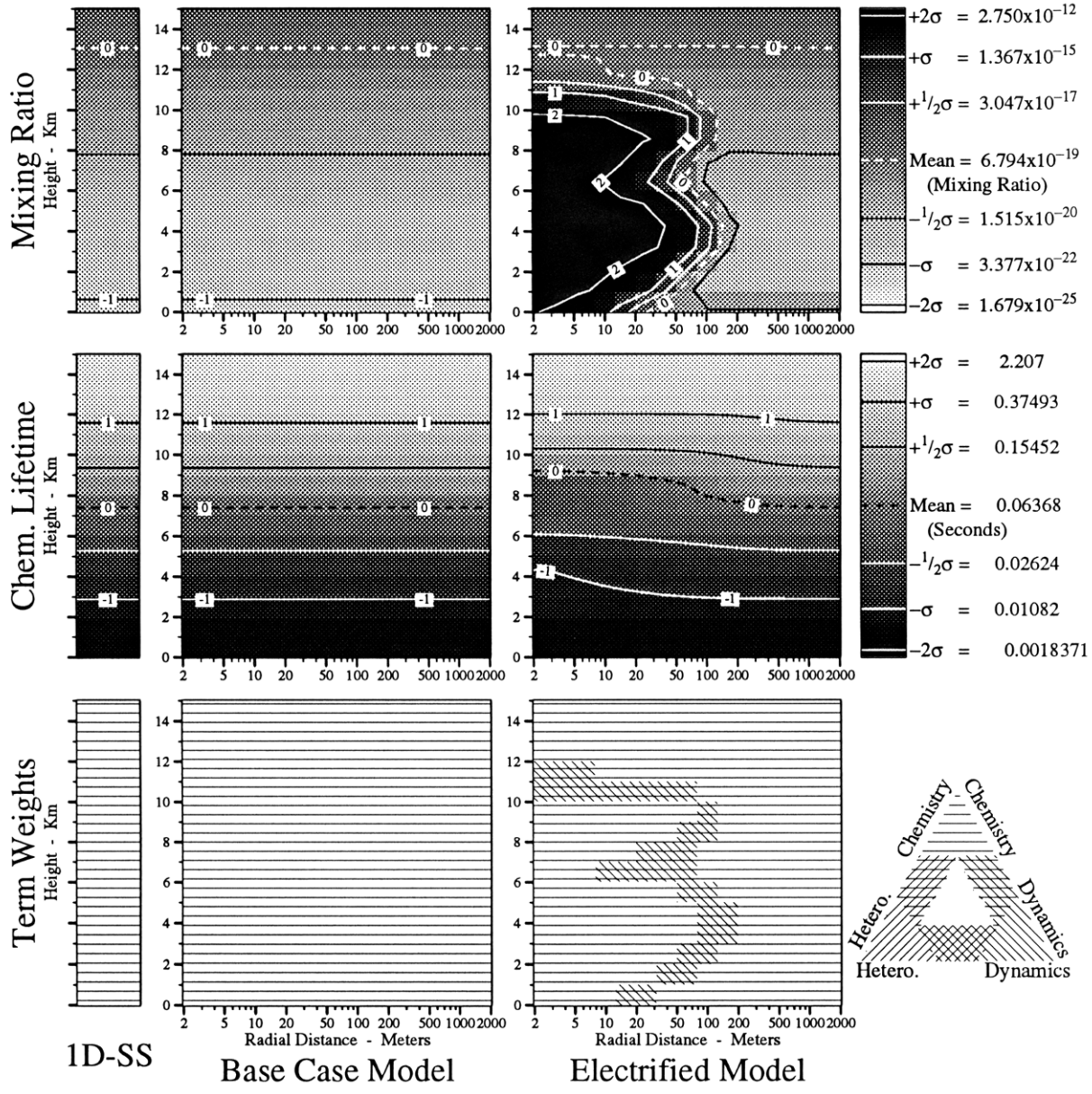

Figure 41. Mixing ratios (χ), lifetimes (τ_c), and term weights of N. See text for definitions of terms and other details.

Table 12. Summary of the chemistry of N in the **inner domain** of the three models. (**a**,**b**) The major terms in the continuity equations for N in the three model runs and (**c**) a summary of its mixing ratios χ and lifetimes τ in the three model runs. In these tables $\Re$ is the specific rate of production of N (molec·cm^{-3}·s^{-1}), τ is the total lifetime (sec) of N and τ_c is its lifetime due to chemical processes (sec). J_i, j_i, k_i, and l_i are photolytic, unimolecular, bimolecular and termolecular rate coefficients respectively for reaction number i as listed in Appendix B , page 184.

a.) The major source terms for N in the inner domain of the three model runs.

1-D Steady-State Model		2-D Base Case Model		2-D Electrified Model	
Log ($\Re$)	Reaction Rate $\Re = k_{yz}$ [y] [z]	Log ($\Re$)	Reaction Rate $\Re = k_{yz}$ [y] [z]	Log ($\Re$)	Reaction Rate $\Re = k_{yz}$ [y] [z]
0.07	j_{117} [N_2]	0.07	j_{117} [N_2]	9.94	j_{132} [N_2]
-0.29	k_{327} [N^+] [O_2]	-0.29	k_{327} [N^+] [O_2]	9.57	k_{327} [N^+] [O_2]
-1.27	k_{226} [O^+] [N_2]	-1.27	k_{226} [O^+] [N_2]	8.64	k_{226} [O^+] [N_2]
-2.47	k_{333} [N^+] [CO_2]	-2.47	k_{333} [N^+] [CO_2]	8.56	$2{\cdot}k_{310}$ [N_2] [e^-]
-2.95	k_{149} [$N(^2D)$] [N_2]	-2.95	k_{149} [$N(^2D)$] [N_2]	7.60	$2{\cdot}k_{406}$ [N_4^+]{NegIon}
-4.78	k_{322} [N_2^+] [N_2O]	-4.78	k_{322} [N_2^+] [N_2O]	7.40	k_{333} [N^+] [CO_2]
...	40 More Reactions	...	40 More Reactions	...	40 More Reactions
0.244 = Log($\Sigma\Re$)		0.244 = Log($\Sigma\Re$)		10.123 = Log($\Sigma\Re$)	

Note: The definitions of the reactive families $\{X\}$ are at the end of Appendix B.

b.) The major sink terms for N in the inner domain of the three model runs.
The reaction rate $\Re$ implicitly contains [N].

1-D Steady-State Model		2-D Base Case Model		2-D Electrified Model	
Log ($\Re$)	Reaction Rate $\Re = k_{yz}$ [y] [N]	Log ($\Re$)	Reaction Rate $\Re = k_{yz}$ [y] [N]	Log ($\Re$)	Reaction Rate $\Re = k_{yz}$ [y] [N]
0.24	k_{458} [O_2]	0.24	k_{458} [O_2]	9.98	k_{458} [O_2]
-3.55	k_{460} [NO]	-2.82	Heterogeneous Loss	9.42	k_{460} [NO]
-4.38	k_{470} [NO_2]	-3.55	Advection/Diffusion	8.70	k_{470} [NO_2]
-4.67	k_{482} [NO_2]	-3.59	k_{460} [NO]	8.54	k_{553} [OH]
-4.74	k_{540} [O_3]	-4.66	k_{470} [NO_2]	8.40	k_{482} [NO_2]
-5.66	k_{553} [OH]	-4.96	k_{482} [NO_2]	6.62	Heterogeneous Loss
...	19 More Reactions	...	19 More Reactions	...	19 More Reactions
0.244 = Log($\Sigma\Re$)		0.244 = Log($\Sigma\Re$)		10.123 = Log($\Sigma\Re$)	

c.) Summary of the lifetimes of N in the inner domain of the three model runs.

	Log(χ)	Log([N]) cm^{-3}	Log($\Sigma\Re$) $cm^{-3}{\cdot}s^{-1}$	Log(τ) sec	Source Log(τ_c) sec	Sink Log(τ_c) sec
1-D Steady-State Model	−20.321	−1.129	0.244	−1.373	−1.373	−1.373
2-D Base Case Model	−20.322	−1.130	0.244	−1.374	−1.374	−1.374
2-D Electrified Model	−10.934	8.258	10.123	−1.865	−1.865	−1.865

Note: τ = [N] / $\Sigma\Re$ or Log(τ) = Log([N]) − Log($\Sigma\Re$).

8.2.4 OH (Hydroxyl) Production

The major source of OH is different in each of the three model runs, although the 1-D and 2-D Base Case runs have the same two most important sources. In the 1-D photochemical model run, OH comes mostly from the reaction of HO_2 and NO while in the 2-D Base Case run, OH comes mostly from the reaction of $O(^1D)$ and H_2O.

In the 2-D Electrified model run, OH comes from HO_2 and NO as in the other two models, but given the large sources of NO and HO_2 in the 2-D Electrified model run, the rate of OH production is 6 orders of magnitude larger in the 2-D Electrified model run than it is in the other two model runs. In the 2-D Electrified model, the second most important source of OH is the reaction of H_2O and H_2O^+ that forms OH and H_3O^+.

The sink processes of OH are also different in the 2-D Electrified model run. In the normal atmospheric models (1-D steady-state and 2-D Base Case model), the dominant loss mechanisms of OH are its reactions with CO and CH_4. In the 2-D Electrified model run, the dominant loss mechanism becomes the formation of HNO_3; herein referred to as $HONO_2$.

OH

Differential Net Production ($P_{I.M.}$ - $P_{B.C.}$) = 14.51 (Kg Year^{-1})

$P_{B.C.}$ = −743.2 $P_{I.M.}$ = −728.7 (Kg Year^{-1})

$\overline{\tau}_c$ = 2.908 $\overline{\tau}_c$ = 2.391 $\overline{\tau}_c$ = 2.328 (Seconds)

$\overline{\chi}$ = 54.06 $\overline{\chi}$ = 12.61 $\overline{\chi}$ = 112.6 (ppQ)

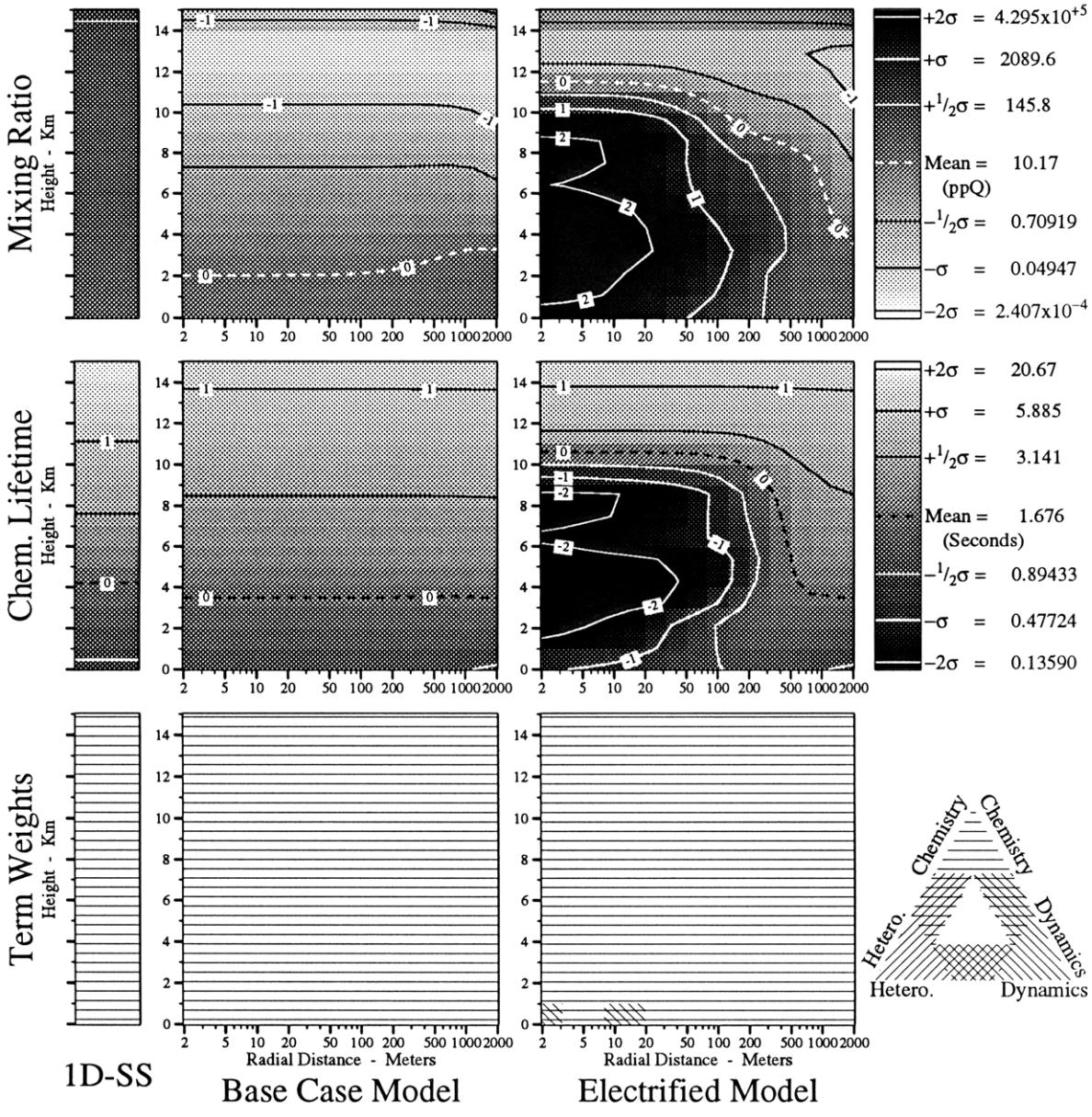

Figure 42. Mixing ratios (χ), lifetimes (τ_c), and term weights of OH. See text for definitions of terms and other details.

Table 13. Summary of the chemistry of OH in the **inner domain** of the three models. (**a**,**b**) The major terms in the continuity equations for OH in the three model runs and (**c**) a summary of its mixing ratios χ and lifetimes τ in the three model runs. In these tables $\Re$ is the specific rate of production of OH (molec·cm^{-3}·s^{-1}), τ is the total lifetime (sec) of OH and τ_c is its lifetime due to chemical processes (sec). J_i, j_i, k_i, and l_i are photolytic, unimolecular, bimolecular and termolecular rate coefficients respectively for reaction number i as listed in Appendix B , page 184.

a.) The major source terms for OH in the inner domain of the three model runs.

1-D Steady-State Model		2-D Base Case Model		2-D Electrified Model	
Log ($\Re$)	Reaction Rate $\Re = k_{yz}$ [y] [z]	Log ($\Re$)	Reaction Rate $\Re = k_{yz}$ [y] [z]	Log ($\Re$)	Reaction Rate $\Re = k_{yz}$ [y] [z]
5.27	k_{55} [HO_2] [NO]	4.75	$2{\cdot}k_{135}$ [$O(^1D)$] [H_2O]	10.26	k_{55} [HO_2] [NO]
5.08	$2{\cdot}k_{135}$ [$O(^1D)$] [H_2O]	4.12	k_{55} [HO_2] [NO]	10.22	k_{358} [OHH_3O^+] [H_2O]
4.87	k_{54} [HO_2] [O_3]	3.36	k_{54} [HO_2] [O_3]	9.92	k_{341} [H_2O^+] [H_2O]
4.72	$2{\cdot}J_5$ [H_2O_2]	2.75	Advection/Diffusion	8.46	k_{426} [HCO_3^-]{PosIon}
4.37	j_{608} [CH_2OOH]	2.26	J_{11} [CH_3OOH]	8.42	$2{\cdot}k_{135}$ [$O(^1D)$] [H_2O]
4.00	J_{11} [CH_3OOH]	2.15	j_{608} [CH_2OOH]	8.05	J_3 [HONO]
...	84 More Reactions	...	84 More Reactions	...	84 More Reactions
5.675 = Log($\Sigma\Re$)		4.861 = Log($\Sigma\Re$)		10.642 = Log($\Sigma\Re$)	

Note: The definitions of the reactive families $\{X\}$ are at the end of Appendix B.

b.) The major sink terms for OH in the inner domain of the three model runs.
The reaction rate $\Re$ implicitly contains [OH].

1-D Steady-State Model		2-D Base Case Model		2-D Electrified Model	
Log ($\Re$)	Reaction Rate $\Re = k_{yz}$ [y] [OH]	Log ($\Re$)	Reaction Rate $\Re = k_{yz}$ [y] [OH]	Log ($\Re$)	Reaction Rate $\Re = k_{yz}$ [y] [OH]
5.38	k_{659} [CO]	4.60	k_{659} [CO]	10.20	k_{31} [HO_2]
5.02	k_{556} [CH_4]	4.26	k_{556} [CH_4]	10.13	k_{94} [NO_2]
4.37	k_{607} [CH_3OOH]	3.87	Heterogeneous Loss	9.74	k_{68} [HONO]
4.30	k_{633} [CH_2O]	3.52	k_{42} [H_2]	9.61	k_{92} [NO]
4.27	k_{42} [H_2]	3.16	k_{668} [DMS]	9.05	k_{659} [CO]
4.14	k_{609} [CH_3OOH]	2.91	k_{52} [O_3]	9.03	k_{66} [HO_2NO_2]
...	62 More Reactions	...	62 More Reactions	...	62 More Reactions
5.675 = Log($\Sigma\Re$)		4.861 = Log($\Sigma\Re$)		10.642 = Log($\Sigma\Re$)	

c.) Summary of the lifetimes of OH in the inner domain of the three model runs.

	Log(χ)	Log([OH]) cm^{-3}	Log($\Sigma\Re$) $cm^{-3}{\cdot}s^{-1}$	Log(τ) sec	Source Log(τ_c) sec	Sink Log(τ_c) sec
1-D Steady-State Model	−13.325	5.867	5.675	0.192	0.192	0.192
2-D Base Case Model	−14.230	4.962	4.861	0.101	0.104	0.148
2-D Electrified Model	−9.721	9.471	10.642	−1.171	−1.171	−1.167

Note: τ = [OH] / $\Sigma\Re$ or Log(τ) = Log([OH]) − Log($\Sigma\Re$).

8.2.5 Major Families of the Model

The primary families formed are in order of average concentration NO_x, O_x, and HO_y. I discuss in this section each of these families; the individual members of these families are presented in Appendix D , page 218. Given the production rates of O, NO, H, and OH it is easy to guess the source regions of the families; they are co-located with the source regions of their members. The chemical lifetimes of the families are measured in hours rather than in seconds, as are their constitutive members (this is the value of talking about a "chemical family"), and consequently we note that not only are there high concentrations of the families in their source regions, but also there is considerable transport of these families out of the model domain.

8.2.5.1 NO_x

The differential net production of NO_x is 4.5×10^7 moles per year (per storm), predominantly reflecting the reversal of the in-cloud loss of 3.8×10^7 moles per year predicted in the Base Case model. There is however a large negative radial gradient in the mixing ratio of NO_x, and the term weights indicate that in this region of the model heterogeneous loss is balanced by dynamic transport. This implies that the actual storm production depends on the assumed heterogeneous-loss rate.

This level of production most likely represents a lower limit because the net production of NO_x is a function of the assumed rate of heterogeneous loss. If the loss rate to cloud particles in the upper model domain is too large (as is may well be) then more NO_x will "survive" the trip from the production regions to the model boundary. The reasons that the assumed heterogeneous-loss rate may be too large are (1) at the temperatures of the upper model domain, liquid water cannot exist and the sticking coefficient to ice is, in gen-

eral, smaller than that to liquid water and (2) the possibility that the drops/ice may become saturated with NO_x, thereby reducing the effective sticking coefficient to zero.

Nevertheless, it is instructive to compare the differential net production with observations. Adopting a global thunderstorm density of 2000 storms and considering just the amount of nitrogen in NO, yields a global production of 1.3 Tg N per year from all thunderstorms. This value can be compared with the 7 Tg $N \cdot yr^{-1}$ calculated by *Chameides et al.* [1987] (C87) based on observations of NO mixing ratios in the outflow of a thunderstorm. These values actually can be considered to agree more closely than they appear to at first glance. The value of 7 Tg $N \cdot yr^{-1}$ was calculated based on an aircraft penetration of the outflow of a thunderstorm. In this penetration, the NO levels rose from a background level of 20 pptv to 440 pptv. By reference to Figure 43 it is noted that the mean inflow NO_x value is between 93 ppt and 17 ppt, reasonably close to the 20 ppt NO observed by C87 (Averaged over the model domain, $NO \approx NO_2$). The mixing ratios in the outflow of the model storm also agree with the values C87 observed in the outflow regions; the $+\frac{1}{2}\sigma$ isopleth has a value of 495 ppt. This isopleth is 1 grid point removed from the model boundary at the outflow region, so the exact location of the outer model domain relative to the position of the aircraft penetration could account for the values observed by C87 that are larger than the model domain's actual boundary values $\approx$ 93 ppt.

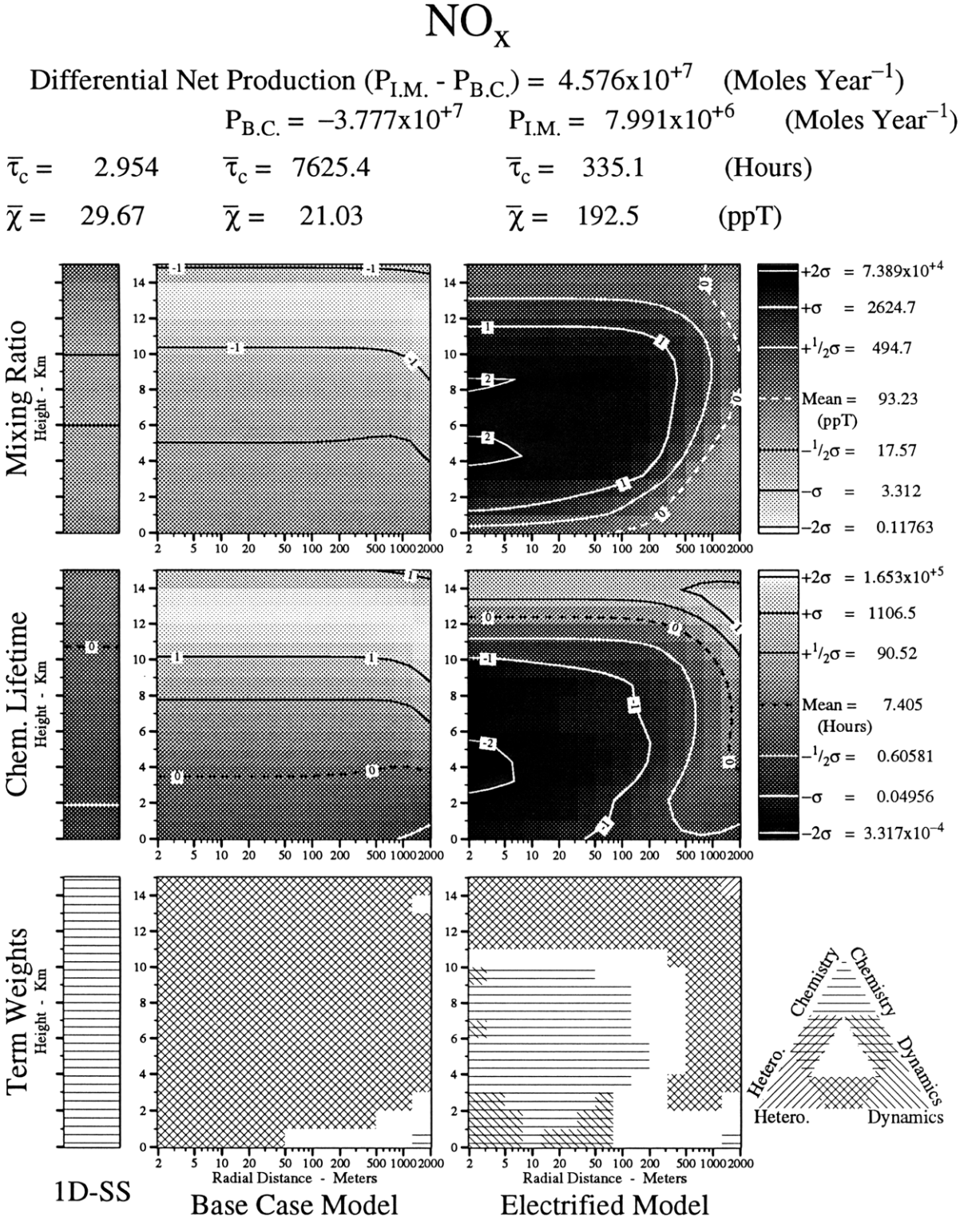

Figure 43. Mixing ratios (χ), lifetimes (τ_c), and term weights of NO_x. See text for definitions of terms and other details.

Table 14. Summary of the chemistry of NO_x in the **inner domain** of the three models. (**a,b**) The major terms in the continuity equations for NO_x in the three model runs and (**c**) a summary of its mixing ratios χ and lifetimes τ in the three model runs. In these tables $\Re$ is the specific rate of production of NO_x (molec·cm^{-3}·s^{-1}), τ is the total lifetime (sec) of NO_x and τ_c is its lifetime due to chemical processes (sec). J_i, j_i, k_i, and l_i are photolytic, unimolecular, bimolecular and termolecular rate coefficients respectively for reaction number i as listed in Appendix B , page 184.

a.) The major source terms for NO_x in the inner domain of the three model runs.

1-D Steady-State Model		2-D Base Case Model		2-D Electrified Model	
Log ($\Re$)	Reaction Rate $\Re = k_{yz}$ [y] [z]	Log ($\Re$)	Reaction Rate $\Re = k_{yz}$ [y] [z]	Log ($\Re$)	Reaction Rate $\Re = k_{yz}$ [y] [z]
4.74	j_{101} [$CH_3O_2NO_2$]	5.90	Advection/Diffusion	10.40	k_{326} [N_2^+] [O_2]
4.69	j_{96} [HO_2NO_2]	4.00	$2 \cdot j_{488}$ [N_2O_3]	9.98	k_{458} [N] [O_2]
4.06	$2 \cdot j_{488}$ [N_2O_3]	3.54	j_{101} [$CH_3O_2NO_2$]	9.95	$2 \cdot j_{488}$ [N_2O_3]
3.66	J_3 [HONO]	3.29	$2 \cdot j_{485}$ [N_2O_4]	9.74	k_{68} [OH] [HONO]
3.53	$2 \cdot j_{485}$ [N_2O_4]	3.27	j_{96} [HO_2NO_2]	9.29	$2 \cdot j_{485}$ [N_2O_4]
3.18	J_8 [NO_3]	2.53	J_8 [NO_3]	9.16	k_{339} [NO^+] [H_2O]
...	80 More Reactions	...	80 More Reactions	...	80 More Reactions
5.108 = Log($\Sigma\Re$)		5.912 = Log($\Sigma\Re$)		10.750 = Log($\Sigma\Re$)	

b.) The major sink terms for NO_x in the inner domain of the three model runs.

1-D Steady-State Model		2-D Base Case Model		2-D Electrified Model	
Log ($\Re$)	Reaction Rate $\Re = k_{yz}$ [y] {NO_x}	Log ($\Re$)	Reaction Rate $\Re = k_{yz}$ [y] {NO_x}	Log ($\Re$)	Reaction Rate $\Re = k_{yz}$ [y] {NO_x}
4.74	k_{100} [CH_3O_2] [NO_2]	5.90	Heterogeneous Loss	10.15	Advection/Diffusion
4.69	k_{95} [HO_2] [NO_2]	4.00	$2 \cdot k_{487}$ [NO] [NO_2]	10.13	k_{94} [OH] [NO_2]
4.06	$2 \cdot k_{487}$ [NO] [NO_2]	3.57	k_{100} [CH_3O_2] [NO_2]	9.95	$2 \cdot k_{487}$ [NO] [NO_2]
3.60	k_{86} [HO_2] [NO_2]	3.47	k_{95} [HO_2] [NO_2]	9.69	k_{263} [CO_3^-] [NO]
3.53	$2 \cdot k_{484}$ [NO_2] [NO_2]	3.29	$2 \cdot k_{484}$ [NO_2] [NO_2]	9.61	k_{92} [OH] [NO]
3.39	k_{94} [OH] [NO_2]	2.65	k_{26} [O_3] [NO_2]	9.59	k_{95} [HO_2] [NO_2]
...	58 More Reactions	...	58 More Reactions	...	58 More Reactions
5.108 = Log($\Sigma\Re$)		5.912 = Log($\Sigma\Re$)		10.750 = Log($\Sigma\Re$)	

c.) Summary of the lifetimes of NO_x in the inner domain of the three model runs.

	Log(χ)	Log(NO_x) cm^{-3}	Log($\Sigma\Re$) $cm^{-3} \cdot s^{-1}$	Log(τ) sec	Source Log(τ_c) sec	Sink Log(τ_c) sec
1-D Steady-State Model	−10.626	8.566	5.108	3.458	3.461	3.458
2-D Base Case Model	−10.680	8.512	5.912	2.600	4.264	4.214
2-D Electrified Model	−7.659	11.533	10.750	0.784	0.784	0.918

Note: $\tau = NO_x / \Sigma\Re$ or Log(τ) = Log(NO_x) − Log($\Sigma\Re$).

8.2.5.2 O_x

The differential net production of O_x is is 4.2×10^8 moles per year (per storm) and just as in the case of NO_x predominantly reflects a decrease in the rate of loss between the Base Case and the Electrified model runs. Because the majority of the O_x is O_3, the differential net production corresponds to an annual, global production of 20 $Tg \cdot year^{-1}$ of O_3. Just as in the case of NO_x, this level of production represents a lower limit because the net production of O_x is again a function of the assumed rate of heterogeneous loss.

8.2.5.3 HO_y

We now arrive at the most water soluble of the three chemical families considered here; the relatively small differential net production is a direct consequence of this solubility. In fact, differential net production is not particularly relevant for a water soluble family, as the members of the family are relatively quickly removed from the gas phase and are not expected to be transported any significant distance.

The aqueous phase concentrations of HO_y must be rather high for just as in the case of NO_x and O_x, there are exceedingly high gas-phase mixing ratios in the inner model domain. The aqueous phase concentration in the inner model domain can be estimated by multiplying the heterogeneous-loss rate (found in Table 16(b) to be $10^{9.45}$ $molec \cdot cm^{-3} \cdot s^{-1}$) by the lifetime of a cloud particle τ_R in the inner model domain (600 seconds *cf.* Figure 18, in Section 3.2.3, page 73) and dividing by the liquid water content M of the same region (6 g $H_2O\ m^{-3}$ *cf.* Figure 17). These calculations yield a result of 1×10^{19} molecules of HO_x per gram of liquid water. This corresponds to a solution 16 millimolar in HO_x, predominately H_2O_2.

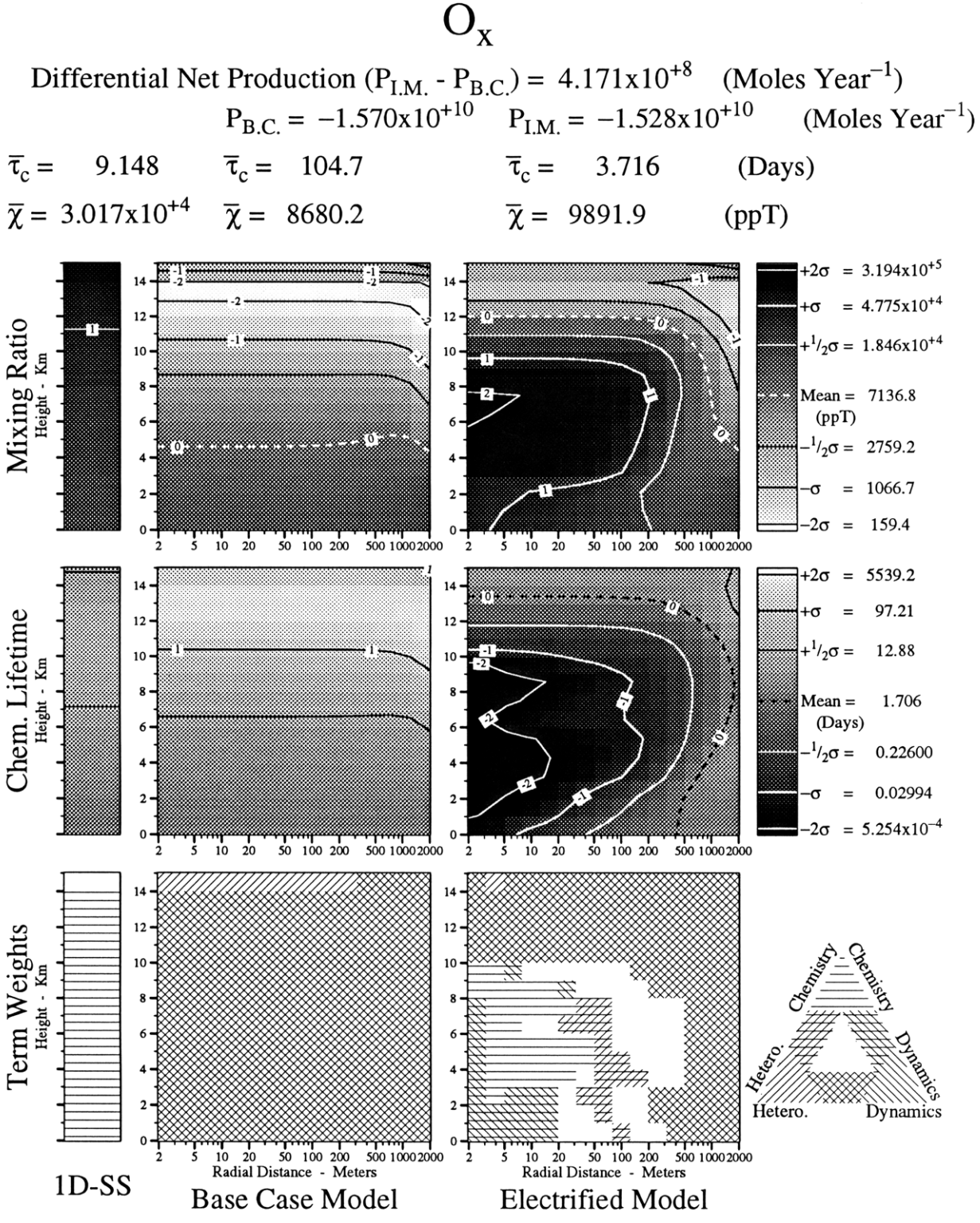

Figure 44. Mixing ratios (χ), lifetimes (τ_c), and term weights of O_x. See text for definitions of terms and other details.

Table 15. Summary of the chemistry of O_x in the **inner domain** of the three models. (**a,b**) The major terms in the continuity equations for O_x in the three model runs and (**c**) a summary of its mixing ratios χ and lifetimes τ in the three model runs. In these tables $\Re$ is the specific rate of production of O_x (molec·cm^{-3}·s^{-1}), τ is the total lifetime (sec) of O_x and τ_c is its lifetime due to chemical processes (sec). J_i, j_i, k_i, and l_i are photolytic, unimolecular, bimolecular and termolecular rate coefficients respectively for reaction number i as listed in Appendix B , page 184.

a.) The major source terms for O_x in the inner domain of the three model runs.

1-D Steady-State Model		2-D Base Case Model		2-D Electrified Model	
Log ($\Re$)	Reaction Rate $\Re = k_{yz}$ [y] [z]	Log ($\Re$)	Reaction Rate $\Re = k_{yz}$ [y] [z]	Log ($\Re$)	Reaction Rate $\Re = k_{yz}$ [y] [z]
5.91	J_7 [NO_2]	8.48	Advection/Diffusion	10.76	$2 \cdot J_{125}$ [O_2]
4.27	Advection/Diffusion	5.76	J_7 [NO_2]	9.98	k_{458} [N] [O_2]
3.18	J_8 [NO_3]	2.53	J_8 [NO_3]	9.43	k_{330} [N^+] [O_2]
1.39	k_{736} [SO] [O_2]	0.51	k_{736} [SO] [O_2]	9.42	k_{460} [N] [NO]
0.37	k_{796} [$CC\ell_3COO_2$] [HO_2]	0.24	k_{458} [N] [O_2]	9.36	j_{131} [O_2]
0.24	k_{458} [N] [O_2]	-0.44	k_{330} [N^+] [O_2]	9.32	k_{227} [O^+] [O_2]
...	101 More Reactions	...	101 More Reactions	...	101 More Reactions
5.919 = Log($\Sigma\Re$)		8.477 = Log($\Sigma\Re$)		10.911 = Log($\Sigma\Re$)	

b.) The major sink terms for O_x in the inner domain of the three model runs.

1-D Steady-State Model		2-D Base Case Model		2-D Electrified Model	
Log ($\Re$)	Reaction Rate $\Re = k_{yz}$ [y] {O_x}	Log ($\Re$)	Reaction Rate $\Re = k_{yz}$ [y] {O_x}	Log ($\Re$)	Reaction Rate $\Re = k_{yz}$ [y] {O_x}
5.76	k_{25} [O_3] [NO]	8.48	Heterogeneous Loss	10.76	Advection/Diffusion
5.05	Heterogeneous Loss	5.47	k_{25} [O_3] [NO]	10.09	k_{258} [CO_4^-] [O_3]
4.87	k_{54} [HO_2] [O_3]	4.45	k_{135} [$O(^1D)$] [H_2O]	9.67	k_{302} [NO_2^-] [O_3]
4.78	k_{135} [$O(^1D)$] [H_2O]	3.36	k_{54} [HO_2] [O_3]	9.64	Heterogeneous Loss
4.02	k_{52} [OH] [O_3]	2.91	k_{52} [OH] [O_3]	9.39	k_{25} [O_3] [NO]
3.06	k_{26} [O_3] [NO_2]	2.65	k_{26} [O_3] [NO_2]	8.45	k_{52} [OH] [O_3]
...	122 More Reactions	...	122 More Reactions	...	122 More Reactions
5.919 = Log($\Sigma\Re$)		8.477 = Log($\Sigma\Re$)		10.911 = Log($\Sigma\Re$)	

c.) Summary of the lifetimes of O_x in the inner domain of the three model runs.

	Log(χ)	Log(O_x) cm^{-3}	Log($\Sigma\Re$) $cm^{-3} \cdot s^{-1}$	Log(τ) sec	Source Log(τ_c) sec	Sink Log(τ_c) sec
1-D Steady-State Model	−7.628	11.564	5.919	5.645	5.654	5.707
2-D Base Case Model	−8.105	11.087	8.477	2.610	5.326	5.576
2-D Electrified Model	−6.964	12.228	10.911	1.317	1.317	1.928

Note: $\tau = O_x / \Sigma\Re$ or $\text{Log}(\tau) = \text{Log}(O_x) - \text{Log}(\Sigma\Re)$.

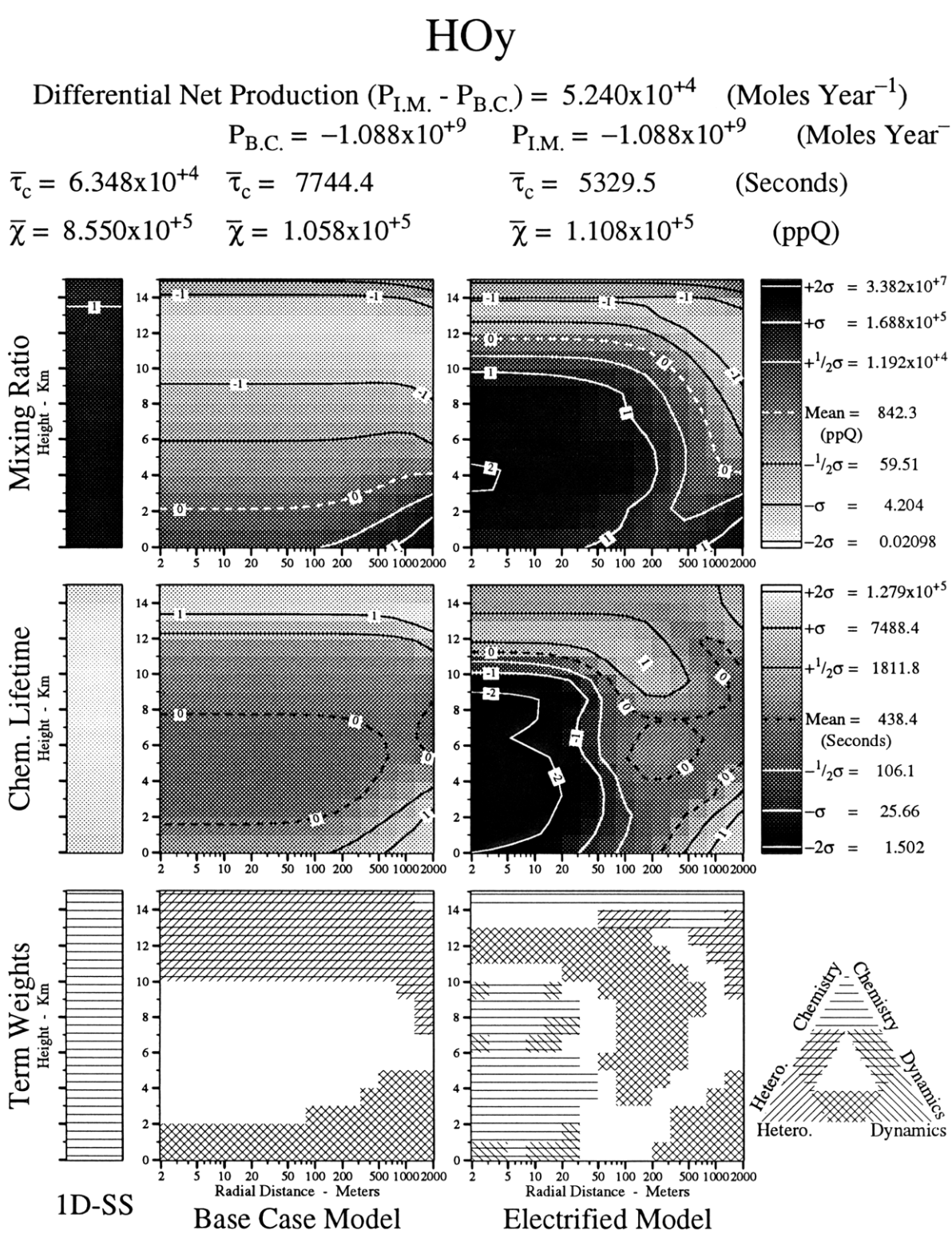

Figure 45. Mixing ratios (χ), lifetimes (τ_c), and term weights of HO_y. See text for definitions of terms and other details.

Table 16. Summary of the chemistry of HO_y in the **inner domain** of the three models. (**a,b**) The major terms in the continuity equations for HO_y in the three model runs and (**c**) a summary of its mixing ratios χ and lifetimes τ in the three model runs. In these tables $\Re$ is the specific rate of production of HO_y (molec·cm^{-3}·s^{-1}), τ is the total lifetime (sec) of HO_y and τ_c is its lifetime due to chemical processes (sec). J_i, j_i, k_i, and l_i are photolytic, unimolecular, bimolecular and termolecular rate coefficients respectively for reaction number i as listed in Appendix B , page 184.

a.) The major source terms for HO_y in the inner domain of the three model runs.

1-D Steady-State Model		2-D Base Case Model		2-D Electrified Model	
Log ($\Re$)	Reaction Rate $\Re = k_{yz}$ [y] [z]	Log ($\Re$)	Reaction Rate $\Re = k_{yz}$ [y] [z]	Log ($\Re$)	Reaction Rate $\Re = k_{yz}$ [y] [z]
5.08	$2{\cdot}k_{135}$ [$O(^1D)$] [H_2O]	5.48	Advection/Diffusion	10.58	k_{280} [O_2^-] [H_2O]
4.84	k_{582} [CH_3O] [O_2]	4.75	$2{\cdot}k_{135}$ [$O(^1D)$] [H_2O]	10.22	k_{358} [OHH_3O^+] [H_2O]
4.70	k_{640} [CHO] [O_2]	3.71	k_{582} [CH_3O] [O_2]	9.92	k_{341} [H_2O^+] [H_2O]
4.49	J_{13} [CH_2O]	3.16	k_{674} [CH_3SOHCH_3] [O_2]	9.18	k_{347} [$W_2H_3O^+$] [e^-]
4.37	j_{608} [CH_2OOH]	3.12	k_{640} [CHO] [O_2]	8.46	k_{426} [HCO_3^-]{PosIon}
4.00	J_{11} [CH_3OOH]	3.05	J_{13} [CH_2O]	8.42	$2{\cdot}k_{135}$ [$O(^1D)$] [H_2O]
...	127 More Reactions	...	127 More Reactions	...	127 More Reactions
5.508 = Log($\Sigma\Re$)		5.568 = Log($\Sigma\Re$)		10.815 = Log($\Sigma\Re$)	

Notes: Read **W** as H_2O. The definitions of the reactive families $\{X\}$ are at the end of Appendix B.

b.) The major sink terms for HO_y in the inner domain of the three model runs.

1-D Steady-State Model		2-D Base Case Model		2-D Electrified Model	
Log ($\Re$)	Reaction Rate $\Re = k_{yz}$ [y] {HO_y}	Log ($\Re$)	Reaction Rate $\Re = k_{yz}$ [y] {HO_y}	Log ($\Re$)	Reaction Rate $\Re = k_{yz}$ [y] {HO_y}
5.02	k_{556} [CH_4] [OH]	5.54	Heterogeneous Loss	10.50	$2{\cdot}k_{31}$ [OH] [HO_2]
4.75	k_{589} [CH_3O_2] [HO_2]	4.26	k_{556} [CH_4] [OH]	10.13	k_{94} [OH] [NO_2]
4.37	k_{607} [CH_3OOH] [OH]	3.16	k_{668} [DMS] [OH]	9.74	k_{68} [OH] [HONO]
4.32	Heterogeneous Loss	2.65	k_{669} [DMS] [OH]	9.61	k_{92} [OH] [NO]
4.31	$2{\cdot}k_{56}$ [OH] [H_2O_2]	2.57	k_{94} [OH] [NO_2]	9.58	Advection/Diffusion
4.30	k_{633} [CH_2O] [OH]	2.54	k_{589} [CH_3O_2] [HO_2]	9.45	Heterogeneous Loss
...	105 More Reactions	...	105 More Reactions	...	105 More Reactions
5.508 = Log($\Sigma\Re$)		5.568 = Log($\Sigma\Re$)		10.815 = Log($\Sigma\Re$)	

c.) Summary of the lifetimes of HO_y in the inner domain of the three model runs.

	Log(χ)	Log(HO_y) cm^{-3}	Log($\Sigma\Re$) $cm^{-3}{\cdot}s^{-1}$	Log(τ) sec	Source Log(τ_c) sec	Sink Log(τ_c) sec
1-D Steady-State Model	−8.990	10.202	5.508	4.694	4.694	4.748
2-D Base Case Model	−12.196	6.996	5.568	1.428	2.178	2.651
2-D Electrified Model	−8.416	10.775	10.815	−0.040	−0.040	0.007

Note: $\tau = HO_y / \Sigma\Re$ or Log(τ) = Log(HO_y) − Log($\Sigma\Re$).

8.2.6 Long-Lived Species

The long lived species (τ_c > 1yr) can generally be into two groups, those that react with OH (*e.g.* CH_4, CO, and OCS) and those that do not (*e.g.* SF_6, CF_4, and N_2O). I now discuss the species that react with OH as a group, using CH_4 as a typical example and then I discuss those compounds that do not react with OH, using SF_6 as an example.

8.2.6.1 Species That React With OH

The long-lived atmospheric species that react (relatively) rapidly with OH have similar in-cloud-loss processes and very long heterogeneous lifetimes. Unlike the chemical families of discussed earlier, these compounds are generally considered completely insoluble in water and hence the dominant balancing terms of the continuity equations for these species are chemical loss and transport (into the loss region). Although there are very high mixing ratios of OH in the inner model domain of the Electrified model run, the dynamic lifetimes are very small compared the the chemical lifetimes in this region and consequently most of the molecules (of CH_4) "survive" the transit through the inner model domain. This is reflected by the very slight decrease in the mixing ratio of CH_4 in the innermost model domain of the Electrified model run.

8.2.6.2 Species That Do Not React With OH

I now discuss those that do not react with OH. The compounds in this model that do not react with OH generally react with electrons or ions. Because these charged species are co-located with the high OH production regions the considerations given for the species that react with OH are applicable here as well. The exceedingly long tropospheric chemical lifetimes shown for SF_6 indicate that electrified convection is probably not a dominant sink

of these compounds.

For comparison of the overall loss rates of SF_6, I a 1-D model of SF_6 loss above the model domain was carried out. In this model, detailed in Appendix E , page 275, electron impact upon SF_6 at altitudes above 100km, where there are high electron densities ($> 100\ cm^{-3}$) does not destroy significant quantities of SF_6. This implies that if SF_6 has any photolysis loss at lower altitudes, then this photolysis is probably the dominant loss mechanism.

CH_4

Differential Net Production ($P_{I.M.}$ - $P_{B.C.}$) = −452.6 (Mg Year^{-1})

	$P_{B.C.}$ = −433.7	$P_{I.M.}$ = −886.3 (Mg Year^{-1})
$\overline{\tau}_c$ = 22.87	$\overline{\tau}_c$ = 1.068x10^{+5}	$\overline{\tau}_c$ = 1.526x10^{+4} (Years)
$\overline{\chi}$ = 2331.2	$\overline{\chi}$ = 2338.5	$\overline{\chi}$ = 2338.5 (ppB)

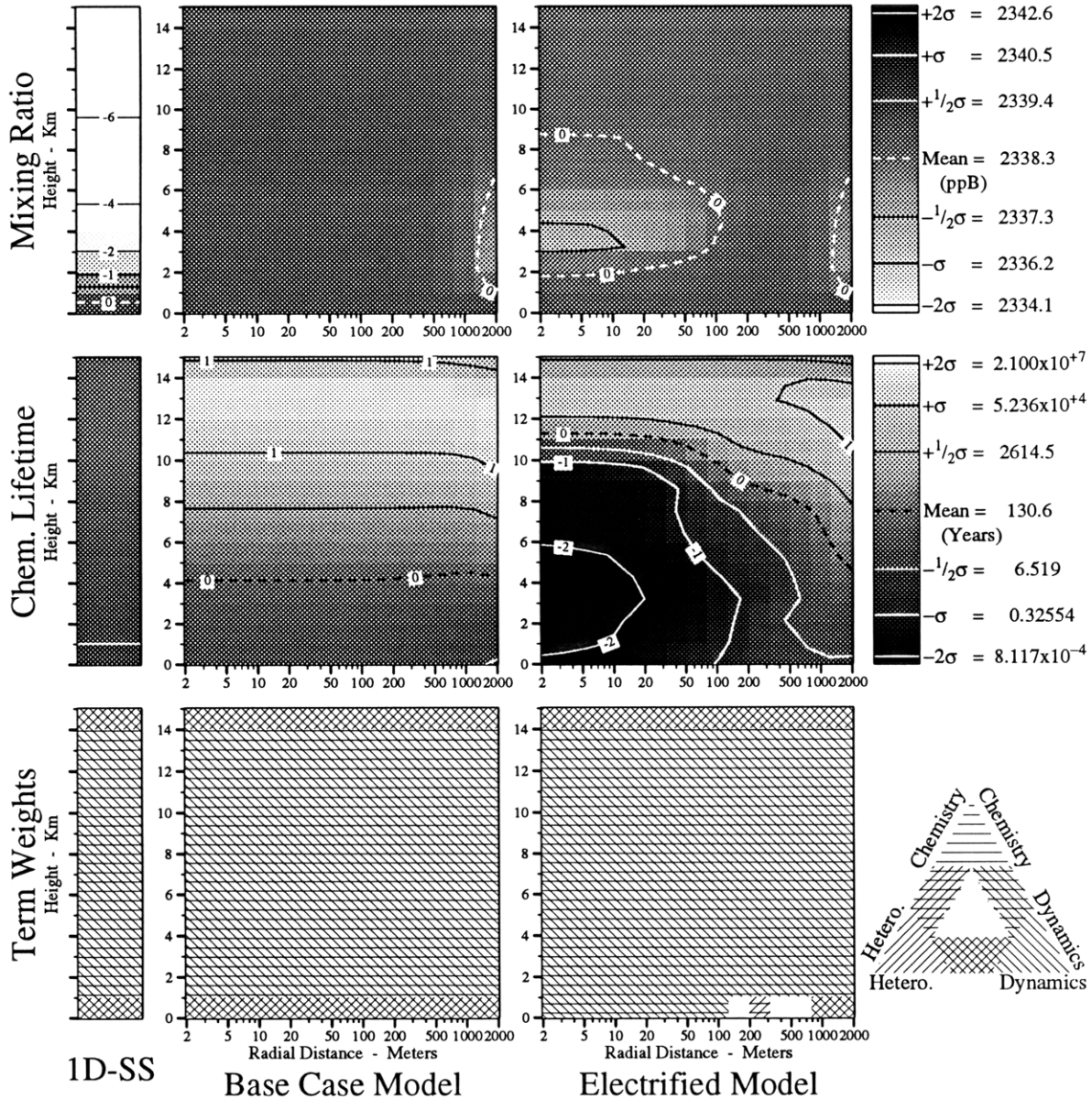

Figure 46. Mixing ratios (χ), lifetimes (τ_c), and term weights of CH_4. See text for definitions of terms and other details.

Table 17. Summary of the chemistry of CH_4 in the **inner domain** of the three models. (**a,b**) The major terms in the continuity equations for CH_4 in the three model runs and (**c**) a summary of its mixing ratios χ and lifetimes τ in the three model runs. In these tables $\Re$ is the specific rate of production of CH_4 (molec·cm^{-3}·s^{-1}), τ is the total lifetime (sec) of CH_4 and τ_c is its lifetime due to chemical processes (sec). J_i, j_i, k_i, and l_i are photolytic, unimolecular, bimolecular and termolecular rate coefficients respectively for reaction number i as listed in Appendix B , page 184.

a.) The major source terms for CH_4 in the inner domain of the three model runs.

1-D Steady-State Model		2-D Base Case Model		2-D Electrified Model	
Log ($\Re$)	Reaction Rate $\Re = k_{yz}$ [y] [z]	Log ($\Re$)	Reaction Rate $\Re = k_{yz}$ [y] [z]	Log ($\Re$)	Reaction Rate $\Re = k_{yz}$ [y] [z]
5.02	Advection/Diffusion	4.26	Advection/Diffusion	8.64	Advection/Diffusion
-4.70	k_{568} [CH_3] [HO_2]	-6.47	k_{568} [CH_3] [HO_2]	1.49	k_{568} [CH_3] [HO_2]
-4.86	k_{570} [CH_3] [H_2O_2]	-8.88	k_{570} [CH_3] [H_2O_2]	-0.73	k_{570} [CH_3] [H_2O_2]
-9.00	k_{566} [CH_3] [H_2]	-9.65	k_{566} [CH_3] [H_2]	-2.39	k_{106} [H] [CH_3]
-9.81	k_{704} [CH_3] [H_2S]	-10.74	k_{704} [CH_3] [H_2S]	-5.00	k_{677} [CH_3SH] [O]
-9.91	k_{677} [CH_3SH] [O]	-11.16	k_{677} [CH_3SH] [O]	-5.43	k_{566} [CH_3] [H_2]
...	5 More Reactions	...	5 More Reactions	...	5 More Reactions
5.017 = Log($\Sigma\Re$)		4.261 = Log($\Sigma\Re$)		8.644 = Log($\Sigma\Re$)	

b.) The major sink terms for CH_4 in the inner domain of the three model runs.
The reaction rate $\Re$ implicitly contains [CH_4].

1-D Steady-State Model		2-D Base Case Model		2-D Electrified Model	
Log ($\Re$)	Reaction Rate $\Re = k_{yz}$ [y] [CH_4]	Log ($\Re$)	Reaction Rate $\Re = k_{yz}$ [y] [CH_4]	Log ($\Re$)	Reaction Rate $\Re = k_{yz}$ [y] [CH_4]
5.02	k_{556} [OH]	4.26	k_{556} [OH]	8.64	k_{556} [OH]
1.51	k_{555} [$O(^1D)$]	1.01	k_{555} [$O(^1D)$]	5.63	k_{825} [$C\ell$]
1.04	k_{825} [$C\ell$]	0.01	k_{554} [$O(^1D)$]	4.94	k_{555} [$O(^1D)$]
0.51	k_{554} [$O(^1D)$]	-0.46	k_{825} [$C\ell$]	3.94	k_{554} [$O(^1D)$]
-0.20	k_{560} [O]	-0.57	k_{560} [O]	3.01	k_{560} [O]
-1.36	k_{559} [O]	-1.70	k_{559} [O]	2.59	k_{833} [$C\ell O$]
...	14 More Reactions	...	14 More Reactions	...	14 More Reactions
5.017 = Log($\Sigma\Re$)		4.261 = Log($\Sigma\Re$)		8.644 = Log($\Sigma\Re$)	

c.) Summary of the lifetimes of CH_4 in the inner domain of the three model runs.

	Log(χ)	Log([CH_4]) cm^{-3}	Log($\Sigma\Re$) cm^{-3}·s^{-1}	Log(τ) sec	Source Log(τ_c) sec	Sink Log(τ_c) sec
1-D Steady-State Model	−5.632	13.560	5.017	8.542	18.027	8.542
2-D Base Case Model	−5.631	13.561	4.261	9.300	20.025	9.300
2-D Electrified Model	−5.631	13.561	8.644	4.916	12.064	4.916

Note: τ = [CH_4] / $\Sigma\Re$ or Log(τ) = Log([CH_4]) − Log($\Sigma\Re$).

SF_6

Differential Net Production ($P_{I.M.}$ - $P_{B.C.}$) = −17.45 (Kg Year^{-1})

$P_{B.C.}$ = −0.04723 $P_{I.M.}$ = −17.49 (Kg Year^{-1})

$\overline{\tau}_c$ = 6.507x10^{+5} $\overline{\tau}_c$ = 6.057x10^{+5} $\overline{\tau}_c$ = 3.483x10^{+5} (Years)

$\overline{\chi}$ = 504.3 $\overline{\chi}$ = 504.5 $\overline{\chi}$ = 504.2 (ppQ)

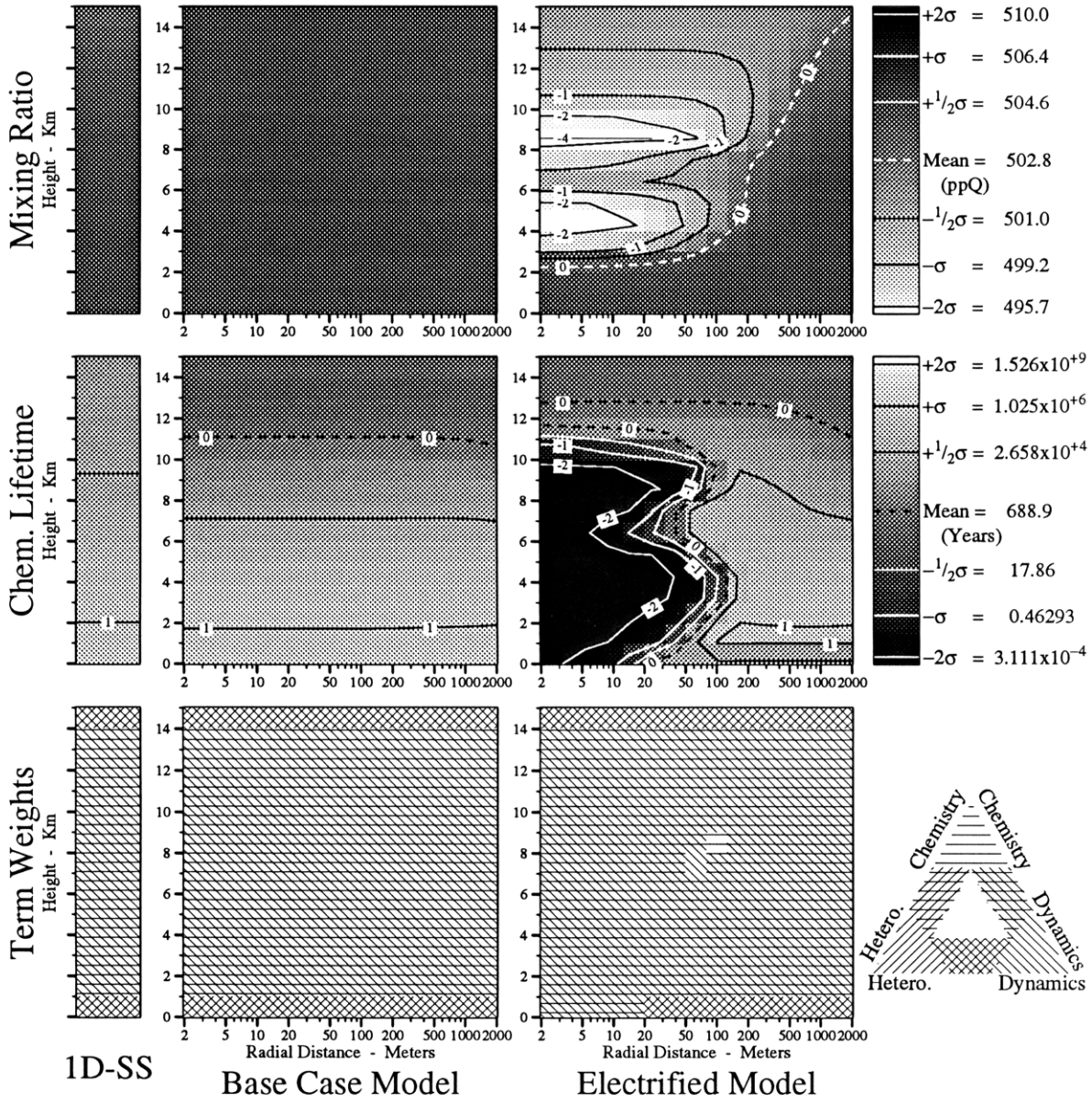

Figure 47. Mixing ratios (χ), lifetimes (τ_c), and term weights of SF_6. See text for definitions of terms and other details.

Table 18. Summary of the chemistry of SF_6 in the **inner domain** of the three models. (**a,b**) The major terms in the continuity equations for SF_6 in the three model runs and (**c**) a summary of its mixing ratios χ and lifetimes τ in the three model runs. In these tables $\Re$ is the specific rate of production of SF_6 (molec·cm^{-3}·s^{-1}), τ is the total lifetime (sec) of SF_6 and τ_c is its lifetime due to chemical processes (sec). J_i, j_i, k_i, and l_i are photolytic, unimolecular, bimolecular and termolecular rate coefficients respectively for reaction number i as listed in Appendix B , page 184.

a.) The major source terms for SF_6 in the inner domain of the three model runs.

1-D Steady-State Model		2-D Base Case Model		2-D Electrified Model	
Log ($\Re$)	Reaction Rate $\Re = k_{yz}\,[y]\,[z]$	Log ($\Re$)	Reaction Rate $\Re = k_{yz}\,[y]\,[z]$	Log ($\Re$)	Reaction Rate $\Re = k_{yz}\,[y]\,[z]$
-5.79	Advection/Diffusion	-5.30	Advection/Diffusion	3.38	Advection/Diffusion
$-\infty$	Flux	$-\infty$	Flux	$-\infty$	Flux
-5.788 = Log($\Sigma\Re$)		-5.299 = Log($\Sigma\Re$)		3.382 = Log($\Sigma\Re$)	

b.) The major sink terms for SF_6 in the inner domain of the three model runs.
The reaction rate $\Re$ implicitly contains [SF_6].

1-D Steady-State Model		2-D Base Case Model		2-D Electrified Model	
Log ($\Re$)	Reaction Rate $\Re = k_{yz}\,[y]\,[SF_6]$	Log ($\Re$)	Reaction Rate $\Re = k_{yz}\,[y]\,[SF_6]$	Log ($\Re$)	Reaction Rate $\Re = k_{yz}\,[y]\,[SF_6]$
-5.79	$k_{200}\,[CO_4^-]$	-5.30	$k_{200}\,[CO_4^-]$	3.38	$k_{200}\,[CO_4^-]$
-8.81	$k_{197}\,[O_4^-]$	-8.41	$k_{197}\,[O_4^-]$	0.59	$k_{197}\,[O_4^-]$
-9.97	$k_{194}\,[O_2^-]$	-9.78	$k_{194}\,[O_2^-]$	-0.23	$k_{194}\,[O_2^-]$
-10.44	$k_{188}\,[e^-]$	-10.44	$k_{188}\,[e^-]$	-0.26	$k_{188}\,[e^-]$
-11.52	j_{120}	-11.52	j_{120}	-4.51	$k_{206}\,[H^-]$
-17.44	$k_{203}\,[O^-]$	-18.20	$k_{203}\,[O^-]$	-6.41	$k_{189}\,[e^-]$
-19.70	$k_{206}\,[H^-]$	-21.31	$k_{206}\,[H^-]$	-6.65	$k_{203}\,[O^-]$
$-\infty$	Deposition	$-\infty$	Deposition	-11.52	j_{120}
$-\infty$	Heterogeneous Loss	$-\infty$	Heterogeneous Loss	$-\infty$	Heterogeneous Loss
...	2 More Reactions	...	2 More Reactions	...	2 More Reactions
-5.788 = Log($\Sigma\Re$)		-5.299 = Log($\Sigma\Re$)		3.382 = Log($\Sigma\Re$)	

c.) Summary of the lifetimes of SF_6 in the inner domain of the three model runs.

	Log(χ)	Log([SF_6]) cm^{-3}	Log($\Sigma\Re$) $cm^{-3}\cdot s^{-1}$	Log(τ) sec	Source Log(τ_c) sec	Sink Log(τ_c) sec
1-D Steady-State Model	−12.297	6.895	−5.788	12.683	+∞	12.683
2-D Base Case Model	−12.297	6.895	−5.299	12.193	+∞	12.193
2-D Electrified Model	−12.301	6.891	3.382	3.509	+∞	3.509

Note: $\tau = [SF_6] / \Sigma\Re$ or $\text{Log}(\tau) = \text{Log}([SF_6]) - \text{Log}(\Sigma\Re)$.

8.3 Global *vs.* Local Influences

To see the regions where lightning is the dominant chemical influence in the region, we chose NO_x as a representative family. The global lightning-induced source strength of NO_x has been estimated by *Chameides et al.* [1987] to be 7 Tg N·yr^{-1} ($\pm$ a factor of 3). *Borucki & Chameides* [1984] reviewed various estimates of the global source strengths of lightning produced NO and estimated it to be 3 Tg N·yr^{-1}. I will therefore use a value of 5 Tg N·yr^{-1} as the global lightning production rate. Assuming 70% of all lightning occurs over land (*cf. Orville & Henderson*, 1986), these data correspond to a terrestrial production rate of 2.9×10^{19} molecules km^{-2} sec^{-1} and an oceanic production rate of 5.3×10^{18} molecules km^{-2} sec^{-1}.

The total anthropogenic NO_x production has been estimated to be 33 Tg N·yr^{-1} (*Logan*, 1983). Given that the Northern Hemisphere has twice as much land as the Southern Hemisphere and $\approx 75\%$ of the anthropogenic NO_x emissions, the anthropogenic NO_x emission rate over land is 9.1×10^{19} molecules km^{-2} sec^{-1} in the Northern Hemisphere and 6.1×10^{19} molecules km^{-2} sec^{-1} in the Southern Hemisphere.

I now seek to compute at what distance from a thunderstorm (on average) the relative strengths of the continental, anthropogenic sources of NO equal lightning sources. We can adopt an approach parallel to that given by *Fay & Rosenzweig* [1980] and consider an industrialized region (or a thunderstorm) as a vertical line source. The equation governing the steady state concentration of a reactive material is then given by

$$\vec{V} \cdot \nabla C = D_h \nabla^2 \cdot C - \frac{C}{\tau_{\text{net}}} \quad , \tag{72}$$

where $\vec{V}$ is the mean wind, D_h is the horizontal diffusivity, τ_{net} is the loss-rate constant, and C is the concentration of the material in question. In our case, we have two sources of

C, lightning and anthropogenic activity. The solution to equation 72 is given as

$$C = \frac{Q}{2\pi h D_h} \exp\left(\frac{wx}{2D_h}\right) K_0\left(r\left[\frac{1}{D_h \tau_{\text{net}}} + \left(\frac{w}{2D_h}\right)^2\right]^{\frac{1}{2}}\right) \quad , \tag{73}$$

where Q is the emission rate, w is the mean wind speed, x is the x axis (aligned in the direction of the mean wind), $K_0(-)$ is the Modified Bessel function of the 0^{th} order, r is the radial distance from the line source, and h = the height of the mixed layer.

Proceeding as in *Prinn* [1986] we may identify the "sphere of influence" with the $1/10^{th}$ folding distance given as

$$L = \ln\left(\frac{1}{10}\right)\left(\frac{\partial \ln C}{\partial r}\right)^{-1} \tag{74}$$

Solving equation 3 with the following numerical values: $D_h = 5\times10^5$ m^2 sec^{-1}; h = 2 km; τ_{net} = 2 days; C_o(x = 100km,y=0km) = 1; and w = 3 m sec^{-1} from 270^o yields Figure 48. As seen in this figure, the "sphere of influence" of a stationary source is of the order of 1000km in the downwind direction, 500 km in the cross-wind direction and 300 km in the upwind direction.

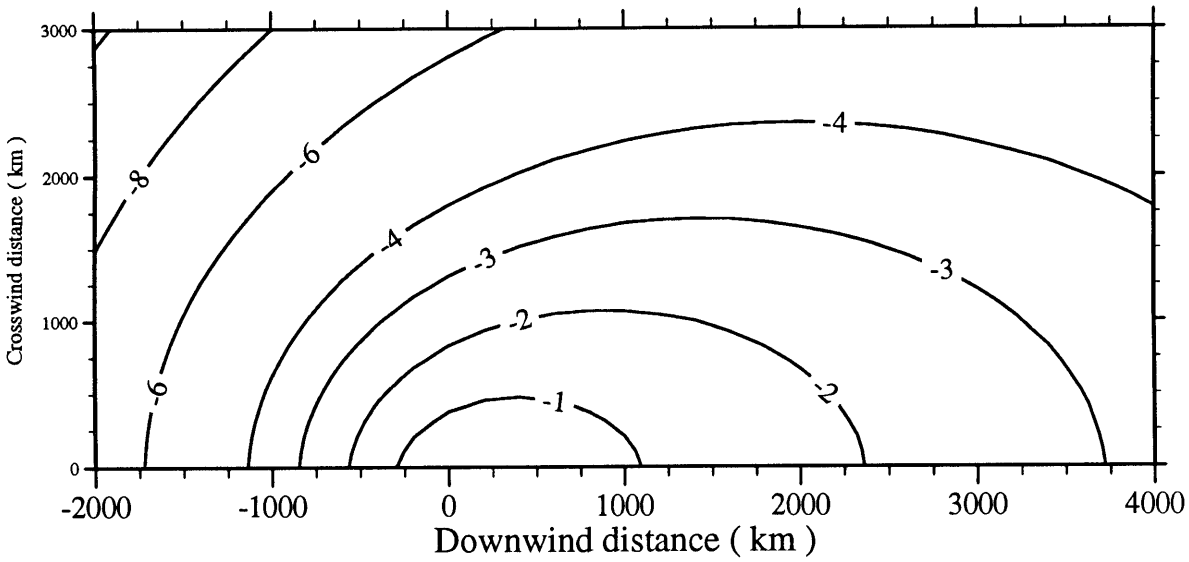

Figure 48. Sphere of influence of a stationary source. This figure shows the spatial distribution of $\mathrm{Log}_{10}\left(C(x,y)/C(0,0)\right)$. A point 1000km directly downwind of a stationary source would have the average concentration 1/10 that of a point co-located with the source.

9 Conclusions and Summary

We began with the observation that the electric fields and plasma surrounding regions of the dielectric breakdown of air (lightning) result in high ion and electron production rates ($> 10^{10}$ $m^{-3} \cdot s^{-1}$). In addition, the high temperatures in the lightning channel ($\approx$ 30,000 K) release large amounts of short wavelength UV radiation.

To examine the resulting ion, electron, and photon reactions, a detailed chemical, but crude dynamical and microphysical model of electrified convection has been developed. This model considered more than 800 reactions among 165 neutrals, ions, water clusters, and the electron; the pressure, temperature and electric field effects upon the reaction coefficients were explicitly considered. This model represents the first effort to model the physical phenomena involved in lightning and corona production, the subsequent chemical reactions, and to quantify these reactions' integrated effects on the chemistry of electrified convection.

The influence of the ion and UV generation mechanisms is pronounced on species such as O_3, where the average mixing ratio increased from 20 ppb in the Base Case run to 100 ppb in the Electrified Case. Locally, even greater increases were noted for many species: the maximum OH mixing ratio rose by 5 orders of magnitude from 5×10^{-5}ppb to 5 ppb near the maximum ion production regions.

The model-domain-averaged effect of lightning on the highly soluble chemical families such as HO_x, is relatively small because of high in-cloud scavenging rates that mask locally-high rates of production. For example, the model-domain-average concentration of HO_x changes by less than 2% between the two model runs (Base Case & Electrified) yet the maximum HO_x mixing ratios in the main ionization regions of the Electrified model are 4 orders of magnitude larger than in the Base Case model run.

In general, the ion and UV-induced reactions contribute equally to the production of both $O(^3P)$ and $O(^1D)$ and consequently are equally important in the overall chemistry of O_3 and OH and other derivative chemical species. Ion processes dominate the production of both the neutral N (and consequently its derivative species, *e.g.* NO) as well as charged species such as O_2^+, O_4^+, N_2^+, N_4^+, and the ions that ultimately derive from them, primarily water clusters $H_3O^+ \cdot (H_2O)_n$.

The Electrified model produces a net loss process for some chemical species, primarily due to enhanced in-cloud OH levels. On a global basis this model accounts for the annual destruction of 1.8 Tg of CO, 0.45 Tg of CH_4, and 2×10^{-4} Tg of OCS. Once again, these are small fractions of the currently estimated annual source strengths of these species (1600 Tg CO, 525 Tg CH_4, and 0.4 Tg OCS).

Although the global budgets of the major chemical families and compounds are not greatly affected by electrified convection, the meso-scale flows in which the thunderstorms are embedded certainly are affected to a greater or lesser extent depending on the assumptions regarding the loss rate of sparingly soluble species in the outflow. While the high rates of anthropogenic NO_x production dominate the budget of NO_x near urban areas where NO_x levels can exceed 200 ppb (*Warneck*, 1988), in the remote troposphere where levels of NO_x are generally $\approx$ 30 ppt (*Noxon*, 1981 & 1983), lightning (and stratospheric injection) can dominate the NO_x budget.

In addition to the meso-scale effects of the thunderstorm outflow, The electric-field-driven capture of ions and the heterogeneous loss of neutrals to cloud particles greatly alters the normal aqueous-phase chemistry of clouds, although this model does not accurately quantify the extent of this perturbation. Nevertheless, high levels (millimolar concentrations) of water-soluble oxidants such as H_2O_2 can reasonably be expected to occur

in the vicinity of active in-cloud corona and lightning.

The quantities of almost all chemical species formed in the cooling hot channel are of little importance when compared with the corresponding quantities formed in the surrounding regions. The only exception is NO_x; while the local mixing ratios of NO and NO_2 can approach 0.01 in the cooled lightning channel, the relatively small volume of the hot lightning channel ($\approx$ 10 m^3) compared to the much larger volume of air surrounding the channel dominated by ion chemistry ($\approx 5 \times 10^7$ m^3) results in $\approx$ 50% of the in-cloud production of NO_x coming from the hot channel. The ion-induced processes occurring in the regions surrounding the lightning channel dominate the production or loss of all other species and chemical families (*e.g.* N_2O, O_x, HO_y).

For the cases of CF_4, SF_6, and $CC\ell_4$ their in-cloud lifetimes are reduced by a factor of $\approx$ 10,000 from their base case tropospheric chemical lifetimes of 2.6×10^6, 2.6×10^4, 1.0×10^4 years respectively. Given the small fraction of the Earth's atmosphere that is in electrified convection ($\approx 6 \times 10^{-4}$), this in-cloud loss reduces their overall tropospheric chemical lifetime by a factor of two. Consequently, these ionic reactions cannot compete with other known loss mechanisms, such as stratospheric or mesospheric photodissociation and electron impact that result in these gases having global lifetimes estimated to be of order centuries for CF_4 and SF_6, and decades for $CC\ell_4$.

References

Atkinson, R., Kinetics and mechanism of the gas-phase reactions of the hydroxyl radical with organic compounds under atmospheric conditions, *Chemical Reviews*, **85**, pp 69 – 201, 1986.

Atkinson, R., D. L. Baulch, R. A. Cox, R. F. Hampson, Jr., J. A. Kerr, and J. Troe, Evaluated kinetic and photochemical data for atmospheric chemistry: supplement III, *J. Physical Chemistry Ref. Data,* **18**, pp 881 – 917, 1989.

Barshay, S. S., and J. S. Lewis, Chemical structure of the deep atmosphere of Jupiter, *Icarus*, **33**, pp 593 – 611, 1978.

Baulch, D. L., D. D. Drysdale, D. G. Horne, and A. C. Lloyd, *Evaluated kinetic data for high temperature reactions.*, Volumes 1, 2 and 3, C.R.C. Press, 1972.

Borucki, W., W. L. Chameides, Lightning: Estimates of the rates of energy dissipation and nitrogen fixation. *Rev. Geophysics and Space Physics* **22-4**, pp 363 – 372, 1984.

Breitbarth, F. W., H. J. Tiller, and R. Reinhardt, Plasma-chemical reactions in weakly decomposed $CC\ell_4$., *Plasma Chemistry and Plasma Processing*, **5**, No. 4 pp 293 – 316, 1985.

Byrne, G. J., A. A. Few, and M. E. Weber, Altitude, thickness and charge concentration of charged regions of four thunderstorms during TRIP 1981 based upon *in situ* balloon electric field measurements. *Geophys. Res. Letters,* **10**, No. 1, pp 39 – 42, 1983.

Chameides, W. L., The implications of CO production in electrical discharges. *Geophys. Res. Letters,* **6**, No. 4, pp 287 – 290, 1979.

Chameides, W. L., and D. D. Davis, The free radical chemistry of cloud droplets and its impact upon the composition of rain, *J. Geophys. Res.,* **87**, No. C7, pp 4863 – 4877, 1982.

Chameides, W. L., D. D. Davis, M. O. Rogers, J. Bradshaw, S. Sandholm, and D. B. Bai, An estimate of the NO_x production rate in electrified clouds based on NO observations from the GTE/CITE 1 observations during fall 1983. *J. Geophys. Res.,* **92**, No. D2, pp 2153 – 2172, 1987.

Chameides, W. L., D. H. Stedman, R. R. Dickerson, D. W. Rusch, and R. J. Cicerone, NO_x production in lightning *J. Atmos. Sciences,* **34**, pp 143 – 149, 1977.

Christophorou, L. G., Electron attachment to molecules in dense gases ("quasi-liquids"), *Chemical Reviews*, **76**, No. 4, 1976.

References

Dalgarno, A., Atmospheric reactions with energetic particles, in *Space Research*, **VII**, pp. 849 – 861, North Holland Publishing Co., Amsterdam, 1967.

Dawson, G. A., Nitrogen fixation by lightning, *J. Atmos. Sciences,* **37**, pp 174 – 178, 1980.

DeMore, W. B., J. J. Margitan, M. J. Molina, R. T. Watson, D. M. Golden, R. F. Hampson, M. J. Kurylo, C. J. Howard, A. R. Ravishankara, Chemical kinetics and photochemical data for use in stratospheric modeling, Evaluation Number 7, NASA & JPL, JPL Publication 85-37, 1985.

DeMore, W. B., M. J. Molina, S. P. Sander, D. M. Golden, R. F. Hampson, M. J. Kurylo, C. J. Howard, A. R. Ravishankara, Chemical kinetics and photochemical data for use in stratospheric modeling, NASA & JPL, JPL Publication 87-41, 1987.

Dickerson, R. R., G. J. Huffman, W. T. Luke, L. J. Nunnermacker, K. E. Pickering, A. C. D. Leslie, C. G. Lindsey, W. G. N. Slinn, T. J. Kelly, P. H. Daum, A. C. Delany, J. P. Greenberg, P. R. Zimmerman, J. F. Boatman, J. D. Ray, and D. H. Stedman, Thunderstorms: an important mechanism in the transport of air pollutants, *Science*, **235**, pp 460 – 465, 1987.

Donahue, N. M., and R. G. Prinn, Nonmethane hydrocarbon chemistry in the remote marine atmosphere, *J. Geophys. Res.*, **95**, No. D11, pp 18,387 – 18,411, 1990.

Eisele, F. L., Identification of tropospheric ions. *J. Geophys. Res.*, **91** No. D7, pp 7897 – 7906, 1986.

Eisele, F. L., First tandem mass spectrometric measurement of troposheric ions. *J. Geophys. Res.*, **93**, No. D1, pp 716 – 724, 1988.

Eisele, F. L., and E. W. McDaniel, Mass spectrometric study of tropospheric ions in the northeast and southwest United States. *J. Geophys. Res.*, **91**, No. D4, pp 5183 – 5188, 1986.

Fay, J. A., and J. J. Rosenzweig, An analytical diffusion model for long distance transport of air pollutants. *Atmospheric Environment*, **14**, pp 355 - 365. 1980.

Fegley, B. Jr., and R. G. Prinn, Equilibrium and nonequilibrium chemistry of Saturn's atmosphere: implications for the observability of PH_3, N_2, CO, and GeH_4, *The Astrophysical Journal*, **299**, pp 1067 – 1078, 1985.

Fehsenfeld, F. C. and E. E. Ferguson, Laboratory studies of negative ion reactions with atmospheric trace constituents, *J. Chemical Physics,* **61**, No. 8, pp 3181 –3193, 1974.

Fels, S. B., Analytic representations of standard atmosphere temperature profiles, *J. Atmos. Sciences,* **43**, No. 2, pp 219 – 221, 1986.

References

Franzblau, E., and C. J. Popp, Nitrogen oxides produced from lightning, *J. Geophys. Res.*, **94**, No. D8, pp 11,089 – 11,104, 1989.

Fuchs, N. A. and A. G. Sutugin, High-dispersed aerosols, *Int. Rev. Aerosol Phys. Chem.*, **2**, pp 1 – 60, 1971.

Gallagher, J. W., E. C. Beaty, J. Dutton, and L. C. Pitchford, An annotated compilation and appraisal of electron swarm data in electronegative gases, *J. Physical Chemistry Ref. Data,* **12**, No. 1, pp 109 – 152, 1983.

Gallimberti, I., The mechanism of the long spark formation, *Journal de Physique* **C7**, No. 7-40, pp 193 – 250, 1979.

Good, A., D. A. Durden, and P.Kebarle, Ion-molecule reactions in pure nitrogen and nitrogen containing traces of water at total pressures 0.5 – 4 torr. kinetics of clustering reactions forming $H^+(H_2O)_n$. *J. Chemical Physics,* **52**, pp 212 – 221, 1970a.

Good, A., D. A. Durden, and P.Kebarle, Mechanism and rate constants of ion-molecule reactions leading to the formation of $H^+(H_2O)_n$ in moist oxygen and air. *J. Chemical Physics,* **52**, pp 222 – 229, 1970b.

Griffing, G. W., Ozone and oxides of nitrogen production during thunderstorms. *J. Geophys. Res.,* **82**, No. 6, pp 943 – 950, 1977.

Griffiths, R. F., J. Latham, and V. Myers, The ionic conductivity of electrified clouds, *Quart. J. Royal Met. Society,* **100**, pp 181 – 190, 1974.

Guo, C., and E. P. Krider, The optical and radiation field signatures produced by lightning return strokes, *J. Geophys. Res.,* **87**, No. C11, pp 8913 – 8922, 1982.

Gurney, K. M.S. Thesis, M.I.T, 1991.

Hameka, H.F., and G.W. Robinson, and C.J. Marsden, Structure of the hydrated electron. *J. Physical Chemistry,* **91**, pp 3150 – 3157, 1987.

Hayakawa, S., *Cosmic ray physics. Nuclear and astrophysical aspects.* Wiley-interscience, Wiley & Sons, New York, NY., 1969.

Heckman, S. J., and E. R. Williams, Corona envelopes and lightning currents, *J. Geophys. Res.,* **94**, No. D11, pp 13,287 – 13,294, 1989.

Hill, R. D., I. Rahmim, and R. G. Rinker, Experimental study of the production of NO, N_2O, and O_3 in a simulated atmospheric corona., *Ind & Eng. Chem. Res.*, **27**, No. 7, pp 1264 – 1269, 1988.

Hill, R. D., R. G. Rinker, and A. Coucouvinos, Nitrous oxide production by lightning, *J. Geophys. Res.,* **89**, No. D1, pp 1411 – 1421, 1984.

References

Hill, R. D., R. G. Rinker, and H. D. Wilson, Atmospheric nitrogen fixation by lightning, *J. Atmos. Sciences,* **37**, pp 179 – 192, 1980.

Hough, A. M., Development of a two-dimensional global tropospheric model: model chemistry, *J. Geophys. Res.,* **96**, No. D4, pp 7325 – 7363, 1991.

Hunter, S. R., and L. G. Christophorou, Electron attachment to the perfluoroalkanes n-C_nF_{2n+2} (N = 1 - 6) using high pressure swarm techniques., *J. Chemical Physics,* **80**, No. 12, pp 6150 – 6164, 1984.

Itikawa, Y., M. Hayashi, A. Ichimura, K. Onda, K. Sakimoto, K. Takayanagi, M. Nakamura, H. Nishimura, and T. Takayanagi, cross sections for collisions of electrons and photons with nitrogen molecules, *J. Physical Chemistry Ref. Data,* **15**, No. 3, pp 985 – 1010, 1986.

Itikawa, Y., A. Ichimura, K. Onda, K. Sakimoto, K. Takayanagi, Y. Hatano, M. Hayashi, H. Nishimura, and S. Tsurubuchi, Cross sections for collisions of electrons and photons with oxygen molecules, *J. Physical Chemistry Ref. Data,* **18**, No. 1, pp 23 – 42, 1989.

Kasting, J., and H. Singh, Nonmethane Hydrocarbons in the Troposphere: Impact on the odd hydrogen and odd nitrogen chemistry, *J. Geophys. Res.,* **91**, 13,239 – 13,256, 1986.

Keenan, T. D., and R. E. Carbone, A preliminary morphology of convective systems in tropical northern Australia, Preprints, *24th Conf. on Radar Meteorology*, Amer. Meteor. Soc., pp 640 – 644, 1989.

Klemp, J. B., and R. B. Wilhelmson, The simulation of three-dimensional convective storm dynamics, *J. Atmos. Sciences,* **35**, No. 6, pp 1070 – 1096, 1978.

Krehbiel, P. R. The electrical structure of thunderstorms, in *The Earth's Electrical Environment*, edited by E. P. Krider and R. G. Roble, pp 90 – 113, National Academy Press, Washington, D. C., 1986.

Levine, J. S., R. E. Huges, W. L. Chameides, and W. E. Howell, N_2O and CO production by electric discharge: atmospheric implications, *Geophys. Res. Letters,* **6**, No. 7, pp 557 – 559, 1979.

Levine, J. S., R. S. Rogowski, G. L. Gregory, W. E. Howell, and J. Fishman, Simultaneous measurements of NO_x, NO and O_3 production in a laboratory discharge: atmospheric implications, *Geophys. Res. Letters,* **8**, No. 4, pp 357 – 369, 1981.

Lin, S.-C., and D. J. Teare, Rate of ionization behind shock waves in air. II. Theoretical interpretations, *The Physica of Fluids*, **6**, No. 3, pp 355 –375, 1963.

Logan, J. A., Nitrogen oxides in the troposphere: Global and regional budgets. *J. Geophys. Res.,* **88** No. C15, pp 10,785 – 10,807, 1983.

References

Logan, J. A., M. J. Prather, S. C. Wofsy, and M. B. McElroy, Tropospheric chemistry: a global perspective, *J. Geophys. Res.*, **86**, No. C8, pp 7210 – 7254, 1981.

McEwan, M. J., and L. F. Phillips, *Chemistry of the Atmosphere.*, Edward Arnold, London pub., 1975.

McFarland, M., D. L. Albritton, F. C. Fehsenfeld, E. E. Ferguson and A. L. Schmeltekopf, Ion mobility and rate constant measurements. II., *J. Chemical Physics,* **59**, pp 6610 – 6628, 1973.

Makina, M and T. Ogawa, Quantitative estimation of the global circuit. *J. Geophys. Res.,* **90**, No. D4, pp 5961 – 5966, 1985.

Markson, R., Aircraft measurements of the atmospheric electrical global circuit during the period 1971 – 1984. *J. Geophys. Res.,* **90**, No. D4, pp 5967 – 5977, 1985.

Markson, R., Tropical convection, ionospheric potentials and global circuit variation. *Nature* **320**, No. 6063, pp 588 – 594, 1986.

Marshall, J. S., and W. McK. Palmer, The distribution of raindrops with size, *J. Met.*, **5**, pp 165 – 166, 1948.

Marshall, T. C., and W. D. Rust, Electric field soundings through thunderstorms, *J. Geophys. Res.,* **96**, No. D12, pp 22,297 – 22,306, 1991.

Martell, E. A., Enhanced ion production in convective storms by transpired radon isotopes and their decay products, *J. Geophys. Res.,* **90**, No. D4, pp 5909 – 5916, 1985.

Mueller, C. K., and R. E. Carbone, The dynamics of a thunderstorm outflow, In the 23^{rd} conference on radar meteorology and the conference on cloud physics, Sept 22-26, 1986, Snowmass, Colo., American Meteorological Society, Boston, Mass.

Musil, D. J., and P. L. Smith, Interior characteristics at mid-levels of thunderstorms in the southeastern United States, *Atmospheric Research*, **24**, pp 149 – 167, 1989.

N.I.S.T. Chemical Kinetics Database Version 4.0, U.S. Department of Commerce, National Institute of Standards and Technology, Standard Reference Data Program, Gaithersburg, MD, 10899, April 1992.

Noxon, J. F., NO_3 and NO_2 in the mid-Pacific troposphere. *J. Geophys. Res.,* **88**, No. C15, pp 11,017 – 11,021, 1983.

Noxon, J. F., NO_x in the mid-Pacific troposphere. *Geophys. Res. Letters,* **8**, No. 12, pp 1223 – 1226, 1981.

Noxon, J. F., Atmospheric nitrogen fixation by lightning. *Geophys. Res. Letters,* **3**, No. 8, pp 463 – 465, 1976.

References

Ogawa, T., Fair weather electricity. *J. Geophys. Res.*, **90**, No. D4, pp 5951 – 5961, 1985.

Orville, R. E., A high-speed time-resolved spectroscopic study of the lightning return stroke: Part I. A qualitative analysis., *J. Atmos. Sciences,* **25**, pp 827 – 838, 1986a.

Orville, R. E., A high-speed time-resolved spectroscopic study of the lightning return stroke: Part II. A quantitative analysis., *J. Atmos. Sciences,* **25**, pp 839 – 851, 1986b.

Orville, R. E., Ozone production during thunderstorms, measured by the absorption of ultraviolet radiation from lightning, *J. Geophys. Res.*, **72**, No. 14, pp 3557 – 3561, 1967.

Orville, R.E., and R.W. Henderson, Global distribution of midnight lightning: September 1977 to August 1978. *Monthly Weather Review,* **114**, No. 12, pp 2640 – 2653, 1986.

Palva, V. Long air gap discharges at les renardieres, 1973 results, *Electra*, No. 35, pp 193 – 210, July 1974.

Paxton, A. H., R. L. Gardner, and L. Baker, Lightning return stroke. A numerical calculation of the optical output, *Phys. Fluids* **29**, No. 8, pp 2736 – 2741, 1986.

Perkins, M.D., and F.L. Eisele, First mass spectrometric measurements of atmospheric ions at ground level, *J. Geophys. Res.*, **89**, No. D6, pp 9649 – 9657, 1984.

Phillips, B. B., Ionic equilibrium and the electrical conductivity in thunderclouds, *Monthly Weather Review,* **95**, pp 854 – 862, 1967.

Pickering, K. E., R. R. Dickerson, G. J. Huffman, J. F. Boatman, and A. Schanot, Trace gas transport in the vicinity of frontal convective clouds. *J. Geophys. Res.*, **93 No. D1**, pp 759 – 773, 1988.

Prinn, R. G., Towards an improved global network for determination of tropospheric ozone climatology and trends. *J. Atmos. Chem.*, **6**, pp 281 – 298, 1988.

Prinn, R., D. Cunnold, P. Simmonds, F. Alyea, R. Boldi, A. Crawford, P. Fraser, D. Gutzler, D. Hartley, R. Rosen, and R. Rasmussen, Global average concentration and trend for hydroxyl radicals deduced from ALE/GAGE trichloroethane (Methyl Chloroform) data for 1978–1990, *J. Geophys. Res.*, **97**, No. D2, pp 2445 – 2462, 1992.

Pruppacher, H. R., and J. D. Klett, *Microphysics of Clouds and Precipitation*, D. Reidel Publishing Co., 1978.

Reiter, R., On the causal relation between nitrogen-oxygen compounds in the troposphere and atmospheric electricity. *Tellus* **XXII**, No. 1, pp 122 – 135, 1970.

Robinson, P. J. and D. R. Easterling, The frequency distribution of thunderstorm durations, *J. Applied Met.*, **27**, pp 77 – 82, 1988.

References

Rosen, J. M., D. J. Hofmann, and W. Gringel, Measurements of ion mobility to 30km, *J. Geophys. Res.,* **90**, No. D4, pp 5876 – 5884, 1985.

Rutledge, S. A., E. R. Williams, and T. D. Keenan, The Down Under Doppler and Electricity Experiment (DUNDEE): overview and preliminary results, *Bulletin American Meteorological Society*, **73**, No. 1, pp 3 – 16, 1992.

Ryan, K. R. and I. C. Plumb, A model for the etching of silicon in SF_6/O_2 plasmas, *Plasma Chemistry and Plasma Processing*, **10**, No. 2, pp 207 –229, 1990.

Standler, R. B., Estimation of corona current beneath thunderclouds. *J. Geophys. Res.,* **85 No. C8**, pp 4541 – 4544, 1980.

Thomason, L. W. and E. P. Krider, The cffects of clouds on the light produced by lightning, *J. Atmos. Sciences,* **39**, 2051 – 2065, 1982.

Thompson, A. M. and R. J. Cicerone, Clouds and wet removal as causes of variability in the trace-Gas composition of the marine troposphere, *J. Geophys. Res.,* **87**, No. C11, pp 8811 – 8826, 1982.

Thompson, A. M. and R. J. Cicerone, Possible perturbations to atmospheric CO, CH_4, and OH, *J. Geophys. Res.,* **91**, No. D10, pp 10,853 – 10,864, 1986.

Thompson, A. M. and R. W. Stewart, Effect of chemical kinetics uncertainties on calculated constituents in a tropospheric photochemical model, *J. Geophys. Res.,* **96**, No. D7, pp 13,089 – 13,108, 1991.

Tuck, A. F., Production of nitrogen oxides by lightning discharges, *Quart. J. Royal Met. Society,* **102**, pp 749 – 755, 1976.

Uman, M. A., *Lightning.*, Advanced Physics Monograph Series, McGraw-Hill Book Co., Pub., 1969.

Uman, M. A., *The lightning discharge.*, International geophysics series, Vol 39, Academic Press, Inc., 1987.

Uman, M. A., and R. E. Orville, Electron density measurement in lightning from Stark-broadening of Hα., *J. Geophys. Res.,* **69**, No. 24, pp 5151 – 5154, 1964.

Uman, M. A., and R. E. Voshall, Time interval between lightning strokes and the initiation of dart leaders., *J. Geophys. Res.,* **73**, No. 2, pp 497 – 506, 1968.

United States Air Force, Air Research and Development Command, Air Force Research Div., Geophysics Research Directorate, *Handbook of Geophysics*, Macmillian Co., Pub., N.Y., N.Y., 1961.

References

Van Brunt, R. J., and M. C. Siddagangappa, Identification of corona discharge-induced SF_6 oxidation mechanisms using $SF_6/^{18}O_2/H_2{}^{16}O$ and $SF_6/^{16}O_2/H_2{}^{18}O$ gas mixtures, *Plasma Chemistry and Plasma Processing*, **8**, No. 2, pp 207 – 223, 1988.

van de Hulst, H. C., *Light scattering by small particles*, Wiley, 470 pp, 1957.

Venugopalan, M. *Reactions under plasma conditions* , Edited by M. Venugopalan, Wiley-Interscience, New York, Publisher, 1971.

Viemeister, P. E., Lightning and the origin of nitrates found in precipitation, *J. Met.*, **17**, pp. 681 – 683, 1960.

Warneck, P., *Chemistry of the Natural Atmosphere*, Academic Press, Inc., Harcourt Brace Jovanovich, Pub., 1988.

Willet, J., Atmospheric electrical implications of ^{222}Rn daughter deposition on vegetated ground, *J. Geophys. Res.*, **90**, No. D4, pp 5901 – 5908, 1985.

Williams, E. R., Large-scale charge separation in thunderclouds, *J. Geophys. Res.*, **90**, No. D4, pp 6013 – 6026, 1985.

Williams, E. R., The tripole structure of thunderstorms, *J. Geophys. Res.*, **94**, No. D11, pp 13,151 – 13,167, 1989.

Willis, P. T., and P. Tattelman, Drop-size distributions associated with intense rainfall, *J. Applied Met.*, **28**, pp 3 – 15, 1989.

Winters, H. F., and M. Inokuti, Total dissociation cross section of CF_4 and other fluoroalkanes for electron impact, *Physical Review A*, **25**, No. 3, pp 1420 – 1429, 1982.

World Meteorological Organization, Global Ozone Research and Monitoring project, Report No. 16, Atmospheric Ozone 1985.

Ziereis, H. and F. Arnold, Gaseous ammonia and ammonium ions in the free troposphere, *Nature*, **321**, pp 503 – 504, 1986.

Zinn, J., C. D. Sutherland, and S. Ganguly, The solar flare of August 18, 1979: incoherent scatter radar data and photochemical model comparisons, *J. Geophys. Res.*, **95**, No. D10, pp 16,705 – 16,718, 1990.

Appendix A Derivation of Photon Flux *vs.* Temperature

I here show that just as the total power radiated by a black body is proportional to T^4, the total photon flux is proportional to T^3. The radiant power emitted by a black body of unit area, at a given wavelength, into a hemisphere is $E(\lambda, T)$ ($W \cdot m^{-2} \cdot m^{-1}$) and is given by

$$E(\lambda, T) = \frac{2\pi hc^2}{\lambda^5 \left[\exp(ch/k\lambda T) - 1\right]}. \qquad A-1$$

Since the energy per photon (ϵ) is a function of wavelength $\epsilon(\lambda) = h\nu = hc/\lambda$, the photon flux per unit wavelength per unit area $\phi(\lambda, T)$ ($\gamma's \cdot s^{-1} \cdot m^{-2} \cdot m^{-1}$) is

$$\phi(\lambda, T) = \frac{E(\lambda, T)}{hc/\lambda} = \frac{2\pi c}{\lambda^4 \left[\exp(ch/k\lambda T) - 1\right]}, \qquad A-2$$

and the total photon flux at a given temperature $\Phi(T)$ is then

$$\Phi(T) = \int_0^\infty \phi(\lambda, T) d\lambda. \qquad A-3$$

This equation is of the form

$$\int_0^\infty \frac{dx}{x^n (e^{a/x} - 1)}, \qquad A-4$$

and can be solved by substituting $y = a/x$ to yield

$$\Phi(T) = \frac{4\pi T^3 k^3}{c^2 h^3} \sum_{i=1}^{\infty} \frac{1}{i^3}, \qquad A-5$$

which is proportional to T^3, and is the photon flux equivalent of the integral of A-1,

$$E(T) = \int_0^\infty E(\lambda, T) d\lambda = \frac{2\pi^5 T^4 k^4}{15 c^2 h^3}, \qquad A-6$$

which is proportional to T^4.

Appendix B The chemical reactions included in the model.

The following table, Table 19, lists all the reactions used in the model. The reactions are grouped by type and no relationship between a reaction's order in table and its relative importance is implied. All the reactions in the table were used in the 1D photochemical steady state model as well as in both the 2D base case (non-electrified) model and the 2D ion (electrified) model. All reactions involving CH_4 (and its oxidation products), as well as all sulfur, chlorine, and fluorine containing compounds were excluded from the explicit, time-marching model runs.

The J_n's represent photolysis reactions while the j_n's represent either unimolecular reactions or the high pressure limit of bimolecular reactions. The units of the rate coefficients are: s^{-1} for the J_n's and the j_n's; $cm^3 \cdot s^{-1}$ for the k_n's; $cm^6 \cdot s^{-1}$ for the l_n's.

Rate coefficients written either as functions (*e.g.* NPD (a, b, c, e, f, g), DependsEV(a, b, c)) or as named variables (*e.g.* O3_3P, IonIon) are, in general, functions of the local temperature, pressure, and the electric field strength. Those reaction with references indicated by **X?** are discussed in the text. The derivation of the rate coefficient for the photolysis reactions (J_n) was given in Section 4.1, page 95 . The definitions of NPD, DependsEV, and the standard 3 body reactions are given at the end of this Appendix.

The references are as follows. **A9** : Atkinson *et al.*, 1989; **A6** : Atkinson, 1986; **B7** : Baulch *et al.*, 1972; **BT** : Breitbarth, *et al.*, 1985; **BS** : Van Brunt & Siddagangappa, 1988; **C6** : Christophorou, 1976; **D7** : DeMoore *et al.*, 1987; **D5** : DeMoore *et al.*, 1985; **FF** : Fehsenfeld & Ferguson, 1974; **GB** : Gallagher *et al.*, 1983; **GD** : Good *et al.*, 1970; **GI** : Gallimberti, 1979; **H4** : Hill *et al.*, 1984; **HC** : Hunter & Christophorou, 1984; **IH** : Itikawa, Hayashi *et al.*, 1986; **II** : Itikawa, Ichimura *et al.*, 1989; **LT** : Lin & Teare, 1963; **MC** : McFarland *et al.*, 1973; **MP** : McEwan & Phillips, 1975; **NB** : N.I.S.T. Chemical Kinetic Data Base, 1992; **NM** : Donahue & Prinn, 1990; **RP** : Ryan & Plumb, 1990; **VE** : Venugopalan, 1971; **WI** : Winters & Inokuti, 1982; **ZN** : Zinn *et al.*, 1990; **X?** : See text for derivation;

TABLE 19. List of Chemical Reactions Included in the Model.

Rx	Ref	Reaction	Rate Coefficient
	Photolysis		
R_1	D7	$O_3 \rightarrow O_2 + O$	J_1= O3_3P
R_2	D7	$O_3 \rightarrow O_2 + O(^1D)$	J_2= O3_1D
R_3	A9	$HONO \rightarrow OH + NO$	J_3= HONO
R_4	A9	$HONO_2 \rightarrow OH + NO_2$	J_4= HONO2
R_5	D5	$H_2O_2 \rightarrow OH + OH$	J_5= H2O2_OH
R_6	D5	$N_2O_5 \rightarrow NO_2 + NO_3$	J_6= N2O5
R_7	D5	$NO_2 \rightarrow NO + O$	J_7= NO2
R_8	D5	$NO_3 \rightarrow NO_2 + O$	J_8= NO3_O
R_9	D5	$NO_3 \rightarrow NO + O_2$	J_9= NO3_O2
R_{10}	D5	$HO_2NO_2 \rightarrow HO_2 + NO_2$	J_{10}= HO2NO2
R_{11}	D5	$CH_3OOH \rightarrow CH_3O + OH$	J_{11}= CH3OOH
R_{12}	D5	$CH_2O \rightarrow CO + H_2$	J_{12}= CH2O_H2
R_{13}	D5	$CH_2O \rightarrow CHO + H$	J_{13}= CH2O_H
R_{14}	NM	$CH_3SCH_2OOH \rightarrow CH_3S + CH_2O + OH$	J_{14}= CH3OOH
R_{15}	NM	$CH_3SCHO \rightarrow CH_3S + CHO$	J_{15}= CH3CHO_1
R_{16}	D9	$CC\ell_4 \rightarrow CC\ell_3 + C\ell$	J_{16}= CCl4
R_{17}	D9	$N_2O \rightarrow N_2 + O(^1D)$	J_{17}= N2O
	N_iO_j and H_iO_j reactions		
R_{18}	NB	$NO_2 + O \rightarrow NO + O_2$	$k_{18} = 8.298 \times 10^{-12}\ (T/298)^{(-0.455)}\ e^{(27.6/T)}$
R_{19}	NB	$O + NO_3 \rightarrow NO_2 + O_2$	$k_{19} = 1. \times 10^{-11}$
R_{20}	NB	$NO_3 + NO_3 \rightarrow NO_2 + NO_2 + O_2$	$k_{20} = 3.894 \times 10^{-16}\ e^{(-136.4/T)}$
R_{21}	NB	$N_2O + O(^1D) \rightarrow NO + NO$	$k_{21} = 6.7 \times 10^{-11}$
R_{22}	NB	$N_2O + O(^1D) \rightarrow N_2 + O_2$	$k_{22} = 4.9 \times 10^{-11}$
R_{23}	NB	$N_2O + NO \rightarrow N_2 + NO_2$	$k_{23} = 7.638 \times 10^{-11}\ e^{(-26880.0/T)}$
R_{24}	NB	$NO_3 + H \rightarrow NO_2 + OH$	$k_{24} = 1.1 \times 10^{-10}$
R_{25}	D7	$O_3 + NO \rightarrow NO_2 + O_2$	$k_{25} = 1.8 \times 10^{-12}\ e^{(-1370/T)}$
R_{26}	D7	$O_3 + NO_2 \rightarrow O_2 + NO_3$	$k_{26} = 1.2 \times 10^{-13}\ e^{(-2450/T)}$
R_{27}	D7	$NO + NO_3 \rightarrow NO_2 + NO_2$	$k_{27} = 1.7 \times 10^{-11}\ e^{(+150/T)}$
R_{28}	NB	$OH + NO_3 \rightarrow NO_2 + HO_2$	$k_{28} = 2.5 \times 10^{-11}$
R_{29}	NB	$O_2 + H_2 \rightarrow OH + OH$	$k_{29} = 2.571 \times 10^{-13}\ e^{(-16200.0/T)}$
R_{30}	NB	$O_2 + H_2 \rightarrow HO_2 + H$	$k_{30} = 7.679 \times 10^{-11}\ e^{(-28590.0/T)}$
R_{31}	NB	$OH + HO_2 \rightarrow H_2O + O_2$	$k_{31} = 6.809 \times 10^{-11}\ (T/298)^{(-0.937)}\ e^{(79.0/T)}$
R_{32}	NB	$OH + N_2O \rightarrow HO_2 + N_2$	$k_{32} = 3.804 \times 10^{-17}$
R_{33}	NB	$HO_2 + N_2O \rightarrow OH + O_2 + N_2$	$k_{33} = 1. \times 10^{-20}$

TABLE 19-2. List of Chemical Reactions Included in the Model (Continued).

Rx	Ref	Reaction	Rate Coefficient
R_{34}	NB	$H + N_2O \rightarrow NH + NO$	$k_{34} = 1.048 \times 10^{-9}\, e^{(-14590.0/T)}$
R_{35}	B7	$OH + NO_2 \rightarrow NO + HO_2$	$k_{35} = 1.55 \times 10^{-11}\, e^{(-3040.0/T)}$
R_{36}	B7	$NO_2 + H \rightarrow NO + OH$	$k_{36} = 5.8 \times 10^{-10}\, e^{(-740.0/T)}$
R_{37}	B7	$N_2O + H \rightarrow N_2 + OH$	$k_{37} = 1.3 \times 10^{-10}\, e^{(-7600.0/T)}$
R_{38}	B7	$N_2 + OH \rightarrow N_2O + H$	$k_{38} = 5.31 \times 10^{-12}\, e^{(-40509.0/T)}$
R_{39}	NB	$H + O_2 \rightarrow OH + O$	$k_{39} = 2.22 \times 10^{-10}\, e^{(-7983.5/T)}$
R_{40}	NB	$H + OH \rightarrow H_2 + O$	$k_{40} = 6.858 \times 10^{-14}\, (T/298)^{(2.800)}\, e^{(-1950.0/T)}$
R_{41}	NB	$H + H_2O \rightarrow OH + H_2$	$k_{41} = 2.979 \times 10^{-10}\, e^{(-10516.1/T)}$
R_{42}	NB	$OH + H_2 \rightarrow H + H_2O$	$k_{42} = 9.804 \times 10^{-13}\, (T/298)^{(1.981)}\, e^{(-1497.1/T)}$
R_{43}	NB	$H + HO_2 \rightarrow O + H_2O$	$k_{43} = 9.18 \times 10^{-11}\, e^{(-971.9/T)}$
R_{44}	NB	$H + HO_2 \rightarrow H_2 + O_2$	$k_{44} = 7.348 \times 10^{-11}\, e^{(-653.4/T)}$
R_{45}	NB	$H + HO_2 \rightarrow OH + OH$	$k_{45} = 1.254 \times 10^{-10}\, e^{(-325.3/T)}$
R_{46}	NB	$OH + O \rightarrow H + O_2$	$k_{46} = 3.833 \times 10^{-11}\, (T/298)^{(-0.439)}\, e^{(-1.9/T)}$
R_{47}	NB	$O + H_2 \rightarrow OH + H$	$k_{47} = 9.466 \times 10^{-14}\, (T/298)^{(3.196)}\, e^{(-2748.1/T)}$
R_{48}	NB	$O(^1D) + H_2 \rightarrow OH + H$	$k_{48} = 1. \times 10^{-10}$
R_{49}	NB	$H_2O + O \rightarrow OH + OH$	$k_{49} = 1.965 \times 10^{-10}\, e^{(-9487.8/T)}$
R_{50}	NB	$O_3 + \{M\} \rightarrow O + O_2 + \{M\}$	$k_{50} = 9.016 \times 10^{-10}\, e^{(-11253.9/T)}$
R_{51}	NB	$O + O_3 \rightarrow O_2 + O_2$	$k_{51} = 1.314 \times 10^{-11}\, e^{(-2149.2/T)}$
R_{52}	NB	$OH + O_3 \rightarrow HO_2 + O_2$	$k_{52} = 1.02 \times 10^{-12}\, e^{(-860.7/T)}$
R_{53}	NB	$H + O_3 \rightarrow OH + O_2$	$k_{53} = 1.399 \times 10^{-10}\, e^{(-459.7/T)}$
R_{54}	D7	$HO_2 + O_3 \rightarrow OH + O_2 + O_2$	$k_{54} = 1.1 \times 10^{-14}\, e^{(-500/T)}$
R_{55}	A9	$HO_2 + NO \rightarrow OH + NO_2$	$k_{55} = 3.7 \times 10^{-12}\, e^{(+240/T)}$
R_{56}	D7	$OH + H_2O_2 \rightarrow H_2O + HO_2$	$k_{56} = 2.9 \times 10^{-12}\, e^{(-160/T)}$
R_{57}	NB	$OH + OH \rightarrow H_2O + O$	$k_{57} = 7.262 \times 10^{-13}\, (T/298)^{(1.493)}\, e^{(269.0/T)}$
R_{58}	NB	$OH + OH \rightarrow H_2O_2$	$k_{58} = \mathrm{NPD}(3.516 \times 10^{-30}, -3.597, -534.3, 4.44 \times 10^{-12}, 0.000, 243.7)$
R_{59}	NB	$HO_2 + HO_2 \rightarrow H_2O_2 + O_2$	$k_{59} = 2.303 \times 10^{-13}\, e^{(600.0/T)}$
R_{60}	NB	$HO_2 + HO_2 + \{M\} \rightarrow H_2O_2 + O_2 + \{M\}$	$l_{60} = 1.678 \times 10^{-33}\, e^{(981.1/T)}$
R_{61}	NB	$HO_2 + O \rightarrow OH + O_2$	$k_{61} = 2.885 \times 10^{-11}\, e^{(207.2/T)}$
		$H_iN_jO_k$ reactions	
R_{62}	NB	$NO_3 + HO_2 \rightarrow HONO_2 + O_2$	$k_{62} = 9.209 \times 10^{-13}$
R_{63}	NB	$NO_3 + CH_2O \rightarrow HONO_2 + CHO$	$k_{63} = 6.298 \times 10^{-16}$
R_{64}	NB	$H_2O + N_2O_5 \rightarrow HONO_2 + HONO_2$	$k_{64} = 1.75 \times 10^{-21}$
R_{65}	NB	$H + HO_2NO_2 \rightarrow H_2O_2 + NO_2$	$k_{65} = 2.461 \times 10^{-14}$
R_{66}	NB	$OH + HO_2NO_2 \rightarrow H_2O + NO_2 + O_2$	$k_{66} = 1.198 \times 10^{-12}\, e^{(335.6/T)}$
R_{67}	NB	$O + HO_2NO_2 \rightarrow OH + NO_2 + O_2$	$k_{67} = 7.651 \times 10^{-11}\, e^{(-3393.7/T)}$
R_{68}	NB	$OH + HONO \rightarrow H_2O + NO_2$	$k_{68} = 1.8 \times 10^{-11}\, e^{(-390.0/T)}$
R_{69}	NB	$HO_2 + NO \rightarrow HNO + O_2$	$k_{69} = 9.103 \times 10^{-19}\, e^{(2819.0/T)}$
R_{70}	NB	$HNO + O_2 \rightarrow NO + HO_2$	$k_{70} = 5.251 \times 10^{-12}\, e^{(-1510.0/T)}$

Note: The definitions of the reactive families $\{X\}$ are at the end of this table.

TABLE 19-3. List of Chemical Reactions Included in the Model (Continued).

Rx	Ref	Reaction	Rate Coefficient
R_{71}	NB	$HNO + O \rightarrow NO + OH$	$k_{71} = 2. \times 10^{-11}$
R_{72}	NB	$HNO + CH_3O \rightarrow NO + CH_3OH$	$k_{72} = 5.251 \times 10^{-11}\ e^{(0.0/T)}$
R_{73}	NB	$HNO + HNO \rightarrow N_2O + H_2O$	$k_{73} = 7.056 \times 10^{-20}\ e^{(3262.0/T)}$
R_{74}	B7	$HNO + H \rightarrow H_2 + NO$	$k_{74} = 3.07 \times 10^{-12}\ e^{(451/T)}$
R_{75}	B7	$HNO + OH \rightarrow H_2O + NO$	$k_{75} = 2.69 \times 10^{-10}\ e^{(-1569.0/T)}$
R_{76}	B7	$NO + H + \{M\} \rightarrow HNO + \{M\}$	$l_{76} = 1.5 \times 10^{-32}\ e^{(300.0/T)}$
R_{77}	B7	$HNO + O_2 \rightarrow NO + H + O_2$	$k_{77} = 1.66 \times 10^{-5}\ e^{(-23150.0/T)}$
R_{78}	B7	$HNO + N_2 \rightarrow NO + H + N_2$	$k_{78} = 1.66 \times 10^{-5}\ e^{(-23150.0/T)}$
R_{79}	B7	$HNO + Ar \rightarrow NO + H + Ar$	$k_{79} = 1.66 \times 10^{-5}\ e^{(-23150.0/T)}$
R_{80}	B7	$H_2 + NO \rightarrow H + HNO$	$k_{80} = 5.25 \times 10^{-11}\ e^{(-27778.0/T)}$
R_{81}	B7	$H_2O + NO \rightarrow HNO + OH$	$k_{81} = 7.4 \times 10^{-10}\ e^{(-36657.0/T)}$
R_{82}	B7	$HONO + O \rightarrow HONO_2$	$k_{82} = 1. \times 10^{-15}$
R_{83}	B7	$H_2O + NO_3 \rightarrow HONO_2 + OH$	$k_{83} = 2.3 \times 10^{-26}$
R_{84}	NB	$NH_2 + O_3 \rightarrow HNO + O + OH$	$k_{84} = 1.914 \times 10^{-12}\ e^{(-709.0/T)}$
R_{85}	NB	$HONO \rightarrow OH + NO$	$j_{85} = 5.495 \times 10^{+12}\ e^{(-24155.0/T)}$
R_{86}	D7	$HO_2 + NO_2 \rightarrow HONO + O_2$	$k_{86} = 1.2 \times 10^{-13}$
R_{87}	NB	$H_2 + NO_2 \rightarrow H + HONO$	$k_{87} = 3.983 \times 10^{-11}\ e^{(-14590.0/T)}$
R_{88}	NB	$H_2O_2 + NO_2 \rightarrow OH + HONO_2$	$k_{88} = 1.001 \times 10^{-18}$
R_{89}	NB	$CH_2OH + H_2O_2 \rightarrow CH_3OH + HO_2$	$k_{89} = 5.003 \times 10^{-15}\ e^{(-1300.0/T)}$
	Standard 3-body reactions		
R_{90}	A9	$O + O_2 \rightarrow O_3$	$l\_N2_{90} = 5.7 \times 10^{-34}\ (T/300)^{(-2.8)}$ $l\_O2_{90} = 6.2 \times 10^{-34}\ (T/300)^{(-2.0)}$ $ki_{90} = 2.8 \times 10^{-12}$ $Fc_{90} = e^{(-T/696)}$
R_{91}	D7	$OH + HONO_2 \rightarrow H_2O + NO_3$	$s3_{91} = 7.2 \times 10^{-15}\ e^{(+785/T)}$ $k2_{91} = 4.1 \times 10^{-16}\ e^{(+1440/T)}$ $k3_{91} = 1.9 \times 10^{-33}\ e^{(+725/T)}$
R_{92}	A9	$OH + NO \rightarrow HONO$	$l\_N2_{92} = 7.4 \times 10^{-31}\ (T/300)^{(-2.4)}$ $l\_O2_{92} = 7.4 \times 10^{-31}\ (T/300)^{(-2.4)}$ $ki_{92} = 1. \times 10^{-11}$ $Fc_{92} = e^{(-T/1300)}$
R_{93}	D7	$H + O_2 \rightarrow HO_2$	$l\_N2_{93} = 5.7 \times 10^{-32}\ (T/300)^{(-1.6)}$ $l\_O2_{93} = 5.7 \times 10^{-32}\ (T/300)^{(-1.6)}$ $ki_{93} = 7.5 \times 10^{-11}$ $Fc_{93} = e^{(-T/502)}$
R_{94}	A9	$OH + NO_2 \rightarrow HONO_2$	$l\_N2_{94} = 2.6 \times 10^{-30}\ (T/300)^{(-2.9)}$ $l\_O2_{94} = 2.2 \times 10^{-30}\ (T/300)^{(-2.9)}$ $ki_{94} = 5.2 \times 10^{-11}$ $Fc_{94} = e^{(-T/353)}$

Note: The definitions of the reactive families $\{X\}$ are at the end of this table.

TABLE 19-4. List of Chemical Reactions Included in the Model (Continued).

Rx	Ref	Reaction	Rate Coefficient
R_{95}	D7	$HO_2 + NO_2 \rightarrow HO_2NO_2$	$l\_N2_{95} = 1.8 \times 10^{-31}\,(T/300)^{(-3.2)}$ $l\_O2_{95} = 1.8 \times 10^{-31}\,(T/300)^{(-3.2)}$ $ki_{95} = 4.7 \times 10^{-12}\,(T/300)^{(-1.4)}$ $Fc_{95} = e^{(-T/517)}$
R_{96}	A9	$HO_2NO_2 \rightarrow HO_2 + NO_2$	$jo\_N2_{96} = 5. \times 10^{-6}\,e^{(-10000/T)}$ $ko\_O2_{96} = 3.6 \times 10^{-6}\,e^{(-10000/T)}$ $ji_{96} = 3.4 \times 10^{+14}\,e^{(-10420/T)}$ $Fc_{96} = e^{(-T/517)}$
R_{97}	NB	$NO_2 + NO_3 \rightarrow N_2O_5$	$k_{97} = \mathrm{NPD}(1.466 \times 10^{-31}, 0.000, 915.1,$ $1.377 \times 10^{-12}, 0.000, 30.4)$
R_{98}	A9	$N_2O_5 \rightarrow NO_2 + NO_3$	$jo\_N2_{98} = 2.2 \times 10^{-3}\,(T/300)^{(-4.4)}\,e^{(-11080/T)}$ $ko\_O2_{98} = 2.2 \times 10^{-3}\,(T/300)^{(-4.4)}\,e^{(-11080/T)}$ $ji_{98} = 9.7 \times 10^{+14}\,(T/300)^{(+0.1)}\,e^{(-11080/T)}$ $Fc_{98} = e^{(-T/280)}$
R_{99}	D7	$CH_3 + O_2 \rightarrow CH_3O_2$	$l\_N2_{99} = 4.5 \times 10^{-31}\,(T/300)^{(-2.0)}$ $l\_O2_{99} = 4.5 \times 10^{-31}\,(T/300)^{(-2.0)}$ $ki_{99} = 1.8 \times 10^{-12}\,(T/300)^{(-2.0)}$ $Fc_{99} = e^{(-T/446)}$
R_{100}	A9	$CH_3O_2 + NO_2 \rightarrow CH_3O_2NO_2$	$l\_N2_{100} = 2.3 \times 10^{-30}\,(T/300)^{(-4.0)}$ $l\_O2_{100} = 2.3 \times 10^{-30}\,(T/300)^{(-4.0)}$ $ki_{100} = 8. \times 10^{-12}$ $Fc_{100} = e^{(-T/327)}$
R_{101}	SA	$CH_3O_2NO_2 \rightarrow CH_3O_2 + NO_2$	$jo\_N2_{101} = 9. \times 10^{-5}\,e^{(-9690/T)}$ $ko\_O2_{101} = ko_{N2}$ $ji_{101} = 1.1 \times 10^{+16}\,e^{(-10560/T)}$ $Fc_{101} = e^{(-T/325)}$
R_{102}	NB	$O + NO \rightarrow NO_2$	$k_{102} = \mathrm{NPD}(1.759 \times 10^{-32}, 0.000, 478.5,$ $2.221 \times 10^{-11}, 0.452, 92.6)$
R_{103}	NB	$CH_3O \rightarrow CH_2O + H$	$j_{103} = \mathrm{NPD}(1.893 \times 10^{-11}, 0.000, -6346.0,$ $6.628 \times 10^{+13}, 0.000, -12630.0)$
R_{104}	NB	$CH_3ONO \rightarrow CH_3O + NO$	$j_{104} = \mathrm{NPD}(8.396 \times 10^{-8}, 0.000, -15480.0,$ $9.749 \times 10^{+17}, 0.000, -22700.0)$
R_{105}	NB	$CH_2O \rightarrow H + CHO$	$j_{105} = \mathrm{NPD}(5.388 \times 10^{-8}, 0.000, -39020.0,$ $3.299 \times 10^{+14}, 0.000, -44950.0)$
R_{106}	NB	$H + CH_3 \rightarrow CH_4$	$k_{106} = \mathrm{NPD}(8.194 \times 10^{-31}, 0.000, 1281.0,$ $8.27 \times 10^{-11}, 0.000, 389.5)$

TABLE 19-5. List of Chemical Reactions Included in the Model (Continued).

Rx	Ref	Reaction	Rate Coefficient
R_{107}	NB	$CH_4 \rightarrow CH_3 + H$	j_{107} = NPD(7.253×10^{-7}, 0.000, −48720.0, $3.272 \times 10^{+15}$, 0.000, −52180.0)
R_{108}	NB	$H + OH \rightarrow H_2O$	k_{108} = NPD(5.451×10^{-30}, −2.630, −809.6, 7.966×10^{-14}, 0.000, −276.3)
R_{109}	NB	$H + CO \rightarrow CHO$	k_{109} = NPD(1.213×10^{-33}, 0.000, −759.2, 1.96×10^{-13}, 0.000, −1366.0)
R_{110}	NB	$O + CO \rightarrow CO_2$	k_{110} = NPD(1.182×10^{-33}, 0.000, −1470.0, 5.681×10^{-15}, 0.000, −1160.0)
R_{111}	NB	$CO_2 \rightarrow CO + O$	j_{111} = NPD(5.088×10^{-10}, 0.000, −51420.0, $8.995 \times 10^{+12}$, 0.000, −65310.0)
R_{112}	NB	$H_2O_2 \rightarrow OH + OH$	j_{112} = NPD(5.797×10^{-1}, −7.009, −29110.0, $2.951 \times 10^{+14}$, 0.000, −24370.0)
R_{113}	NB	$NO_2 + O \rightarrow NO_3$	k_{113} = NPD(1.466×10^{-32}, 0.000, 532.0, 2.163×10^{-11}, 0.000, 2.8)
		Cosmic ray ionizations	
R_{114}	X3	$O_2 \rightarrow O_2^+ + e$	j_{114} = 0.50×IonizationRate
R_{115}	X3	$O_2 \rightarrow O + O^+ + e$	j_{115} = 0.25×IonizationRate
R_{116}	X3	$N_2 \rightarrow N_2^+ + e$	j_{116} = 0.50×IonizationRate
R_{117}	X3	$N_2 \rightarrow N + N^+ + e$	j_{117} = 0.25×IonizationRate
R_{118}	X3	$CO_2 \rightarrow CO_2^+ + e$	j_{118} = IonizationRate
R_{119}	X3	$H_2O \rightarrow H_2O^+ + e$	j_{119} = IonizationRate
R_{120}	X3	$SF_6 \rightarrow SF_5 + F$	j_{120} = IonizationRate
R_{121}	X3	$CC\ell_4 \rightarrow CC\ell_3 + C\ell$	j_{121} = IonizationRate
R_{122}	X3	$CF_4 \rightarrow CF_3 + F$	j_{122} = IonizationRate
		Lightning-induced photolysis	
R_{123}	X4	$O_3 \rightarrow O_2 + O$	J_{123}= 0.05 × O3_L_Photo
R_{124}	X4	$O_3 \rightarrow O_2 + O(^1D)$	J_{124}= 0.95 × O3_L_Photo
R_{125}	X4	$O_2 \rightarrow O + O$	J_{125}= O2_L_Photo
R_{126}	X4	$O^- \rightarrow O + e$	J_{126}= O_L_PhotoFrag
R_{127}	X4	$O_2^- \rightarrow O_2 + e$	J_{127}= O2_L_PhotoFrag
R_{128}	X4	$O_3^- \rightarrow O_3 + e$	J_{128}= O3_L_PhotoFrag
		Lightning-induced ionization	
R_{129}	X5	$O_2 \rightarrow O_2^+ + e$	j_{129} = 0.79×L_Ion_P
R_{130}	X5	$N_2 \rightarrow N_2^+ + e$	j_{130} = 0.79×L_Ion_P
R_{131}	X5	$O_2 \rightarrow O + O^+ + e$	j_{131} = 0.21×L_Ion_P
R_{132}	X5	$N_2 \rightarrow N + N^+ + e$	j_{132} = 0.21×L_Ion_P

TABLE 19-6. List of Chemical Reactions Included in the Model (Continued).

Rx	Ref	Reaction	Rate Coefficient
		N and O Excited-state chemistry	
R_{133}	A9	$O(^1D) + N_2 \rightarrow O + N_2$	$k_{133} = 1.8 \times 10^{-11}\, e^{(+107/T)}$
R_{134}	A9	$O(^1D) + O_2 \rightarrow O + O_2$	$k_{134} = 3.2 \times 10^{-11}\, e^{(+67/T)}$
R_{135}	A9	$O(^1D) + H_2O \rightarrow OH + OH$	$k_{135} = 2.2 \times 10^{-10}$
R_{136}	A9	$O(^1D) + H_2O \rightarrow O + H_2O$	$k_{136} = 1.2 \times 10^{-11}$
R_{137}	A9	$O(^1D) + H_2O \rightarrow H_2 + O_2$	$k_{137} = 2.3 \times 10^{-12}$
R_{138}	A9	$O(^1D) + O_3 \rightarrow O_2 + O_2$	$k_{138} = 1.2 \times 10^{-10}$
R_{139}	A9	$O(^1D) + O_3 \rightarrow O_2 + O + O$	$k_{139} = 1.2 \times 10^{-10}$
R_{140}	H4	$O + O_3 \rightarrow O_2(^1D) + O_2$	$k_{140} = 1.314 \times 10^{-12}\, e^{(-2149.2/T)}$
R_{141}	H4	$O_2(^1D) + O_3 \rightarrow O_2 + O_2 + O$	$k_{141} = 4.5 \times 10^{-11}\, e^{(-2800.0/T)}$
R_{142}	H4	$O_2(^1D) + N \rightarrow O_2 + N$	$k_{142} = 3. \times 10^{-15}$
R_{143}	H4	$O_2(^1D) + O \rightarrow O_2 + O$	$k_{143} = 1. \times 10^{-16}$
R_{144}	H4	$O_2(^1D) + N_2 \rightarrow O_2 + N_2$	$k_{144} = 2.1 \times 10^{-15}$
R_{145}	H4	$O_2(^1D) + O_2 \rightarrow O_2 + O_2$	$k_{145} = 2.4 \times 10^{-18}$
R_{146}	MP	$O_2(^1D) + O_2^- \rightarrow O_2 + O_2 + e$	$k_{146} = 2. \times 10^{-10}$
R_{147}	VE	$O_2(^1D) + O^- \rightarrow O_3 + e$	$k_{147} = 3. \times 10^{-10}$
R_{148}	B7	$N(^2D) + O_2 \rightarrow NO + O$	$k_{148} = 7.5 \times 10^{-12}\, (300.0/T)^{(0.5)}$
R_{149}	H4	$N(^2D) + N_2 \rightarrow N + N_2$	$k_{149} = 1.6 \times 10^{-14}$
R_{150}	B7	$N(^2D) + NO \rightarrow N_2 + O$	$k_{150} = 6. \times 10^{-11}$
R_{151}	H4	$N(^2D) + NO \rightarrow NO + N$	$k_{151} = 6. \times 10^{-11}$
R_{152}	H4	$N(^2D) + N_2O \rightarrow NO + N_2$	$k_{152} = 2. \times 10^{-10}$
R_{153}	MP	$N_2 + e \rightarrow N_2(S) + e$	$k_{153} = 1. \times 10^{-11}$
R_{154}	MP	$N_2(S) + O(^1D) \rightarrow NO + N$	$k_{154} = 1. \times 10^{-11}$
R_{155}	MP	$N_2(S) + O_2 \rightarrow N_2 + O_2$	$k_{155} = 3.8 \times 10^{-12}$
R_{156}	VE	$N_2(S) + O^+ \rightarrow NO^+ + N$	$k_{156} = 2. \times 10^{-12}$
		SF_6, $CC\ell_4$, and CF_4 reactions	
R_{157}	NB	$CF_3 + F \rightarrow CF_4$	$k_{157} = \text{NPD}(7.7 \times 10^{-27}, 0.000, 0.0,$ $2. \times 10^{-11}, 0.000, 0.0)$
R_{158}	NB	$CF_2 + F \rightarrow CF_3$	$k_{158} = \text{NPD}(3. \times 10^{-29}, 0.000, 0.0,$ $1.3 \times 10^{-11}, 0.000, 0.0)$
R_{159}	NB	$COF_2 + O(^1D) \rightarrow CO_2 + F + F$	$k_{159} = 2.1 \times 10^{-11}$
R_{160}	NB	$CF_3 + O \rightarrow COF_2 + F$	$k_{160} = 3.1 \times 10^{-11}$
R_{161}	NB	$CF_2 + O \rightarrow COF + F$	$k_{161} = 1.4 \times 10^{-11}$
R_{162}	NB	$CF_2 + O \rightarrow CO + F + F$	$k_{162} = 4. \times 10^{-12}$
R_{163}	NB	$COF + O \rightarrow CO_2 + F$	$k_{163} = 9.3 \times 10^{-11}$
R_{164}	NB	$COF + F \rightarrow COF_2$	$k_{164} = \text{NPD}(6.5 \times 10^{-29}, 0.000, 0.0,$ $1.4 \times 10^{-11}, 0.000, 0.0)$
R_{165}	NB	$CF_3OO + O \rightarrow COF_2 + F + O_2$	$k_{165} = 1. \times 10^{-11}$

TABLE 19-7. List of Chemical Reactions Included in the Model (Continued).

Rx	Ref	Reaction	Rate Coefficient
R_{166}	NB	$F + CO \rightarrow COF$	$k_{166} = \text{NPD}(8.1 \times 10^{-32}, 0.000, 0.0, 9.4 \times 10^{-11}, 0.000, 0.0)$
R_{167}	NB	$F + O_2 \rightarrow FO_2$	$k_{167} = \text{NPD}(1.6 \times 10^{-32}, 0.000, 0.0, 3. \times 10^{-11}, 0.000, 0.0)$
R_{168}	NB	$F + FO_2 \rightarrow F + F + O_2$	$k_{168} = 5. \times 10^{-11}$
R_{169}	NB	$O + FO_2 \rightarrow FO + O_2$	$k_{169} = 5. \times 10^{-11}$
R_{170}	NB	$O + FO \rightarrow F + O_2$	$k_{170} = 5. \times 10^{-11}$
R_{171}	NB	$CF_3 + O_2 \rightarrow CF_3OO$	$k_{171} = \text{NPD}(6.725 \times 10^{-29}, -5.708, -386.4, 3.77 \times 10^{-12}, 0.000, 243.7)$
R_{172}	NB	$CF_3 + O_2 \rightarrow CF_3O + O$	$k_{172} = 8.814 \times 10^{-12}\ e^{(-8852.0/T)}$
R_{173}	NB	$CF_3 + H \rightarrow CF_2 + HF$	$k_{173} = 9.104 \times 10^{-11}$
R_{174}	NB	$F + H_2O \rightarrow HF + OH$	$k_{174} = 1.4 \times 10^{-11}$
R_{175}	NB	$F + H_2 \rightarrow HF + H$	$k_{175} = 6.576 \times 10^{-11}\ (T/298)^{(0.579)}\ e^{(-312.4/T)}$
R_{176}	NB	$F + HO_2 \rightarrow HF + O_2$	$k_{176} = 8.303 \times 10^{-11}$
R_{177}	NB	$F + CH_4 \rightarrow HF + CH_3$	$k_{177} = 2.597 \times 10^{-10}\ e^{(-379.8/T)}$
R_{178}	NB	$F + HONO_2 \rightarrow HF + NO_3$	$k_{178} = 6.906 \times 10^{-12}\ e^{(367.1/T)}$
R_{179}	NB	$F + NH_3 \rightarrow HF + NH_2$	$k_{179} = 2.895 \times 10^{-10}\ e^{(-685.3/T)}$
R_{180}	SA	$COF_2 + H_2O \rightarrow CO_2 + HF + HF$	$k_{180} = 2. \times 10^{-6}$
R_{181}	NB	$CC\ell_4 + O(^1D) \rightarrow CC\ell_3 + C\ell O$	$k_{181} = 3.3 \times 10^{-10}$
R_{182}	HC	$CF_4 + e \rightarrow CF_3 + F^-$	$k_{182} =$ e_k_CF3_F_M
R_{183}	WI	$CF_4 + e \rightarrow CF_3 + F + e$	$k_{183} = 0.5$ e_k_CF3
R_{184}	WI	$CF_4 + e \rightarrow CF_2 + F + F + e$	$k_{184} = 0.5$ e_k_CF3
R_{185}	BT	$CC\ell_4 + e \rightarrow CC\ell_3 + C\ell^-$	$k_{185} =$ e_k_CCl3_Cl_M
R_{186}	BT	$CC\ell_4 + e \rightarrow CC\ell_3 + C\ell + e$	$k_{186} = 4.5 \times 10^{-8}$
R_{187}	BT	$CC\ell_4 + e \rightarrow CC\ell_3^+ + C\ell + e + e$	$k_{187} =$ e_k_CCl3_P
R_{188}	RP	$SF_6 + e \rightarrow SF_5 + F^-$	$k_{188} =$ e_k_SF5_F_M
R_{189}	RP	$SF_6 + e \rightarrow SF_5 + F + e$	$k_{189} =$ e_k_SF5
R_{190}	RP	$SF_5 + O_2 \rightarrow SO_2F_2 + F + F + F$	$k_{190} = 1. \times 10^{-16}$
R_{191}	BS	$SF_5 + O \rightarrow SOF_4 + F$	$k_{191} = 2. \times 10^{-11}$
R_{192}	BS	$SF_5 + OH \rightarrow SOF_4 + HF$	$k_{192} = 1.6 \times 10^{-11}$
R_{193}	BS	$SOF_4 + H_2O \rightarrow SO_2F_2 + HF + HF$	$k_{193} = 1. \times 10^{-21}$
R_{194}	XX	$SF_6 + O_2^- \rightarrow SF_5 + F^- + O_2$	$k_{194} = 1. \times 10^{-10}$
R_{195}	XX	$CF_4 + O_2^- \rightarrow CF_3 + F^- + O_2$	$k_{195} = 1. \times 10^{-12}$
R_{196}	XX	$CC\ell_4 + O_2^- \rightarrow CC\ell_3 + C\ell^- + O_2$	$k_{196} = 1. \times 10^{-10}$
R_{197}	XX	$SF_6 + O_4^- \rightarrow SF_5 + F^- + O_2 + O_2$	$k_{197} = 1. \times 10^{-11}$
R_{198}	XX	$CF_4 + O_4^- \rightarrow CF_3 + F^- + O_2 + O_2$	$k_{198} = 1. \times 10^{-13}$
R_{199}	XX	$CC\ell_4 + O_4^- \rightarrow CC\ell_3 + C\ell^- + O_2 + O_2$	$k_{199} = 1. \times 10^{-11}$
R_{200}	XX	$SF_6 + CO_4^- \rightarrow SF_5 + F^- + CO_2 + O_2$	$k_{200} = 1. \times 10^{-11}$

TABLE 19-8. List of Chemical Reactions Included in the Model (Continued).

Rx	Ref	Reaction	Rate Coefficient
R_{201}	XX	$CF_4 + CO_4^- \rightarrow CF_3 + F^- + CO_2 + O_2$	$k_{201} = 1. \times 10^{-13}$
R_{202}	XX	$CC\ell_4 + CO_4^- \rightarrow CC\ell_3 + C\ell^- + CO_2 + O_2$	$k_{202} = 1. \times 10^{-11}$
R_{203}	XX	$SF_6 + O^- \rightarrow SF_5 + F^- + O$	$k_{203} = 1. \times 10^{-10}$
R_{204}	XX	$CF_4 + O^- \rightarrow CF_3 + F^- + O$	$k_{204} = 1. \times 10^{-12}$
R_{205}	XX	$CC\ell_4 + O^- \rightarrow CC\ell_3 + C\ell^- + O$	$k_{205} = 1. \times 10^{-10}$
R_{206}	XX	$SF_6 + H^- \rightarrow SF_5 + F^- + H$	$k_{206} = 1. \times 10^{-10}$
R_{207}	XX	$CF_4 + H^- \rightarrow CF_3 + F^- + H$	$k_{207} = 1. \times 10^{-12}$
R_{208}	XX	$CC\ell_4 + H^- \rightarrow CC\ell_3 + C\ell^- + H$	$k_{208} = 1. \times 10^{-10}$
		O_2 Positive ion reactions	
R_{209}	II	$O_2 + e \rightarrow O_2^+ + e + e$	$k_{209} =$ O2_Ion
R_{210}	II	$O_2 + e \rightarrow O + O + e$	$k_{210} =$ O2_Dis
R_{211}	II	$O_2 + e \rightarrow O + O^+ + e + e$	$k_{211} =$ O2_DisIon
R_{212}	ZN	$O_4^+ + N_2 \rightarrow O_2^+ + O_2 + N_2$	$k_{212} = 1.11 \times 10^{-6} (T/300)^{(-5.2)} e^{(-5007.0/T)}$
R_{213}	ZN	$O_4^+ + O_2 \rightarrow O_2^+ + O_2 + O_2$	$k_{213} = 1.11 \times 10^{-10}$
R_{214}	ZN	$O_4^+ + O \rightarrow O_2^+ + O_3$	$k_{214} = 1. \times 10^{-11}$
R_{215}	ZN	$O_4^+ + N_2 \rightarrow N_2O_2^+ + O_2$	$k_{215} = 4.61 \times 10^{-12} (T/300)^{(2.5)} e^{(-2650.0/T)}$
R_{216}	ZN	$O_4^+ + H_2O \rightarrow WO_2^+ + O_2$	$k_{216} = 2.2 \times 10^{-9}$
R_{217}	ZN	$O_4^+ + e \rightarrow O + O + O_2$	$k_{217} = 2. \times 10^{-6} (300.0/T)$
R_{218}	MP	$O_2^+ + N \rightarrow NO^+ + O$	$k_{218} = 1.8 \times 10^{-10}$
R_{219}	ZN	$O_2^+ + NO \rightarrow NO^+ + O_2$	$k_{219} = 4.5 \times 10^{-10}$
R_{220}	ZN	$O_2^+ + N_2 \rightarrow NO^+ + NO$	$k_{220} = 1. \times 10^{-16}$
R_{221}	H4	$O_2^+ + N_2 \rightarrow N_2^+ + O_2$	$k_{221} = 1. \times 10^{-10}$
R_{222}	ZN	$O_2^+ + NO_2 \rightarrow NO_2^+ + O_2$	$k_{222} = 6.6 \times 10^{-10}$
R_{223}	ZN	$O_2^+ + O_2 + \{M\} \rightarrow O_4^+ + \{M\}$	$l_{223} = 5. \times 10^{-30} (T/300)^{(-4.7)}$
R_{224}	ZN	$O_2^+ + N_2 + \{M\} \rightarrow N_2O_2^+ + \{M\}$	$l_{224} = 9. \times 10^{-31} (T/300)^{(-2.0)}$
R_{225}	X?	$O_2^+ + H_2O \rightarrow H_2O^+ + O_2$	$k_{225} = 1. \times 10^{-10}$
R_{226}	X7	$O^+ + N_2 \rightarrow NO^+ + N$	$k_{226} =$ DependsEV(−10.27591, 2.2889980, −0.38392840, −0.85343900)
R_{227}	X7	$O^+ + O_2 \rightarrow O_2^+ + O$	$k_{227} =$ DependsEV(−10.29551, 1.2033180, 0.17122480, −0.41260120)
R_{228}	MP	$O^+ + CO_2 \rightarrow O_2^+ + CO$	$k_{228} = 1.2 \times 10^{-9}$
R_{229}	MP	$O^+ + H_2O \rightarrow H_2O^+ + O$	$k_{229} = 2.3 \times 10^{-9}$
R_{230}	MP	$O^+ + H_2 \rightarrow OH^+ + H$	$k_{230} = 2. \times 10^{-9}$
R_{231}	MP	$O^+ + NO \rightarrow NO^+ + O$	$k_{231} = 1. \times 10^{-12}$
R_{232}	MP	$O^+ + NO_2 \rightarrow NO_2^+ + O$	$k_{232} = 1.6 \times 10^{-9}$
R_{233}	MP	$O^+ + N_2O \rightarrow N_2O^+ + O$	$k_{233} = 2.2 \times 10^{-10}$
R_{234}	MP	$O^+ + N_2O \rightarrow NO^+ + NO$	$k_{234} = 2.3 \times 10^{-10}$

Note: W_nX represents $(H_2O)_n \cdot X$ in these reactions. The definitions of the reactive families $\{X\}$ are at the end of this table.

TABLE 19-9. List of Chemical Reactions Included in the Model (Continued).

Rx	Ref	Reaction	Rate Coefficient
R_{235}	H4	$O^+ + N_2O \rightarrow O_2^+ + N_2$	$k_{235} = 2. \times 10^{-11}$
R_{236}	ZN	$CO^+ + NO \rightarrow NO^+ + CO$	$k_{236} = 3.3 \times 10^{-10}$
R_{237}	ZN	$CO^+ + O_2 \rightarrow O_2^+ + CO$	$k_{237} = 2. \times 10^{-10}$
R_{238}	ZN	$CO^+ + CO_2 \rightarrow CO_2^+ + CO$	$k_{238} = 1.1 \times 10^{-9}$
R_{239}	ZN	$CO^+ + H_2O \rightarrow H_2O^+ + CO$	$k_{239} = 1.1 \times 10^{-9}$
R_{240}	ZN	$CO_2^+ + NO \rightarrow NO^+ + CO_2$	$k_{240} = 1.2 \times 10^{-10}$
R_{241}	ZN	$CO_2^+ + O_2 \rightarrow O_2^+ + CO_2$	$k_{241} = 5. \times 10^{-11}$
		O_2 Negative ion reactions	
R_{242}	XX	$e + H_2O \rightarrow OH^- + H$	$k_{242} = 1. \times 10^{-12}$
R_{243}	MP	$e + O_2 + O_2 \rightarrow O_2^- + O_2$	$l_{243} = 1.4 \times 10^{-29}\ (300/T)\ e^{(-600/T)}$
R_{244}	MP	$e + O_2 + N_2 \rightarrow O_2^- + N_2$	$l_{244} = 1. \times 10^{-31}$
R_{245}	VE	$e + O_2 + H_2O \rightarrow O_2^- + H_2O$	$l_{245} = 1.4 \times 10^{-29}$
R_{246}	VE	$e + O_2 + CO_2 \rightarrow O_2^- + CO_2$	$l_{246} = 3.3 \times 10^{-30}$
R_{247}	H4	$e + N_2O \rightarrow N_2O^+ + e + e$	$k_{247} = 3.3 \times 10^{-14}$
R_{248}	MP	$e + O_3 \rightarrow O^- + O_2$	$k_{248} = 9. \times 10^{-12}$
R_{249}	ZN	$e + O \rightarrow O^-$	$k_{249} = 1.3 \times 10^{-15}$
R_{250}	VE	$e + O_2 \rightarrow O_2^-$	$k_{250} = 1. \times 10^{-20}$
R_{251}	MP	$O_4^- + O \rightarrow O_3^- + O_2$	$k_{251} = 4 \times 10^{-10}$
R_{252}	MP	$O_4^- + O \rightarrow O^- + O_2 + O_2$	$k_{252} = 3 \times 10^{-10}$
R_{253}	MP	$O_4^- + O_2 \rightarrow O_2^- + O_2 + O_2$	$k_{253} = 2. \times 10^{-14}$
R_{254}	MP	$O_4^- + CO_2 \rightarrow CO_4^- + O_2$	$k_{254} = 4.3 \times 10^{-10}$
R_{255}	MP	$O_4^- + NO \rightarrow OONO^- + O_2$	$k_{255} = 2.5 \times 10^{-10}$
R_{256}	MP	$OONO^- + NO \rightarrow NO_2^- + NO_2$	$k_{256} = 1.5 \times 10^{-11}$
R_{257}	MP	$CO_4^- + O_2 \rightarrow O_4^- + CO_2$	$k_{257} = 1.02 \times 10^{-11}\ (T/300)^{(-0.1)}\ e^{(-2433.0/T)}$
R_{258}	MP	$CO_4^- + O_3 \rightarrow O_3^- + O_2 + CO_2$	$k_{258} = 1.3 \times 10^{-10}$
R_{259}	MP	$CO_4^- + O \rightarrow CO_3^- + O_2$	$k_{259} = 1.5 \times 10^{-10}$
R_{260}	MP	$CO_4^- + NO \rightarrow OONO^- + CO_2$	$k_{260} = 4.8 \times 10^{-11}$
R_{261}	MP	$CO_3^- + O \rightarrow e + CO_2 + O_2$	$k_{261} = 2. \times 10^{-11}$
R_{262}	ZN	$CO_3^- + O \rightarrow O_2^- + CO_2$	$k_{262} = 1.1 \times 10^{-10}$
R_{263}	MP	$CO_3^- + NO \rightarrow NO_2^- + CO_2$	$k_{263} = 9. \times 10^{-12}$
R_{264}	ZN	$O_3^- + O \rightarrow O_2^- + O_2$	$k_{264} = 3.2 \times 10^{-10}$
R_{265}	MP	$O_3^- + NO \rightarrow NO_2^- + O_2$	$k_{265} = 1 \times 10^{-11}$
R_{266}	MP	$O_3^- + NO_2 \rightarrow O_2 + O_2^- + NO$	$k_{266} = 2.8 \times 10^{-10}$
R_{267}	ZN	$O_3^- + CO_2 \rightarrow O_2 + CO_3^-$	$k_{267} = 5.5 \times 10^{-10}\ (T/300)^{(-0.5)}$
R_{268}	MP	$O_2^- + H \rightarrow O^- + OH$	$k_{268} = 0.5 \times 10^{-9}$
R_{269}	MP	$O_2^- + H \rightarrow O + OH^-$	$k_{269} = 0.5 \times 10^{-9}$
R_{270}	MP	$O_2^- + H \rightarrow H^- + O_2$	$k_{270} = 0.5 \times 10^{-9}$
R_{271}	MP	$O_2^- + H_2 \rightarrow OH^- + OH$	$k_{271} = 1 \times 10^{-12}$
R_{272}	ZN	$O_2^- + O_3 \rightarrow O_3^- + O_2$	$k_{272} = 4 \times 10^{-10}$
R_{273}	MP	$O_2^- + NO_2 \rightarrow NO_2^- + O_2$	$k_{273} = 8 \times 10^{-10}$
R_{274}	MP	$O_2^- + N_2O \rightarrow O_3^- + N_2$	$k_{274} = 1. \times 10^{-12}$

TABLE 19-10. List of Chemical Reactions Included in the Model (Continued).

Rx	Ref	Reaction	Rate Coefficient
R_{275}	ZN	$O_2^- + O \rightarrow O_3 + e$	$k_{275} = 1.5 \times 10^{-10}$
R_{276}	ZN	$O_2^- + O \rightarrow O^- + O_2$	$k_{276} = 1.5 \times 10^{-10}$
R_{277}	MP	$O_2^- + O_2 \rightarrow O_2 + O_2 + e$	$k_{277} = 2.7 \times 10^{-10} (T/300)^{(0.5)} e^{(-5590.0/T)}$
R_{278}	MP	$O_2^- + N_2 \rightarrow O_2 + N_2 + e$	$k_{278} = 1.9 \times 10^{-12} (T/300)^{(1.5)} e^{(-4990.0/T)}$
R_{279}	ZN	$O_2^- + O_2 + \{M\} \rightarrow O_4^- + \{M\}$	$l_{279} = 3.5 \times 10^{-31} (300/T)$
R_{280}	XX	$O_2^- + H_2O \rightarrow OH^- + H + O_2$	$k_{280} = 1.4 \times 10^{-9}$
R_{281}	ZN	$O_2^- + CO_2 + \{M\} \rightarrow CO_4^- + \{M\}$	$l_{281} = 2. \times 10^{-29} (300/T)$
R_{282}	MP	$O_2^- + N \rightarrow NO_2 + e$	$k_{282} = 5. \times 10^{-10}$
R_{283}	ZN	$O^- + O_2 \rightarrow O_3 + e$	$k_{283} = 3. \times 10^{-11}$
R_{284}	ZN	$O^- + O_2 + \{M\} \rightarrow O_3^- + \{M\}$	$l_{284} = 1.1 \times 10^{-30} (300/T)$
R_{285}	VE	$O^- + O_2 \rightarrow O + O_2 + e$	$k_{285} = 2.3 \times 10^{-9} e^{(-26000.0/T)}$
R_{286}	VE	$O^- + N_2 \rightarrow O + N_2 + e$	$k_{286} = 2.3 \times 10^{-9} e^{(-26000.0/T)}$
R_{287}	VE	$O^- + N_2 \rightarrow N_2O + e$	$k_{287} = 1. \times 10^{-16}$
R_{288}	MP	$O^- + NO \rightarrow NO_2 + e$	$k_{288} = 1.6 \times 10^{-10}$
R_{289}	MP	$O^- + CO \rightarrow CO_2 + e$	$k_{289} = 4.4 \times 10^{-10}$
R_{290}	ZN	$O^- + CO_2 + \{M\} \rightarrow CO_3^- + \{M\}$	$l_{290} = 3.1 \times 10^{-28} (300/T)$
R_{291}	ZN	$O^- + O \rightarrow O_2 + e$	$k_{291} = 1.9 \times 10^{-10}$
R_{292}	MP	$O^- + H_2 \rightarrow H_2O + e$	$k_{292} = 6.4 \times 10^{-10}$
R_{293}	MP	$O^- + O_3 \rightarrow O_2^- + O_2$	$k_{293} = 8. \times 10^{-10}$
R_{294}	MP	$O^- + O_3 \rightarrow O_3^- + O$	$k_{294} = 5.3 \times 10^{-10}$
R_{295}	MP	$O^- + N \rightarrow NO + e$	$k_{295} = 2.2 \times 10^{-10}$
R_{296}	MP	$O^- + H_2 \rightarrow OH^- + H$	$k_{296} = 3.3 \times 10^{-11}$
R_{297}	FF	$O^- + H_2O \rightarrow OH^- + OH$	$k_{297} = 6. \times 10^{-12}$
R_{298}	MP	$O^- + NO_2 \rightarrow NO_2^- + O$	$k_{298} = 1.2 \times 10^{-9}$
R_{299}	MP	$O^- + NO_2 \rightarrow O_2^- + NO$	$k_{299} = 1.8 \times 10^{-11}$
R_{300}	MP	$O^- + N_2O \rightarrow NO^- + NO$	$k_{300} = 2 \times 10^{-10}$
R_{301}	MP	$O^- + CH_4 \rightarrow OH^- + CH_3$	$k_{301} = 1 \times 10^{-10}$
R_{302}	MP	$NO_2^- + O_3 \rightarrow NO_3^- + O_2$	$k_{302} = 1.8 \times 10^{-11}$
R_{303}	MP	$NO_2^- + NO_2 \rightarrow NO_3^- + NO$	$k_{303} = 4. \times 10^{-12}$
R_{304}	MP	$NO_2^- + H \rightarrow OH^- + NO$	$k_{304} = 3. \times 10^{-10}$
R_{305}	MP	$OH^- + NO_2 \rightarrow NO_2^- + OH$	$k_{305} = 1.2 \times 10^{-9}$
R_{306}	MP	$OH^- + O \rightarrow HO_2 + e$	$k_{306} = 3. \times 10^{-10}$
R_{307}	MP	$OH^- + H \rightarrow H_2O + e$	$k_{307} = 3. \times 10^{-10}$
R_{308}	MP	$OH^- + CO_2 + \{M\} \rightarrow HCO_3^- + \{M\}$	$l_{308} = 1. \times 10^{-29}$
		N_2 Positive ion reactions	
R_{309}	IH	$N_2 + e \rightarrow N_2^+ + e + e$	k_{309} = N2_Ion
R_{310}	IH	$N_2 + e \rightarrow N + N + e$	k_{310} = N2_Dis
R_{311}	IH	$N_2 + e \rightarrow N^+ + N + e + e$	k_{311} = N2_DisIon
R_{312}	ZN	$N_4^+ + O \rightarrow O^+ + N_2 + N_2$	$k_{312} = 3. \times 10^{-10}$
R_{313}	ZN	$N_4^+ + O_2 \rightarrow O_2^+ + N_2 + N_2$	$k_{313} = 2.5 \times 10^{-10}$

Note: The definitions of the reactive families $\{X\}$ are at the end of this table.

TABLE 19-11. List of Chemical Reactions Included in the Model (Continued).

Rx	Ref	Reaction	Rate Coefficient
R_{314}	MP	$N_4^+ + H_2O \rightarrow H_2O^+ + N_2 + N_2$	$k_{314} = 1.9 \times 10^{-9}$
R_{315}	ZN	$N_2^+ + N_2 + \{M\} \rightarrow N_4^+ + \{M\}$	$l_{315} = 5. \times 10^{-29}\ (300/T)$
R_{316}	MP	$N_2^+ + H_2O \rightarrow H_2O^+ + N_2$	$k_{316} = 1. \times 10^{-10}$
R_{317}	XX	$N_2^+ + O_2 \rightarrow O_2^+ + N_2$	$k_{317} = \text{DependsEV}(-11.034200, 0.78235110, 1.7330660, 0.49174980)$
R_{318}	MP	$N_2^+ + O \rightarrow O^+ + N_2$	$k_{318} = 1.4 \times 10^{-10}\ (T/300)^{(-0.44)}$
R_{319}	MP	$N_2^+ + O \rightarrow NO^+ + N$	$k_{319} = 1.4 \times 10^{-10}\ (T/300)^{(-0.44)}$
R_{320}	MP	$N_2^+ + N \rightarrow N^+ + N_2$	$k_{320} = 1. \times 10^{-11}$
R_{321}	MP	$N_2^+ + NO \rightarrow NO^+ + N_2$	$k_{321} = 3.3 \times 10^{-10}$
R_{322}	H4	$N_2^+ + N_2O \rightarrow NO^+ + N_2 + N$	$k_{322} = 3.9 \times 10^{-10}$
R_{323}	H4	$N_2^+ + N_2O \rightarrow N_2O^+ + N_2$	$k_{323} = 7. \times 10^{-10}$
R_{324}	MP	$N_2^+ + CO \rightarrow CO^+ + N_2$	$k_{324} = 7. \times 10^{-11}$
R_{325}	MP	$N_2^+ + CO_2 \rightarrow CO_2^+ + N_2$	$k_{325} = 9. \times 10^{-10}$
R_{326}	LT	$N_2^+ + O_2 \rightarrow NO + NO^+$	$k_{326} = 1. \times 10^{-10}$
R_{327}	ZN	$N^+ + O_2 \rightarrow O_2^+ + N$	$k_{327} = 2.8 \times 10^{-10}$
R_{328}	ZN	$N^+ + O_2 \rightarrow O_2^+ + N(^2D)$	$k_{328} = 8.4 \times 10^{-11}$
R_{329}	MP	$N^+ + O_2 \rightarrow NO^+ + O$	$k_{329} = 5. \times 10^{-11}$
R_{330}	MP	$N^+ + O_2 \rightarrow NO^+ + O(^1D)$	$k_{330} = 2. \times 10^{-10}$
R_{331}	MP	$N^+ + O_2 \rightarrow O^+ + NO$	$k_{331} = 2.8 \times 10^{-11}$
R_{332}	MP	$N^+ + CO \rightarrow CO^+ + N$	$k_{332} = 5. \times 10^{-10}$
R_{333}	MP	$N^+ + CO_2 \rightarrow CO_2^+ + N$	$k_{333} = 1.3 \times 10^{-9}$
R_{334}	H4	$N^+ + N_2O \rightarrow NO^+ + N_2$	$k_{334} = 2.8 \times 10^{-10}$
R_{335}	LT	$N^+ + NO \rightarrow NO^+ + N$	$k_{335} = 1. \times 10^{-10}$
R_{336}	LT	$N^+ + NO \rightarrow N_2^+ + O$	$k_{336} = 1. \times 10^{-10}$
R_{337}	LT	$N^+ + NO \rightarrow N_2 + O^+$	$k_{337} = 1. \times 10^{-10}$
R_{338}	ZN	$NO + e \rightarrow NO^+ + e + e$	$k_{338} = 1. \times 10^{-11}$
R_{339}	ZN	$NO^+ + H_2O \rightarrow H_2O^+ + NO$	$k_{339} = 1. \times 10^{-10}$
	Cluster reactions		
R_{340}	ZN	$H_2O^+ + O_2 \rightarrow O_2^+ + H_2O$	$k_{340} = 2. \times 10^{-10}$
R_{341}	ZN	$H_2O^+ + H_2O \rightarrow H_3O^+ + OH$	$k_{341} = 1.8 \times 10^{-9}$
R_{342}	ZN	$H_3O^+ + H_2O + N_2 \rightarrow WH_3O^+ + N_2$	$l_{342} = 3.4 \times 10^{-27}\ (T/300)^{(-4.0)}$
R_{343}	ZN	$H_3O^+ + H_2O + O_2 \rightarrow WH_3O^+ + O_2$	$l_{343} = 3.7 \times 10^{-27}\ (T/300)^{(-2.0)}$
R_{344}	ZN	$WH_3O^+ + H_2O + N_2 \rightarrow W_2H_3O^+ + N_2$	$l_{344} = 2.3 \times 10^{-27}\ (T/300)^{(-2.0)}$
R_{345}	ZN	$WH_3O^+ + H_2O + O_2 \rightarrow W_2H_3O^+ + O_2$	$l_{345} = 2. \times 10^{-27}\ (T/300)^{(-4.0)}$
R_{346}	ZN	$W_2H_3O^+ + N_2 \rightarrow WH_3O^+ + H_2O + N_2$	$k_{346} = 6.44 \times 10^{-1}\ (T/300)^{(-1.6)}\ e^{(-11220.0/T)}$

Note: W_nX represents $(H_2O)_n \cdot X$ in these reactions. The definitions of the reactive families $\{X\}$ are at the end of this table.

TABLE 19-12. List of Chemical Reactions Included in the Model (Continued).

Rx	Ref	Reaction	Rate Coefficient
R_{347}	ZN	$W_2H_3O^+ + e \rightarrow H + H_2O + H_2O + H_2O$	$k_{347} = 3. \times 10^{-6} (T/300)^{(-0.1)}$
R_{348}	ZN	$WH_3O^+ + e \rightarrow H + H_2O + H_2O$	$k_{348} = 2.5 \times 10^{-6} (T/300)^{(-0.1)}$
R_{349}	ZN	$N_2O_2^+ + \{M\} \rightarrow O_2^+ + N_2 + \{M\}$	$k_{349} = 1.1 \times 10^{-6} (T/300)^{(-5.3)} e^{(-2357.0/T)}$
R_{350}	ZN	$N_2O_2^+ + O_2 \rightarrow O_4^+ + N_2$	$k_{350} = 1. \times 10^{-9}$
R_{351}	ZN	$N_2O_2^+ + H_2O \rightarrow WO_2^+ + N_2$	$k_{351} = 4. \times 10^{-9}$
R_{352}	ZN	$WO_2^+ + O_2 \rightarrow O_2^+ + H_2O + O_2$	$k_{352} = 1. \times 10^{-10}$
R_{353}	ZN	$WO_2^+ + H_2 \rightarrow H_3O^+ + HO_2$	$k_{353} = 3. \times 10^{-10}$
R_{354}	ZN	$WO_2^+ + H \rightarrow H_3O^+ + O_2$	$k_{354} = 1. \times 10^{-9}$
R_{355}	ZN	$WO_2^+ + e \rightarrow O + O + H_2O$	$k_{355} = 1.5 \times 10^{-6} (300/T)^{(0.2)}$
R_{356}	ZN	$WO_2^+ + H_2O \rightarrow H_3O^+ + O_2 + OH$	$k_{356} = 8.63 \times 10^{-6} e^{(-4400.0/T)}$
R_{357}	ZN	$WO_2^+ + H_2O \rightarrow OHH_3O^+ + O_2$	$k_{357} = 1.87 \times 10^{-9}$
R_{358}	ZN	$OHH_3O^+ + H_2O \rightarrow WH_3O^+ + OH$	$k_{358} = 1.4 \times 10^{-9}$
R_{359}	ZN	$OHH_3O^+ + NO \rightarrow NO^+ + H_2O + H_2O$	$k_{359} = 3. \times 10^{-10}$
R_{360}	ZN	$OHH_3O^+ + e \rightarrow H_2O + H + OH$	$k_{360} = 2. \times 10^{-6} (T/300)^{(-0.2)}$
R_{361}	ZN	$NO^+ + N_2 + \{M\} \rightarrow N_2NO^+ + \{M\}$	$l_{361} = 2. \times 10^{-31} (T/300)^{(-4.4)}$
R_{362}	ZN	$N_2NO^+ + \{M\} \rightarrow NO^+ + N_2 + \{M\}$	$k_{362} = 1.83 \times 10^{-7} (T/300)^{(-8.1)} e^{(-2558.0/T)}$
R_{363}	ZN	$N_2NO^+ + H_2O \rightarrow WNO^+ + N_2$	$k_{363} = 1. \times 10^{-9}$
R_{364}	ZN	$N_2NO^+ + CO_2 \rightarrow NOCO_2^+ + N_2$	$k_{364} = 1. \times 10^{-9}$
R_{365}	ZN	$NOCO_2^+ + H_2O \rightarrow WNO^+ + CO_2$	$k_{365} = 1. \times 10^{-9}$
R_{366}	ZN	$NOCO_2^+ + N_2 \rightarrow N_2NO^+ + CO_2$	$k_{366} = 3.03 \times 10^{-9} (T/300)^{(-1.3)} e^{(-2338.0/T)}$
R_{367}	ZN	$NOCO_2^+ + \{M\} \rightarrow NO^+ + CO_2 + \{M\}$	$k_{367} = 1.44 \times 10^{-5} (T/300)^{(-11.0)} e^{(-4896.0/T)}$
R_{368}	ZN	$NO^+ + H_2O + \{M\} \rightarrow WNO^+ + \{M\}$	$l_{368} = 1.5 \times 10^{-28} (300/T)^{(-2)}$
R_{369}	ZN	$WNO^+ + H_2O + \{M\} \rightarrow W_2NO^+ + \{M\}$	$l_{369} = 1.1 \times 10^{-27} (300/T)^{(-4.7)}$
R_{370}	ZN	$W_2NO^+ + H_2O + \{M\} \rightarrow W_3NO^+ + \{M\}$	$l_{370} = 1.6 \times 10^{-27} (300/T)^{(-4.7)}$
R_{371}	ZN	$W_3NO^+ + \{M\} \rightarrow W_2NO^+ + H_2O + \{M\}$	$k_{371} = 7.41 \times 10^{-1} (300/T)^{(-4.3)} e^{(-8025.0/T)}$
R_{372}	ZN	$W_3NO^+ + H_2O \rightarrow W_2H_3O^+ + HONO$	$k_{372} = 7. \times 10^{-11}$
R_{373}	ZN	$W_3NO^+ + e \rightarrow NO + H_2O + H_2O + H_2O$	$k_{373} = 3. \times 10^{-6} (T/300)^{(-0.2)}$
R_{374}	ZN	$W_2NO^+ + e \rightarrow NO + H_2O + H_2O$	$k_{374} = 3. \times 10^{-6} (T/300)^{(-0.2)}$
R_{375}	ZN	$WNO^+ + e \rightarrow NO + H_2O$	$k_{375} = 1.5 \times 10^{-6} (T/300)^{(-0.2)}$
R_{376}	ZN	$WNO^+ + OH \rightarrow H_3O^+ + NO_2$	$k_{376} = 6. \times 10^{-11}$
R_{377}	ZN	$NO^+ + CO_2 + \{M\} \rightarrow NOCO_2^+ + \{M\}$	$l_{377} = 9.5 \times 10^{-30} (T/300)^{(-6.0)}$

Note: W_nX represents $(H_2O)_n \cdot X$ in these reactions. The definitions of the reactive families $\{X\}$ are at the end of this table.

TABLE 19-13. List of Chemical Reactions Included in the Model (Continued).

Rx	Ref	Reaction	Rate Coefficient
		Electron recombinations	
R_{378}	H4	$O_4^+ + e \rightarrow O_2 + O_2$	$k_{378} = 1.5 \times 10^{-6}\,(300/T)$
R_{379}	H4	$O_2^+ + e + \{M\} \rightarrow O_2 + \{M\}$	$l_{379} = 1. \times 10^{-26}\,(300/T)^{(2.5)}$
R_{380}	H4	$O_2^+ + e + e \rightarrow O_2 + e$	$l_{380} = 1. \times 10^{-19}\,(300/T)^{(4.5)}$
R_{381}	X9	$O^+ + e + \{M\} \rightarrow O + \{M\}$	l_{381} = Uni_ElectronCapture
R_{382}	H4	$O^+ + e + e \rightarrow O + e$	$l_{382} = 1.9 \times 10^{-19}\,(300.0/T)^{(4.5)}$
R_{383}	H4	$N_4^+ + e \rightarrow N_2 + N_2$	$k_{383} = 2.1 \times 10^{-6}\,(300/T)$
R_{384}	H4	$N_2^+ + e + e \rightarrow N_2 + e$	$l_{384} = 1. \times 10^{-19}\,(300/T)^{(4.5)}$
R_{385}	H4	$N_2^+ + e + \{M\} \rightarrow N_2 + \{M\}$	$l_{385} = 1. \times 10^{-26}\,(300/T)^{(2.5)}$
R_{386}	X9	$N^+ + e + \{M\} \rightarrow N + \{M\}$	l_{386} = Uni_ElectronCapture
R_{387}	H4	$N^+ + e + e \rightarrow N + e$	$l_{387} = 1.9 \times 10^{-19}\,(300.0/T)^{(4.5)}$
R_{388}	X9	$H_2O^+ + e \rightarrow OH + H$	k_{388} = Multi_ElectronCapture
R_{389}	ZN	$H_3O^+ + e \rightarrow H + H_2O$	$k_{389} = 1.3 \times 10^{-6}\,(300/T)^{(0.7)}$
R_{390}	H4	$NO^+ + e + \{M\} \rightarrow NO + \{M\}$	$l_{390} = 1. \times 10^{-26}\,(300/T)^{(2.5)}$
R_{391}	H4	$NO^+ + e + e \rightarrow NO + e$	$l_{391} = 1.9 \times 10^{-19}\,(300.0/T)^{(4.5)}$
R_{392}	X9	$NO_2^+ + e \rightarrow N + O + O$	k_{392} = Multi_ElectronCapture
R_{393}	X9	$N_2O^+ + e \rightarrow N + N + O$	k_{393} = Multi_ElectronCapture
R_{394}	H4	$N_2O^+ + e + e \rightarrow N_2O + e$	$l_{394} = 1.9 \times 10^{-19}\,(300/T)^{(4.5)}$
R_{395}	H4	$N_2O^+ + e + \{M\} \rightarrow N_2O + \{M\}$	$l_{395} = 1. \times 10^{-26}\,(300/T)^{(2.5)}$
R_{396}	X9	$OH^+ + e \rightarrow O + H$	k_{396} = Multi_ElectronCapture
R_{397}	X9	$CO^+ + e \rightarrow C + O$	k_{397} = Multi_ElectronCapture
R_{398}	X9	$CO_2^+ + e \rightarrow C + O + O$	k_{398} = Multi_ElectronCapture
R_{399}	X9	$N_2O_2^+ + e \rightarrow NO + NO$	k_{399} = Multi_ElectronCapture
		Ion recombinations	
R_{400}	X9	$N_2O_2^+ + \{NegIon\} \rightarrow NO + NO$	k_{400} = IonIon
R_{401}	X9	$O^+ + \{NegIon\} \rightarrow O(^1D)$	k_{401} = IonIon
R_{402}	X9	$O_2^+ + \{NegIon\} \rightarrow O + O(^1D)$	k_{402} = IonIon
R_{403}	X9	$O_4^+ + \{NegIon\} \rightarrow O + O + O_2$	k_{403} = IonIon
R_{404}	X9	$N^+ + \{NegIon\} \rightarrow N(^2D)$	k_{404} = IonIon
R_{405}	X9	$N_2^+ + \{NegIon\} \rightarrow N + N(^2D)$	k_{405} = IonIon
R_{406}	X9	$N_4^+ + \{NegIon\} \rightarrow N + N + N_2$	k_{406} = IonIon
R_{407}	X9	$NO^+ + \{NegIon\} \rightarrow N + O(^1D)$	k_{407} = IonIon
R_{408}	X9	$NO_2^+ + \{NegIon\} \rightarrow NO + O$	k_{408} = IonIon
R_{409}	X9	$N_2O^+ + \{NegIon\} \rightarrow N_2 + O$	k_{409} = IonIon
R_{410}	X9	$H_2O^+ + \{NegIon\} \rightarrow OH + H$	k_{410} = IonIon
R_{411}	X9	$H_3O^+ + \{NegIon\} \rightarrow H_2O + H$	k_{411} = IonIon
R_{412}	X9	$OH^+ + \{NegIon\} \rightarrow O + H$	k_{412} = IonIon
R_{413}	X9	$CO^+ + \{NegIon\} \rightarrow C + O$	k_{413} = IonIon

Note: The definitions of the reactive families $\{X\}$ are at the end of this table.

TABLE 19-14. List of Chemical Reactions Included in the Model (Continued).

Rx	Ref	Reaction	Rate Coefficient
R_{414}	X9	$CO_2^+ + \{NegIon\} \rightarrow C + O + O$	k_{414} = IonIon
R_{415}	X9	$CC\ell_3^+ + \{NegIon\} \rightarrow CC\ell_2 + C\ell$	k_{415} = IonIon
R_{416}	X9	$O^- + \{PosIon\} \rightarrow O(^1D)$	k_{416} = IonIon
R_{417}	X9	$O_2^- + \{PosIon\} \rightarrow O + O$	k_{417} = IonIon
R_{418}	X9	$O_3^- + \{PosIon\} \rightarrow O_2 + O$	k_{418} = IonIon
R_{419}	X9	$O_4^- + \{PosIon\} \rightarrow O_2 + O_2$	k_{419} = IonIon
R_{420}	X9	$H^- + \{PosIon\} \rightarrow H$	k_{420} = IonIon
R_{421}	X9	$NO_2^- + \{PosIon\} \rightarrow NO + O$	k_{421} = IonIon
R_{422}	X9	$NO^- + \{PosIon\} \rightarrow N + O$	k_{422} = IonIon
R_{423}	X9	$CO_3^- + \{PosIon\} \rightarrow CO_2 + O$	k_{423} = IonIon
R_{424}	X9	$CO_4^- + \{PosIon\} \rightarrow CO_2 + O_2$	k_{424} = IonIon
R_{425}	X9	$OONO^- + \{PosIon\} \rightarrow NO + O_2$	k_{425} = IonIon
R_{426}	X9	$HCO_3^- + \{PosIon\} \rightarrow CO_2 + OH$	k_{426} = IonIon
R_{427}	X9	$NO_3^- + \{PosIon\} \rightarrow NO_2 + O$	k_{427} = IonIon
		Thermal ionizations & recombinations	
R_{428}	LT	$N + O \rightarrow NO^+ + e$	$k_{428} = 5. \times 10^{-11}\, T^{-1/2}\, e^{(-32500.0/T)}$
R_{429}	LT	$NO^+ + e \rightarrow N + O$	$k_{429} = 0.2{\times}3. \times 10^{-3}\, (T)^{(-3/2)}$
R_{430}	LT	$NO^+ + e \rightarrow N(^2D) + O$	$k_{430} = 0.4{\times}3. \times 10^{-3}\, (T)^{(-3/2)}$
R_{431}	LT	$NO^+ + e \rightarrow N + O(^1D)$	$k_{431} = 0.4{\times}3. \times 10^{-3}\, (T)^{(-3/2)}$
R_{432}	LT	$N + N \rightarrow N_2^+ + e$	$k_{432} = 9. \times 10^{-11}\, T^{-1/2}\, e^{(-67300.0/T)} \times (1 + T\,(1.3 \times 10^{-4+}T\ 3.3 \times 10^{-8)})$
R_{433}	LT	$N_2^+ + e \rightarrow N + N(^2D)$	$k_{433} = 0.9{\times}3. \times 10^{-3}\, (T)^{(-3/2)}$
R_{434}	LT	$N_2^+ + e \rightarrow N + N$	$k_{434} = 0.1{\times}3. \times 10^{-3}\, (T)^{(-3/2)}$
R_{435}	LT	$O + O \rightarrow O_2^+ + e$	$k_{435} = 3.2 \times 10^{-11}\, T^{-1/2}\, e^{(-80100.0/T)} \times (1 + T\,(7.5 \times 10^{-5+}T\ 2.2 \times 10^{-8)})$
R_{436}	LT	$O_2^+ + e \rightarrow O + O(^1D)$	$k_{436} = 0.9{\times}2. \times 10^{-3}\, (T)^{(-3/2)}$
R_{437}	LT	$O_2^+ + e \rightarrow O + O$	$k_{437} = 0.1{\times}2. \times 10^{-3}\, (T)^{(-3/2)}$
		High T. reactions of N_iO_j	
R_{438}	B7	$N_2 + O \rightarrow N + N + O$	$k_{438} = 3.16 \times 10^{-7}\, e^{(-112450.0/T)}\, T^{-1/2}$
R_{439}	B7	$N_2 + O_2 \rightarrow N + N + O_2$	$k_{439} = 3.16 \times 10^{-7}\, e^{(-112450.0/T)}\, T^{-1/2}$
R_{440}	B7	$N_2 + NO \rightarrow N + N + NO$	$k_{440} = 3.16 \times 10^{-7}\, e^{(-112450.0/T)}\, T^{-1/2}$
R_{441}	B7	$N_2 + N_2 \rightarrow N + N + N_2$	$k_{441} = 7.81 \times 10^{-7}\, e^{(-112450.0/T)}\, T^{-1/2}$
R_{442}	B7	$N_2 + N \rightarrow N + N + N$	$k_{442} = 6.81 \times 10^{-2}\, e^{(-112450.0/T)}\, T^{-3/2}$
R_{443}	B7	$N + N + O \rightarrow N_2 + O$	$l_{443} = 2.76 \times 10^{-32}\, T^{-1/2}$
R_{444}	B7	$N + N + NO \rightarrow N_2 + NO$	$l_{444} = 2.76 \times 10^{-32}\, T^{-1/2}$
R_{445}	B7	$N + N + O_2 \rightarrow N_2 + O_2$	$l_{445} = 2.76 \times 10^{-32}\, T^{-1/2}$
R_{446}	B7	$N + N + N_2 \rightarrow N_2 + N_2$	$l_{446} = 7.17 \times 10^{-32}\, T^{-1/2}$
R_{447}	B7	$N + N + N \rightarrow N + N_2$	$l_{447} = 6.23 \times 10^{-27}\, T^{-3/2}$

Note: The definitions of the reactive families $\{X\}$ are at the end of this table.

TABLE 19-15. List of Chemical Reactions Included in the Model (Continued).

Rx	Ref	Reaction	Rate Coefficient
R_{448}	B7	$O + O + O \rightarrow O_2 + O$	$l_{448} = 3.86 \times 10^{-30}\, T^{-1}\, e^{(-171.0/T)}$
R_{449}	B7	$O + O + O_2 \rightarrow O_2 + O_2$	$l_{449} = 3.86 \times 10^{-30}\, T^{-1}\, e^{(-171.0/T)}$
R_{450}	B7	$O + O + N_2 \rightarrow O_2 + N_2$	$l_{450} = 1.93 \times 10^{-30}\, T^{-1}\, e^{(-171.0/T)}$
R_{451}	B7	$O + O + N \rightarrow O_2 + N$	$l_{451} = 2.5 \times 10^{-30}\, T^{-1}\, e^{(-171.0/T)}$
R_{452}	B7	$O + O + Ar \rightarrow O_2 + Ar$	$l_{452} = 2.5 \times 10^{-30}\, T^{-1}\, e^{(-171.0/T)}$
R_{453}	B7	$O_2 + O \rightarrow O + O + O$	$k_{453} = 1.35 \times 10^{-4}\, T^{-1}\, e^{(-59700.0/T)}$
R_{454}	B7	$O_2 + O_2 \rightarrow O_2 + O + O$	$k_{454} = 4.48 \times 10^{-5}\, T^{-1}\, e^{(-59700.0/T)}$
R_{455}	B7	$O_2 + N_2 \rightarrow N_2 + O + O$	$k_{455} = 2.24 \times 10^{-5}\, T^{-1}\, e^{(-59700.0/T)}$
R_{456}	B7	$O_2 + N \rightarrow N + O + O$	$k_{456} = 7. \times 10^{-5}\, T^{-1}\, e^{(-59700.0/T)}$
R_{457}	B7	$O_2 + Ar \rightarrow Ar + O + O$	$k_{457} = 7.04 \times 10^{-5}\, T^{-1}\, e^{(-59700.0/T)}$
R_{458}	B7	$N + O_2 \rightarrow NO + O$	$k_{458} = 1.1 \times 10^{-14}\, T\, e^{(-3150.0/T)}$
R_{459}	B7	$NO + O \rightarrow N + O_2$	$k_{459} = 2.59 \times 10^{-15}\, T\, e^{(-19450.0/T)}$
R_{460}	B7	$N + NO \rightarrow N_2 + O$	$k_{460} = 3.4 \times 10^{-11}$
R_{461}	B7	$N_2 + O \rightarrow N + NO$	$k_{461} = 1.3 \times 10^{-10}\, e^{(-38000.0/T)}$
R_{462}	B7	$NO + NO \rightarrow N_2O + O$	$k_{462} = 2.16 \times 10^{-12}\, e^{(-32100.0/T)}$
R_{463}	H4	$N + O + N_2 \rightarrow NO + N_2$	$l_{463} = 1.1 \times 10^{-32}\, (300.0/T)^{(0.5)}$
R_{464}	H4	$N + O + O_2 \rightarrow NO + O_2$	$l_{464} = 1.1 \times 10^{-32}\, (300.0/T)^{(0.95)}$
R_{465}	B7	$NO + \{M\} \rightarrow N + O + \{M\}$	$k_{465} = 6.46 \times 10^{-4}\, T^{-3/2}\, e^{(-75000.0/T)}$
R_{466}	B7	$N_2 + O_2 \rightarrow N_2O + O$	$k_{466} = 9.96 \times 10^{-11}\, e^{(-55200.0/T)}$
R_{467}	B7	$N_2 + O_2 \rightarrow NO + NO$	$k_{467} = 7.64 \times 10^{+0}\, (T)^{(-2.5)}\, e^{(-64700.0/T)}$
R_{468}	B7	$NO + NO \rightarrow N_2 + O_2$	$k_{468} = 2.92 \times 10^{-11}\, e^{(-32214.0/T)}$
R_{469}	B7	$NO + NO \rightarrow NO_2 + N$	$k_{469} = 1.86 \times 10^{-13}\, e^{(-39200/T)}$
R_{470}	B7	$NO_2 + N \rightarrow NO + NO$	$k_{470} = 5.98 \times 10^{-12}$
R_{471}	B7	$N_2O + Ar \rightarrow N_2 + O + Ar$	$k_{471} = 8.3 \times 10^{-10}\, e^{(-29000.0/T)}$
R_{472}	B7	$N_2O + O_2 \rightarrow N_2 + O + O_2$	$k_{472} = 1.6 \times 10^{-9}\, e^{(-29000.0/T)}$
R_{473}	B7	$N_2O + N_2 \rightarrow N_2 + O + N_2$	$k_{473} = 1.6 \times 10^{-9}\, e^{(-29000.0/T)}$
R_{474}	B7	$N_2O + N_2O \rightarrow N_2 + O + N_2O$	$k_{474} = 8.3 \times 10^{-9}\, e^{(-29000.0/T)}$
R_{475}	B7	$N_2 + O + Ar \rightarrow N_2O + Ar$	$l_{475} = 3.9 \times 10^{-35}\, e^{(-10400.0/T)}$
R_{476}	B7	$N_2 + O + O_2 \rightarrow N_2O + O_2$	$l_{476} = 8. \times 10^{-34}\, e^{(-10400.0/T)}$
R_{477}	B7	$N_2 + O + N_2 \rightarrow N_2O + N_2$	$l_{477} = 8. \times 10^{-34}\, e^{(-10400.0/T)}$
R_{478}	B7	$N_2 + O(^1D) + \{M\} \rightarrow N_2O + \{M\}$	$l_{478} = 3.5 \times 10^{-37}\, (T/300)^{(-0.6)}$
R_{479}	H4	$N + NO + \{M\} \rightarrow N_2O + \{M\}$	$l_{479} = 1. \times 10^{-34}\, e^{(-1000.0/T)}$
R_{480}	B7	$N_2 + O \rightarrow N_2O$	$k_{480} = 1. \times 10^{-24}$
R_{481}	B7	$NO + O_2 \rightarrow NO_2 + O$	$k_{481} = 2.82 \times 10^{-12}\, e^{(-23400.0/T)}$
R_{482}	B7	$N + NO_2 \rightarrow N_2O + O$	$k_{482} = 3. \times 10^{-12}$
R_{483}	B7	$N_2O + O \rightarrow N + NO_2$	$k_{483} = 4.15 \times 10^{-1}\, (T)^{(-2.5)}\, e^{(-43000.0/T)}$
R_{484}	NB	$NO_2 + NO_2 \rightarrow N_2O_4$	$k_{484} = \mathrm{NPD}(1.269 \times 10^{-28}, -12.700, -3433.0, 8.303 \times 10^{-13}, -1.100, -0.0)$
R_{485}	NB	$N_2O_4 \rightarrow NO_2 + NO_2$	$j_{485} = \mathrm{NPD}(1.034 \times 10^{-7}, 0.000, -5010.0, 8.7 \times 10^{+16}, 0.000, -7948.0)$
R_{486}	NB	$NO_3 \rightarrow NO + O_2$	$j_{486} = \mathrm{NPD}(2.213 \times 10^{-13}, 0.000, -1811.0, 2.5 \times 10^{+6}, 0.000, -6100.0)$

Note: The definitions of the reactive families $\{X\}$ are at the end of this table.

TABLE 19-16. List of Chemical Reactions Included in the Model (Continued).

Rx	Ref	Reaction	Rate Coefficient
R_{487}	NB	$NO + NO_2 \rightarrow N_2O_3$	$k_{487} = \text{NPD}(9.108 \times 10^{-33}, 0.000, -0.0, 3.398 \times 10^{-12}, 0.000, -0.0)$
R_{488}	NB	$N_2O_3 \rightarrow NO + NO_2$	$j_{488} = \text{NPD}(1.034 \times 10^{-7}, 0.000, -5010.0, 8.7 \times 10^{+16}, 0.000, -7948.0)$
R_{489}	NB	$N_2O_3 + H_2O \rightarrow HONO + HONO$	$k_{489} = 6.298 \times 10^{-11}\ e^{(-4468.0/T)}$
R_{490}	B7	$NO_2 + \{M\} \rightarrow NO + O + \{M\}$	$k_{490} = 1.83 \times 10^{-8}\ e^{(-33000.0/T)}$
R_{491}	B7	$NO + NO + O_2 \rightarrow NO_2 + NO_2$	$l_{491} = 3.31 \times 10^{-39}\ e^{(530.0/T)}$
R_{492}	B7	$NO_2 + NO_2 \rightarrow NO + NO + O_2$	$k_{492} = 3.32 \times 10^{-12}\ e^{(-13540.0/T)}$
R_{493}	B7	$NO_2 + NO_3 \rightarrow NO + NO_2 + O_2$	$k_{493} = 2.3 \times 10^{-13}\ e^{(-1600.0/T)}$
R_{494}	B7	$O_2 + NO_2 + NO \rightarrow NO_2 + NO_3$	$l_{494} = 8. \times 10^{-41}\ e^{(400.0/T)}$
R_{495}	B7	$NO_2 + O_2 \rightarrow O_3 + NO$	$k_{495} = 2.79 \times 10^{-12}\ e^{(-25400.0/T)}$
R_{496}	B7	$NO_2 + NO_2 \rightarrow NO + NO_3$	$k_{496} = 6.47 \times 10^{-13}\ e^{(-12000.0/T)}$
	High T. reactions of $H_iC_jO_k$		
R_{497}	B7	$H_2O_2 + O_2 \rightarrow HO_2 + HO_2$	$k_{497} = 9. \times 10^{-11}\ e^{(-20000.0/T)}$
R_{498}	B7	$H_2O + HO_2 \rightarrow H_2O_2 + OH$	$k_{498} = 4.7 \times 10^{-11}\ e^{(-16500.0/T)}$
R_{499}	B7	$H_2O_2 + H \rightarrow H_2 + HO_2$	$k_{499} = 2.8 \times 10^{-12}\ e^{(-1900.0/T)}$
R_{500}	B7	$H_2 + HO_2 \rightarrow H_2O_2 + H$	$k_{500} = 1.2 \times 10^{-12}\ e^{(-9400.0/T)}$
R_{501}	B7	$H_2O_2 + H \rightarrow H_2O + OH$	$k_{501} = 4. \times 10^{-11}\ e^{(-2000.0/T)}$
R_{502}	B7	$H_2O_2 + CH_2 \rightarrow CH_3 + HO_2$	$k_{502} = 1. \times 10^{-14}$
R_{503}	B7	$H_2O_2 + O \rightarrow HO_2 + OH$	$k_{503} = 2.62 \times 10^{-13}\ (T/298)^{(2.6)}\ e^{(-1498.0/T)}$
R_{504}	B7	$H + H + \{M\} \rightarrow H_2 + \{M\}$	$l_{504} = 1.35 \times 10^{-32}\ (T/298)^{(-1.2)}\ e^{(-65/T)}$
R_{505}	B7	$H_2 + \{M\} \rightarrow H + H + \{M\}$	$k_{505} = 2.15 \times 10^{-9}\ e^{(-51570.0/T)}$
R_{506}	B7	$H_2O + Ar \rightarrow H + OH + Ar$	$k_{506} = 2.9 \times 10^{-10}\ e^{(-50323.0/T)}$
R_{507}	B7	$H_2O + N_2 \rightarrow H + OH + N_2$	$k_{507} = 5.8 \times 10^{-9}\ e^{(-52900.0/T)}$
R_{508}	B7	$H_2O + N \rightarrow H + OH + N$	$k_{508} = 5.8 \times 10^{-9}\ e^{(-52900.0/T)}$
R_{509}	B7	$H_2O + O_2 \rightarrow H + OH + O_2$	$k_{509} = 2.7 \times 10^{-7}\ e^{(-57491.0/T)}$
R_{510}	B7	$H_2O + O \rightarrow H + OH + O$	$k_{510} = 2.7 \times 10^{-7}\ e^{(-57491.0/T)}$
R_{511}	B7	$H_2O + OH \rightarrow H + OH + OH$	$k_{511} = 2.7 \times 10^{-7}\ e^{(-57491.0/T)}$
R_{512}	B7	$H_2O + H_2O \rightarrow H + OH + H_2O$	$k_{512} = 2.7 \times 10^{-7}\ e^{(-57491.0/T)}$
R_{513}	B7	$OH + OH \rightarrow H_2 + O_2$	$k_{513} = 1.17 \times 10^{-11}\ e^{(-24500.0/T)}$
R_{514}	B7	$OH + OH \rightarrow H + HO_2$	$k_{514} = 2. \times 10^{-11}\ e^{(-20200.0/T)}$
R_{515}	B7	$H + O + \{M\} \rightarrow OH + \{M\}$	$l_{515} = 4.36 \times 10^{-32}\ (T/298)^{(-1.0)}$
R_{516}	B7	$OH + \{M\} \rightarrow H + O + \{M\}$	$k_{516} = 4. \times 10^{-9}\ e^{(-50000.0/T)}$
R_{517}	B7	$H + NO \rightarrow N + OH$	$k_{517} = 2.2 \times 10^{-10}\ e^{(-24345.0/T)}$
R_{518}	B7	$CO_2 + O \rightarrow CO + O_2$	$k_{518} = 4.57 \times 10^{-11}\ e^{(-26666.20/T)}$
R_{519}	NB	$CO_2 + N \rightarrow CO + O + N$	$k_{519} = 5.088 \times 10^{-11}\ e^{(-51420.0/T)}$
R_{520}	NB	$CO_2 + N_2 \rightarrow CO + O + N_2$	$k_{520} = 5.088 \times 10^{-11}\ e^{(-51420.0/T)}$
R_{521}	NB	$CO_2 + O_2 \rightarrow CO + O + O_2$	$k_{521} = 5.088 \times 10^{-11}\ e^{(-51420.0/T)}$
R_{522}	NB	$CO_2 + H \rightarrow CO + OH$	$k_{522} = 4.043 \times 10^{-10}\ e^{(-13280.0/T)}$
R_{523}	B7	$CO + O_2 \rightarrow CO_2 + O$	$k_{523} = 8.91 \times 10^{-12}\ e^{(-24120.0/T)}$

Note: The definitions of the reactive families $\{X\}$ are at the end of this table.

TABLE 19-17. List of Chemical Reactions Included in the Model (Continued).

Rx	Ref	Reaction	Rate Coefficient
R_{524}	B7	$CO + NO_2 \rightarrow CO_2 + NO$	$k_{524} = 1.04 \times 10^{-8}\ e^{(-18561.0/T)}$
R_{525}	B7	$CO + \{M\} \rightarrow C + O + \{M\}$	$k_{525} = 1.4 \times 10^{+6}\ (T)^{(-3.52)}\ e^{(-128700.0/T)}$
R_{526}	B7	$C + O + \{M\} \rightarrow CO + \{M\}$	$l_{526} = 9.1 \times 10^{-22}\ (T)^{(-3.08)}\ e^{(+2114.0/T)}$
R_{527}	B7	$CN + O \rightarrow CO + N$	$k_{527} = 2.31 \times 10^{-11}\ e^{(-98/T)}$
R_{528}	NB	$CH + N_2 \rightarrow HCN + N$	$k_{528} = \text{NPD}(2.603 \times 10^{-31}, 0.000, -0.0, 4.75 \times 10^{-14}, 0.000, 345.6)$
		High temperature quench	
R_{529}	NB	$CN + CH_4 \rightarrow HCN + CH_3$	$k_{529} = 1.325 \times 10^{-11}\ e^{(-875.0/T)}$
R_{530}	NB	$CN + H_2 \rightarrow HCN + H$	$k_{530} = 8.726 \times 10^{-13}\ (T/298)^{(2.437)}\ e^{(-1067.0/T)}$
R_{531}	NB	$CN + O_2 \rightarrow NCO + O$	$k_{531} = 8.929 \times 10^{-12}\ (T/298)^{(0.011)}\ e^{(167.1/T)}$
R_{532}	NB	$CN + CO_2 \rightarrow NCO + CO$	$k_{532} = 1.57 \times 10^{-11}\ e^{(-1956.0/T)}$
R_{533}	NB	$CN + NO \rightarrow NCO + N$	$k_{533} = 1.544 \times 10^{-10}\ e^{(-21050.0/T)}$
R_{534}	NB	$CN + NO \rightarrow N_2 + CO$	$k_{534} = 6.717 \times 10^{-14}\ e^{(92.2/T)}$
R_{535}	NB	$NCO + O_2 \rightarrow NO + CO_2$	$k_{535} = 1.319 \times 10^{-12}$
R_{536}	NB	$O + NCO \rightarrow NO + CO$	$k_{536} = 4.826 \times 10^{-11}\ e^{(-335.5/T)}$
R_{537}	NB	$H + NCO \rightarrow NH + CO$	$k_{537} = 9.969 \times 10^{-11}\ e^{(-208.1/T)}$
R_{538}	NB	$N + NCO \rightarrow CN + NO$	$k_{538} = 1.66 \times 10^{-12}\ e^{(0.0/T)}$
R_{539}	NB	$N + NCO \rightarrow N_2 + CO$	$k_{539} = 3.321 \times 10^{-11}\ e^{(0.0/T)}$
R_{540}	B7	$N + O_3 \rightarrow NO + O_2$	$k_{540} = 7. \times 10^{-16}$
R_{541}	NB	$NCO \rightarrow N + CO$	$j_{541} = 1.979 \times 10^{-18}\ e^{(23480.0/T)}$
R_{542}	NB	$HCN \rightarrow H + CN$	$j_{542} = 1.115 \times 10^{-8}\ e^{(-53170.0/T)}$
R_{543}	NB	$O + HCN \rightarrow OH + CN$	$k_{543} = 2.237 \times 10^{-9}\ e^{(-14680.0/T)}$
R_{544}	NB	$O + HCN \rightarrow H + NCO$	$k_{544} = 7.524 \times 10^{-13}\ (T/298)^{(1.652)}\ e^{(-3563.0/T)}$
R_{545}	NB	$O + HCN \rightarrow CO + NH$	$k_{545} = 4.267 \times 10^{-13}\ (T/298)^{(1.322)}\ e^{(-3580.0/T)}$
R_{546}	NB	$OH + HCN \rightarrow H_2O + CN$	$k_{546} = 1.185 \times 10^{-11}\ e^{(-4279.0/T)}$
R_{547}	NB	$OH + HCN \rightarrow NH_2 + CO$	$k_{547} = 1.07 \times 10^{-13}\ e^{(-5892.0/T)}$
R_{548}	NB	$H + HCN \rightarrow CN + H_2$	$k_{548} = 6.313 \times 10^{-10}\ e^{(-12400.0/T)}$
R_{549}	B7	$C + O_2 \rightarrow CO + O$	$k_{549} = 3.1 \times 10^{-11}\ (T/298)^{(0.5)}$
R_{550}	B7	$C + N_2 \rightarrow CN + N$	$k_{550} = 5. \times 10^{-11}\ (T/298)^{(0.5)}$
R_{551}	B7	$NH + O_2 \rightarrow HNO + O$	$k_{551} = 1.66 \times 10^{-10}\ e^{(-503/T)}$
R_{552}	B7	$H + N_2 \rightarrow NH + N$	$k_{552} = 3.93 \times 10^{-10}\ e^{(-72564.0/T)}$
R_{553}	B7	$OH + N \rightarrow H + NO$	$k_{553} = 4.05 \times 10^{-11}\ e^{(61.0/T)}$
		CH_4 Oxidation	
R_{554}	NB	$CH_4 + O(^1D) \rightarrow CH_2O + H_2$	$k_{554} = 1.4 \times 10^{-11}$
R_{555}	NB	$CH_4 + O(^1D) \rightarrow CH_3 + OH$	$k_{555} = 1.4 \times 10^{-10}$
R_{556}	NB	$CH_4 + OH \rightarrow CH_3 + H_2O$	$k_{556} = 3.398 \times 10^{-13}\ (T/298)^{(2.317)}\ e^{(-1130.0/T)}$
R_{557}	NB	$CH_4 + HO_2 \rightarrow CH_3 + H_2O_2$	$k_{557} = 1.216 \times 10^{-11}\ e^{(-10321.5/T)}$
R_{558}	NB	$CH_4 + NO_2 \rightarrow CH_3 + HONO$	$k_{558} = 2.959 \times 10^{-12}\ e^{(-14354.2/T)}$

Note: The definitions of the reactive families $\{X\}$ are at the end of this table.

TABLE 19-18. List of Chemical Reactions Included in the Model (Continued).

Rx	Ref	Reaction	Rate Coefficient
R_{559}	NB	$CH_4 + O \rightarrow CH_3 + OH$	$k_{559} = 4.57 \times 10^{-12} (T/298)^{(1.782)} e^{(-3982.3/T)}$
R_{560}	NB	$CH_4 + O \rightarrow CH_2 + H_2O$	$k_{560} = 5.498 \times 10^{-12} e^{(-3372.0/T)}$
R_{561}	NB	$CH_4 + H \rightarrow CH_3 + H_2$	$k_{561} = 5.008 \times 10^{-13} (T/298)^{(3.053)} e^{(-3995.9/T)}$
R_{562}	NB	$CH_4 + O_2 \rightarrow CH_3 + HO_2$	$k_{562} = 5.249 \times 10^{-10} e^{(-28508.8/T)}$
R_{563}	NB	$CH_3 + O_2 \rightarrow CH_3O + O$	$k_{563} = 7.062 \times 10^{-11} e^{(-15367.5/T)}$
R_{564}	NB	$CH_3 + O_2 \rightarrow CH_2O + OH$	$k_{564} = 9.076 \times 10^{-20} (T/298)^{(6.429)} e^{(3122.4/T)}$
R_{565}	NB	$CH_3 + O_3 \rightarrow CH_3O_2 + O$	$k_{565} = 5.653 \times 10^{-12} e^{(-315.0/T)}$
R_{566}	NB	$CH_3 + H_2 \rightarrow CH_4 + H$	$k_{566} = 7.387 \times 10^{-15} (T/298)^{(3.527)} e^{(-3775.3/T)}$
R_{567}	NB	$CH_3 + HO_2 \rightarrow CH_3O + OH$	$k_{567} = 3.298 \times 10^{-11}$
R_{568}	NB	$CH_3 + HO_2 \rightarrow CH_4 + O_2$	$k_{568} = 6. \times 10^{-12}$
R_{569}	NB	$CH_3 + H_2O \rightarrow CH_4 + OH$	$k_{569} = 1.2 \times 10^{-14} (T/298)^{(2.900)} e^{(-7480.0/T)}$
R_{570}	NB	$CH_3 + H_2O_2 \rightarrow CH_4 + HO_2$	$k_{570} = 2.001 \times 10^{-14} e^{(300.0/T)}$
R_{571}	NB	$CH_3 + NO_2 \rightarrow CH_3O + NO$	$k_{571} = 2.062 \times 10^{-11} e^{(56.9/T)}$
R_{572}	NB	$CH_3 + N_2O \rightarrow CH_3O + N_2$	$k_{572} = 2.324 \times 10^{-17}$
R_{573}	NB	$CH_3 + O \rightarrow CH_2O + H$	$k_{573} = 1.224 \times 10^{-10} e^{(-37.4/T)}$
R_{574}	NB	$CH_3 + CH_3O_2 \rightarrow CH_3O + CH_3O$	$k_{574} = 4.001 \times 10^{-11}$
R_{575}	NB	$CH_3O \rightarrow CH_2OH$	$j_{575} = 2.651 \times 10^{+4} e^{(-4433.4/T)}$
R_{576}	NB	$CH_3O + H \rightarrow CH_2O + H_2$	$k_{576} = 3.308 \times 10^{-11} e^{(0.4/T)}$
R_{577}	NB	$CH_3O + OH \rightarrow CH_2O + H_2O$	$k_{577} = 3. \times 10^{-11}$
R_{578}	NB	$CH_3O + HO_2 \rightarrow CH_2O + H_2O_2$	$k_{578} = 5.003 \times 10^{-13}$
R_{579}	NB	$CH_3O + NO \rightarrow CH_2O + HNO$	$k_{579} = 5.012 \times 10^{-12}$
R_{580}	NB	$CH_3O + NO_2 \rightarrow CH_2O + HONO$	$k_{580} = 8.321 \times 10^{-13}$
R_{581}	NB	$CH_3O + O \rightarrow CH_2O + OH$	$k_{581} = 1. \times 10^{-11}$
R_{582}	NB	$CH_3O + O_2 \rightarrow CH_2O + HO_2$	$k_{582} = 8.605 \times 10^{-14} e^{(-1117.4/T)}$
R_{583}	NB	$CH_3O + CH_3O_2 \rightarrow CH_2O + CH_3OOH$	$k_{583} = 5.003 \times 10^{-13}$
R_{584}	NB	$CH_3O + CO \rightarrow CH_3 + CO_2$	$k_{584} = 2.61 \times 10^{-11} e^{(-5938.3/T)}$
R_{585}	A9	$CH_3O + NO \rightarrow CH_3ONO$	$k_{585} = 2 \times 10^{-11}$
R_{586}	A9	$CH_3O + NO_2 \rightarrow CH_3ONO_2$	$k_{586} = 1.2 \times 10^{-11}$
R_{587}	NB	$CH_3O_2 + \{M\} \rightarrow CH_3 + O_2 + \{M\}$	$k_{587} = 2.019 (T/298)^{(-10.020)} e^{(-16731.0/T)}$
R_{588}	NB	$CH_3O_2 + OH \rightarrow CH_3OH + O_2$	$k_{588} = 1. \times 10^{-10}$
R_{589}	NB	$CH_3O_2 + HO_2 \rightarrow O_2 + CH_3OOH$	$k_{589} = 7.651 \times 10^{-14} e^{(1298.7/T)}$
R_{590}	NB	$CH_3O_2 + H_2O_2 \rightarrow HO_2 + CH_3OOH$	$k_{590} = 4.001 \times 10^{-12} e^{(-5000.0/T)}$
R_{591}	NB	$CH_3O_2 + H \rightarrow CH_3O + OH$	$k_{591} = 1.6 \times 10^{-10}$
R_{592}	NB	$CH_3O_2 + NO \rightarrow CH_3O + NO_2$	$k_{592} = 1.004 \times 10^{-11} (T/298)^{(-1.503)} e^{(-95.1/T)}$
R_{593}	NB	$CH_3O_2 + O \rightarrow CH_3O + O_2$	$k_{593} = 7.032 \times 10^{-11} e^{(1.9/T)}$
R_{594}	NB	$CH_3O_2 + CH_2O \rightarrow CHO + CH_3OOH$	$k_{594} = 3.296 \times 10^{-12} e^{(-5870.2/T)}$
R_{595}	NB	$CH_3O_2 + CH_3OH \rightarrow CH_2OH + CH_3OOH$	$k_{595} = 3. \times 10^{-12} e^{(-6900.0/T)}$
R_{596}	NB	$CH_3O_2 + H_2 \rightarrow CH_3OOH + H$	$k_{596} = 5.003 \times 10^{-11} e^{(-13100.0/T)}$

Note: The definitions of the reactive families $\{X\}$ are at the end of this table.

TABLE 19-19. List of Chemical Reactions Included in the Model (Continued).

Rx	Ref	Reaction	Rate Coefficient
R_{597}	NB	$CH_3O_2 + CH_3O_2 \rightarrow CH_3O + CH_3O + O_2$	$k_{597} = 2.367 \times 10^{-13}\ e^{(169.3/T)}$
R_{598}	NB	$CH_3O_2 + NO_3 \rightarrow NO_2 + CH_3O + O_2$	$k_{598} = 2.303 \times 10^{-12}$
R_{599}	NB	$CH_3OH + NO_3 \rightarrow HONO_2 + CH_2OH$	$k_{599} = 1.251 \times 10^{-12}\ e^{(-2562.0/T)}$
R_{600}	A6	$CH_3OH + OH \rightarrow CH_3O + H_2O$	$k_{600} = 1.7 \times 10^{-12}\ e^{(-806/T)}$
R_{601}	A6	$CH_3OH + OH \rightarrow CH_2OH + H_2O$	$k_{601} = 9.8 \times 10^{-12}\ e^{(-806/T)}$
R_{602}	NB	$CH_3ONO \rightarrow CH_2O + HNO$	$j_{602} = 3.143 \times 10^{+11}\ e^{(-17329.6/T)}$
R_{603}	NB	$CH_3ONO + H \rightarrow CH_3OH + NO$	$k_{603} = 2.019 \times 10^{-13}\ e^{(-956.0/T)}$
R_{604}	NB	$CH_3ONO + O_3 \rightarrow CH_3ONO_2 + O_2$	$k_{604} = 6.764 \times 10^{-13}\ e^{(-5315.0/T)}$
R_{605}	NB	$CH_3OOH + H \rightarrow CH_3O + H_2O$	$k_{605} = 2.8 \times 10^{-13}\ e^{(-946.0/T)}$
R_{606}	NB	$CH_3OOH + H \rightarrow H_2 + CH_3O_2$	$k_{606} = 2.8 \times 10^{-13}\ e^{(-946.0/T)}$
R_{607}	NB	$CH_3OOH + OH \rightarrow CH_2OOH + H_2O$	$k_{607} = 1. \times 10^{-11}$
R_{608}	NB	$CH_2OOH \rightarrow CH_2O + OH$	$j_{608} = 5. \times 10^{+4}$
R_{609}	NB	$CH_3OOH + OH \rightarrow CH_3O_2 + H_2O$	$k_{609} = 5.9 \times 10^{-12}$
R_{610}	NB	$CH_3OOH + OH \rightarrow CH_2O + H_2O + OH$	$k_{610} = 2.9 \times 10^{-12}\ e^{((-900+712)/T)}$
R_{611}	A9	$CH_3ONO_2 \rightarrow CH_3O + NO_2$	$j_{611} = 1.7 \times 10^{+17}\ e^{(-20125/T)}$
R_{612}	NB	$CH_2 + CO_2 \rightarrow CH_2O + CO$	$k_{612} = 3.901 \times 10^{-14}$
R_{613}	NB	$CH_2 + O \rightarrow CHO + H$	$k_{613} = 5.014 \times 10^{-11}$
R_{614}	NB	$CH_2 + H_2O \rightarrow CH_3 + OH$	$k_{614} = 1.6 \times 10^{-16}$
R_{615}	NB	$CH_2 + H_2 \rightarrow CH_3 + H$	$k_{615} = 5.003 \times 10^{-15}$
R_{616}	NB	$CH_2 + OH \rightarrow CH_2O + H$	$k_{616} = 3. \times 10^{-11}$
R_{617}	NB	$CH_2 + H \rightarrow CH + H_2$	$k_{617} = 2.719 \times 10^{-10}\ e^{(-205.7/T)}$
R_{618}	NB	$CH_2 + CO \rightarrow CH_2CO$	$k_{618} = 1. \times 10^{-15}$
R_{619}	NB	$CH_2 + O_2 \rightarrow CO + H_2O$	$k_{619} = 4.001 \times 10^{-13}$
R_{620}	NB	$CH_2 + O_2 \rightarrow H + H + CO_2$	$k_{620} = 9.959 \times 10^{-12}$
R_{621}	NB	$CH_2 + O_2 \rightarrow CH_2O + O$	$k_{621} = 9.959 \times 10^{-12}$
R_{622}	NB	$CH_2 + NO \rightarrow CO + NH_2$	$k_{622} = 2.5 \times 10^{-10}$
R_{623}	NB	$CH_2 + H_2O \rightarrow CH_2OH + H$	$k_{623} = 9.49 \times 10^{-12}\ e^{(380/T)}$
R_{624}	NB	$CH_2 + CH_3OH \rightarrow CH_3 + CH_2OH$	$k_{624} = 5.299 \times 10^{-23}\ (T/298)^{(3.200)}\ e^{(-3609.0/T)}$
R_{625}	NB	$CH_2 + CH_3OH \rightarrow CH_3 + CH_3O$	$k_{625} = 2.4 \times 10^{-23}\ (T/298)^{(3.100)}\ e^{(-3490.0/T)}$
R_{626}	NB	$CH_2 + CH_3O_2 \rightarrow CH_2O + CH_3O$	$k_{626} = 3. \times 10^{-11}$
R_{627}	NB	$CH_2O + \{M\} \rightarrow CO + H_2 + \{M\}$	$k_{627} = 7.503 \times 10^{-9}\ e^{(-17762.7/T)}$
R_{628}	NB	$CH_2O + O_2 \rightarrow CHO + HO_2$	$k_{628} = 2.976 \times 10^{-11}\ e^{(-19583.7/T)}$
R_{629}	NB	$CH_2O + O \rightarrow CHO + OH$	$k_{629} = 6.786 \times 10^{-11}\ e^{(-1778.7/T)}$
R_{630}	NB	$CH_2O + HO_2 \rightarrow CH_2OH + O_2$	$k_{630} = 5.626 \times 10^{-12}\ e^{(-9622.0/T)}$
R_{631}	NB	$CH_2O + HO_2 \rightarrow CHO + H_2O_2$	$k_{631} = 4.148 \times 10^{-12}\ e^{(-5899.7/T)}$
R_{632}	NB	$CH_2O + H \rightarrow CHO + H_2$	$k_{632} = 5.243 \times 10^{-12}\ (T/298)^{(1.875)}\ e^{(-1390.1/T)}$
R_{633}	NB	$CH_2O + OH \rightarrow CHO + H_2O$	$k_{633} = 4.103 \times 10^{-12}\ (T/298)^{(1.251)}\ e^{(268.6/T)}$

Note: The definitions of the reactive families $\{X\}$ are at the end of this table.

TABLE 19-20. List of Chemical Reactions Included in the Model (Continued).

Rx	Ref	Reaction	Rate Coefficient
R_{634}	NB	$CH_2CO \rightarrow CH_2 + CO$	$j_{634} = \text{NPD}(6.099 \times 10^{-9}, 0.000, -29850.0, 2.984 \times 10^{+14}, 0.000, -35720.0)$
R_{635}	D7	$CH_2OH + O_2 \rightarrow CH_2O + HO_2$	$k_{635} = 9.6 \times 10^{-12}$
R_{636}	NB	$O + CH_2CO \rightarrow CH_2O + CO$	$k_{636} = 0.5\ 3.875 \times 10^{-12}\ e^{(-649.1/T)}$
R_{637}	NB	$O + CH_2CO \rightarrow CH_2 + CO_2$	$k_{637} = 0.5\ 3.875 \times 10^{-12}\ e^{(-649.1/T)}$
R_{638}	NB	$OH + CH_2CO \rightarrow CHO + CH_2O$	$k_{638} = 4.648 \times 10^{-11}$
R_{639}	NB	$H + CH_2CO \rightarrow CH_3 + CO$	$k_{639} = 5.699 \times 10^{-11}\ e^{(-1916.0/T)}$
R_{640}	A9	$CHO + O_2 \rightarrow CO + HO_2$	$k_{640} = 3.5 \times 10^{-12}\ e^{(+140/T)}$
R_{641}	NB	$CHO + O \rightarrow CO_2 + H$	$k_{641} = 4.991 \times 10^{-11}$
R_{642}	NB	$CHO + O \rightarrow CO + OH$	$k_{642} = 4.991 \times 10^{-11}$
R_{643}	NB	$CHO + OH \rightarrow CO + H_2O$	$k_{643} = 5.003 \times 10^{-11}$
R_{644}	NB	$CHO + H \rightarrow CO + H_2$	$k_{644} = 1.797 \times 10^{-10}\ e^{(-37.9/T)}$
R_{645}	NB	$CHO + H \rightarrow CH_2O$	$k_{645} = 7.766 \times 10^{-14}\ e^{(2285.0/T)}$
R_{646}	NB	$CHO + H_2O \rightarrow CH_2O + OH$	$k_{646} = 1.794 \times 10^{-11}\ e^{(-14121.8/T)}$
R_{647}	NB	$CHO + H_2O_2 \rightarrow CH_2O + HO_2$	$k_{647} = 1.699 \times 10^{-13}\ e^{(-3486.0/T)}$
R_{648}	NB	$CHO + H_2 \rightarrow CH_2O + H$	$k_{648} = 2.662 \times 10^{-13}\ (T/298)^{(2.000)}\ e^{(-8972.0/T)}$
R_{649}	NB	$CHO + \{M\} \rightarrow CO + H + \{M\}$	$k_{649} = 3.805 \times 10^{-10}\ e^{(-8688.8/T)}$
R_{650}	NB	$CHO + CHO \rightarrow CH_2O + CO$	$k_{650} = 3.054 \times 10^{-11}\ e^{(16.4/T)}$
R_{651}	NB	$CHO + CH_2 \rightarrow CH_3 + CO$	$k_{651} = 3. \times 10^{-11}$
R_{652}	NB	$CHO + CH_3 \rightarrow CH_4 + CO$	$k_{652} = 2.001 \times 10^{-10}$
R_{653}	NB	$CHO + CH_2OH \rightarrow CH_3OH + CO$	$k_{653} = 2.001 \times 10^{-10}$
R_{654}	NB	$CHO + CH_2OH \rightarrow CH_2O + CH_2O$	$k_{654} = 3. \times 10^{-10}$
R_{655}	NB	$CHO + CH_3O \rightarrow CH_3OH + CO$	$k_{655} = 1.5 \times 10^{-10}$
R_{656}	NB	$CHO + CH_4 \rightarrow CH_2O + CH_3$	$k_{656} = 1.359 \times 10^{-13}\ (T/298)^{(2.850)}\ e^{(-11330.0/T)}$
R_{657}	NB	$CHO + CH_3OH \rightarrow CH_2O + CH_2OH$	$k_{657} = 2.4 \times 10^{-13}\ (T/298)^{(2.900)}\ e^{(-6596.0/T)}$
R_{658}	NB	$CHO + NO \rightarrow CO + HNO$	$k_{658} = 8.609 \times 10^{-12}\ e^{(86.7/T)}$
R_{659}	NB	$CO + OH \rightarrow CO_2 + H$	$k_{659} = 1.53 \times 10^{-14}\ (T/298)^{(1.898)}\ e^{(716.5/T)}$
R_{660}	NB	$CO + HO_2 \rightarrow CO_2 + OH$	$k_{660} = 7.11 \times 10^{-10}\ e^{(-12218.2/T)}$
R_{661}	NB	$CO_2 + CH \rightarrow CHO + CO$	$k_{661} = 5.532 \times 10^{-12}\ e^{(-324.1/T)}$
R_{662}	NB	$CH + H_2O \rightarrow CH_2OH$	$k_{662} = 9.489 \times 10^{-12}\ e^{(380.0/T)}$
R_{663}	NB	$CH + H_2 \rightarrow CH_2 + H$	$k_{663} = 1.291 \times 10^{-11}\ (T/298)^{(1.849)}\ e^{(-807.7/T)}$
R_{664}	NB	$CH + O \rightarrow CO + H$	$k_{664} = 7.113 \times 10^{-11}\ e^{(-30.6/T)}$
R_{665}	NB	$CH + O_2 \rightarrow CO + OH$	$k_{665} = 3.298 \times 10^{-11}$
R_{666}	NB	$CH + NO \rightarrow CO + NH$	$k_{666} = 2.502 \times 10^{-10}$
R_{667}	NB	$CH + N_2O \rightarrow CHO + N_2$	$k_{667} = 6.906 \times 10^{-11}$
		DMS Oxidation	
R_{668}	NM	$DMS + OH \rightarrow CH_3SOHCH_3$	$k_{668} = 3.5 \times 10^{-12}\ e^{(+353/T)}$
R_{669}	NB	$DMS + OH \rightarrow CH_3SCH_2 + H_2O$	$k_{669} = 1.359 \times 10^{-11}\ e^{(-332.0/T)}$
R_{670}	NB	$DMS + O \rightarrow CH_3SCH_2 + OH$	$k_{670} = 1.42 \times 10^{-11}\ e^{(366.0/T)}$
R_{671}	NB	$DMS + CH_3 \rightarrow CH_3SCH_2 + CH_4$	$k_{671} = 6.921 \times 10^{-13}\ e^{(-4613.0/T)}$

Note: The definitions of the reactive families $\{X\}$ are at the end of this table.

TABLE 19-21. List of Chemical Reactions Included in the Model (Continued).

Rx	Ref	Reaction	Rate Coefficient
R_{672}	NB	$DMS + H \rightarrow CH_3SH + CH_3$	$k_{672} = 1.005 \times 10^{-11}\, e^{(-1114.6/T)}$
R_{673}	NB	$DMS + NO_3 \rightarrow CH_3SCH_2 + HONO_2$	$k_{673} = 1.762 \times 10^{-13}\, e^{(500.0/T)}$
R_{674}	NM	$CH_3SOHCH_3 + O_2 \rightarrow CH_3SOCH_3 + HO_2$	$k_{674} = 5.53 \times 10^{-15}\, e^{(+910/T)}$
R_{675}	NM	$CH_3SOHCH_3 \rightarrow DMS + OH$	$j_{675} = 1 \times 10^{-16}\, e^{(-6550/T)}$
R_{676}	NM	$CH_3SCH_2 + O_2 \rightarrow CH_3SCH_2O_2$	$k_{676} = 9.6 \times 10^{-12}$
R_{677}	NB	$CH_3SH + O \rightarrow SO + CH_4$	$k_{677} = 0.9\ 1.138 \times 10^{-11}\, e^{(-512.1/T)}$
R_{678}	NB	$CH_3SH + O \rightarrow CH_3S + OH$	$k_{678} = 0.1\ 1.138 \times 10^{-11}\, e^{(-512.1/T)}$
R_{679}	NB	$CH_3SH + OH \rightarrow CH_3S + H_2O$	$k_{679} = 1.055 \times 10^{-11}\, e^{(356.2/T)}$
R_{680}	NB	$CH_3SH + H \rightarrow H_2 + CH_3S$	$k_{680} = 2.474 \times 10^{-11}\, e^{(-1026.0/T)}$
R_{681}	NB	$CH_3SH + H \rightarrow H_2S + CH_3$	$k_{681} = 1.146 \times 10^{-11}\, e^{(-841.0/T)}$
R_{682}	NB	$CH_3SH + NO_3 \rightarrow CH_3S + HONO_2$	$k_{682} = 5.058 \times 10^{-13}\, e^{(169.9/T)}$
R_{683}	NM	$CH_3SOCH_3 + OH \rightarrow CH_3SOCH_2 + H_2O$	$k_{683} = 9.6 \times 10^{-12}\, e^{(-234/T)}$
R_{684}	NM	$CH_3SOCH_3 + OH \rightarrow CH_3SOOHCH_3$	$k_{684} = 3.5 \times 10^{-12}\, e^{(+353/T)}$
R_{685}	NM	$CH_3SCH_2O_2 + HO_2 \rightarrow CH_3SCH_2OOH + O_2$	$k_{685} = 3.2 \times 10^{-12}$
R_{686}	NM	$CH_3SCH_2O_2 + NO \rightarrow CH_3S + CH_2O + NO_2$	$k_{686} = 4.2 \times 10^{-12}\, e^{(180/T)}$
R_{687}	NM	$CH_3SCH_2O_2 + CH_3O_2 \rightarrow CH_3SCH_2OH + CH_2O + O_2$	$k_{687} = 2.13 \times 10^{-13}$
R_{688}	NM	$CH_3SCH_2O_2 + CH_3O_2 \rightarrow CH_3SCHO + CH_3OH + O_2$	$k_{688} = 2.13 \times 10^{-13}$
R_{689}	NM	$CH_3SCH_2OOH + OH \rightarrow CH_3SCH_2O_2 + H_2O$	$k_{689} = 5.9 \times 10^{-12}$
R_{690}	NM	$CH_3SCH_2OOH + OH \rightarrow CH_3SCHO + H_2O + OH$	$k_{690} = 2.9 \times 10^{-12}\, e^{((-367+782)/T)}$
R_{691}	NM	$CH_3SCH_2OH + OH \rightarrow CH_3SCHOH + H_2O$	$k_{691} = 2.9 \times 10^{-12}\, e^{((-367+435)/T)}$
R_{692}	NM	$CH_3SCHOH + O_2 \rightarrow CH_3SCHO + HO_2$	$k_{692} = 9.6 \times 10^{-12}$
R_{693}	NM	$CH_3SCHO + OH \rightarrow CH_3S + CO + H_2O$	$k_{693} = 1.3 \times 10^{-12}\, e^{((+111+718)/T)}$
R_{694}	NM	$CH_3SOOHCH_3 + O_2 \rightarrow CH_3SO_2CH_3 + HO_2$	$k_{694} = 9.7 \times 10^{-12}$
R_{695}	NM	$CH_3SOCH_2 + O_2 \rightarrow CH_3 + SO_2 + CH_2O$	$k_{695} = 1 \times 10^{-15}$
R_{696}	NM	$CH_3SO_2CH_3 + OH \rightarrow CH_3SO_2CH_2 + H_2O$	$k_{696} = 9.6 \times 10^{-12}\, e^{(-234/T)}$
R_{697}	NM	$CH_3SO_2CH_2 + O_2 \rightarrow CH_3SO_3 + CH_2O$	$k_{697} = 1 \times 10^{-15}$
R_{698}	NM	$CH_3SO_3 + HO_2 \rightarrow CH_3SO_2OH + O_2$	$k_{698} = 3.2 \times 10^{-12}$

TABLE 19-22. List of Chemical Reactions Included in the Model (Continued).

Rx	Ref	Reaction	Rate Coefficient
R_{699}	NM	$CH_3S + O_2 \rightarrow CH_3 + SO_2$	$k_{699} = 2. \times 10^{-18}$
R_{700}	NM	$CH_3S + O_3 \rightarrow CH_3SO + O_2$	$k_{700} = 4.1 \times 10^{-12}$
R_{701}	NM	$CH_3SO + NO_2 \rightarrow CH_3SO_2 + NO$	$k_{701} = 1.2 \times 10^{-11}$
R_{702}	NM	$CH_3SO + O_3 \rightarrow CH_3SO_2 + O_2$	$k_{702} = 1.2 \times 10^{-12}$
R_{703}	NM	$CH_3SO_2 + OH \rightarrow CH_3SO_2OH$	$k_{703} = 1. \times 10^{-12}$
		H_2S, OCS, and CS_2 Oxidation	
R_{704}	NB	$CH_3 + H_2S \rightarrow CH_4 + SH$	$k_{704} = 1.936 \times 10^{-13}\ e^{(-1077.0/T)}$
R_{705}	NB	$O + H_2S \rightarrow OH + SH$	$k_{705} = 1.021 \times 10^{-11}\ e^{(-1827.0/T)}$
R_{706}	NB	$OH + H_2S \rightarrow H_2O + SH$	$k_{706} = 1.043 \times 10^{-11}\ e^{(-221.5/T)}$
R_{707}	NB	$H + H_2S \rightarrow H_2 + SH$	$k_{707} = 2.302 \times 10^{-11}\ e^{(-938.2/T)}$
R_{708}	NB	$O_3 + H_2S \rightarrow H_2O + SO_2$	$k_{708} = 2.626 \times 10^{-12}\ e^{(-2617.0/T)}$
R_{709}	NB	$C\ell + H_2S \rightarrow HC\ell + SH$	$k_{709} = 6.254 \times 10^{-11}\ e^{(-11.0/T)}$
R_{710}	NB	$HSO + NO_2 \rightarrow HOSO + NO$	$k_{710} = 9.599 \times 10^{-12}\ e^{(-0.0/T)}$
R_{711}	NB	$HSO + O_3 \rightarrow O_2 + O_2 + SH$	$k_{711} = 2.542 \times 10^{-13}\ e^{(-384.0/T)}$
R_{712}	NB	$HOSO + O_2 \rightarrow HO_2 + SO_2$	$k_{712} = 3.001 \times 10^{-13}\ e^{(0.0/T)}$
R_{713}	NB	$HOSO_2 + O_2 \rightarrow HO_2 + SO_3$	$k_{713} = 1. \times 10^{-12}\ e^{(-266.0/T)}$
R_{714}	NB	$OCS + H \rightarrow CO + SH$	$k_{714} = 2.313 \times 10^{-11}\ e^{(-2137.5/T)}$
R_{715}	NB	$OCS + OH \rightarrow CO_2 + SH$	$k_{715} = 1.612 \times 10^{-13}\ e^{(-1150.8/T)}$
R_{716}	NB	$OCS + O \rightarrow CO + SO$	$k_{716} = 1.438 \times 10^{-11}\ e^{(-2103.5/T)}$
R_{717}	NB	$OCS + O \rightarrow CO_2 + S$	$k_{717} = 8.321 \times 10^{-11}\ e^{(-5527.0/T)}$
R_{718}	NB	$OCS + NO_3 \rightarrow CO + SO + NO_2$	$k_{718} = 1. \times 10^{-15}$
R_{719}	NB	$CS_2 \rightarrow CS + S$	$j_{719} = 4.171 \times 10^{-10}\ e^{(-37390.0/T)}$
R_{720}	NB	$CS_2 + O \rightarrow SO + CS$	$k_{720} = 2.685 \times 10^{-11}\ e^{(-629.3/T)}$
R_{721}	NB	$CS_2 + O \rightarrow OCS + S$	$k_{721} = 3.649 \times 10^{-12}\ e^{(-701.0/T)}$
R_{722}	NB	$CS_2 + O_2 \rightarrow CS + SO_2$	$k_{722} = 1.66 \times 10^{-12}\ e^{(-16100.0/T)}$
R_{723}	NB	$CS_2 + OH \rightarrow CS_2OH$	$k_{723} = 1.719 \times 10^{-14}\ e^{(877.0/T)}$
R_{724}	NB	$CS_2 + OH \rightarrow SH + OCS$	$k_{724} = 4.298 \times 10^{-13}$
R_{725}	NB	$O + CS \rightarrow CO + S$	$k_{725} = 2.629 \times 10^{-10}\ e^{(-758.3/T)}$
R_{726}	NB	$CS + O_2 \rightarrow OCS + O$	$k_{726} = 4.172 \times 10^{-16}\ e^{(-2106.0/T)}$
R_{727}	NB	$CS + O_3 \rightarrow OCS + O_2$	$k_{727} = 3.16 \times 10^{-16}$
R_{728}	NB	$CS + NO_2 \rightarrow OCS + NO$	$k_{728} = 7.9 \times 10^{-17}$
R_{729}	NB	$NO_3 + CS \rightarrow OCS + NO_2$	$k_{729} = 1.12 \times 10^{-17}$
R_{730}	NB	$CS_2OH \rightarrow CS_2 + OH$	$j_{730} = 2.36 \times 10^{+10}\ e^{(-4189.0/T)}$
R_{731}	NB	$CS_2OH + O_2 \rightarrow OCS + HOSO$	$k_{731} = 7.566 \times 10^{-14}\ e^{(121.0/T)}$

TABLE 19-23. List of Chemical Reactions Included in the Model (Continued).

Rx	Ref	Reaction	Rate Coefficient
		Inorganic S chemistry	
R_{732}	NB	$S + O_2 \rightarrow SO + O$	$k_{732} = 5.585 \times 10^{-12}\, e^{(-266.2/T)}$
R_{733}	NB	$S + NO_2 \rightarrow SO + NO$	$k_{733} = 5.198 \times 10^{-11}\, e^{(59.6/T)}$
R_{734}	NB	$SO + O \rightarrow SO_2$	$k_{734} = \text{NPD}(1.031 \times 10^{-32}, 0.000, 1229.0, 5.299 \times 10^{-11}, 0.000, -0.0)$
R_{735}	NB	$SO + O_3 \rightarrow SO_2 + O_2$	$k_{735} = 4.263 \times 10^{-12}\, e^{(-1145.0/T)}$
R_{736}	NB	$SO + O_2 \rightarrow SO_2 + O$	$k_{736} = 1.798 \times 10^{-13}\, e^{(-2313.0/T)}$
R_{737}	NB	$SO + OH \rightarrow H + SO_2$	$k_{737} = 8.595 \times 10^{-11}$
R_{738}	NB	$SO + NO_2 \rightarrow SO_2 + NO$	$k_{738} = 1.397 \times 10^{-11}\, e^{(0.1/T)}$
R_{739}	NB	$SO_2 + OH \rightarrow HOSO_2$	$k_{739} = \text{NPD}(2.169 \times 10^{-32}, 0.000, 849.5, 1.5 \times 10^{-12}, 0.000, 0.0)$
R_{740}	NB	$SO_2 + O \rightarrow SO_3$	$k_{740} = \text{NPD}(1.259 \times 10^{-32}, 0.000, -636.9, 8.19 \times 10^{-8}, 0.000, -1258.0)$
R_{741}	NB	$SO_2 \rightarrow SO + O$	$j_{741} = 5.627 \times 10^{-10}\, e^{(-37350.0/T)}$
R_{742}	NB	$SO_2 + HO_2 \rightarrow OH + SO_3$	$k_{742} = 8.694 \times 10^{-16}$
R_{743}	NB	$SO_2 + O \rightarrow O_2 + SO$	$k_{743} = 9.007 \times 10^{-12}\, e^{(-9837.0/T)}$
R_{744}	NB	$SO_2 + NO_2 \rightarrow NO + SO_3$	$k_{744} = 2.583 \times 10^{-13}\, e^{(-9181.0/T)}$
R_{745}	NB	$SO_2 + NO_3 \rightarrow NO_2 + SO_3$	$k_{745} = 6.97 \times 10^{-21}$
R_{746}	NB	$SO_2 + CH_3O_2 \rightarrow CH_3O + SO_3$	$k_{746} = 2. \times 10^{-17}$
R_{747}	NB	$SO_2 + O_3 \rightarrow O_2 + SO_3$	$k_{747} = 3. \times 10^{-12}\, e^{(-7000/T)}$
R_{748}	NB	$SO_3 \rightarrow SO_2 + O$	$j_{748} = 5.251 \times 10^{-9}\, e^{(-31870.0/T)}$
R_{749}	NB	$SO_3 + H_2O \rightarrow H_2SO_4$	$k_{749} = 9.104 \times 10^{-13}$
R_{750}	NB	$SO_3 + O \rightarrow O_2 + SO_2$	$k_{750} = \text{NPD}(2.815 \times 10^{-30}, 0.000, -0.0, 3.02 \times 10^{-11}, 0.000, -4436.0)$
R_{751}	NB	$SO + SO_3 \rightarrow SO_2 + SO_2$	$k_{751} = 1.992 \times 10^{-15}$
R_{752}	NB	$SH + CH_3 \rightarrow CH_3SH$	$k_{752} = 1.66 \times 10^{-11}\, e^{(0.0/T)}$
R_{753}	NB	$SH + O_3 \rightarrow HSO + O_2$	$k_{753} = 1.101 \times 10^{-11}\, e^{(-317.9/T)}$
R_{754}	NB	$SH + HO_2 \rightarrow HSO + OH$	$k_{754} = 1.001 \times 10^{-11}$
R_{755}	NB	$SH + O_2 \rightarrow SO + OH$	$k_{755} = 1. \times 10^{-19}$
R_{756}	NB	$SH + O \rightarrow H + SO$	$k_{756} = 1.6 \times 10^{-10}$
R_{757}	NB	$SH + NO_2 \rightarrow HSO + NO$	$k_{757} = 1.722 \times 10^{-11}\, e^{(314.8/T)}$
		NH_3 Oxidation	
R_{758}	B7	$NH_3 + \{M\} \rightarrow NH_2 + H + \{M\}$	$k_{758} = 1.5 \times 10^{-8}\, e^{(-42400.0/T)}$
R_{759}	B7	$H + NH_2 + \{M\} \rightarrow NH_3 + \{M\}$	$l_{759} = 1.3 \times 10^{-33}\, e^{(8300.0/T)}$
R_{760}	B7	$NH_2 + OH \rightarrow NH_3 + O$	$k_{760} = 9.96 \times 10^{-14}\, e^{(-2500.0/T)}$
R_{761}	B7	$NH_2 + NH_2 \rightarrow NH_3 + NH$	$k_{761} = 6.64 \times 10^{-12}\, e^{(-2800.0/T)}$
R_{762}	NB	$O + NH_3 \rightarrow OH + NH_2$	$k_{762} = 1.13 \times 10^{-11}\, e^{(-3482.0/T)}$
R_{763}	NB	$O(^1D) + NH_3 \rightarrow OH + NH_2$	$k_{763} = 2.502 \times 10^{-10}$

Note: The definitions of the reactive families $\{X\}$ are at the end of this table.

TABLE 19-24. List of Chemical Reactions Included in the Model (Continued).

Rx	Ref	Reaction	Rate Coefficient
R_{764}	NB	$O_2 + NH_3 \rightarrow NH_2 + HO_2$	$k_{764} = 1.66 \times 10^{-12}\ e^{(-30950.0/T)}$
R_{765}	NB	$OH + NH_3 \rightarrow H_2O + NH_2$	$k_{765} = 2.999 \times 10^{-13}\ (T/298)^{(1.690)}\ e^{(-209.6/T)}$
R_{766}	NB	$H + NH_3 \rightarrow H_2 + NH_2$	$k_{766} = 4.966 \times 10^{-11}\ e^{(-6478.0/T)}$
R_{767}	NB	$NH_2 + H_2O \rightarrow NH_3 + OH$	$k_{767} = 9.959 \times 10^{-15}$
R_{768}	NB	$NH_2 + H_2 \rightarrow NH_3 + H$	$k_{768} = 8.853 \times 10^{-12}\ e^{(-4782.0/T)}$
R_{769}	NB	$NH_2 + CH_4 \rightarrow NH_3 + CH_3$	$k_{769} = 4.031 \times 10^{-12}\ e^{(-4865.0/T)}$
R_{770}	NB	$NH_2 + O \rightarrow H_2 + NO$	$k_{770} = 5.504 \times 10^{-13}\ e^{(-203.6/T)}$
R_{771}	NB	$NH_2 + O \rightarrow HNO + H$	$k_{771} = 3.399 \times 10^{-11}\ e^{(52.8/T)}$
R_{772}	NB	$NH_2 + O_2 \rightarrow NH + HO_2$	$k_{772} = 1.66 \times 10^{-10}\ e^{(-25160.0/T)}$
R_{773}	NB	$NH_2 + O_2 \rightarrow HNO + OH$	$k_{773} = 3.351 \times 10^{-12}\ e^{(-16320.0/T)}$
R_{774}	NB	$NH_2 + NO \rightarrow N_2 + H_2O$	$k_{774} = 1.889 \times 10^{-12}\ e^{(576.9/T)}$
R_{775}	NB	$NH + O_2 \rightarrow NO + OH$	$k_{775} = 3. \times 10^{-14}$
R_{776}	NB	$NH + H_2 \rightarrow NH_2 + H$	$k_{776} = 1. \times 10^{-11}$
		MethylChloroform Oxidation	
R_{777}	NB	$CC\ell_3CH_3 + OH \rightarrow CC\ell_3CH_2 + H_2O$	$k_{777} = 1.401 \times 10^{-12}\ (T/298)^{(1.239)}\ e^{(-1408.0/T)}$
R_{778}	X2	$CC\ell_3CH_2 + O_2 \rightarrow CC\ell_3CH_2OO$	$k_{778} = 5. \times 10^{-13}$
R_{779}	X2	$CC\ell_3CH_2OO + NO_2 \rightarrow CC\ell_3CH_2O_2NO_2$	$k_{779} = 1. \times 10^{-11}$
R_{780}	X2	$CC\ell_3CH_2OO + HO_2 \rightarrow CC\ell_3CH_2OOH + O_2$	$k_{780} = 3.4 \times 10^{-13}\ e^{(800/T)}$
R_{781}	X2	$CC\ell_3CH_2OO + NO \rightarrow CC\ell_3CH_2O + NO_2$	$k_{781} = 1.5 \times 10^{-11}\ (T/300)^{(-1.2)}$
R_{782}	X2	$CC\ell_3CH_2OO + CH_3O_2 \rightarrow CC\ell_3CH_2O + CH_3O + O_2$	$k_{782} = 6.8 \times 10^{-13}$
R_{783}	X2	$CC\ell_3CH_2O_2NO_2 \rightarrow CC\ell_3CH_2OO + NO_2$	$j_{783} = 2. \times 10^{-6}$
R_{784}	X2	$CC\ell_3CH_2O_2NO_2 \rightarrow CC\ell_3CH_2O + NO_3$	$j_{784} = 2. \times 10^{-6}$
R_{785}	X2	$CC\ell_3CH_2O_2NO_2 + \{M\} \rightarrow CC\ell_3CH_2OO + NO_2 + \{M\}$	$k_{785} = 1. \times 10^{+15}\ e^{(-11000/T)}$
R_{786}	X2	$CC\ell_3CH_2OOH + OH \rightarrow CC\ell_3CH_2OO + H_2O$	$k_{786} = 1.7 \times 10^{-12}\ e^{(220/T)}$
R_{787}	X2	$CC\ell_3CH_2OOH \rightarrow CC\ell_3CH_2O + OH$	J_{787}= CH3OOH
R_{788}	X2	$CC\ell_3CH_2OOH + OH \rightarrow CC\ell_3CHO + H_2O + OH$	$k_{788} = 1.7 \times 10^{-13}\ e^{(220/T)}$
R_{789}	X2	$CC\ell_3CH_2O + O_2 \rightarrow CC\ell_3CHO + HO_2$	$k_{789} = 3.7 \times 10^{-14}\ e^{(-460/T)}$
R_{790}	X2	$CC\ell_3CHO + OH \rightarrow CC\ell_3CO + H_2O$	$k_{790} = 6.9 \times 10^{-12}\ e^{(260/T)}$

Note: The definitions of the reactive families $\{X\}$ are at the end of this table.

TABLE 19-25. List of Chemical Reactions Included in the Model (Continued).

Rx	Ref	Reaction	Rate Coefficient
R_{791}	X2	$CCl_3CHO + NO_3 \rightarrow CCl_3CO + HONO_2$	$k_{791} = 1.4 \times 10^{-12}\, e^{(-1860/T)}$
R_{792}	X2	$CCl_3CHO \rightarrow CCl_3CO + H$	J_{792}= CH3CHO_3
R_{793}	X2	$CCl_3CHO \rightarrow CCl_3 + CHO$	J_{793}= CH3CHO_1
R_{794}	X2	$CCl_3CO + O_2 \rightarrow CCl_3COO_2$	$l\_N2_{794} = 4.5 \times 10^{-31}\, (T/300)^{(-2.0)}$ $l\_O2_{794} = 4.5 \times 10^{-31}\, (T/300)^{(-2.0)}$ $ki_{794} = 1.8 \times 10^{-12}\, (T/300)^{(-2.0)}$ $Fc_{794} = e^{(-T/446)}$
R_{795}	X2	$CCl_3COO_2 + HO_2 \rightarrow CCl_3COOOH + O_2$	$k_{795} = 0.667\, 4.3 \times 10^{-13}\, e^{(+1040/T)}$
R_{796}	X2	$CCl_3COO_2 + HO_2 \rightarrow CCl_3COOH + O_3$	$k_{796} = 0.333\, 4.3 \times 10^{-13}\, e^{(+1040/T)}$
R_{797}	X2	$CCl_3COO_2 + NO \rightarrow CCl_3COO + NO_2$	$k_{797} = 1.4 \times 10^{-11}$
R_{798}	X2	$CCl_3COO_2 + NO_2 \rightarrow CCl_3COO_2NO_2$	$k_{798} = 8 \times 10^{-12}$
R_{799}	X2	$CCl_3COO_2 + CH_3O_2 \rightarrow CCl_3COO + CH_3O + O_2$	$k_{799} = 1.4 \times 10^{-11}$
R_{800}	X2	$CCl_3COO \rightarrow CCl_3 + CO_2$	$j_{800} = 1 \times 10^{+7}$
R_{801}	X2	$CCl_3COO_2NO_2 \rightarrow CCl_3COO_2 + NO_2$	$j_{801} = 2.2 \times 10^{+16}\, e^{(-13435/T)}$
R_{802}	X2	$CCl_3COO_2NO_2 \rightarrow CCl_3COO_2 + NO_2$	J_{802}= PAN
R_{803}	X2	$CCl_3COOH \rightarrow CCl_3 + CO_2 + OH$	J_{803}= CH3OOH
R_{804}	X2	$CCl_3COOH + OH \rightarrow CCl_3COO_2 + H_2O$	$k_{804} = 5.9 \times 10^{-12}$
R_{805}	X2	$CCl_3COOH + OH \rightarrow CCl_3 + CO_2 + H_2O$	$k_{805} = 1.3 \times 10^{-12}\, e^{(-170/T)}$
R_{806}	NB	$CCl_3 + O_2 \rightarrow CCl_3O_2$	k_{806} = NPD(4.969×10^{-32}, 0.000, 892.1, 4.504×10^{-9}, −10.990, −2295.0)
R_{807}	NB	$CCl_3 + O \rightarrow COCl_2 + Cl$	$k_{807} = 4.2 \times 10^{-11}$
R_{808}	NB	$CCl_3 + H_2 \rightarrow CHCl_3 + H$	$k_{808} = 8.322 \times 10^{-12}\, e^{(-7196.0/T)}$
R_{809}	NB	$O + CHCl_3 \rightarrow OH + CCl_3$	$k_{809} = 4.184 \times 10^{-12}\, e^{(-2389.0/T)}$
R_{810}	NB	$OH + CHCl_3 \rightarrow H_2O + CCl_3$	$k_{810} = 2.453 \times 10^{-12}\, (T/298)^{(0.566)}\, e^{(-942.8/T)}$
R_{811}	NB	$NO_3 + CHCl_3 \rightarrow HONO_2 + CCl_3$	$k_{811} = 8.516 \times 10^{-13}\, e^{(-2814.0/T)}$
R_{812}	NB	$Cl + CHCl_3 \rightarrow HCl + CCl_3$	$k_{812} = 2.4 \times 10^{-11}\, e^{(-1877/T)}$
R_{813}	X2	$CCl_3O_2 + NO_2 \rightarrow CCl_3O_2NO_2$	$k_{813} = 1. \times 10^{-11}$
R_{814}	X2	$CCl_3O_2 + HO_2 \rightarrow CCl_3OOH + O_2$	$k_{814} = 3.4 \times 10^{-13}\, e^{(800/T)}$
R_{815}	X2	$CCl_3O_2 + NO \rightarrow COCl_2 + Cl + NO_2$	$k_{815} = 1.5 \times 10^{-11}\, (T/300)^{(-1.2)}$
R_{816}	X2	$CCl_3O_2 + CH_3O_2 \rightarrow COCl_2 + Cl + CH_3O + O_2$	$k_{816} = 6.8 \times 10^{-13}$

TABLE 19-26. List of Chemical Reactions Included in the Model (Continued).

Rx	Ref	Reaction	Rate Coefficient
R_{817}	X2	$CC\ell_3O_2NO_2 \rightarrow CC\ell_3O_2 + NO_2$	$jo\_N2_{817} = 9. \times 10^{-5}\ e^{(-9690/T)}$ $ko\_O2_{817} = ko_{N2}$ $ji_{817} = 1.1 \times 10^{+16}\ e^{(-10560/T)}$ $Fc_{817} = e^{(-T/325)}$
R_{818}	X2	$CC\ell_3OOH + OH \rightarrow CC\ell_3O_2 + H_2O$	$k_{818} = 1.7 \times 10^{-12}\ e^{(220/T)}$
R_{819}	X2	$CC\ell_3OOH \rightarrow COC\ell_2 + C\ell + OH$	J_{819}= CH3OOH
R_{820}	X2	$COC\ell_2 + H_2O \rightarrow CO_2 + HC\ell + HC\ell$	$k_{820} = 2. \times 10^{-6}$
R_{821}	ZN	$CC\ell_2 + O_2 \rightarrow COC\ell_2 + O$	$k_{821} = 2. \times 10^{-10}$
		Inorganic Cℓ chemistry	
R_{822}	NB	$C\ell + H_2O \rightarrow OH + HC\ell$	$k_{822} = 2.788 \times 10^{-11}\ e^{(-8670.0/T)}$
R_{823}	NB	$C\ell + H_2 \rightarrow HC\ell + H$	$k_{823} = 2.866 \times 10^{-11}\ e^{(-2249.0/T)}$
R_{824}	NB	$C\ell + HO_2 \rightarrow HC\ell + O_2$	$k_{824} = 4.366 \times 10^{-11}\ e^{(-14.5/T)}$
R_{825}	NB	$C\ell + CH_4 \rightarrow HC\ell + CH_3$	$k_{825} = 1.713 \times 10^{-11}\ e^{(-1514.0/T)}$
R_{826}	NB	$C\ell + OH \rightarrow O + HC\ell$	$k_{826} = 9.8 \times 10^{-12}\ e^{(-2860.0/T)}$
R_{827}	NB	$C\ell + H_2O_2 \rightarrow HC\ell + HO_2$	$k_{827} = 1.222 \times 10^{-11}\ e^{(-995.7/T)}$
R_{828}	NB	$NO_3 + C\ell \rightarrow C\ell O + NO_2$	$k_{828} = 2.601 \times 10^{-11}$
R_{829}	NB	$C\ell O + O \rightarrow C\ell + O_2$	$k_{829} = 4.586 \times 10^{-11}\ e^{(-30.4/T)}$
R_{830}	NB	$C\ell O + NO \rightarrow C\ell + NO_2$	$k_{830} = 6.957 \times 10^{-12}\ e^{(276.9/T)}$
R_{831}	NB	$SO + C\ell O \rightarrow SO_2 + C\ell$	$k_{831} = 2.87 \times 10^{-11}\ e^{(-0.8/T)}$
R_{832}	NB	$C\ell O + H_2 \rightarrow HC\ell + OH$	$k_{832} = 5. \times 10^{-16}$
R_{833}	NB	$C\ell O + CH_4 \rightarrow CH_3 + O + HC\ell$	$k_{833} = 1. \times 10^{-12}$
R_{834}	NB	$C\ell O + CO \rightarrow CO_2 + C\ell$	$k_{834} = 1. \times 10^{-12}$
		End of Reactions	

TABLE 19-1. The Chemical reactions included in the model (continued).

The following are the definitions of the chemical families in the model

Family	Members
$\{M\}$	$\equiv\Sigma\{ O_2 + N_2 \}$
$\{NegIon\}$	$\equiv\Sigma\{ O^- + O_2^- + O_3^- + O_4^- + H^- + NO_2^- + NO^- + CO_3^- + CO_4^- \}$
$\{PosIon\}$	$\equiv\Sigma\{ O^+ + O_2^+ + O_4^+ + N^+ + N_2^+ + N_4^+ + NO^+ + NO_2^+ + N_2O^+ + H_2O^+ + H_3O^+ + OH^+ + CO^+ + CO_2^+ + CC\ell_3^+ + N_2O_2^+ \}$
$\{O_x\}$	$\equiv\Sigma\{ O_3 + O + O(^1D) \}$
$\{HO_y\}$	$\equiv\Sigma\{ OH + H + HO_2 + 2\times H_2O_2 + HO_2NO_2 \}$
$\{NO_x\}$	$\equiv\Sigma\{ NO + NO_2 \}$
$\{NO_z\}$	$\equiv\Sigma\{ \{NO_x\} + NO_3 + 2\times N_2O_3 + 2\times N_2O_4 + 2\times N_2O_5 + HNO + HONO + HO_2NO_2 + CH_3O_2NO_2 \}$
$\{NO_t\}$	$\equiv\Sigma\{ \{NO_z\} + HONO_2 \}$

Definition of NPD(a, b, c, d, e, f)

This function is a pressure (and temperature) dependent three body reaction coefficient. In this function a, b, and c determine the low-pressure limit, d, e, and f determine the high-pressure limit. These two limits are then combined to yield the rate at an intermediate pressure.

$$k_l = [\ \mathrm{M}\ ] \times a \times (\mathrm{T}/298)^b \times \exp(c/\mathrm{T}) \quad \text{and} \quad k_\infty = d \times (\mathrm{T}/298)^e \times \exp(f/\mathrm{T})$$

$$\alpha = \left(1 + (\log_{10}(k_l/k_\infty))^2\right)^{-1}$$

$$\mathrm{NPD} = \left(\frac{k_l}{1 + k_l/k_\infty}\right) \times 0.6^\alpha$$

Definition of DependsEV(a, b, c)

This function depends on both the strength of the local electric field, expressed as a mean electron energy, eV, as well as the lightning flash rate $f_L(z)$ (each flash is assumed to have a duration of 0.01 sec.).

$$\beta = \log_{10}(eV) \quad \text{and} \quad k_{eV} = a + b\beta + c\beta^2$$

$$\mathrm{DependsEV} = 0.01 \times f_L(z) \times k_{eV}$$

Definition of IonIon

This temperature dependent function is for ion–ion collisions.

$$\mathrm{IonIon} = 5.0 \times 10^{-7} \times (\mathrm{T}/300)^{-0.455}$$

Definition of ElectronCapture

Two electron capture rates are uese, one for bimolecular collisions between polyatomic molecules and electrons (Multi_Electron_Capture) and one for trimolecular collisions between monoatomic species and electrons (Uni_Electron_Capture).

$$\mathrm{Multi\_Electron\_Capture} = 4.0 \times 10^{-8} \times (\mathrm{T}/300)^{-0.455}$$

and

$$\mathrm{Uni\_Electron\_Capture} = 5.0 \times 10^{-25} \times (\mathrm{T}/300)^{-0.455}$$

Appendix C Thermodynamic Equilibrium Composition of Air as a Function of Temperature.

This Appendix presents the computed thermodynamic equilibrium composition of air as a function of temperature. The air is assumed to have the same elemental composition as average earth air, and is a 1 bar pressure.

In the 4 figures that follow, each graph has the same scales; on the X-axis is the temperature in thousands of degrees Kelvin and along the Y-axis is the common Logarithm of the mixing ratio.

Figure 49 shows the Nitrogen, Oxygen, and Hydrogen systems along with the electron. In this figure, chemical species are arranged in a two-dimensional grid, going up the page changes a chemical compound from neutral to positive to negative, and going across the page changes the compound. A general pattern in these figures is that there is either an abrupt change in the mixing ratio or a maximum in the mixing ratio in the range $6,000\text{K} - 3,000\text{K}$.

Thermodynamic Equilibrium Composition of Air as a Function of Temperature.

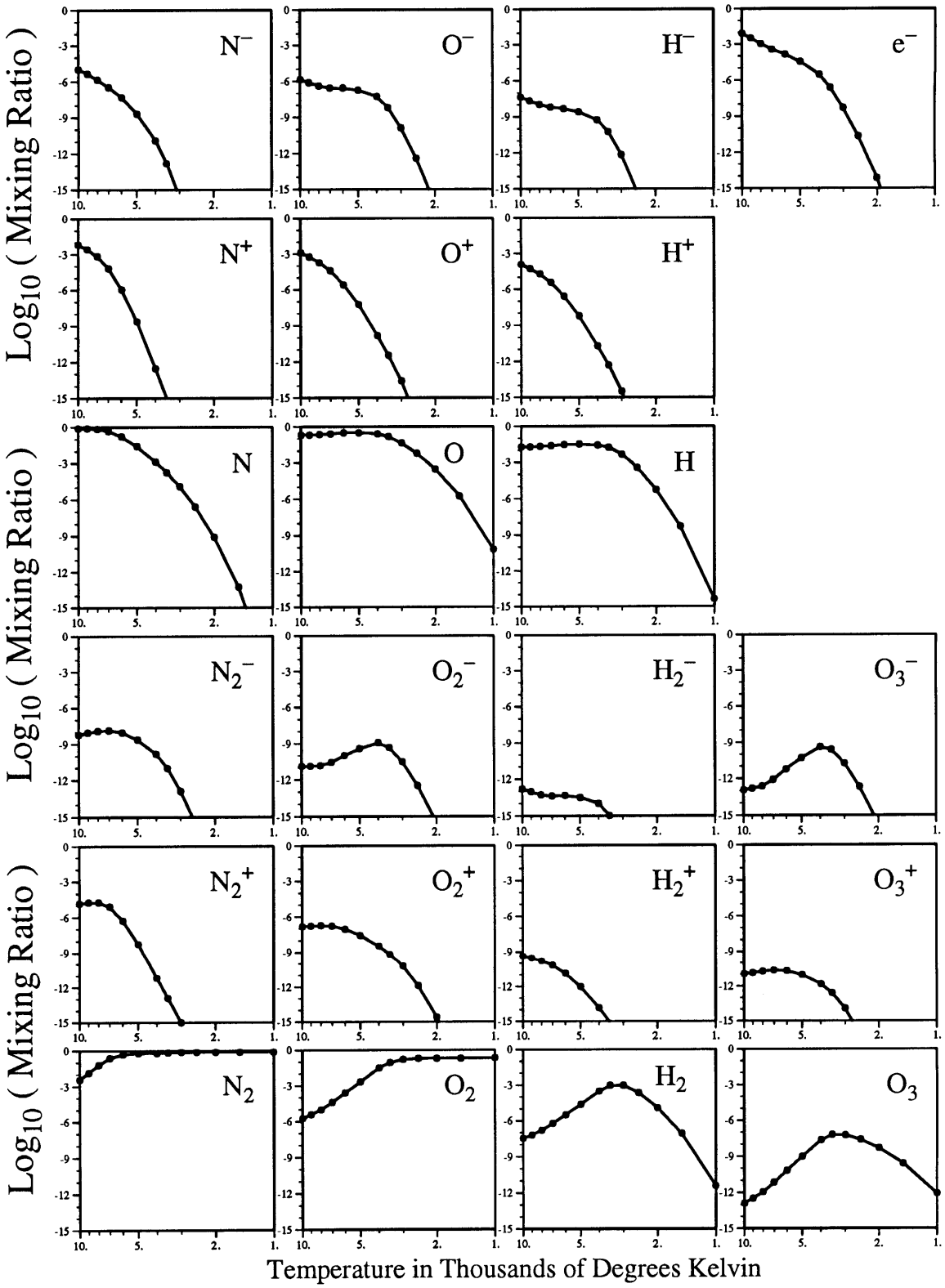

Figure 49a. The calculated thermodynamic equilibrium composition of air at 1 bar. Theses are the major N, O, and H containing chemical species.

Thermodynamic Equilibrium Composition of Air as a Function of Temperature.

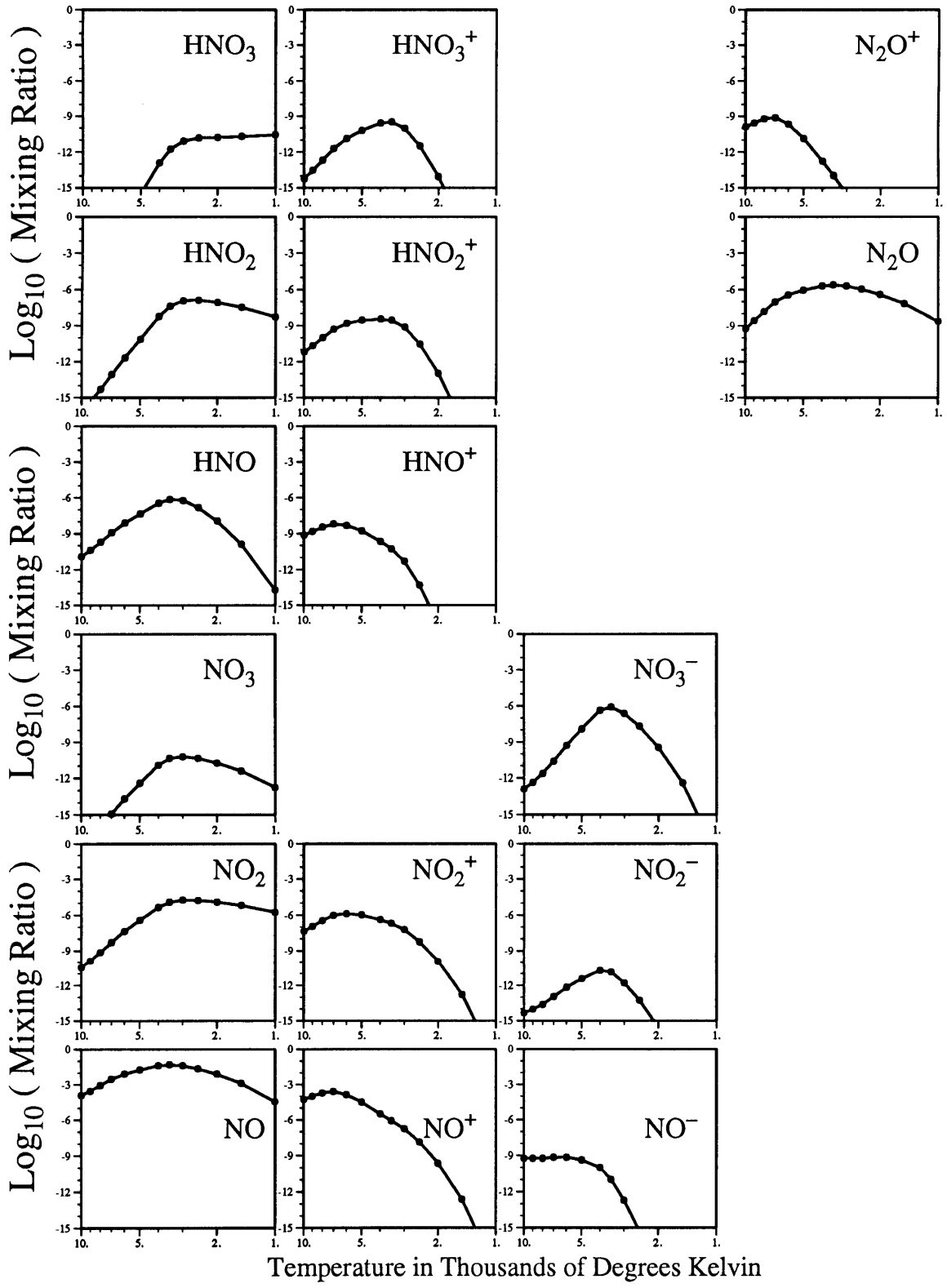

Figure 49b. The calculated thermodynamic equilibrium composition of air at 1 bar. Theses are the major $H_iN_jO_k$ compounds.

Thermodynamic Equilibrium Composition of Air as a Function of Temperature.

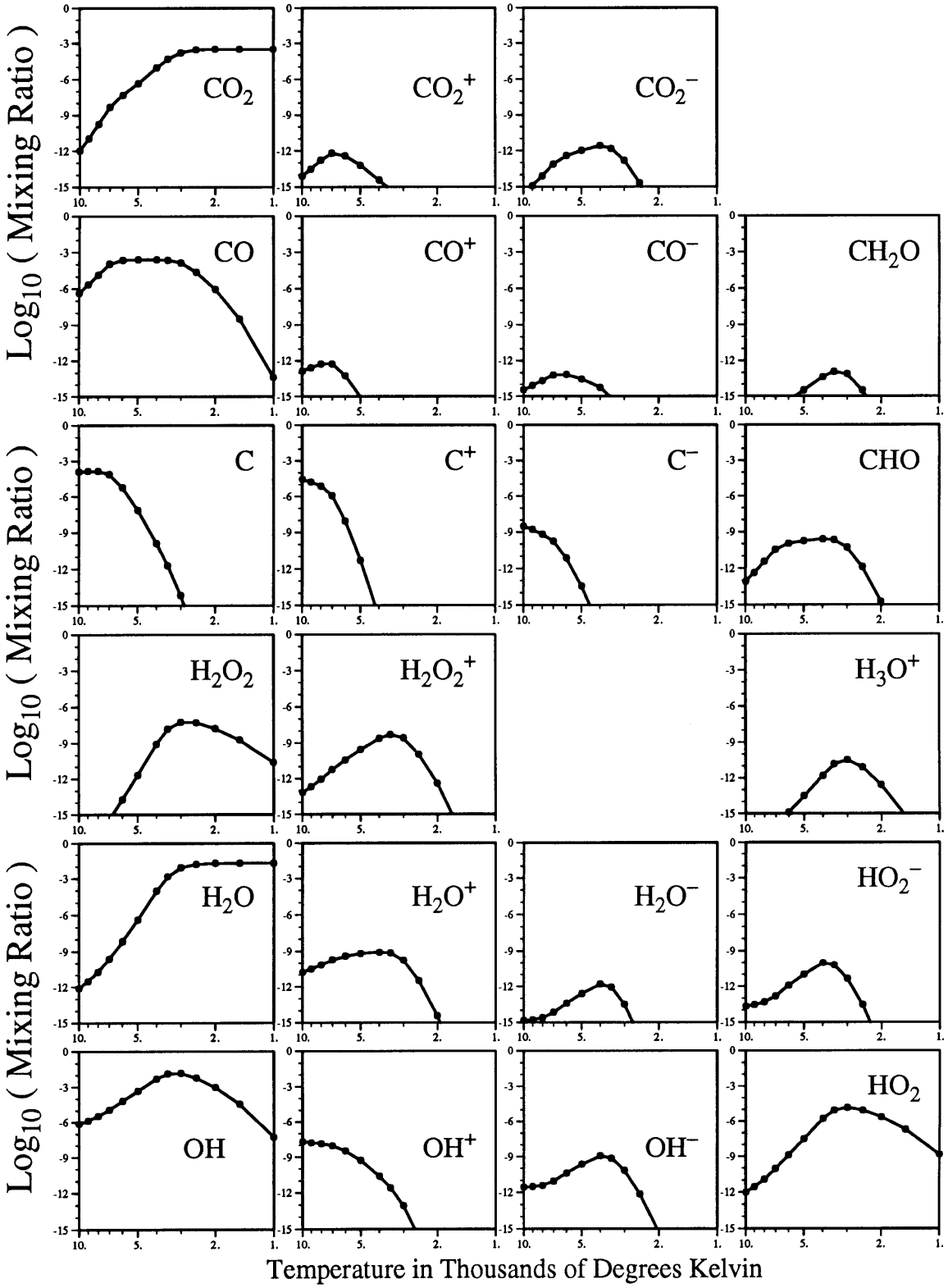

Figure 49c. The calculated thermodynamic equilibrium composition of air at 1 bar. Theses are the major $H_iC_jO_k$ compounds.

Thermodynamic Equilibrium Composition of Air as a Function of Temperature.

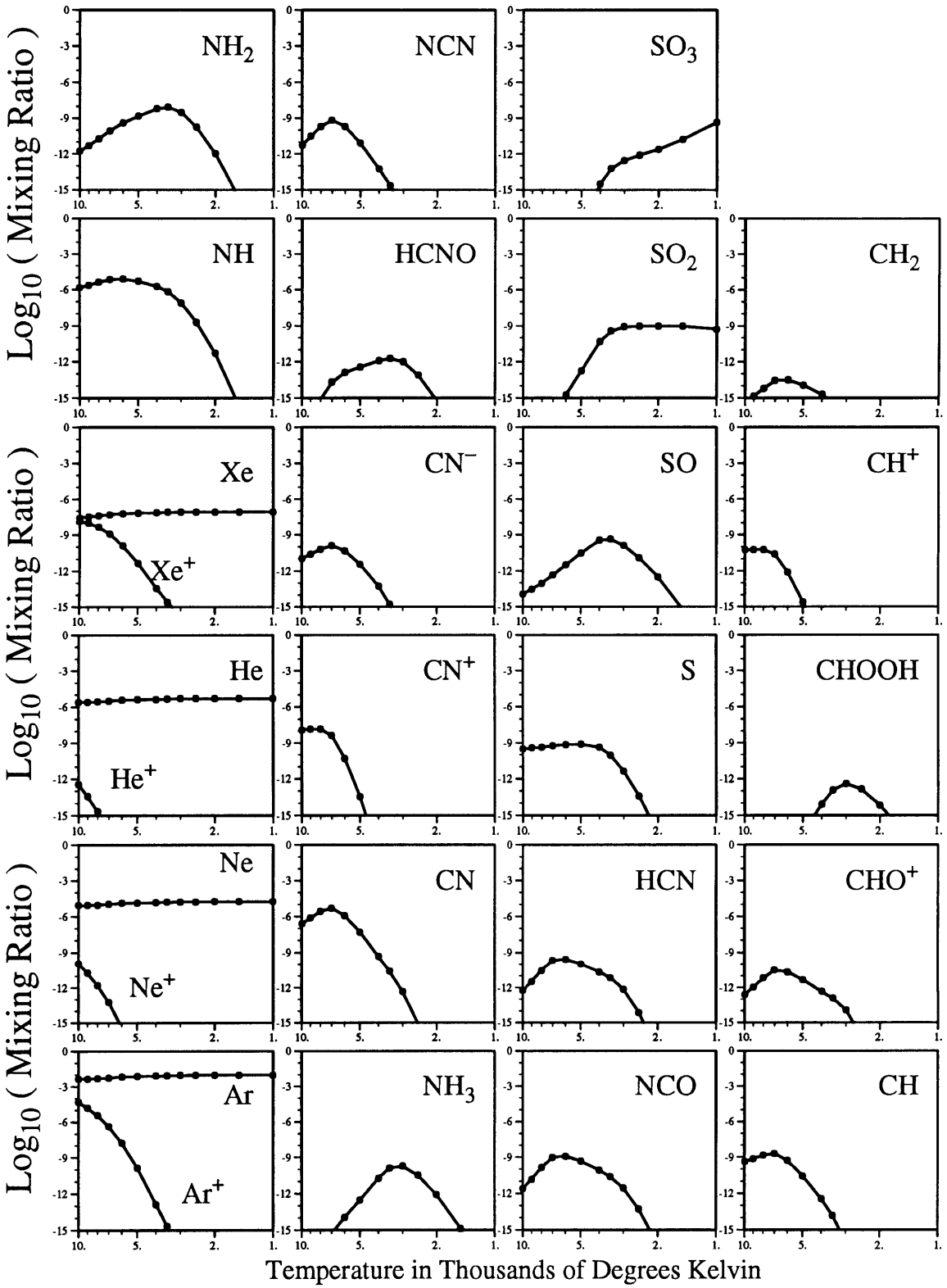

Figure 49d. The calculated thermodynamic equilibrium composition of air at 1 bar. Theses are most of the minor compounds.

Appendix D Summary Maps and Tables for Selected Compounds

This appendix displays maps of the mixing ratios, lifetimes, and term weights for the major chemical species modeled. Each compound is summarized on two pages of data; one comprising primarily half-tone maps and one of tables. Each half-tone map page displays summaries of the mixing ratios χ, chemical lifetimes τ, and **term weights** for the major chemical species modeled. These summaries are laid out in a 3 by 3 grid in the following manner. The top row of figures represent the distribution of mixing ratio for the species throughout the model domain, the second row displays the corresponding chemical lifetimes, and the bottom row shows the relative importance of the different types of processes in the continuity equation for the species (**term weights**). The meaning of the phrase **term weights** was explained in Section 8.2.1.1, page 138.

Each of the three columns represents a different model run, the left-most column is the 1-D state state model, the center column is the Base Case model run (*i.e.* the 2-D steady-state model with no lightning produced ions nor ultra-violet light included), and the right most column is the Electrified model run, (*i.e.* the 2-D steady-state run with lightning produced ions and ultra-violet light included).

This 3 by 3 grid is bounded on the right-most edge by the legends for each of the three rows. Immediately above the 3 by 3 grid are the mass weighted average mixing ratios $\bar{\chi}$ and chemical lifetimes $\bar{\tau_c}$ for each of the three model runs. Above these summaries are the net mass production (outflow - inflow) of the chemical species in question in both the Base Case and Electrified model runs (there is no transport in the 1-D model). Here P_{BC} is the net production in the Base Case model and P_{IM} is the net production in the Electrified model case. Above these figures is presented the difference in the net production between these two model runs (Differential Net Production; P_{IM} - P_{BC}).

On the page after the 3 by 3 grid of half-tone maps are 3 tables that summarize the major sources and sinks for the compound in question. Beginning at the top, the first table **(a.)** lists the major source terms and **(b.)** the major sink terms in the continuity equation. These terms have units molec·cm^{-3}·s^{-1} and can be considered the specific production (or loss) rate $\Re$ of the compound in question. Since these models are steady state ones, the sum of the source $\Re$'s (shown at the bottom of each column in the source **(a.)** table must equal sum of the sink $\Re$'s (shown at the bottom of each column in the sink **(b.)** table.

The lower-most table summarizes the domain averaged mixing ratio χ, number density [..] and total specific production rate $\Sigma\Re$ in each of the three steady-state model runs. As noted at the bottom of this table, τ = [..] / $\Sigma\Re$. Since non-chemical terms (*e.g.* Advection/Diffusion) are sometimes the dominant ones, also listed in the final two columns of this table are the chemical lifetimes τ_c of the compound in question.

O_2^+

Differential Net Production ($P_{I.M.} - P_{B.C.}$) = 3.354×10^{-14} (Kg Year^{-1})

$P_{B.C.} = 4.358 \times 10^{-10}$ $P_{I.M.} = 4.358 \times 10^{-10}$ (Kg Year^{-1})

$\bar{\tau}_c = 6.600 \times 10^{-10}$ $\bar{\tau}_c = 6.600 \times 10^{-10}$ $\bar{\tau}_c = 6.600 \times 10^{-10}$ (Seconds)

$\bar{\chi} = 2.045 \times 10^{-26}$ $\bar{\chi} = 2.045 \times 10^{-26}$ $\bar{\chi} = 1.937 \times 10^{-20}$ (Mixing Ratio)

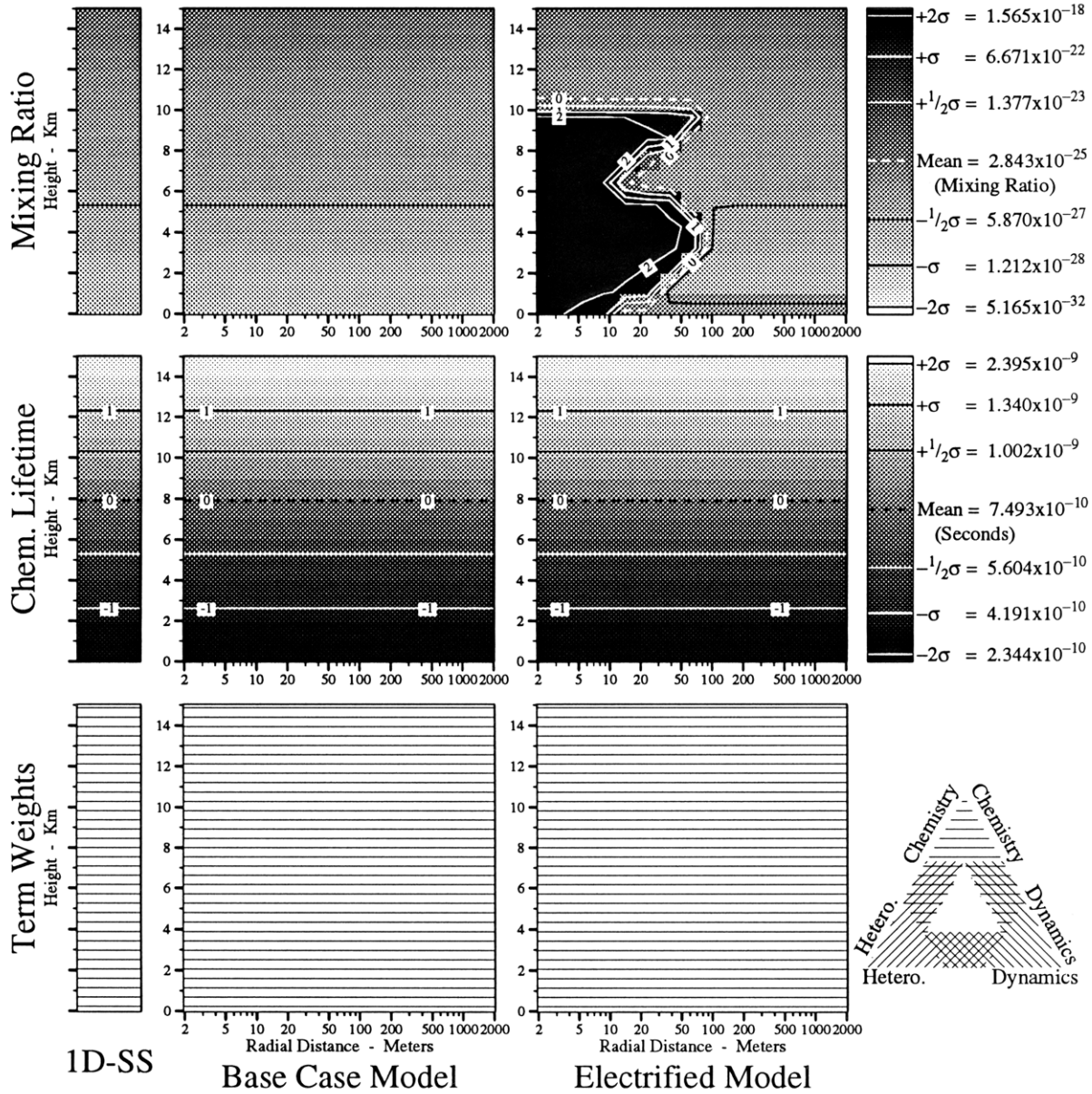

Figure 50. Mixing ratios (χ), lifetimes (τ_c), and term weights of O_2^+. See text for definitions of terms and other details.

Table 20. Summary of the chemistry of O_2^+ in the **inner domain** of the three models. (**a**,**b**) The major terms in the continuity equations for O_2^+ in the three model runs and (**c**) a summary of its mixing ratios χ and lifetimes τ in the three model runs. In these tables $\Re$ is the specific rate of production of O_2^+ (molec·cm^{-3}·s^{-1}), τ is the total lifetime (sec) of O_2^+ and τ_c is its lifetime due to chemical processes (sec). J_i, j_i, k_i, and l_i are photolytic, unimolecular, bimolecular and termolecular rate coefficients respectively for reaction number i as listed in Appendix B , page 184.

a.) The major source terms for O_2^+ in the inner domain of the three model runs.

1-D Steady-State Model		2-D Base Case Model		2-D Electrified Model	
Log (ℜ)	Reaction Rate $\Re = k_{yz}\,[y]\,[z]$	Log (ℜ)	Reaction Rate $\Re = k_{yz}\,[y]\,[z]$	Log (ℜ)	Reaction Rate $\Re = k_{yz}\,[y]\,[z]$
1.87	$k_{313}\,[N_4^+]\,[O_2]$	1.87	$k_{313}\,[N_4^+]\,[O_2]$	11.88	$k_{313}\,[N_4^+]\,[O_2]$
1.56	$k_{213}\,[O_4^+]\,[O_2]$	1.56	$k_{213}\,[O_4^+]\,[O_2]$	11.53	$k_{213}\,[O_4^+]\,[O_2]$
0.86	$k_{349}\,[N_2O_2^+]\{M\}$	0.86	$k_{349}\,[N_2O_2^+]\{M\}$	10.94	$k_{349}\,[N_2O_2^+]\{M\}$
0.67	$k_{317}\,[N_2^+]\,[O_2]$	0.67	$k_{317}\,[N_2^+]\,[O_2]$	10.81	$k_{340}\,[H_2O^+]\,[O_2]$
0.59	$k_{340}\,[H_2O^+]\,[O_2]$	0.59	$k_{340}\,[H_2O^+]\,[O_2]$	10.80	$k_{352}\,[WO_2^+]\,[O_2]$
0.58	$k_{352}\,[WO_2^+]\,[O_2]$	0.58	$k_{352}\,[WO_2^+]\,[O_2]$	10.62	$k_{317}\,[N_2^+]\,[O_2]$
...	15 More Reactions	...	15 More Reactions	...	15 More Reactions
2.120 = Log(Σℜ)		2.120 = Log(Σℜ)		12.134 = Log(Σℜ)	

Notes: Read **W** as H_2O. The definitions of the reactive families $\{X\}$ are at the end of Appendix B.

b.) The major sink terms for O_2^+ in the inner domain of the three model runs.
The reaction rate ℜ implicitly contains $[O_2^+]$.

1-D Steady-State Model		2-D Base Case Model		2-D Electrified Model	
Log (ℜ)	Reaction Rate $\Re = k_{yz}\,[y]\,[O_2^+]$	Log (ℜ)	Reaction Rate $\Re = k_{yz}\,[y]\,[O_2^+]$	Log (ℜ)	Reaction Rate $\Re = k_{yz}\,[y]\,[O_2^+]$
1.92	$k_{221}\,[N_2]$	1.92	$k_{221}\,[N_2]$	11.93	$k_{221}\,[N_2]$
1.53	$l_{223}\,[O_2]\{M\}$	1.53	$l_{223}\,[O_2]\{M\}$	11.54	$l_{223}\,[O_2]\{M\}$
1.15	$l_{224}\,[N_2]\{M\}$	1.15	$l_{224}\,[N_2]\{M\}$	11.20	$l_{224}\,[N_2]\{M\}$
-0.79	$k_{225}\,[H_2O]$	-0.79	$k_{225}\,[H_2O]$	9.44	$k_{225}\,[H_2O]$
-4.08	$k_{220}\,[N_2]$	-4.08	$k_{220}\,[N_2]$	7.18	$k_{402}\,\{NegIon\}$
-8.21	$k_{222}\,[NO_2]$	-7.78	Heterogeneous Loss	5.93	$k_{220}\,[N_2]$
...	10 More Reactions	...	10 More Reactions	...	10 More Reactions
2.120 = Log(Σℜ)		2.120 = Log(Σℜ)		12.134 = Log(Σℜ)	

Note: The definitions of the reactive families $\{X\}$ are at the end of Appendix B.

c.) Summary of the lifetimes of O_2^+ in the inner domain of the three model runs.

	Log(χ)	Log($[O_2^+]$) cm^{-3}	Log(Σℜ) $cm^{-3}\cdot s^{-1}$	Log(τ) sec	Source Log(τ_c) sec	Sink Log(τ_c) sec
1-D Steady-State Model	−26.268	−7.077	2.120	−9.197	−9.197	−9.197
2-D Base Case Model	−26.268	−7.077	2.120	−9.197	−9.197	−9.197
2-D Electrified Model	−16.334	2.858	12.134	−9.276	−9.276	−9.276

Note: $\tau = [O_2^+] / \Sigma\Re$ or $\text{Log}(\tau) = \text{Log}([O_2^+]) - \text{Log}(\Sigma\Re)$.

N_2^+

Differential Net Production ($P_{I.M.} - P_{B.C.}$) = 2.935×10^{-15} (Kg Year^{-1})

$P_{B.C.} = 5.903 \times 10^{-11}$ $P_{I.M.} = 5.903 \times 10^{-11}$ (Kg Year^{-1})

$\overline{\tau}_c = 1.463 \times 10^{-10}$ $\overline{\tau}_c = 1.463 \times 10^{-10}$ $\overline{\tau}_c = 1.463 \times 10^{-10}$ (Seconds)

$\overline{\chi} = 4.272 \times 10^{-27}$ $\overline{\chi} = 4.272 \times 10^{-27}$ $\overline{\chi} = 2.162 \times 10^{-21}$ (Mixing Ratio)

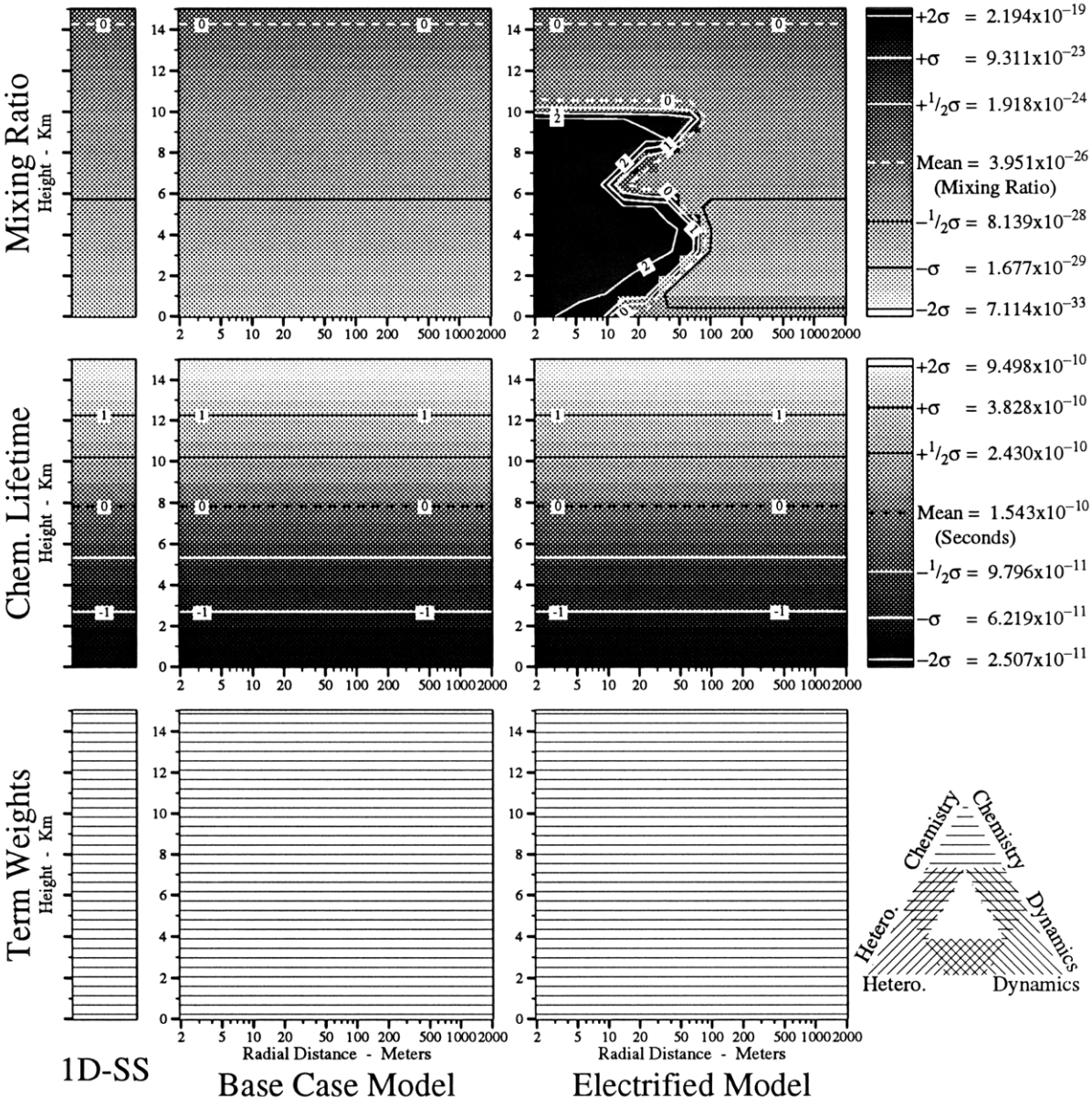

Figure 51. Mixing ratios (χ), lifetimes (τ_c), and term weights of N_2^+. See text for definitions of terms and other details.

Table 21. Summary of the chemistry of N_2^+ in the **inner domain** of the three models. (**a**,**b**) The major terms in the continuity equations for N_2^+ in the three model runs and (**c**) a summary of its mixing ratios χ and lifetimes τ in the three model runs. In these tables $\Re$ is the specific rate of production of N_2^+ (molec·cm^{-3}·s^{-1}), τ is the total lifetime (sec) of N_2^+ and τ_c is its lifetime due to chemical processes (sec). J_i, j_i, k_i, and l_i are photolytic, unimolecular, bimolecular and termolecular rate coefficients respectively for reaction number i as listed in Appendix B , page 184.

a.) The major source terms for N_2^+ in the inner domain of the three model runs.

1-D Steady-State Model		2-D Base Case Model		2-D Electrified Model	
Log ($\Re$)	Reaction Rate $\Re = k_{yz}\,[y]\,[z]$	Log ($\Re$)	Reaction Rate $\Re = k_{yz}\,[y]\,[z]$	Log ($\Re$)	Reaction Rate $\Re = k_{yz}\,[y]\,[z]$
1.92	$k_{221}\,[O_2^+]\,[N_2]$	1.92	$k_{221}\,[O_2^+]\,[N_2]$	11.93	$k_{221}\,[O_2^+]\,[N_2]$
0.37	$j_{116}\,[N_2]$	0.37	$j_{116}\,[N_2]$	10.51	$j_{130}\,[N_2]$
-11.08	$k_{336}\,[N^+]\,[NO]$	-11.06	$k_{336}\,[N^+]\,[NO]$	2.26	$k_{336}\,[N^+]\,[NO]$
-13.75	Advection/Diffusion	-121.66	$k_{432}\,[N]\,[N]$	0.37	$j_{116}\,[N_2]$
-121.66	$k_{432}\,[N]\,[N]$	$-\infty$	$j_{130}\,[N_2]$	-2.65	$k_{309}\,[N_2]\,[e^-]$
$-\infty$	Flux	$-\infty$	$k_{309}\,[N_2]\,[e^-]$	-102.07	$k_{432}\,[N]\,[N]$
...	2 More Reactions	...	2 More Reactions	...	2 More Reactions
1.934 = Log($\Sigma\Re$)		1.934 = Log($\Sigma\Re$)		11.947 = Log($\Sigma\Re$)	

b.) The major sink terms for N_2^+ in the inner domain of the three model runs.
The reaction rate $\Re$ implicitly contains $[N_2^+]$.

1-D Steady-State Model		2-D Base Case Model		2-D Electrified Model	
Log ($\Re$)	Reaction Rate $\Re = k_{yz}\,[y]\,[N_2^+]$	Log ($\Re$)	Reaction Rate $\Re = k_{yz}\,[y]\,[N_2^+]$	Log ($\Re$)	Reaction Rate $\Re = k_{yz}\,[y]\,[N_2^+]$
1.89	$l_{315}\,[N_2]\{M\}$	1.89	$l_{315}\,[N_2]\{M\}$	11.91	$l_{315}\,[N_2]\{M\}$
0.67	$k_{317}\,[O_2]$	0.67	$k_{317}\,[O_2]$	10.62	$k_{317}\,[O_2]$
0.44	$k_{326}\,[O_2]$	0.44	$k_{326}\,[O_2]$	10.40	$k_{326}\,[O_2]$
-1.45	$k_{325}\,[CO_2]$	-1.45	$k_{325}\,[CO_2]$	8.51	$k_{325}\,[CO_2]$
-1.77	$k_{316}\,[H_2O]$	-1.77	$k_{316}\,[H_2O]$	8.45	$k_{316}\,[H_2O]$
-4.52	$k_{323}\,[N_2O]$	-4.52	$k_{323}\,[N_2O]$	6.22	k_{405} {NegIon}
...	14 More Reactions	...	14 More Reactions	...	14 More Reactions
1.934 = Log($\Sigma\Re$)		1.934 = Log($\Sigma\Re$)		11.947 = Log($\Sigma\Re$)	

Note: The definitions of the reactive families $\{X\}$ are at the end of Appendix B.

c.) Summary of the lifetimes of N_2^+ in the inner domain of the three model runs.

	Log(χ)	Log($[N_2^+]$) cm^{-3}	Log($\Sigma\Re$) cm^{-3}·s^{-1}	Log(τ) sec	Source Log(τ_c) sec	Sink Log(τ_c) sec
1-D Steady-State Model	−27.169	−7.977	1.934	−9.911	−9.911	−9.911
2-D Base Case Model	−27.169	−7.977	1.934	−9.911	−9.911	−9.911
2-D Electrified Model	−17.287	1.905	11.947	−10.042	−10.042	−10.042

Note: $\tau = [N_2^+] / \Sigma\Re$ or $\text{Log}(\tau) = \text{Log}([N_2^+]) - \text{Log}(\Sigma\Re)$.

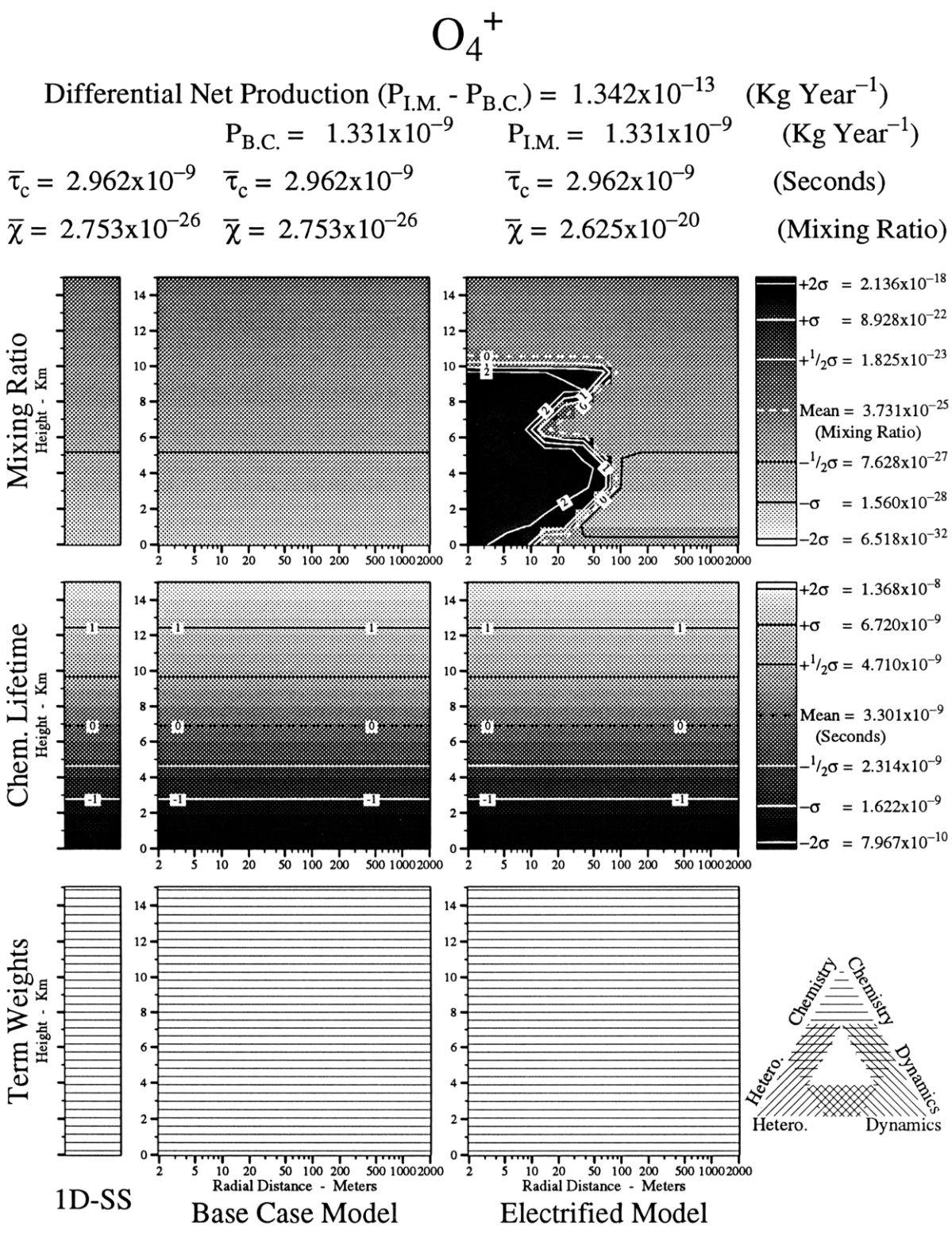

Figure 52. Mixing ratios (χ), lifetimes (τ_c), and term weights of O_4^+. See text for definitions of terms and other details.

Table 22. Summary of the chemistry of O_4^+ in the **inner domain** of the three models. (**a**,**b**) The major terms in the continuity equations for O_4^+ in the three model runs and (**c**) a summary of its mixing ratios χ and lifetimes τ in the three model runs. In these tables $\Re$ is the specific rate of production of O_4^+ (molec·cm^{-3}·s^{-1}), τ is the total lifetime (sec) of O_4^+ and τ_c is its lifetime due to chemical processes (sec). J_i, j_i, k_i, and l_i are photolytic, unimolecular, bimolecular and termolecular rate coefficients respectively for reaction number i as listed in Appendix B , page 184.

a.) The major source terms for O_4^+ in the inner domain of the three model runs.

1-D Steady-State Model		2-D Base Case Model		2-D Electrified Model	
Log ($\Re$)	Reaction Rate $\Re = k_{yz}$ [y] [z]	Log ($\Re$)	Reaction Rate $\Re = k_{yz}$ [y] [z]	Log ($\Re$)	Reaction Rate $\Re = k_{yz}$ [y] [z]
1.53	l_{223} [O_2^+] [O_2]{M}	1.53	l_{223} [O_2^+] [O_2]{M}	11.54	l_{223} [O_2^+] [O_2]{M}
0.82	k_{350} [$N_2O_2^+$] [O_2]	0.82	k_{350} [$N_2O_2^+$] [O_2]	10.83	k_{350} [$N_2O_2^+$] [O_2]
-12.81	Advection/Diffusion	$-\infty$	Flux	$-\infty$	Flux
$-\infty$	Flux	$-\infty$	Advection/Diffusion	$-\infty$	Advection/Diffusion
1.610 = Log($\Sigma\Re$)		1.610 = Log($\Sigma\Re$)		11.618 = Log($\Sigma\Re$)	

Note: The definitions of the reactive families $\{X\}$ are at the end of Appendix B.

b.) The major sink terms for O_4^+ in the inner domain of the three model runs.
The reaction rate $\Re$ implicitly contains [O_4^+].

1-D Steady-State Model		2-D Base Case Model		2-D Electrified Model	
Log ($\Re$)	Reaction Rate $\Re = k_{yz}$ [y] [O_4^+]	Log ($\Re$)	Reaction Rate $\Re = k_{yz}$ [y] [O_4^+]	Log ($\Re$)	Reaction Rate $\Re = k_{yz}$ [y] [O_4^+]
1.56	k_{213} [O_2]	1.56	k_{213} [O_2]	11.53	k_{213} [O_2]
0.66	k_{216} [H_2O]	0.66	k_{216} [H_2O]	10.88	k_{216} [H_2O]
-2.11	k_{212} [N_2]	-2.11	k_{212} [N_2]	8.06	k_{212} [N_2]
-4.02	k_{215} [N_2]	-4.02	k_{215} [N_2]	7.31	k_{403} {NegIon}
-9.77	k_{403} {NegIon}	-7.60	Heterogeneous Loss	6.14	k_{215} [N_2]
-11.92	Heterogeneous Loss	-9.36	Advection/Diffusion	3.71	Heterogeneous Loss
-14.63	k_{214} [O]	-12.51	k_{403} {NegIon}	2.41	k_{217} [e^-]
...	4 More Reactions	...	4 More Reactions	...	4 More Reactions
1.610 = Log($\Sigma\Re$)		1.610 = Log($\Sigma\Re$)		11.618 = Log($\Sigma\Re$)	

Note: The definitions of the reactive families $\{X\}$ are at the end of Appendix B.

c.) Summary of the lifetimes of O_4^+ in the inner domain of the three model runs.

	Log(χ)	Log([O_4^+]) cm^{-3}	Log($\Sigma\Re$) cm^{-3}·s^{-1}	Log(τ) sec	Source Log(τ_c) sec	Sink Log(τ_c) sec
1-D Steady-State Model	−26.097	−6.905	1.610	−8.514	−8.514	−8.514
2-D Base Case Model	−26.097	−6.905	1.610	−8.514	−8.514	−8.514
2-D Electrified Model	−16.202	2.990	11.618	−8.629	−8.629	−8.629

Note: $\tau = [O_4^+] / \Sigma\Re$ or Log(τ) = Log([O_4^+]) − Log($\Sigma\Re$).

N_4^+

Differential Net Production ($P_{I.M.} - P_{B.C.}$) = 8.804×10^{-14} (Kg Year^{-1})

$P_{B.C.} = 1.022 \times 10^{-9}$ $P_{I.M.} = 1.022 \times 10^{-9}$ (Kg Year^{-1})

$\bar{\tau}_c = 1.421 \times 10^{-9}$ $\bar{\tau}_c = 1.421 \times 10^{-9}$ $\bar{\tau}_c = 1.421 \times 10^{-9}$ (Seconds)

$\bar{\chi} = 2.659 \times 10^{-26}$ $\bar{\chi} = 2.659 \times 10^{-26}$ $\bar{\chi} = 2.549 \times 10^{-20}$ (Mixing Ratio)

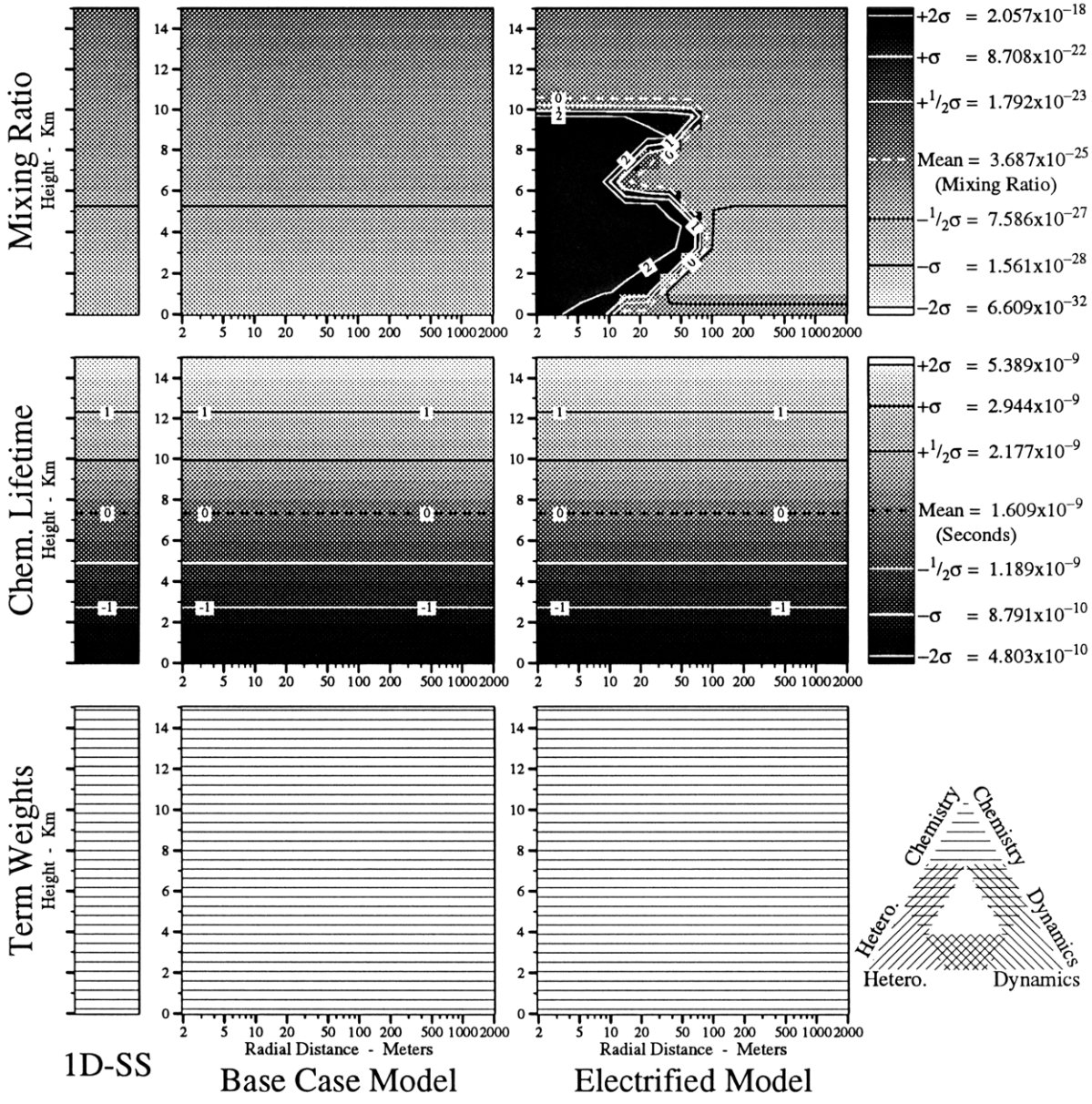

Figure 53. Mixing ratios (χ), lifetimes (τ_c), and term weights of N_4^+. See text for definitions of terms and other details.

Table 23. Summary of the chemistry of N_4^+ in the **inner domain** of the three models. (**a,b**) The major terms in the continuity equations for N_4^+ in the three model runs and (**c**) a summary of its mixing ratios χ and lifetimes τ in the three model runs. In these tables $\Re$ is the specific rate of production of N_4^+ (molec·cm^{-3}·s^{-1}), τ is the total lifetime (sec) of N_4^+ and τ_c is its lifetime due to chemical processes (sec). J_i, j_i, k_i, and l_i are photolytic, unimolecular, bimolecular and termolecular rate coefficients respectively for reaction number i as listed in Appendix B , page 184.

a.) The major source terms for N_4^+ in the inner domain of the three model runs.

1-D Steady-State Model		2-D Base Case Model		2-D Electrified Model	
Log ($\Re$)	Reaction Rate $\Re = k_{yz}$ [y] [z]	Log ($\Re$)	Reaction Rate $\Re = k_{yz}$ [y] [z]	Log ($\Re$)	Reaction Rate $\Re = k_{yz}$ [y] [z]
1.89	l_{315} [N_2^+] [N_2]{M}	1.89	l_{315} [N_2^+] [N_2]{M}	11.91	l_{315} [N_2^+] [N_2]{M}
-12.92	Advection/Diffusion	$-\infty$	Advection/Diffusion	$-\infty$	Advection/Diffusion
$-\infty$	Flux	$-\infty$	Flux	$-\infty$	Flux
1.894 = Log($\Sigma\Re$)		1.894 = Log($\Sigma\Re$)		11.913 = Log($\Sigma\Re$)	

Note: The definitions of the reactive families $\{X\}$ are at the end of Appendix B.

b.) The major sink terms for N_4^+ in the inner domain of the three model runs.
The reaction rate $\Re$ implicitly contains [N_4^+].

1-D Steady-State Model		2-D Base Case Model		2-D Electrified Model	
Log ($\Re$)	Reaction Rate $\Re = k_{yz}$ [y] [N_4^+]	Log ($\Re$)	Reaction Rate $\Re = k_{yz}$ [y] [N_4^+]	Log ($\Re$)	Reaction Rate $\Re = k_{yz}$ [y] [N_4^+]
1.87	k_{313} [O_2]	1.87	k_{313} [O_2]	11.88	k_{313} [O_2]
0.60	k_{314} [H_2O]	0.60	k_{314} [H_2O]	10.83	k_{314} [H_2O]
-9.84	k_{406} {NegIon}	-7.65	Heterogeneous Loss	7.30	k_{406} {NegIon}
-11.96	Heterogeneous Loss	-9.42	Advection/Diffusion	3.70	Heterogeneous Loss
-13.21	k_{312} [O]	-12.57	k_{406} {NegIon}	2.42	k_{383} [e^-]
-18.88	k_{383} [e^-]	-13.99	k_{312} [O]	1.74	k_{312} [O]
$-\infty$	Advection/Diffusion	-18.88	k_{383} [e^-]	0.95	Advection/Diffusion
$-\infty$	Deposition	$-\infty$	Deposition	$-\infty$	Deposition
1.894 = Log($\Sigma\Re$)		1.894 = Log($\Sigma\Re$)		11.913 = Log($\Sigma\Re$)	

Note: The definitions of the reactive families $\{X\}$ are at the end of Appendix B.

c.) Summary of the lifetimes of N_4^+ in the inner domain of the three model runs.

	Log(χ)	Log([N_4^+]) cm^{-3}	Log($\Sigma\Re$) cm^{-3}·s^{-1}	Log(τ) sec	Source Log(τ_c) sec	Sink Log(τ_c) sec
1-D Steady-State Model	−26.143	−6.951	1.894	−8.845	−8.845	−8.845
2-D Base Case Model	−26.143	−6.951	1.894	−8.845	−8.845	−8.845
2-D Electrified Model	−16.215	2.977	11.913	−8.936	−8.936	−8.936

Note: $\tau = [N_4^+] / \Sigma\Re$ or Log(τ) = Log([N_4^+]) − Log($\Sigma\Re$).

NO^+

Differential Net Production ($P_{I.M.} - P_{B.C.}$) = 1.572×10^{-13} (Kg Year^{-1})

$P_{B.C.} = 1.127 \times 10^{-8}$ $P_{I.M.} = 1.127 \times 10^{-8}$ (Kg Year^{-1})

$\bar{\tau}_c = 1.365 \times 10^{-8}$ $\bar{\tau}_c = 1.365 \times 10^{-8}$ $\bar{\tau}_c = 1.365 \times 10^{-8}$ (Seconds)

$\bar{\chi} = 1.985 \times 10^{-24}$ $\bar{\chi} = 1.985 \times 10^{-24}$ $\bar{\chi} = 3.087 \times 10^{-20}$ (Mixing Ratio)

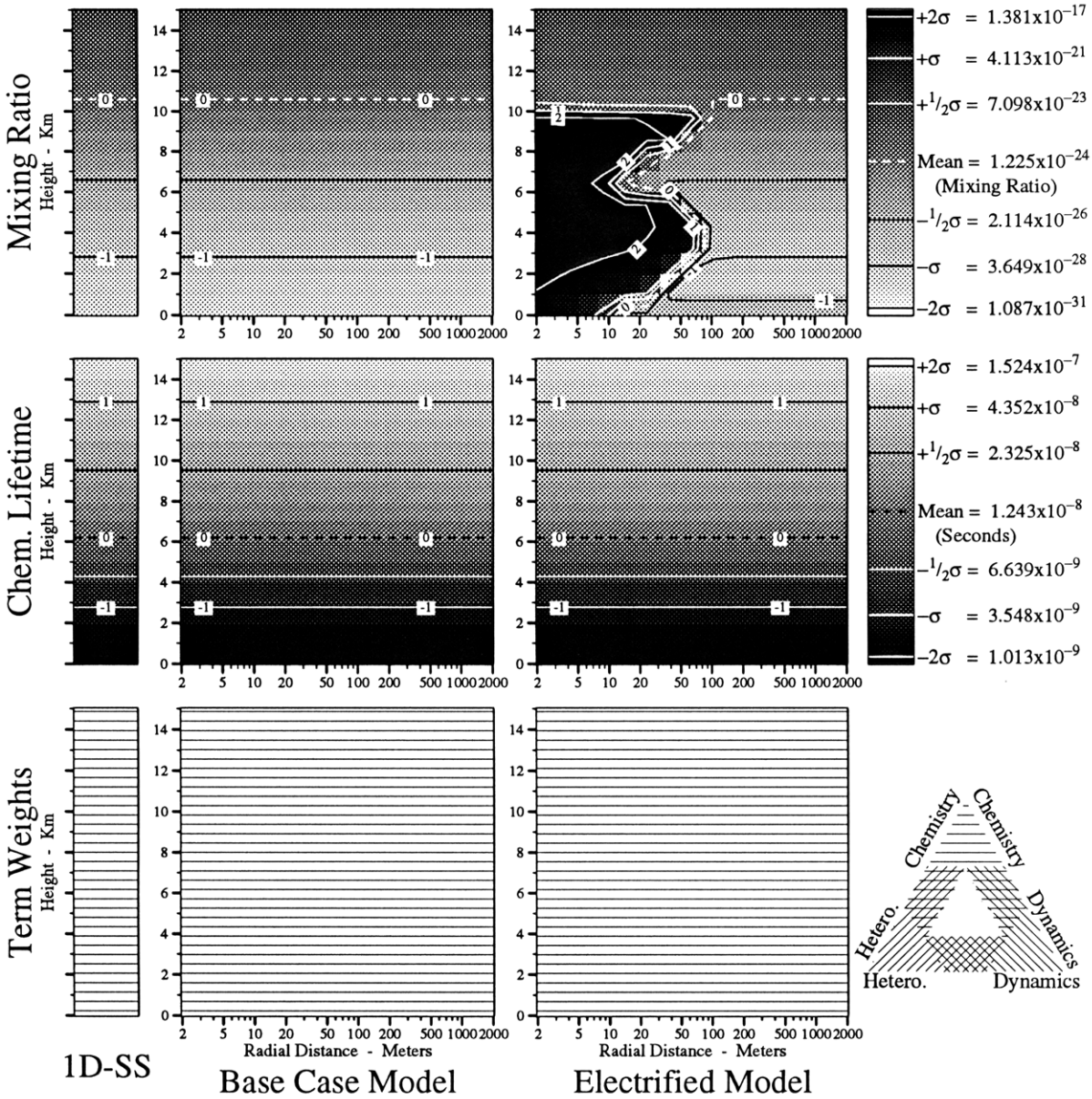

Figure 54. Mixing ratios (χ), lifetimes (τ_c), and term weights of NO^+. See text for definitions of terms and other details.

Table 24. Summary of the chemistry of NO^+ in the **inner domain** of the three models. (**a**,**b**) The major terms in the continuity equations for NO^+ in the three model runs and (**c**) a summary of its mixing ratios χ and lifetimes τ in the three model runs. In these tables $\Re$ is the specific rate of production of NO^+ (molec·cm^{-3}·s^{-1}), τ is the total lifetime (sec) of NO^+ and τ_c is its lifetime due to chemical processes (sec). J_i, j_i, k_i, and l_i are photolytic, unimolecular, bimolecular and termolecular rate coefficients respectively for reaction number i as listed in Appendix B , page 184.

a.) The major source terms for NO^+ in the inner domain of the three model runs.

1-D Steady-State Model		2-D Base Case Model		2-D Electrified Model	
Log ($\Re$)	Reaction Rate $\Re = k_{yz}$ [y] [z]	Log ($\Re$)	Reaction Rate $\Re = k_{yz}$ [y] [z]	Log ($\Re$)	Reaction Rate $\Re = k_{yz}$ [y] [z]
1.20	k_{362} [N_2NO^+]{M}	1.20	k_{362} [N_2NO^+]{M}	10.77	k_{362} [N_2NO^+]{M}
0.44	k_{326} [N_2^+] [O_2]	0.44	k_{326} [N_2^+] [O_2]	10.40	k_{326} [N_2^+] [O_2]
-0.44	k_{330} [N^+] [O_2]	-0.44	k_{330} [N^+] [O_2]	9.43	k_{330} [N^+] [O_2]
-0.76	k_{367} [$NOCO_2^+$]{M}	-0.76	k_{367} [$NOCO_2^+$]{M}	8.83	k_{329} [N^+] [O_2]
-1.04	k_{329} [N^+] [O_2]	-1.04	k_{329} [N^+] [O_2]	8.74	k_{367} [$NOCO_2^+$]{M}
-1.27	k_{226} [O^+] [N_2]	-1.27	k_{226} [O^+] [N_2]	8.64	k_{226} [O^+] [N_2]
...	18 More Reactions	...	18 More Reactions	...	18 More Reactions
1.286 = Log($\Sigma\Re$)		1.286 = Log($\Sigma\Re$)		10.943 = Log($\Sigma\Re$)	

Note: The definitions of the reactive families $\{X\}$ are at the end of Appendix B.

b.) The major sink terms for NO^+ in the inner domain of the three model runs.
The reaction rate $\Re$ implicitly contains [NO^+].

1-D Steady-State Model		2-D Base Case Model		2-D Electrified Model	
Log ($\Re$)	Reaction Rate $\Re = k_{yz}$ [y] [NO^+]	Log ($\Re$)	Reaction Rate $\Re = k_{yz}$ [y] [NO^+]	Log ($\Re$)	Reaction Rate $\Re = k_{yz}$ [y] [NO^+]
1.21	l_{361} [N_2]{M}	1.21	l_{361} [N_2]{M}	10.78	l_{361} [N_2]{M}
0.39	l_{368} [H_2O]{M}	0.39	l_{368} [H_2O]{M}	10.38	l_{368} [H_2O]{M}
-0.38	l_{377} [CO_2]{M}	-0.38	l_{377} [CO_2]{M}	9.18	l_{377} [CO_2]{M}
-0.72	k_{339} [H_2O]	-0.72	k_{339} [H_2O]	9.16	k_{339} [H_2O]
-9.17	k_{407} {NegIon}	-7.17	Heterogeneous Loss	7.31	k_{407} {NegIon}
-11.55	Heterogeneous Loss	-8.83	Advection/Diffusion	3.72	Heterogeneous Loss
...	7 More Reactions	...	7 More Reactions	...	7 More Reactions
1.286 = Log($\Sigma\Re$)		1.286 = Log($\Sigma\Re$)		10.943 = Log($\Sigma\Re$)	

Note: The definitions of the reactive families $\{X\}$ are at the end of Appendix B.

c.) Summary of the lifetimes of NO^+ in the inner domain of the three model runs.

	Log(χ)	Log([NO^+]) cm^{-3}	Log($\Sigma\Re$) cm^{-3}·s^{-1}	Log(τ) sec	Source Log(τ_c) sec	Sink Log(τ_c) sec
1-D Steady-State Model	−25.671	−6.479	1.286	−7.765	−7.765	−7.765
2-D Base Case Model	−25.671	−6.479	1.286	−7.765	−7.765	−7.765
2-D Electrified Model	−16.138	3.054	10.943	−7.889	−7.889	−7.889

Note: τ = [NO^+] / $\Sigma\Re$ or Log(τ) = Log([NO^+]) − Log($\Sigma\Re$).

H_2O^+

Differential Net Production ($P_{I.M.} - P_{B.C.}$) = 1.415×10^{-15} (Kg Year^{-1})

$P_{B.C.} = 6.809 \times 10^{-12}$ $P_{I.M.} = 6.811 \times 10^{-12}$ (Kg Year^{-1})

$\overline{\tau}_c = 1.757 \times 10^{-9}$ $\overline{\tau}_c = 1.757 \times 10^{-9}$ $\overline{\tau}_c = 1.757 \times 10^{-9}$ (Seconds)

$\overline{\chi} = 4.635 \times 10^{-28}$ $\overline{\chi} = 4.635 \times 10^{-28}$ $\overline{\chi} = 2.505 \times 10^{-21}$ (Mixing Ratio)

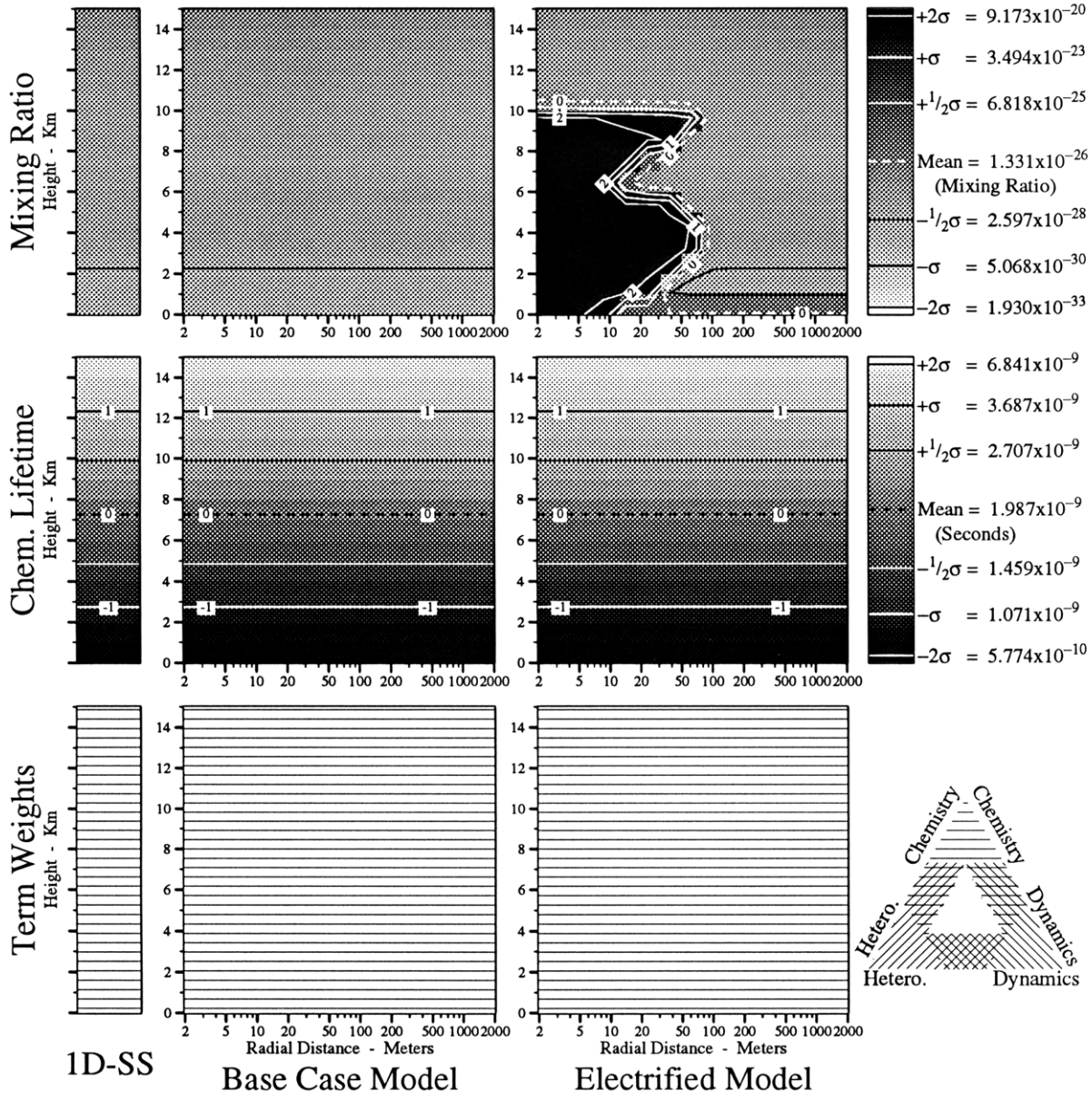

Figure 55. Mixing ratios (χ), lifetimes (τ_c), and term weights of H_2O^+. See text for definitions of terms and other details.

Table 25. Summary of the chemistry of H_2O^+ in the **inner domain** of the three models. (**a**,**b**) The major terms in the continuity equations for H_2O^+ in the three model runs and (**c**) a summary of its mixing ratios χ and lifetimes τ in the three model runs. In these tables $\Re$ is the specific rate of production of H_2O^+ (molec·cm^{-3}·s^{-1}), τ is the total lifetime (sec) of H_2O^+ and τ_c is its lifetime due to chemical processes (sec). J_i, j_i, k_i, and l_i are photolytic, unimolecular, bimolecular and termolecular rate coefficients respectively for reaction number i as listed in Appendix B , page 184.

a.) The major source terms for H_2O^+ in the inner domain of the three model runs.

1-D Steady-State Model		2-D Base Case Model		2-D Electrified Model	
Log ($\Re$)	Reaction Rate $\Re = k_{yz}\,[y]\,[z]$	Log ($\Re$)	Reaction Rate $\Re = k_{yz}\,[y]\,[z]$	Log ($\Re$)	Reaction Rate $\Re = k_{yz}\,[y]\,[z]$
0.60	$k_{314}\,[N_4^+]\,[H_2O]$	0.60	$k_{314}\,[N_4^+]\,[H_2O]$	10.83	$k_{314}\,[N_4^+]\,[H_2O]$
-0.72	$k_{339}\,[NO^+]\,[H_2O]$	-0.72	$k_{339}\,[NO^+]\,[H_2O]$	9.44	$k_{225}\,[O_2^+]\,[H_2O]$
-0.79	$k_{225}\,[O_2^+]\,[H_2O]$	-0.79	$k_{225}\,[O_2^+]\,[H_2O]$	9.16	$k_{339}\,[NO^+]\,[H_2O]$
-1.36	$k_{229}\,[O^+]\,[H_2O]$	-1.36	$k_{229}\,[O^+]\,[H_2O]$	8.63	$k_{229}\,[O^+]\,[H_2O]$
-1.77	$k_{316}\,[N_2^+]\,[H_2O]$	-1.77	$k_{316}\,[N_2^+]\,[H_2O]$	8.45	$k_{316}\,[N_2^+]\,[H_2O]$
-1.82	$j_{119}\,[H_2O]$	-1.82	$j_{119}\,[H_2O]$	2.93	$k_{239}\,[CO^+]\,[H_2O]$
...	3 More Reactions	...	3 More Reactions	...	3 More Reactions
0.642 = Log($\Sigma\Re$)		0.642 = Log($\Sigma\Re$)		10.859 = Log($\Sigma\Re$)	

b.) The major sink terms for H_2O^+ in the inner domain of the three model runs.
The reaction rate $\Re$ implicitly contains $[H_2O^+]$.

1-D Steady-State Model		2-D Base Case Model		2-D Electrified Model	
Log ($\Re$)	Reaction Rate $\Re = k_{yz}\,[y]\,[H_2O^+]$	Log ($\Re$)	Reaction Rate $\Re = k_{yz}\,[y]\,[H_2O^+]$	Log ($\Re$)	Reaction Rate $\Re = k_{yz}\,[y]\,[H_2O^+]$
0.59	$k_{340}\,[O_2]$	0.59	$k_{340}\,[O_2]$	10.81	$k_{340}\,[O_2]$
-0.29	$k_{341}\,[H_2O]$	-0.29	$k_{341}\,[H_2O]$	9.92	$k_{341}\,[H_2O]$
-11.43	k_{410} {NegIon}	-8.97	Heterogeneous Loss	6.30	k_{410} {NegIon}
-13.15	Heterogeneous Loss	-10.99	Advection/Diffusion	2.70	Heterogeneous Loss
-14.37	Advection/Diffusion	-14.10	k_{410} {NegIon}	0.04	Advection/Diffusion
-22.14	$k_{388}\,[e^-]$	-22.14	$k_{388}\,[e^-]$	-0.32	$k_{388}\,[e^-]$
$-\infty$	Deposition	$-\infty$	Deposition	$-\infty$	Deposition
0.642 = Log($\Sigma\Re$)		0.642 = Log($\Sigma\Re$)		10.859 = Log($\Sigma\Re$)	

Note: The definitions of the reactive families $\{X\}$ are at the end of Appendix B.

c.) Summary of the lifetimes of H_2O^+ in the inner domain of the three model runs.

	Log(χ)	Log($[H_2O^+]$) cm^{-3}	Log($\Sigma\Re$) cm^{-3}·s^{-1}	Log(τ) sec	Source Log(τ_c) sec	Sink Log(τ_c) sec
1-D Steady-State Model	−27.411	−8.219	0.642	−8.861	−8.861	−8.861
2-D Base Case Model	−27.411	−8.219	0.642	−8.861	−8.861	−8.861
2-D Electrified Model	−17.222	1.970	10.859	−8.889	−8.889	−8.889

Note: $\tau = [H_2O^+] / \Sigma\Re$ or Log(τ) = Log($[H_2O^+]$) − Log($\Sigma\Re$).

O_2^-

Differential Net Production ($P_{I.M.}$ - $P_{B.C.}$) = -1.902×10^{-9} (Kg Year^{-1})

$P_{B.C.} = 8.823 \times 10^{-9}$ $P_{I.M.} = 6.922 \times 10^{-9}$ (Kg Year^{-1})

$\overline{\tau}_c = 5.747 \times 10^{-8}$ $\overline{\tau}_c = 5.747 \times 10^{-8}$ $\overline{\tau}_c = 5.747 \times 10^{-8}$ (Seconds)

$\overline{\chi} = 1.580 \times 10^{-25}$ $\overline{\chi} = 9.691 \times 10^{-25}$ $\overline{\chi} = 2.259 \times 10^{-20}$ (Mixing Ratio)

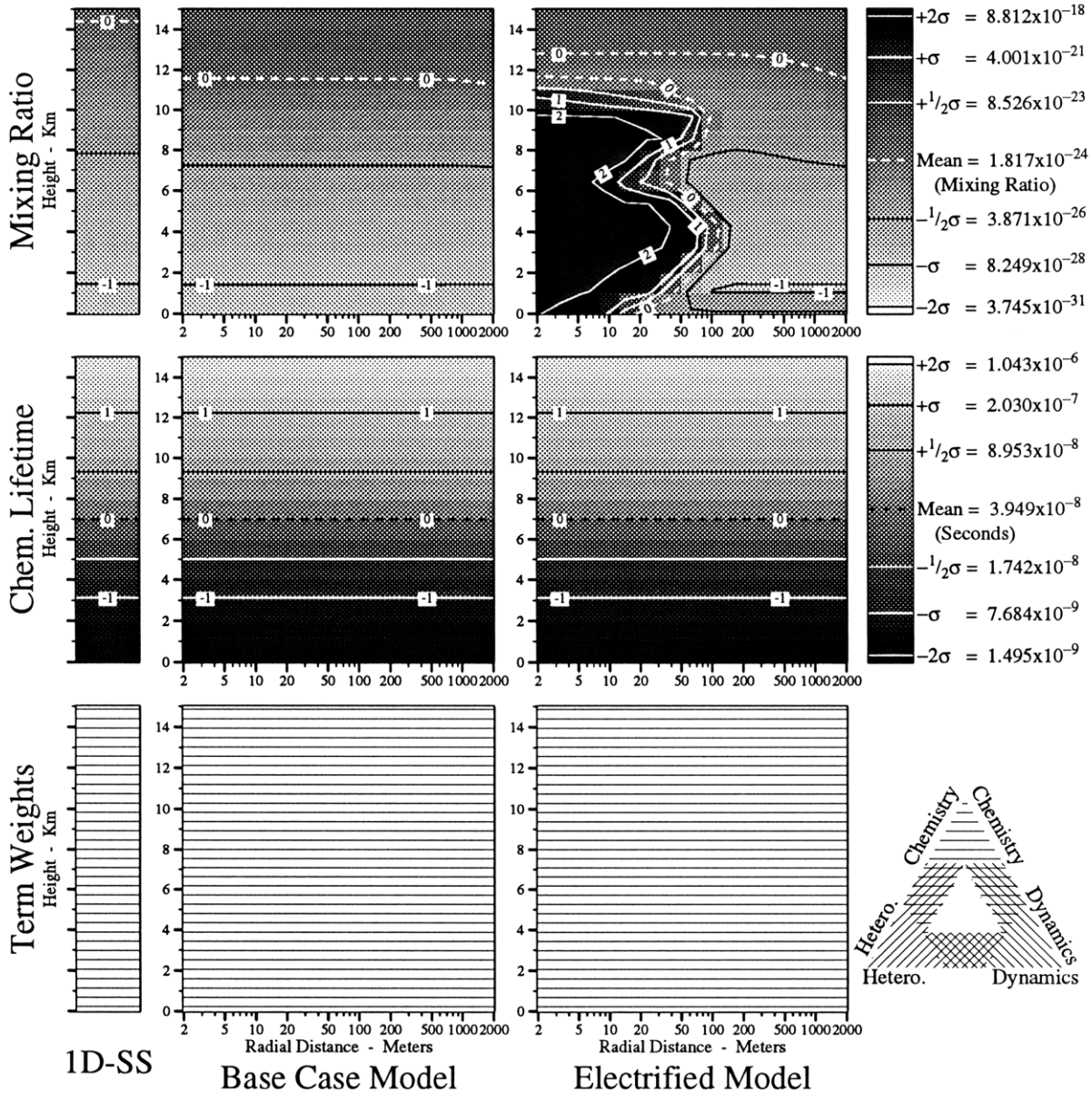

Figure 56. Mixing ratios (χ), lifetimes (τ_c), and term weights of O_2^-. See text for definitions of terms and other details.

Table 26. Summary of the chemistry of O_2^- in the **inner domain** of the three models. (**a**,**b**) The major terms in the continuity equations for O_2^- in the three model runs and (**c**) a summary of its mixing ratios χ and lifetimes τ in the three model runs. In these tables $\Re$ is the specific rate of production of O_2^- (molec·cm^{-3}·s^{-1}), τ is the total lifetime (sec) of O_2^- and τ_c is its lifetime due to chemical processes (sec). J_i, j_i, k_i, and l_i are photolytic, unimolecular, bimolecular and termolecular rate coefficients respectively for reaction number i as listed in Appendix B , page 184.

a.) The major source terms for O_2^- in the inner domain of the three model runs.

1-D Steady-State Model		2-D Base Case Model		2-D Electrified Model	
Log ($\Re$)	Reaction Rate $\Re = k_{yz}$ [y] [z]	Log ($\Re$)	Reaction Rate $\Re = k_{yz}$ [y] [z]	Log ($\Re$)	Reaction Rate $\Re = k_{yz}$ [y] [z]
0.53	l_{243} [e^-] [O_2] [O_2]	0.53	l_{243} [e^-] [O_2] [O_2]	10.58	l_{243} [e^-] [O_2] [O_2]
0.11	k_{253} [O_4^-] [O_2]	0.51	k_{253} [O_4^-] [O_2]	9.94	l_{244} [e^-] [O_2] [N_2]
-0.09	l_{244} [e^-] [O_2] [N_2]	-0.09	l_{244} [e^-] [O_2] [N_2]	9.64	l_{245} [e^-] [O_2] [H_2O]
-0.49	l_{245} [e^-] [O_2] [H_2O]	-0.49	l_{245} [e^-] [O_2] [H_2O]	9.51	k_{253} [O_4^-] [O_2]
-1.99	l_{246} [e^-] [O_2] [CO_2]	-1.99	l_{246} [e^-] [O_2] [CO_2]	8.04	l_{246} [e^-] [O_2] [CO_2]
-3.55	k_{262} [CO_3^-] [O]	-7.09	k_{262} [CO_3^-] [O]	7.01	k_{262} [CO_3^-] [O]
...	7 More Reactions	...	7 More Reactions	...	7 More Reactions
0.764 = Log($\Sigma\Re$)		0.888 = Log($\Sigma\Re$)		10.733 = Log($\Sigma\Re$)	

b.) The major sink terms for O_2^- in the inner domain of the three model runs.
The reaction rate $\Re$ implicitly contains [O_2^-].

1-D Steady-State Model		2-D Base Case Model		2-D Electrified Model	
Log ($\Re$)	Reaction Rate $\Re = k_{yz}$ [y] [O_2^-]	Log ($\Re$)	Reaction Rate $\Re = k_{yz}$ [y] [O_2^-]	Log ($\Re$)	Reaction Rate $\Re = k_{yz}$ [y] [O_2^-]
0.52	k_{280} [H_2O]	0.60	k_{280} [H_2O]	10.58	k_{280} [H_2O]
0.37	l_{279} [O_2]{M}	0.54	l_{279} [O_2]{M}	10.18	l_{279} [O_2]{M}
-0.72	l_{281} [CO_2]{M}	-0.55	l_{281} [CO_2]{M}	9.09	l_{281} [CO_2]{M}
-4.61	k_{272} [O_3]	-5.26	k_{272} [O_3]	6.03	k_{272} [O_3]
-5.93	k_{271} [H_2]	-5.74	k_{271} [H_2]	5.48	k_{273} [NO_2]
-6.16	k_{274} [N_2O]	-5.97	k_{274} [N_2O]	3.82	k_{271} [H_2]
...	18 More Reactions	...	18 More Reactions	...	18 More Reactions
0.764 = Log($\Sigma\Re$)		0.888 = Log($\Sigma\Re$)		10.733 = Log($\Sigma\Re$)	

Note: The definitions of the reactive families $\{X\}$ are at the end of Appendix B.

c.) Summary of the lifetimes of O_2^- in the inner domain of the three model runs.

	Log(χ)	Log([O_2^-]) cm^{-3}	Log($\Sigma\Re$) cm^{-3}·s^{-1}	Log(τ) sec	Source Log(τ_c) sec	Sink Log(τ_c) sec
1-D Steady-State Model	−25.939	−6.748	0.764	−7.511	−7.511	−7.511
2-D Base Case Model	−25.734	−6.542	0.888	−7.431	−7.431	−7.431
2-D Electrified Model	−16.269	2.923	10.733	−7.810	−7.810	−7.810

Note: $\tau = [O_2^-] / \Sigma\Re$ or Log(τ) = Log([O_2^-]) − Log($\Sigma\Re$).

O_4^-

Differential Net Production ($P_{I.M.} - P_{B.C.}$) = -7.286×10^{-7} (Kg Year^{-1})

$P_{B.C.} = 2.996 \times 10^{-6}$ $P_{I.M.} = 2.267 \times 10^{-6}$ (Kg Year^{-1})

$\overline{\tau}_c = 5.976 \times 10^{-7}$ $\overline{\tau}_c = 5.976 \times 10^{-7}$ $\overline{\tau}_c = 5.976 \times 10^{-7}$ (Seconds)

$\overline{\chi} = 3.903 \times 10^{-24}$ $\overline{\chi} = 1.322 \times 10^{-22}$ $\overline{\chi} = 1.349 \times 10^{-18}$ (Mixing Ratio)

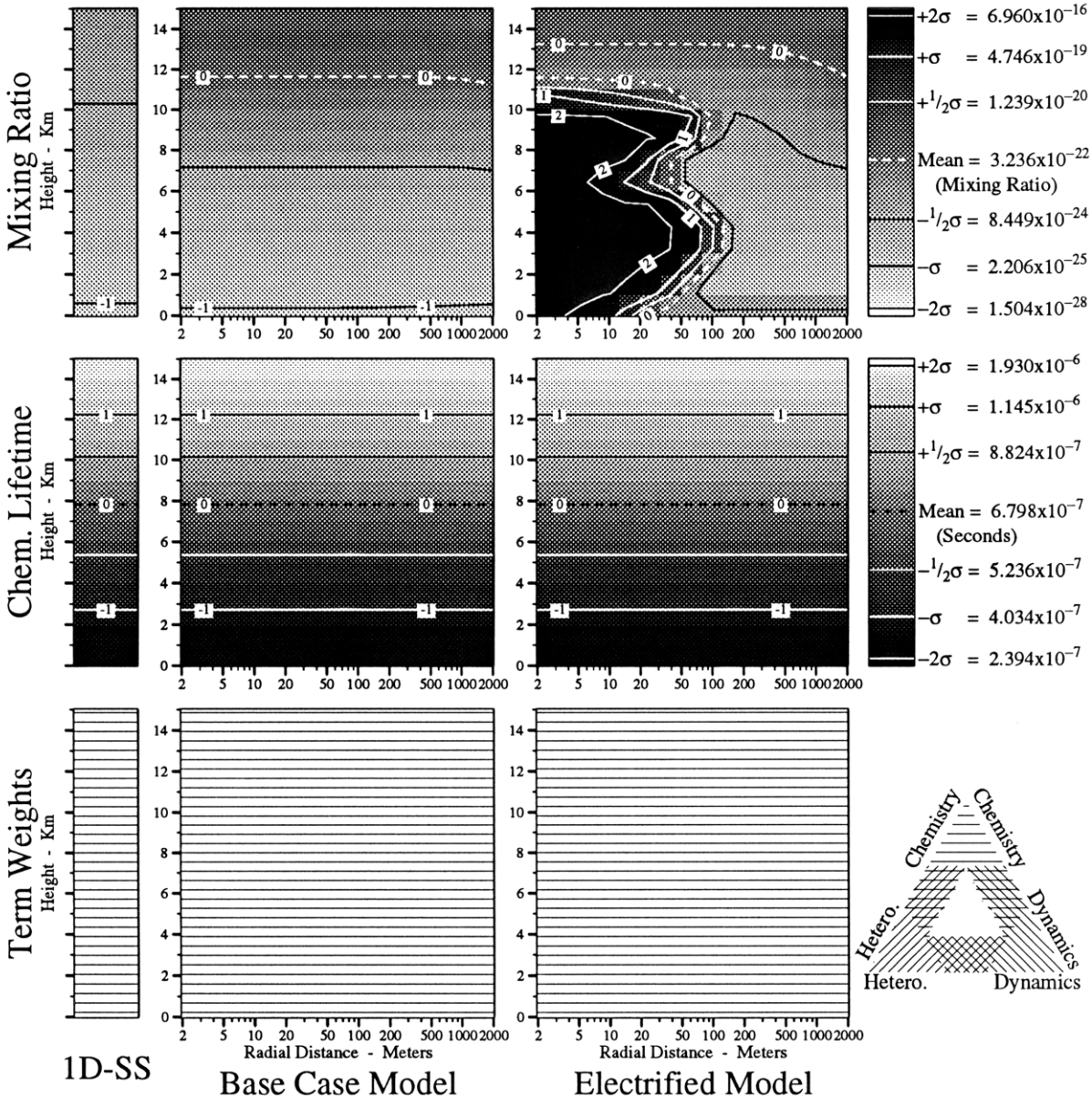

Figure 57. Mixing ratios (χ), lifetimes (τ_c), and term weights of O_4^-. See text for definitions of terms and other details.

Table 27. Summary of the chemistry of O_4^- in the **inner domain** of the three models. (**a**,**b**) The major terms in the continuity equations for O_4^- in the three model runs and (**c**) a summary of its mixing ratios χ and lifetimes τ in the three model runs. In these tables $\Re$ is the specific rate of production of O_4^- (molec·cm^{-3}·s^{-1}), τ is the total lifetime (sec) of O_4^- and τ_c is its lifetime due to chemical processes (sec). J_i, j_i, k_i, and l_i are photolytic, unimolecular, bimolecular and termolecular rate coefficients respectively for reaction number i as listed in Appendix B , page 184.

a.) The major source terms for O_4^- in the inner domain of the three model runs.

1-D Steady-State Model		2-D Base Case Model		2-D Electrified Model	
Log ($\Re$)	Reaction Rate $\Re = k_{yz}$ [y] [z]	Log ($\Re$)	Reaction Rate $\Re = k_{yz}$ [y] [z]	Log ($\Re$)	Reaction Rate $\Re = k_{yz}$ [y] [z]
1.59	k_{257} [CO_4^-] [O_2]	2.00	k_{257} [CO_4^-] [O_2]	10.95	k_{257} [CO_4^-] [O_2]
0.37	l_{279} [O_2^-] [O_2]{M}	0.54	l_{279} [O_2^-] [O_2]{M}	10.18	l_{279} [O_2^-] [O_2]{M}
-10.80	Advection/Diffusion	$-\infty$	Flux	$-\infty$	Flux
$-\infty$	Flux	$-\infty$	Advection/Diffusion	$-\infty$	Advection/Diffusion
1.615 = Log($\Sigma\Re$)		2.011 = Log($\Sigma\Re$)		11.017 = Log($\Sigma\Re$)	

Note: The definitions of the reactive families $\{X\}$ are at the end of Appendix B.

b.) The major sink terms for O_4^- in the inner domain of the three model runs.
The reaction rate $\Re$ implicitly contains [O_4^-].

1-D Steady-State Model		2-D Base Case Model		2-D Electrified Model	
Log ($\Re$)	Reaction Rate $\Re = k_{yz}$ [y] [O_4^-]	Log ($\Re$)	Reaction Rate $\Re = k_{yz}$ [y] [O_4^-]	Log ($\Re$)	Reaction Rate $\Re = k_{yz}$ [y] [O_4^-]
1.60	k_{254} [CO_2]	2.00	k_{254} [CO_2]	11.00	k_{254} [CO_2]
0.11	k_{253} [O_2]	0.51	k_{253} [O_2]	9.51	k_{253} [O_2]
-6.14	k_{255} [NO]	-4.88	Heterogeneous Loss	6.71	k_{255} [NO]
-6.34	k_{199} [$CC\ell_4$]	-5.80	k_{255} [NO]	5.41	Heterogeneous Loss
-8.66	k_{198} [CF_4]	-5.94	k_{199} [$CC\ell_4$]	3.60	k_{419} {PosIon}
-8.81	k_{197} [SF_6]	-6.59	Advection/Diffusion	3.42	k_{251} [O]
-9.62	Heterogeneous Loss	-8.27	k_{198} [CF_4]	3.30	k_{252} [O]
...	5 More Reactions	...	5 More Reactions	...	5 More Reactions
1.615 = Log($\Sigma\Re$)		2.011 = Log($\Sigma\Re$)		11.017 = Log($\Sigma\Re$)	

Note: The definitions of the reactive families $\{X\}$ are at the end of Appendix B.

c.) Summary of the lifetimes of O_4^- in the inner domain of the three model runs.

	Log(χ)	Log([O_4^-]) cm^{-3}	Log($\Sigma\Re$) cm^{-3}·s^{-1}	Log(τ) sec	Source Log(τ_c) sec	Sink Log(τ_c) sec
1-D Steady-State Model	−23.814	−4.622	1.615	−6.237	−6.237	−6.237
2-D Base Case Model	−23.376	−4.184	2.011	−6.195	−6.195	−6.195
2-D Electrified Model	−14.494	4.698	11.017	−6.320	−6.320	−6.320

Note: $\tau = [O_4^-] / \Sigma\Re$ or Log(τ) = Log([O_4^-]) − Log($\Sigma\Re$).

HCO_3^-

Differential Net Production ($P_{I.M.}$ - $P_{B.C.}$) = −0.25573 (Kg Year^{-1})

$P_{B.C.}$ = −614.8 $P_{I.M.}$ = −615.1 (Kg Year^{-1})

$\overline{\tau}_c$ = 0.76458 $\overline{\tau}_c$ = 102.0 $\overline{\tau}_c$ = 810.6 (Years)

$\overline{\chi}$ = 2.216x10^{-14} $\overline{\chi}$ = 7.811x10^{-16} $\overline{\chi}$ = 1.918x10^{-13} (Mixing Ratio)

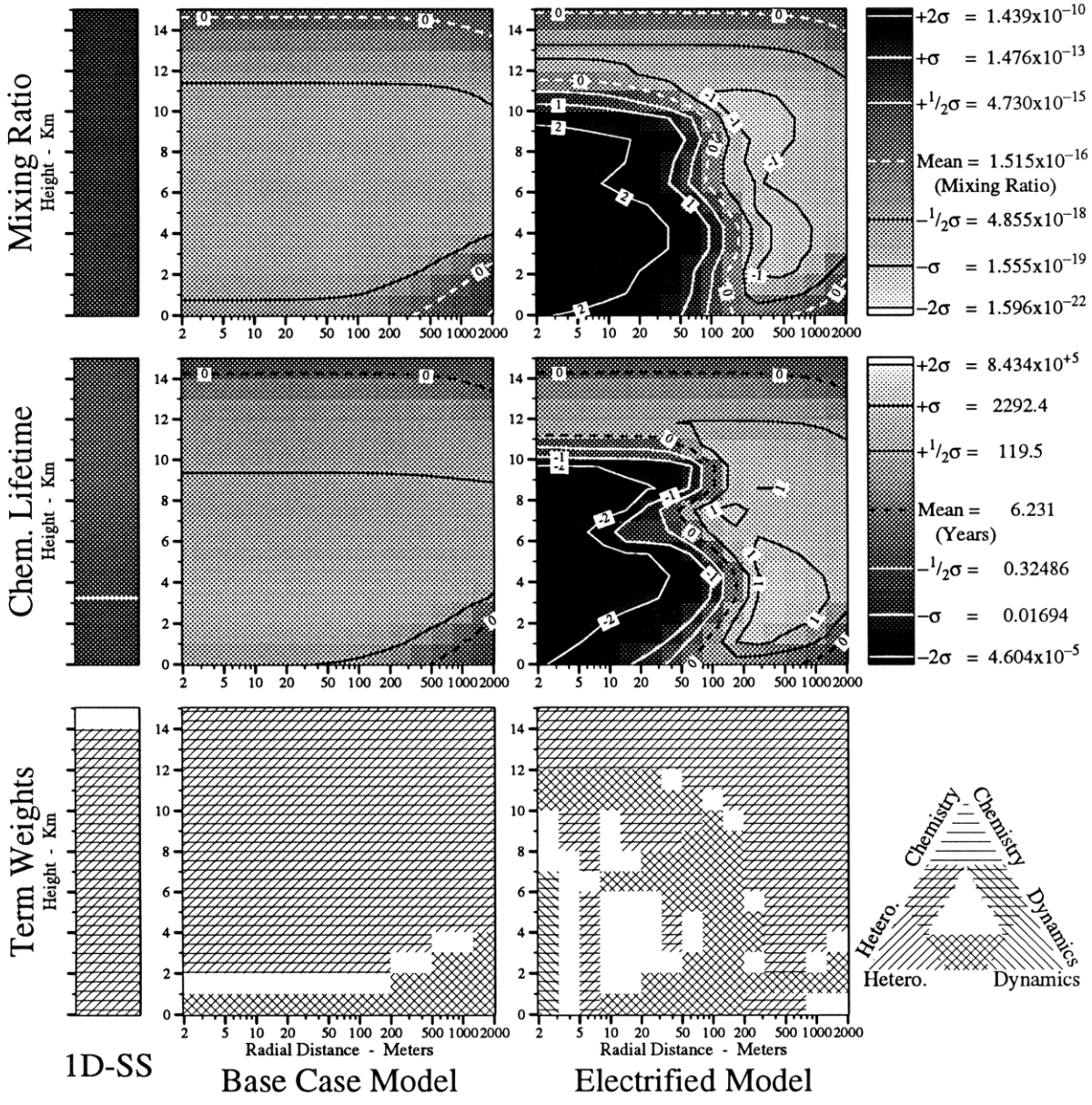

Figure 58. Mixing ratios (χ), lifetimes (τ_c), and term weights of HCO_3^-. See text for definitions of terms and other details.

Table 28. Summary of the chemistry of HCO_3^- in the **inner domain** of the three models. (**a**,**b**) The major terms in the continuity equations for HCO_3^- in the three model runs and (**c**) a summary of its mixing ratios χ and lifetimes τ in the three model runs. In these tables $\Re$ is the specific rate of production of HCO_3^- (molec·cm^{-3}·s^{-1}), τ is the total lifetime (sec) of HCO_3^- and τ_c is its lifetime due to chemical processes (sec). J_i, j_i, k_i, and l_i are photolytic, unimolecular, bimolecular and termolecular rate coefficients respectively for reaction number i as listed in Appendix B , page 184.

a.) The major source terms for HCO_3^- in the inner domain of the three model runs.

1-D Steady-State Model		2-D Base Case Model		2-D Electrified Model	
Log ($\Re$)	Reaction Rate $\Re = k_{yz}$ [y] [z]	Log ($\Re$)	Reaction Rate $\Re = k_{yz}$ [y] [z]	Log ($\Re$)	Reaction Rate $\Re = k_{yz}$ [y] [z]
0.52	l_{308} [OH^-] [CO_2]{M}	0.60	l_{308} [OH^-] [CO_2]{M}	10.58	l_{308} [OH^-] [CO_2]{M}
$-\infty$	Advection/Diffusion	-0.32	Advection/Diffusion	$-\infty$	Advection/Diffusion
$-\infty$	Flux	$-\infty$	Flux	$-\infty$	Flux
0.518 = Log($\Sigma\Re$)		0.650 = Log($\Sigma\Re$)		10.577 = Log($\Sigma\Re$)	

Note: The definitions of the reactive families $\{X\}$ are at the end of Appendix B.

b.) The major sink terms for HCO_3^- in the inner domain of the three model runs.
The reaction rate $\Re$ implicitly contains [HCO_3^-].

1-D Steady-State Model		2-D Base Case Model		2-D Electrified Model	
Log ($\Re$)	Reaction Rate $\Re = k_{yz}$ [y] [HCO_3^-]	Log ($\Re$)	Reaction Rate $\Re = k_{yz}$ [y] [HCO_3^-]	Log ($\Re$)	Reaction Rate $\Re = k_{yz}$ [y] [HCO_3^-]
0.51	Heterogeneous Loss	0.65	Heterogeneous Loss	10.57	Heterogeneous Loss
-1.26	Advection/Diffusion	-8.50	k_{426} {PosIon}	8.46	k_{426} {PosIon}
-1.74	k_{426} {PosIon}	$-\infty$	Deposition	8.08	Advection/Diffusion
$-\infty$	Deposition	$-\infty$	Advection/Diffusion	$-\infty$	Deposition
0.518 = Log($\Sigma\Re$)		0.650 = Log($\Sigma\Re$)		10.577 = Log($\Sigma\Re$)	

Note: The definitions of the reactive families $\{X\}$ are at the end of Appendix B.

c.) Summary of the lifetimes of HCO_3^- in the inner domain of the three model runs.

	Log(χ)	Log([HCO_3^-]) cm^{-3}	Log($\Sigma\Re$) cm^{-3}·s^{-1}	Log(τ) sec	Source Log(τ_c) sec	Sink Log(τ_c) sec
1-D Steady-State Model	−13.750	5.442	0.518	4.923	4.923	7.177
2-D Base Case Model	−17.729	1.463	0.650	0.813	0.861	9.967
2-D Electrified Model	−9.342	9.850	10.577	−0.727	−0.727	1.388

Note: τ = [HCO_3^-] / $\Sigma\Re$ or Log(τ) = Log([HCO_3^-]) − Log($\Sigma\Re$).

CO_3^-

Differential Net Production ($P_{I.M.}$ - $P_{B.C.}$) = −0.08055 (Kg Year^{-1})

$P_{B.C.}$ = 0.07523 $P_{I.M.}$ = −0.0053254 (Kg Year^{-1})

$\overline{\tau}_c$ = 702.5 $\overline{\tau}_c$ = 7086.5 $\overline{\tau}_c$ = 303.1 (Seconds)

$\overline{\chi}$ = 3.205x10^{-16} $\overline{\chi}$ = 5.129x10^{-17} $\overline{\chi}$ = 3.785x10^{-14} (Mixing Ratio)

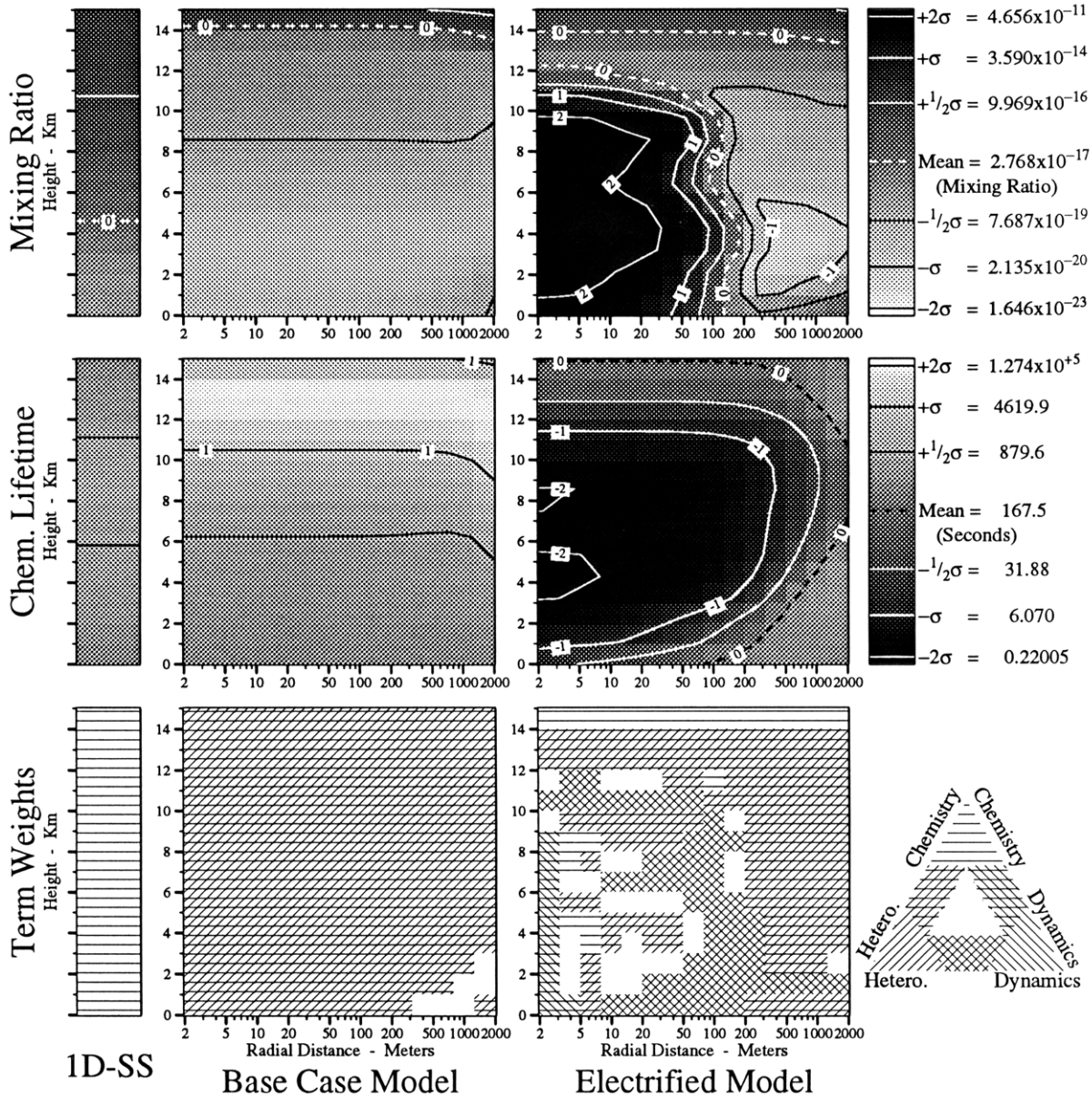

Figure 59. Mixing ratios (χ), lifetimes (τ_c), and term weights of CO_3^-. See text for definitions of terms and other details.

Table 29. Summary of the chemistry of CO_3^- in the **inner domain** of the three models. (**a**,**b**) The major terms in the continuity equations for CO_3^- in the three model runs and (**c**) a summary of its mixing ratios χ and lifetimes τ in the three model runs. In these tables $\Re$ is the specific rate of production of CO_3^- (molec·cm^{-3}·s^{-1}), τ is the total lifetime (sec) of CO_3^- and τ_c is its lifetime due to chemical processes (sec). J_i, j_i, k_i, and l_i are photolytic, unimolecular, bimolecular and termolecular rate coefficients respectively for reaction number i as listed in Appendix B , page 184.

a.) The major source terms for CO_3^- in the inner domain of the three model runs.

1-D Steady-State Model		2-D Base Case Model		2-D Electrified Model	
Log ($\Re$)	Reaction Rate $\Re = k_{yz}$ [y] [z]	Log ($\Re$)	Reaction Rate $\Re = k_{yz}$ [y] [z]	Log ($\Re$)	Reaction Rate $\Re = k_{yz}$ [y] [z]
0.08	k_{267} [O_3^-] [CO_2]	-0.30	k_{267} [O_3^-] [CO_2]	10.09	k_{267} [O_3^-] [CO_2]
-2.49	Advection/Diffusion	-7.71	l_{290} [O^-] [CO_2]{M}	5.78	k_{259} [CO_4^-] [O]
-7.01	l_{290} [O^-] [CO_2]{M}	-8.49	k_{259} [CO_4^-] [O]	3.87	l_{290} [O^-] [CO_2]{M}
-8.10	k_{259} [CO_4^-] [O]	$-\infty$	Advection/Diffusion	$-\infty$	Flux
$-\infty$	Flux	$-\infty$	Flux	$-\infty$	Advection/Diffusion
0.086 = Log($\Sigma\Re$)		-0.304 = Log($\Sigma\Re$)		10.089 = Log($\Sigma\Re$)	

Note: The definitions of the reactive families $\{X\}$ are at the end of Appendix B.

b.) The major sink terms for CO_3^- in the inner domain of the three model runs.
The reaction rate $\Re$ implicitly contains [CO_3^-].

1-D Steady-State Model		2-D Base Case Model		2-D Electrified Model	
Log ($\Re$)	Reaction Rate $\Re = k_{yz}$ [y] [CO_3^-]	Log ($\Re$)	Reaction Rate $\Re = k_{yz}$ [y] [CO_3^-]	Log ($\Re$)	Reaction Rate $\Re = k_{yz}$ [y] [CO_3^-]
0.08	k_{263} [NO]	-0.31	Heterogeneous Loss	9.86	Heterogeneous Loss
-1.95	Heterogeneous Loss	-2.24	Advection/Diffusion	9.69	k_{263} [NO]
-3.55	k_{262} [O]	-2.59	k_{263} [NO]	7.86	k_{423} {PosIon}
-4.30	k_{261} [O]	-7.09	k_{262} [O]	7.30	Advection/Diffusion
-4.42	k_{423} {PosIon}	-7.83	k_{261} [O]	7.01	k_{262} [O]
$-\infty$	Advection/Diffusion	-9.38	k_{423} {PosIon}	6.27	k_{261} [O]
$-\infty$	Deposition	$-\infty$	Deposition	$-\infty$	Deposition
0.086 = Log($\Sigma\Re$)		-0.304 = Log($\Sigma\Re$)		10.089 = Log($\Sigma\Re$)	

Note: The definitions of the reactive families $\{X\}$ are at the end of Appendix B.

c.) Summary of the lifetimes of CO_3^- in the inner domain of the three model runs.

	Log(χ)	Log([CO_3^-]) cm^{-3}	Log($\Sigma\Re$) cm^{-3}·s^{-1}	Log(τ) sec	Source Log(τ_c) sec	Sink Log(τ_c) sec
1-D Steady-State Model	−16.098	3.094	0.086	3.009	3.010	3.013
2-D Base Case Model	−18.793	0.399	−0.304	0.703	0.703	2.988
2-D Electrified Model	−10.046	9.146	10.089	−0.943	−0.943	−0.555

Note: τ = [CO_3^-] / $\Sigma\Re$ or Log(τ) = Log([CO_3^-]) − Log($\Sigma\Re$).

$O(^3P)$

Differential Net Production ($P_{I.M.} - P_{B.C.}$) = 0.07623 (Kg Year^{-1})

$P_{B.C.}$ = −0.30518 $P_{I.M.}$ = −0.22895 (Kg Year^{-1})

$\overline{\tau}_c$ = 3.915x10^{-5} $\overline{\tau}_c$ = 3.915x10^{-5} $\overline{\tau}_c$ = 3.915x10^{-5} (Seconds)

$\overline{\chi}$ = 2.843x10^{-16} $\overline{\chi}$ = 2.532x10^{-17} $\overline{\chi}$ = 1.377x10^{-16} (Mixing Ratio)

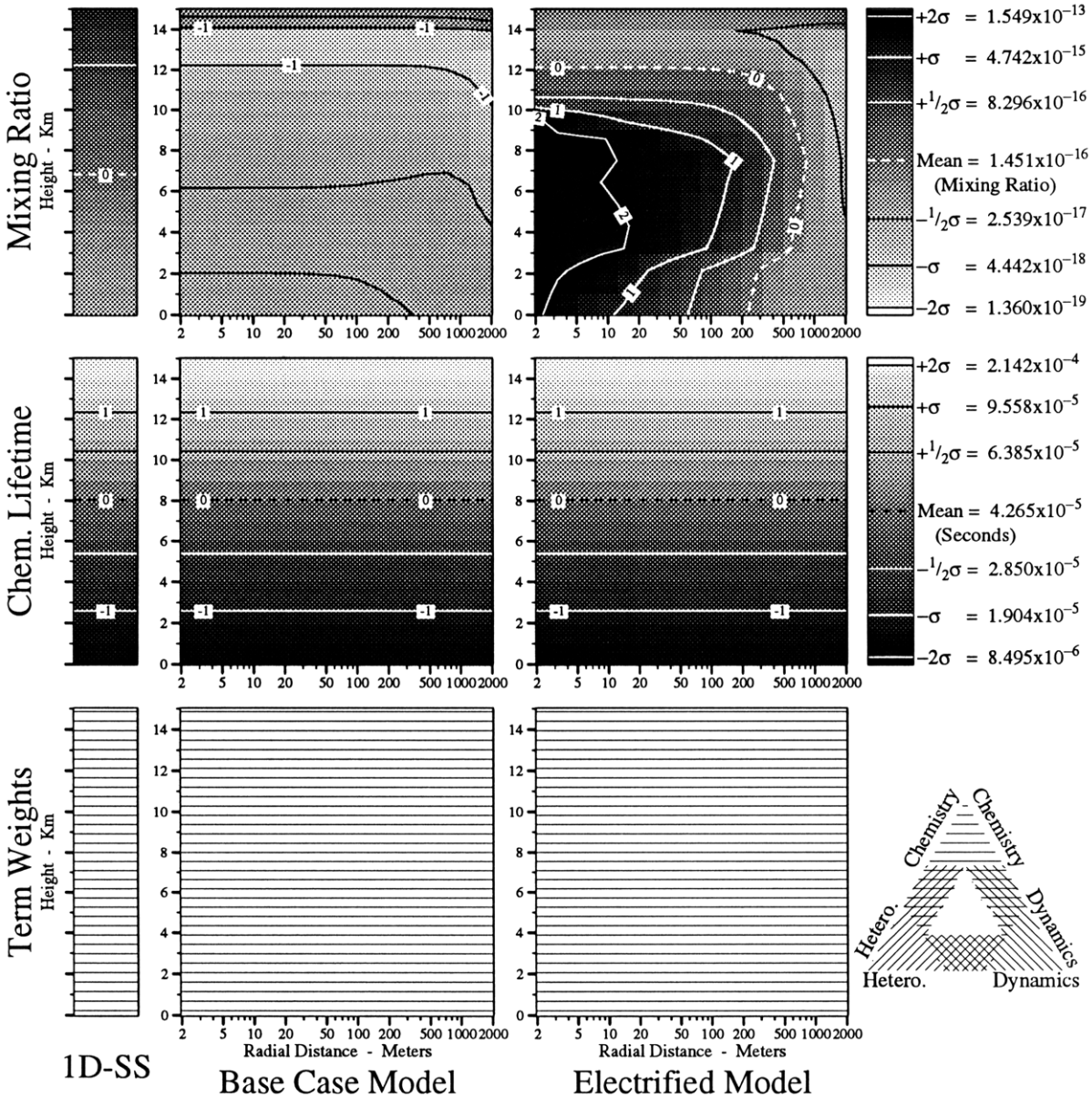

Figure 60. Mixing ratios (χ), lifetimes (τ_c), and term weights of O. See text for definitions of terms and other details.

Table 30. Summary of the chemistry of O in the **inner domain** of the three models. (**a**,**b**) The major terms in the continuity equations for O in the three model runs and (**c**) a summary of its mixing ratios χ and lifetimes τ in the three model runs. In these tables $\Re$ is the specific rate of production of O (molec·cm^{-3}·s^{-1}), τ is the total lifetime (sec) of O and τ_c is its lifetime due to chemical processes (sec). J_i, j_i, k_i, and l_i are photolytic, unimolecular, bimolecular and termolecular rate coefficients respectively for reaction number i as listed in Appendix B , page 184.

a.) The major source terms for O in the inner domain of the three model runs.

1-D Steady-State Model		2-D Base Case Model		2-D Electrified Model	
Log ($\Re$)	Reaction Rate $\Re = k_{yz}$ [y] [z]	Log ($\Re$)	Reaction Rate $\Re = k_{yz}$ [y] [z]	Log ($\Re$)	Reaction Rate $\Re = k_{yz}$ [y] [z]
7.68	J_1 [O_3]	7.20	J_1 [O_3]	10.76	$2 \cdot J_{125}$ [O_2]
6.33	k_{133} [$O(^1D)$] [N_2]	5.81	k_{133} [$O(^1D)$] [N_2]	9.98	k_{458} [N] [O_2]
5.94	k_{134} [$O(^1D)$] [O_2]	5.76	J_7 [NO_2]	9.75	k_{133} [$O(^1D)$] [N_2]
5.91	J_7 [NO_2]	5.43	k_{134} [$O(^1D)$] [O_2]	9.42	k_{460} [N] [NO]
3.61	k_{50} [O_3]{M}	3.36	k_{50} [O_3]{M}	9.36	k_{134} [$O(^1D)$] [O_2]
3.52	k_{136} [$O(^1D)$] [H_2O]	3.19	k_{136} [$O(^1D)$] [H_2O]	9.36	j_{131} [O_2]
...	101 More Reactions	...	101 More Reactions	...	101 More Reactions
7.717 = Log($\Sigma\Re$)		7.236 = Log($\Sigma\Re$)		10.941 = Log($\Sigma\Re$)	

Note: The definitions of the reactive families $\{X\}$ are at the end of Appendix B.

b.) The major sink terms for O in the inner domain of the three model runs.
The reaction rate $\Re$ implicitly contains [O].

1-D Steady-State Model		2-D Base Case Model		2-D Electrified Model	
Log ($\Re$)	Reaction Rate $\Re = k_{yz}$ [y] [O]	Log ($\Re$)	Reaction Rate $\Re = k_{yz}$ [y] [O]	Log ($\Re$)	Reaction Rate $\Re = k_{yz}$ [y] [O]
7.72	k_{90} [O_2]	7.24	k_{90} [O_2]	10.94	k_{90} [O_2]
0.99	k_{61} [HO_2]	1.36	k_{670} [DMS]	7.19	k_{61} [HO_2]
0.86	k_{670} [DMS]	0.91	Heterogeneous Loss	7.01	k_{262} [CO_3^-]
0.51	k_{593} [CH_3O_2]	-0.15	k_{18} [NO_2]	6.97	k_{18} [NO_2]
0.38	k_{18} [NO_2]	-0.57	k_{560} [CH_4]	6.63	k_{46} [OH]
0.20	k_{51} [O_3]	-0.60	k_{51} [O_3]	6.27	k_{261} [CO_3^-]
...	92 More Reactions	...	92 More Reactions	...	92 More Reactions
7.717 = Log($\Sigma\Re$)		7.236 = Log($\Sigma\Re$)		10.941 = Log($\Sigma\Re$)	

c.) Summary of the lifetimes of O in the inner domain of the three model runs.

	Log(χ)	Log([O]) cm^{-3}	Log($\Sigma\Re$) cm^{-3}·s^{-1}	Log(τ) sec	Source Log(τ_c) sec	Sink Log(τ_c) sec
1-D Steady-State Model	−16.029	3.162	7.717	−4.555	−4.555	−4.555
2-D Base Case Model	−16.604	2.588	7.236	−4.649	−4.649	−4.649
2-D Electrified Model	−12.822	6.370	10.941	−4.571	−4.571	−4.571

Note: τ = [O] / $\Sigma\Re$ or Log(τ) = Log([O]) − Log($\Sigma\Re$).

$O(^1D)$

Differential Net Production ($P_{I.M.} - P_{B.C.}$) = 5.726×10^{-7} (Kg Year^{-1})

$P_{B.C.} = -1.355 \times 10^{-6}$ $P_{I.M.} = -7.828 \times 10^{-7}$ (Kg Year^{-1})

$\overline{\tau}_c = 2.552 \times 10^{-9}$ $\overline{\tau}_c = 2.552 \times 10^{-9}$ $\overline{\tau}_c = 2.552 \times 10^{-9}$ (Seconds)

$\overline{\chi} = 9.950 \times 10^{-22}$ $\overline{\chi} = 1.144 \times 10^{-22}$ $\overline{\chi} = 1.167 \times 10^{-21}$ (Mixing Ratio)

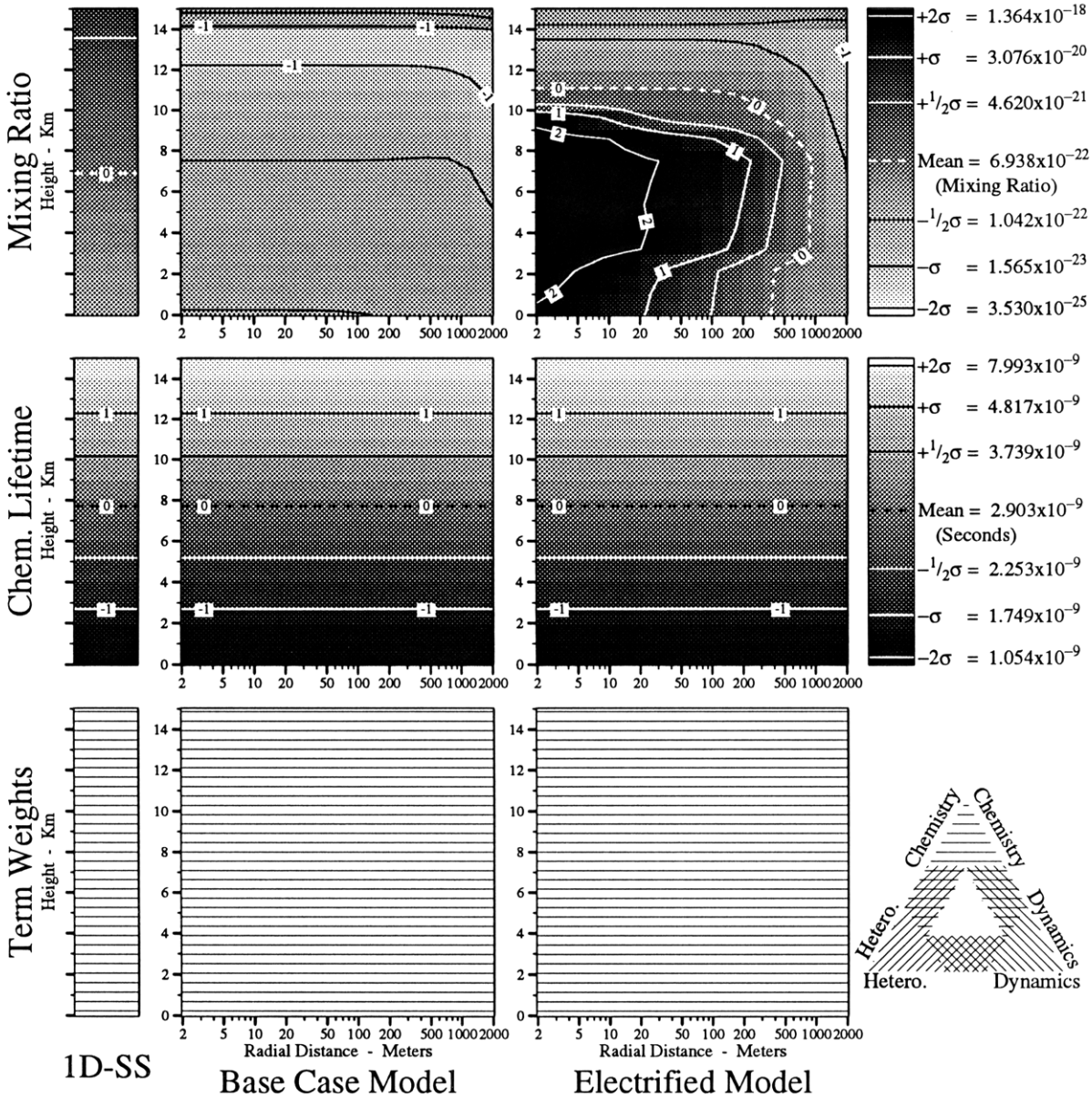

Figure 61. Mixing ratios (χ), lifetimes (τ_c), and term weights of $O(^1D)$. See text for definitions of terms and other details.

Table 31. Summary of the chemistry of $O(^1D)$ in the **inner domain** of the three models. (**a**,**b**) The major terms in the continuity equations for $O(^1D)$ in the three model runs and (**c**) a summary of its mixing ratios χ and lifetimes τ in the three model runs. In these tables $\Re$ is the specific rate of production of $O(^1D)$ (molec·cm^{-3}·s^{-1}), τ is the total lifetime (sec) of $O(^1D)$ and τ_c is its lifetime due to chemical processes (sec). J_i, j_i, k_i, and l_i are photolytic, unimolecular, bimolecular and termolecular rate coefficients respectively for reaction number i as listed in Appendix B , page 184.

a.) The major source terms for $O(^1D)$ in the inner domain of the three model runs.

1-D Steady-State Model		2-D Base Case Model		2-D Electrified Model	
Log ($\Re$)	Reaction Rate $\Re = k_{yz}$ [y] [z]	Log ($\Re$)	Reaction Rate $\Re = k_{yz}$ [y] [z]	Log ($\Re$)	Reaction Rate $\Re = k_{yz}$ [y] [z]
6.48	J_2 [O_3]	5.98	J_2 [O_3]	9.73	J_{124} [O_3]
-0.44	k_{330} [N^+] [O_2]	-0.44	k_{330} [N^+] [O_2]	9.43	k_{330} [N^+] [O_2]
-7.81	j_{17} [N_2O]	-6.10	Advection/Diffusion	7.31	k_{407} [NO^+]{NegIon}
-9.17	k_{407} [NO^+]{NegIon}	-7.81	j_{17} [N_2O]	7.18	k_{402} [O_2^+]{NegIon}
-9.61	Advection/Diffusion	-11.92	k_{407} [NO^+]{NegIon}	7.16	J_2 [O_3]
-9.97	k_{402} [O_2^+]{NegIon}	-12.70	k_{402} [O_2^+]{NegIon}	4.95	k_{401} [O^+]{NegIon}
...	6 More Reactions	...	6 More Reactions	...	6 More Reactions
6.484 = Log($\Sigma\Re$)		5.978 = Log($\Sigma\Re$)		9.910 = Log($\Sigma\Re$)	

Note: The definitions of the reactive families $\{X\}$ are at the end of Appendix B.

b.) The major sink terms for $O(^1D)$ in the inner domain of the three model runs.
The reaction rate $\Re$ implicitly contains [$O(^1D)$].

1-D Steady-State Model		2-D Base Case Model		2-D Electrified Model	
Log ($\Re$)	Reaction Rate $\Re = k_{yz}$ [y] [$O(^1D)$]	Log ($\Re$)	Reaction Rate $\Re = k_{yz}$ [y] [$O(^1D)$]	Log ($\Re$)	Reaction Rate $\Re = k_{yz}$ [y] [$O(^1D)$]
6.33	k_{133} [N_2]	5.81	k_{133} [N_2]	9.75	k_{133} [N_2]
5.94	k_{134} [O_2]	5.43	k_{134} [O_2]	9.36	k_{134} [O_2]
4.78	k_{135} [H_2O]	4.45	k_{135} [H_2O]	8.12	k_{135} [H_2O]
3.52	k_{136} [H_2O]	3.19	k_{136} [H_2O]	6.86	k_{136} [H_2O]
2.80	k_{137} [H_2O]	2.47	k_{137} [H_2O]	6.14	k_{137} [H_2O]
1.51	k_{555} [CH_4]	1.01	k_{555} [CH_4]	4.94	k_{555} [CH_4]
...	14 More Reactions	...	14 More Reactions	...	14 More Reactions
6.484 = Log($\Sigma\Re$)		5.978 = Log($\Sigma\Re$)		9.910 = Log($\Sigma\Re$)	

c.) Summary of the lifetimes of $O(^1D)$ in the inner domain of the three model runs.

	Log(χ)	Log([$O(^1D)$]) cm^{-3}	Log($\Sigma\Re$) cm^{-3}·s^{-1}	Log(τ) sec	Source Log(τ_c) sec	Sink Log(τ_c) sec
1-D Steady-State Model	−21.353	−2.162	6.484	−8.646	−8.646	−8.646
2-D Base Case Model	−21.924	−2.732	5.978	−8.710	−8.710	−8.710
2-D Electrified Model	−17.932	1.260	9.910	−8.651	−8.651	−8.651

Note: τ = [$O(^1D)$] / $\Sigma\Re$ or Log(τ) = Log([$O(^1D)$]) − Log($\Sigma\Re$).

H

Differential Net Production ($P_{I.M.} - P_{B.C.}$) = 1.071×10^{-7} (Kg Year^{-1})

$P_{B.C.} = -4.399 \times 10^{-6}$ $P_{I.M.} = -4.291 \times 10^{-6}$ (Kg Year^{-1})

$\overline{\tau}_c = 5.250 \times 10^{-7}$ $\overline{\tau}_c = 5.251 \times 10^{-7}$ $\overline{\tau}_c = 5.251 \times 10^{-7}$ (Seconds)

$\overline{\chi} = 6.497 \times 10^{-21}$ $\overline{\chi} = 1.319 \times 10^{-21}$ $\overline{\chi} = 3.273 \times 10^{-19}$ (Mixing Ratio)

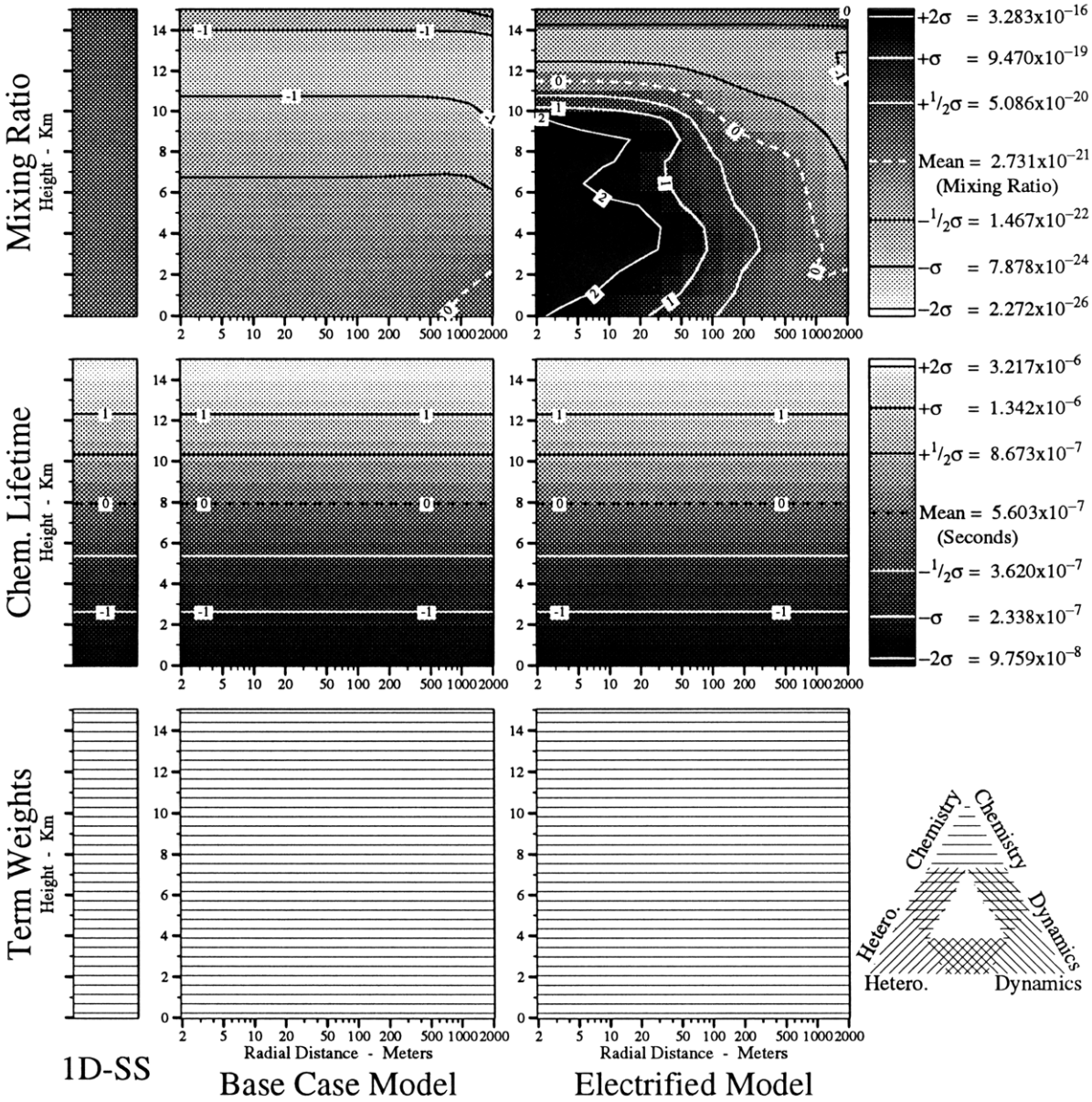

Figure 62. Mixing ratios (χ), lifetimes (τ_c), and term weights of H. See text for definitions of terms and other details.

Table 32. Summary of the chemistry of H in the **inner domain** of the three models. (**a**,**b**) The major terms in the continuity equations for H in the three model runs and (**c**) a summary of its mixing ratios χ and lifetimes τ in the three model runs. In these tables $\Re$ is the specific rate of production of H (molec·cm^{-3}·s^{-1}), τ is the total lifetime (sec) of H and τ_c is its lifetime due to chemical processes (sec). J_i, j_i, k_i, and l_i are photolytic, unimolecular, bimolecular and termolecular rate coefficients respectively for reaction number i as listed in Appendix B , page 184.

a.) The major source terms for H in the inner domain of the three model runs.

1-D Steady-State Model		2-D Base Case Model		2-D Electrified Model	
Log ($\Re$)	Reaction Rate $\Re = k_{yz}$ [y] [z]	Log ($\Re$)	Reaction Rate $\Re = k_{yz}$ [y] [z]	Log ($\Re$)	Reaction Rate $\Re = k_{yz}$ [y] [z]
5.38	k_{659} [CO] [OH]	4.60	k_{659} [CO] [OH]	10.58	k_{280} [O_2^-] [H_2O]
4.49	J_{13} [CH_2O]	3.52	k_{42} [OH] [H_2]	9.18	k_{347} [$W_2H_3O^+$] [e^-]
4.27	k_{42} [OH] [H_2]	3.05	J_{13} [CH_2O]	9.05	k_{659} [CO] [OH]
0.74	k_{48} [$O(^1D)$] [H_2]	0.60	k_{280} [O_2^-] [H_2O]	8.54	k_{553} [OH] [N]
0.52	k_{280} [O_2^-] [H_2O]	0.23	k_{48} [$O(^1D)$] [H_2]	7.95	k_{242} [e^-] [H_2O]
-0.22	$2{\cdot}k_{620}$ [CH_2] [O_2]	-0.60	$2{\cdot}k_{620}$ [CH_2] [O_2]	7.89	k_{42} [OH] [H_2]
...	67 More Reactions	...	67 More Reactions	...	67 More Reactions
5.465 = Log($\Sigma\Re$)		4.644 = Log($\Sigma\Re$)		10.611 = Log($\Sigma\Re$)	

Note: Read **W** as H_2O.

b.) The major sink terms for H in the inner domain of the three model runs.
The reaction rate $\Re$ implicitly contains [H].

1-D Steady-State Model		2-D Base Case Model		2-D Electrified Model	
Log ($\Re$)	Reaction Rate $\Re = k_{yz}$ [y] [H]	Log ($\Re$)	Reaction Rate $\Re = k_{yz}$ [y] [H]	Log ($\Re$)	Reaction Rate $\Re = k_{yz}$ [y] [H]
5.47	k_{93} [O_2]	4.64	k_{93} [O_2]	10.61	k_{93} [O_2]
-0.05	l_{759} [NH_2]{M}	-1.30	k_{53} [O_3]	6.00	k_{53} [O_3]
-0.13	k_{53} [O_3]	-3.72	Heterogeneous Loss	5.31	k_{36} [NO_2]
-3.12	k_{36} [NO_2]	-3.96	k_{36} [NO_2]	4.69	k_{45} [HO_2]
-3.24	k_{591} [CH_3O_2]	-5.02	k_{109} [CO]	3.92	k_{304} [NO_2^-]
-3.41	k_{45} [HO_2]	-5.06	k_{591} [CH_3O_2]	3.91	k_{44} [HO_2]
...	49 More Reactions	...	49 More Reactions	...	49 More Reactions
5.465 = Log($\Sigma\Re$)		4.644 = Log($\Sigma\Re$)		10.611 = Log($\Sigma\Re$)	

Note: The definitions of the reactive families $\{X\}$ are at the end of Appendix B.

c.) Summary of the lifetimes of H in the inner domain of the three model runs.

	Log(χ)	Log([H]) cm^{-3}	Log($\Sigma\Re$) cm^{-3}·s^{-1}	Log(τ) sec	Source Log(τ_c) sec	Sink Log(τ_c) sec
1-D Steady-State Model	−20.270	−1.078	5.465	−6.543	−6.543	−6.543
2-D Base Case Model	−21.201	−2.009	4.644	−6.653	−6.653	−6.653
2-D Electrified Model	−15.111	4.081	10.611	−6.530	−6.530	−6.530

Note: τ = [H] / $\Sigma\Re$ or Log(τ) = Log([H]) − Log($\Sigma\Re$).

NO

Differential Net Production ($P_{I.M.}$ - $P_{B.C.}$) = 1199.7 (Mg Year^{-1})

$P_{B.C.}$ = −196.0 $P_{I.M.}$ = 1003.7 (Mg Year^{-1})

$\overline{\tau}_c$ = 4.546	$\overline{\tau}_c$ = 688.9	$\overline{\tau}_c$ = 202.9 (Minutes)
$\overline{\chi}$ = 13.73	$\overline{\chi}$ = 9.017	$\overline{\chi}$ = 115.8 (ppT)

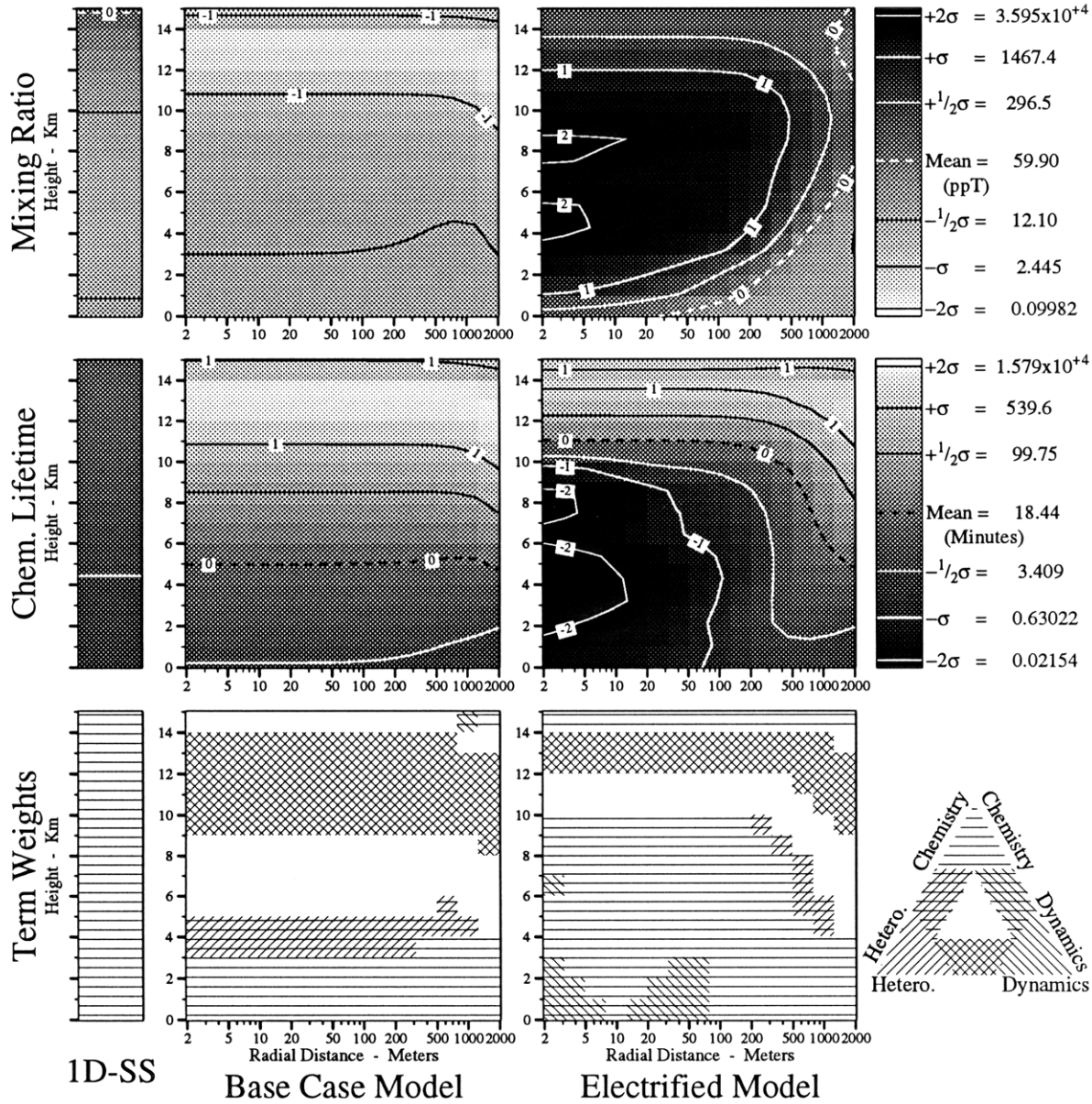

Figure 63. Mixing ratios (χ), lifetimes (τ_c), and term weights of NO. See text for definitions of terms and other details.

Table 33. Summary of the chemistry of NO in the **inner domain** of the three models. (**a**,**b**) The major terms in the continuity equations for NO in the three model runs and (**c**) a summary of its mixing ratios χ and lifetimes τ in the three model runs. In these tables $\Re$ is the specific rate of production of NO (molec·cm^{-3}·s^{-1}), τ is the total lifetime (sec) of NO and τ_c is its lifetime due to chemical processes (sec). J_i, j_i, k_i, and l_i are photolytic, unimolecular, bimolecular and termolecular rate coefficients respectively for reaction number i as listed in Appendix B , page 184.

a.) The major source terms for NO in the inner domain of the three model runs.

1-D Steady-State Model		2-D Base Case Model		2-D Electrified Model	
Log ($\Re$)	Reaction Rate $\Re = k_{yz}$ [y] [z]	Log ($\Re$)	Reaction Rate $\Re = k_{yz}$ [y] [z]	Log ($\Re$)	Reaction Rate $\Re = k_{yz}$ [y] [z]
5.91	J_7 [NO_2]	5.76	J_7 [NO_2]	10.40	k_{326} [N_2^+] [O_2]
3.76	j_{488} [N_2O_3]	5.19	Advection/Diffusion	9.98	k_{458} [N] [O_2]
3.66	J_3 [HONO]	3.70	j_{488} [N_2O_3]	9.64	j_{488} [N_2O_3]
2.93	k_{70} [HNO] [O_2]	1.61	J_9 [NO_3]	9.16	k_{339} [NO^+] [H_2O]
2.26	J_9 [NO_3]	1.61	k_{70} [HNO] [O_2]	9.05	k_{148} [$N(^2D)$] [O_2]
2.24	Advection/Diffusion	0.96	J_3 [HONO]	9.00	$2{\cdot}k_{470}$ [NO_2] [N]
...	68 More Reactions	...	68 More Reactions	...	68 More Reactions
5.915 = Log($\Sigma\Re$)		5.867 = Log($\Sigma\Re$)		10.648 = Log($\Sigma\Re$)	

b.) The major sink terms for NO in the inner domain of the three model runs.
The reaction rate $\Re$ implicitly contains [NO].

1-D Steady-State Model		2-D Base Case Model		2-D Electrified Model	
Log ($\Re$)	Reaction Rate $\Re = k_{yz}$ [y] [NO]	Log ($\Re$)	Reaction Rate $\Re = k_{yz}$ [y] [NO]	Log ($\Re$)	Reaction Rate $\Re = k_{yz}$ [y] [NO]
5.76	k_{25} [O_3]	5.62	Heterogeneous Loss	10.26	k_{55} [HO_2]
5.27	k_{55} [HO_2]	5.47	k_{25} [O_3]	9.78	Advection/Diffusion
4.76	k_{592} [CH_3O_2]	4.12	k_{55} [HO_2]	9.69	k_{263} [CO_3^-]
3.76	k_{487} [NO_2]	3.70	k_{487} [NO_2]	9.64	k_{487} [NO_2]
2.93	k_{69} [HO_2]	3.69	k_{592} [CH_3O_2]	9.61	k_{92} [OH]
2.79	k_{92} [OH]	2.09	k_{686} [$CH_3SCH_2O_2$]	9.42	k_{460} [N]
...	50 More Reactions	...	50 More Reactions	...	50 More Reactions
5.915 = Log($\Sigma\Re$)		5.867 = Log($\Sigma\Re$)		10.648 = Log($\Sigma\Re$)	

c.) Summary of the lifetimes of NO in the inner domain of the three model runs.

	Log(χ)	Log([NO]) cm^{-3}	Log($\Sigma\Re$) $cm^{-3}{\cdot}s^{-1}$	Log(τ) sec	Source Log(τ_c) sec	Sink Log(τ_c) sec
1-D Steady-State Model	−11.011	8.180	5.915	2.266	2.266	2.266
2-D Base Case Model	−10.964	8.228	5.867	2.361	2.464	2.729
2-D Electrified Model	−8.028	11.164	10.648	0.516	0.516	0.583

Note: τ = [NO] / $\Sigma\Re$ or Log(τ) = Log([NO]) − Log($\Sigma\Re$).

NO_2

Differential Net Production ($P_{I.M.}$ - $P_{B.C.}$) = 265.2 (Mg Year^{-1})

$P_{B.C.}$ = −1436.7 $P_{I.M.}$ = −1171.5 (Mg Year^{-1})

$\overline{\tau}_c$ =	224.9	$\overline{\tau}_c$ = 238.5	$\overline{\tau}_c$ = 232.7	(Seconds)
$\overline{\chi}$ =	15.94	$\overline{\chi}$ = 12.02	$\overline{\chi}$ = 76.68	(ppT)

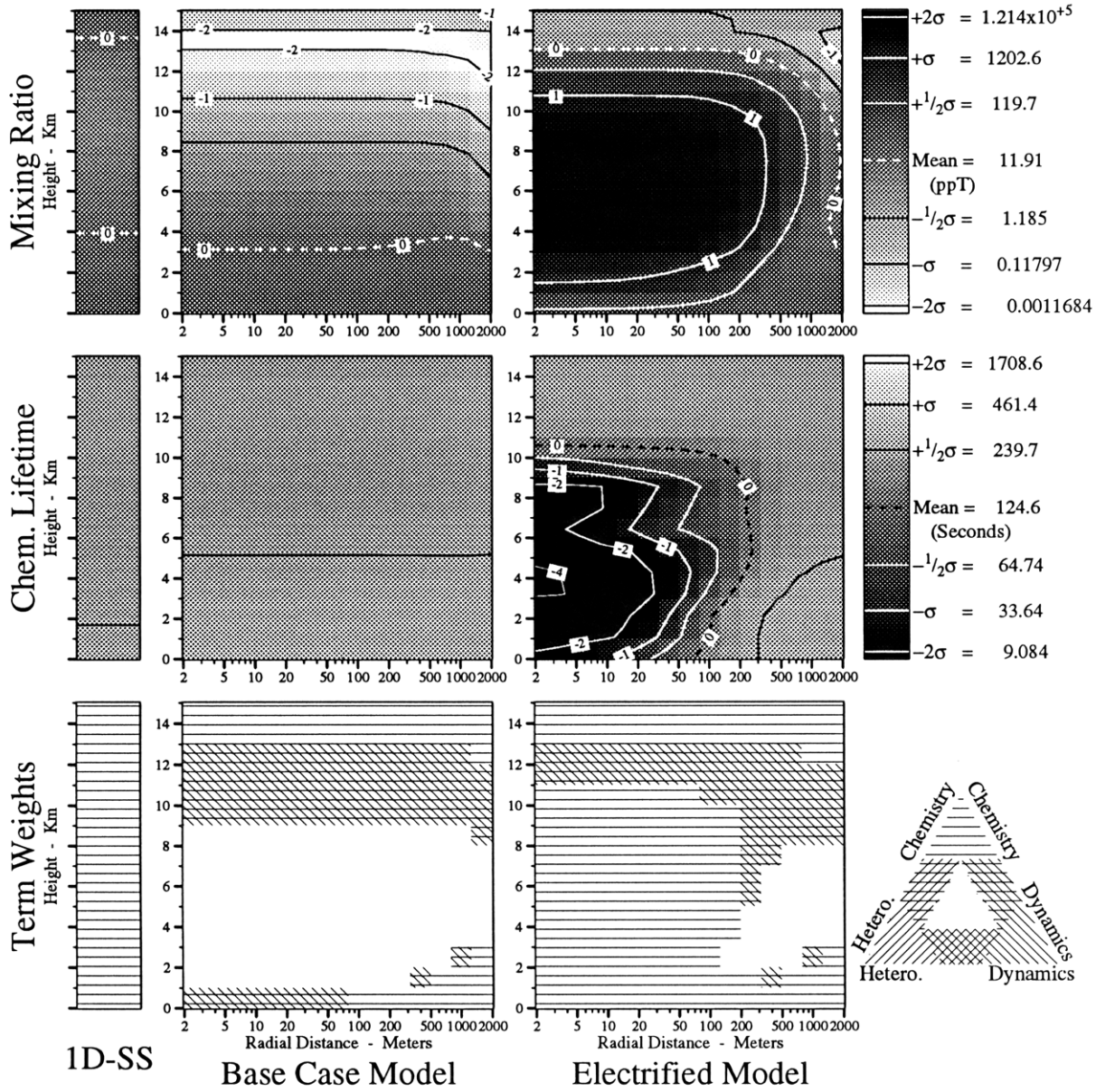

Figure 64. Mixing ratios (χ), lifetimes (τ_c), and term weights of NO_2. See text for definitions of terms and other details.

Table 34. Summary of the chemistry of NO_2 in the **inner domain** of the three models. (**a,b**) The major terms in the continuity equations for NO_2 in the three model runs and (**c**) a summary of its mixing ratios χ and lifetimes τ in the three model runs. In these tables $\Re$ is the specific rate of production of NO_2 (molec·cm^{-3}·s^{-1}), τ is the total lifetime (sec) of NO_2 and τ_c is its lifetime due to chemical processes (sec). J_i, j_i, k_i, and l_i are photolytic, unimolecular, bimolecular and termolecular rate coefficients respectively for reaction number i as listed in Appendix B , page 184.

a.) The major source terms for NO_2 in the inner domain of the three model runs.

1-D Steady-State Model		2-D Base Case Model		2-D Electrified Model	
Log ($\Re$)	Reaction Rate $\Re = k_{yz}$ [y] [z]	Log ($\Re$)	Reaction Rate $\Re = k_{yz}$ [y] [z]	Log ($\Re$)	Reaction Rate $\Re = k_{yz}$ [y] [z]
5.76	k_{25} [O_3] [NO]	5.81	Advection/Diffusion	10.26	k_{55} [HO_2] [NO]
5.27	k_{55} [HO_2] [NO]	5.47	k_{25} [O_3] [NO]	9.74	k_{68} [OH] [HONO]
4.76	k_{592} [CH_3O_2] [NO]	4.12	k_{55} [HO_2] [NO]	9.64	j_{488} [N_2O_3]
4.74	j_{101} [$CH_3O_2NO_2$]	3.70	j_{488} [N_2O_3]	9.39	k_{25} [O_3] [NO]
4.69	j_{96} [HO_2NO_2]	3.69	k_{592} [CH_3O_2] [NO]	9.29	$2 \cdot j_{485}$ [N_2O_4]
3.76	j_{488} [N_2O_3]	3.54	j_{101} [$CH_3O_2NO_2$]	9.03	k_{66} [OH] [HO_2NO_2]
...	44 More Reactions	...	44 More Reactions	...	44 More Reactions
5.969 = Log($\Sigma\Re$)		5.985 = Log($\Sigma\Re$)		10.538 = Log($\Sigma\Re$)	

b.) The major sink terms for NO_2 in the inner domain of the three model runs.
The reaction rate $\Re$ implicitly contains [NO_2].

1-D Steady-State Model		2-D Base Case Model		2-D Electrified Model	
Log ($\Re$)	Reaction Rate $\Re = k_{yz}$ [y] [NO_2]	Log ($\Re$)	Reaction Rate $\Re = k_{yz}$ [y] [NO_2]	Log ($\Re$)	Reaction Rate $\Re = k_{yz}$ [y] [NO_2]
5.91	J_7	5.76	J_7	10.13	k_{94} [OH]
4.74	k_{100} [CH_3O_2]	5.57	Heterogeneous Loss	9.91	Advection/Diffusion
4.69	k_{95} [HO_2]	3.70	k_{487} [NO]	9.64	k_{487} [NO]
3.76	k_{487} [NO]	3.57	k_{100} [CH_3O_2]	9.59	k_{95} [HO_2]
3.60	k_{86} [HO_2]	3.47	k_{95} [HO_2]	9.29	$2 \cdot k_{484}$ [NO_2]
3.53	$2 \cdot k_{484}$ [NO_2]	3.29	$2 \cdot k_{484}$ [NO_2]	8.91	J_7
...	41 More Reactions	...	41 More Reactions	...	41 More Reactions
5.969 = Log($\Sigma\Re$)		5.985 = Log($\Sigma\Re$)		10.538 = Log($\Sigma\Re$)	

c.) Summary of the lifetimes of NO_2 in the inner domain of the three model runs.

	Log(χ)	Log([NO_2]) cm^{-3}	Log($\Sigma\Re$) cm^{-3}·s^{-1}	Log(τ) sec	Source Log(τ_c) sec	Sink Log(τ_c) sec
1-D Steady-State Model	−10.856	8.336	5.969	2.367	2.367	2.367
2-D Base Case Model	−10.998	8.193	5.985	2.208	2.684	2.422
2-D Electrified Model	−7.901	11.291	10.538	0.753	0.753	0.878

Note: τ = [NO_2] / $\Sigma\Re$ or Log(τ) = Log([NO_2]) − Log($\Sigma\Re$).

HONO

Differential Net Production ($P_{I.M.}$ - $P_{B.C.}$) = 0.0024630 (Mg Year^{-1})

$P_{B.C.}$ = −68.09 $P_{I.M.}$ = −68.08 (Mg Year^{-1})

$\bar{\tau}_c$ = 1381.1 $\bar{\tau}_c$ = 1384.5 $\bar{\tau}_c$ = 1381.4 (Seconds)

$\bar{\chi}$ = 525.2 $\bar{\chi}$ = 167.7 $\bar{\chi}$ = 6768.1 (ppQ)

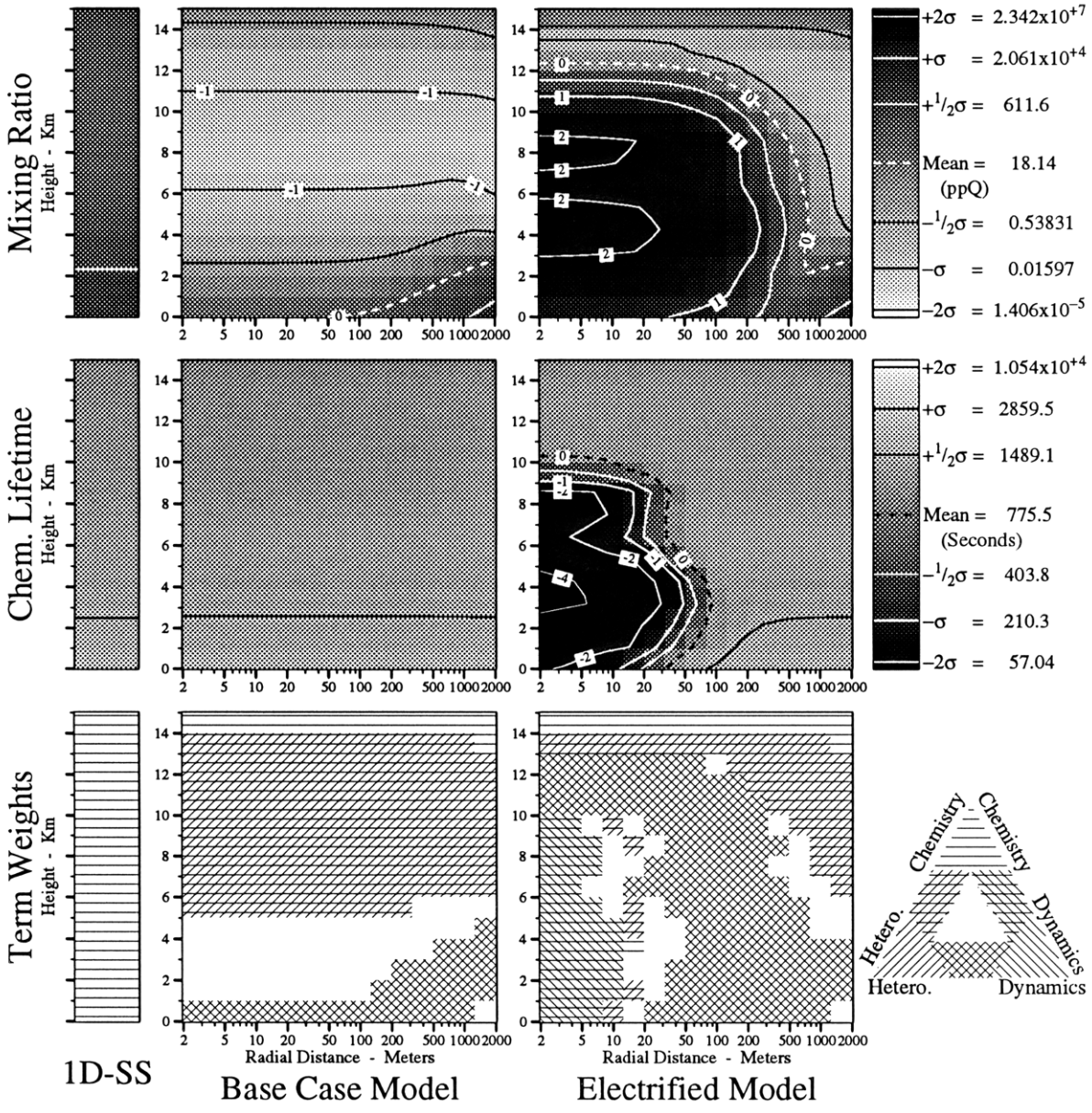

Figure 65. Mixing ratios (χ), lifetimes (τ_c), and term weights of HONO. See text for definitions of terms and other details.

Table 35. Summary of the chemistry of HONO in the **inner domain** of the three models. (**a,b**) The major terms in the continuity equations for HONO in the three model runs and (**c**) a summary of its mixing ratios χ and lifetimes τ in the three model runs. In these tables $\Re$ is the specific rate of production of HONO (molec·cm^{-3}·s^{-1}), τ is the total lifetime (sec) of HONO and τ_c is its lifetime due to chemical processes (sec). J_i, j_i, k_i, and l_i are photolytic, unimolecular, bimolecular and termolecular rate coefficients respectively for reaction number i as listed in Appendix B , page 184.

a.) The major source terms for HONO in the inner domain of the three model runs.

1-D Steady-State Model		2-D Base Case Model		2-D Electrified Model	
Log (ℜ)	Reaction Rate ℜ = k_{yz} [y] [z]	Log (ℜ)	Reaction Rate ℜ = k_{yz} [y] [z]	Log (ℜ)	Reaction Rate ℜ = k_{yz} [y] [z]
3.60	k_{86} [HO_2] [NO_2]	2.80	Advection/Diffusion	10.44	k_{372} [W_3NO^+] [H_2O]
2.79	k_{92} [OH] [NO]	2.37	k_{86} [HO_2] [NO_2]	9.61	k_{92} [OH] [NO]
1.61	Advection/Diffusion	2.07	k_{92} [OH] [NO]	8.49	k_{86} [HO_2] [NO_2]
0.49	k_{372} [W_3NO^+] [H_2O]	0.49	k_{372} [W_3NO^+] [H_2O]	5.56	$2{\cdot}k_{489}$ [N_2O_3] [H_2O]
0.02	$2{\cdot}k_{489}$ [N_2O_3] [H_2O]	-0.04	$2{\cdot}k_{489}$ [N_2O_3] [H_2O]	4.02	k_{580} [CH_3O] [NO_2]
-2.46	k_{580} [CH_3O] [NO_2]	-3.64	k_{580} [CH_3O] [NO_2]	-10.23	k_{87} [H_2] [NO_2]
...	3 More Reactions	...	3 More Reactions	...	3 More Reactions
3.664 = Log(Σℜ)		2.992 = Log(Σℜ)		10.501 = Log(Σℜ)	

Note: Read **W** as H_2O.

b.) The major sink terms for HONO in the inner domain of the three model runs.
The reaction rate ℜ implicitly contains [HONO].

1-D Steady-State Model		2-D Base Case Model		2-D Electrified Model	
Log (ℜ)	Reaction Rate ℜ = k_{yz} [y] [HONO]	Log (ℜ)	Reaction Rate ℜ = k_{yz} [y] [HONO]	Log (ℜ)	Reaction Rate ℜ = k_{yz} [y] [HONO]
3.66	J_3	2.99	Heterogeneous Loss	10.21	Heterogeneous Loss
1.43	k_{68} [OH]	0.96	J_3	10.00	Advection/Diffusion
1.02	Heterogeneous Loss	-1.77	k_{68} [OH]	9.74	k_{68} [OH]
-5.15	k_{82} [O]	-8.11	k_{82} [O]	8.05	J_3
-18.56	j_{85}	-21.02	j_{85}	3.19	k_{82} [O]
$-\infty$	Advection/Diffusion	$-\infty$	Advection/Diffusion	-15.59	j_{85}
$-\infty$	Deposition	$-\infty$	Deposition	$-\infty$	Deposition
3.664 = Log(Σℜ)		2.992 = Log(Σℜ)		10.501 = Log(Σℜ)	

c.) Summary of the lifetimes of HONO in the inner domain of the three model runs.

	Log(χ)	Log([HONO]) cm^{-3}	Log(Σℜ) cm^{-3}·s^{-1}	Log(τ) sec	Source Log(τ_c) sec	Sink Log(τ_c) sec
1-D Steady-State Model	−12.352	6.840	3.664	3.176	3.180	3.177
2-D Base Case Model	−15.027	4.164	2.992	1.173	1.612	3.206
2-D Electrified Model	−8.015	11.177	10.501	0.676	0.676	1.424

Note: τ = [HONO] / Σℜ or Log(τ) = Log([HONO]) − Log(Σℜ).

HONO$_2$

Differential Net Production ($P_{I.M.}$ - $P_{B.C.}$) = 0.000 (Gg Year^{-1})

$P_{B.C.}$ = −29.90 $P_{I.M.}$ = −29.90 (Gg Year^{-1})

$\overline{\tau}_c$ = 26.05 $\overline{\tau}_c$ = 35.74 $\overline{\tau}_c$ = 33.17 (Days)

$\overline{\chi}$ = 2.429x10^{+5} $\overline{\chi}$ = 4.971x10^{+4} $\overline{\chi}$ = 5.320x10^{+4} (ppQ)

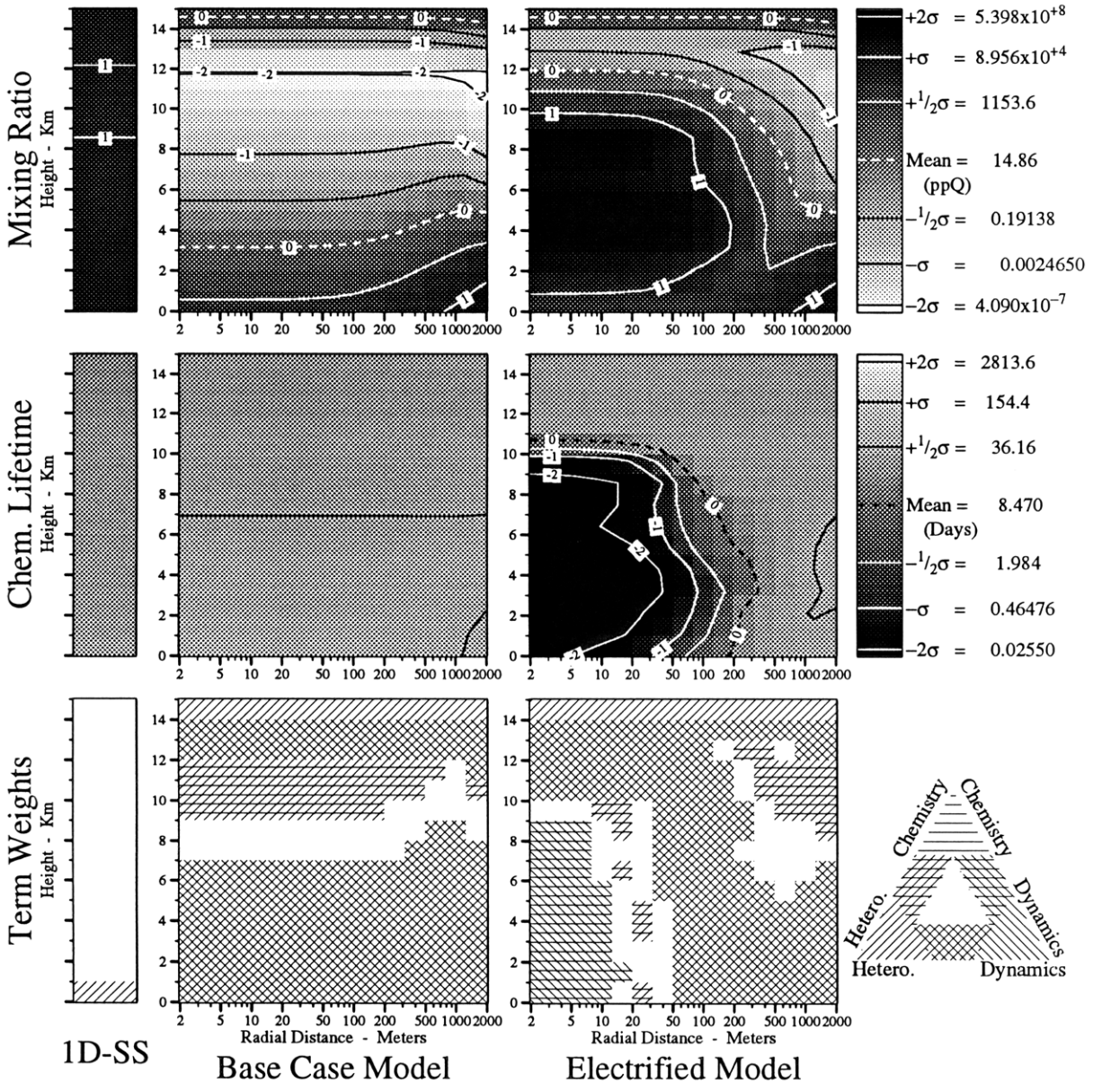

Figure 66. Mixing ratios (χ), lifetimes (τ_c), and term weights of HONO$_2$. See text for definitions of terms and other details.

Table 36. Summary of the chemistry of $HONO_2$ in the **inner domain** of the three models. (**a,b**) The major terms in the continuity equations for $HONO_2$ in the three model runs and (**c**) a summary of its mixing ratios χ and lifetimes τ in the three model runs. In these tables $\Re$ is the specific rate of production of $HONO_2$ (molec·cm^{-3}·s^{-1}), τ is the total lifetime (sec) of $HONO_2$ and τ_c is its lifetime due to chemical processes (sec). J_i, j_i, k_i, and l_i are photolytic, unimolecular, bimolecular and termolecular rate coefficients respectively for reaction number i as listed in Appendix B , page 184.

a.) The major source terms for $HONO_2$ in the inner domain of the three model runs.

1-D Steady-State Model		2-D Base Case Model		2-D Electrified Model	
Log ($\Re$)	Reaction Rate $\Re = k_{yz}$ [y] [z]	Log ($\Re$)	Reaction Rate $\Re = k_{yz}$ [y] [z]	Log ($\Re$)	Reaction Rate $\Re = k_{yz}$ [y] [z]
3.64	Advection/Diffusion	5.07	Advection/Diffusion	10.13	k_{94} [OH] [NO_2]
3.39	k_{94} [OH] [NO_2]	2.57	k_{94} [OH] [NO_2]	5.91	k_{62} [NO_3] [HO_2]
0.86	k_{673} [DMS] [NO_3]	0.74	k_{673} [DMS] [NO_3]	4.24	$2{\cdot}k_{64}$ [H_2O] [N_2O_5]
0.41	k_{62} [NO_3] [HO_2]	-0.81	$2{\cdot}k_{64}$ [H_2O] [N_2O_5]	3.73	k_{673} [DMS] [NO_3]
0.35	k_{88} [H_2O_2] [NO_2]	-1.21	k_{62} [NO_3] [HO_2]	3.41	k_{88} [H_2O_2] [NO_2]
0.25	$2{\cdot}k_{64}$ [H_2O] [N_2O_5]	-3.13	k_{63} [NO_3] [CH_2O]	3.19	k_{82} [HONO] [O]
...	8 More Reactions	...	8 More Reactions	...	8 More Reactions
3.838 = Log($\Sigma\Re$)		5.073 = Log($\Sigma\Re$)		10.126 = Log($\Sigma\Re$)	

b.) The major sink terms for $HONO_2$ in the inner domain of the three model runs.
The reaction rate $\Re$ implicitly contains [$HONO_2$].

1-D Steady-State Model		2-D Base Case Model		2-D Electrified Model	
Log ($\Re$)	Reaction Rate $\Re = k_{yz}$ [y] [$HONO_2$]	Log ($\Re$)	Reaction Rate $\Re = k_{yz}$ [y] [$HONO_2$]	Log ($\Re$)	Reaction Rate $\Re = k_{yz}$ [y] [$HONO_2$]
3.73	Heterogeneous Loss	5.07	Heterogeneous Loss	9.88	Heterogeneous Loss
2.95	J_4	-0.43	J_4	9.74	Advection/Diffusion
2.83	k_{91} [OH]	-1.01	k_{91} [OH]	8.21	k_{91} [OH]
-12.38	k_{178} [F]	-16.91	k_{178} [F]	4.28	J_4
$-\infty$	Advection/Diffusion	$-\infty$	Advection/Diffusion	-1.33	k_{178} [F]
$-\infty$	Deposition	$-\infty$	Deposition	$-\infty$	Deposition
3.838 = Log($\Sigma\Re$)		5.073 = Log($\Sigma\Re$)		10.126 = Log($\Sigma\Re$)	

c.) Summary of the lifetimes of $HONO_2$ in the inner domain of the three model runs.

	Log(χ)	Log([$HONO_2$]) cm^{-3}	Log($\Sigma\Re$) cm^{-3}·s^{-1}	Log(τ) sec	Source Log(τ_c) sec	Sink Log(τ_c) sec
1-D Steady-State Model	−9.617	9.575	3.838	5.736	6.180	6.377
2-D Base Case Model	−12.924	6.268	5.073	1.195	3.693	6.600
2-D Electrified Model	−8.335	10.857	10.126	0.731	0.731	2.647

Note: τ = [$HONO_2$] / $\Sigma\Re$ or Log(τ) = Log([$HONO_2$]) − Log($\Sigma\Re$).

HO_2NO_2

Differential Net Production ($P_{I.M.}$ - $P_{B.C.}$) = 0.52991 (Mg Year^{-1})

$P_{B.C.}$ = −106.3 $P_{I.M.}$ = −105.8 (Mg Year^{-1})

$\overline{\tau}_c$ = 8.260 $\overline{\tau}_c$ = 11.22 $\overline{\tau}_c$ = 11.16 (Hours)

$\overline{\chi}$ = 1.239x10^{+4} $\overline{\chi}$ = 264.9 $\overline{\chi}$ = 3757.6 (ppQ)

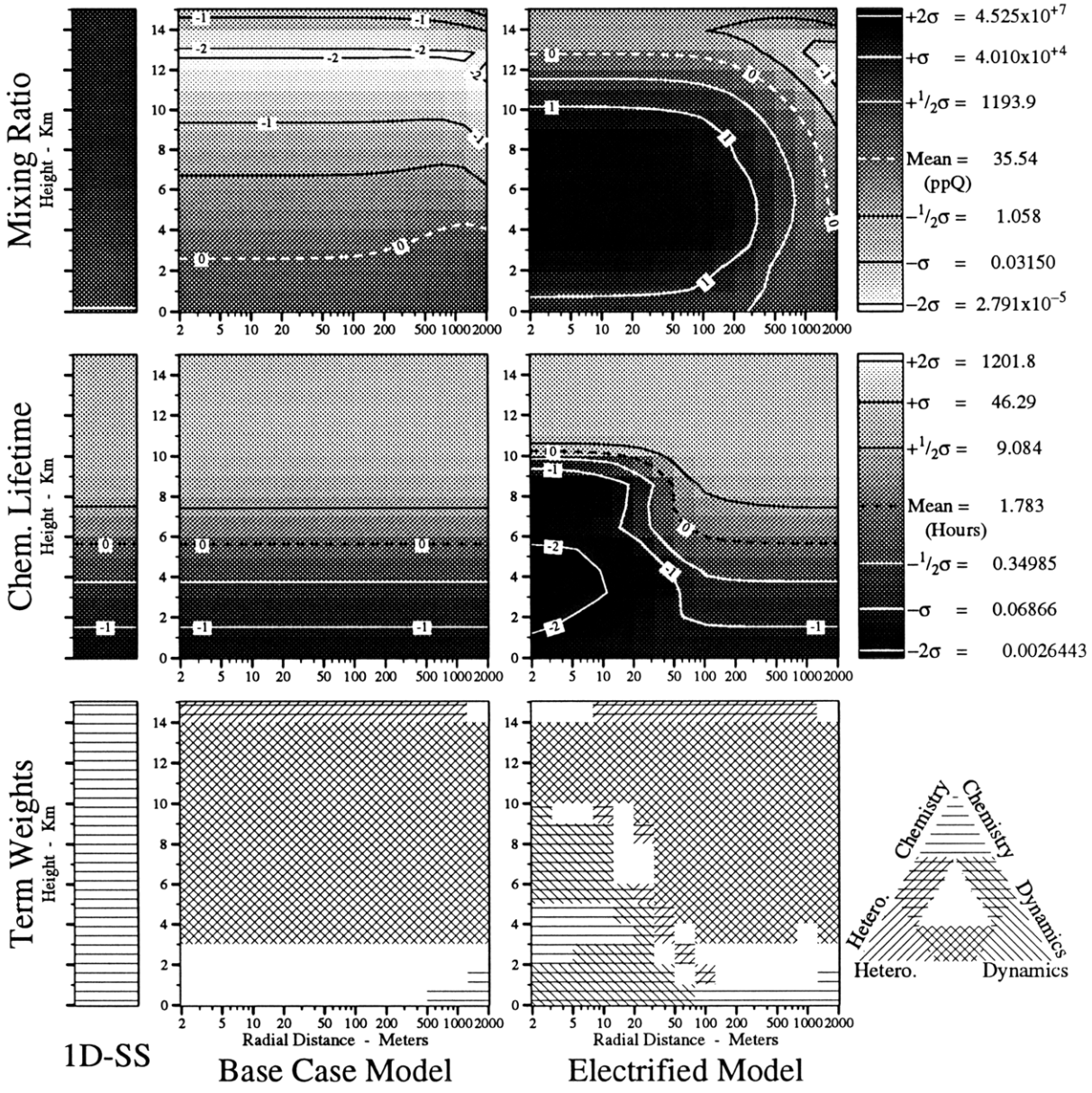

Figure 67. Mixing ratios (χ), lifetimes (τ_c), and term weights of HO_2NO_2. See text for definitions of terms and other details.

Table 37. Summary of the chemistry of HO_2NO_2 in the **inner domain** of the three models. (**a**,**b**) The major terms in the continuity equations for HO_2NO_2 in the three model runs and (**c**) a summary of its mixing ratios χ and lifetimes τ in the three model runs. In these tables $\Re$ is the specific rate of production of HO_2NO_2 (molec·cm^{-3}·s^{-1}), τ is the total lifetime (sec) of HO_2NO_2 and τ_c is its lifetime due to chemical processes (sec). J_i, j_i, k_i, and l_i are photolytic, unimolecular, bimolecular and termolecular rate coefficients respectively for reaction number i as listed in Appendix B , page 184.

a.) The major source terms for HO_2NO_2 in the inner domain of the three model runs.

1-D Steady-State Model		2-D Base Case Model		2-D Electrified Model	
Log ($\Re$)	Reaction Rate $\Re = k_{yz}$ [y] [z]	Log ($\Re$)	Reaction Rate $\Re = k_{yz}$ [y] [z]	Log ($\Re$)	Reaction Rate $\Re = k_{yz}$ [y] [z]
4.69	k_{95} [HO_2] [NO_2]	3.86	Advection/Diffusion	9.59	k_{95} [HO_2] [NO_2]
1.58	Advection/Diffusion	3.47	k_{95} [HO_2] [NO_2]	$-\infty$	Advection/Diffusion
$-\infty$	Flux	$-\infty$	Flux	$-\infty$	Flux
4.695 = Log($\Sigma\Re$)		4.011 = Log($\Sigma\Re$)		9.592 = Log($\Sigma\Re$)	

b.) The major sink terms for HO_2NO_2 in the inner domain of the three model runs.
The reaction rate $\Re$ implicitly contains [HO_2NO_2].

1-D Steady-State Model		2-D Base Case Model		2-D Electrified Model	
Log ($\Re$)	Reaction Rate $\Re = k_{yz}$ [y] [HO_2NO_2]	Log ($\Re$)	Reaction Rate $\Re = k_{yz}$ [y] [HO_2NO_2]	Log ($\Re$)	Reaction Rate $\Re = k_{yz}$ [y] [HO_2NO_2]
4.69	j_{96}	3.92	Heterogeneous Loss	9.31	Advection/Diffusion
2.77	J_{10}	3.27	j_{96}	9.03	k_{66} [OH]
2.54	k_{66} [OH]	0.21	J_{10}	8.88	Heterogeneous Loss
1.79	Heterogeneous Loss	-0.35	k_{66} [OH]	7.36	j_{96}
-4.71	k_{67} [O]	-7.10	k_{67} [O]	5.14	J_{10}
-6.66	k_{65} [H]	-9.57	k_{65} [H]	1.56	k_{65} [H]
$-\infty$	Deposition	$-\infty$	Deposition	1.54	k_{67} [O]
$-\infty$	Advection/Diffusion	$-\infty$	Advection/Diffusion	$-\infty$	Deposition
4.695 = Log($\Sigma\Re$)		4.011 = Log($\Sigma\Re$)		9.592 = Log($\Sigma\Re$)	

c.) Summary of the lifetimes of HO_2NO_2 in the inner domain of the three model runs.

	Log(χ)	Log([HO_2NO_2]) cm^{-3}	Log($\Sigma\Re$) cm^{-3}·s^{-1}	Log(τ) sec	Source Log(τ_c) sec	Sink Log(τ_c) sec
1-D Steady-State Model	−11.101	8.091	4.695	3.396	3.396	3.396
2-D Base Case Model	−13.520	5.672	4.011	1.661	2.202	2.402
2-D Electrified Model	−8.676	10.516	9.592	0.923	0.923	1.478

Note: τ = [HO_2NO_2] / $\Sigma\Re$ or Log(τ) = Log([HO_2NO_2]) − Log($\Sigma\Re$).

O_3

Differential Net Production ($P_{I.M.}$ - $P_{B.C.}$) = 20.02 (Gg Year^{-1})

$P_{B.C.}$ = −753.4 $P_{I.M.}$ = −733.4 (Gg Year^{-1})

$\overline{\tau}_c$ = 117.2 $\overline{\tau}_c$ = 117.3 $\overline{\tau}_c$ = 110.0 (Minutes)

$\overline{\chi}$ = 3.017x10^{+4} $\overline{\chi}$ = 8680.2 $\overline{\chi}$ = 9891.9 (ppT)

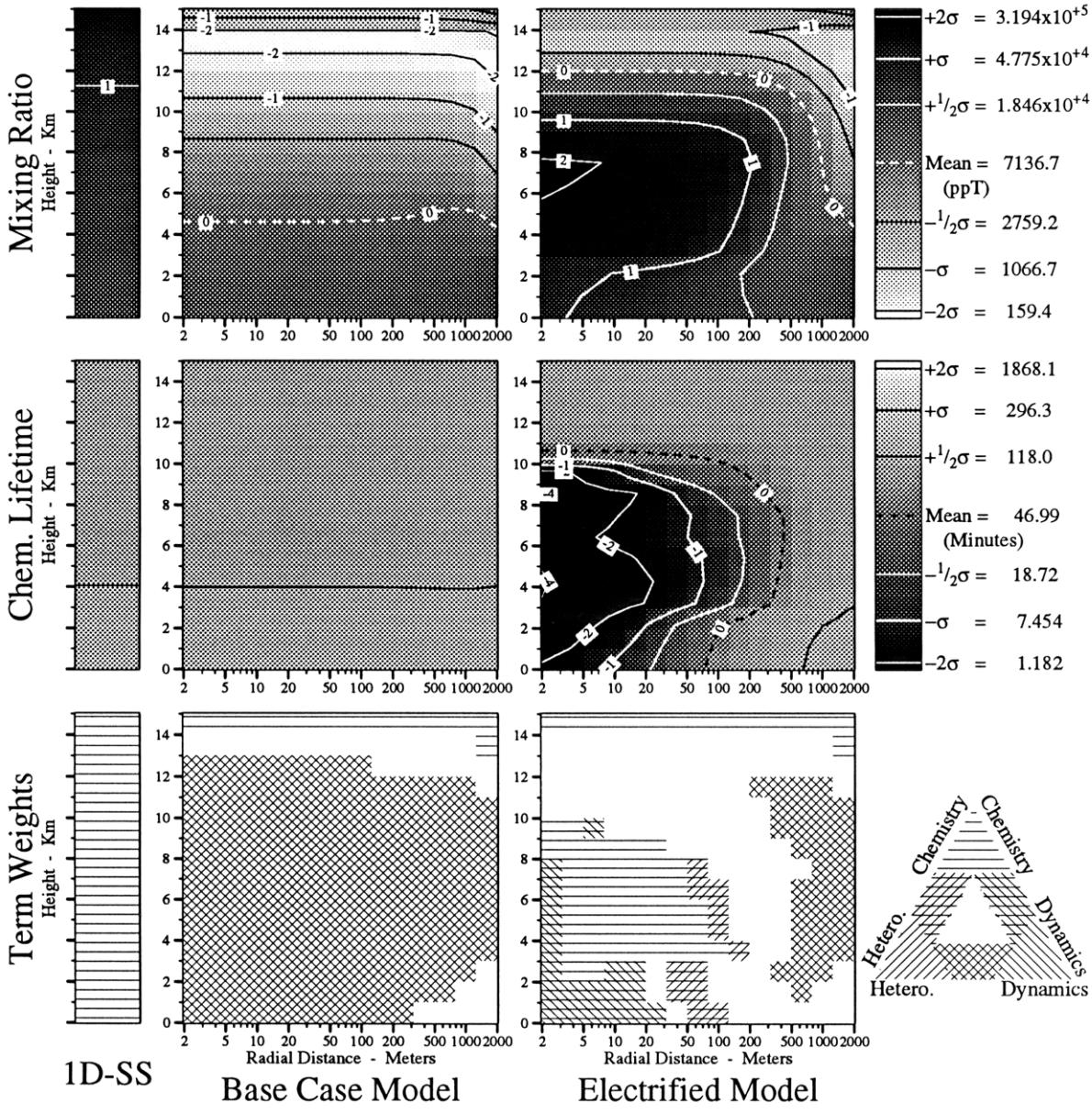

Figure 68. Mixing ratios (χ), lifetimes (τ_c), and term weights of O_3. See text for definitions of terms and other details.

Table 38. Summary of the chemistry of O_3 in the **inner domain** of the three models. (**a**,**b**) The major terms in the continuity equations for O_3 in the three model runs and (**c**) a summary of its mixing ratios χ and lifetimes τ in the three model runs. In these tables $\Re$ is the specific rate of production of O_3 (molec·cm^{-3}·s^{-1}), τ is the total lifetime (sec) of O_3 and τ_c is its lifetime due to chemical processes (sec). J_i, j_i, k_i, and l_i are photolytic, unimolecular, bimolecular and termolecular rate coefficients respectively for reaction number i as listed in Appendix B , page 184.

a.) The major source terms for O_3 in the inner domain of the three model runs.

1-D Steady-State Model		2-D Base Case Model		2-D Electrified Model	
Log (ℜ)	Reaction Rate ℜ = k_{yz} [y] [z]	Log (ℜ)	Reaction Rate ℜ = k_{yz} [y] [z]	Log (ℜ)	Reaction Rate ℜ = k_{yz} [y] [z]
7.72	k_{90} [O] [O_2]	8.48	Advection/Diffusion	10.94	k_{90} [O] [O_2]
4.27	Advection/Diffusion	7.24	k_{90} [O] [O_2]	4.46	k_{283} [O^-] [O_2]
0.37	k_{796} [$CC\ell_3COO_2$] [HO_2]	-2.18	k_{796} [$CC\ell_3COO_2$] [HO_2]	3.22	k_{796} [$CC\ell_3COO_2$] [HO_2]
-6.35	k_{283} [O^-] [O_2]	-7.10	k_{283} [O^-] [O_2]	2.20	J_{128} [O_3^-]
-13.27	k_{275} [O_2^-] [O]	-13.96	k_{275} [O_2^-] [O]	1.34	k_{275} [O_2^-] [O]
-14.63	k_{214} [O_4^+] [O]	-15.43	k_{214} [O_4^+] [O]	0.27	k_{214} [O_4^+] [O]
...	4 More Reactions	...	4 More Reactions	...	4 More Reactions
7.717 = Log(Σℜ)		8.501 = Log(Σℜ)		10.940 = Log(Σℜ)	

b.) The major sink terms for O_3 in the inner domain of the three model runs.
The reaction rate ℜ implicitly contains [O_3].

1-D Steady-State Model		2-D Base Case Model		2-D Electrified Model	
Log (ℜ)	Reaction Rate ℜ = k_{yz} [y] [O_3]	Log (ℜ)	Reaction Rate ℜ = k_{yz} [y] [O_3]	Log (ℜ)	Reaction Rate ℜ = k_{yz} [y] [O_3]
7.68	J_1	8.48	Heterogeneous Loss	10.76	Advection/Diffusion
6.48	J_2	7.20	J_1	10.09	k_{258} [CO_4^-]
5.76	k_{25} [NO]	5.98	J_2	9.73	J_{124}
5.05	Heterogeneous Loss	5.47	k_{25} [NO]	9.67	k_{302} [NO_2^-]
4.87	k_{54} [HO_2]	3.36	k_{50} {M}	9.64	Heterogeneous Loss
4.02	k_{52} [OH]	3.36	k_{54} [HO_2]	9.39	k_{25} [NO]
...	30 More Reactions	...	30 More Reactions	...	30 More Reactions
7.717 = Log(Σℜ)		8.501 = Log(Σℜ)		10.940 = Log(Σℜ)	

Note: The definitions of the reactive families $\{X\}$ are at the end of Appendix B.

c.) Summary of the lifetimes of O_3 in the inner domain of the three model runs.

	Log(χ)	Log([O_3]) cm^{-3}	Log(Σℜ) cm^{-3}·s^{-1}	Log(τ) sec	Source Log(τ_c) sec	Sink Log(τ_c) sec
1-D Steady-State Model	−7.628	11.564	7.717	3.847	3.847	3.848
2-D Base Case Model	−8.105	11.087	8.501	2.586	3.851	3.857
2-D Electrified Model	−6.964	12.228	10.940	1.287	1.287	1.818

Note: τ = [O_3] / Σℜ or Log(τ) = Log([O_3]) − Log(Σℜ).

HO_2

Differential Net Production ($P_{I.M.}$ - $P_{B.C.}$) = 0.67444 (Mg Year^{-1})

	$P_{B.C.}$ = −280.0	$P_{I.M.}$ = −279.3 (Mg Year^{-1})
$\overline{\tau}_c$ = 281.1	$\overline{\tau}_c$ = 5359.7	$\overline{\tau}_c$ = 198.4 (Seconds)
$\overline{\chi}$ = 6974.6	$\overline{\chi}$ = 1870.7	$\overline{\chi}$ = 2448.3 (ppQ)

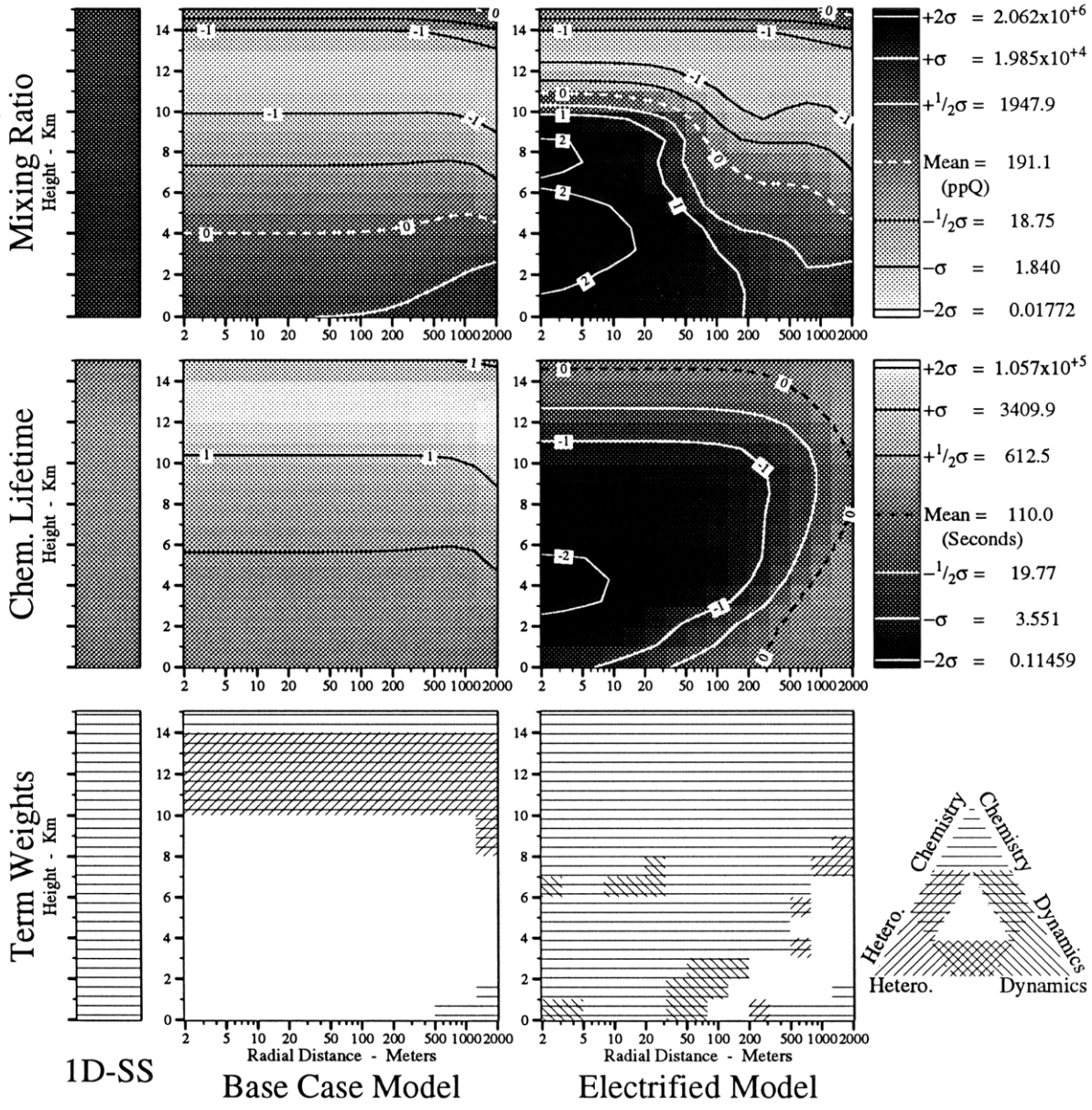

Figure 69. Mixing ratios (χ), lifetimes (τ_c), and term weights of HO_2. See text for definitions of terms and other details.

Table 39. Summary of the chemistry of HO_2 in the **inner domain** of the three models. **(a,b)** The major terms in the continuity equations for HO_2 in the three model runs and **(c)** a summary of its mixing ratios χ and lifetimes τ in the three model runs. In these tables $\Re$ is the specific rate of production of HO_2 (molec·cm^{-3}·s^{-1}), τ is the total lifetime (sec) of HO_2 and τ_c is its lifetime due to chemical processes (sec). J_i, j_i, k_i, and l_i are photolytic, unimolecular, bimolecular and termolecular rate coefficients respectively for reaction number i as listed in Appendix B , page 184.

a.) The major source terms for HO_2 in the inner domain of the three model runs.

1-D Steady-State Model		2-D Base Case Model		2-D Electrified Model	
Log (ℜ)	Reaction Rate ℜ = k_{yz} [y] [z]	Log (ℜ)	Reaction Rate ℜ = k_{yz} [y] [z]	Log (ℜ)	Reaction Rate ℜ = k_{yz} [y] [z]
5.47	k_{93} [H] [O_2]	4.85	Advection/Diffusion	10.61	k_{93} [H] [O_2]
4.84	k_{582} [CH_3O] [O_2]	4.64	k_{93} [H] [O_2]	8.45	k_{52} [OH] [O_3]
4.70	k_{640} [CHO] [O_2]	3.71	k_{582} [CH_3O] [O_2]	8.18	k_{582} [CH_3O] [O_2]
4.69	j_{96} [HO_2NO_2]	3.27	j_{96} [HO_2NO_2]	8.16	k_{56} [OH] [H_2O_2]
4.02	k_{52} [OH] [O_3]	3.16	k_{674} [CH_3SOHCH_3] [O_2]	7.96	k_{70} [HNO] [O_2]
4.01	k_{56} [OH] [H_2O_2]	3.12	k_{640} [CHO] [O_2]	7.90	k_{640} [CHO] [O_2]
...	31 More Reactions	...	31 More Reactions	...	31 More Reactions
5.692 = Log(Σℜ)		5.098 = Log(Σℜ)		10.620 = Log(Σℜ)	

b.) The major sink terms for HO_2 in the inner domain of the three model runs.
The reaction rate ℜ implicitly contains [HO_2].

1-D Steady-State Model		2-D Base Case Model		2-D Electrified Model	
Log (ℜ)	Reaction Rate ℜ = k_{yz} [y] [HO_2]	Log (ℜ)	Reaction Rate ℜ = k_{yz} [y] [HO_2]	Log (ℜ)	Reaction Rate ℜ = k_{yz} [y] [HO_2]
5.27	k_{55} [NO]	5.02	Heterogeneous Loss	10.26	k_{55} [NO]
4.87	k_{54} [O_3]	4.12	k_{55} [NO]	10.20	k_{31} [OH]
4.86	2·k_{59} [HO_2]	3.47	k_{95} [NO_2]	9.59	k_{95} [NO_2]
4.75	k_{589} [CH_3O_2]	3.36	k_{54} [O_3]	9.23	2·k_{59} [HO_2]
4.69	k_{95} [NO_2]	2.60	2·k_{59} [HO_2]	8.94	2·l_{60} [HO_2]{M}
4.58	2·l_{60} [HO_2]{M}	2.54	k_{589} [CH_3O_2]	8.68	Advection/Diffusion
...	31 More Reactions	...	31 More Reactions	...	31 More Reactions
5.692 = Log(Σℜ)		5.098 = Log(Σℜ)		10.620 = Log(Σℜ)	

Note: The definitions of the reactive families $\{X\}$ are at the end of Appendix B.

c.) Summary of the lifetimes of HO_2 in the inner domain of the three model runs.

	Log(χ)	Log([HO_2]) cm^{-3}	Log(Σℜ) cm^{-3}·s^{-1}	Log(τ) sec	Source Log(τ_c) sec	Sink Log(τ_c) sec
1-D Steady-State Model	−11.114	8.078	5.692	2.386	2.386	2.386
2-D Base Case Model	−12.428	6.764	5.098	1.665	2.025	2.470
2-D Electrified Model	−9.261	9.931	10.620	−0.689	−0.689	−0.681

Note: τ = [HO_2] / Σℜ or Log(τ) = Log([HO_2]) − Log(Σℜ).

H_2O_2

Differential Net Production ($P_{I.M.}$ - $P_{B.C.}$) = 0.000 (Gg Year^{-1})

$P_{B.C.}$ = −18.33 $P_{I.M.}$ = −18.33 (Gg Year^{-1})

$\overline{\tau}_c$ = 58.70 $\overline{\tau}_c$ = 69.54 $\overline{\tau}_c$ = 65.98 (Hours)

$\overline{\chi}$ = 4.178x10^{-10} $\overline{\chi}$ = 5.183x10^{-11} $\overline{\chi}$ = 5.222x10^{-11} (Mixing Ratio)

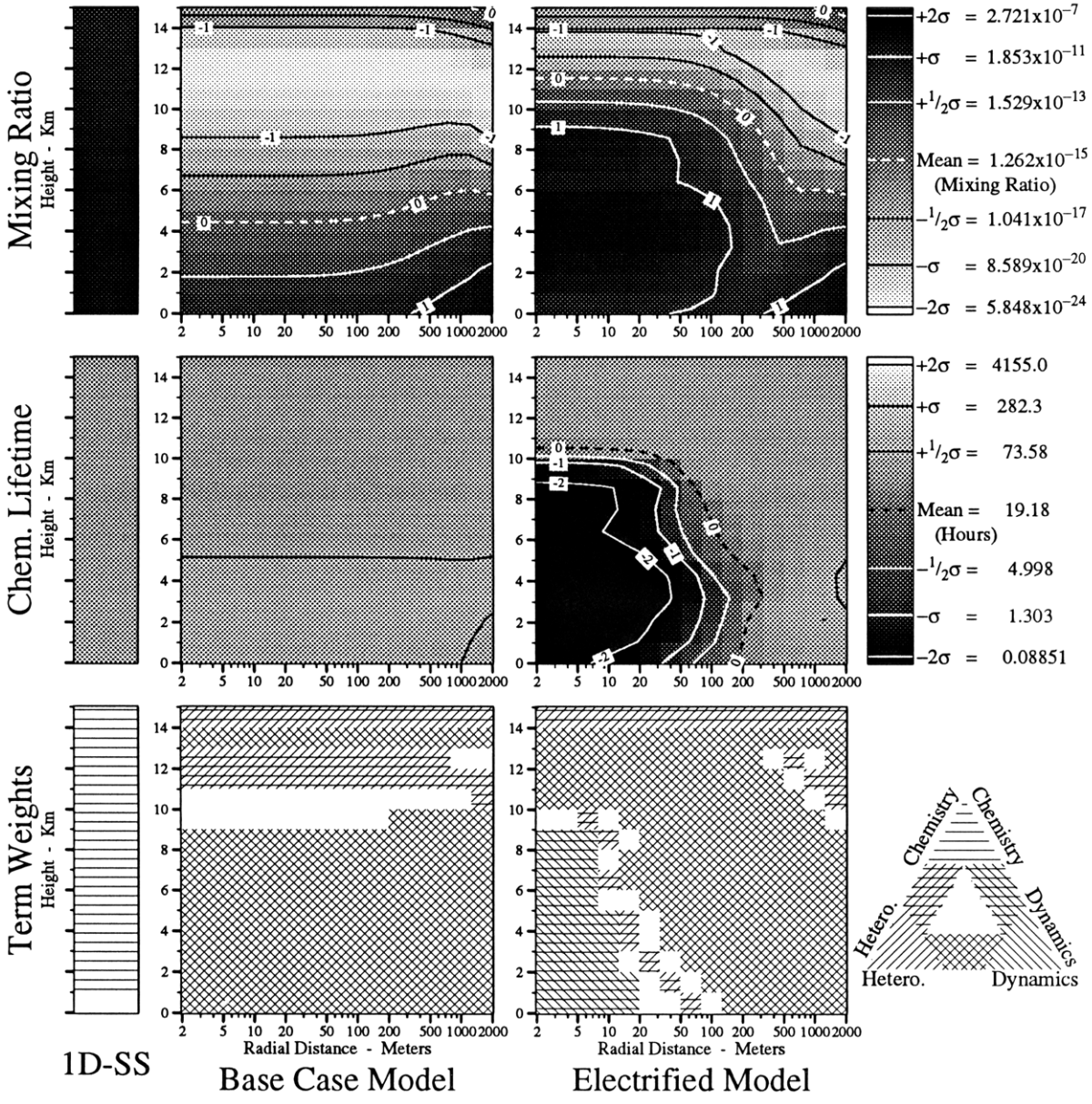

Figure 70. Mixing ratios (χ), lifetimes (τ_c), and term weights of H_2O_2. See text for definitions of terms and other details.

Table 40. Summary of the chemistry of H_2O_2 in the **inner domain** of the three models. (**a,b**) The major terms in the continuity equations for H_2O_2 in the three model runs and (**c**) a summary of its mixing ratios χ and lifetimes τ in the three model runs. In these tables $\Re$ is the specific rate of production of H_2O_2 (molec·cm^{-3}·s^{-1}), τ is the total lifetime (sec) of H_2O_2 and τ_c is its lifetime due to chemical processes (sec). J_i, j_i, k_i, and l_i are photolytic, unimolecular, bimolecular and termolecular rate coefficients respectively for reaction number i as listed in Appendix B , page 184.

a.) The major source terms for H_2O_2 in the inner domain of the three model runs.

1-D Steady-State Model		2-D Base Case Model		2-D Electrified Model	
Log ($\Re$)	Reaction Rate $\Re = k_{yz}$ [y] [z]	Log ($\Re$)	Reaction Rate $\Re = k_{yz}$ [y] [z]	Log ($\Re$)	Reaction Rate $\Re = k_{yz}$ [y] [z]
4.55	k_{59} [HO_2] [HO_2]	5.05	Advection/Diffusion	8.92	k_{59} [HO_2] [HO_2]
4.28	l_{60} [HO_2] [HO_2]{M}	2.29	k_{59} [HO_2] [HO_2]	8.64	l_{60} [HO_2] [HO_2]{M}
0.30	k_{58} [OH] [OH]	2.08	l_{60} [HO_2] [HO_2]{M}	8.36	k_{58} [OH] [OH]
-2.99	k_{578} [CH_3O] [HO_2]	-1.18	k_{58} [OH] [OH]	2.86	k_{578} [CH_3O] [HO_2]
-3.24	k_{631} [CH_2O] [HO_2]	-5.16	k_{578} [CH_3O] [HO_2]	1.56	k_{65} [H] [HO_2NO_2]
-5.78	k_{557} [CH_4] [HO_2]	-5.42	k_{631} [CH_2O] [HO_2]	-1.62	k_{631} [CH_2O] [HO_2]
...	5 More Reactions	...	5 More Reactions	...	5 More Reactions
4.741 = Log($\Sigma\Re$)		5.053 = Log($\Sigma\Re$)		9.177 = Log($\Sigma\Re$)	

Note: The definitions of the reactive families $\{X\}$ are at the end of Appendix B.

b.) The major sink terms for H_2O_2 in the inner domain of the three model runs.
The reaction rate $\Re$ implicitly contains [H_2O_2].

1-D Steady-State Model		2-D Base Case Model		2-D Electrified Model	
Log ($\Re$)	Reaction Rate $\Re = k_{yz}$ [y] [H_2O_2]	Log ($\Re$)	Reaction Rate $\Re = k_{yz}$ [y] [H_2O_2]	Log ($\Re$)	Reaction Rate $\Re = k_{yz}$ [y] [H_2O_2]
4.42	J_5	5.05	Heterogeneous Loss	8.89	Heterogeneous Loss
4.02	Heterogeneous Loss	0.69	J_5	8.76	Advection/Diffusion
4.01	k_{56} [OH]	-0.10	k_{56} [OH]	8.16	k_{56} [OH]
3.91	Advection/Diffusion	-3.14	k_{88} [NO_2]	4.42	J_5
0.35	k_{88} [NO_2]	-6.01	k_{590} [CH_3O_2]	3.41	k_{88} [NO_2]
-1.83	k_{590} [CH_3O_2]	-6.05	k_{503} [O]	3.13	k_{827} [Cℓ]
...	11 More Reactions	...	11 More Reactions	...	11 More Reactions
4.741 = Log($\Sigma\Re$)		5.053 = Log($\Sigma\Re$)		9.177 = Log($\Sigma\Re$)	

c.) Summary of the lifetimes of H_2O_2 in the inner domain of the three model runs.

	Log(χ)	Log([H_2O_2]) cm^{-3}	Log($\Sigma\Re$) cm^{-3}·s^{-1}	Log(τ) sec	Source Log(τ_c) sec	Sink Log(τ_c) sec
1-D Steady-State Model	−9.298	9.894	4.741	5.153	5.153	5.332
2-D Base Case Model	−12.944	6.248	5.053	1.195	3.746	5.491
2-D Electrified Model	−9.307	9.885	9.177	0.708	0.708	1.730

Note: τ = [H_2O_2] / $\Sigma\Re$ or Log(τ) = Log([H_2O_2]) − Log($\Sigma\Re$).

DMS

Differential Net Production ($P_{I.M.}$ - $P_{B.C.}$) = −85.90 (Mg Year^{-1})

$P_{B.C.}$ = −32.17 $P_{I.M.}$ = −118.1 (Mg Year^{-1})

$\overline{\tau}_c$ =	0.90853	$\overline{\tau}_c$ = 924.5	$\overline{\tau}_c$ = 181.1	(Days)
$\overline{\chi}$ =	14.51	$\overline{\chi}$ = 53.47	$\overline{\chi}$ = 51.04	(ppT)

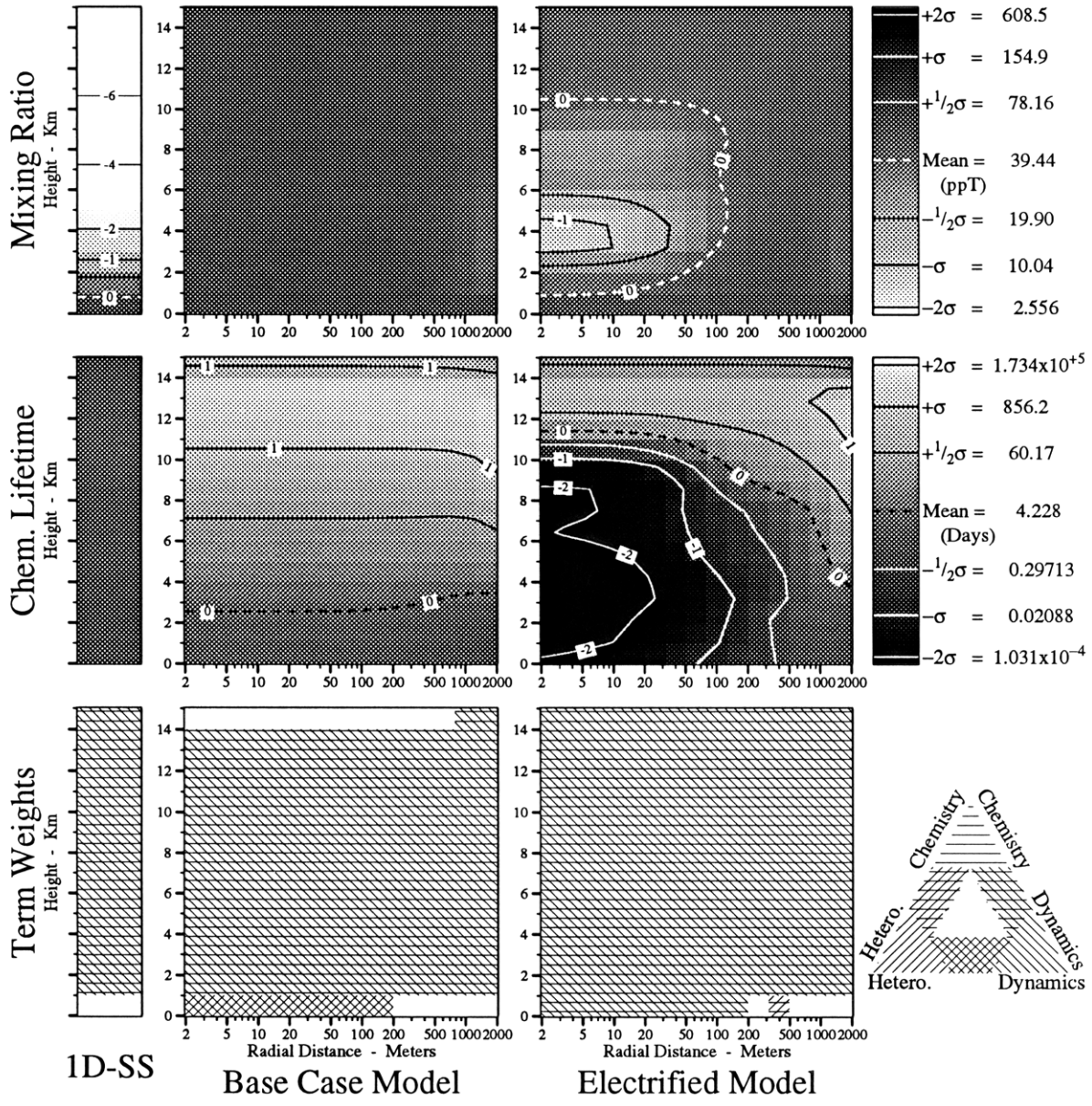

Figure 71. Mixing ratios (χ), lifetimes (τ_c), and term weights of DMS. See text for definitions of terms and other details.

Table 41. Summary of the chemistry of DMS in the **inner domain** of the three models. (**a**,**b**) The major terms in the continuity equations for DMS in the three model runs and (**c**) a summary of its mixing ratios χ and lifetimes τ in the three model runs. In these tables $\Re$ is the specific rate of production of DMS (molec·cm^{-3}·s^{-1}), τ is the total lifetime (sec) of DMS and τ_c is its lifetime due to chemical processes (sec). J_i, j_i, k_i, and l_i are photolytic, unimolecular, bimolecular and termolecular rate coefficients respectively for reaction number i as listed in Appendix B , page 184.

a.) The major source terms for DMS in the inner domain of the three model runs.

1-D Steady-State Model		2-D Base Case Model		2-D Electrified Model	
Log ($\Re$)	Reaction Rate $\Re = k_{yz}$ [y] [z]	Log ($\Re$)	Reaction Rate $\Re = k_{yz}$ [y] [z]	Log ($\Re$)	Reaction Rate $\Re = k_{yz}$ [y] [z]
3.37	Advection/Diffusion	3.28	Advection/Diffusion	7.22	Advection/Diffusion
-28.91	j_{675} [CH_3SOHCH_3]	-29.07	j_{675} [CH_3SOHCH_3]	-25.27	j_{675} [CH_3SOHCH_3]
$-\infty$	Flux	$-\infty$	Flux	$-\infty$	Flux
3.368 = Log($\Sigma\Re$)		3.281 = Log($\Sigma\Re$)		7.220 = Log($\Sigma\Re$)	

b.) The major sink terms for DMS in the inner domain of the three model runs.
The reaction rate $\Re$ implicitly contains [DMS].

1-D Steady-State Model		2-D Base Case Model		2-D Electrified Model	
Log ($\Re$)	Reaction Rate $\Re = k_{yz}$ [y] [DMS]	Log ($\Re$)	Reaction Rate $\Re = k_{yz}$ [y] [DMS]	Log ($\Re$)	Reaction Rate $\Re = k_{yz}$ [y] [DMS]
3.24	k_{668} [OH]	3.16	k_{668} [OH]	7.11	k_{668} [OH]
2.75	k_{669} [OH]	2.65	k_{669} [OH]	6.58	k_{669} [OH]
0.86	k_{673} [NO_3]	1.36	k_{670} [O]	4.55	k_{670} [O]
0.86	k_{670} [O]	0.74	k_{673} [NO_3]	3.73	k_{673} [NO_3]
-5.59	k_{672} [H]	-5.71	k_{672} [H]	-0.44	k_{672} [H]
-12.64	k_{671} [CH_3]	-12.81	k_{671} [CH_3]	-9.03	k_{671} [CH_3]
$-\infty$	Deposition	$-\infty$	Deposition	$-\infty$	Deposition
$-\infty$	Heterogeneous Loss	$-\infty$	Heterogeneous Loss	$-\infty$	Heterogeneous Loss
$-\infty$	Advection/Diffusion	$-\infty$	Advection/Diffusion	$-\infty$	Advection/Diffusion
3.368 = Log($\Sigma\Re$)		3.281 = Log($\Sigma\Re$)		7.220 = Log($\Sigma\Re$)	

c.) Summary of the lifetimes of DMS in the inner domain of the three model runs.

	Log(χ)	Log([DMS]) cm^{-3}	Log($\Sigma\Re$) $cm^{-3}\cdot s^{-1}$	Log(τ) sec	Source Log(τ_c) sec	Sink Log(τ_c) sec
1-D Steady-State Model	−11.030	8.162	3.368	4.794	37.071	4.794
2-D Base Case Model	−10.209	8.983	3.281	5.702	38.054	5.702
2-D Electrified Model	−10.532	8.660	7.220	1.440	33.928	1.440

Note: τ = [DMS] / $\Sigma\Re$ or Log(τ) = Log([DMS]) − Log($\Sigma\Re$).

OCS

Differential Net Production ($P_{I.M.}$ - $P_{B.C.}$) = −217.9 (Kg Year^{-1})

$P_{B.C.}$ = −492.8 $P_{I.M.}$ = −710.7 (Kg Year^{-1})

$\overline{\tau}_c$ = 31.21	$\overline{\tau}_c$ = 1.004x10^{+5}	$\overline{\tau}_c$ = 1.588x10^{+4}	(Years)
$\overline{\chi}$ = 917.3	$\overline{\chi}$ = 921.9	$\overline{\chi}$ = 921.9	(ppT)

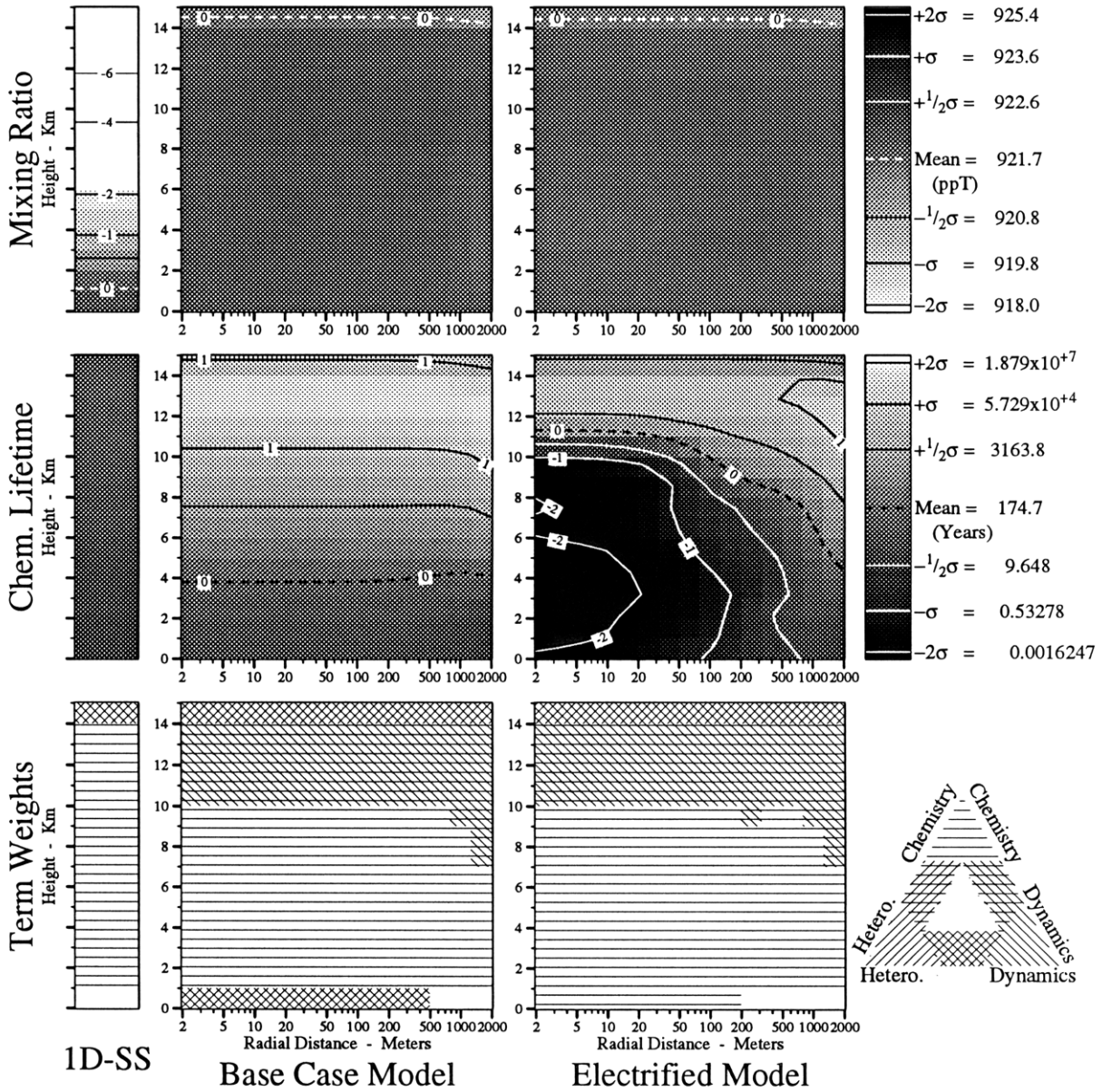

Figure 72. Mixing ratios (χ), lifetimes (τ_c), and term weights of OCS. See text for definitions of terms and other details.

Table 42. Summary of the chemistry of OCS in the **inner domain** of the three models. (**a**,**b**) The major terms in the continuity equations for OCS in the three model runs and (**c**) a summary of its mixing ratios χ and lifetimes τ in the three model runs. In these tables $\Re$ is the specific rate of production of OCS (molec·cm^{-3}·s^{-1}), τ is the total lifetime (sec) of OCS and τ_c is its lifetime due to chemical processes (sec). J_i, j_i, k_i, and l_i are photolytic, unimolecular, bimolecular and termolecular rate coefficients respectively for reaction number i as listed in Appendix B , page 184.

a.) The major source terms for OCS in the inner domain of the three model runs.

1-D Steady-State Model		2-D Base Case Model		2-D Electrified Model	
Log ($\Re$)	Reaction Rate $\Re = k_{yz}$ [y] [z]	Log ($\Re$)	Reaction Rate $\Re = k_{yz}$ [y] [z]	Log ($\Re$)	Reaction Rate $\Re = k_{yz}$ [y] [z]
1.02	Advection/Diffusion	0.33	Advection/Diffusion	4.77	Advection/Diffusion
0.83	k_{731} [CS_2OH] [O_2]	-0.03	k_{724} [CS_2] [OH]	4.32	k_{731} [CS_2OH] [O_2]
0.81	k_{724} [CS_2] [OH]	-0.04	k_{731} [CS_2OH] [O_2]	4.29	k_{724} [CS_2] [OH]
-1.31	k_{726} [CS] [O_2]	-1.80	k_{726} [CS] [O_2]	1.70	k_{726} [CS] [O_2]
-2.29	k_{721} [CS_2] [O]	-2.76	k_{721} [CS_2] [O]	0.79	k_{721} [CS_2] [O]
-4.88	k_{727} [CS] [O_3]	-5.86	k_{727} [CS] [O_3]	-1.01	k_{727} [CS] [O_3]
...	3 More Reactions	...	3 More Reactions	...	3 More Reactions
1.374 = Log($\Sigma\Re$)		0.600 = Log($\Sigma\Re$)		4.996 = Log($\Sigma\Re$)	

b.) The major sink terms for OCS in the inner domain of the three model runs.
The reaction rate $\Re$ implicitly contains [OCS].

1-D Steady-State Model		2-D Base Case Model		2-D Electrified Model	
Log ($\Re$)	Reaction Rate $\Re = k_{yz}$ [y] [OCS]	Log ($\Re$)	Reaction Rate $\Re = k_{yz}$ [y] [OCS]	Log ($\Re$)	Reaction Rate $\Re = k_{yz}$ [y] [OCS]
1.37	k_{715} [OH]	0.59	k_{715} [OH]	4.99	k_{715} [OH]
-0.52	k_{718} [NO_3]	-1.13	k_{718} [NO_3]	2.43	k_{718} [NO_3]
-1.09	k_{716} [O]	-1.50	k_{716} [O]	2.13	k_{716} [O]
-5.04	k_{714} [H]	-5.81	k_{714} [H]	0.09	k_{714} [H]
-5.93	k_{717} [O]	-6.25	k_{717} [O]	-2.77	k_{717} [O]
$-\infty$	Heterogeneous Loss	$-\infty$	Heterogeneous Loss	$-\infty$	Heterogeneous Loss
...	2 More Reactions	...	2 More Reactions	...	2 More Reactions
1.374 = Log($\Sigma\Re$)		0.600 = Log($\Sigma\Re$)		4.996 = Log($\Sigma\Re$)	

c.) Summary of the lifetimes of OCS in the inner domain of the three model runs.

	Log(χ)	Log([OCS]) cm^{-3}	Log($\Sigma\Re$) $cm^{-3}\cdot s^{-1}$	Log(τ) sec	Source Log(τ_c) sec	Sink Log(τ_c) sec
1-D Steady-State Model	−9.037	10.155	1.374	8.781	9.034	8.781
2-D Base Case Model	−9.035	10.157	0.600	9.557	9.887	9.557
2-D Electrified Model	−9.035	10.157	4.996	5.160	5.551	5.160

Note: τ = [OCS] / $\Sigma\Re$ or Log(τ) = Log([OCS]) − Log($\Sigma\Re$).

CO

Differential Net Production ($P_{I.M.} - P_{B.C.}$) = −1.813 (Gg Year^{-1})

$P_{B.C.}$ = −1.584 $P_{I.M.}$ = −3.398 (Gg Year^{-1})

$\overline{\tau}_c$ = 0.23523 $\overline{\tau}_c$ = 602.7 $\overline{\tau}_c$ = 84.40 (Years)

$\overline{\chi}$ = 100.7 $\overline{\chi}$ = 122.6 $\overline{\chi}$ = 122.5 (ppB)

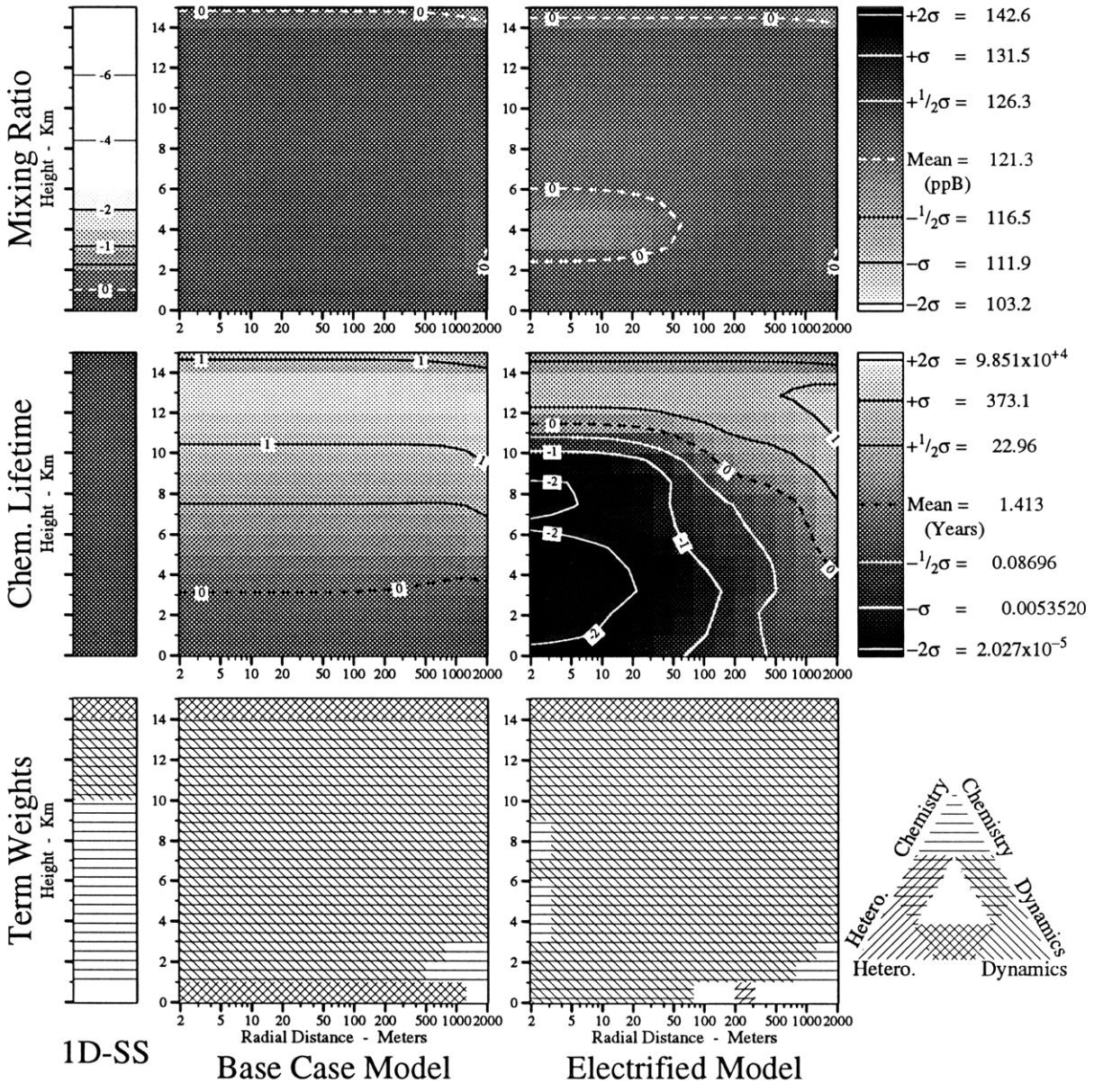

Figure 73. Mixing ratios (χ), lifetimes (τ_c), and term weights of CO. See text for definitions of terms and other details.

Table 43. Summary of the chemistry of CO in the **inner domain** of the three models. (**a,b**) The major terms in the continuity equations for CO in the three model runs and (**c**) a summary of its mixing ratios χ and lifetimes τ in the three model runs. In these tables $\Re$ is the specific rate of production of CO (molec·cm^{-3}·s^{-1}), τ is the total lifetime (sec) of CO and τ_c is its lifetime due to chemical processes (sec). J_i, j_i, k_i, and l_i are photolytic, unimolecular, bimolecular and termolecular rate coefficients respectively for reaction number i as listed in Appendix B , page 184.

a.) The major source terms for CO in the inner domain of the three model runs.

1-D Steady-State Model		2-D Base Case Model		2-D Electrified Model	
Log ($\Re$)	Reaction Rate $\Re = k_{yz}$ [y] [z]	Log ($\Re$)	Reaction Rate $\Re = k_{yz}$ [y] [z]	Log ($\Re$)	Reaction Rate $\Re = k_{yz}$ [y] [z]
5.15	Advection/Diffusion	4.56	Advection/Diffusion	9.01	Advection/Diffusion
4.70	k_{640} [CHO] [O_2]	3.26	J_{12} [CH_2O]	7.90	k_{640} [CHO] [O_2]
4.70	J_{12} [CH_2O]	3.12	k_{640} [CHO] [O_2]	7.38	k_{228} [O^+] [CO_2]
1.98	k_{693} [CH_3SCHO] [OH]	0.16	k_{693} [CH_3SCHO] [OH]	4.90	k_{693} [CH_3SCHO] [OH]
-0.52	k_{718} [OCS] [NO_3]	-1.13	k_{718} [OCS] [NO_3]	4.60	j_{541} [NCO]
-1.09	k_{716} [OCS] [O]	-1.50	k_{716} [OCS] [O]	4.50	J_{12} [CH_2O]
...	47 More Reactions	...	47 More Reactions	...	47 More Reactions
5.385 = Log($\Sigma\Re$)		4.598 = Log($\Sigma\Re$)		9.048 = Log($\Sigma\Re$)	

b.) The major sink terms for CO in the inner domain of the three model runs.
The reaction rate $\Re$ implicitly contains [CO].

1-D Steady-State Model		2-D Base Case Model		2-D Electrified Model	
Log ($\Re$)	Reaction Rate $\Re = k_{yz}$ [y] [CO]	Log ($\Re$)	Reaction Rate $\Re = k_{yz}$ [y] [CO]	Log ($\Re$)	Reaction Rate $\Re = k_{yz}$ [y] [CO]
5.38	k_{659} [OH]	4.60	k_{659} [OH]	9.05	k_{659} [OH]
-1.38	k_{110} [O]	-1.73	k_{110} [O]	4.00	k_{324} [N_2^+]
-3.68	k_{834} [CℓO]	-4.11	k_{834} [CℓO]	3.58	k_{332} [N^+]
-4.28	k_{109} [H]	-5.02	k_{109} [H]	1.90	k_{110} [O]
-6.06	k_{324} [N_2^+]	-5.95	k_{324} [N_2^+]	1.30	k_{834} [CℓO]
-6.35	k_{332} [N^+]	-6.27	k_{332} [N^+]	0.89	k_{109} [H]
...	11 More Reactions	...	11 More Reactions	...	11 More Reactions
5.385 = Log($\Sigma\Re$)		4.598 = Log($\Sigma\Re$)		9.048 = Log($\Sigma\Re$)	

c.) Summary of the lifetimes of CO in the inner domain of the three model runs.

	Log(χ)	Log([CO]) cm^{-3}	Log($\Sigma\Re$) cm^{-3}·s^{-1}	Log(τ) sec	Source Log(τ_c) sec	Sink Log(τ_c) sec
1-D Steady-State Model	−6.973	12.219	5.385	6.834	7.216	6.834
2-D Base Case Model	−6.908	12.284	4.598	7.685	8.785	7.685
2-D Electrified Model	−6.915	12.277	9.048	3.229	4.265	3.229

Note: τ = [CO] / $\Sigma\Re$ or Log(τ) = Log([CO]) − Log($\Sigma\Re$).

N_2O

Differential Net Production ($P_{I.M.}$ - $P_{B.C.}$) = 541.3 (Mg Year^{-1})

$P_{B.C.}$ = −23.56 $P_{I.M.}$ = 517.8 (Mg Year^{-1})

$\overline{\tau}_c$ = 1106.3 $\overline{\tau}_c$ = 4.747x10^{+5} $\overline{\tau}_c$ = 1.382x10^{+5} (Years)

$\overline{\chi}$ = 325.9 $\overline{\chi}$ = 326.3 $\overline{\chi}$ = 326.3 (ppB)

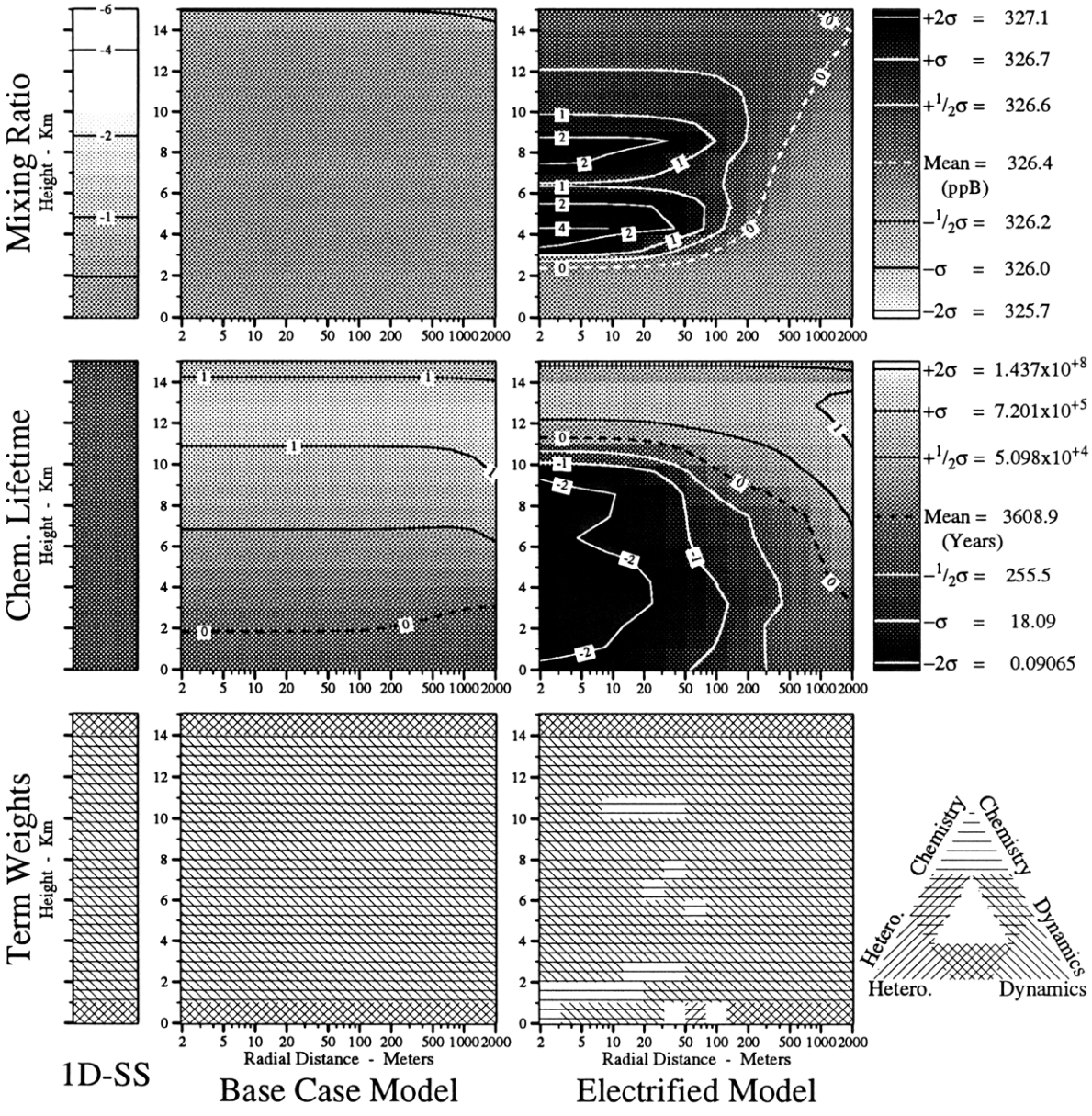

Figure 74. Mixing ratios (χ), lifetimes (τ_c), and term weights of N_2O. See text for definitions of terms and other details.

Table 44. Summary of the chemistry of N_2O in the **inner domain** of the three models. (**a**,**b**) The major terms in the continuity equations for N_2O in the three model runs and (**c**) a summary of its mixing ratios χ and lifetimes τ in the three model runs. In these tables $\Re$ is the specific rate of production of N_2O (molec·cm^{-3}·s^{-1}), τ is the total lifetime (sec) of N_2O and τ_c is its lifetime due to chemical processes (sec). J_i, j_i, k_i, and l_i are photolytic, unimolecular, bimolecular and termolecular rate coefficients respectively for reaction number i as listed in Appendix B , page 184.

a.) The major source terms for N_2O in the inner domain of the three model runs.

1-D Steady-State Model		2-D Base Case Model		2-D Electrified Model	
Log ($\Re$)	Reaction Rate $\Re = k_{yz}$ [y] [z]	Log ($\Re$)	Reaction Rate $\Re = k_{yz}$ [y] [z]	Log ($\Re$)	Reaction Rate $\Re = k_{yz}$ [y] [z]
2.21	Advection/Diffusion	1.37	Advection/Diffusion	8.40	k_{482} [N] [NO_2]
-0.35	l_{478} [N_2] [$O(^1D)$]{M}	-0.80	l_{478} [N_2] [$O(^1D)$]{M}	3.39	l_{479} [N] [NO]{M}
-1.79	k_{480} [N_2] [O]	-2.30	k_{480} [N_2] [O]	3.08	l_{478} [N_2] [$O(^1D)$]{M}
-4.67	k_{482} [N] [NO_2]	-4.96	k_{482} [N] [NO_2]	1.43	k_{480} [N_2] [O]
-8.63	l_{477} [N_2] [O] [N_2]	-8.88	l_{477} [N_2] [O] [N_2]	-0.45	k_{287} [O^-] [N_2]
-9.20	l_{476} [N_2] [O] [O_2]	-9.45	l_{476} [N_2] [O] [O_2]	-0.63	l_{395} [N_2O^+] [e^-]{M}
...	10 More Reactions	...	10 More Reactions	...	10 More Reactions
2.206 = Log($\Sigma\Re$)		1.375 = Log($\Sigma\Re$)		8.402 = Log($\Sigma\Re$)	

Note: The definitions of the reactive families $\{X\}$ are at the end of Appendix B.

b.) The major sink terms for N_2O in the inner domain of the three model runs.
The reaction rate $\Re$ implicitly contains [N_2O].

1-D Steady-State Model		2-D Base Case Model		2-D Electrified Model	
Log ($\Re$)	Reaction Rate $\Re = k_{yz}$ [y] [N_2O]	Log ($\Re$)	Reaction Rate $\Re = k_{yz}$ [y] [N_2O]	Log ($\Re$)	Reaction Rate $\Re = k_{yz}$ [y] [N_2O]
2.18	k_{32} [OH]	1.35	k_{32} [OH]	8.40	Advection/Diffusion
0.82	k_{33} [HO_2]	-0.17	k_{21} [$O(^1D)$]	5.80	k_{32} [OH]
0.34	k_{21} [$O(^1D)$]	-0.31	k_{22} [$O(^1D)$]	5.44	k_{323} [N_2^+]
0.20	k_{22} [$O(^1D)$]	-0.42	k_{33} [HO_2]	5.18	k_{322} [N_2^+]
-4.52	k_{323} [N_2^+]	-4.52	k_{323} [N_2^+]	4.64	k_{152} [$N(^2D)$]
-4.78	k_{322} [N_2^+]	-4.78	k_{322} [N_2^+]	3.77	k_{334} [N^+]
...	22 More Reactions	...	22 More Reactions	...	22 More Reactions
2.206 = Log($\Sigma\Re$)		1.375 = Log($\Sigma\Re$)		8.402 = Log($\Sigma\Re$)	

c.) Summary of the lifetimes of N_2O in the inner domain of the three model runs.

	Log(χ)	Log([N_2O]) cm^{-3}	Log($\Sigma\Re$) cm^{-3}·s^{-1}	Log(τ) sec	Source Log(τ_c) sec	Sink Log(τ_c) sec
1-D Steady-State Model	−6.487	12.705	2.206	10.499	13.037	10.499
2-D Base Case Model	−6.486	12.705	1.375	11.330	13.494	11.330
2-D Electrified Model	−6.486	12.706	8.402	4.304	4.304	6.653

Note: τ = [N_2O] / $\Sigma\Re$ or Log(τ) = Log([N_2O]) − Log($\Sigma\Re$).

CCl_4

Differential Net Production ($P_{I.M.}$ - $P_{B.C.}$) = −7.120 (Mg Year^{-1})

$P_{B.C.}$ = −0.19307 $P_{I.M.}$ = −7.313 (Mg Year^{-1})

$\overline{\tau}_c$ = 1.467x10^{+4} $\overline{\tau}_c$ = 2.208x10^{+4} $\overline{\tau}_c$ = 1.416x10^{+4} (Years)

$\overline{\chi}$ = 149.1 $\overline{\chi}$ = 149.9 $\overline{\chi}$ = 149.8 (ppT)

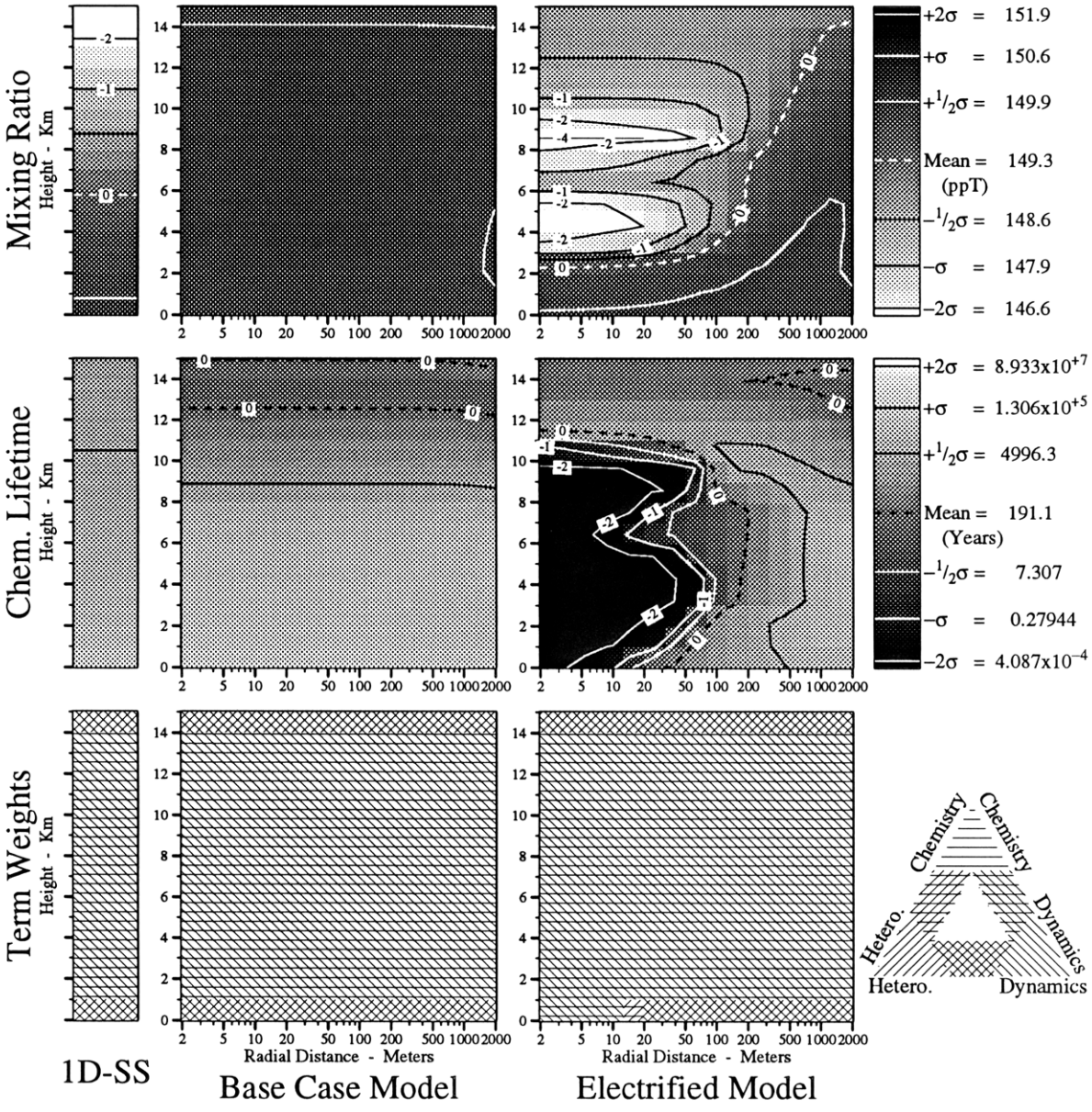

Figure 75. Mixing ratios (χ), lifetimes (τ_c), and term weights of $CC\ell_4$. See text for definitions of terms and other details.

Table 45. Summary of the chemistry of $CC\ell_4$ in the **inner domain** of the three models. (**a**,**b**) The major terms in the continuity equations for $CC\ell_4$ in the three model runs and (**c**) a summary of its mixing ratios χ and lifetimes τ in the three model runs. In these tables $\Re$ is the specific rate of production of $CC\ell_4$ (molec·cm^{-3}·s^{-1}), τ is the total lifetime (sec) of $CC\ell_4$ and τ_c is its lifetime due to chemical processes (sec). J_i, j_i, k_i, and l_i are photolytic, unimolecular, bimolecular and termolecular rate coefficients respectively for reaction number i as listed in Appendix B , page 184.

a.) The major source terms for $CC\ell_4$ in the inner domain of the three model runs.

1-D Steady-State Model		2-D Base Case Model		2-D Electrified Model	
Log (ℜ)	Reaction Rate ℜ = k_{yz} [y] [z]	Log (ℜ)	Reaction Rate ℜ = k_{yz} [y] [z]	Log (ℜ)	Reaction Rate ℜ = k_{yz} [y] [z]
-2.27	Advection/Diffusion	-2.52	Advection/Diffusion	5.97	Advection/Diffusion
$-\infty$	Flux	$-\infty$	Flux	$-\infty$	Flux
-2.267 = Log(Σℜ)		-2.515 = Log(Σℜ)		5.970 = Log(Σℜ)	

b.) The major sink terms for $CC\ell_4$ in the inner domain of the three model runs. The reaction rate ℜ implicitly contains [$CC\ell_4$].

1-D Steady-State Model		2-D Base Case Model		2-D Electrified Model	
Log (ℜ)	Reaction Rate ℜ = k_{yz} [y] [$CC\ell_4$]	Log (ℜ)	Reaction Rate ℜ = k_{yz} [y] [$CC\ell_4$]	Log (ℜ)	Reaction Rate ℜ = k_{yz} [y] [$CC\ell_4$]
-2.31	k_{181} [$O(^1D)$]	-2.81	k_{181} [$O(^1D)$]	5.85	k_{202} [CO_4^-]
-3.32	k_{202} [CO_4^-]	-2.83	k_{202} [CO_4^-]	5.35	k_{186} [e^-]
-4.61	k_{186} [e^-]	-4.61	k_{186} [e^-]	3.06	k_{199} [O_4^-]
-6.34	k_{199} [O_4^-]	-5.94	k_{199} [O_4^-]	2.24	k_{196} [O_2^-]
-7.50	k_{196} [O_2^-]	-7.31	k_{196} [O_2^-]	1.11	k_{181} [$O(^1D)$]
-9.04	j_{121}	-9.04	j_{121}	0.39	k_{185} [e^-]
-9.39	J_{16}	-9.39	J_{16}	-2.04	k_{208} [H^-]
-9.57	k_{185} [e^-]	-9.56	k_{185} [e^-]	-4.18	k_{205} [O^-]
-14.97	k_{205} [O^-]	-15.73	k_{205} [O^-]	-9.05	j_{121}
...	5 More Reactions	...	5 More Reactions	...	5 More Reactions
-2.267 = Log(Σℜ)		-2.515 = Log(Σℜ)		5.970 = Log(Σℜ)	

c.) Summary of the lifetimes of $CC\ell_4$ in the inner domain of the three model runs.

	Log(χ)	Log([$CC\ell_4$]) cm^{-3}	Log(Σℜ) cm^{-3}·s^{-1}	Log(τ) sec	Source Log(τ_c) sec	Sink Log(τ_c) sec
1-D Steady-State Model	−9.825	9.366	−2.267	11.634	+∞	11.634
2-D Base Case Model	−9.824	9.368	−2.515	11.883	+∞	11.883
2-D Electrified Model	−9.829	9.363	5.970	3.392	+∞	3.392

Note: τ = [$CC\ell_4$] / Σℜ or Log(τ) = Log([$CC\ell_4$]) − Log(Σℜ).

CF_4

Differential Net Production ($P_{I.M.}$ - $P_{B.C.}$) = −14.90 (Kg Year^{-1})

$P_{B.C.}$ = −3.578 $P_{I.M.}$ = −18.48 (Kg Year^{-1})

$\overline{\tau}_c$ = 6.501x10^{+7} $\overline{\tau}_c$ = 6.051x10^{+7} $\overline{\tau}_c$ = 3.480x10^{+7} (Years)

$\overline{\chi}$ = 70.01 $\overline{\chi}$ = 70.03 $\overline{\chi}$ = 70.03 (ppT)

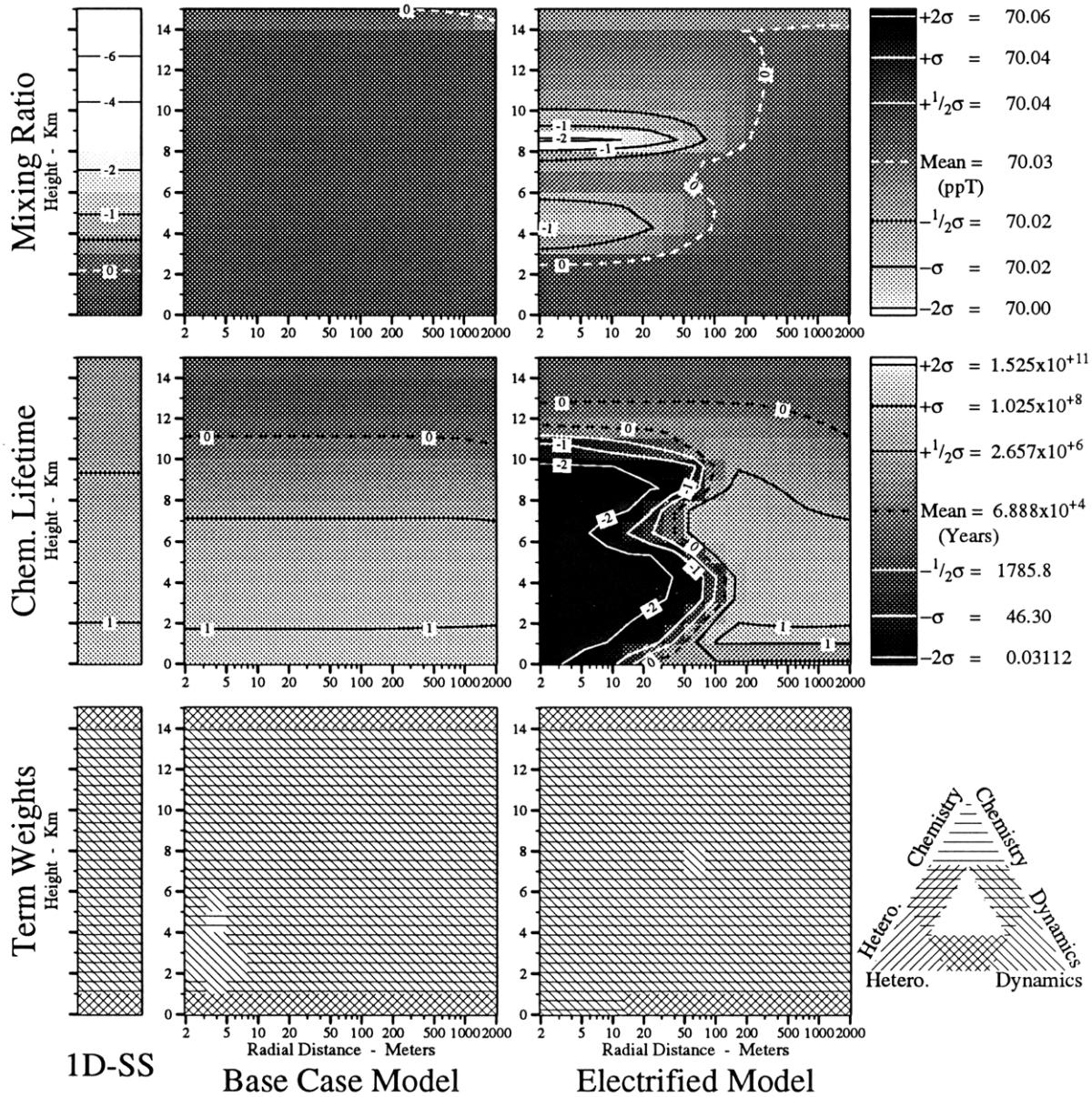

Figure 76. Mixing ratios (χ), lifetimes (τ_c), and term weights of CF_4. See text for definitions of terms and other details.

Table 46. Summary of the chemistry of CF_4 in the **inner domain** of the three models. (**a,b**) The major terms in the continuity equations for CF_4 in the three model runs and (**c**) a summary of its mixing ratios χ and lifetimes τ in the three model runs. In these tables $\Re$ is the specific rate of production of CF_4 (molec·cm^{-3}·s^{-1}), τ is the total lifetime (sec) of CF_4 and τ_c is its lifetime due to chemical processes (sec). J_i, j_i, k_i, and l_i are photolytic, unimolecular, bimolecular and termolecular rate coefficients respectively for reaction number i as listed in Appendix B , page 184.

a.) The major source terms for CF_4 in the inner domain of the three model runs.

1-D Steady-State Model		2-D Base Case Model		2-D Electrified Model	
Log ($\Re$)	Reaction Rate $\Re = k_{yz}\,[y]\,[z]$	Log ($\Re$)	Reaction Rate $\Re = k_{yz}\,[y]\,[z]$	Log ($\Re$)	Reaction Rate $\Re = k_{yz}\,[y]\,[z]$
-5.65	Advection/Diffusion	-5.16	Advection/Diffusion	3.53	Advection/Diffusion
-34.30	k_{157} [CF_3] [F]	-33.08	k_{157} [CF_3] [F]	-15.18	k_{157} [CF_3] [F]
$-\infty$	Flux	$-\infty$	Flux	$-\infty$	Flux
-5.646 = Log($\Sigma\Re$)		-5.155 = Log($\Sigma\Re$)		3.534 = Log($\Sigma\Re$)	

b.) The major sink terms for CF_4 in the inner domain of the three model runs.
The reaction rate $\Re$ implicitly contains [CF_4].

1-D Steady-State Model		2-D Base Case Model		2-D Electrified Model	
Log ($\Re$)	Reaction Rate $\Re = k_{yz}\,[y]\,[CF_4]$	Log ($\Re$)	Reaction Rate $\Re = k_{yz}\,[y]\,[CF_4]$	Log ($\Re$)	Reaction Rate $\Re = k_{yz}\,[y]\,[CF_4]$
-5.65	k_{201} [CO_4^-]	-5.16	k_{201} [CO_4^-]	3.53	k_{201} [CO_4^-]
-8.66	k_{198} [O_4^-]	-8.27	k_{198} [O_4^-]	0.74	k_{198} [O_4^-]
-9.37	j_{122}	-9.37	j_{122}	-0.07	k_{195} [O_2^-]
-9.83	k_{195} [O_2^-]	-9.64	k_{195} [O_2^-]	-3.42	k_{184} [e^-]
-17.30	k_{204} [O^-]	-18.06	k_{204} [O^-]	-3.42	k_{183} [e^-]
-19.55	k_{207} [H^-]	-21.17	k_{207} [H^-]	-4.35	k_{207} [H^-]
$-\infty$	k_{183} [e^-]	$-\infty$	k_{183} [e^-]	-6.50	k_{204} [O^-]
$-\infty$	Advection/Diffusion	$-\infty$	Advection/Diffusion	-9.37	j_{122}
...	4 More Reactions	...	4 More Reactions	...	4 More Reactions
-5.646 = Log($\Sigma\Re$)		-5.156 = Log($\Sigma\Re$)		3.534 = Log($\Sigma\Re$)	

c.) Summary of the lifetimes of CF_4 in the inner domain of the three model runs.

	Log(χ)	Log([CF_4]) cm^{-3}	Log($\Sigma\Re$) $cm^{-3}\cdot s^{-1}$	Log(τ) sec	Source Log(τ_c) sec	Sink Log(τ_c) sec
1-D Steady-State Model	−10.155	9.037	−5.646	14.683	43.340	14.683
2-D Base Case Model	−10.155	9.037	−5.156	14.193	42.120	14.193
2-D Electrified Model	−10.155	9.037	3.534	5.504	24.219	5.504

Note: τ = [CF_4] / $\Sigma\Re$ or Log(τ) = Log([CF_4]) − Log($\Sigma\Re$).

Clusters

Differential Net Production ($P_{I.M.} - P_{B.C.}$) = -5.764 (Moles Year^{-1})

$P_{B.C.} = -2.310 \times 10^{+4}$ $P_{I.M.} = -2.311 \times 10^{+4}$ (Moles Year^{-1})

$\overline{\tau}_c = 4.390 \times 10^{+4}$ $\overline{\tau}_c = 6992.6$ $\overline{\tau}_c = 853.2$ (Seconds)

$\overline{\chi} = 2.292 \times 10^{-13}$ $\overline{\chi} = 1.824 \times 10^{-15}$ $\overline{\chi} = 2.618 \times 10^{-13}$ (Mixing Ratio)

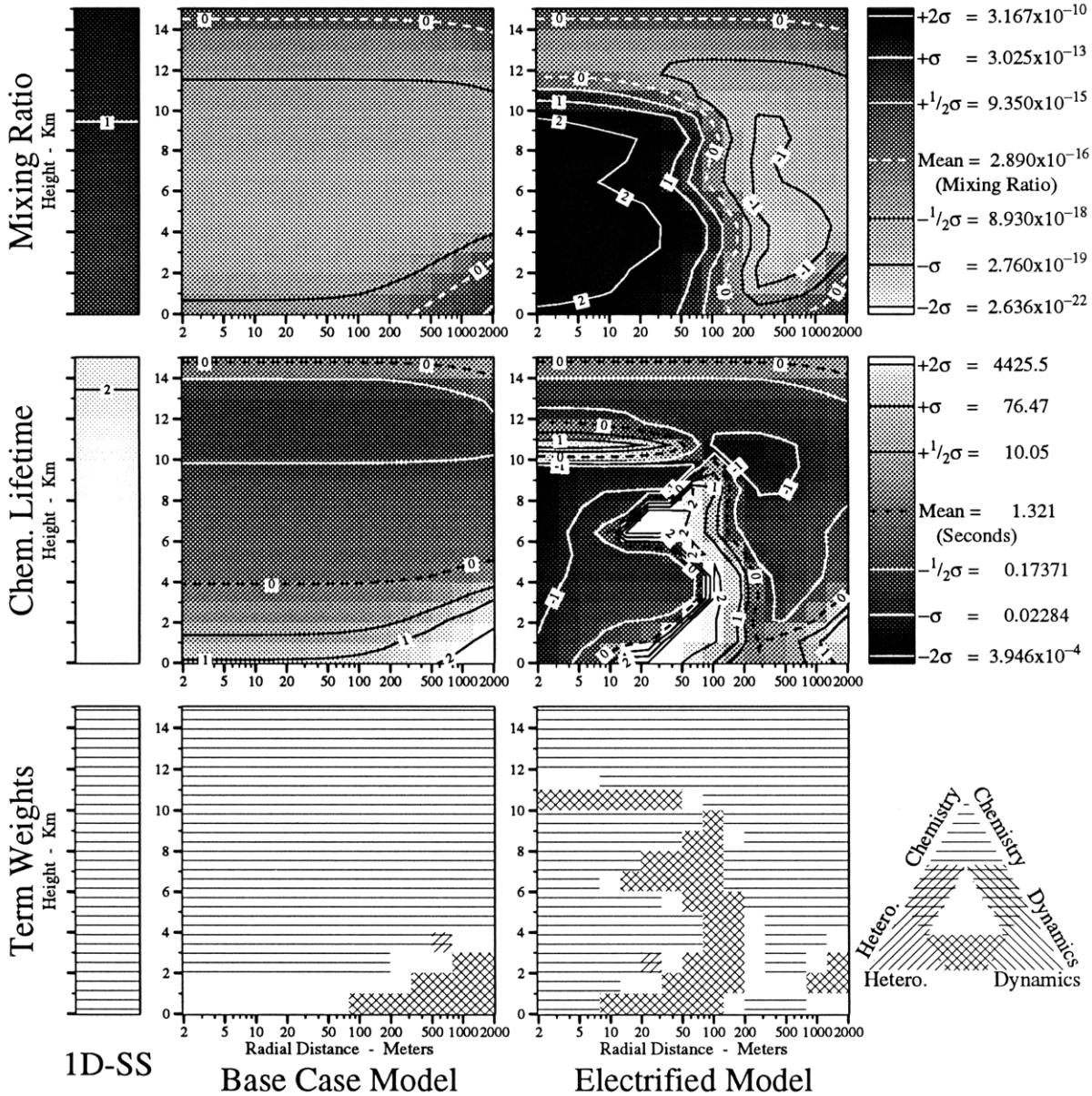

Figure 77. Mixing ratios (χ), lifetimes (τ_c), and term weights of Clusters. See text for definitions of terms and other details.

Table 47. Summary of the chemistry of Clusters in the **inner domain** of the three models. (**a**,**b**) The major terms in the continuity equations for Clusters in the three model runs and (**c**) a summary of its mixing ratios χ and lifetimes τ in the three model runs. In these tables $\Re$ is the specific rate of production of Clusters (molec·cm^{-3}·s^{-1}), τ is the total lifetime (sec) of Clusters and τ_c is its lifetime due to chemical processes (sec). J_i, j_i, k_i, and l_i are photolytic, unimolecular, bimolecular and termolecular rate coefficients respectively for reaction number i as listed in Appendix B , page 184.

a.) The major source terms for Clusters in the inner domain of the three model runs.

1-D Steady-State Model		2-D Base Case Model		2-D Electrified Model	
Log ($\Re$)	Reaction Rate $\Re = k_{yz}$ [y] [z]	Log ($\Re$)	Reaction Rate $\Re = k_{yz}$ [y] [z]	Log ($\Re$)	Reaction Rate $\Re = k_{yz}$ [y] [z]
1.21	l_{361} [NO^+] [N_2]{M}	1.21	l_{361} [NO^+] [N_2]{M}	11.20	l_{224} [O_2^+] [N_2]{M}
1.15	l_{224} [O_2^+] [N_2]{M}	1.15	l_{224} [O_2^+] [N_2]{M}	10.88	k_{216} [O_4^+] [H_2O]
0.66	k_{216} [O_4^+] [H_2O]	0.66	k_{216} [O_4^+] [H_2O]	10.78	l_{361} [NO^+] [N_2]{M}
0.39	l_{368} [NO^+] [H_2O]{M}	0.39	l_{368} [NO^+] [H_2O]{M}	10.38	l_{368} [NO^+] [H_2O]{M}
0.06	Advection/Diffusion	-0.00	Advection/Diffusion	9.92	k_{341} [H_2O^+] [H_2O]
-0.29	k_{341} [H_2O^+] [H_2O]	-0.29	k_{341} [H_2O^+] [H_2O]	9.18	l_{377} [NO^+] [CO_2]{M}
...	3 More Reactions	...	3 More Reactions	...	3 More Reactions
1.595 = Log($\Sigma\Re$)		1.594 = Log($\Sigma\Re$)		11.516 = Log($\Sigma\Re$)	

Note: The definitions of the reactive families $\{X\}$ are at the end of Appendix B.

b.) The major sink terms for Clusters in the inner domain of the three model runs.

1-D Steady-State Model		2-D Base Case Model		2-D Electrified Model	
Log ($\Re$)	Reaction Rate $\Re = k_{yz}$ [y] {Clusters}	Log ($\Re$)	Reaction Rate $\Re = k_{yz}$ [y] {Clusters}	Log ($\Re$)	Reaction Rate $\Re = k_{yz}$ [y] {Clusters}
1.20	k_{362} [N_2NO^+]{M}	1.20	k_{362} [N_2NO^+]{M}	10.94	k_{349} [$N_2O_2^+$]{M}
0.86	k_{349} [$N_2O_2^+$]{M}	0.86	k_{349} [$N_2O_2^+$]{M}	10.83	k_{350} [$N_2O_2^+$] [O_2]
0.82	k_{350} [$N_2O_2^+$] [O_2]	0.82	k_{350} [$N_2O_2^+$] [O_2]	10.80	k_{352} [WO_2^+] [O_2]
0.75	Heterogeneous Loss	0.74	Heterogeneous Loss	10.77	k_{362} [N_2NO^+]{M}
0.58	k_{352} [WO_2^+] [O_2]	0.58	k_{352} [WO_2^+] [O_2]	10.70	Heterogeneous Loss
-0.76	k_{367} [$NOCO_2^+$]{M}	-0.76	k_{367} [$NOCO_2^+$]{M}	9.18	k_{347} [$W_2H_3O^+$] [e^-]
...	14 More Reactions	...	14 More Reactions	...	14 More Reactions
1.595 = Log($\Sigma\Re$)		1.594 = Log($\Sigma\Re$)		11.516 = Log($\Sigma\Re$)	

Notes: Read **W** as H_2O. The definitions of the reactive families $\{X\}$ are at the end of Appendix B.

c.) Summary of the lifetimes of Clusters in the inner domain of the three model runs.

	Log(χ)	Log(Clusters) cm^{-3}	Log($\Sigma\Re$) cm^{-3}·s^{-1}	Log(τ) sec	Source Log(τ_c) sec	Sink Log(τ_c) sec
1-D Steady-State Model	−13.160	6.032	1.595	4.436	4.449	4.503
2-D Base Case Model	−17.624	1.568	1.594	−0.026	−0.014	0.040
2-D Electrified Model	−9.207	9.985	11.516	−1.531	−1.531	−1.458

Note: τ = Clusters / $\Sigma\Re$ or Log(τ) = Log(Clusters) − Log($\Sigma\Re$).

Appendix E Extended Altitude Model

High altitude SF_6 loss

To model the chemical lifetime of a compound with a loss mechanism high above the model domain ($Z_{loss} \gg$ 20km), a 1D steady state model was run for the region up to 150 km. The 1976 U.S. Standard Atmosphere was used for the required vertical distributions of atmospheric density ρ_{air} ($kg \cdot m^{-3}$) and temperature T; the vertical distribution of the transport coefficient $K_{transp.}$ ($m^2 \cdot s^{-1}$) is from *Gurney* [1990] for the region 0 – 80 km and extrapolated from 80 – 150 km. The vertical distributions of ρ_{air}, T, and $K_{transp.}$ are shown in Figure 78.

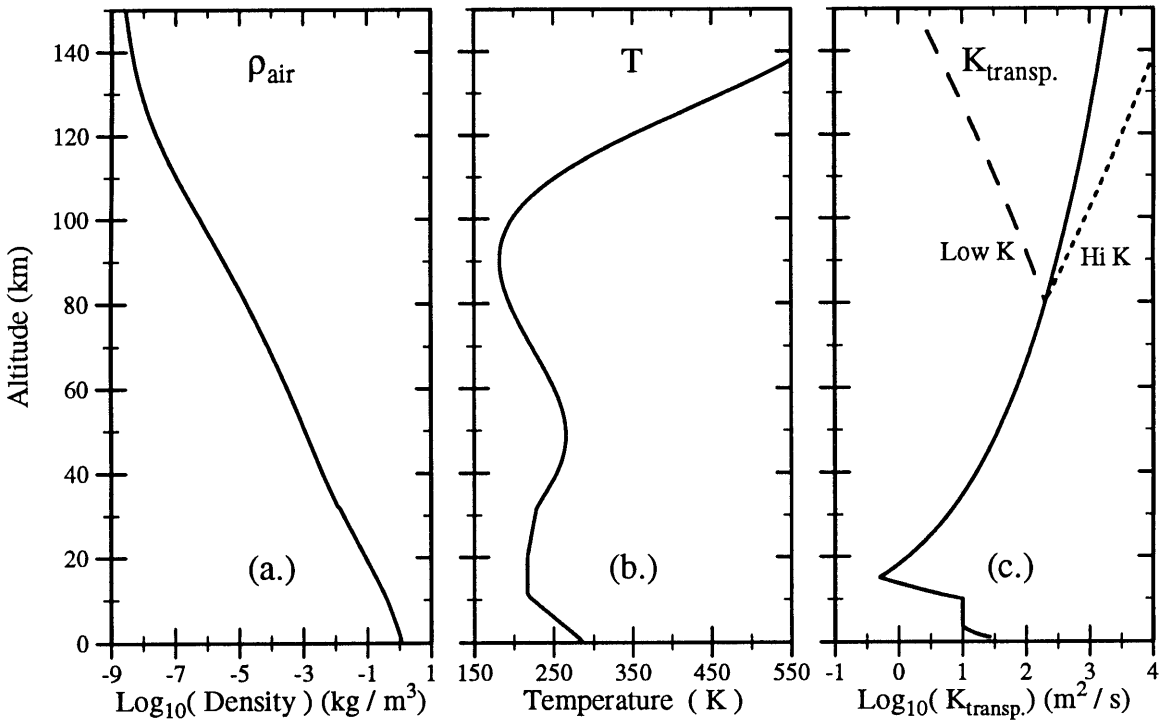

Figure 78. (a.) Atmospheric density ρ_{air}, (b.) Tempreature T, and (c.) the Transport coefficient $K_{transp.}$ *vs.* Height in the extended altitude model. See text for **Low K** and **Hi K**.

To determine the sensitivity of the results to the extrapolation of $K_{transp.}$, models were run wherein the values of $K(z)_{transp.}$ were varied from their nominal values above 80 km. These runs used the values of $K(z)_{transp.}$ indicated by **Low**$K(z)$ and **Hi**$K(z)$ on Figure 78.

In this model the only reaction considered is the loss of SF_6 due to its reaction with the electron

$$R_{188} \qquad SF_6 + e \rightarrow SF_5 + F^- \qquad k_{188} = e\_k\_SF5,$$

and the vertical distribution of the electron number density [e^-] (cm^{-3}) is from *U.S.A.F.*, [1961]. The rate coefficient for this reaction (e_k_SF5) is derived from the measurements the electron capture cross-section summarized by *Gallagher et. al.* [1983] and is a sensitive function of the mean electron energy. The thermal electron capture cross-section of SF_6 is a decreasing function of increasing electron energy that is maximal at thermal electron energies with a value of $\approx 200 \times 10^{-22}$ m^{-2} and decreases to $\approx 10 \times 10^{-22}$ m^{-2} at E/N values of 10^{-18} $V{\cdot}m^{-1}$ / $molec{\cdot}m^{-3}$.

The resulting vertical variations of the mixing ratio of SF_6 and its lifetime are shown in Figure 79. It can be seen in this figure that most of the destruction occurs at the upper model domain, where there is an upper boundary condition of infinite loss at 150 km. This indicates that even with the high electron number densities and temperatures found in the mesosphere and lower thermosphere, the bulk of the SF_6 would be lost at altitudes above 150 km in this model.

Complete Destruction at Altitude Z_{loss} Model

To simplify the analysis of other compounds with loss mechanisms at high altitudes, another 1D model was run wherein the **only** loss was at a prescribed altitude Z_{loss}. This loss was made very large, so it can be considered an infinite loss mechanism for all practical purposes.

By varying the altitude of this complete destruction (Z_{loss}), is is possible to compute the atmospheric lifetime τ of a compound as a function of its (assumed) altitude of destruction. The results of this model are shown in in Figure 80. as can be seen from this graph, the chemical lifetime rises rapidly from $<$ 1 year to $\approx$ 70 years as the height of the destruction increases from 10 to 30 km. Averaging over the whole interval $0 - 150$ km, crudely speaking, the atmospheric lifetime increases by a factor of 10 as the height of destruction increases by 20 km.

Increasing the assumed value of $K_{transp.}$ in the thermosphere leads to a decrease in the atmospheric lifetime for loss processes in the thermosphere. For example, increasing the values of $K(z)_{transp.}$ from **Low K(z)** to **Hi K(z)** results in decreasing the atmospheric lifetime (τ) of a compound with a complete loss process at 100 km from 34,000 years to 6,300 years respectively.

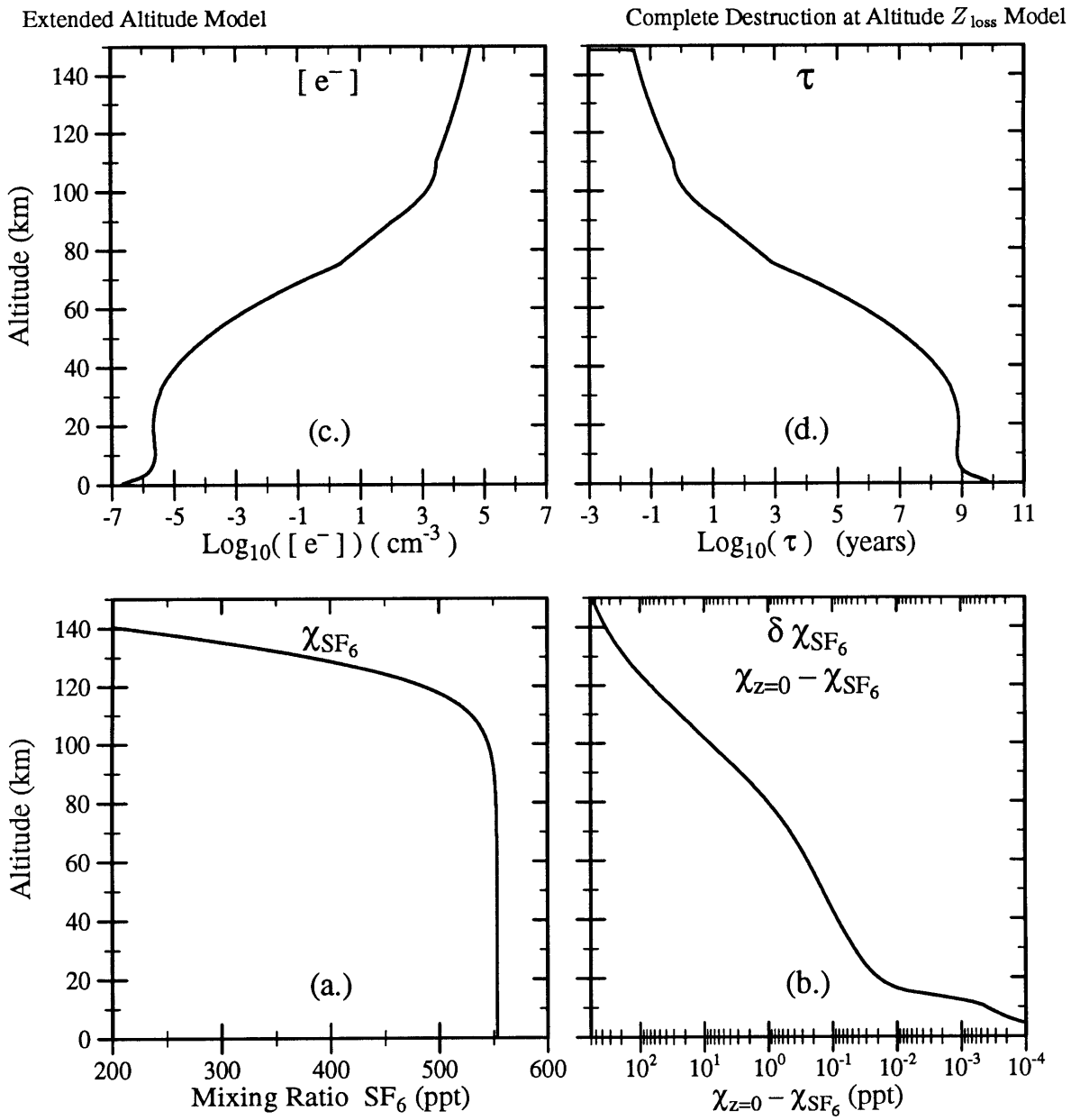

Figure 79. Vertical variations in the mixing ratio χ_{SF_6} (a.,b.) and lifetime τ (c.) of SF_6 in the extended altitude model along with the prescribed electron number density $[e^-]$ (d.). $\delta\chi_{SF_6}$ is defined to be the difference between the local mixing ratio χ_{SF_6} and the mixing ratio at the ground $\chi_{z=0}$.

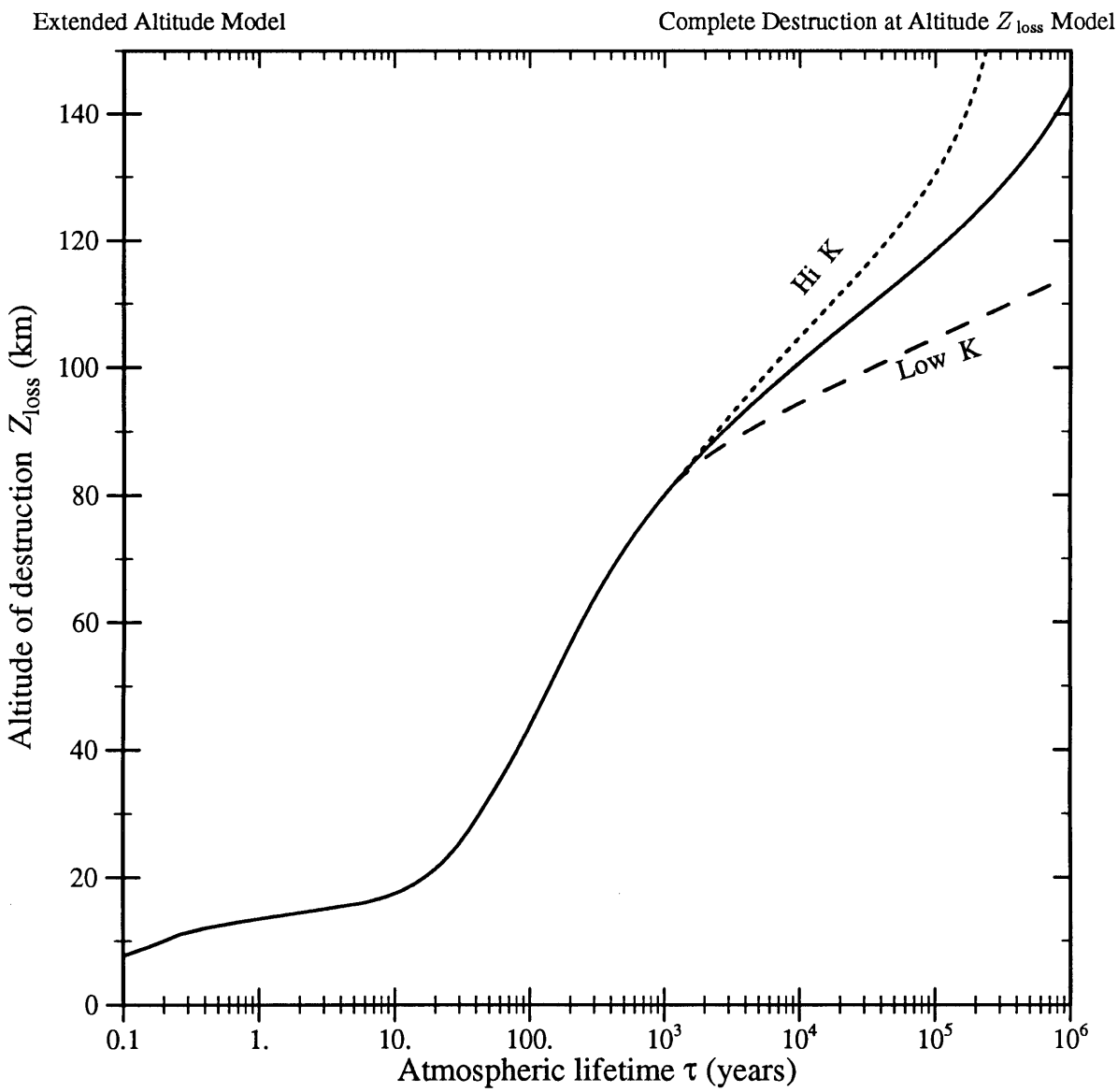

Figure 80. Atmospheric lifetime τ *vs.* Altitude of destruction Z_{loss} in the extended altitude model. See text for **Low K** and **Hi K**.

Appendix F Symbols and Their Meanings

Table 48. List of Symbols and Their Meanings.

Symbol	Definition/Name	Value	Units	Page(s)
α_0, α_1	Grid spacing coefficients	–	–	43, 45, 48
$\alpha_{i,j}$	Finite-difference coefficient	–	s^{-1}	50
α_K	Diffusion scaling coefficient	10 – 50	–	62
α_W	Constant	0.667	–	57
β	Power of polynomial	$0 \ldots \pm 5$	–	43, 45–47
$B(T, \lambda)$	Planck function	–	$W \cdot m^{-2} \cdot sr^{-1} \cdot m^{-1}$	91
c	Speed of light in vacuum	2.998×10^8	$m \cdot s^{-1}$	91
χ_i	Mixing ratio of species i	10^{-9}	$molec_i \cdot molec_{air}^{-1}$	32, 34, 36, 50
$\bar{\chi}$	Domain-average mixing ratio	–	–	138
dBZ	Radar reflectivity	0 – 6	$mm^6 \cdot m^{-3}$	71, 72
$\vec{\vec{D}}$	Diffusion tensor	100	$m^2 \cdot s^{-1}$	33
δ	Radial grid spacing	1 – 1000	m	37
D	Cloud particle's diameter	–	cm	66
E_{BD}	Breakdown strength of air	$\approx 0.5 \times 10^6$	$V \cdot m^{-1}$	30, 78
E_ℓ	Local field when channel **is** conductive	–	$V \cdot m^{-1}$	69
E_a	Local field when channel **is not** conductive	–	$V \cdot m^{-1}$	69
$\vec{E}(r, z)$	Electric field	$10^2 – 10^6$	$V \cdot m^{-1}$	33, 36
$E_r(r, z)$	Radial electric field	$10^2 – 10^6$	$V \cdot m^{-1}$	37, 39, 75
$E_z(r, z)$	Vertical electric field	$10^2 – 10^4$	$V \cdot m^{-1}$	39, 74, 76
e^-	Charge of electron	1.6×10^{-19}	Coulombs (C)	80
$E_\pm$	Ionization energy	≈ 16	$eV \cdot ion\ pair^{-1}$	79, 83
ϵ	Gray body emissivity	0.05	–	87–89
ε_0	Permittivity of free space	8.85×10^{-12}	$C^2 \cdot N^{-1} \cdot m^{-2}$	78
ε	Radial power law for $\vec{E}(r, z)$	0 – 3	–	42, 48, 49
eV	Electron volt	1.6×10^{-19}	J	79

... Continued next page ...

Table 48–B. List of Symbols and Meanings – continued.

Symbol	Definition/Name	Value	Units	Page(s)
f_ℓ	Fraction of time channel is conductive	0.01	–	69
$f_L(z)$	Lightning flash rate	0 – 0.3	strokes·s^{-1}	212
F_i	Flux into region	–	molec$_i$·m^{-3}s^{-1}	34
$F(r)$	General function of r	–	varies	41
$\Gamma(T, \lambda)$	Outward photon flux	–	Photons·m^{-2}·s^{-1}·m^{-1}	90
$\Gamma(\delta\lambda)$	Photons per meter of channel	–	Photons·m^{-1}	90
h	Planck's constant	6.63×10^{-34}	J·Hz^{-1}	91
H_i	Heterogeneous loss rate	10^{-2}	s^{-1}	34
H_o	Determines height of W_{max}	5	km	57
i	Chemical species (compound) i	–	–	32
$\Im_C$	"Chemical Importance"	–	–	138
$\Im_D$	"Dynamic Importance"	–	–	138
$\Im_H$	"Hetero. Importance"	–	–	138
$I(z)$	cosmic-ray energy deposition	$O[10^4]$	MeV·m^{-3}·s^{-1}	83, 97
$j(\theta, z)$	cosmic-ray radiance	$O[10^7]$	MeV·m^{-2}·s^{-1}·sr^{-1}	83
$J(z)$	cosmic-ray irradiance	$O[10^7]$	MeV·m^{-2}·s^{-1}	83
k	Boltzmann's constant (R/N$_A$)	1.38×10^{-23}	J·K^{-1}	68
κ	Dielectric strength	–	–	80
K_{eddy}	Eddy diffusion coefficient	5 – 125	m^2·s^{-1}	33, 62–64
K_{TE}	Thermodynamic Equilibrium constant	–	varies	107
$K_{transp.}$	Transport coefficient	1 – 1000	m^2·s^{-1}	275
ℓ	Mean free path	$O[10^{-6}]$	cm	33, 68
λ	Induced charge on channel	1	C·km^{-1}	75–78, 81
Λ	Marshall-Palmer distribution coeff.	–	cm^{-1}	66
L_i	Chemical loss	–	molec$_i$·m^{-3}·s^{-1}	32, 35, 36

... Continued next page ...

Table 48–C. List of Symbols and Meanings – continued.

Symbol	Definition/Name	Value	Units	Page(s)
M	Cloud liquid water content	0 – 6	g $H_2O \cdot m^{-3}$	71, 72
m	Mass of species i (MW/N_A)	$O[10^{-25}]$	kg	68
mol	Mole	–	mol	33
MW_{AIR}	Molecular Weight of air	0.0289	$kg \cdot mol^{-1}$	33
molec	Molecule	–	molec	33
μ	Electrostatic energy density	–	$J \cdot m^{-3}$	78, 81
μ^*	Total electrostatic energy	–	J	78, 80, 81
μ_{jj}	Ion mobility of specie i	–	$(m \cdot s^{-1}) / (V \cdot m^{-1})$	33, 37, 69
$\vec{\vec{\mu_i}}$	Ion mobility tensor	–	$(m \cdot s^{-1}) / (V \cdot m^{-1})$	33, 36, 69
N_A	Avogadro's constant	6.02×10^{23}	$molec \cdot mol^{-1}$	33
$N(D)$	Number density distribution	–	$cm^{-3} \cdot cm^{-1}$	66, 68
ν	Photon frequency = c/λ	–	Hz	91
N	Number of grid points per dimension	15	–	38, 43, 46
Ω	Resistance	–	ohm (V/A)	20
$\bar{\omega}_0$	Single-scattering albedo	1	–	92
ϕ	Scavenging rate	$10^{-1} - 10^3$	s^{-1}	67
$\varphi(\lambda, z)$	UV flux	$O[10^{13}]$	$cm^{-2} \cdot s^{-1}$	95
P_i	Chemical production	–	$molec_i \cdot m^{-3} \cdot s^{-1}$	32, 35, 36
Ψ	In-cloud photon free mean path	$O[3]$	m	92
q_i	Number of charges on specie i	± 1	–	33
R	Production rate of liquid water	0 – 10	mg $H_2O \cdot m^{-3} \cdot s^{-1}$	71, 72
$R_{channel}$	Channel radius	2	cm	76, 91
$\Re$	Specific production rate	–	$molec \cdot cm^{-3} \cdot s^{-1}$	139, 143
$\Re_f$	"Reactive Flux"	–	$molec \cdot cm^{-3} \cdot s^{-1}$	138
ρ_{air}^{-1}	Density of air	1 (at STP)	$kg \cdot m^{-3}$	33, 275

... Continued next page ...

Table 48–D. List of Symbols and Meanings – continued.

Symbol	Definition/Name	Value	Units	Page(s)
$\varrho_{\text{air}}^{-1}$	Number density of air	10^{25} (at STP)	molec·m^{-3}	33, 35, 97
$\rho_{\pm}$	Net space charge	10^{-9}	C·m^{-3}	75, 76
R_{inner}	Domain's inner boundary	2	m	38, 43, 46
R_{outer}	Domain's outer boundary	2000	m	38, 43, 46
R_o	Radial decay scale of W_{max}	1	km	57
SA	Cloud particle specific surface area	0 – 0.3	m^2·m^{-3}	71, 72
$\sigma(\lambda, T)$	Reaction cross-section	$O[10^{-20}]$	cm^2·molec^{-1}	95
τ	Overall lifetime of species i	–	s	28
τ_c	Chemical lifetime of species i	–	s	28
$\bar{\tau_c}$	Domain-average chemical lifetime	–	s	138
τ_d^r	Vertically averaged dynamic lifetime	–	s	57, 60, 61
$\tau_d^{r,z}$	Local dynamic lifetime	–	s	57, 61
τ_h	Heterogeneous loss lifetime	–	s	34
τ_{IC}^{-1}	Loss rate due to ion capture	± 1	s^{-1}	69, 71
τ_R	Lifetime due to rainout	–	s	73
τ_{storm}	In-cloud chemical lifetime of i	–	s	28
τ_{trop}	Tropospheric chemical lifetime of i	–	s	28
$T(t)$	Channel temperature at time t	$10^4 - 10^2$	K	91
t	Time	–	seconds (s)	32
$U(r, z)$	Radial wind velocity	0 – 1	m·s^{-1}	57–59, 119
υ	Ion pairs required to reduce the electric field from E to E_{BD}	–	Ion Pairs·m^{-3}	80, 81
$\vec{V}$	Velocity vector	–	m·s^{-1}	33
$W(r, z)$	Vertical wind velocity	0 – 12	m·s^{-1}	58, 59, 62, 63, 65, 119
W	Watt	–	J·s^{-1}	91
W_{max}	Maximum vertical velocity	12	m·s^{-1}	57, 62

... Continued next page ...

Table 48–E. List of Symbols and Meanings – continued.

Symbol	Definition/Name	Value	Units	Page(s)
ξ	Sticking coefficient	$0.1 - 10^{-4}$	–	65, 67–70
z	Height above the ground	$0 - 15$	km	57
Z_{loss}	Altitude of destruction	–	km	275, 276, 278

Key Word Index

K

L

M

N

O

P

R

W

X

Abbreviated Table of Contents